CT Abdomen
A Pattern Approach

CT Abdomen
A Pattern Approach

D Karthikeyan DMRD DNB
Consultant Radiologist
Bharat Heart Scans
Chennai

Deepa Chegu DMRD
Consultant Radiologist
Bharat Scans
Chennai

JAYPEE BROTHERS
MEDICAL PUBLISHERS (P) LTD
New Delhi

Published by

Jitendar P Vij
Jaypee Brothers Medical Publishers (P) Ltd
B-3 EMCA House, 23/23B Ansari Road, Daryaganj
New Delhi 110 002, India
Phones: +91-11-23272143, +91-11-23272703, +91-11-23282021, +91-11-23245672, Rel: 32558559
Fax: +91-11-23276490, +91-11-23245683
e-mail: jaypee@jaypeebrothers.com
Visit our website: www.jaypeebrothers.com

Branches

- 2/B, Akruti Society, Jodhpur Gam Road Satellite
  Ahmedabad 380 015
  Phones: +91-079-26926233, Rel: +91-079-32988717, Fax: +91-079-26927094
  e-mail: jpamdvd@rediffmail.com
- 202 Batavia Chambers, 8 Kumara Krupa Road
  Kumara Park East, **Bangalore** 560 001
  Phones: +91-80-22285971, +91-80-22382956, Rel: +91-80-32714073, Fax: +91-80-22281761
  e-mail: jaypeemedpubbgl@eth.net
- 282 IIIrd Floor, Khaleel Shirazi Estate, Fountain Plaza
  Pantheon Road, **Chennai** 600 008
  Phones: +91-44-28193265, +91-44-28194897, Rel: +91-44-32972089, Fax: +91-44-28193231
  e-mail: jpchen@eth.net
- 4-2-1067/1-3, 1st Floor, Balaji Building, Ramkote Cross Road
  Hyderabad 500 095, Phones: +91-40-66610020, +91-40-24758498, Rel:+91-40-32940929
  Fax:+91-40-24758499, e-mail: jpmedpub@rediffmail.com
- No. 41/3098, B and B1, Kuruvi Building, St. Vincent Road
  Kochi 682 018, Kerala, Phone: 0484-4036109
- 1-A Indian Mirror Street, Wellington Square
  Kolkata 700 013, Phones: +91-33-22451926, +91-33-22276404, +91-33-22276415, Rel: +91-33-32901926
  Fax: +91-33-22456075, e-mail: jpbcal@dataone.in
- 106 Amit Industrial Estate, 61 Dr SS Rao Road
  Near MGM Hospital, Parel, **Mumbai** 400 012
  Phones: +91-22-24124863, +91-22-24104532, Rel: +91-22-32926896
  Fax: +91-22-24160828, e-mail: jpmedpub@bom7.vsnl.net.in
- "KAMALPUSHPA" 38, Reshimbag
  Opp. Mohota Science College, Umred Road
  Nagpur 440 009 (MS)
  Phones: Rel: 3245220, Fax: 0712-2704275
  e-mail: jaypeenagpur@dataone.in

CT Abdomen: A Pattern Approach

First Edition: **2007**

ISBN 81-8061-958-3

Typeset at JPBMP typesetting unit
Printed at Gopsons Papers Ltd, Sector 60, Noida

We wish to Dedicate this book to our parents without whose inspiration and moral support this book would not have been possible.

Dr L Dhamodaran
And
Mrs Meera

Dr Hariprasad Chegu, Director,
MEdRc,Edu tech.
And
Mrs Bharathi

Preface

There are many comprehensive books on Abdominal Imaging, but very few practical easy to use books focusing on CT scan of abdomen. This book is aimed at radiology residents, junior radiologists and clinicians providing them with an abundantly illustrated guide to the various abdominal pathologies. We have tried to provide high resolution axial CT image for all the common pathologies so as to develop a pattern approach. Text and tabular columns are from our experience, gleaned from standard textbooks and from reputed radiology journals. This book best serves its purpose as a companion guide to be used at the time of reporting a scan.

D Karthikeyan
Deepa Chegu

Acknowledgements

We wish to thank all the staff and referring physicians in our Hospital for their constant support.

Special mention goes to our technicians Mr Parthiban, Mr Murugesan and Mr Manoharan for their help and support.

We wish to thank our brother Vinod Chegu for his encouragement.

We wish to thank our teachers for instilling in us the basic foundation of radiology.

Contents

1. **Axial Anatomy** *1*
2. **Liver** *14*
3. **Gallbladder and Biliary Tract** *68*
4. **Spleen** *89*
5. **Pancreas** *102*
6. **Genitourinary System** *137*
7. **Adrenal Gland** *222*
8. **Gastrointestinal System** *232*
9. **Abdominal Trauma** *358*

Index *377*

CD Content

Pictorial Review of Interesting Cases

CHAPTER

1

Axial Anatomy

NORMAL AXIAL CT ANATOMY

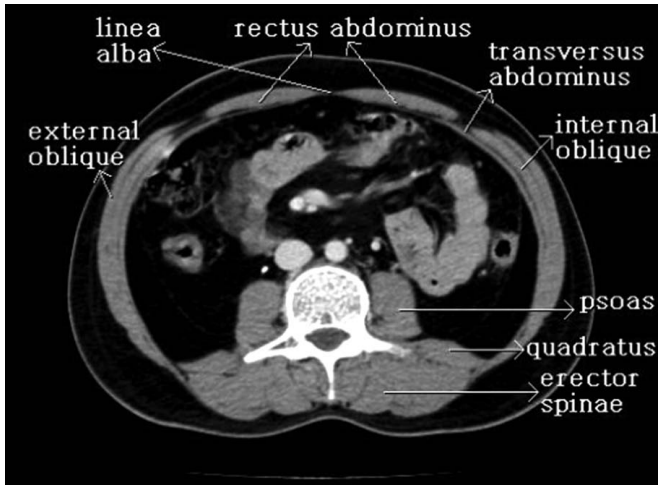

FIGURE 1.1: Axial CT sections showing abdominal wall muscles.

Liver Segments

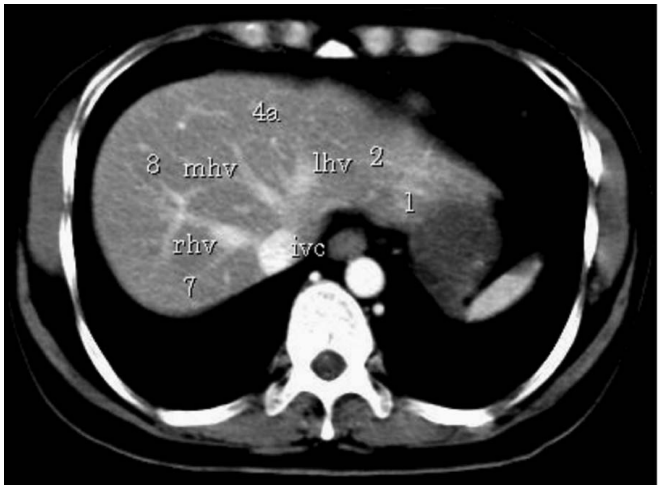

FIGURE 1.2

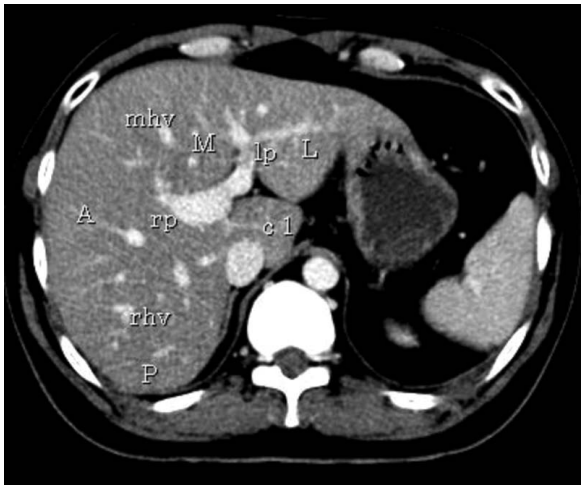

FIGURE 1.3

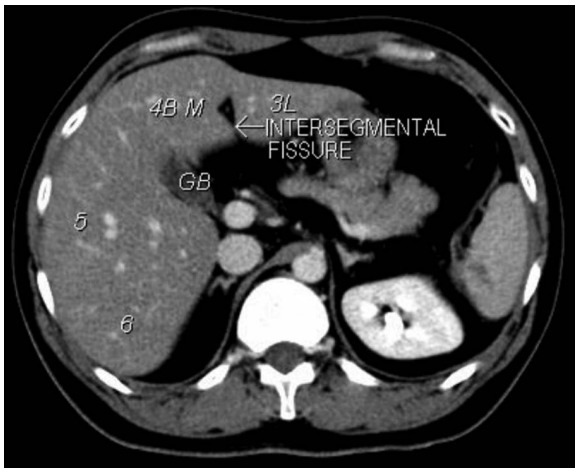

FIGURE 1.4

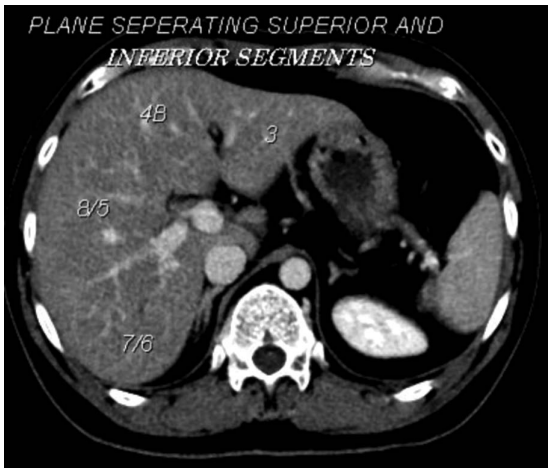

FIGURE 1.5

SURFACE REFORMATION

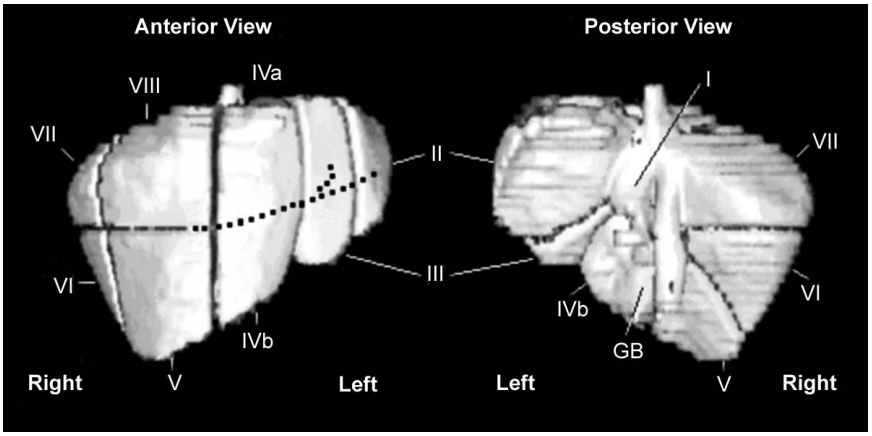

FIGURE 1.6

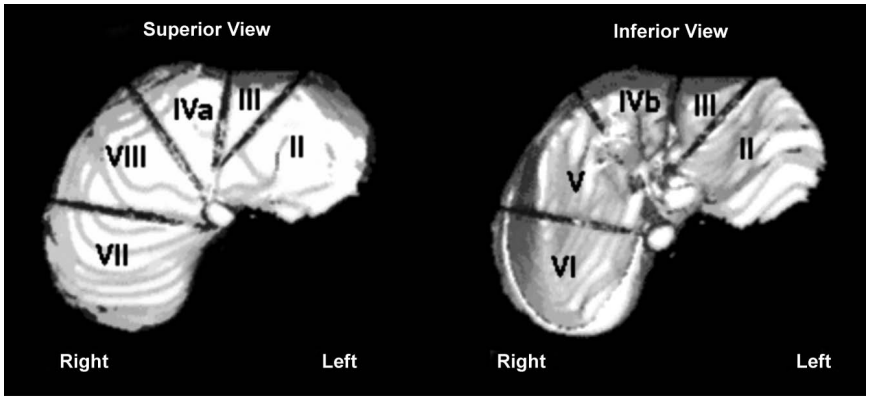

I. caudate
II. left posterolateral segment
III. left anterolateral segment
IVa. left superomedial segment
IVb. left inferomedial segment
V. right anteroinferior segment
VI. right posteroinferior segment
VII. right posterosuperior segment
VIII. right anterosuperior segment

FIGURE 1.7

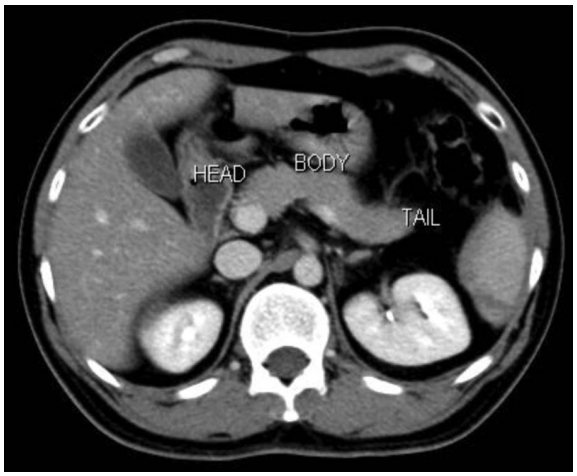

FIGURE 1.8: Pancreas.

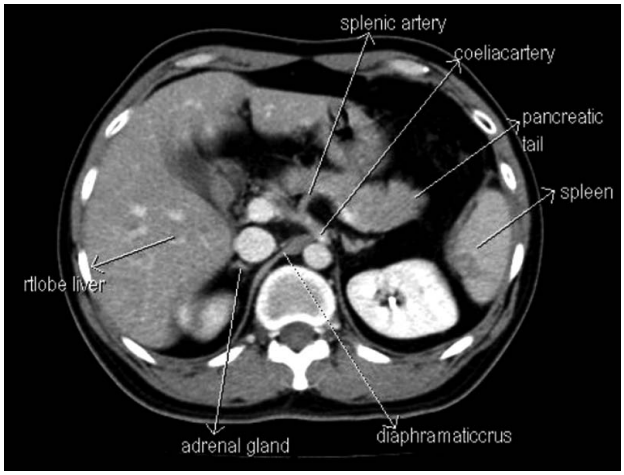

FIGURE 1.9: Axial section at the celiac axis level.

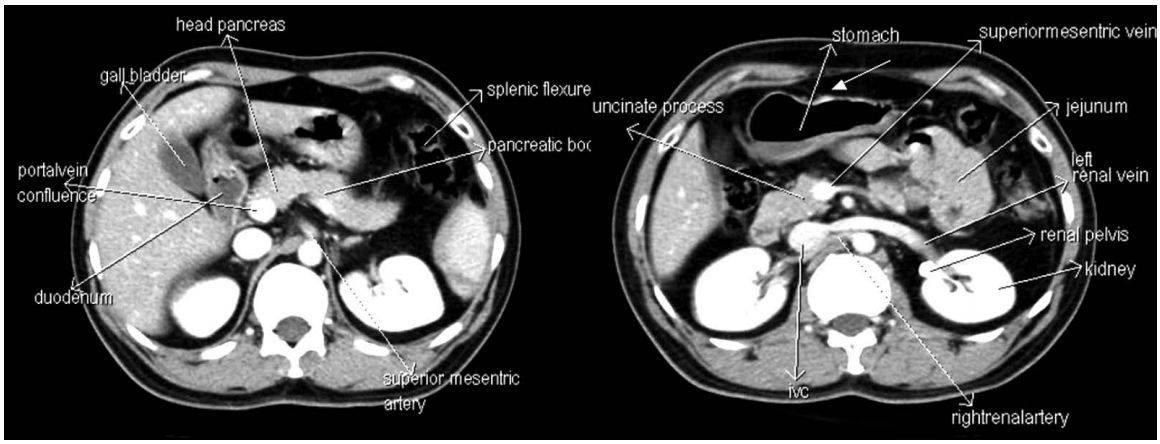

FIGURE 1.10: Axial sections at the level of SMA.

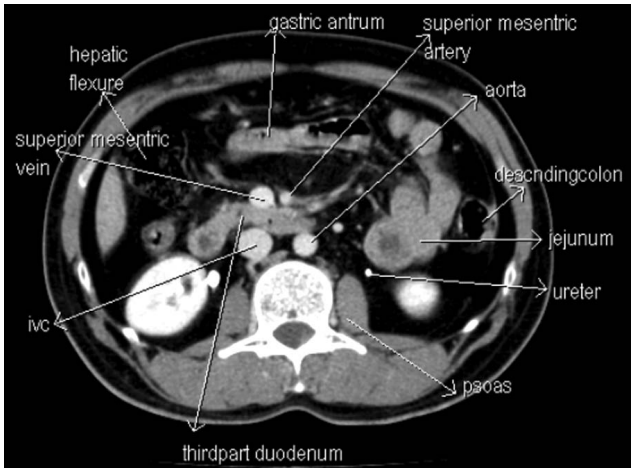

FIGURE 1.11

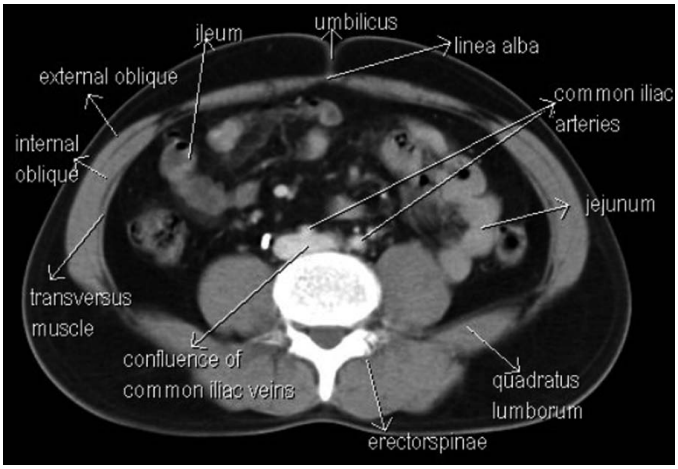

FIGURE 1.12: Axial section at the level of umbilicus.

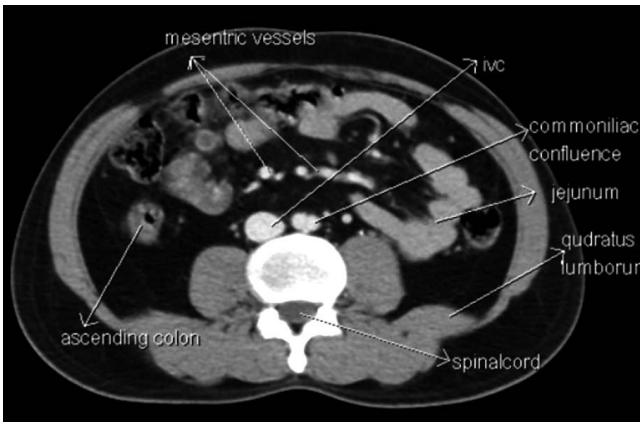

FIGURE 1.13

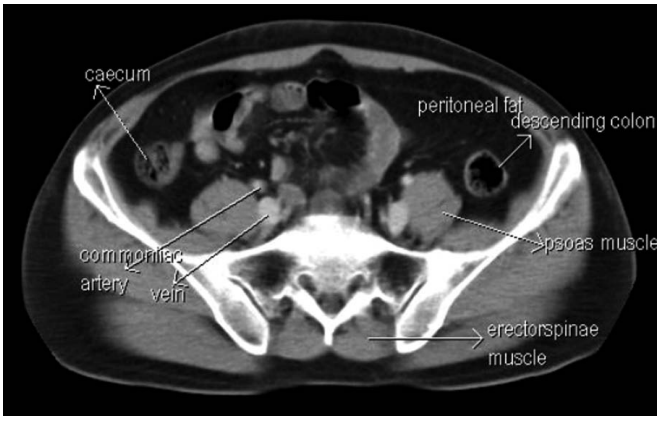

FIGURE 1.14: Axial section at the level of caecum.

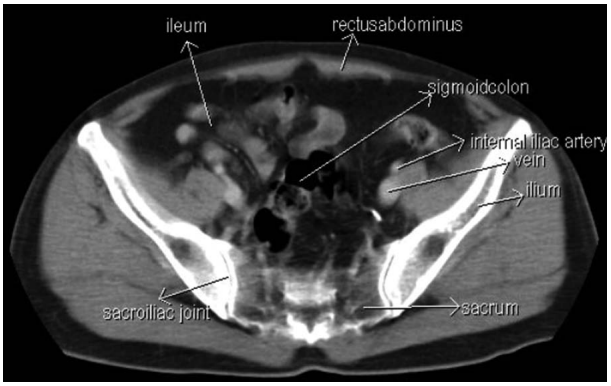

FIGURE 1.15

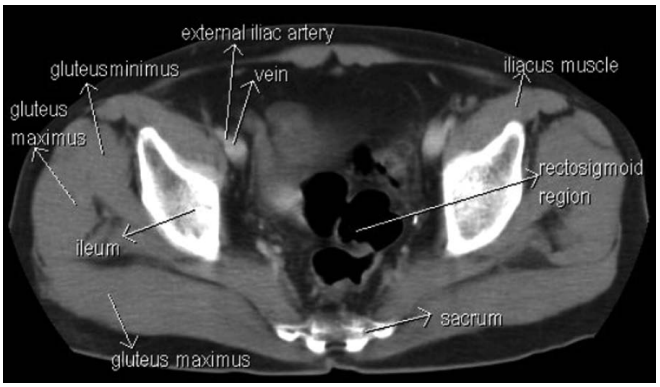

FIGURE 1.16

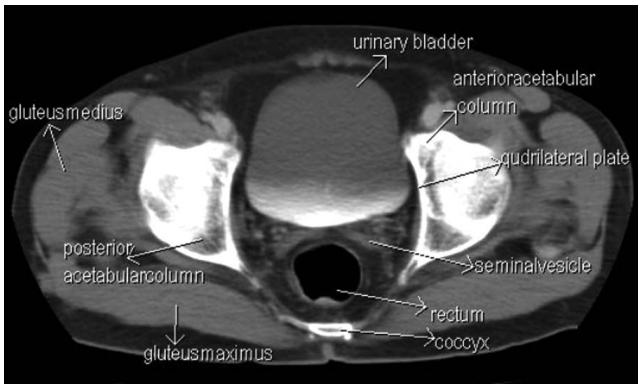

FIGURE 1.17: Axial section at the level of urinary bladder.

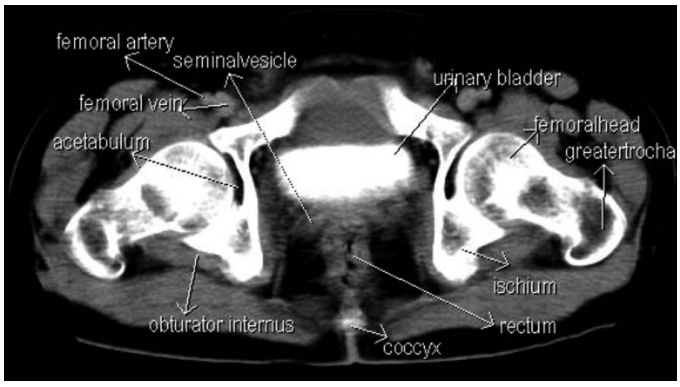

FIGURE 1.18

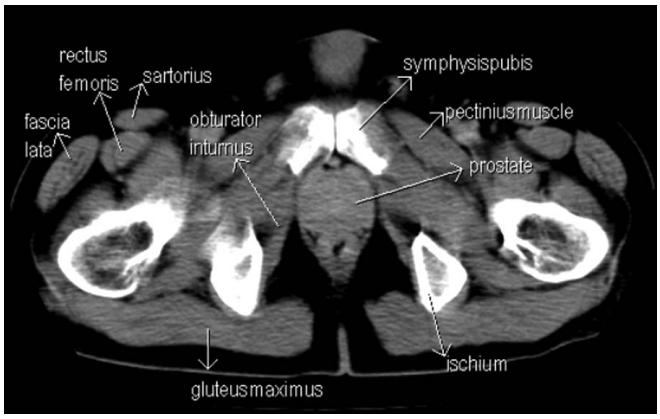

FIGURE 1.19

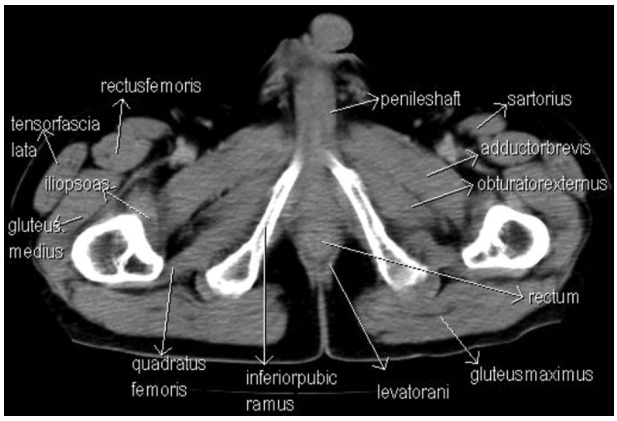

FIGURE 1.20

Uterus and Ovaries

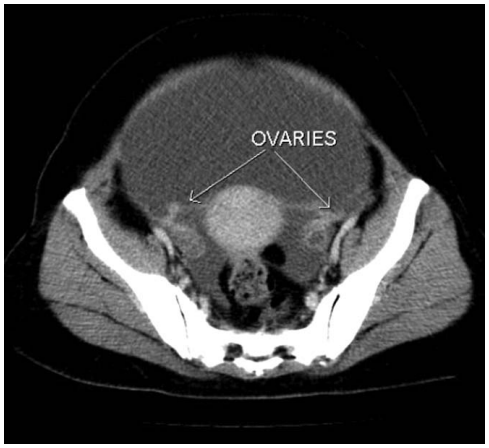

FIGURE 1.21

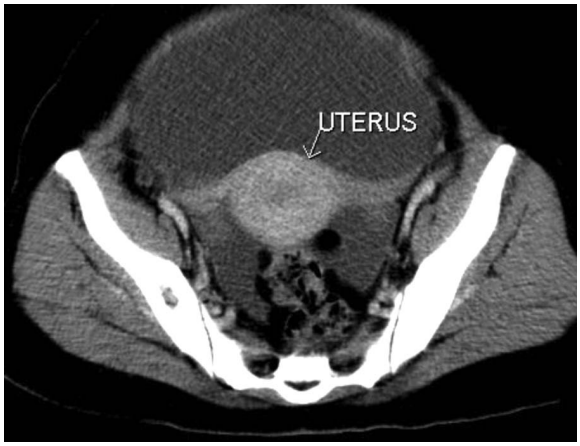

FIGURE 1.22

Muscles and Pelvic Structures

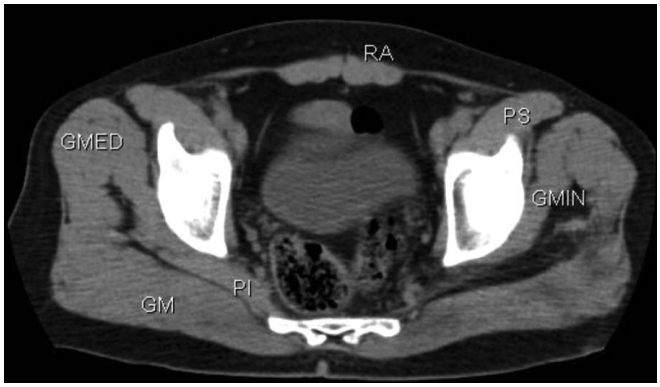

FIGURE 1.23: Axial section at the level of acetabular roof. RA—Rectus abdominus, PS—Psoas, GMIN—Gluteus minimus GMED—Gluteus medius, GM—Gluteus maximus, PI—Piriformis.

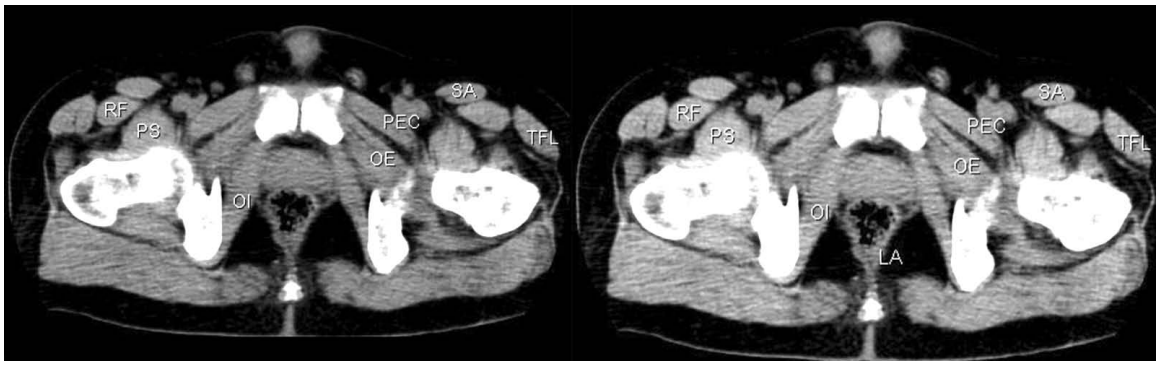

FIGURE 1.24: Axial CT at the level of pubic symphysis. OI—Obturator internus, OE—Obturator externus, SA—Sartorius, PEC—Pectineus, PS—Psoas, RF—Rectus femoris.

Individual Bowel Patterns

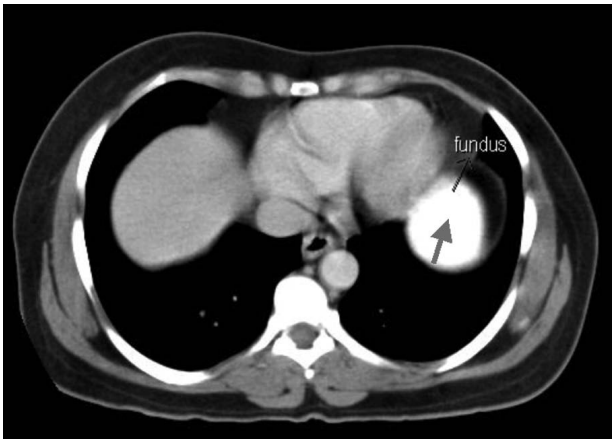

FIGURE 1.25

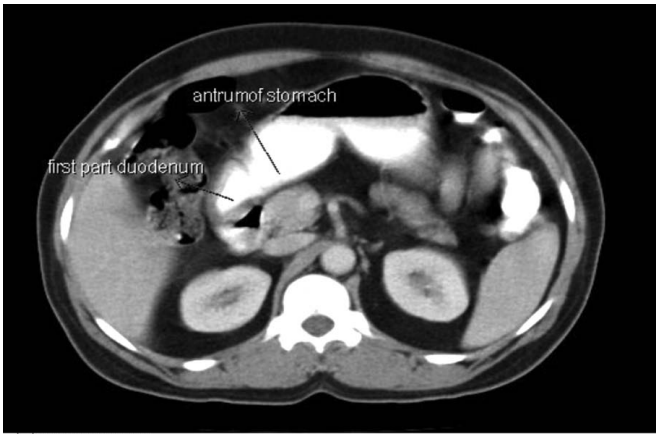

FIGURE 1.26

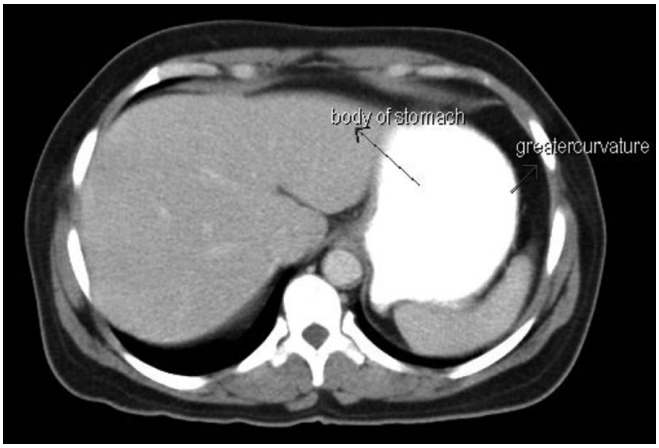

FIGURE 1.27

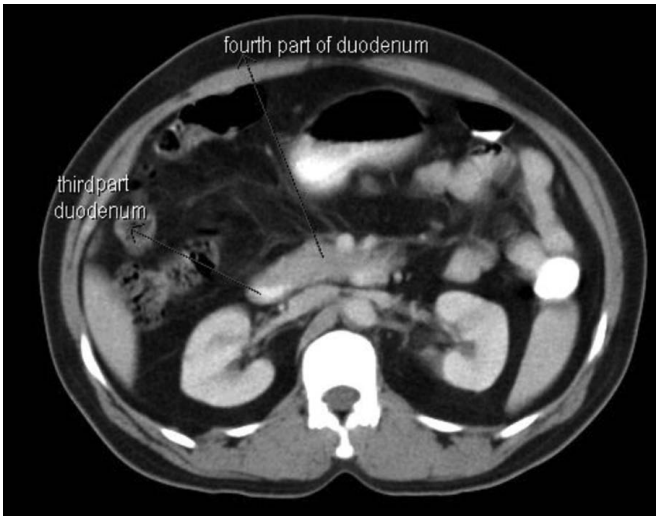

FIGURE 1.28

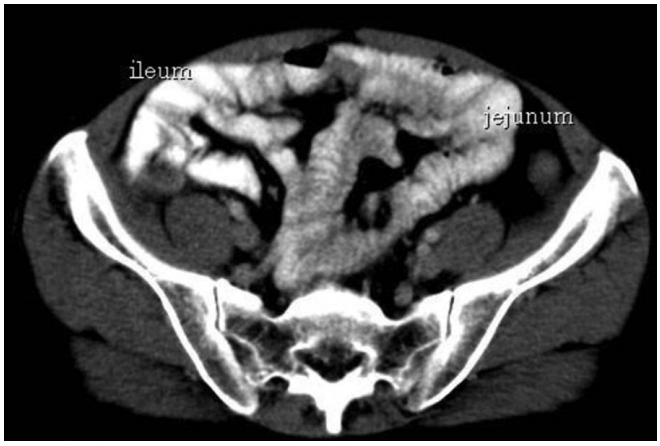

FIGURE 1.29

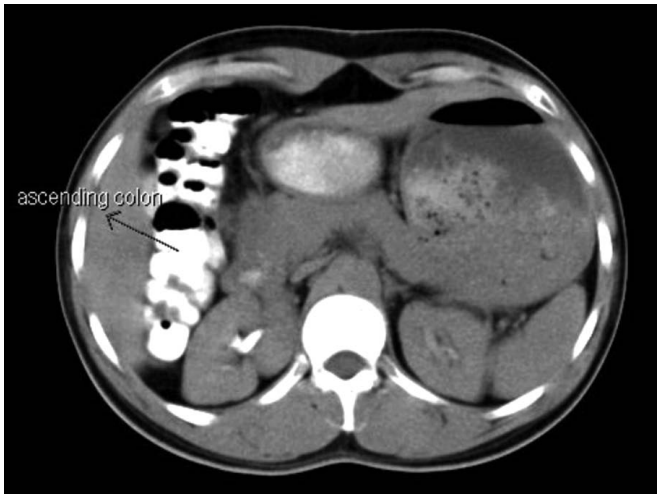

FIGURE 1.30

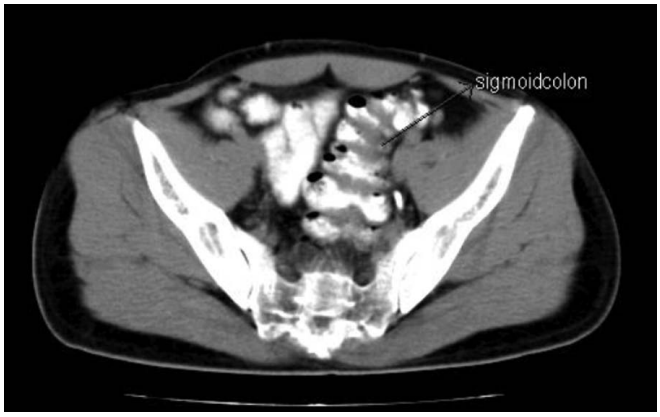

FIGURE 1.31

CT Peritoneogram—Showing Peritoneal Spaces

Peritoneal Spaces

The peritoneal cavity is divided into two main compartments, the supramesocolic and the inframesocolic, by the transverse colon and its mesentery connecting it to the posterior abdominal wall. The root of the transverse mesocolon subextends across the infra-ampullary segment of the descending duodenum, the head of the pancreas, and continues along the lower edge of the body and tail of the pancreas.

The Supramesocolic Compartment

The supramesocolic compartment can be arbitrarily divided into right and left supramesocolic peritoneal spaces. These regions can also be divided into a number of subspaces, which are normally in communication, but often become separated by inflammatory membranes in disease.

Right Supramesocolic Space

The right supramesocolic space has three subextends spaces: (a) the right subphrenic space; (b) the right subhepatic space, which can be further divided arbitrarily into anterior and posterior areas; and (c) the lesser sac. The right

subphrenic space extends over the diaphragmatic surface of the right lobe of the liver to the right coronary ligament posteroinferiorly and the falciform ligament medially, which separates it from the left subphrenic space. In the presence of infected fluid, pyogenic membranes may divide the right subphrenic space into anterior and posterior compartments.

The right subhepatic space can be arbitrarily divided into anterior and posterior spaces. The anterior right subhepatic space is limited inferiorly by the transverse colon and its mesentery. The posterior right subhepatic space, also known as the hepatorenal fossa or Morison's pouch, extends posteriorly to the parietal peritoneum overlying the right kidney. Superiorly the right subhepatic space is bounded by the inferior surface of the right lobe of the liver.

It communicates freely with the right subphrenic space and the right paracolic gutter. In the supine patient, the posterior right subhepatic space (the hepatorenal fossa or Morison's pouch) is more dependent than the right paracolic gutter, and thus under the force of gravity, fluid collections are common in this location.

The lesser sac extends to the left, behind the stomach and anterior to the pancreas. It is considered to be part of the right supramesocolic space, as embryologically the growth of the liver into the right peritoneal space stretches the dorsal mesentery and forms the future lesser sac posterior to the stomach. It communicates with the rest of the peritoneal cavity through a narrow inlet, the epiploic foramen (foramen of Winslow), between the inferior vena cava and the free margin of the hepatoduodenal ligament. The lesser sac lies posterior to the lesser omentum, stomach, duodenal bulb and gastrocolic ligament.

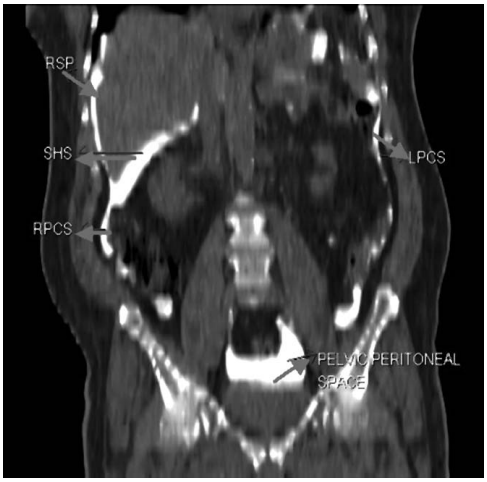

FIGURE 1.32: Coronal CT reformation after CT peritoneogram revealing the peritoneal spaces. RSP—right subphrenic space, SHS—subhepatic space, RPCS—right paracolic space, LPCS—left paracolic space.

A prominent oblique fold of peritoneum is raised on the posterior wall of the lesser sac by the left gastric artery, dividing it into two major recesses. The smaller superior recess completely encloses the caudate lobe of the liver. At the porta hepatis this recess lies posterior to the portal vein. Superiorly it extends deep into the fissure for the ligamentum venosum and posteriorly lies adjacent to the right diaphragmatic crus. The larger inferior recess lies between the stomach and the pancreas. It is bounded inferiorly by the transverse colon and its mesentery, but can extend for a variable distance between the leaves of the greater omentum. To the left it is bounded by the gastrosplenic and splenorenal ligaments which meet at the splenic hilum.

Left Supramesocolic Space

The left supramesocolic space has four arbitrary subspaces, which are in communication in normal anatomy : (a) the anterior left perihepatic space; (b) the posterior left perihepatic space, surrounding the lateral segment of the left hepatic lobe; (c) the anterior left subphrenic spaces;and (d) the posterior left subphrenic (perisplenic) space, superior to gastric fundus and spleen.

The left anterior perihepatic space is bounded medially by the falciform ligament, posteriorly by the liver surface and left coronary ligament, and anteriorly by the diaphragm. It communicates superiorly and to the left with the left anterior perihepatic space is bounded medially by the falciform ligament, posteriorly by the liver surface and left coronary ligament, and anteriorly by the diaphragm. It communicates superiorly and to the left with the left anterior subphrenic space, and inferiorly with the greater peritoneal cavity over the surface of the transverse mesocolon.

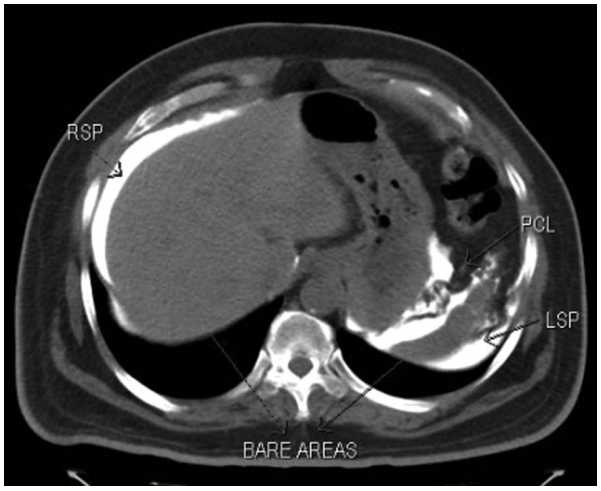

FIGURE 1.33: CT peritoneogram showing right subphrenic space (RSP), left subphrenic space (LSP), phrenicolic ligament (PCL).

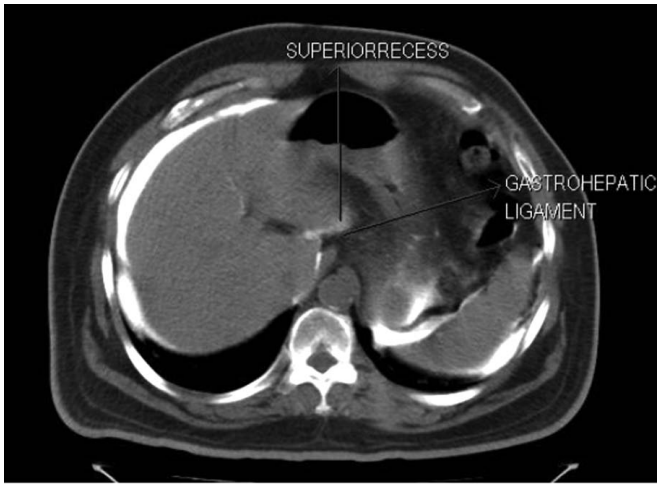

FIGURE 1.34: CT peritoneogram showing the gastro-hepatic ligament.

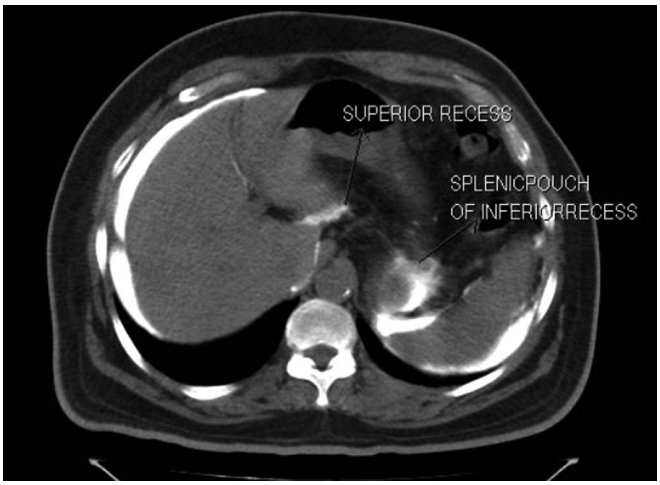

FIGURE 1.35: CT peritoneogram showing the recess of lesser sac.

The Inframesocolic Compartment

The inframesocolic compartment is divided into two unequal spaces posteriorly by the root of the small bowel mesentery, as this runs from the duodenojejunal flexure in the left upper quadrant to the ileocaecal valve in the right lower quadrant. It also contains the right and left paracolic gutter lateral to the ascending and descending colon.

The Right Inframesocolic Space

This triangular space is smaller than its counterpart on the left. It is bounded by the transverse colon superiorly and to the right, and by the root of the small bowel mesentery, as this runs from the duodenojejunal flexure to the ileocaecal junction inferiorly and to the left.

The Left Inframesocolic Space

This space is larger than its counterpart on the right and is in free communication with the pelvis on the right of the midline. The sigmoid colon and its associated mesentery form a partial barrier on the left of the midline.

The Paracolic Gutters

These are the peritoneal recesses on the posterior gastroabdominal wall lateral to the ascending and descending colon. The right paracolic gutter is continuous superiorly with the right subhepatic and subphrenic spaces. It is larger than the left paracolic gutter, which is partially separated from the left subphrenic spaces by the phrenicocolic ligament. Both paracolic spaces are in continuity with the pelvic peritoneal spaces.

The Pelvic Peritoneal Spaces

Inferiorly the peritoneum is reflected over the fundus of the bladder, the anterior and posterior surface of the uterus and upper posterior vagina in females, and on to the front of the rectum at the junction of its middle and lower thirds. The urinary bladder subdivides the pelvis into right and left paravesical spaces. In men parathere is only one potential space for fluid collection posterior to the bladder, the rectovesical pouch.

In women there are two potential spaces posterior to the bladder, the uterovesical pouch, and posterior to the uterus the deeper rectouterine pouch (pouch of Douglas). The layers of peritoneum on the anterior and posterior surcolon faces of the uterus are reflected laterally to the pelvic side walls as the broad ligaments, containing the uterine (Fallopian) tubes.

Omentum

- This is a **double-layered sheet or fold of peritoneum**.
- The lesser and greater omentum attach the stomach to the body wall or to other abdominal organs.

The Lesser Omentum

- This fold of peritoneum connects the **lesser curvature of the stomach** and the **proximal part of the duodenum** to the **liver**.
- Individually, these connections are referred to as the **gastrohepatic ligament** and the **hepatoduodenal ligament**.
- The lesser omentum lies **posterior to the left lobe of the liver** and is attached to the liver in the **fissure for the ligamentum venosum**.
- It is also attached to the **porta hepatis**, the transverse fissure or gate (L. *porta*) on the inferior surface of the liver through which the bile duct, vessels, and nerves enter or leave the liver.

The Greater Omentum

- This is a fat-laden fold of peritoneum that hangs down from the **greater curvature of the stomach** and connects the stomach with the **diaphragm**, **spleen**, and **transverse colon**.
- This double-layered peritoneal fold normally fuses during the fetal period, thereby **obliterating the inferior recess of the omental bursa**.
- As a result, the apron-like greater omentum is **composed of four layers of peritoneum**.
- After passing inferiorly as far as the pelvis, the greater omentum **loops back on itself**, overlying and **attaching to the transverse colon**.

Peritoneal Ligaments

- A peritoneal ligament is a **double layer of peritoneum** that connects an organ with another organ or with the abdominal wall.
- Ligaments may contain blood vessels or remnants of vessels (e.g. the falciform ligament contains the ligamentum teres, a remnant of the fetal umbilical vein).

- The greater omentum is divided into **3 parts**:
  1. The apron-like part, called the **gastrocolic ligament**, is attached to the **transverse colon**.
  2. The left part, called the **gastrosplenic ligament** (gastrolienal ligament), connects the hilum of the spleen to the greater curvature and fundus of the stomach.
  3. The superior part called the **gastrophrenic ligament** is attached to the diaphragm and the posterior aspect of the fundus and the esophagus.
- The **falciform ligament** extends from the liver to the anterior abdominal wall and the diaphragm.
- The **ligamentum teres** is the obliterated remnant of the **left umbilical vein**, lying in the free edge of the falciform ligament and extending from the groove for the ligamentum teres to the umbilicus.
- The **superior (anterior) and inferior (posterior) layers of the coronary ligament** are reflections of the peritoneum, which surround the bare area of the liver.
- The **left and right triangular ligaments** are where the layers of the coronary ligament meet to the left and right respectively.
- The falciform, coronary and triangular ligaments are **derived from** that part of the **ventral mesogastrium connecting the liver to the body wall**.
- The gastrohepatic and hepatoduodenal ligaments are **derived from** that part of the **ventral mesogastrium connecting the stomach and the liver**.
- The gastrosplenic and gastrophrenic, as well as the lienorenal and phrenicolienal ligaments are **derived from the dorsal mesogastrium**.

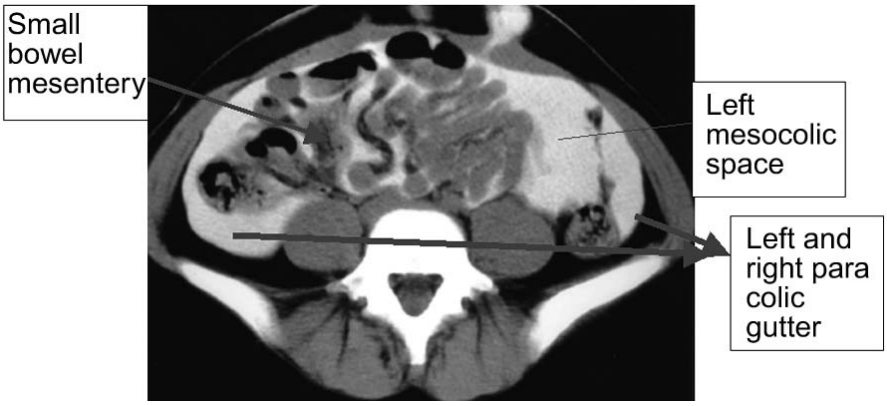

FIGURE 1.36: CT peritoneogram showing folds of mesentery.

The Peritoneal Folds

- A peritoneal fold (L. *plica*) is a reflection of peritoneum with more or less sharp borders. Often it is formed by peritoneum that covers blood vessels, ducts, and obliterated fetal vessels.
- Several folds are visible on the **parietal peritoneum** on the **interior** of the anterior abdominal wall.
- The **median umbilical fold** contains the **urachus**, which extends from the urinary bladder to the umbilicus.
- The **medial umbilical folds** are raised by the obliterated umbilical arteries, extending from the internal iliac arteries to the umbilicus.
- The **lateral umbilical folds** are raised by the inferior epigastric arteries, extending from the deep inguinal rings on each side to the arcuate lines.

Peritoneal Pouches

- The **rectouterine pouch** (in females) separating the rectum from the bladder.
- The **rectovesical pouch** (in males) separating the rectum from the bladder.
- The **vesicouterine pouch** (in females) separating the bladder from the uterus.

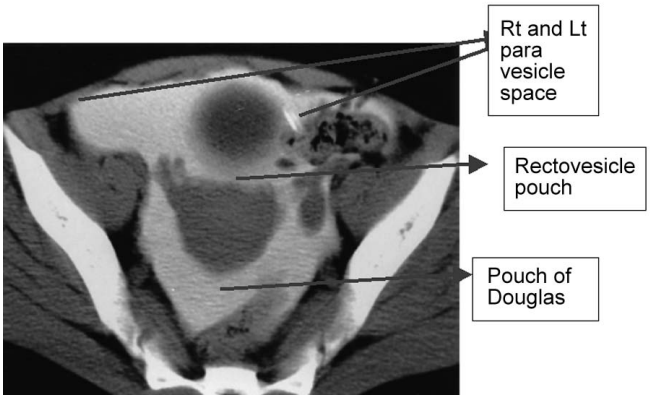

FIGURE 1.37: CT peritoneogram showing pelvic spaces.

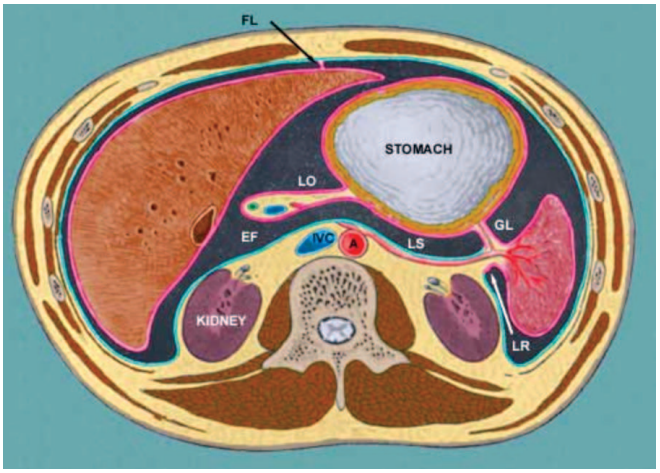

FIGURE 1.38

- Falciform ligament (FL)
- Lienorenal ligament (LR)
- Gastrolienal ligament (GL)
- Lesser omentum (LO)

RETROPERITONEUM

Extra peritoneal space is divided into the anterior and posterior pararenal space and the perinephric space by the anterior and posterior layers of the renal fascia. Both these fascia fuse to form the lateral conal fascia behind the descending colon.

ANTERIOR PARARENAL COMPARTMENT

The anterior pararenal compartment lies between the anterior renal fascia and the posterior parietal peritoneum. The lateral border is defined by the lateroconal fascia and the compartment is potentially contiguous across the midline. Contents include pancreas, the descending, horizontal and terminal portions of duodenum, the ascending and descending colon.

Perinephric Compartment

Formed by fusion of the anterior (gerotas) and posterior (zuckercandles) fascia superiorly it fuses with the diaphragmatic fascia and laterally with the lateroconal fascia.

The inferior portion of the space is open towards the iliac fossa. Medially the posterior renal fascia fuses with the quadratus and psoas fascia.

Contents include adrenals, kidneys, renal vasculature, proximal part of renal collecting system.

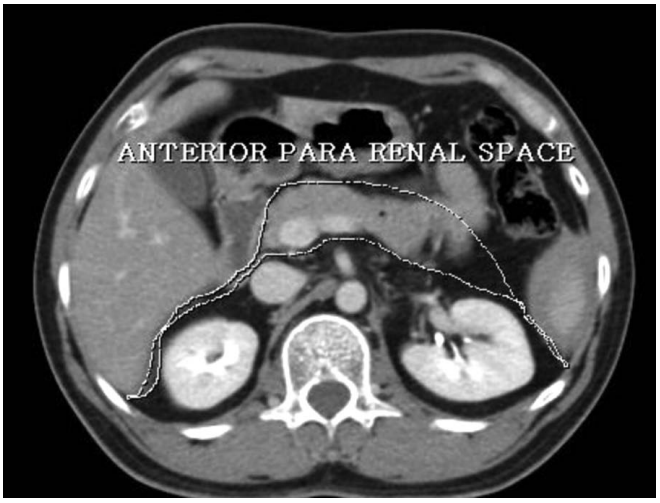

FIGURE 1.39

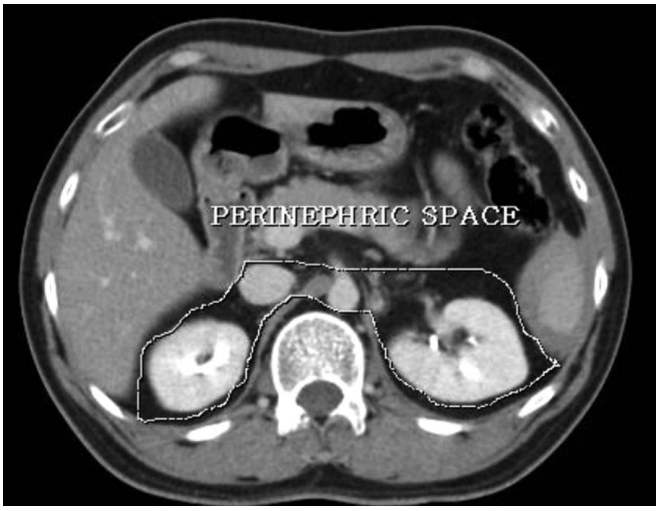

FIGURE 1.40

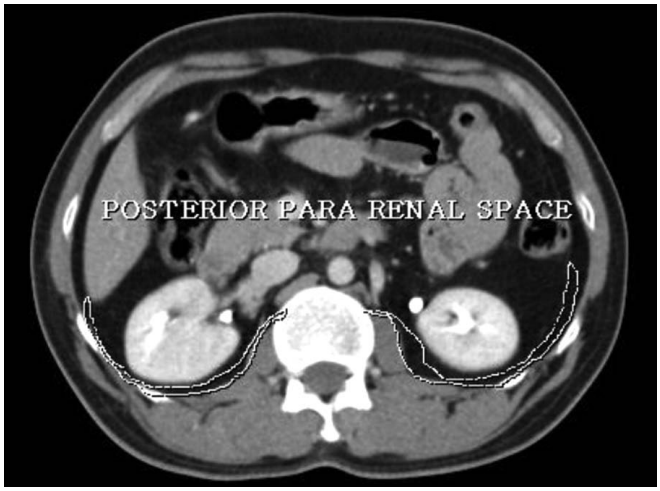

FIGURE 1.41

Posterior Pararenal Compartment

It lies between the posterior renal fascia and the transversalis fascia, it contains fat tissue and continues laterally as the peritoneal fat. The space is open inferiorly at the iliac crest. Medially the space is contained by the fusion of the transversalis and psoas fascias.

CHAPTER

2

Liver

INTRODUCTION

CT is today probably the most reproducible way for imaging the liver. With advent of newer CT technology newer strategies of evaluating the liver have been devised.

Spiral CT (SCT) has been available since 1989. SCTmade acquirement of anatomically consecutive axial sections through the liver in a single breath-hold and to repeat this procedure in several phases after intravascular injection of contrast medium possible.

Availability of contrast media injectors also contributed to the standardization of this injection to more accurately depict the different vascular phases during distribution of contrast medium enabling both detection and characterization of focal liver lesions.

Dedicated methods, such as CT arterial portography (CTAP), where CT is performed during arterial injection of contrast media after selective catheterization of the superior mesenteric artery, has been considered as one of the gold-standard methods for detection of focal liver lesions. This method is not so widely performed any more due to the development of less invasive and less costly methods. Furthermore, irregular liver perfusion on CTAP may sometimes simulate focal liver lesions and result in false negative and false positive lesions.

Since the end of the 1990s, multi-detector (MD) spiral CT has also been clinically available. Today's MDCT systems have an array of either 8, 16 or 32, 64 X-ray detectors. It is now technically feasible to obtain 0.5 mm thick slices through the liver within a breath-hold. Use of 2. 5 mm thick slices compared to 5 and 10 mm slices has been reported to result in an increased sensitivity for detection of focal liver lesions.

First, an early arterial phase is acquired that enables reconstruction of angiographic images of the arterial supply to the liver. Then, late arterial (parenchymal, portal vein inflow) and portal venous (hepatic venous) phases that enable detection of hyper- and hypovascular liver tumors, respectively, are performed. To obtain early arterial phase and reconstruct angiographic images is of interest before liver surgery to visualise the anatomy of the arterial vascular supply to the liver.

The two major objectives of diagnostic imaging of the liver in the oncologic patient population are detection and characterization of the liver tumor, and detection of extrahepatic disease. While detection of hepatic tumors is of obvious importance in staging and management, the high prevalence of benign liver masses (estimated to be in excess of 20% in the general adult population) makes characterization equally important.

Focal hepatic lesions are detected by difference in attenuation between the normal and abnormal hepatic tissues unlike lungs were the intrinsic contrast is more, in liver the difference is only about 10-30 HU making the use of intravenous contrast mandatory.

TECHNICAL PRINCIPLES OF CONTRAST ENHANCED CT

Intravenous iodinated contrast media are used routinely for CT evaluation of the liver to overcome the lack of inherent density difference between pathological conditions affecting the liver and hepatic parenchyma. There are two physiological principles that allow us to target contrast enhancement, the dual blood supply of the liver and the hemodynamics of hepatic tumors.

The liver is unique among abdominal viscera in having a dual blood supply, with the portal vein supplying some 75 to 80% of flow and the hepatic artery the remaining 20 to 25%. Liver tumors, however, generally receive nearly all their blood supply from the hepatic artery. It is also useful, though not stringently defined, to consider whether a specific hepatic tumor is typically hypovascular or hypervascular relative to the vascularity of the liver. Hypovascular tumors are usually best detected as low-density lesions against a background of a maximally enhanced liver achieved during the so-called portal venous dominant phase of hepatic enhancement, as defined below. Hypervascular tumors, however, receive a rich hepatic arterial flow and enhance to a similar degree as liver parenchyma and may not be detected on this phase of enhancement. Using a helical CT scanner, we can obtain CT sections through the liver in both the arterial dominant and portal venous dominant phases of enhancement. This is often referred to as a biphasic or multiphasic CT protocol.

Technical errors that result in suboptimal liver CT evaluation include the following:

- A conventional CT scanner generally requires 100 to 120 sec to complete a scan of the upper abdomen, resulting in at least some sections of the liver being scanned at an inopportune phase of enhancement.
- Using an insufficient volume of contrast medium. While helical CT allows substantial reductions of contrast material for protocols requiring only opacification of vessels optimal liver CT protocols require administration of about 2 mL/kg of contrast medium. For an average-size adult, this would equate to 125 to 150 mL of contrast medium.
- Using a slow injection (<2. 5 mL/sec) or drip infusion of contrast material. This will inevitably result in a diminished contrast between the liver tumor and parenchyma.
- Obtaining scans too early or too late for the lesion in question.
- Using a CT slice thickness (collimation) >7 mm. Thin sections (2.5-7 mm) are essential to minimize "partial volume artifact, " which results when a small lesion does not fill the entire CT slice (the pixel, or picture element).

NONENHANCED CT

Nonenhanced CT scans still have an important role. Certain tumors are characterized by focal hemorrhage, fat, or calcification, all of which are more easily recognized before contrast enhancement of the liver. Nonenhanced scans are always obtained in CT evaluation of the cirrhotic liver because regenerating nodules are easier to recognize and to distinguish from other focal hepatic masses with the added information provided by the noncontrast images.

Hepatic Arterial Phase [HAP]

The HAP images should be obtained with a scan delay of 30 to 35 sec, using an injection rate of 4 or 5 mL/sec. Earlier scan delays of only 20 to 25 sec, were used with injection rates of 2. 5 to 3 ml per second, but these have proved less useful in the detection of hypervascular tumors. During the HAP hypervascular tumors receive concentrated contrast material from the hepatic artery undiluted because of their lack of portal venous supply. Later, when the portal vein becomes densely opacified the liver parenchyma will enhance maximally, often obscuring the detection of hypervascular tumors. A properly obtained arterial dominant set of images can be recognized by the heterogeneous enhancement of the spleen and kidneys (cortex more than medulla), minimal enhancement of

the liver, dense opacification of the hepatic artery, some enhancement of the portal vein, and no enhancement of the hepatic veins [see Fig. 2.43A].

Portal Venous Phase (PVP)

PVP images should be obtained in all abdominal CT scans. The timing for optimal PVP images varies according to a number of variables, including the patient's circulation time and the rate of IV contrast medium injection. For patients with normal cardiac output and using a helical scanner with an injection rate of 3 to 5 mL/sec, a scan delay of about 70 sec is recommended. Many CT scanners have a computerized bolus-tracking feature that allows the CT technologist to perform rapid repeated low-dose scans over the liver following the initiation of the IV contrast bolus. When the liver enhancement has reached a certain threshold above baseline (e. g. 50 Hounsfield units, or HU), the helical scan sequence through the entire liver is initiated. A properly obtained PVP series of images can be recognized by the dense homogeneous enhancement of the liver, spleen, and kidneys and by opacification of all large abdominal blood vessels, including the hepatic and portal veins, which are hyperdense to the viscera and muscle [see Fig. 2.43D].

The equilibrium phase of hepatic enhancement begins at about 100 to 120 sec after the start of the IV contrast bolus. During this phase the enhancement curves of the liver and hepatic tumors become parallel, and contrast is dispersed throughout the interstitial tissues of the body. Equilibrium phase images can be recognized by the homogeneous enhancement of all abdominal viscera and the excretion of contrast-opacified urine by the kidneys. Blood vessels, lymph nodes, and abdominal viscera are all nearly the same density.

Delayed CT images of the liver may be obtained 10 to 15 min after the initiation of contrast injection and are useful for specific indications. Tumors with a large component of fibrosis demonstrate prolonged hyperdense enhancement of the stroma. This feature has proved to be particularly characteristic of cholangiocarcinoma.

In patients with primary sclerosing cholangitis or a focal hepatic mass that is associated with intrahepatic bile duct obstruction, routine delayed phase images in addition to the standard portal venous dominant phase series are recommended. We also commonly obtain delayed images in cases of hepatic masses felt to possibly represent cavernous hemangioma, where progressive centripetal enhancement of the hemangioma is one of its characteristic features.

In evaluating the cirrhotic liver for HCC or other focal nodular lesions, both nonenhanced and biphasic scanning (HAP and PVP) are mandatory. The differentiation among regenerating nodules, dysplastic nodules, and various stages of HCC requires an assessment of the hemodynamic nature of the nodule. Demonstration of a hypervascular mass on the HAP phase of a biphasic CT scan is highly suggestive of HCC. Not only are most HCC hypervascular, but the cirrhotic liver receives less portal venous inflow due to portal hypertension, further increasing the conspicuity of HCC relative to the liver on the HAP images.

Hypovascular tumors are the most common neoplasms of the liver, encompassing most metastatic lesions. During the HAP (arterial phase) of contrast delivery, no significant enhancement of these tumors or the liver occurs; therefore, it is not important to survey the liver during the HAP for detection of these lesions. The ideal means of CT detection of hypovascular tumors would be by catheterizing the splenic or superior mesenteric artery and injecting contrast material about 30 sec prior to CT scanning [no longer practised].

CT ARTERIAL PORTOGRAPHY

CT arterial portography (CTAP) is recognized as the most sensitive test for detecting individual liver lesions. CT sections are obtained during infusion of contrast material through a catheter placed in the super-mesenteric or splenic artery, producing a more consistent and homogeneous enhancement of the normal hepatic parenchyma. Normal parenchyma is enhanced preferentially to liver tumors, because tumors derive their blood flow exclusively

or predominantly from the hepatic artery, while normal parenchyma receives 80% of its blood flow from the portal vein.

For CTAP, 100 to 150 ml of 60% iodinated contrast is infused through the SMA or splenic artery catheter at a rate of 1 to 3 ml per second. CT scans are initiated 20 seconds after the start of the infusion and are obtained in rapid incremental fashion. After the dynamic phase scans have been obtained, rescanning the liver during the equilibrium phase of contrast enhancement or after a delay of 4 to 6 hours helps to avoid misdiagnoses caused by abnormalities of hepatic perfusion. Perfusion defects are a common and troubling potential pitfall. Peripheral wedge shaped lesions are almost invariably caused by perfusion, although attention should be directed to the apex of the wedge, for diagnosis of a possible tumor causing the perfusion defect.

CTAP detects approximately 90% of all liver masses, exceeding the ability of non-contrast MR and contrast-enhanced CT (which detect about 2/3 of lesions).

CT Arteriography

The single most sensitive CT technique for the demonstration of hypervascular liver tumors is CT arteriography, during which contrast is injected into a selectively catheterized hepatic artery while CT sections are obtained. Another technique that requires selective catheterization of the hepatic artery is Lipiodol-enhanced CT. Lipiodol (iodized poppy seed oil) is known to concentrate semi-selectively in hepatic tumors, especially HCC. Because Lipiodol is often mixed with chemotherapeutic agents as part of an intra-arterial chemoembolization regimen, it may prove useful for both diagnosis and therapy of HCC To allow for clearance of Lipiodol from a nontumor-bearing liver, hepatic CT should be delayed for 10 to 14 days after arterial injection of this contrast agent. In areas where HCC is endemic, both CT arteriography and Lipiodol-enhanced CT are widely employed.

Hepatic CT angiography (CTA) has proved useful in several settings. To evaluate the vascular anatomy of potential liver transplantation donors, for patients being considered for surgical implantation of a chemotherapy pump, CTA can obviate catheter angiography. Vascular complications following liver transplantation can also be demonstrated accurately and noninvasively by CTA. CTA can also be used as an adjunct to the standard CT protocols to further characterize the hemodynamics and potential resectability of hepatic tumors.

CT Protocols

Our routine abdominal CT protocol consists of a axial plain survey of liver. Spiral CT scan of the abdomen and pelvis after oral and intravenous administration of contrast material. Typically, 100 mL (300 mg/mL iodine) of iohexol is injected at a rate of 2-3 mL/sec. Beginning 25 seconds after initiation of the contrast material injection, a 30-second breath-hold arterial phase helical CT scan was acquired with section thickness of 5 mm and pitch (usually 1. 0–1. 6) sufficient to cover the entire liver within the breath-hold period.

A breath-hold portal venous phase scan was obtained 60–70 seconds after initiation of the injection. Images were reconstructed at 3-mm intervals through the lesions with use of standard soft-tissue (window width, 400 HU; level, 40 HU) and liver (window width, 150 HU; level, 50–80 HU) display settings.

HEPATIC INFECTIONS

Hepatic infections may be caused by bacterial (85%), fungal (9%), or parasitic (6%) infections. The most common causative agents are *E. coli*, streptococci, actinomyces, candida, *Entamoeba histolytica* and echinococcus.

Pyogenic Hepatic Abscess

Pyogenic hepatic abscess is a localized collection of pus in the liver with destruction of the hepatic parenchyma. Pyogenic abscesses, particularly when multiple, may be caused by hematogenous dissemination (of either

gastrointestinal infection via the portal vein or disseminated sepsis via the hepatic artery), ascending cholangitis, or superinfection of necrotic tissue. A solitary hepatic abscess is often cryptogenic and has no clear-cut predisposing cause. Over one-half of liver abscesses are polymicrobic. *Escherichia coli* is the most common bacterium, but other anaerobic and aerobic organisms can be involved. Pyogenic abscesses demonstrate no sex predilection but most commonly involve middle-aged patients.

Most hepatic abscesses are bacterial, fungal or amebic in origin. CT has a very high sensitivity in detecting pyogenic abscesses, which appear as single or multiloculated masses with low attenuation values (0-40 HU). In contrast material–enhanced CT, they appear as multiple small, well-defined hypoattenuating lesions. Faint rim enhancement and perilesional edema can be seen, findings that help differentiate them from hepatic cysts. At contrast-enhanced CT, large abscesses are generally well-defined and hypoattenuating; they may be unilocular with smooth margins or complex with internal septa and an irregular contour. Rim enhancement is relatively uncommon, as is the presence of gas.

Most fully developed abscesses present a peripheral rim demonstrating contrast enhancement. The "cluster" sign may be sometimes seen with small coalescent lesions.

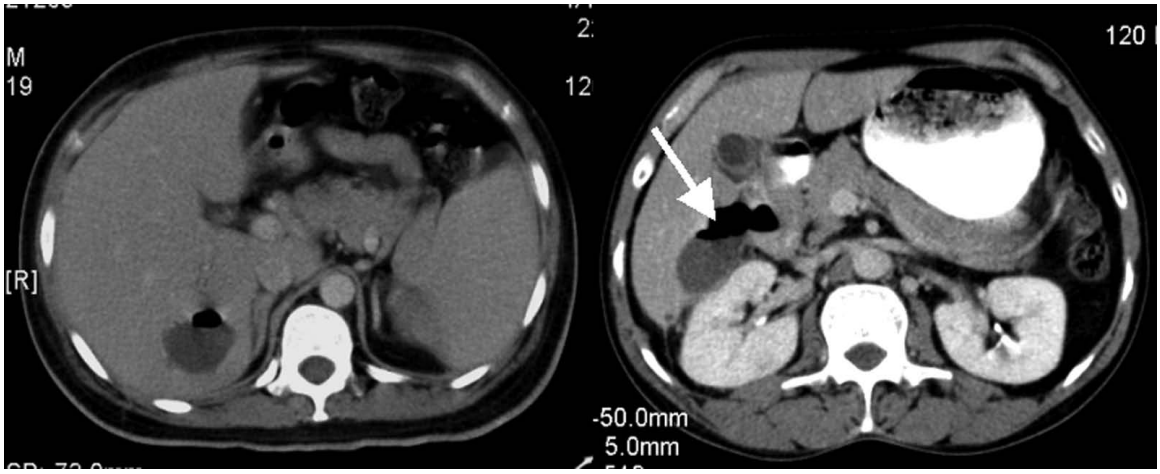

FIGURES 2.1A and B: Axial CECT reveals a well marginated lesion in right lobe liver segment six region showing air fluid level (arrow).

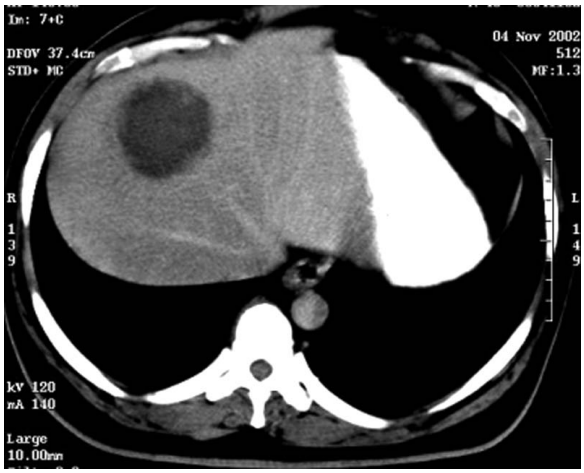

FIGURE 2.2: Axial CECT reveals a well marginated hypodense lesion showing an irregular capsular wall in segment 8 of right lobe.

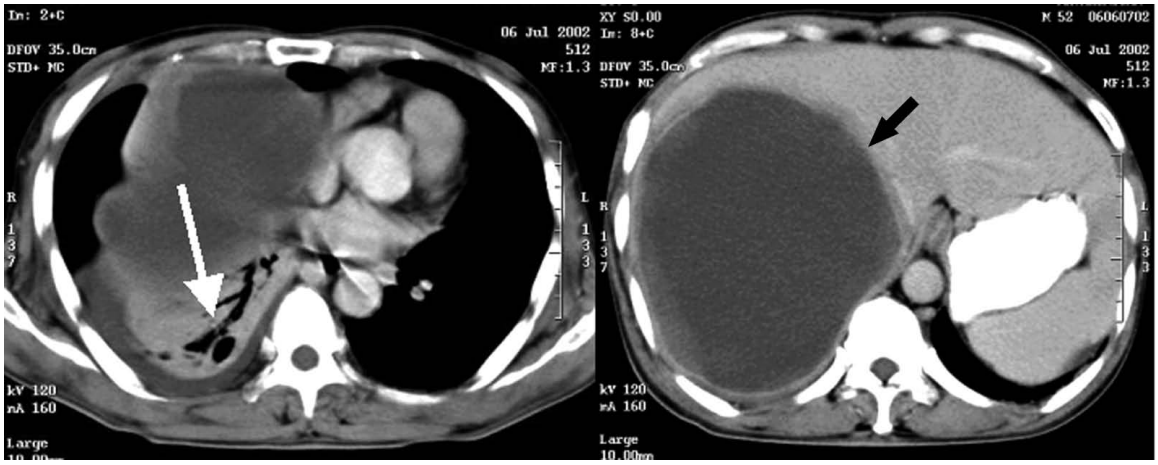

FIGURES 2.3A and B: (A) Axial CECT reveals right pleural effusion with right basal pneumonitis (arrow), (B) axial CECT reveals a large hypodense lesion in the right lobe liver with a well defined capsule (arrow). Feature of a liver abscess with sympathetic effusion and secondary pneumonitis.

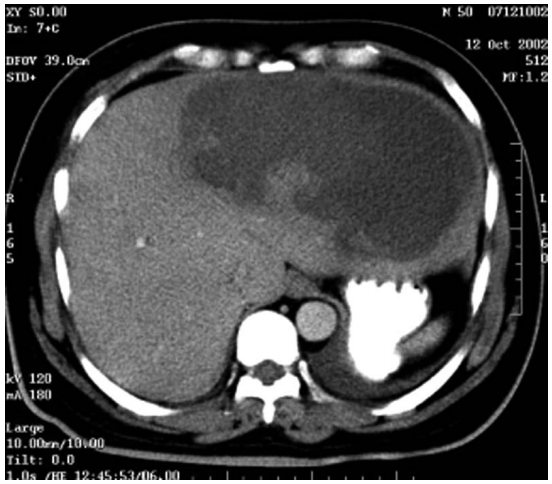

FIGURE 2.4: Axial CECT reveals a large well marginated lesion in the left lobe of liver with shaggy nodular posterior margin.

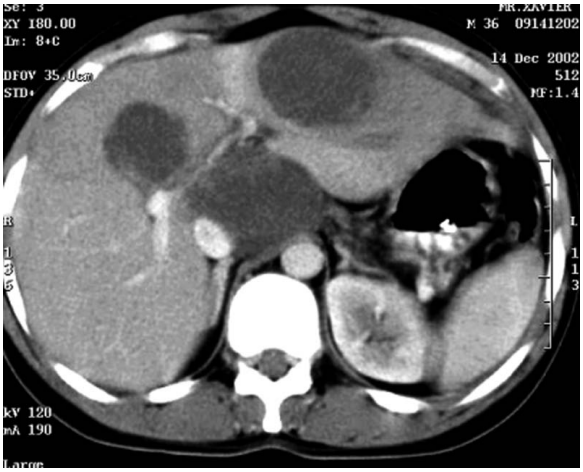

FIGURE 2.5: Axial CECT reveals multiple well marginated lesions showing capsular enhancement involving the caudate lobe and left lobe liver.

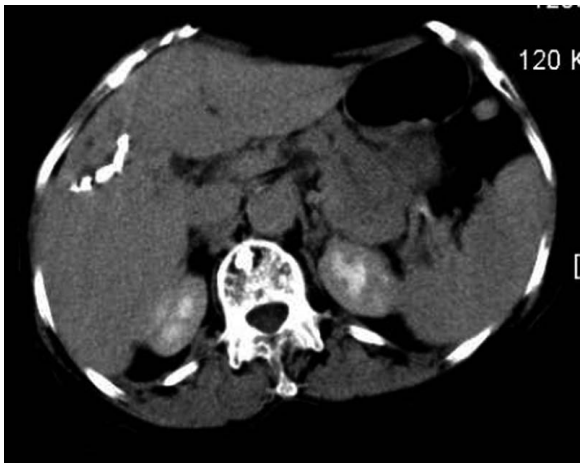

FIGURE 2.6: Axial CECT reveals a peripheral heterogenous lesion with calcification of the posterior wall suggestive of a chronic abscess.

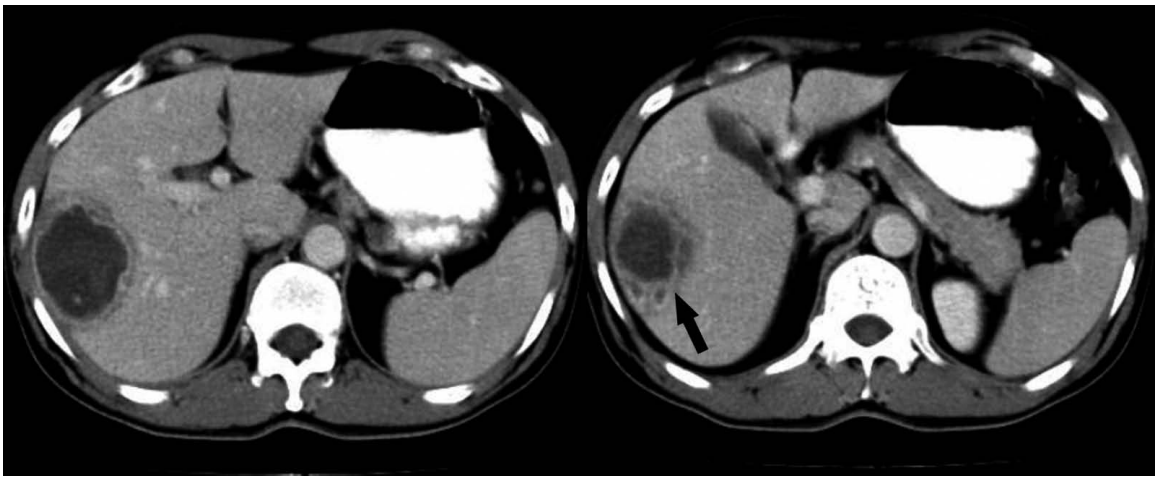

FIGURES 2.7A and B: Axial CECT reveals a well marginated lesion in the right lobe inferior segment showing capsular enhancement with adjacent satellite nodules.

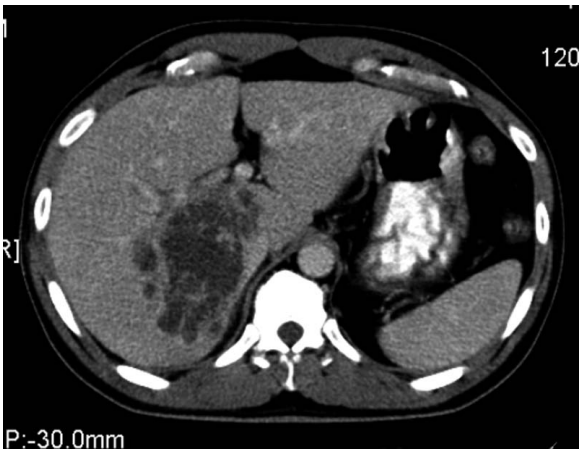

FIGURE 2.8: Axial CECT reveals a well-defined septated lesion in the right lobe – features of a chronic abscess.

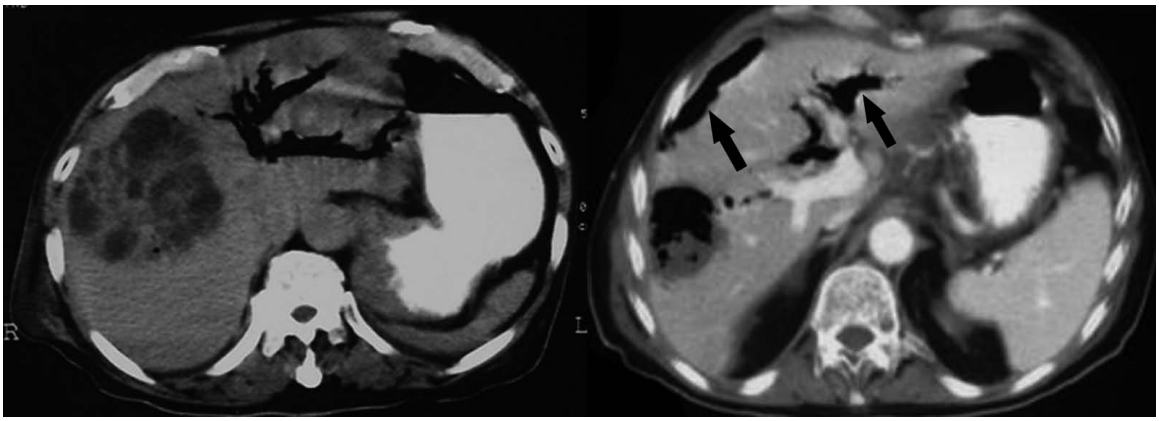

FIGURES 2.9A and B: (A) Axial CECT reveals a well marginated heterogenous lesion in the right lobe liver with pneumobilia. (B) Axial CECT reveals a air containing lesion in the right lobe with pneumobilia with air in the right subdiaphragmatic region.

Amebic Abscess

Entamoeba histolytica is endemic worldwide, with an estimated 10% of the world's population being infected. It is most prevalent in India, Africa, the Far East, and Central and South America. Amebic liver abscess is the most common extraintestinal complication of amebiasis, occurring in 8. 5% of cases. Hepatic infection occurs because colonic trophozoites ascend via the portal vein and invade the parenchyma.

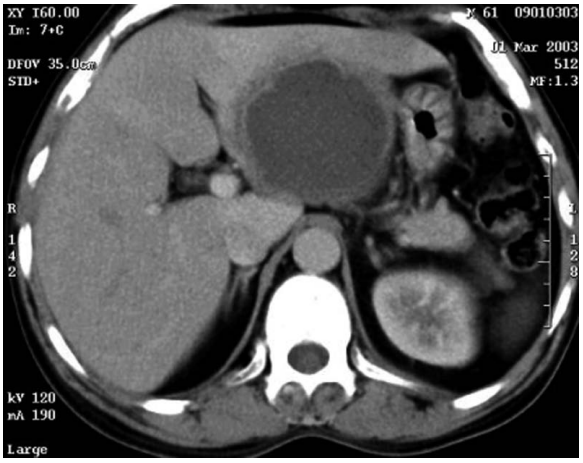

FIGURE 2.10: Axial CECT showing a capsulated segment 3 abscess.

Contrast-enhanced CT, amebic abscesses usually appear as rounded, well-defined lesions with attenuation values that indicate the presence of complex fluid (10-20 HU). An enhancing wall 3-15 mm in thickness and a peripheral zone of edema around the abscess are common and somewhat characteristic for this lesion. The central abscess cavity may show multiple septa or fluid-debris levels and, rarely, air bubbles or hemorrhage. Extrahepatic extension of amebic abscess is relatively common, and involvement of the chest wall, pleural cavity, pericardium, and adjacent viscera has been reported.

Hydatid Disease

Hydatid disease is a worldwide zoonosis produced by the larval stage of the *Echinococcus* tapeworm. Humans become infected by ingestion of eggs of the tapeworm *E granulosus,* either by eating contaminated food or from contact with dogs. The ingested embryos invade the intestinal mucosal wall and proceed to the liver via the portal venous system. Although the liver filters out most of these embryos, those that are not destroyed become hepatic hydatid cysts. The two main types are caused by *E. granulosus (cysticus) and E. multilocularis (alveolaris)*. Imaging findings depend on the stage of the disease. Hydatid cysts may be unilocular, may contain daughter cysts and may be partially calcified. Calcifications are seen in 20-30% and are mostly curvilinear.

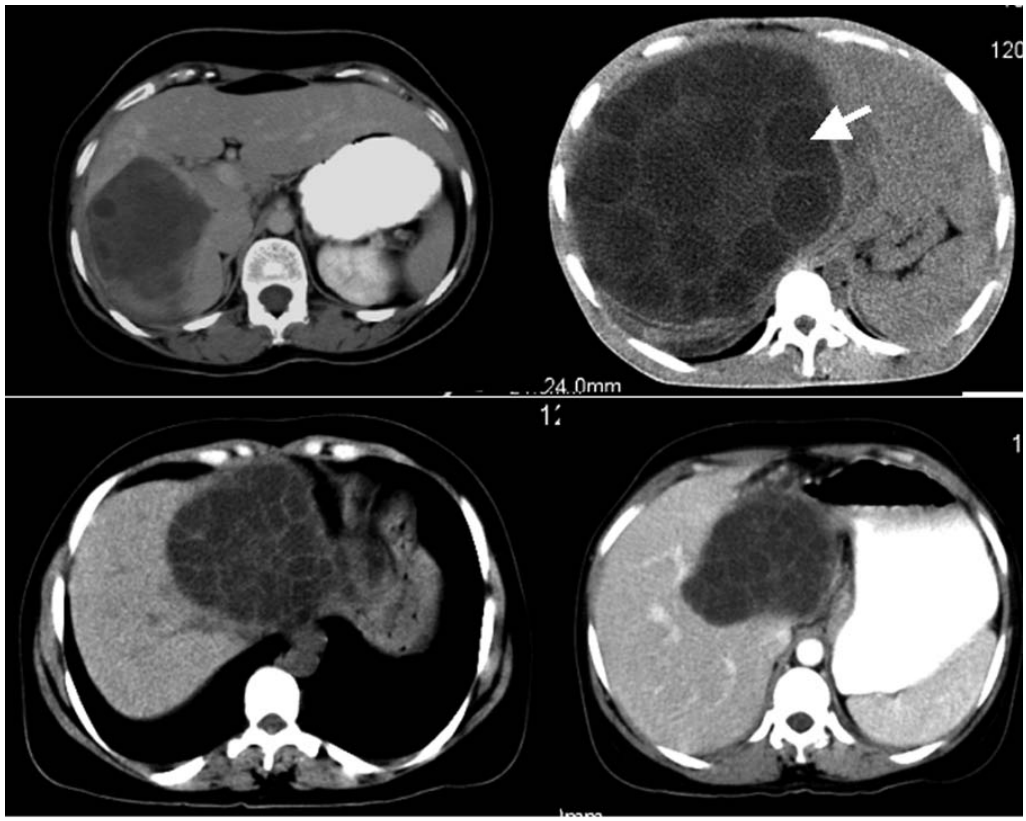

FIGURES 2.11A to D: Axial CECT reveals well defined lesions showing multiple intralesional daughter cysts (arrow).

Hepatic Granuloma

Granulomatous hepatitis may be bacterial (caused by Mycobacterium or Bartonella), fungal (aspergillosis) or parasitic (schistosomiasis, leishmaniasis, larva migrans). Infectious granulomas have to be differentiated from systemic diseases as sarcoid and chronic granulomatous disease.

At contrast-enhanced CT, fungal microabscesses usually appear as multiple round, discrete areas of low attenuation, generally ranging from 2 to 20 mm. These microabscesses usually enhance centrally after intravenous administration of contrast medium, although peripheral enhancement may occur.

Tuberculosis

Tuberculosis is one of the most common infectious diseases, with a worldwide distribution and a variety of clinical manifestations. Tuberculosis is known to involve the liver in different ways. Generally, tuberculosis of the liver is classified as either a miliary form, which is part of generalized miliary tuberculosis, or a local form, which is further subdivided into focal or nodular tuberculosis (i.e., tuberculous hepatic abscess and tuberculoma) and tubular or hepatobiliary tuberculosis (i.e. tuberculosis involving the intrahepatic ducts). Miliary tuberculosis of the liver is most common and is reported to occur in 50-80% of all patients with terminal pulmonary tuberculosis.

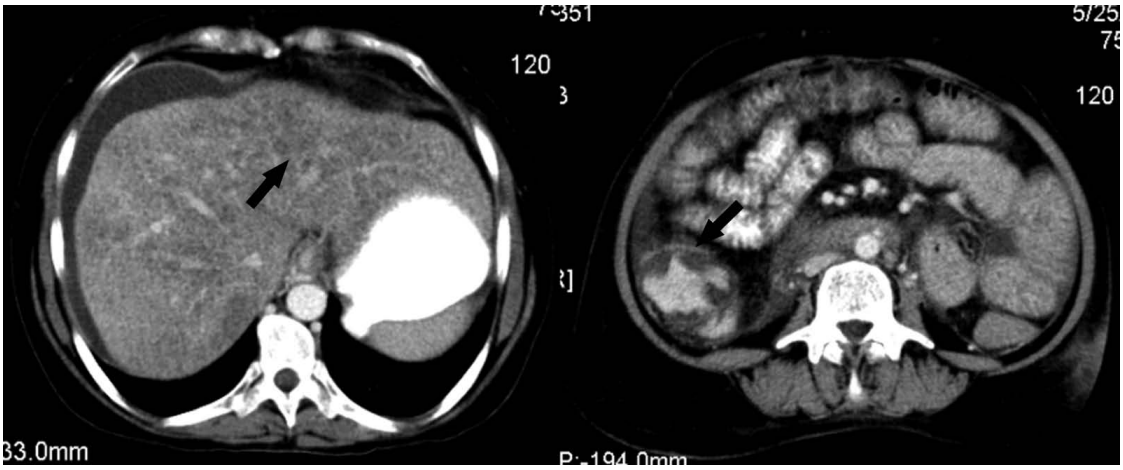

FIGURES 2.12A and B: Axial CECT reveals hepatomegaly with multiple ill-defined hypodense infiltrative lesions involving both lobes of liver. Figure 2.12b Axial CECT in the same patient reveals circumferential caecal thickening with rim of pericaecal fluid-imaging features suggestive of tuberculosis.

Miliary tuberculosis is usually not detected at imaging, and hepatomegaly may be the only radiologic abnormality. In the healing stage of tuberculosis, CT may show diffuse hepatic calcifications (approximately 50% of cases). At US, detectable tuberculomas usually manifest as round, hypoechoic masses.

Fungal Abscess

Candidiasis (see Fig. 4.14)

Candidiasis is the most frequently encountered systemic fungal infection in immunocompromised hosts and has increased in frequency in recent years. In these patients clinical presentation with a combination of persistent fever, abdominal symptoms, and an elevated serum alkaline phosphatase is quite characteristic. At CT, hepatic candidiasis typically appears as multiple small rounded lesions with decreased attenuation evenly distributed throughout the liver. Their size varies between 0.5 and 3 cm in diameter. A peripheral enhancement may occur as well as in "target" lesions, a small central zone of high density representing the hyphae.

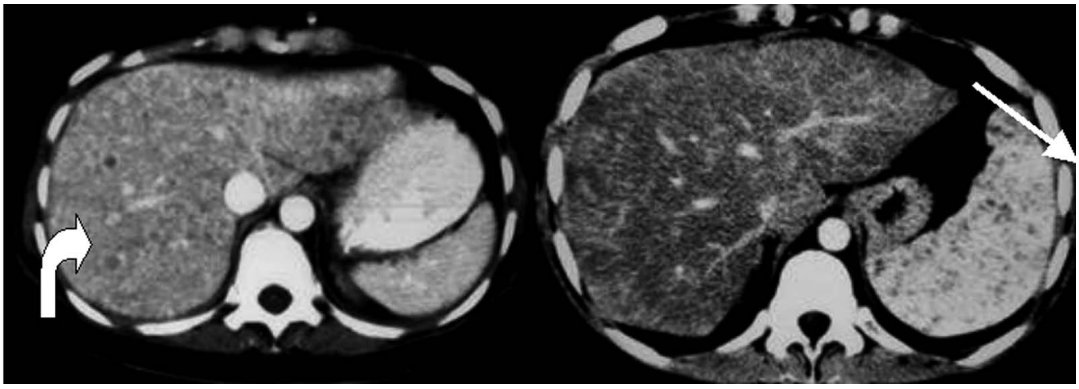

FIGURES 2.13A and B: Axial CECT in two different patients reveals multiple nodular hypodense lesions involving both lobes of liver (curved arrow) and spleen (arrow in B). Both cases were proved to be due to candida infection.

Mucormycosis

Mucormycosis is produced by zygomycosis species: rhizopus, rhizomucor, mucor, and apophysomices. Incidence is increased in immunocompromised patients (diabetes). The fungus invades arteries leading to infarction and necrosis. Manifestation is mostly rhinocerebral while liver may be involved with dissemination. Disseminated mucor uniformly fatal disease. CT shows hypodense necrotic lesions, located around vessels without mass effect. They are usually well defined and display no peripheral enhancement.

Diffuse Inflammation

Most viral infections lead to a diffuse inflammatory reaction of hepatic parenchyma. Additionally, systemic bacterial infections may also produce a similar hepatic inflammation. Malaria and systemic toxoplasmosis are further causes of diffuse hepatitis. Diagnosis is usually easily made by clinical symptoms and blood tests. Imaging is rarely helpful in establishing the diagnosis. Acute viral hepatitis is a systemic infection that affects the liver and is usually caused by one of five viral agents: hepatitis A virus, hepatitis B virus (HBV), hepatitis C virus, the HBV-associated delta agent or hepatitis D virus, and hepatitis E virus. A vast array of other viruses may also produce hepatitis, including herpes viruses, yellow fever virus, rubella virus, Coxsackie virus, and adenovirus. Although these viruses can be distinguished by their molecular and antigenic properties, all types of viral hepatitis produce clinically similar illnesses. These illnesses range from asymptomatic, inapparent infections to fulminant, fatal acute infections (common to all types of viruses), and from subclinical persistent infections to rapidly progressive chronic liver disease with cirrhosis (common to the blood-borne types [HBV and hepatitis C or D virus]).

In chronic hepatitis, the hepatic inflammation and necrosis continue for at least 6 months. Complications that occur during end-stage chronic hepatitis include ascites, edema, variceal bleeding, hepatic encephalopathy, coagulopathy, hypersplenism, and development of hepatocellular carcinoma.

In acute viral hepatitis, the major histologic findings are *(a)* necrosis of random isolated liver cells or small cell clusters, *(b)* diffuse liver cell injury, *(c)* reactive changes in Kupffer cells and sinusoidal lining cells and an inflammatory infiltrate in portal tracts, and *(d)* evidence of hepatocytic regeneration during the recovery phase. Confluent necrosis may lead to bridging necrosis connecting portal, central, or portal-to-central regions of adjacent lobules, signifying a more severe form of acute hepatitis.

The morphologic features of chronic hepatitis are variable. In the mildest form, an inflammatory infiltrate is limited to portal tracts. The histologic hallmark of progressive disease is piecemeal necrosis, whereby chronic inflammatory cells extend out from portal tracts into adjacent parenchyma, with associated necrosis of hepatocytes

in the limiting plate. Continued loss of hepatocytes resulting in fibrous septum formation accompanied by hepatocyte regeneration determines progression of disease to cirrhosis.

The imaging features of acute hepatitis are nonspecific, and the diagnosis is usually based on serologic, virologic, and clinical findings. Probably the most important role of radiology in patients with suspected hepatitis is to help rule out other diseases that produce similar clinical and biochemical abnormalities, such as extrahepatic cholestasis, diffuse metastatic disease, and cirrhosis.

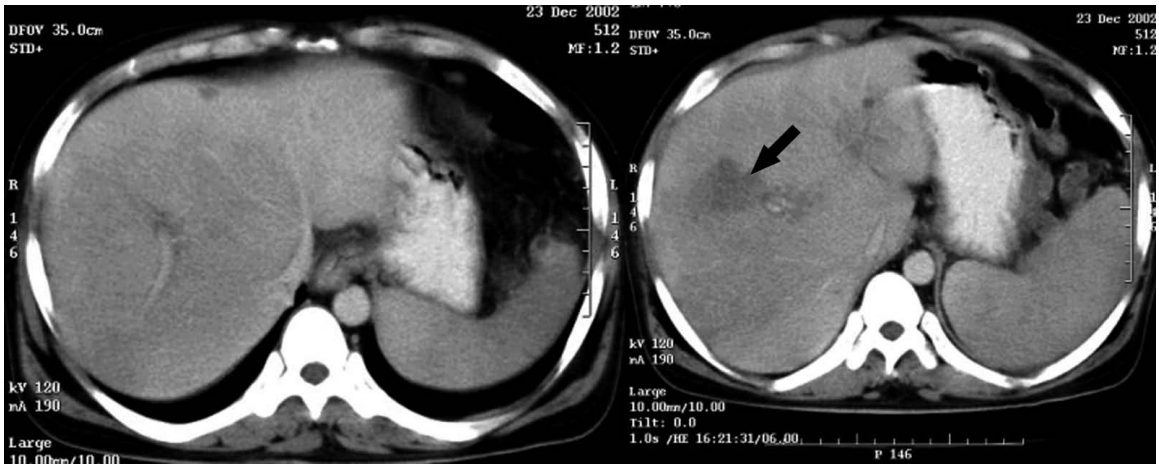

FIGURES 2.14A and B: CT imaging, findings in acute viral hepatitis are nonspecific and include hepatomegaly and periportal edema. At CT, heterogeneous enhancement and well-defined regions of low attenuation may be present.

Peliosis Hepatis

Some hepatic infections have a vascular involvement as leading manifestation. Septic portal vein thrombosis (pylephlebitis) is one of these characteristic manifestations that represent an acute bacterial infection of the portal system from a primary gastrointestinal source (diverticulitis). Mortality without adequate treatment is 50%.

Other vascular alterations may be the formation of blood filled cavities in bacterial or viral infections (tuberculosis, *Bartonella henselae*, HIV) or arterial invasion with consecutive parenchymal necrosis by fungi or parasites (mucor, fasciola hepatica) and are characterized by formation of blood filled spaces (peliotic cavities). At CT liver parenchyma may display a diffusely low density due to multiple small cavities. Lesions with diameter of more than 1 cm in diameter appear hypodense and may show a vessel-like enhancement following infection of contrast.

Benign Liver Tumors

Hepatocyte Origin

1. Focal nodular hyperplasia (FNH)
2. Hepatocellular adenoma (HCA)
3. Nodular regenerative hyperplasia (NRH)

Biliary Origin

1. Simple cyst/polycystic liver disease
2. Biliary hamartoma (Von Meyenburg complex)
3. Biliary cystadenoma

Mesenchymal Origin

1. Hemangioma
2. Mesenchymal hamartoma
3. Infantile hemangioendothelioma
4. Angiomyolipoma
5. Rare mesenchymal tumors (lipoma, inflammatory pseudotumor, leiomyoma, lymphangioma).

Hemangioma (see Figs 2.37 to 2.39)

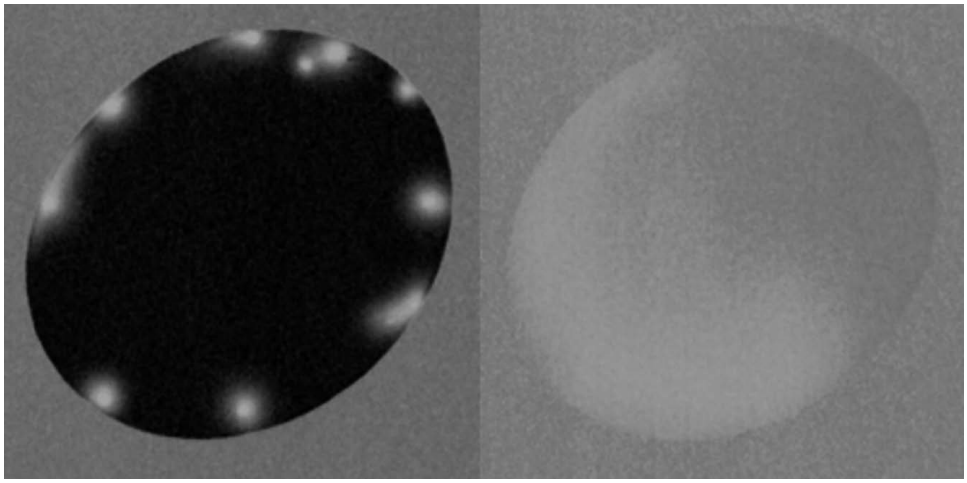

FIGURE 2.15: Schematic showing peripheral puddling in with persistent delayed opacification.

Pathology

Hemangiomas are mesodermal in origin. They are composed of blood filled cavernous vascular spaces that are lined by single layer of flat endothelium cells supported by a thin, fibrous stroma. Grossly its solitary, well circumscribed and range in size from few mm to 25 cm. Hemangiomas larger than 10 cm are refered to as *giant hemangiomas.*

Incidence

It is the second most common benign tumor of the liver exceeded only liver metastasis. It is more common in females, with male to female ratio being 1:5.

Non-contrast CT appearances–low density masses with lobulated well-defined margins, 10-20% show calcifications. On contrast enhanced CT hemangiomas show characteristic peripheral nodular enhancement with centripetal filling on delayed images. Central low attenuation may represent a scar/necrosis.

Diagnostic Triad of Hemangioma: Peripheral Filling, Delayed Filling, and Persistence of Enhancement

Forty-six percent of hemangiomas show atypical patterns of contrast enhancement-hyperdense lesion on NECT; absent, mixed or central enhancement during bolus dynamic phase or incomplete isodense fill in on delayed scans.

Complications of Hemangioma

Spontaneous rupture, thrombocytopenia (platelet sequestration), and hypofibrinogenemia.

Focal Nodular Hyperplasia FNH (Figs 2.40A and B)

FNH is the second most common solid benign tumor of the liver.

FIGURE 2.16: Schematic showing the central scar.

Pathology

It is a tumor-like mass having a central scar with surrounding nodules of hepatocytes. Vessels course the lesion and are abundant in the central scar. It is postulated that an underlying congenital vascular malformation may trigger the formation of hepatocyte hyperplasia. Grossly they are circumscribed masses seen on the surface of the liver. Majority of them are smaller than 5 cm multiple FNH have been reported, thought to be a hyperplastic response to an underlying vascular lesion. No normal portal venous structures are present in the FNH, though bile ducts and arterial vessels course through it. Hemorrhage, necrosis, and calcification are rare features.

It is more common in women in 3rd-5th decade of life.

It is usually a incidental finding and associated with oral contraceptive use.

Except for the central scar, FNH resembles hepatic adenomas on noncontrast CT.

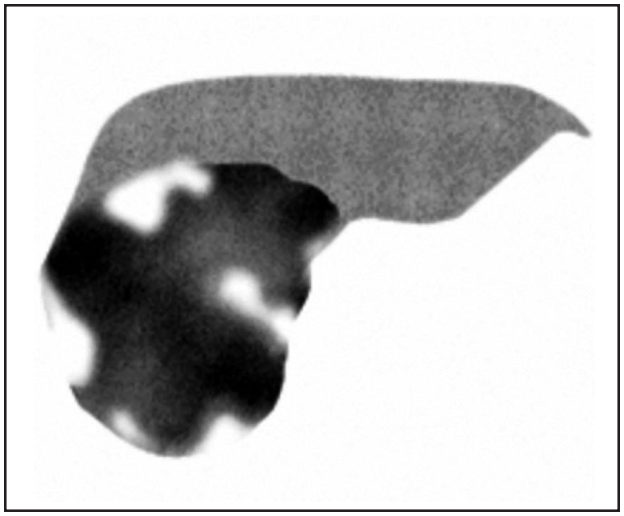

On NECT it appears as a homogenous isodense liver mass and can be seen only if they deform the liver contours or possess a prominent low density central scar. On CECT-FNH show rapid enhancement appearing hyperdense to liver in arterial phase, with a steady decrease in attenuation during portal phase when it appears isodense to the liver. Delayed scans show enhancement of central scars.

Hepatocellular adenoma: It is an uncommon solid primary liver tumor.

FIGURE 2.17: Schematic showing puddling in of contrast—there is no delayed persistence of contrast enhancement.

Tumor of hepatocytes arranged in cords that may form bile. Portal tracts are absent in hepatic adenomas. Grossly it is a large solitary tumor 8-10 cm. Hemorrhage and infarcts are common.

Hepatic adenomas are associated with oral contraceptive use in women, anabolic steroids in men, type I and type III glycogen storage disease in children.

On non-contrast CT hepatic adenomas appear isodense with liver but may appear as a hypodense mass due to fat and glycogen, or heterogenous with foci of necrosis.

Hyperdense areas of hemorrhage can be seen. On contrast enhanced CT-hepatic adenomas show centripetal enhancement with no delayed persistence because of arteriovenous shunting.

Complications

Spontaneous rupture and hemoperitoneum.

Nodular Regenerative Hyperplasia

Nodular regenerative hyperplasia is a rare condition and is characterized by diffuse nodular areas and is not associated with fibrosis or any hepatic injury. Grossly there are multiple nodules on the external surface of liver simulate metastasis. They are usually multiple and range in size from few mm to 6 cm.

Rare 6% prevalence, incidental or present with portal hypertension. It is associated with a variety of systemic diseases such as rheumatoid arthritis, polyarteritis nodosa, CML, myelofibrosis, Hodgkin's, CLL, Felty's syndrome.

CT findings Normal liver to that of a liver with focal nodules of varying attenuation that are primarily hypodense. Central hemorrhage within a large nodule may produce complex mass with variable density.

Hepatic Cysts

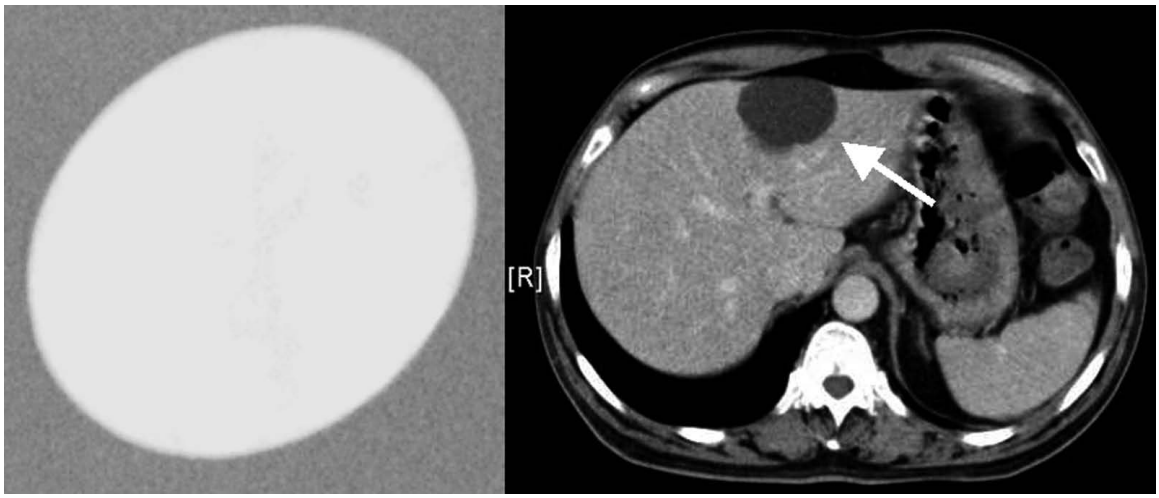

FIGURE 2.18: Schematic and axial CECT showing a typical simple cyst (arrow).

Liver cysts can be developmental, infectious (parasitic) or traumatic.

A simple hepatic (bile duct) cyst is a single, unilocular cyst lined by a layer of cuboidal, bile duct epithelium. They are solitary or multiple. The wall is a thin layer of fibrous tissue and adjacent liver is normal. Wall is 1 mm or less in thickness and typically occurs just beneath the surface of the liver, although some may occur deeper. These are usually asymptomatic and are seen incidentally during imaging.

Incidence

1-14%. They are more prevalent in women, with female to male ratio of 5:1.

On CT scan liver cysts are thin walled sharply marginated lesions having water density (0-15 HU) with absence of internal structures, and no enhancement after administration of contrast administration.

Complication

Hemorrhage, infection.

MALIGNANT HEPATIC TUMORS

Primary hepatic malignancies may arise from any cell type within the liver. They are broadly classified as epithelial or mesenchymal based on their cell of origin. Of all hepatic neoplasms (benign and malignant), 93% are malignant epithelial neoplasms, and 1.1% are mesenchymal malignancies.

Classification of Malignant Tumors

EPITHELIAL TUMORS
- **Hepatocellular origin**
  - Hepatocellular carcinoma
  - Fibrocellular carcinoma
  - Sclerosing carcinoma
- **Cholangiocellular**
  - Cholangiocarcinoma
  - Biliary cystadenocarcinoma
- **Mixed cellular origin**
  - Combined hepatocellular and cholangiocarcinoma

MESENCHYMAL TUMORS
- **Vascular origin**
  - Epithelioid hemangioendothelioma
  - Angiosarcoma
- **Sarcomas**
- **Lymphomas**

Hepatocellular Carcinoma

Also known as hepatoma is much more common in Asia and Africa than in European and North American populations.

Hepatoma is more common in males than in females.

Risk Factors for Hepatoma

Most hepatocellular carcinomas occur in patients who have chronic liver disease.

1. Cirrhosis of liver: Regenerative process associated with cirrhosis is suspected as the underlying cause of a large proportion of hepatocelluar carcinoma. HCC is more common in macronodular form of cirrhosis than micronodular form. Adenomatous hyperplastic nodules and intermediate between regenerative nodule and HCC, is found to contain dysplastic hepatocytes.

2. Alcohol related cirrhosis (macronodular form) is a most common cause of HCC.
3. Persistent infection with hepatitis B virus and hepatitis C virus.
4. Patients with primary hemochromatosis develop cirrhosis are at increased risk of HCC.
5. Aflatoxins produced by Aspergillus flavus fungi are responsible for HCC.
6. Long-term exposure to radiation emitted by Thorotrast.
7. Patients with glycogen storage disease type I and alpha I-antitrypsin deficiency are also at increased risk of developing HCC.

There are 3 CT patterns of hepatoma in the liver: a solitary mass, a dominant mass with smaller satellite lesions (i.e. multifocal hepatoma, 20%), and diffuse involvement. Diffuse involvement is more common in patients with cirrhosis.

HCCs have varied appearance on CT (see pages 36-39).

Most HCCs appear as hypodense masses on noncontrast CT. Some of the lesions are isodense to liver with a hypoattenuating rim, representing tumor capsule or may protrude beyond the contour of the organ.

It may have heterogenous density due to hemorrhage, necrosis or fibrosis. Fatty infiltration may also occur within the HCC.

Calcification is uncommon in HCC.

Following dynamic contrast administration, most tumors become well delineated displaying their full extent of involvement. HCC receives its blood supply from the hepatic artery. Tumor tissue becomes hyperdense in arterial phase and hypodense on portal venous phase. Areas of scar tissue and necrosis remain unenhanced and of low attenuation.

Vascular Effects of HCC

Vascular effects of HCC include arterioportal shunting which is seen as early and prolonged enhancement of portal vein. Neoplastic invasion of portal vein or hepatic vein or IVC causes absent luminal enhancement and expansion of the affected vessel. Tumor thrombus itself may show some enhancement which differentiates it from bland thrombus. Portal venous involvement results in obstruction of blood flow to the involved segment. Wedge-shaped areas of decreased attenuation may result. These changes are particularly prominent when using CTAP.

Invasion of biliary tree by HCC causes biliary obstruction and dilatation of system.

Fibrolamellar hepatoma is a distinctive type of hepatoma which occurs predominantly in older children and young adults. Fibrolamellar carcinomas occur without a background of cirrhosis. Although it is a malignant lesion, the prognosis is better than typical hepatoma, with 25% of patients having resectable lesions. Alpha-fetoprotein levels are usually not elevated. Fibrolamellar hepatoma is typically a well-circumscribed solitary lesion showing uniform contrast enhancement. Often contains central calcifications in 1/3 of lesions and central scarring. Areas of necrosis and fibrosis remain unenhanced. The differential diagnosis includes adenoma or focal nodular hyperplasia.

Although the advent of spiral CT with arterial phase imaging has significantly improved our ability to detect these hypervascular tumors, the diagnosis of HCC at CT remains a challenge for several reasons.

- Small HCC often display transient enhancement and proper timing of image acquisition is critical.
- Although regenerating nodules are usually not seen on CT, occasionally a regenerating or dysplastic nodule can be confused with a small HCC.
- It may be quite difficult to detect a multifocal type of HCC among the diffuse heterogeneity associated with cirrhosis.
- It is important to distinguish HCC from other focal abnormalities related to flow phenomenon or focal fat deposition or fibrosis commonly present in the cirrhotic liver.

CT Pitfalls in the Diagnosis of HCC

Occasionally, peripheral hyperenhancing areas are seen on the **HAP**. These **transient hepatic attenuation differences** (THAD) fade on the **PVP** and are thought to represent areas of normal parenchyma with predominant hepatic arterial perfusion due to segmental portal vein occlusion, or small hepatic arterial to portal venous branch fistulae. They often occur distal to HCC but can be differentiated from the tumor by their wedge shape and peripheral location.

Other focal lesions such as confluent fibrosis or focal fatty infiltration are common in the cirrhotic liver but should be recognized based on their geographic shape and enhancement characteristics.

Cholangiocarcinoma (see also page 83)

Cholangiocarcinoma is the second most common primary hepatic tumor, and is a malignancy arising from the bile ducts. Cholangiocarcinoma is associated with chronic bile duct inflammation. Peak age of onset is 6th to 7th decade. Patients present with painless jaundice.

Intrahepatic cholangiocarcinoma presents late and extrahepatic cholangiocarcinoma presents earlier with painless jaundice.

Presdisposing factors include:
Inflammatory bowel disease-ulcerative colitis, Crohn's disease, sclerosing cholangitis, Clonorchis sinensis infestation, biliary tract stones, gallstones, choledochal cyst, Caroli's disease.
Chronic inflammation of bile ducts is the basic element leading to cholangiocarcinoma.

Intrahepatic CCA occurs peripherally in the liver from the small intrahepatic bile ducts. Mass is usually heterogeneous, but hypodense relative to the liver on unenhanced scans. High attenuation areas in the mass may be seen because of mucinous material, as these tumors produce mucin which accumulate in bile ducts, and mimic stones.

Low attenuation areas within the mass may be due to mucin or necrosis. Contrast enhanced CT show heterogeneous enhancement in peripheral form of CCA.

In CCA alpha-fetoprotein is not elevated, but bilirubin is higher than HCC.

Extrahepatic form is the most common form of this tumor. It is typically sclerosing and infiltrative. Fifty percent of lesions arise at the common duct bifurcation or in the distal bile duct. The so-called Klatskin tumor is a small stricturing cholangiocarcinoma arising at the junction of the left and right hepatic ducts.

It is diificult to visualize a mass in CT. Typical finding on CT is dilatation of IHBR with nonunion of the dilated ducts at the hilum. Occasionally a mass may be seen at the hilum which is hypodense to the adjacent liver parenchyma on CECT. On delayed scans the density of the hypodense mass may increase in the density.

These lesions produce bilobar biliary duct obstruction and are nearly always unresectable. The differential diagnosis includes central metastasis or possibly lymphoma. Peripheral cholangiocarcinoma may occasionally be resectable when it does not involve the IVC or caudate lobe.

CCA should be suspected if there is an abrupt end to the biliary dilatation without a visible mass, especially if it occurs between hilum and pancreatic head.

Lobar atrophy is common with hilar CCA.

Staging of CCA:
Stage I: tumor below the confluence
Stage II: tumor at the confluence
Stage III: unilateral extension into 2nd order ducts.
Stage IV: bilateral multifocal involvement

Differentiating ICC from HCC

Contrast enhancement features

- Marked filling in favors HCC
- Heterogeneous enhancement favors HCC
- Delayed central to peripheral fill in favors ICC

Tumor margins

- Lobulation favors ICC, HCC well encapsulated
- Capsular retraction more common in ICC
- Biliary dilatation peripheral to the tumor favors ICC

Angiosarcoma (see Figs 2.35A and B)

Hepatic angiosarcoma is a rare, aggressive sarcoma that occurs predominantly in men. It is the most common primary malignant mesenchymal neoplasm of the liver. The average age at presentation is 53 years, and the male-to-female ratio is 3:1. Signs and symptoms at presentation are often nonspecific, although one half of patients have hepatomegaly. Jaundice, ascites, thrombocytopenia, and acute hemoperitoneum may be presenting features. Most patients (60%) present with evidence of metastatic disease, most commonly to the lung and spleen.

Angiosarcoma has well-established associations with exposure to vinyl chloride, arsenic, radiation, and the radiographic contrast agent Thorotrast. Thorotrast accumulates in the reticuloendothelial system and induces HCC, cholangiocarcinoma, or angiosarcoma with a latency of 20 to 30 years.

Grossly, hepatic angiosarcoma commonly has a multinodular or multifocal pattern but may also manifest as a solitary large mass. The tumor extends to a subcapsular location and has a propensity to rupture and bleed. Histologically, hepatic angiosarcoma has a spectrum of appearances and may present a variety of appearances within the same tumor. The malignant cells of angiosarcoma may grow along existing vascular channels, have an arrangement of sinusoidal or large cavernous spaces, or form nodules, masses, or poorly organized vessels. Patients exposed to Thorotrast, vinyl chloride, or arsenicals may have concurrent fibrosis or cirrhosis.

Nonenhanced CT scans typically demonstrate a hypoattenuating mass. There may be foci of hyperattenuation within the tumor that represent acute or active intratumoral hemorrhage. Several case reports in the medical literature have described the contrast enhancement pattern of angiosarcoma as mimicking that of a benign hepatic hemangioma. Another variant is that of multiple nodules diffusely replacing the parenchyma.

The presence of fluid-fluid levels and layering of contrast-opacified blood with nonopacified blood is evidence of intratumoral hemorrhage.

Epithelioid Hemangioendothelioma

Epithelioid hemangioendothelioma is a rare malignant neoplasm of vascular origin that arises in the liver, soft tissue, and bone. It occurs primarily in adults and predominantly in women. The clinical presentation is often nonspecific, with signs and symptoms of abdominal pain, weakness, anorexia, jaundice, and hepatosplenomegaly. Many patients are asymptomatic, however, and their tumors are discovered incidentally. There are no well-established risk factors. Suggested associations with oral contraceptives, vinyl chloride, occupational contaminants, major liver trauma, and viral hepatitis have been reported.

Gross pathology reveals multiple small nodules within the periphery of the liver. The peripheral edge of the tumor is often hyperemic. Larger lesions may form from confluent masses. Histologically, epithelioid

hemangioendothelioma is composed of dendritic and epithelioid cells within a fibrous myxoid stroma. The epithelioid cells stain positive for factor VIII–related antigen, confirming an endothelial origin. The tumor is infiltrative with intravascular tumor growth into terminal portal and hepatic vein branches and obliteration of adjacent hepatic sinusoids. The lesions tend to be peripheral in location and may have a retracted or flattened liver capsule adjacent to the tumor.

The lesions of epithelioid hemangioendothelioma are hypodense to normal liver in nonenhanced CT scans. They are more conspicuous on contrast enhanced CT-scans. There is peripheral enhancement of the tumor after intravenous contrast administration, and a second, outer-peripheral hypoattenuating rim may occasionally be seen. Calcification and capsular retraction are well depicted by CT scanning when present.

Hepatic Lymphoma (see Figs 2.36A and B)

Primary hepatic lymphoma occurs primarily in middle-aged men. Solid organ transplant recipients have a higher incidence of primary hepatic lymphoma (post-transplantation lymphoproliferative disorder). Grossly, lymphoma may appear within the liver as a solitary mass, as a miliary pattern, as are multifocal masses, or as a diffusely infiltration lesion.

Hepatic lymphoma may appear as solitary, multifocal, or diffusely infiltrative lesions. The sonographic appearance has been described as hypoechoic relative to the adjacent liver parenchyma with enhanced through transmission. The lesions may also appear anechoic.

The most commonly reported appearance of primary hepatic lymphoma on CT scanning is a solitary hypodense mass. The enhancement pattern following intravenous administration of contrast material is variable. Low-density necrosis may be present within the mass.

Biliary Cystadenocarcinoma

Biliary cystadenocarcinoma and its benign counterpart, biliary cystadenoma, are rare cystic neoplasms of the liver that occur primarily in middle-aged women. There are two distinct histologic variants of biliary cystadenocarcinoma. Biliary cystadenocarcinoma with ovarian stroma is found only in women and typically has a good prognosis. Biliary cystadenocarcinoma without ovarian stroma can occur in both men and women and has a poor prognosis.

Biliary cystadenocarcinomas are multilocular cystic masses that have a fibrous capsule. Polypoid masses, nodularity, and septations may be present on the internal surface in both the benign and malignant varieties. The fluid content within the cyst may be hemorrhagic, mucinous, bilious, or mixed. Focal calcifications may occur within the wall of the cyst or in the internal septations. Histologically, malignant epithelial cells that resemble pancreatic and ovarian mucinous cystic neoplasms line the cysts in cystadenocarcinoma.

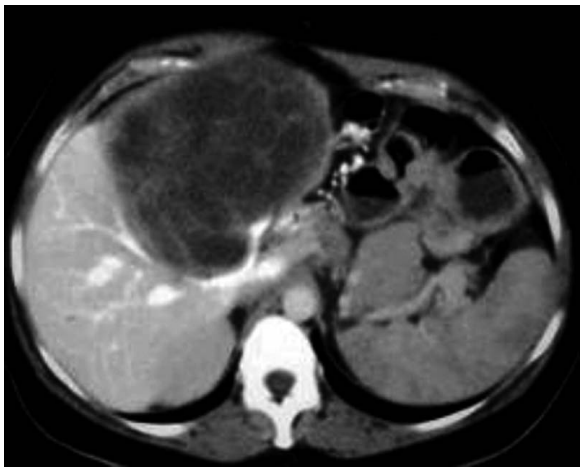

CT scans typically identify a water-density, multiloculated cyst. The attenuation of the cyst fluid is increased when hemorrhage is present. In addition to mural and septal calcification, soft-tissue density septations and nodules may be present. CT scanning may not demonstrate septations that are visualized by ultrasound imaging. The nodules and septae may enhance following contrast administration.

FIGURE 2.19: Axial CECT reveals a large hypodense septated lesion in the left lobe of liver displacing the portal and hepatic vascular radicles.

Box 2.1: Tumor and tumor like lesions of the liver

	Benign liver tumors	Malignant liver tumors
PRIMARY TUMORS		
Epithelial tumors		
Hepatocellular	Hepatocellular adenoma	Hepatocellular carcinoma Fibrolamellar carcinoma
Cholangiocellular	Bile duct adenoma Biliary papillomatosis	Cholangiocellular carcinoma Bile duct cystadenocarcinoma
Mesenchymal tumors	Hemangioma	Angiosarcoma
Vascular tumors	Hemangioendothelioma (children)	Hemangiosarcoma Malignant epithelioid Hemangioendothelioma
	Angiomyolipoma	
		Embryonal sarcoma Leiomyosarcoma Non-Hodgkin's lymphoma and Hodgkin's disease
Mixed type		Hepatoblastoma
SECONDARY TUMORS		
	Parasitic infections	Metastases
TUMOR-LIKE LESIONS		
	Cysts Focal nodular hyperplasia Nodular regenerative hyperplasia Mesenchymal hamartoma Peliosis hepatis Inflammatory pseudotumors	

Table 2.1: Arterial phase enhancement patterns of HCC, hemangioma, FNH, and metastasis

Diagnosis	*Enhancement Pattern*
HCC	Homogeneous
HCC	Abnormal internal vessels or variegated
Hemangioma	Peripheral puddles
FNH	Homogeneous
Metastasis	Complete ring
Metastasis	Incomplete ring
Metastasis	No enhancement

PEDIATRIC LIVER MASSES

Classification

Benign epithelial tumors

- Focal nodular hyperplasia
- Hepatocellular adenoma
- Hepatic cysts

Benign mesenchymal tumors

- Mesenchymal hamartoma
- Hemangioendothelioma
- Hemangioma

Malignant epithelial tumors
- Hepatoblastoma
- Hepatocellular carcinoma
- Fibrolamellar carcinoma

Malignant mesenchymal tumors
- Undifferentiated embryonal sarcoma
- Embryonal rhabdomyosarcoma
- Angiosarcoma

Metastases
- Neuroblastoma
- Burkitt's lymphoma
- Sarcomas
- Wilms' tumor
- Other

APPROACH TO LIVER MASSES

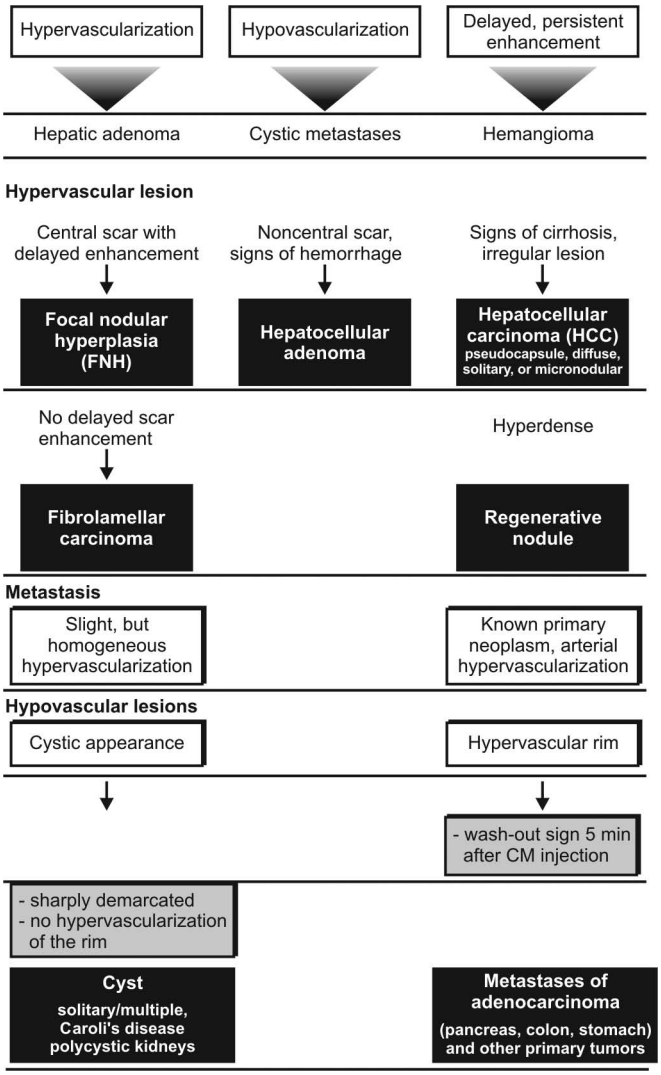

FIGURE 2.20:

PEDIATRIC LIVER TUMOR

Infantile hemangioendothelioma	Less than 1 year	Solid vascular lesion with calcific specks
Mesoblastic hamartoma	Less than 2 years	Predominantly cystic
Hepatoblastoma	Less than 3 years	Solid, vascular, may have calcification, AFP positive, usually solitary
Hepatocellular carcinoma	More than 4 years	Solid, vascular, may have calcification, AFP positive
Embryonal rhabdomyoma	Less than 5 years	Predominantly solid, vascularity, AFP – negative.
Undifferentiated embryonal sarcoma	More than 6 years	Predominantly cystic with few solid components, AFP—negative
Metastasis	Any age group	Solid and cystic, solitary or multiple lesion

Hepatoblastoma

A three-year-old female child with abdominal distention.

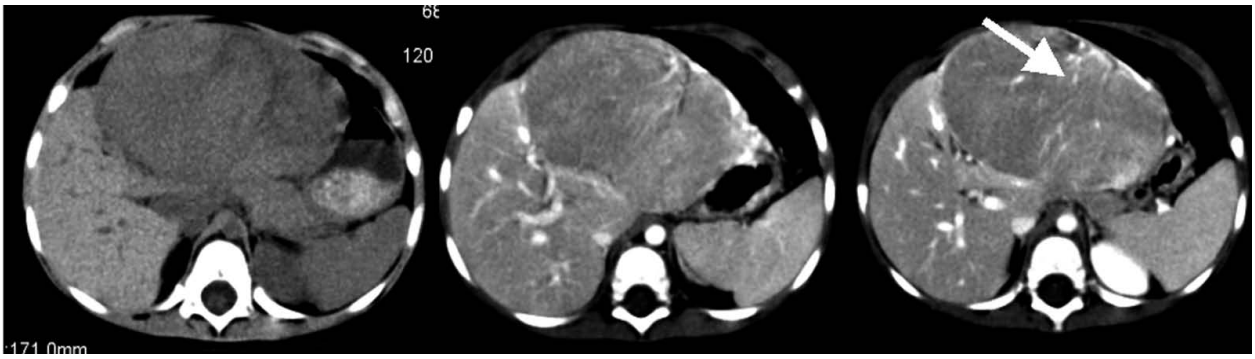

FIGURES 2.21A to C: (A) Axial NECT of liver reveals a well marginated mixed dense mass involving the left lobe of liver. (B,C) Axial CECT sections show variable degree of enhancement with multiple tumor vessels (arrow in C).

A 6-year-old boy with a liver mass noted in USG.

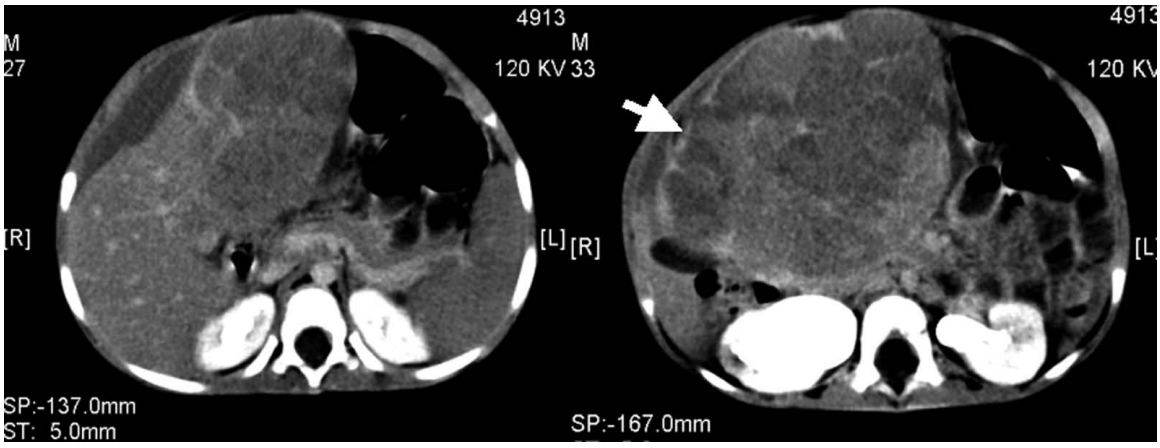

FIGURES 2.22A and B: Axial CECT reveals a heterogeneously enhancing liver mass involving the left lobe of liver with linear enhancing areas of neovascularity with capsular enhancement (arrow in B).

Patterns of Hepatocellular Carcinoma

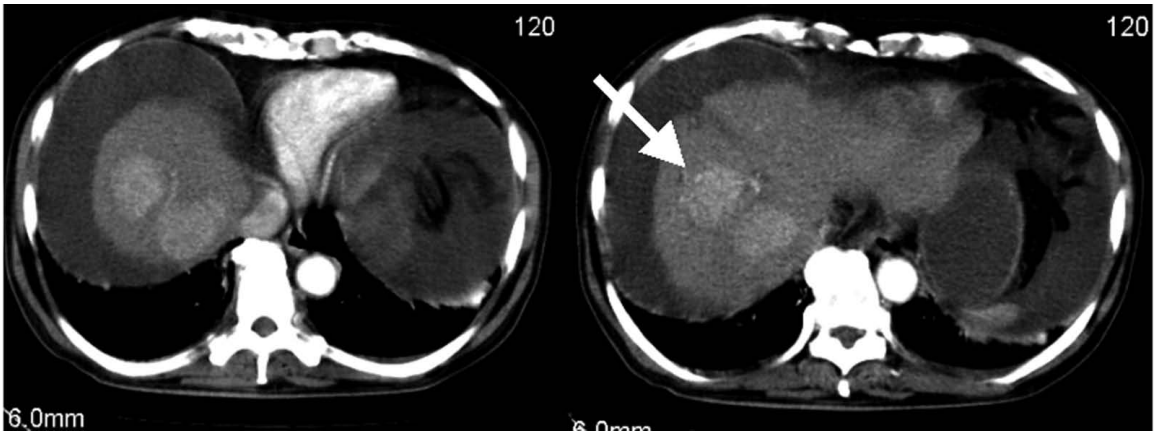

FIGURES 2.23A and B: Axial CECT reveals shrunken liver with nodular margins and ascites. Superior segment shows two enhancing nodular lesions with tumor vessels (arrow in B).

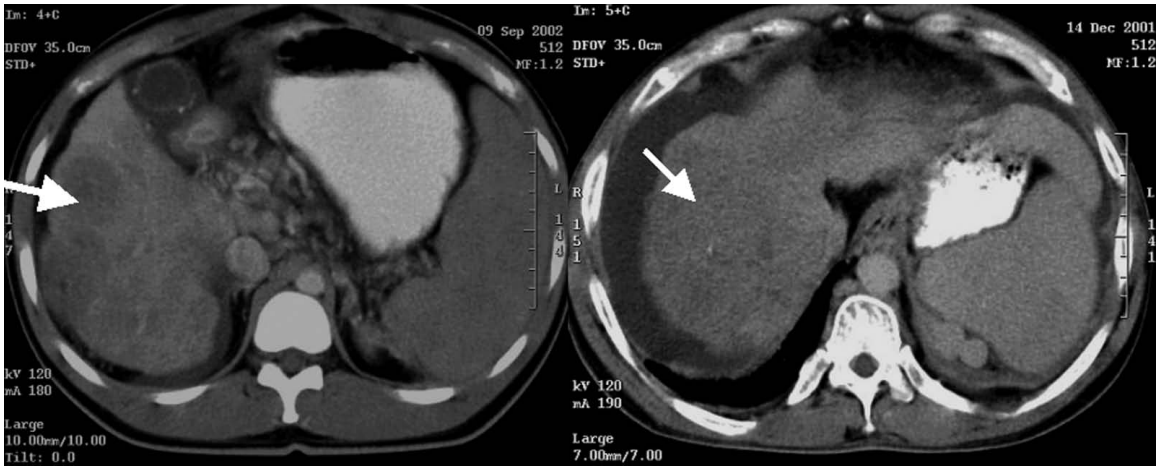

FIGURES 2.24A and B: Axial CECT reveals nodular hypodense lesions (arrow in A) with irregular infiltrative parenchymal architecture suggestive of a infiltrative HCC (arrow in B) in a background of cirrhosis.

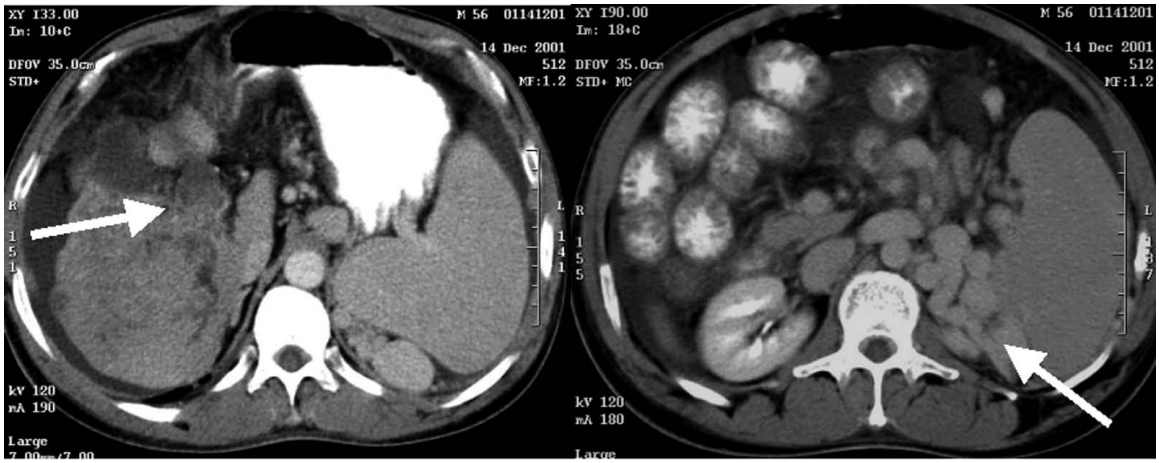

FIGURES 2.25A and B: Axial CECT shows nodular shrunken liver with right segmental portal vein thrombus (arrow) (B) Axial CECT shows splenomegaly with extensive splenic hilar and splenorenal collaterals (arrow).

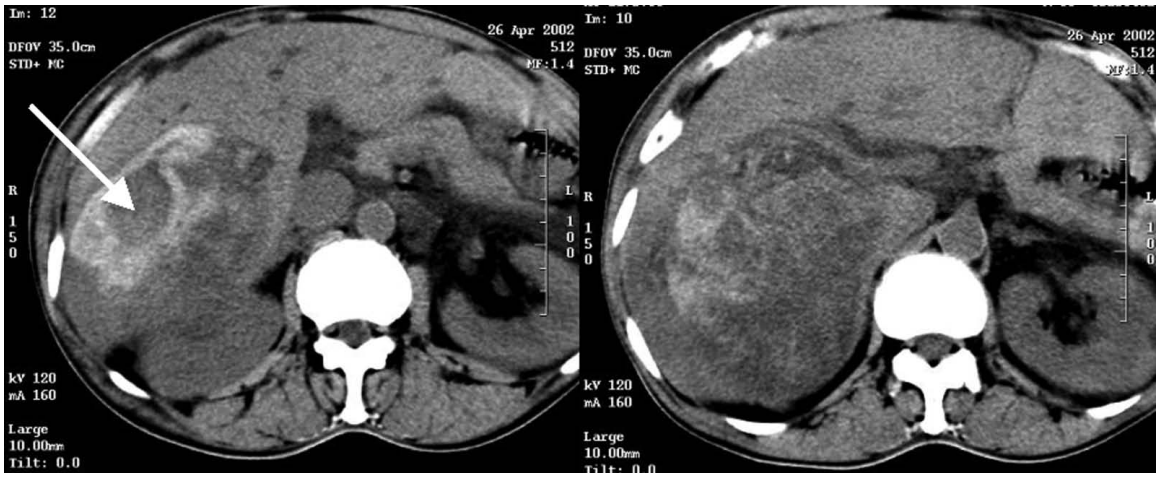

FIGURES 2.26Aand B: Axial NECT in a known case of HCC reveals a hypodense lesion showing areas of hyperdensity suggestive of acute bleed (arrow in A).

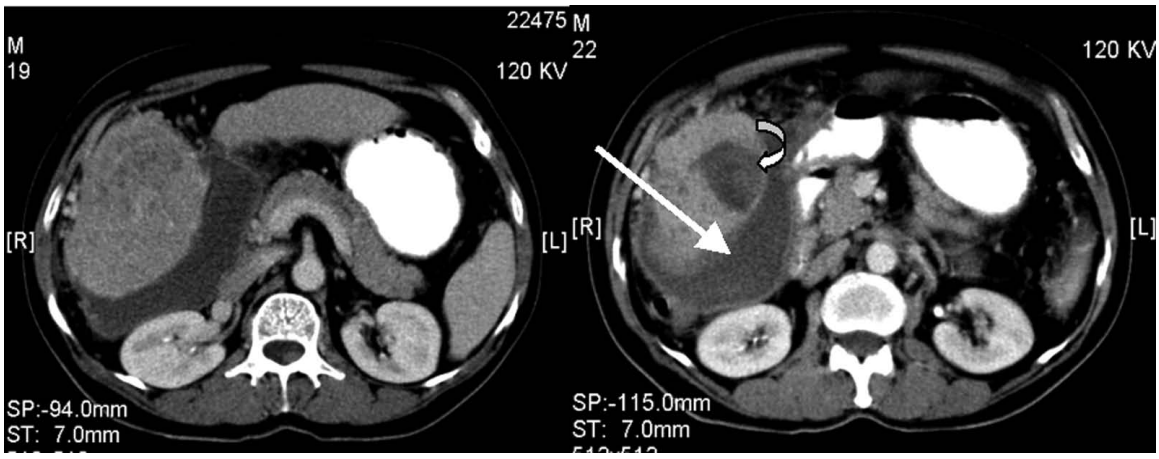

FIGURES 2.27A and B: Axial CECT in a case of HCC reveals a heterogeneous lesion in the right lower lobe of liver (curved arrow in B) with a well marginated subcapsular collection suggestive of bleed due to spontaneous rupture (arrow in B).

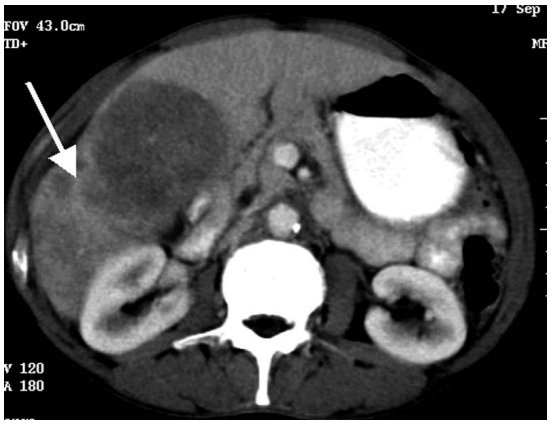

FIGURE 2.28: Axial CECT reveals a well marginated hypodense lesion in right lobe with adjacent satellite nodules (arrow).

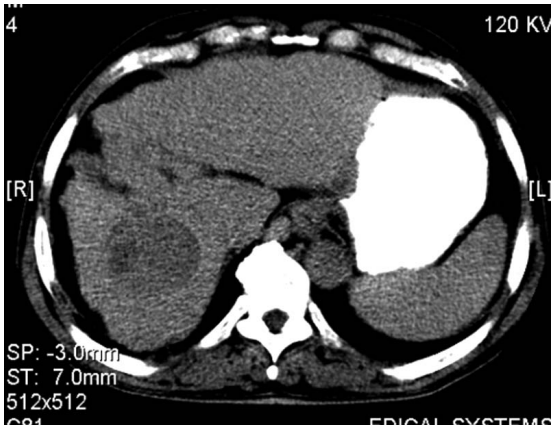

FIGURE 2.29: Axial CT delayed post contrast scan reveals a well defined hypodense lesion in right lobe segment 6 region showing capsular enhancement. Note the background changes of cirrhosis with shrunken nodular margins.

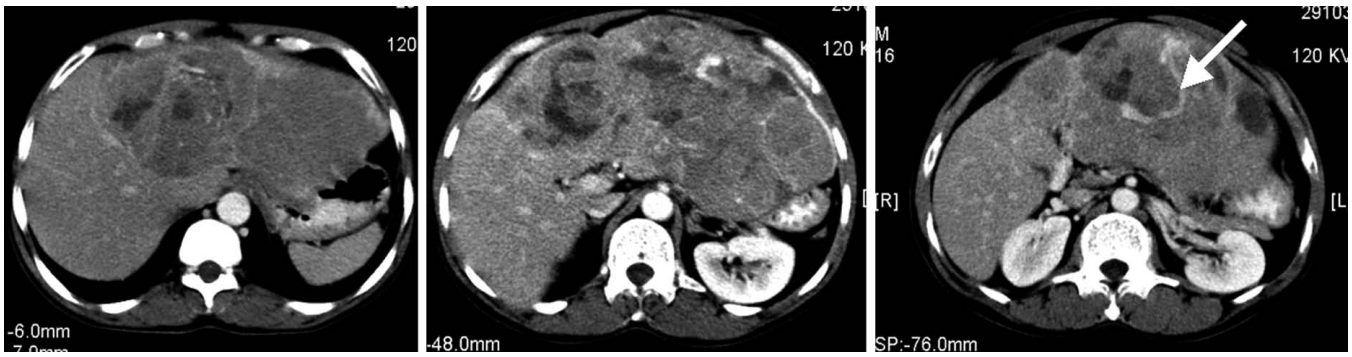

FIGURES 2.30A to C: Axial CECT reveals a large left lobe liver mass showing a large capsular and parenchymal tumor vessel (arrow in C).

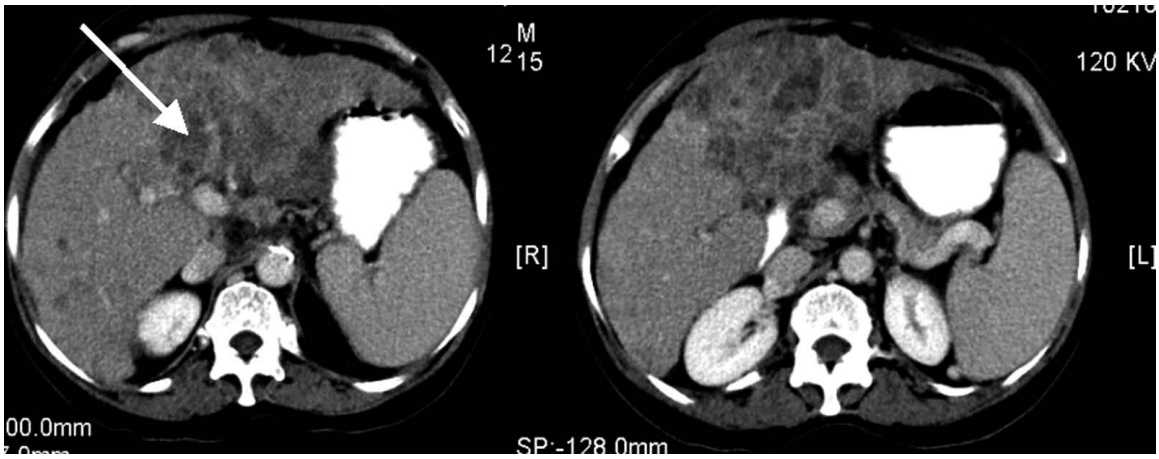

FIGURES 2.31A and B: Axial CECT reveals a infiltrative lesion replacing the left lobe liver encasing the left segmental portal vein (arrow in A).

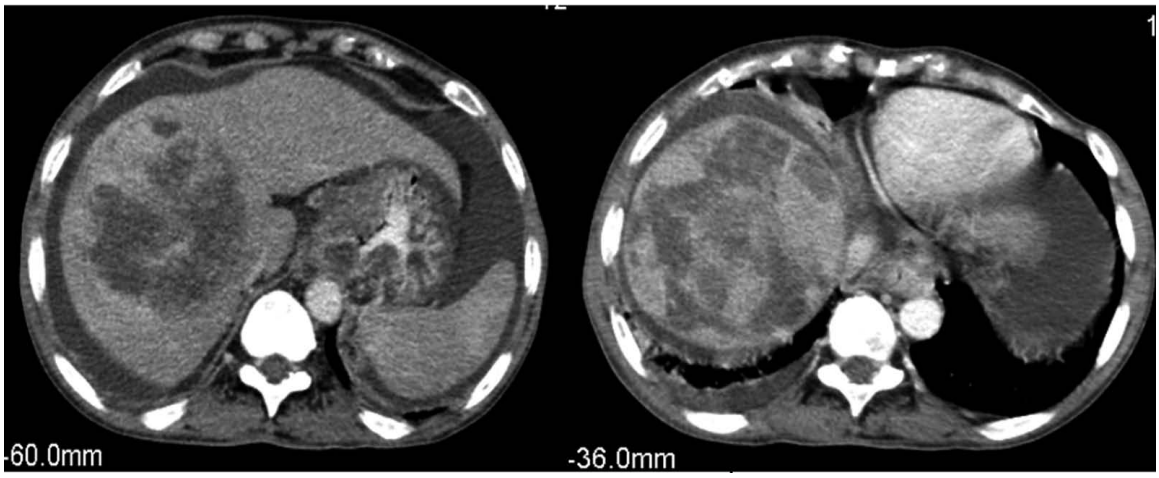

FIGURES 2.32A and B: Axial CECT reveals a right lobe liver variably enhancing well marginated mass with ascites.

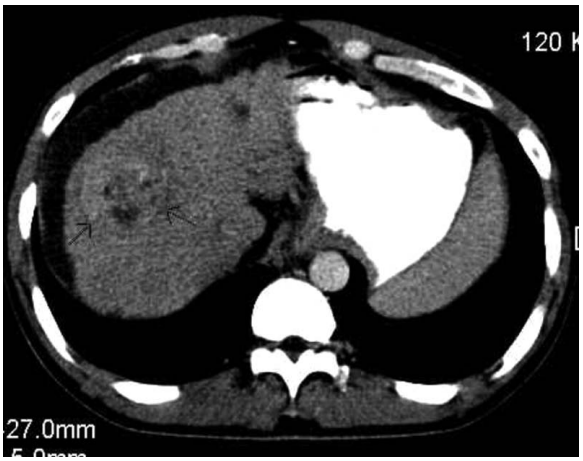

FIGURE 2.33: Axial CECT reveals a well marginated variably enhancing lesion in right lobe of liver, showing tumor vessels, liver shows features of cirrhosis.

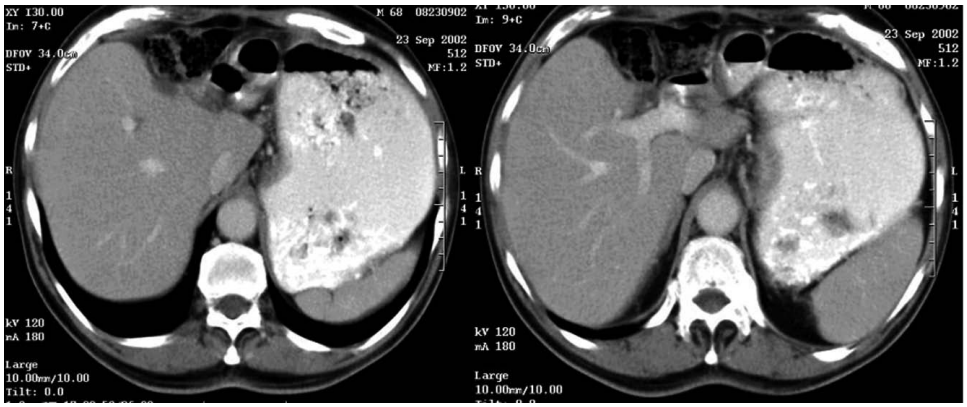

FIGURES 2.34A and B: Axial CECT in a case of left lobe liver HCC - post left lobectomy note the migration of the colon and stomach.

Angiosarcoma

A sixty-two-year old male with jaundice and right upper quadrant pain.

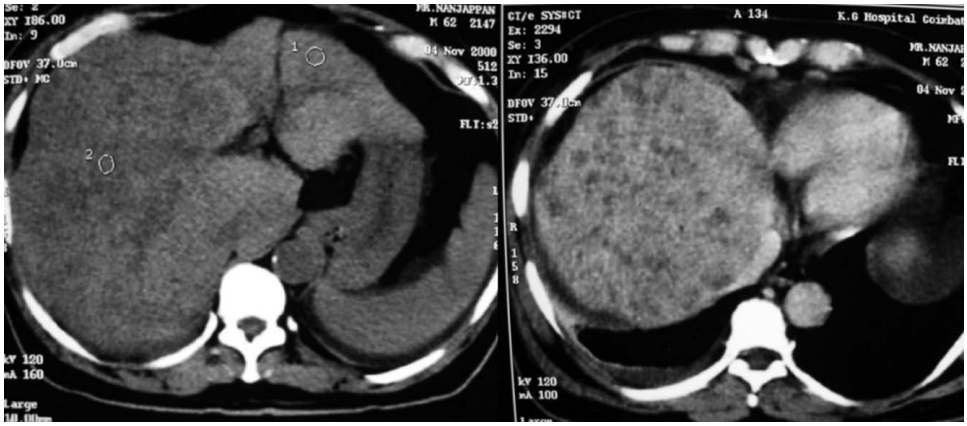

FIGURES 2.35A and B: Axial NECT reveals enlarged liver with multiple hypodense infiltrative lesions, (B) Axial CECT reveals multiple discrete hypodense regions which are not enhancing.

Non-Hodgkin's Lymphoma

A 37-year-old male presenting with abdominal pain and a mass in the left lower chest. FNAB from the lesion in the liver showed features suggestive of NHL.

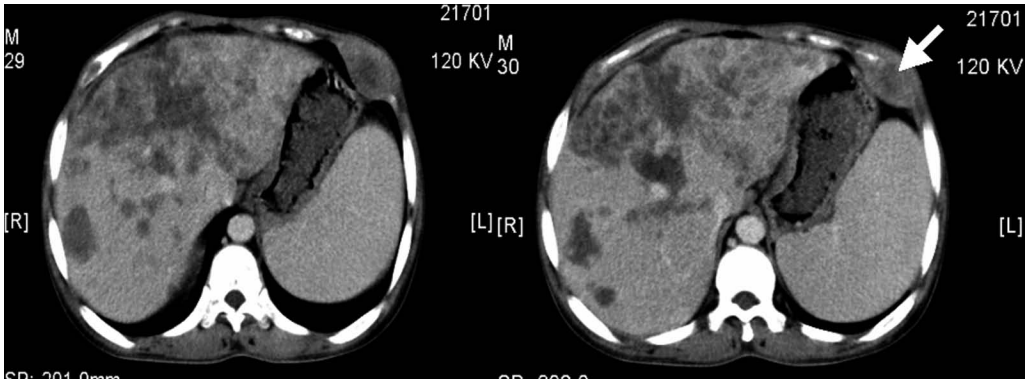

FIGURES 2.36A and B: Axial CECT reveals multiple hypodense lesions involving both lobes of liver with ill-defined margins, left anterior chest wall shows a soft tissue deposit (arrow in B).

Hemangioma

A 57-year-old female with a incidental mass found in USG.

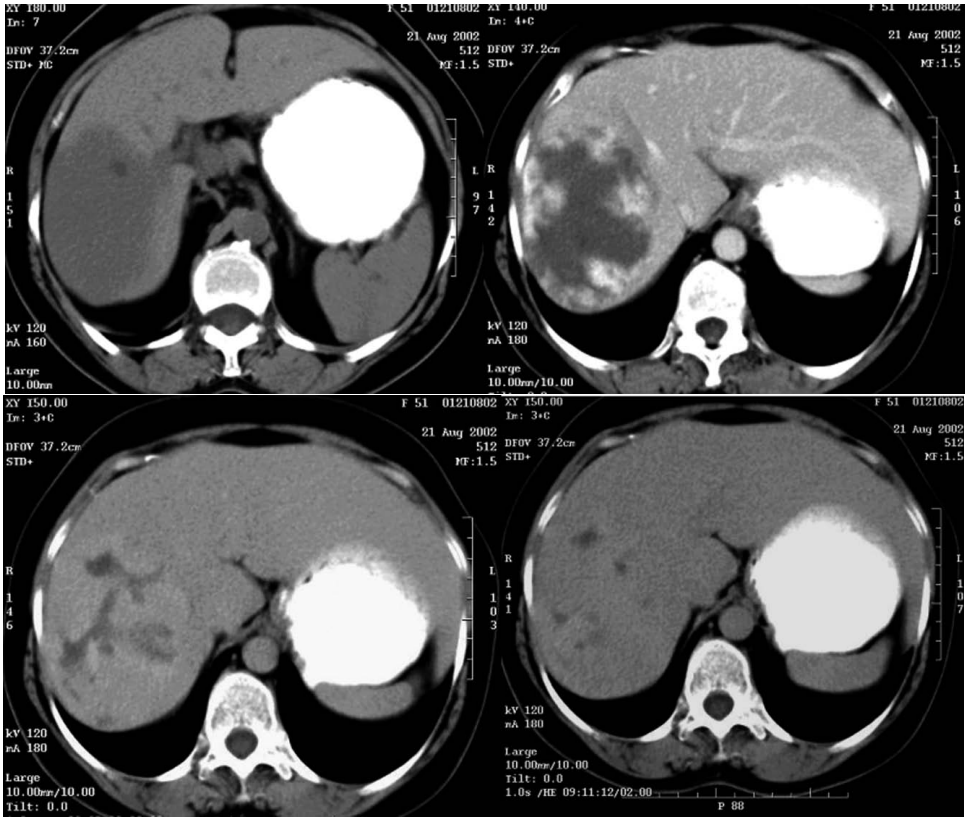

FIGURES 2.37A to D: (A) Plain axial CT showing a hypodense lesion in right lobe segment 7 region, (B) CECT showing peripheral contrast filling in, (C,D) 10 minute delayed scan shows complete filling in of contrast with central non-enhancing scar.

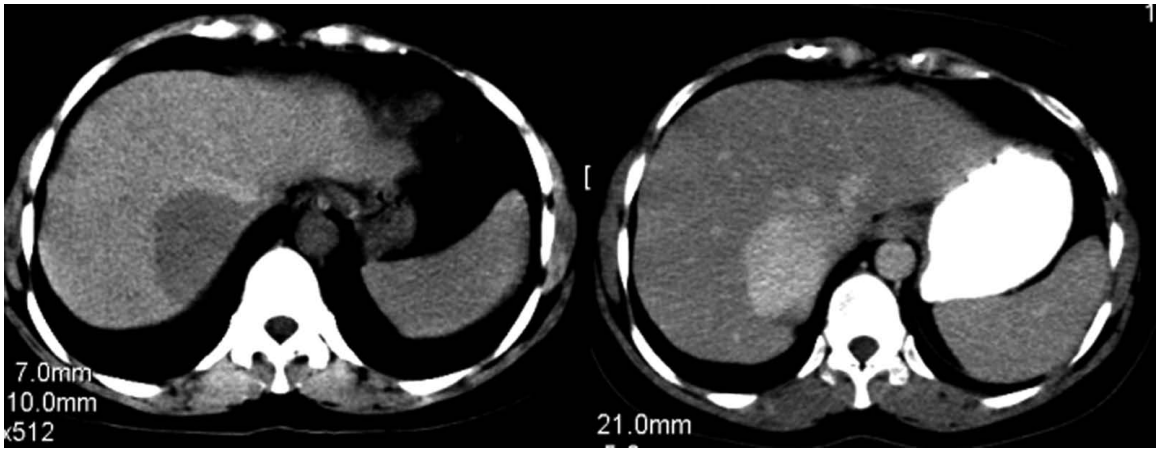

FIGURES 2.38A and B: Axial plain and CECT reveals a peripheral well marginated lesion in right lobe liver showing complete filling in on sequential CECT – hemangioma.

Atypical Delayed Filling is seen in Hemangioma

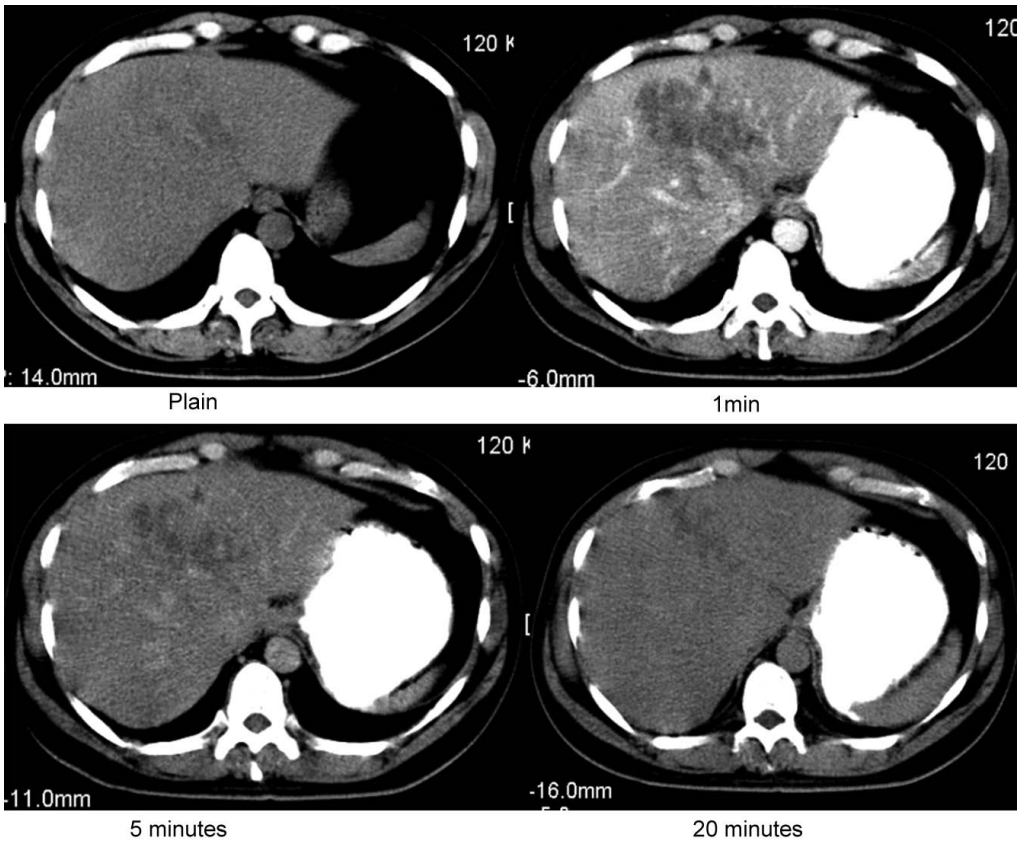

FIGURES 2.39A to D: Axial plain and CECT in a patient with a incidentally detected liver mass showing a very slow diffuse filling in of contrast over a period of 20 minutes, note the absence of the typical nodular filling usually seen.

Focal Nodular Hyperplasia

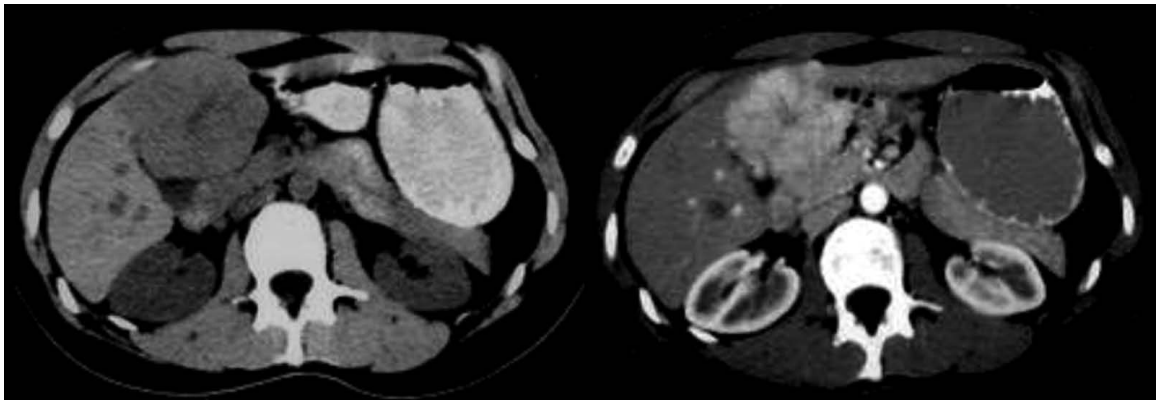

FIGURES 2.40A and B: Axial plain and CECT shows a left lobe liver well marginated lesion with central scar showing diffuse contrast fill in during the arterial phase.

Simple Cysts

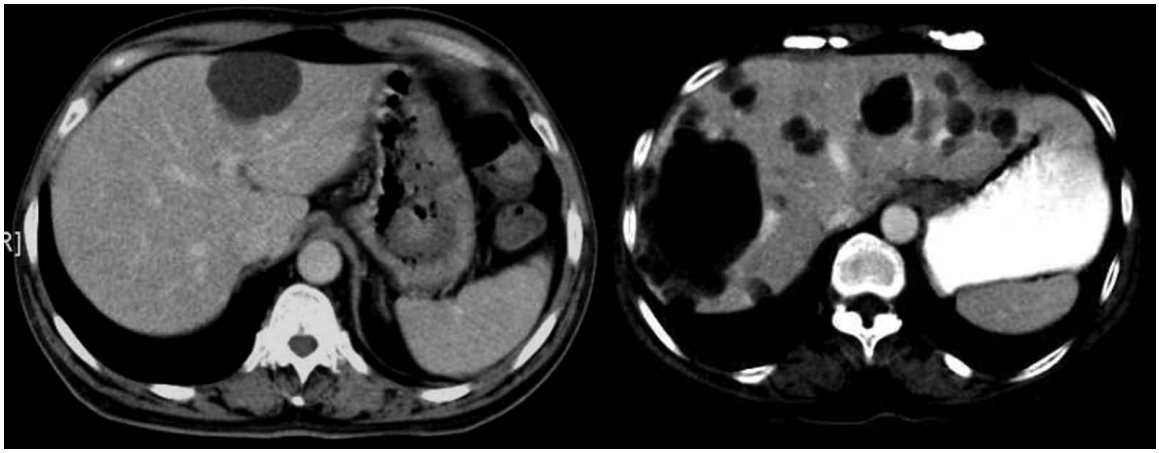

FIGURES 2.41A and B: (A) Axial CECT shows a well marginated hypodense non-enhancing lesion in left lobe liver. (B) Axial CECT reveals multiple well marginated hypodense lesions involving both lobes of liver.

Pseudo Mass

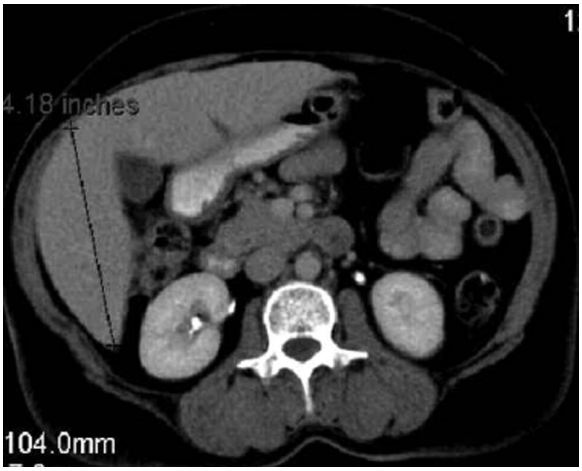

FIGURE 2.42: Axial CECT reveals a enlongated inferior segment of right lobe of liver—Riedel's lobe.

Hepatic metastasic diseases is the most common malignancy of non-cirrhotic liver. It is approximately twenty times more common than primary hepatic neoplasms. The most common metastatic tumors to the liver are colon, breast, lung, pancreas, melanoma and sarcomas. Metastatic disease in the liver usually appears as focal, discrete lesions, but diffuse infiltrative involvement of the liver may be seen in breast cancer or lymphoma, and rarely with colon or lung primaries.

For small lesions < 15 mm in size, benign tumors (hemangioma, cyst) must be considered in the differential of metastatic disease, even if multiple abnormalities are found.

In patients with suspected metastatic disease, cross-sectional imaging is critical.

Blood Supply

The liver is unique because of its dual blood supply from the portal vein and hepatic artery. Approximately 20% of the blood supply is from the hepatic artery and 80% from the portal vein. For most abdominal primary tumors the liver represents the first site to be involved in hematogeneous metastatic spread. It is hypothesized that once tumor cells invade the portal venous system, they seed the hepatic parenchyma, which may represent a favorable environment for tumor growth. The blood supply to tiny or microscopic metastases is primarily from the portal venous system. However, by the time metastases are large enough to be detected by imaging, they receive the majority of their blood from the hepatic artery. It is interesting to note that a significant number of liver metastases up to 1. 5 cm in size have a distinct residual portal venous blood supply to the tumor periphery. Such dual vascularity in the smallest of lesions may partly explain some of the difficulty in detecting such lesions with imaging techniques.

Metastases are nearly always multiple. As a general rule, they are more frequently encountered in the right lobe than the left. This is likely due to the large mass of the right lobe and, accordingly, its greater blood flow. Furthermore, laminar flow in the portal vein plays a role because metastases from the gastrointestinal tract spread to the liver via the superior mesenteric vein, which preferentially flows into the right lobe.

Detection By Imaging

Detection of metastatic disease by imaging is based on lesion size, lesion-to-liver contrast difference, and lesion-to-liver edge definition. To maximize the detection of lesions, it is critical to perform imaging techniques with high spatial resolution. High-spatial resolution imaging can be maximized with thin collimation computed tomography (CT), magnetic resonance imaging (MRI), or ultrasound (US). Thin collimation imaging also results in improved lesion-to-liver edge definition because partial volume artifacts will be reduced.

Because the composition of metastatic deposits differs from the background liver (metastases usually contain more water), they may be detected on CT or MRI studies performed without the administration of contrast material. However, the lesion-to-liver contrast difference will be maximized by selectively enhancing the background liver parenchyma by the administration of contrast material. With CT and MRI, the most common approach to enhance the parenchyma is to inject iodine-containing contrast or gadolinium-containing contrast material, respectively.

There are several methods available to screen the liver for metastatic disease. Choice of modality will be based on clinical scenario. Table 2.2 lists the sensitivity of a variety of cross-sectional imaging techniques for the detection of individual metastases.

Table 2.2: Sensitivity of imaging for detecting individual metastases

Type	*Detection Rate (%)*
Transabdominal sonography	40-70
Noncontrast CT	50
Incremental (nonspiral) contrast-enhanced CT	60-75
Spiral contrast-enhanced CT	80-85
Magnetic resonance imaging	80-85
CT arterial portography	85-95
Intraoperative ultrasound	90-96

Imaging Appearances

Metastasic lesions may be hyper, hypo or isodense, cystic, complex, calcified or diffusely infiltrative on CT scans. Most metastasis are hypovascular showing a complete ring of enhancement. During the portal phase the ring enhances still, some metastases will show peripheral areas of low attenuation surrounding an enhanced center on delayed images.

Hyperdense metastases are usually hypervascular in nature the primary neoplasms being melanoma, carcinoid, renal cell carcinoma, pancreatic islet cell tumor, choriocarcinoma, pheochromocytoma and thyroid. Precontrast scans are a must in detecting these lesions as they become isodense on contrast scans. Depending on the size the margins tend to be irregular with or without necrosis.

Calcified lesions can be noted from mucinous GIT tumors, and from primary ovarian, breast, lung, renal and thyroid cancer.

Majority of liver metastases are hypodense because these lesions are usually hypovascular and the administration of intravenous contrast increase the density difference aiding in lesion detection.

Cystic metastases are seen in mucinous carcinoma of colon and cystadenocarcinoma of ovary.

Morphologic Pattern Based on the Primary Site

Pattern	*Site*
Expanding massive lesion	Colon, GB, testis
Infiltrative	
1. Massive	Lung, breast, pancreas
2. Diffuse	Breast, pancreas, lung
Uniformly multifocal	Breast, lung
Coelomic spread	Colon, ovary, stomach
Miliary	Prostate, germ cell

Images

A 65-year-old male case of Ca bronchus.

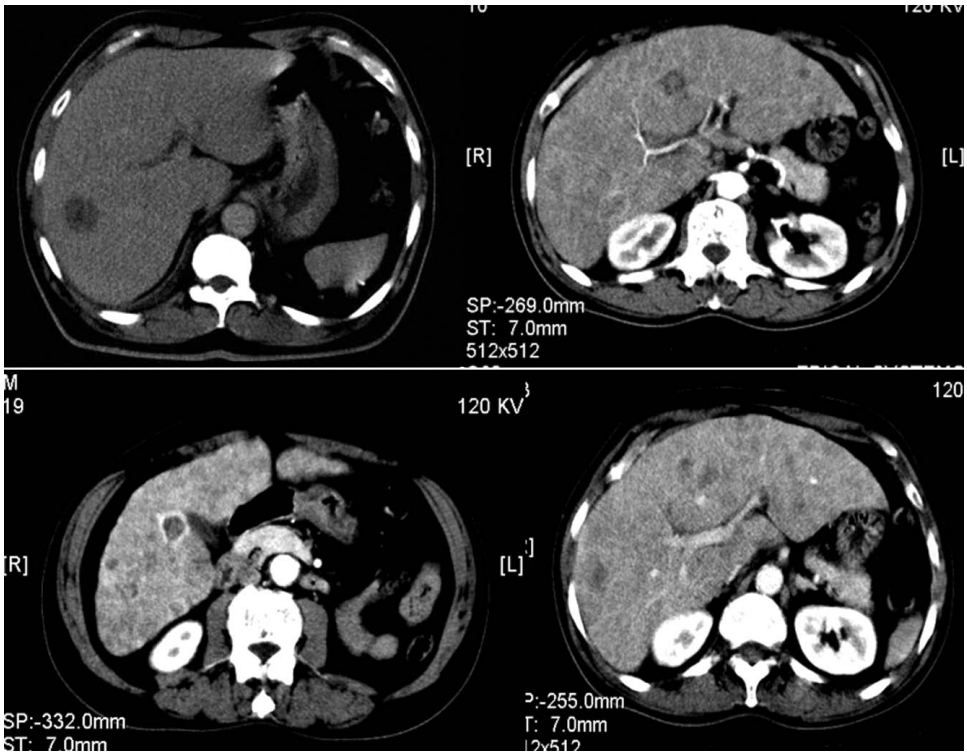

FIGURES 2.43A to D: (A) Axial NECT, reveals a hypodense lesion in segment 6, (B,C) Axial CECT in arterial phase reveals multiple ill-defined hypodensities in both lobes of liver with a rim enhancing lesion in segment 4B, (D) Axial CECT in portal phase reveals multiple hypodense lesion in both lobes.

A 53-year-old female patient with a history of Ca cervix.

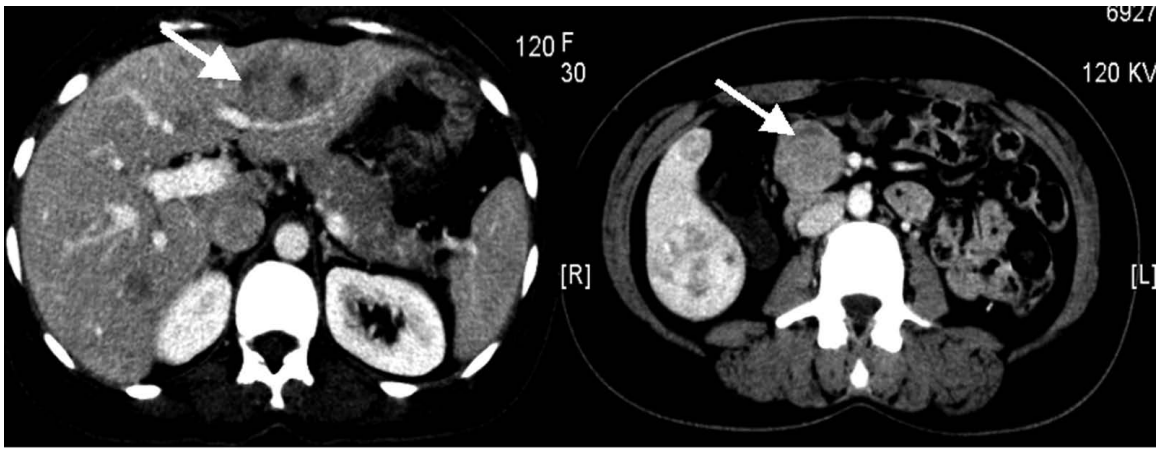

FIGURES 2.44A and B: Axial CECT reveals multiple well marginated lesions showing variable enhancement (arrow in A) involving both lobes of liver with a hypodense precaval soft tissue suggestive of lymph node.

A 67-year-old male patient case of Ca stomach.

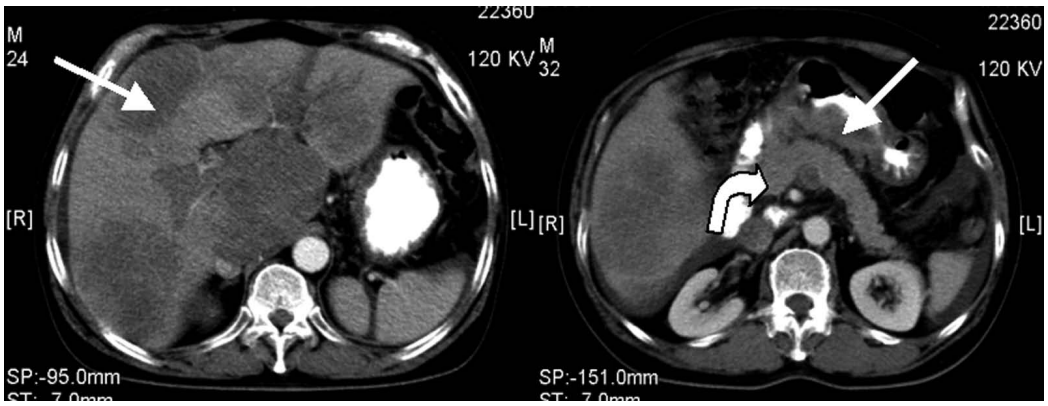

FIGURES 2.45A and B: Axial CECT reveals multiple hypodense lesions involving the liver (arrow in A), eccentric thickening of the stomach wall noted involving the distal body (arrow in B). There is alteration or the SMA/SMV axis with thrombosis of the SMV (curved arrow in B).

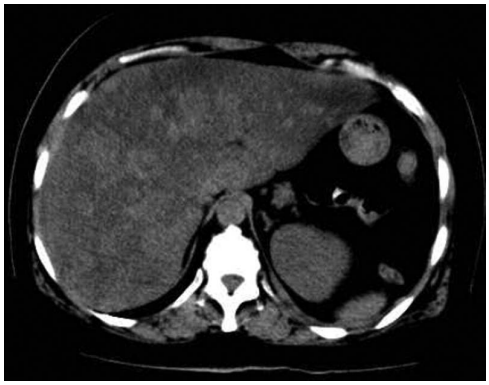

FIGURE 2.46: Axial NECT in a case of Ca bronchus reveals multiple hyperdense nodular areas involving both lobes of liver. This case illustrates the significance of a plain study in evaluation of suspected metastasis.

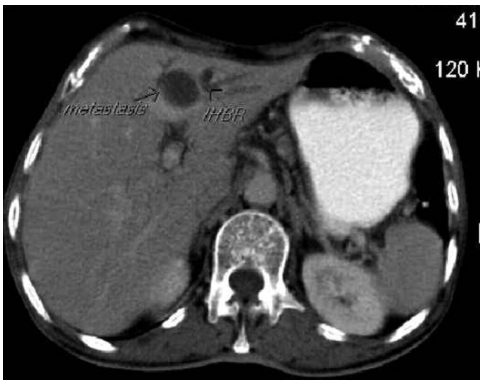

FIGURE 2.47: Axial CECT reveals a hypodense well marginated lesion in the left lobe liver causing segmental biliary dilatation (known case of bronchogenic carcinoma).

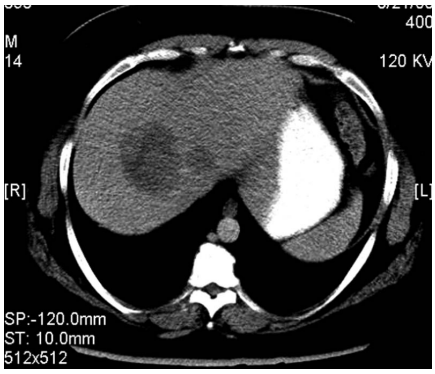

FIGURE 2.48: Axial delayed CECT in a patient with seminoma of testis shows a well marginated hypodense lesion in the right lobe with an adjacent smaller nodule. Delayed imaging is useful in cases were early phases do not delineate lesions adequately.

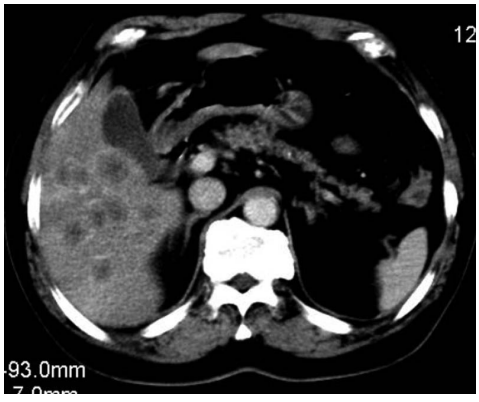

FIGURE 2.49: Axial CECT in a case of carcinoma sigmoid colon shows multiple nodular lesions in right lobe of liver showing a capsular enhancement with central low attenuation due to necrosis with a peripheral gray zone – this differential attenuation is a classical feature usually seen in metastasis.

Diffuse Liver Disease

Wide variety of disease processes are associated with diffuse involvement of the hepatic parenchyma. Regardless of the underlying etiology, many of these chronic parenchymal insults ultimately lead to the development of hepatic cirrhosis, characterized pathologically by a combination of parenchyma necrosis, regenerative nodules and extensive fibrosis.

Pattern of Involvement

Diffuse: Any process that affects the entire liver.

Geographic: Focal, non-mass-like processes of the liver or processes that affect a large area of the liver, including a segment or lobe.

DIFFUSE LIVER DISEASE: CT TECHNIQUE

- Non-contrast CT
- Decreased density: liver-spleen attenuation difference >10HU
- Increased density (> 75 HU)
- CECT
- Contour
- Morphologic changes of the liver

DIFFUSE CHANGES

Low Attenuation

Fatty liver: Fatty infiltration or metamorphosis is a commonly recognized process of the liver. Causes are protean diabetes, steroids, obesity, toxic or infectious hepatitis, TPN, hypertriglyceridemia and malnutrition.

On CT diffuse fatty change is recognized on pre-contrast scans with the following:

1. Low density liver (generally 10-20 HU less than spleen)
2. Prominent vessels, relative to the liver (appear as if enhanced)
3. Gallbladder may appear dense.

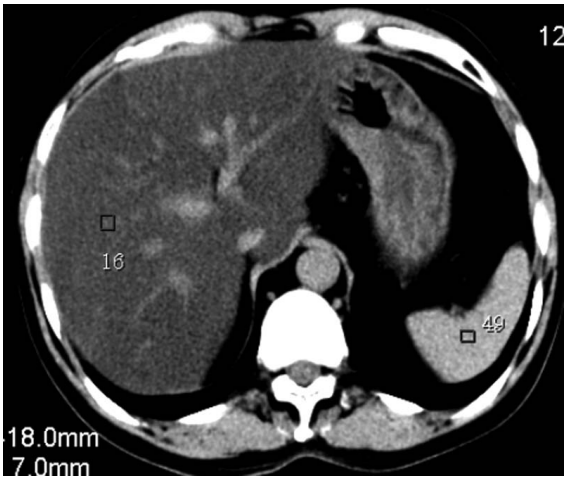

FIGURE 2.50: Axial CECT reveals low attenuation liver (16 HU), compare it with splenic attenuation.

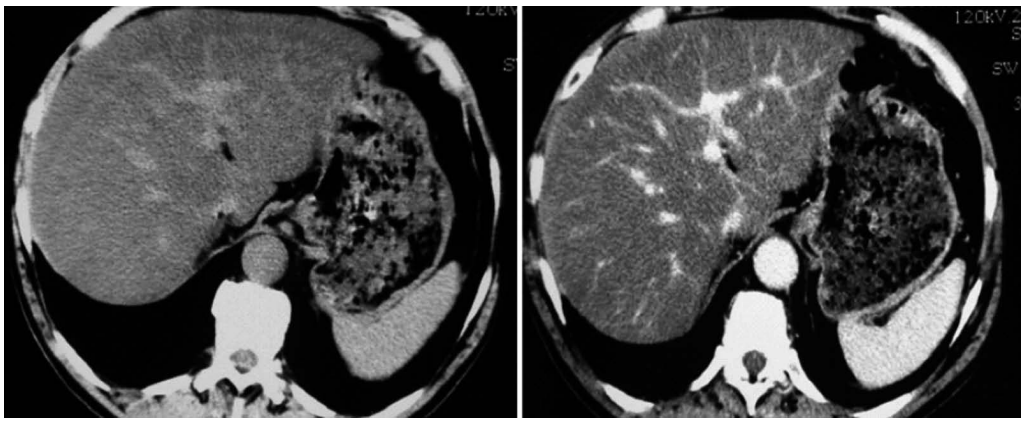

FIGURES 2.51A and B: Axial plain and CECT showing fatty liver.

Hepatitis: Acute viral, toxic or alcoholic hepatitis is not a CT diagnosis. However, these patients can be scanned for other reasons, or to evaluate the abdominal symptoms caused by hepatitis, before the hepatitis is discovered.

The following can be found:

- Hepatomegaly
- Heterogenous liver attenuation with areas of fatty change
- Diffuse fatty change
- Periportal edema
- Gallbladder wall thickening (the thickest gallbladder walls are found in hepatitis).

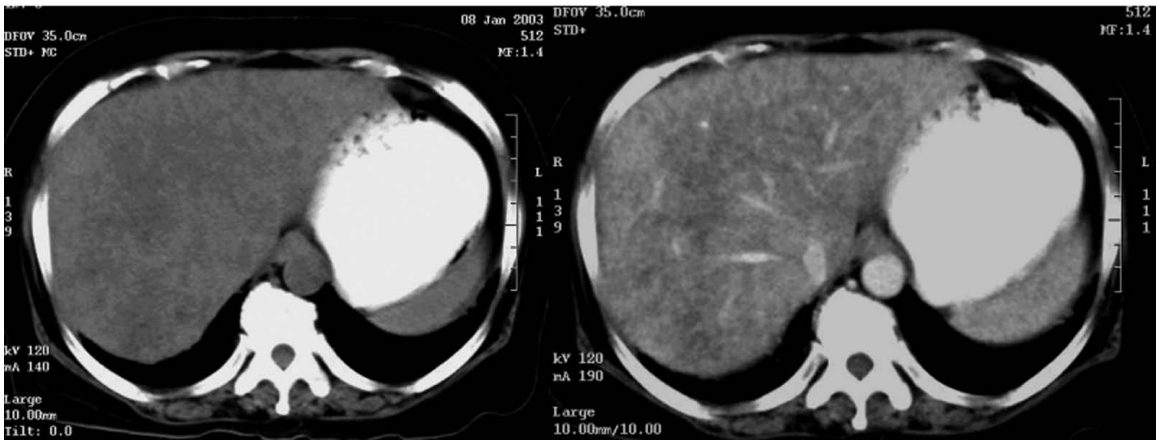

FIGURES 2.52A and B: Axial plain and CECT in a case of viral hepatitis reveals a mottled appearance with patchy enhancement.

High Attenuation

Non-CECT increased density (> 75 HU).

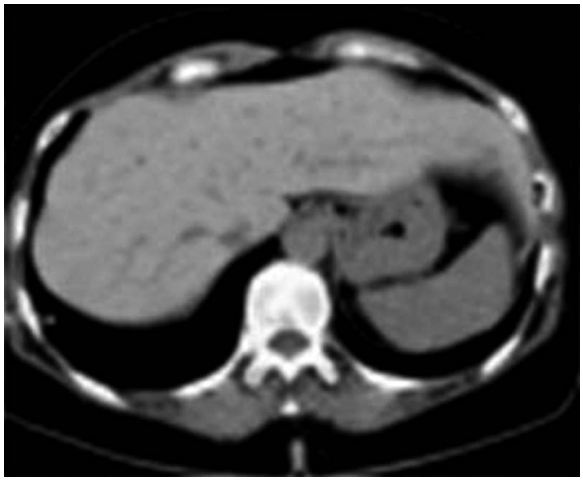

FIGURE 2.53: Axial plain CT shows hyperdense liver compared to spleen.

The causes of increased liver density are iron deposition, Wilson's disease, glycogen storage disease and drug deposition (Amiodarone).

The most common cause of increased liver attenuation is excessive iron deposition. Excessive iron in the liver can be from primary or secondary hemochromatosis. On CT, the liver is dense relative to the spleen, often greater than 25-30 HU on precontrast CT.

Type 1a glycogen storage disease (von Gierke's disease) can cause increases in hepatic parenchymal attenuation. Wilson's disease is said to increase the hepatic attenuation secondary to copper deposition.

Infiltrative Process

Metastatic disease: Metastatic disease can be diffuse and infiltrative. The entire liver can be involved, but diffuse metastatic disease is generally more geographic.

Lymphoma and sarcoidosis: Both lymphoma and sarcoidosis have similar appearances in both their diffuse and focal forms. There is usually hepatosplenomegaly and upper abdominal lymphadenopathy. The lymphadenopathy

with lymphoma is generally more bulky especially when the liver is involved. When focal, the nodules in sarcoidosis are smaller than in lymphoma. Both lymphoma and sarcoidosis can mimic the other granulomatous diseases like histoplasmosis and tuberculosis.

Cirrhosis

Cirrhosis is a pathological process in the liver associated with irreversible injury. The most common causes are alcohol-induced cirrhosis, hepatitis B and C. Pathologically necrosis, micro- and/or macronodular regeneration, bridging fibrosis and fatty change characterize the process of cirrhosis. The imaging changes generally reflect the pathological process occurring, usually a combination of the above changes. Early in cirrhosis, there is often no radiologic change seen.

The diagnosis of cirrhosis on CT are:

1. Nodular or mass-like contour
2. Relative atrophy of right lobe and hypertrophy of left and caudate lobes
3. Splenomegaly
4. Collateral vessels
5. Upper abdominal lymphadenopathy.

Primary Sclerosing Cholangitis

Primary sclerosing cholangitis (PCS) is an uncommon chronic cholestatic liver disease of unknown etiology. Cholangiocarcinoma develops in 9 to 15% of patients with PCS and carries a dismal prognosis.

The following combination of findings is suggestive of PCS at CT:

- Severe hypertrophy of the caudate lobe (pseudotumor)
- Marked resorption of the posterior segment of the right hepatic lobe
- Segmental dilatation of intrahepatic biliary radicals.

Primary Biliary Cirrhosis

Primary biliary cirrhosis (PBC) is an autoimmune disorder of unknown cause characterized by progressive destruction of the intrahepatic bile ducts. Ninety percent of affected patients are female, usually 40 to 60 years old. On CT, the appearance of diffuse hepatic hypertrophy with little atrophy and diffuse lace-like fibrosis is suggestive of the disease. The nodularity of the liver can be quite pronounced and occasionally mimic a neoplastic process.

Cirrhosis in Metabolic Disorders

Hemochromatosis

Idiopathic hemochromatosis is an autosomal recessive disorder of iron metabolism characterized by excessive accumulation of iron in the liver, heart, pancreas and pituitary gland. At CT, the liver parenchyma is of uniformly high density.

A similar appearance can be found in patients with iron overload resulting from multiple transfusions or amiodarone use.

Wilson's Disease

Wilson's disease is an uncommon autosomal recessive disorder of copper metabolism resulting in pathological accumulation of copper in many organs and tissues. A low plasma level of ceruloplasmin and increased hepatic copper content at liver biopsy confirm the diagnosis.

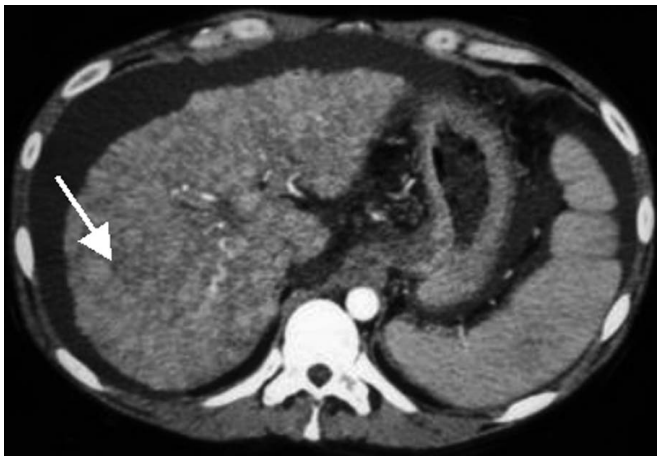

FIGURE 2.54: Axial CECT shows shrunken nodular liver with hyperdense nodules (arrow) in a patient on treatment for Wilson's disease. Note the associated ascites.

Multiple hyperdense nodules, due to the high copper content are characteristically seen on non-contrast CT. These nodules enhance minimally after contrast.

Post Sinusoidal Hepatic Disease

Budd-Chiari Syndrome

Budd-Chiari syndrome arises from obstruction to the hepatic venous outflow. Level of obstruction may be at the level intrahepatic venules, the hepatic veins or IVC that is, obstruction may be at any site from the efferent veins to the lobule to the inferior vena cava. Severe chronic venous congestion may lead to centrilobular fibrosis and cirrhosis. A variety of disease processes have been associated with this entity, including polycythemia vera, abnormality of coagulation factors such as antithrombin C deficiency, protein S and C deficiency, oral contraceptive use, paroxysmal nocturnal hemoglobinuria and membranous web in the inferior vena cava. The underlying etiology remains unknown in upto 25% of cases.

Obstruction to the hepatic venous outflow produces morphologic alteration of the liver and hepatic attenuation changes that can be recognized at CT.

- Hypertrophy of the caudate lobe. The caudate lobe has its own separate venous drainage into the inferior vena cava and usually maintains normal hepatic outflow.
- Heterogeneous enhancement of the liver parenchyma. This appearance is likely related to stagnation of portal venous flow in areas with poor venous drainage. Linear hypoattenuating areas predominantly distributed at the periphery are also common and may represent areas of fibrosis.
- The hepatic veins are poorly visualized or thrombosed.

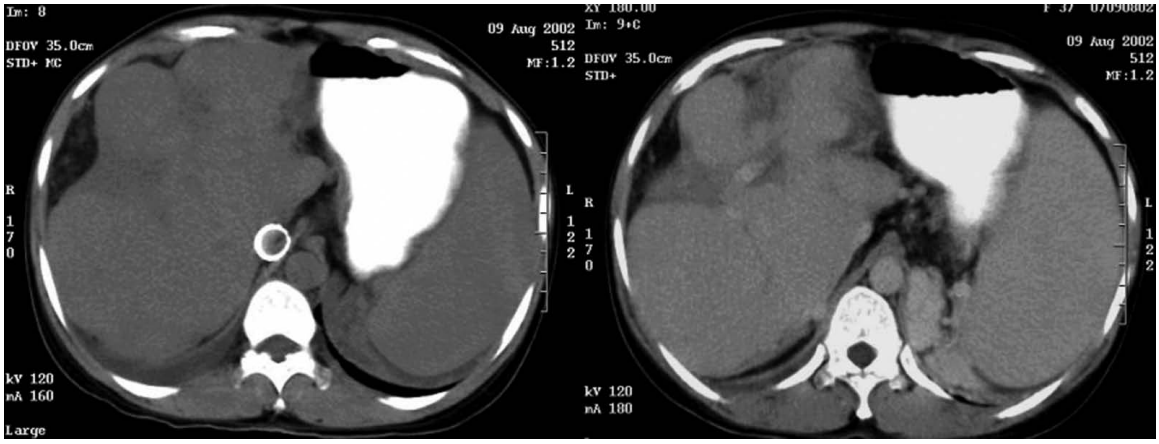

FIGURES 2.55A and B: Axial plain and CECT in a case of Budd-Chiari reveals nodular liver, note the filter in IVC.

- **Cardiac cirrhosis:** Cardiac cirrhosis produces changes on CT similar to Budd-Chiari syndrome and is usually related to severe and prolonged right sided heart failure or constrictive pericarditis. In these patients, however, the hepatic veins and the inferior vena cava are markedly dilated.

Cardiac Cirrhosis

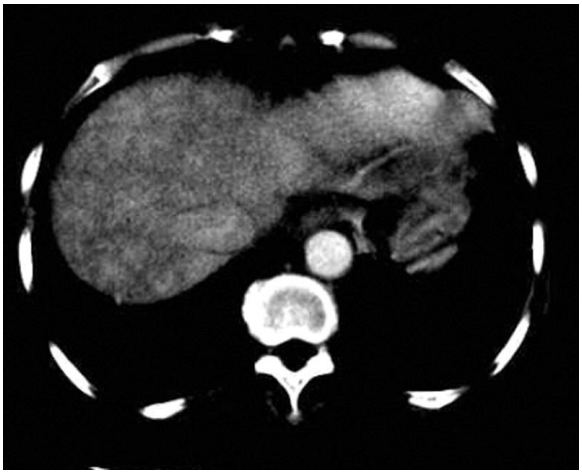

FIGURE 2.56: Axial CECT reveals heterogeneous parenchymal enhancement with nodularity in a case of chronic CCF. IVC appears dilated reflecting venous congestion.

Geographic Changes

Focal Fatty Metamorphosis

While fatty change can be diffuse, it can attain a focal, nodular or geographic shape. Rarely, it is indistinguishable from a focal mass. Recognition is based upon a high degree of suspicion, absence of mass effect and vessels coursing through the focal fat. Common sites for focal fatty change or focal sparing include:

1. Posterior aspect of segment 4 (medial segment) anterior to right portal vein.
2. Adjacent to the gallbladder fossa.
3. Adjacent to the falciform ligament, either in the lateral segment or more commonly in the medial segment.

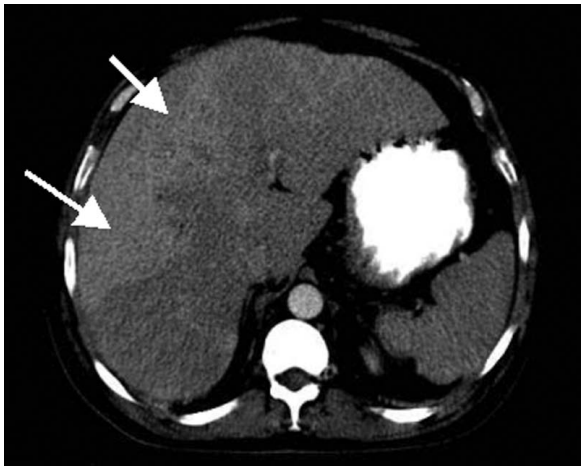

FIGURE 2.57: Axial CECT reveals fatty liver with geographical areas of normal attenuation (arrow).

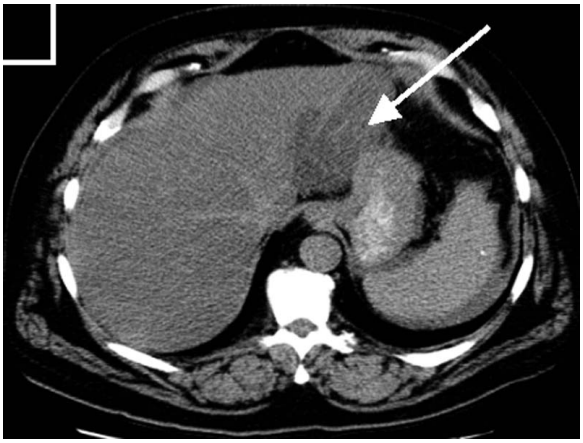

FIGURE 2.58: Axial CECT reveals focal fat infiltration in segment 4a (arrow).

Hepatic Infarction

Hepatic infarction is rare because the liver is supplied by both arterial and portal blood. Causes for infarction include prolonged profound hypotension and abrupt thrombosis, resection or embolization of the hepatic artery or a major branch. These are visualized as low density, wedged shaped areas in the liver. While typically wedge shaped and peripheral in appearance, infarcts of the liver can also be central and round.

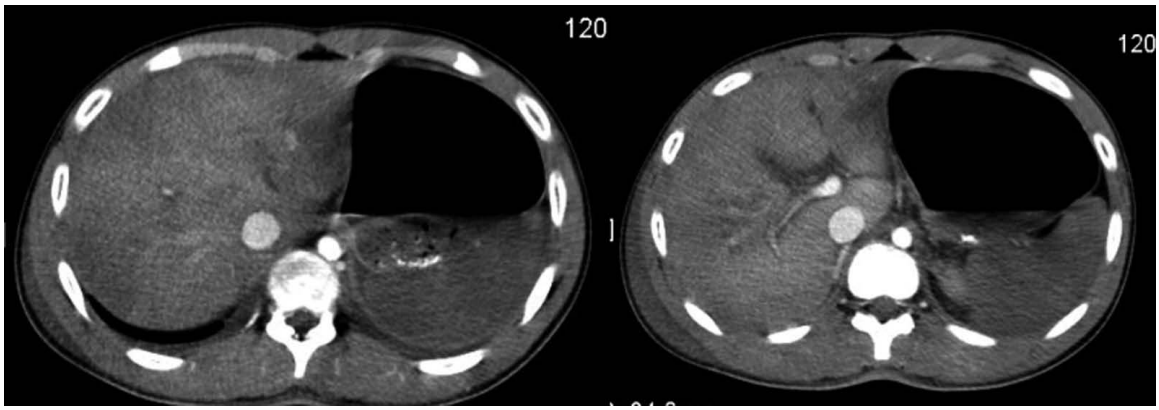

FIGURE 2.59A and B: Axial CECT reveals hypodense liver and spleen with enhancing adrenal, aorta is smaller than IVC - features suggestive of hypovolemia in a patient with shock due to multiple pelvic fractures.

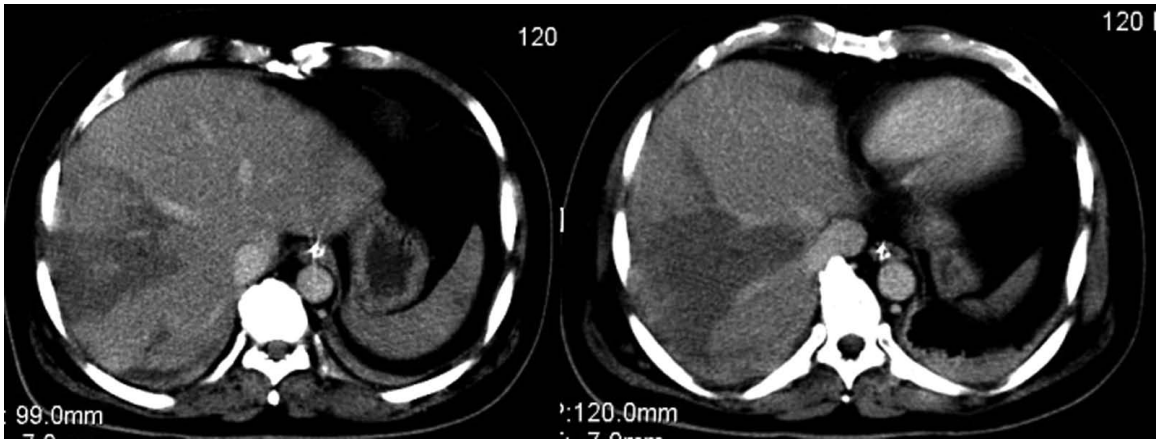

FIGURE 2.60A and B: Axial CECT in a patient with septicemia and shock reveals wedge shaped areas of hypodensity with preserved architecture – Imaging features are suggestive of perfusion defects.

Metastatic Disease and Pseudo-cirrhosis

Diffuse, focal but near-confluent metastatic disease is an unusual pattern of neoplastic involvement of the liver. Breast carcinoma is the most common primary neoplasm to present with this appearance, but melanoma and neuroendocrine tumors can also have this appearance. This pattern can be recognized with the following findings:

- Enlarged liver with a nodular contour
- No alteration in size of lobes unlike cirrhosis
- Attenuated hepatic vessels, especially the hepatic veins.

Lymphoma

Diffuse hepatic lymphoma when present is almost never recognized radiographically. When the liver is involved with non-Hodgkin's and Hodgkin's disease, it is usually diffuse or infiltrative. The liver may be enlarged and may have a nodular contour as with diffuse metastatic disease. Vessels are attenuated especially the hepatic veins.

Discussion on Specific Pathological Processes

Hepatic Cirrhosis

Hepatic cirrhosis is characterized pathologically by a progressive replacement of the normal liver parenchyma by fibrosis and regenerating nodules. Although the liver may appear normal in the early stage of the disease and in up to 25% of patients with end stage disease, the distortion of the hepatic parenchyma caused by established cirrhosis generally produces alterations in hepatic morphology that are easily recognized on CT.

Classification

Micronodular: < 3 mm nodules (upto 1 cm) also called Laennec's cirrhosis.
Macronodular: > 3 mm nodules (upto 5 cm) also called postnecrotic cirrhosis.
Mixed micro and macronodular cirrhosis.

Etiology

- Alcohol
- Infectious hepatitis
- Primary biliary cirrhosis
- Nutritional cirrhosis
- Hemochromatosis
- Wilson's disease
- Congestive cirrhosis
- Cryptogenic cirrhosis
- Indian childhood cirrhosis.

CT Findings

- **The liver surface** is irregular, with fine nodules reflecting micronodular cirrhosis and larger nodules reflecting macronodular cirrhosis.
- **The shape of the liver** is altered. The liver may be small and shrunken or display a combination of segmental atrophy and hypertrophy. There is atrophy of right lobe (seg 5-8) and medial segment of left lobe (4a, 4b). Hypertrophy of lateral segment of left lobe (2, 3) and caudate lobe.
- Caudate to right lobe ratio greater than 65 is specific for cirrhosis. Normal is 37.

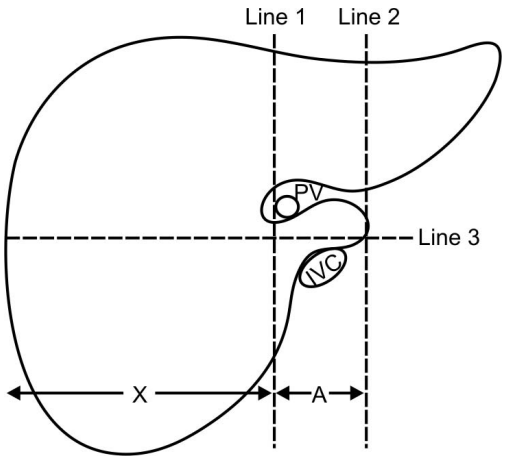

FIGURE 2.61: Caudate lobe/right lobe ratio.

Caudate lobe is measured from its most medial aspect to the right lateral wall of the main portal vein, just caudal to its bifurcation. The right lobe is measured from the same portion of the main portal vein to the right lateral margin of the liver.

- **The hepatic parenchyma** displays heterogeneous attenuation and inhomogeneous enhancement. This heterogeneity is most pronounced on unenhanced scans and is caused by fatty infiltration, focal fibrosis and intraparenchymal iron deposition.

Regenerative nodules are seen as tiny hypoattenuating areas less than 1 cm compactly placed in the entire liver. Hyperattenuating regenerative nodules may be seen due to iron deposition within the nodules.

Dysplastic nodules should be suspected when a dominant nodule is seen in the company of smaller nodules. It has been shown as a grade of malignancy increases hepatic arterial flow to nodular lesions tend to increase and the portal venous supply tend to decrease.

Early HCC's are seen as iso-attenuating on all phases of CT. As early HCC is usually hypovascular. Advanced HCC's appear hypervascular in arterial phase.

Features of portal hypertension, ascites, splenomegaly, enlarged porto-splenic axis and presence of portosystemic shunts.

- **Prominent hepatic fissures, prominent gallbladder fossa.**
- **Alteration in the gallbladder IVC axis.**

Stages of Cirrhosis

Stage I: Portal pressure is only slightly elevated. Portal and hepatic arterial flow are hepatopetal. Portosystemic collaterals are absent.

Stage II: Diversion of portal flow into portosystemic collaterals.

Stage III: End stage. Characterized by portal flow reversal with only the hepatic artery supplying the liver.

Micronodular Cirrhosis

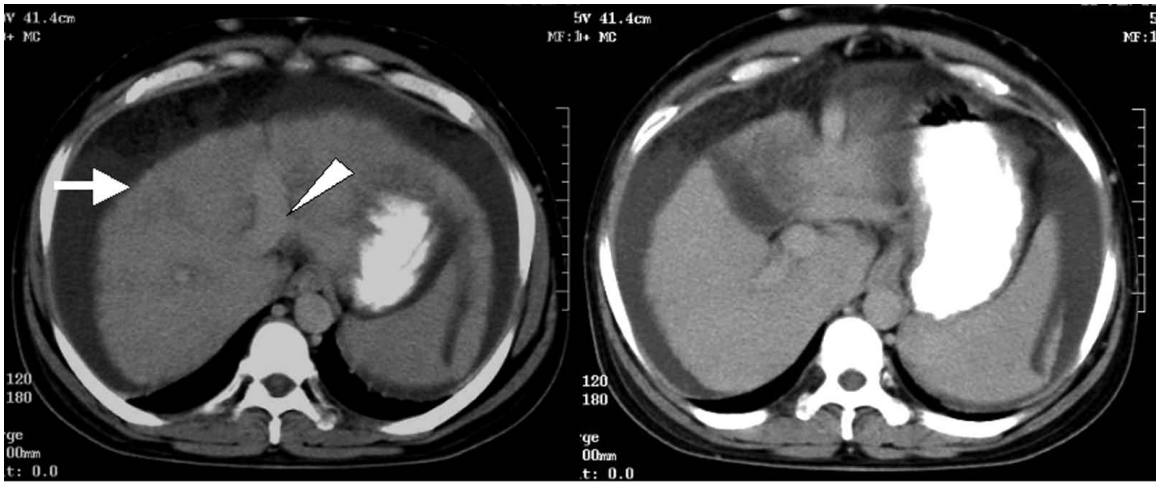

FIGURES 2.62A and B: Axial CECT shows shrunken liver with irregular nodular margins (arrow) with ascites. Note the prominent left segmental portal veins in Figure A (arrowhead).

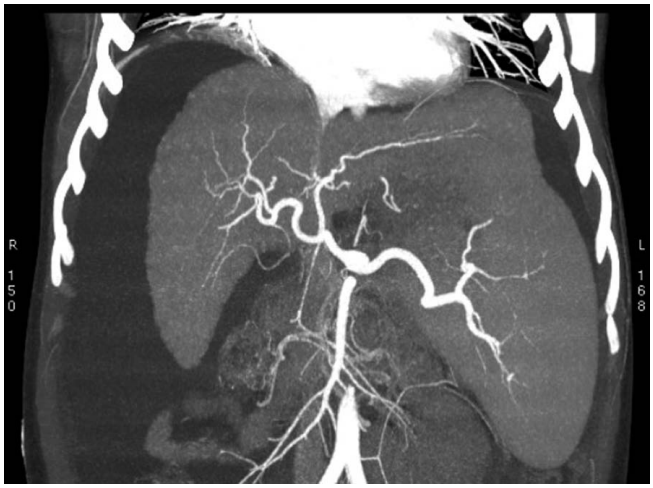

FIGURE 2.62C: Coronal MIP in a young boy with idiopathic cirrhosis showing the typical shrunken nodular liver with enlarged spleen.

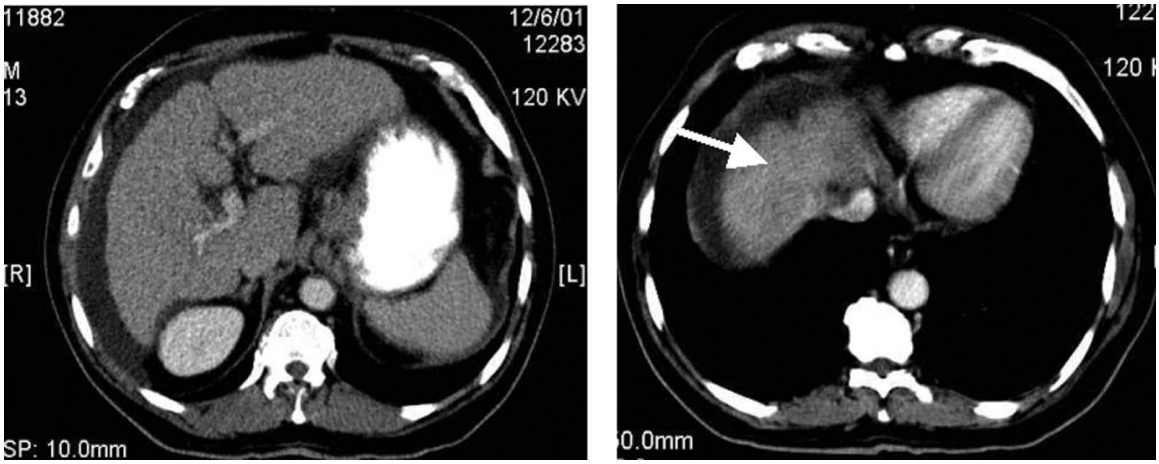

FIGURES 2.63A and B: Axial CECT showing shrunken liver with nodular margins (arrow).

Redistributed Lobar Volumes

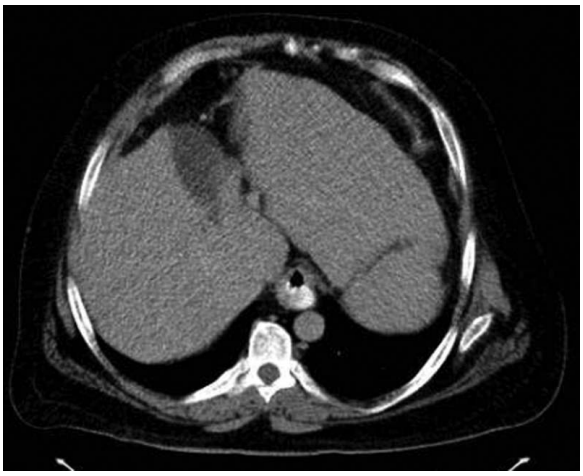

FIGURE 2.64: Axial NECT reveals shrunken right lobe with hypertrophy of left lobe.

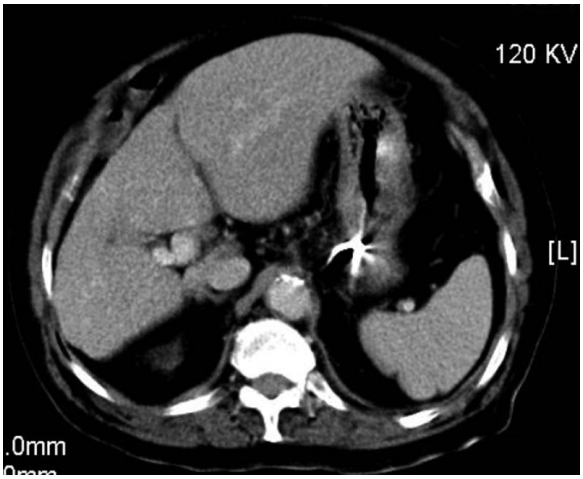

FIGURE 2.65: Axial CECT reveals hypertrophy of left lobe liver.

Lobar Hypertrophy

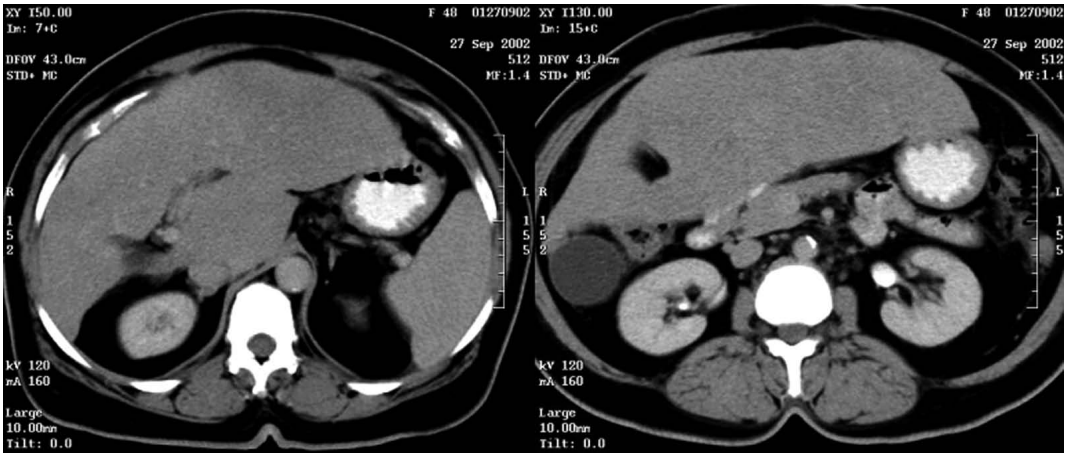

FIGURES 2.66A and B: Axial CECT reveals atrophy of the right lobe with lobar hypertrophy of the left lobe and caudate lobe.

Macronodular Cirrhosis

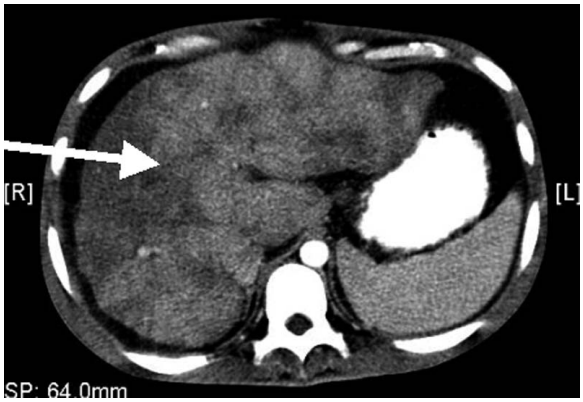

FIGURE 2.67: Axial CECT reveals shrunken liver with macronodules (arrow).

Expanded GB Fossae

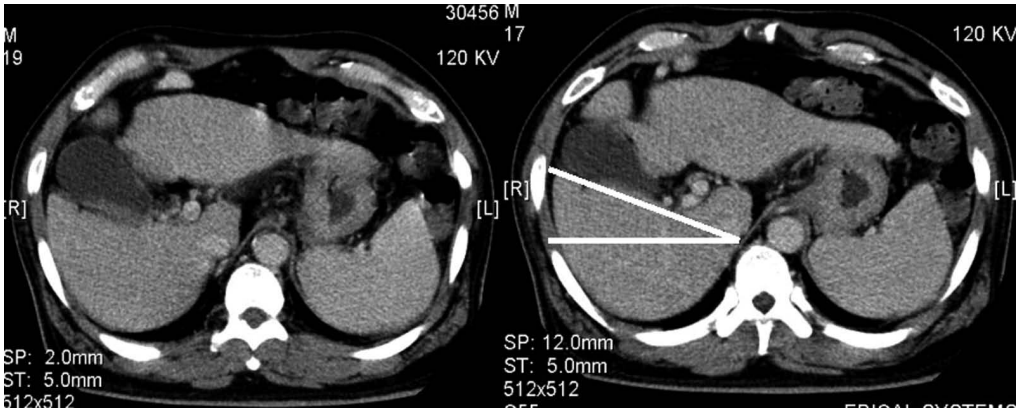

FIGURES 2.68A and B: Shrunken liver alteration in the axis of gallbladder. The GB and interlobar fissure also undergo counterclockwise rotation in patients with cirrhotic liver morphology. This alteration can be quantitated by measuring the GB angle. This angle is determined by drawing a line through the interlobar fissure, GB neck and /or medial aspect of the anterior segment of right hepatic lobe and IVC. Another line is drawn coronally through the IVC parallel to the patients back (B)

In normal patients the angle is 46 degrees, but in cirrhotics it is reduced to 35 degrees.

Portosystemic Collaterals

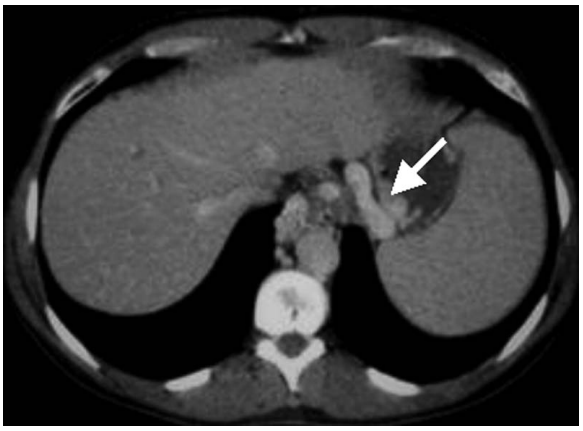

FIGURE 2.69: CECT axial CT reveals shrunken liver with multiple GO junction varices (arrow).

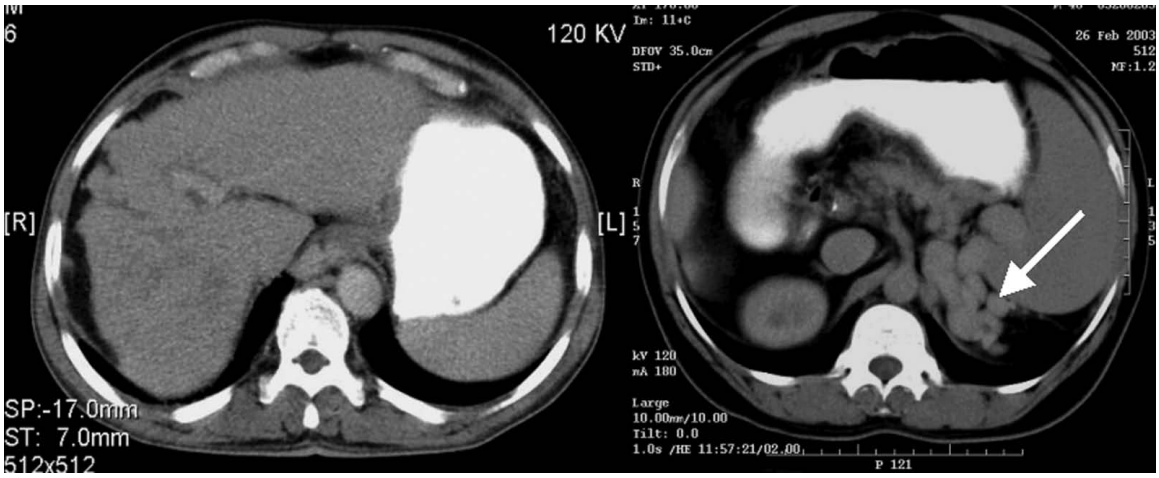

FIGURES 2.70A and B: Axial CECT reveals shrunken nodular liver with splenic hilar and splenorenal collaterals (arrow in B).

Nodular Lesions in Cirrhosis

1. **Regenerative nodule**—Localized proliferation of hepatocytes and their supporting stroma. Regenerative nodules are not easily demonstrated at CT but may usually be detected as tiny hyperattenuating nodules on nonenhanced scans if the nodules have undergone iron deposition or are surrounded by fibrotic stroma. They become isoattenuating to the liver on portal venous phase images.
2. **Cirrhotic nodule**—Regenerative nodule completely surrounded by fibrosis.
3. **Dysplastic nodule**—Cluster of hepatocytes less than 1 mm with evidence of histological dysplasia.
4. **HCC**—When HCC is encountered in a noncirrhotic patient, it is usually a solitary, large, heterogeneous mass that is hypoattenuating to the liver on nonenhanced and portal venous phase images and heterogeneously hyperattenuating on arterial phase images. The large (multiacinar) regenerative nodules are typically small (0.5-4 cm), multiple, homogeneously enhancing lesions that are brightly hyperattenuating on hepatic arterial phase images and slightly hyperattenuating on portal venous phase images.

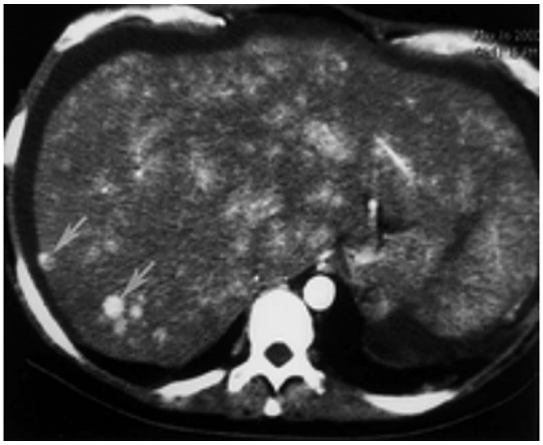

FIGURE 2.71: Axial CECT reveals multiple dysplastic nodules (arrow).

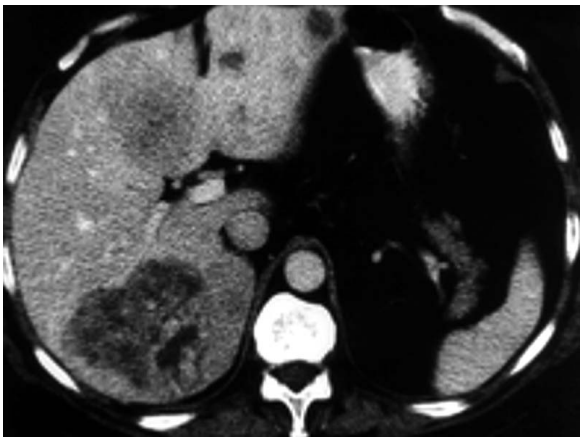

FIGURE 2.72: Axial CECT reveals multiple heterogeneously enhancing lesions in both lobes of liver—suggestive of multicentric hepatoma.

- Regenerative or hyperplastic nodules
  - Monoacinar regenerative nodules
    - Diffuse nodular hyperplasia (with fibrosis)
    - Nodular regenerative hyperplasia
  - Multiacinar regenerative nodules
    - Large regenerative nodule (if > 0.5 cm)
  - Lobar or segmental hyperplasia
  - Cirrhotic nodule
  - Focal nodular hyperplasia
- Dysplastic or neoplastic lesions
  - Hepatocellular adenoma
  - Dysplastic nodule
  - Hepatocellular carcinoma

Portal Hypertension

Definition: Portal vein pressure more than 12 mmHg or 30 cm of water.

Types: Hyperkinetic (increased flow through portal vein)
Obstructive (increased resistance to blood flow)

Etiology:

I. Hyperkinetic: Arterioportal fistula
II. Increased portal venous resistance:
  A. Intrahepatic:
    1. Presinusoidal—hepatic schistosomiasis, congenital hepatic fibrosis, sarcoidosis, lymphoma.
    2. Postsinusoidal—hepatic cirrhosis, veno occlusive disease.
  B. Extrahepatic –
    1. Prehepatic: Portal vein occlusion or thrombosis—congenital absence of portal vein, inflammatory process-omphalitis, acute/chronic pancreatitis, ulcerative colitis, tumors- pancreatic, Ca stomach, HCC dehydration, oral contraceptive pills, hypercoagulable states.
    2. Posthepatic: Hepatic venous outflow obstruction.

Collateral Pathways in Portal Hypertension

Cirrhosis causes obstruction to the splanchnic blood flow. As a result, portal venous blood is diverted away from the liver and flows from a high pressure portal venous system into a low pressure systemic venous system via a variety of porto-systemic collateral pathways. Venous collateral develop to the portal venous bed.

Portohepatic collaterals develop in cases of prehepatic portal hypertension (portal/splenic vein thrombosis) these collaterals are hepatopetal and conduct blood to liver bypassing the obstruction and drain into the intrahepatic venous radicles. Collaterals in case of portal vein occlusion include periportal collaterals like cavernoma and gallbladder bed collaterals.

Collaterals in case of splenic vein thrombus include short gastric veins, peripancreatic and gastroepiploic collaterals.

Portosystemic collaterals develop due to any cause of portal hypertension (pre, post and hepatic causes). They are hepato fugal and conduct blood to IVC or SVC.

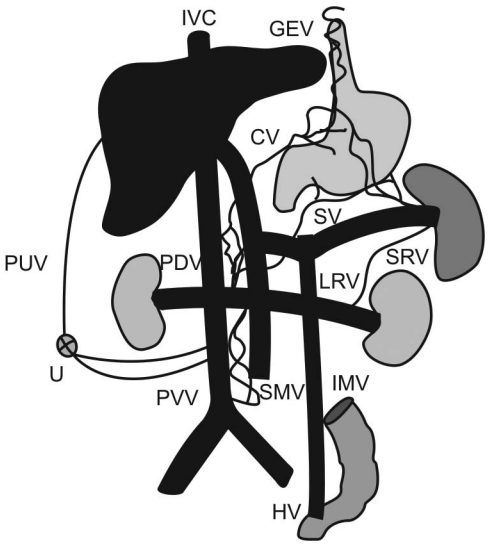

FIGURE 2.73: Schematic showing collateral pathways in portal hypertension.

Collaterals draining into SVC territory include coronary veins and short gastric veins. Collaterals draining into IVC territory include paraumbilical and splenorenal, splenoretroperitoneal, mesenteric and peripancreatic collaterals.

Portosystemic collaterals are of two types they are developed and tributary collaterals. Developed collaterals are those which arise from preexisting vessels that normally do not function as collaterals and do not function as tributaries of portal vein, these are paraumbilical, splenorenal and splenoretroperitoneal veins.

Tributary collaterals arise from the tributaries of the portal venous system these are coronary veins, short gastric veins superior and inferior mesenteric veins. They reach the systemic veins by the azygous and hemiazygous veins.

Four major pathways of porto-systemic collateralization are well demonstrated on CT.

- The coronary or short gastric vein divert portal blood through esophageal, paraesophageal and gastric varices into the azygous system and the inferior vena cava. Gastroesophageal varices are the most common source of severe bleeding in the cirrhotic patient. Coronary vein dimension of more than 7 mm correlates well with severe portal hypertension.
- The paraumbilical vein carries blood from the left portal vein towards superficial veins of the anterior abdominal wall and may produce the classic "caput medusae" appearance on physical examination.
- Spontaneous splenorenal shunts drain blood from splenic varices into the left renal vein at the leval of the left renal hilum. Like paraumbilical collaterals, these are desirable routes of decompression of the portal system as they are not associated with gastrointestinal bleeding.
- The superior hemorrhoidal vein carry portal blood into the systemic veins through rectal and hemorrhoidal varices and may be a source of rectal bleeding.
- Retroperitoneal GI tract veins anastomose with renal, lumbar and phrenic veins.

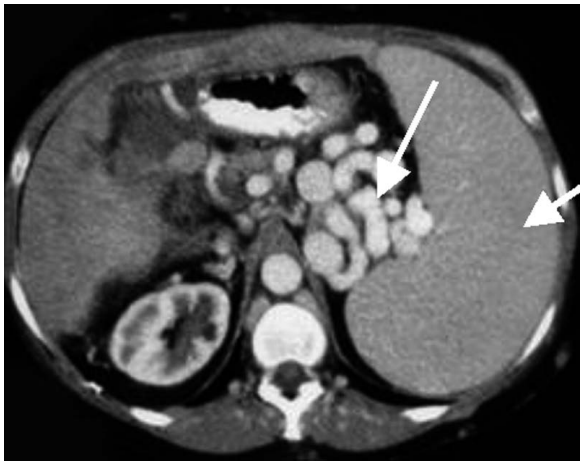

FIGURE 2.74: Axial CECT reveals splenomegaly with multiple splenic hilar collaterals.

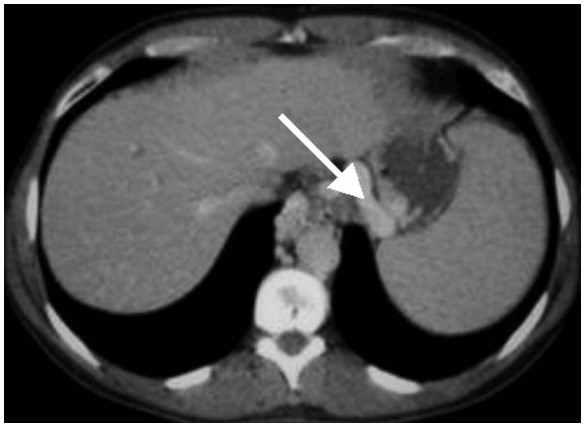

FIGURE 2.75: Axial CECT in a case of cirrhosis reveals nodular enhancing venous collaterals in the GI junction and gastric fundus.

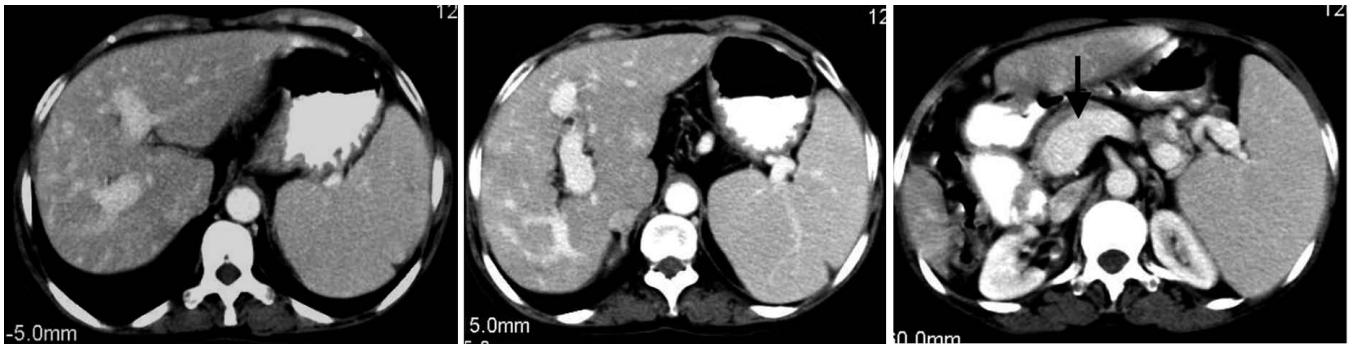

FIGURES 2.76A to C: Axial CECT reveals splenomegaly, main portal vein (arrow) and segmental portal veins are enlarged.

Portal Venous Occlusion

Portal vein can be affected in a number of neoplastic or inflammatory disease, they usually reflect pathological process in the liver, spleen, pancreas, or the gut.

Absence of enhancement of the portal veins on the PVP is diagnostic. In chronic PVT, the main portal vein may become fibrotic and obliterated and replaced by multiple serpiginous collateral channels, the so called "cavernous transformation" of the portal vein.

The prevalence of PVT complicating cirrhosis is relatively low and should raise suspicion for the presence of an underlying hepatocellular carcinoma.

CT Appearances of Thrombosed Veins

Thrombi are readily identified on CECT as low attenuation intraluminal filling defect.

When segmental occlusions occur local collateral pathways take over:

1. Cavernomatous transformation – in response to thrombosis of main portal vein
2. Perigastric collateral in response to splenic vein thrombosis.

If vessels larger than 6 mm are present in the gastrohepatic ligament varices are present similarly vessels greater than 4 mm in the perisplenic area is considered as a collateral.

Diseases Causing Segmental Occlusion of the Portal Vein

Intrahepatic and main portal vein occlusions are usually caused by HCC, metastatic disease and Budd-Chiari syndrome. Pancreatitis, pancreatic Ca, splenectomy are causes for splenic vein thrombosis.

CT Diagnosis of Malignant Thrombosis of the Portal Vein

Hepatocellular carcinoma has a propensity to invade the portal vein or its branches. Differentiation between bland and tumor thrombus is best achieved by evaluating the pattern of enhancement of the thrombus in the HAP. Early enhancement of the hypervascular tumor thrombus or the presence of multiple small vessels giving a striated appearance to the thrombus are highly suggestive of malignant thrombus.

Signs of Malignant Thrombi

Rail sign—abnormal enhancement at the margin of thrombus.

Thread and streak sign—linear enhancement within the thrombus.

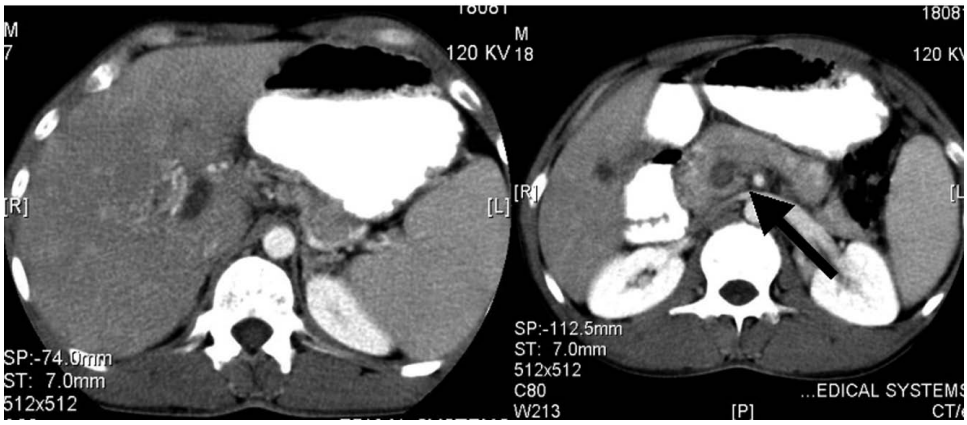

FIGURES 2.77A and B: Axial CECT showing nonenhancing acute portal vein thrombus.

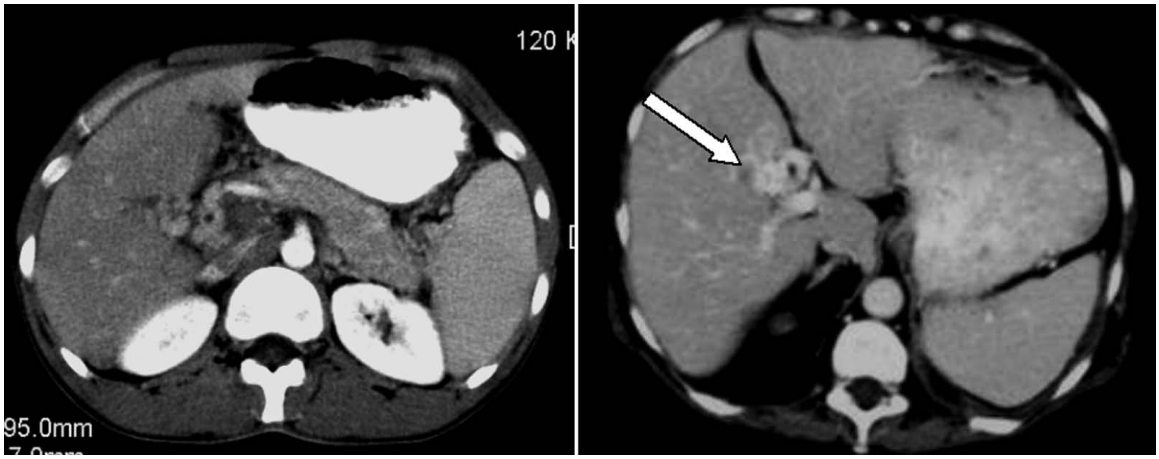

FIGURES 2.78A and B: Axial CECT reveals hypodense nonenhancing filling defect in the portal confluence with conglomerate nodular enhancing vessels in the porta (arrow).

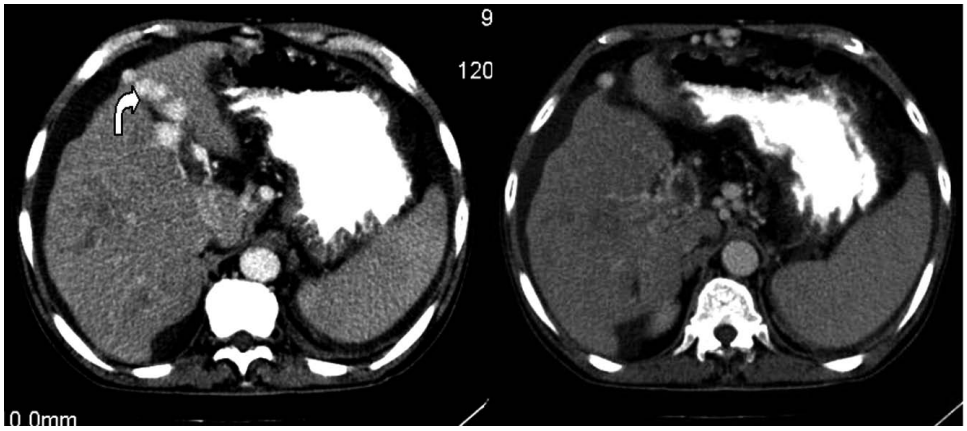

FIGURES 2.79A and B: Axial CECT reveals shrunken liver portal vein at porta and left segmental vein shows thrombus (arrow in B), linear enhancing structure (arrow in A) seen is the recanalized umbilical vein.

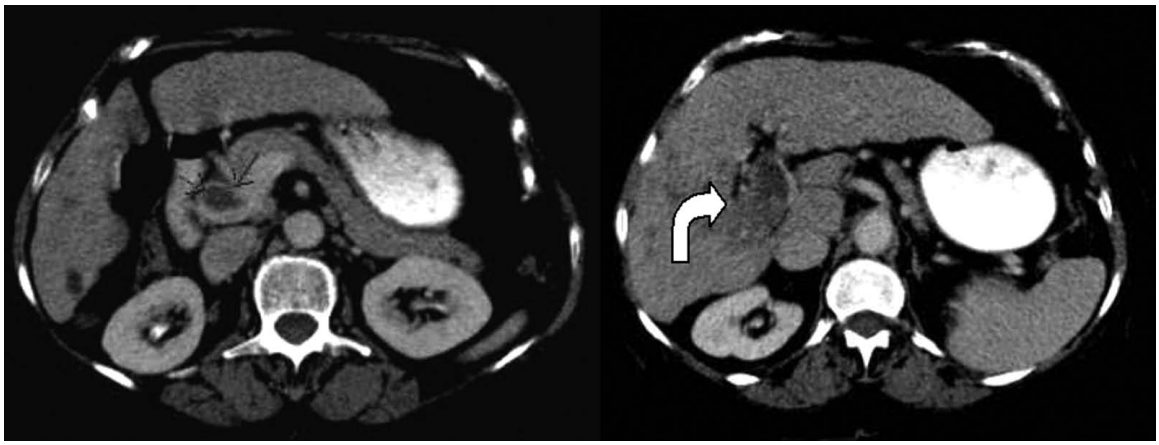

FIGURES 2.80A and B: Axial CECT reveals shrunken liver, portal vein at porta and left segmental vein shows thrombus (arrow in B).

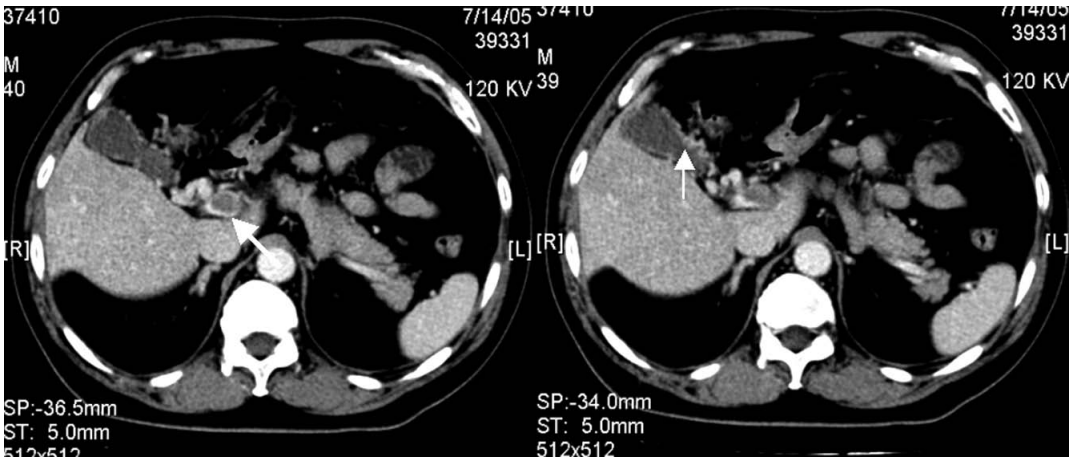

FIGURES 2.81A and B: Axial CECT showing partially recanalized portal vein thrombus (arrow in A), with multiple pericholecystic collaterals (arrow in B).

Malignant Thrombus

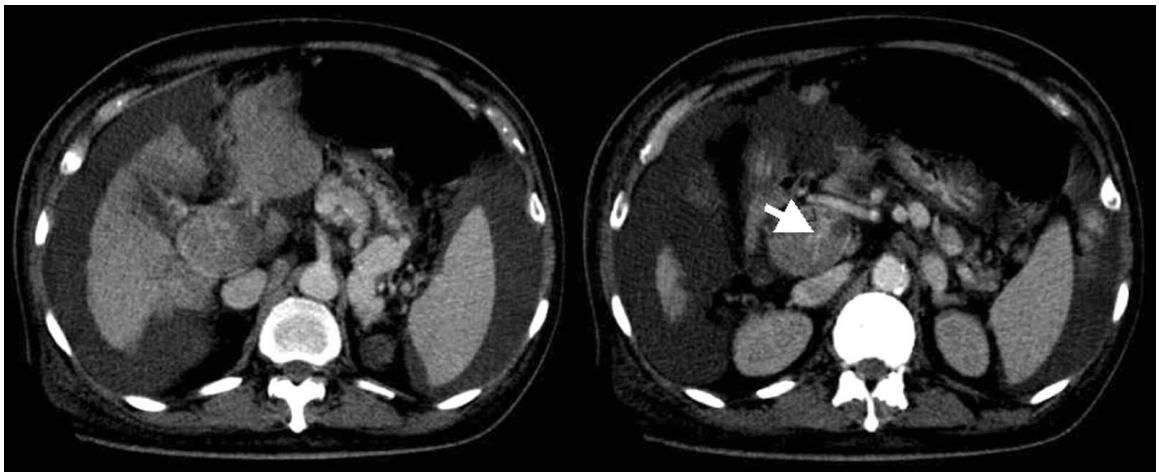

FIGURES 2.82A and B: Axial CECT in a case of cirrhosis with a infiltrative HCC reveals a thrombus in the main portal vein showing streaky areas of enhancement (arrow in B) suggestive of a tumor thrombus.

Miscellaneous Conditions-Cystic Lesions of Liver

Cystic lesions of the liver in the adult can be classified as developmental, neoplastic, inflammatory, or miscellaneous. Although in some cases it is difficult to distinguish these entities with imaging criteria alone, certain cystic focal liver lesions have classic computed tomographic (CT) and magnetic resonance (MR) imaging features, which are important for the radiologist to understand and recognize. Lesions with such features include simple (bile duct) cyst, autosomal dominant polycystic liver disease, biliary hamartoma, Caroli disease, undifferentiated (embryonal) sarcoma, biliary cystadenoma and cystadenocarcinoma, cystic subtypes of primary liver neoplasms, cystic metastases, pyogenic and amebic abscesses, intrahepatic hydatid cyst, extrapancreatic pseudocyst, and intrahepatic hematoma and biloma. Specific CT and MR imaging findings that are important to recognize are the size of the lesion; the presence and thickness of a wall; the presence of septa, calcifications, or internal nodules; the enhancement pattern; the MR cholangiographic appearance; and the signal intensity spectrum. In addition, access to critical clinical information remains extremely important. The most important clinical parameters defined include age and gender, clinical history, and symptoms.

Developmental Lesion

Hepatic (Bile Duct) Cyst

Simple hepatic cysts are benign developmental lesions that do not communicate with the biliary tree. The current theory regarding the origin of true hepatic cysts is that they originate from hamartomatous tissue. Hepatic cysts are common and are presumed to be present in 2. 5% of the population. They are more often discovered in women and are almost always asymptomatic. Simple hepatic cysts can be solitary or multiple, with the latter being the more typical scenario. At histopathologic analysis, true hepatic cysts contain serous fluid and are lined by a nearly imperceptible wall consisting of cuboidal epithelium, identical to that of bile ducts, and a thin underlying rim of fibrous stroma.

A hepatic cyst appears as a homogeneous and hypoattenuating lesion on nonenhanced CT scans, with no enhancement of its wall or content after intravenous administration of contrast material.

Polycystic Liver Disease

Hepatic cysts can also be part of polycystic liver disease, an autosomal dominant disorder often found in association with renal polycystic disease. Although hepatic cysts are found in 40% of cases of autosomal dominant polycystic disease involving the kidneys, they may be seen without identifiable renal involvement at radiography. Usually, patients with autosomal dominant polycystic liver disease are asymptomatic and liver dysfunction occurs only sporadically. However, advanced disease can result in hepatomegaly, liver failure, or Budd-Chiari syndrome. In these more severe cases, percutaneous interventional alcohol ablation has been useful as an alternative to partial liver resection or even transplantation.

Polycystic liver disease typically appears as multiple homogeneous and hypoattenuating cystic lesions with a regular outline on nonenhanced CT scans, with no wall or content enhancement on contrast-enhanced images.

Bile Duct Hamartoma

Bile duct hamartomas, also called von Meyenburg complexes, originate from embryonic bile ducts that fail to involute. They are generally without clinical manifestations and are usually encountered as an incidental finding at imaging, laparotomy, or autopsy. At pathologic analysis, they appear as grayish-white nodular lesions 0.1-1.5 cm in diameter that do not communicate with the biliary tree and are scattered throughout the liver parenchyma.

Nonenhanced CT has shown multiple hypoattenuating, cyst like hepatic nodules occurring throughout both lobes of the liver and typically measuring less than 1.5 cm in diameter. The latter feature is the most essential one in the differential diagnosis from multiple simple cysts. Furthermore, simple cysts are typically regularly outlined, whereas bile duct hamartomas have a more irregular outline. Bile duct hamartomas do not exhibit a characteristic pattern of enhancement after intravenous administration of iodinated contrast material.

Caroli Disease

Caroli disease, also known as congenital communicating cavernous ectasia of the biliary tract, is a rare, autosomal recessive developmental abnormality characterized by saccular dilatation of the intrahepatic bile ducts, multiple intrahepatic calculi, and associated cystic renal disease. Two forms of Caroli disease have been described: a less common pure form (type 1) and a more complex form (type 2), which is associated with other ductal plate abnormalities, such as hepatic fibrosis. The abnormality may be segmental or diffuse. Clinical symptoms are usually restricted to recurrent attacks of right upper quadrant pain, fever, and, more rarely, jaundice. The prevalence of cholangiocarcinoma is higher in patients with this disease than in the general population.

CT typically shows hypoattenuating dilated cystic structures of varying size that communicate with the biliary tree. The presence of tiny dots with strong contrast enhancement within the dilated intrahepatic bile ducts (the "central dot" sign) is considered very suggestive of Caroli disease. At histopathologic analysis, these intraluminal dots correspond to intraluminal portal vein radicals.

Neoplastic Lesions

Undifferentiated Embryonal Sarcoma

Undifferentiated embryonal sarcoma is a rare malignant hepatic tumor that occurs predominantly in older children and adolescents (mean age, 12 years), although it can occur in young adults as well.

At cross-sectional imaging, the tumor typically appears as a large (10-25 cm-diameter), solitary, predominantly cystic mass with well-defined borders; occasionally, a pseudocapsule separates the mass from normal liver tissue. Internal calcifications have been reported sporadically. Although undifferentiated embryonal sarcoma appears predominantly solid at gross examination (83% of cases), CT usually demonstrates a discordant cystic appearance

due to the high water content of the myxoid stroma, which is typical of undifferentiated embryonal sarcoma. Intratumoral hemorrhage may be not on contrast-enhanced CT heterogeneous enhancement is present in the solid, usually peripheral portions of the mass, especially on delayed images.

Biliary Cystadenoma and Cystadenocarcinoma

Biliary cystadenomas are rare, usually slow growing, multilocular cystic tumors that represent less than 5% of intrahepatic cystic masses of biliary origin. Although they are generally intrahepatic (85%), extrahepatic lesions have been reported. Among intrahepatic cystadenomas, 55% occur in the right lobe, 29% occur in the left lobe, and 16% occur in both lobes. Biliary cystadenomas range in diameter from 1. 5 to 35 cm. They occur predominantly in middle-aged women (mean age, 38 years) and are considered premalignant lesions. Symptoms are usually related to the mass effect of the lesion and consist of intermittent pain or biliary obstruction. At microscopy, a single layer of mucin-secreting cells lines the cyst wall. The fluid within the tumor can be proteinaceous, mucinous, and occasionally gelatinous, purulent, or hemorrhagic due to trauma.

At CT, a biliary cystadenoma appears as a solitary cystic mass with a well-defined thick fibrous capsule, mural nodules, internal septa, and rarely capsular calcification. Polypoid, pedunculated excrescences are seen more commonly in biliary cystadenocarcinoma than in cystadenoma, although papillary areas and polypoid projections have been reported in cystadenomas without frank malignancy.

Cystic Subtypes of Primary Liver Neoplasms

Cystic subtypes of primary liver neoplasms are rare and are usually related to internal necrosis following disproportionate growth or systemic and locoregional treatment. Hepatocellular carcinoma and giant cavernous hemangioma are the two most common primary neoplasms of the liver that rarely manifest as an entirely or partially cystic mass.

Cystic Metastases

Metastases to the liver are common, and a variety of often nonspecific appearances have been reported. Most hepatic metastases are solid, but some have a complete or partially cystic appearance. In general, two different pathologic mechanisms can explain the cyst like appearance of hepatic metastases. First, hypervascular metastatic tumors with rapid growth may lead to necrosis and cystic degeneration. This mechanism is frequently demonstrated in metastases from neuroendocrine tumors, sarcoma, melanoma, and certain subtypes of lung and breast carcinoma. Contrast-enhanced CT and MR imaging typically demonstrate multiple lesions with strong enhancement of the peripheral viable and irregularly defined tissue. Second, cystic metastases may also be seen with mucinous adenocarcinomas, such as colorectal or ovarian carcinoma. Ovarian metastases commonly spread by means of peritoneal seeding rather than hematogenously. Therefore, they appear on cross-sectional images as cystic serosal implants on both the visceral peritoneal surface of the liver and the parietal peritoneum of the diaphragm. This appearance is in contradistinction to that of most other cystic hepatic lesions, which are intraparenchymal.

Abscess

Abscesses can be classified as pyogenic, amebic, or fungal. Pyogenic hepatic abscesses are most commonly caused by *Clostridium* species and gram-negative bacteria, such as *Escherichia coli* and *Bacteroides* species, which enter the liver via the portal venous system or biliary tree. Ascending cholangitis and portal phlebitis are the most frequent causes of pyogenic hepatic abscesses. An amebic abscess results from infection with the protozoan *Entamoeba histolytica* and is the most commonly encountered hepatic abscess on a worldwide basis. Fungal abscesses are most

often caused by *Candida albicans*. Clinical symptoms of abscesses are related to the coexistence of sepsis and the presence of one or more space-occupying lesions.

In general, the presence of air within a lesion, although uncommon, is diagnostic of a gas-forming organism if there is no history of instrumentation or rupture into a hollow viscus. Air is easily recognizable at CT by measuring the Hounsfield units (range, -1, 000 to -100 HU). At MR imaging, air appears as a signal void and is therefore more difficult to differentiate from calcifications. However, the shape and location (air-fluid level) should enable correct diagnosis. The overall appearance of a hepatic abscess at cross-sectional imaging varies according to the pathologic stage of the infection. Abscesses have a unilocular cystic appearance in subacute stages, in which necrosis and liquefaction predominate. In more acute stages, abscesses frequently manifest as a cluster of small low-attenuation or high-signal-intensity lesions, which represent different locations of contamination. This coalescent, grouped appearance is especially suggestive of pyogenic infection.

Abscesses usually appear as thick-walled lesions with homogeneous low attenuation at CT. In addition to the enhancing abscess wall, contrast-enhanced CT typically show increased peripheral rim enhancement, which is secondary to increased capillary permeability in the surrounding liver parenchyma (the "double target" sign).

Intrahepatic Hydatid Cyst

Hepatic echinococcus is an endemic disease in the Mediterranean basin and other sheep-raising countries. Humans become infected by ingestion of eggs of the tapeworm *Echinococcus granulosus*, either by eating contaminated food or from contact with dogs. The ingested embryos invade the intestinal mucosal wall and proceed to the liver by entering the portal venous system. Although the liver filters most of these embryos, those that are not destroyed then become hepatic hydatid cysts.

At CT, a hydatid cyst usually appears as a well-defined hypoattenuating lesion with a distinguishable wall. Coarse calcifications of the wall are present in 50% of cases, and daughter cysts are identified in approximately 75% of patients. MR imaging clearly demonstrates the pericyst, the matrix, and daughter cysts.

Hepatic Extrapancreatic Pseudocyst

Although pancreatic pseudocysts can form anywhere in the abdomen, intrahepatic occurrence is rare. They occur predominantly in the left lobe of the liver as a result of extension of fluid from the lesser sac into the leaves of the hepatogastric ligament. Clinical symptoms are usually related to the underlying inflammatory pancreatic disease. Elevated serum and urinary amylase levels should arouse suspicion for this condition.

Correct diagnosis is not difficult with imaging when other signs of acute pancreatitis are present. At CT, a mature intrahepatic pseudocyst appears as a well-defined, subcapsular, homogeneous, hypoattenuating mass surrounded by a thin fibrous capsule. In more acute settings, the attenuation of the fluid within the cyst may be higher due to hemorrhage and necrotic debris, and the lesion may be less distinctly defined.

Hematoma

Surgery and trauma are the two most common causes of hepatic bleeding. Hemorrhage within a solid liver neoplasm, especially a hepatocellular adenoma, is a third well-known mechanism by which intra- or perihepatic hematoma can be induced. Symptomatic manifestations depend on the severity of the bleeding, the location, and the time frame during which the hemorrhage occurred.

At CT, the appearance of an intrahepatic hemorrhage depends on the cause of the bleeding and the lag time between the traumatic event and the imaging procedure. In an acute or subacute setting, hemorrhage has a higher

attenuation value than pure fluid due to the presence of aggregated fibrin components. In chronic cases, a hematoma has attenuation identical to that of pure fluid. Frequently, the cause of the hemorrhage can be detected at CT. In posttraumatic cases, coexistent features such as hepatic lacerations, rib fractures, or perihepatic fluid will be present. In hemorrhage induced by surgery, the location of the hematoma (along the surgical plane) will often be a clue to the diagnosis. The presence of a perihepatic hematoma in combination with a hemorrhagic mass is highly suggestive of hepatocellular adenoma. Because of the paramagnetic effect of methemoglobin, MR imaging is even more suitable than CT for detection and characterization of hemorrhage.

Biloma

Bilomas result from rupture of the biliary system, which can be spontaneous, traumatic, or iatrogenic following surgery or interventional procedures. Bilomas can be intrahepatic or perihepatic. Extravasation of bile into the liver parenchyma generates an intense inflammatory reaction, thereby inducing formation of a well-defined pseudocapsule. Clinical manifestations depend on the location and size of the biloma.

At CT imaging, a biloma usually appears as a well-defined or slightly irregular cystic mass without septa or calcifications. Also, the pseudocapsule is usually not readily identifiable. This imaging appearance, in combination with the clinical history and location, should enable correct diagnosis.

Focal Liver Lesions

- Hemangioma
- Focal nodular hyperplasia (FNH)
- Hepatocellular adenoma (HCA)
- Metastasis
- Hepatocellular carcinoma (HCC)
- Focal fatty change (FFC)
- Cyst (Bile duct cyst)
- Abscess

Female Predominance

- HCA (almost)
- Hemangioma
- FNH (overwhelming)

Male Predominance

- HCC
- Abscess

Pathology based on Age

- 60's – Cyst, Metastasis, HCC
- 50's – Cyst, Hemangioma, Metastasis, Abscess
- 40's – FNH, Abscess
- 30's – HCA

Symptomatic

- HCC
- HCA
- Metastasis (primary)
- Abscess

Incidentaloma

- Hemangioma
- Cyst
- FNH
- FFC

CHAPTER

3

Gallbladder and Biliary Tract

INTRODUCTION

The gallbladder in fasting patients are always seen in CT scans and although gallstones are always visible. CT is not used as a primary examination for detecting gallstones because of lower sensitivity.

Role of CT in evaluating gallbladder involves (1) staging of malignancies, (2) evaluating the complications of cholecystitis.

Helical scanning of bile ducts has proved useful in three areas (1) detection of CBD stones, (2) determining the extent of cholangiocellular malignancies, (3) preoperative planning with the emergence of high resolution thin scanners minimally dilated intra- and extrahepatic bile ducts are now easily visible. Entire CBD is routinely visible. CT has a accuracy of 96%. In detecting biliary obstruction. Ninety percent in determining the level of obstruction, 70% in identifying the cause of obstruction.

CT Techniques

Gallbladder—is usually scanned as part of routine abdominal scanning we use a 7 /7 mm,
Acquisition with IV and oral contrast, thin sections 3-5 mm are reformatted as required.

Biliary tree—CT is very effective in defining the site and etiology of the obstruction.
CT of biliary tree most often involves three basic questions:

1. Is biliary obstruction present?
2. Level of obstruction and etiology.
3. Stage of the disease process.

Hallmark of biliary obstruction in CT is the presence of dilated biliary tree, non-CECT reveals these as low attenuation structures.

Extrahepatic ductal dilatation occurs early in the course of diseases. Duct dimensions should measure less than 8 mm. Using the short axis of the duct avoids artificially increasing the diameter owing to the oblique course of the duct.

Sequential section help to define the degree of transition, abrupt as in the case of malignancy or gradually tapering as in the case of benign stricture.

Evaluating the duct wall distal to the obstruction gives a clue to the etiology negative contrast with water or milk can be given if distal CBD calculus is considered.

Technique

For evaluating stones in biliary tree an initial non-CECT using 3 mm collimation is done, if negative routine study using oral contrast is used, scanning using a small field of view (FOV), in the region of distal CBD increases the spatial resolution.

CONGENITAL LESIONS

Normal variants of gallbladder can be divided into those of number, position and shape.

Gallbladder Number

- Agenesis is very rare, in many cases it is not of clinical significance but may predispose to biliary tract disease like choledocholithiasis. It is associated with anomalies of GIT, GUT, CVS and skeletal system.
- Accessory gallbladder is a anomaly of duplication divided into two types: (1) bilobed GB—gallbladder separated into two chambers by a septum with a single neck (Fig. 3.1), (2) double GB—two separate gallbladder with 2 separate cystic ducts.

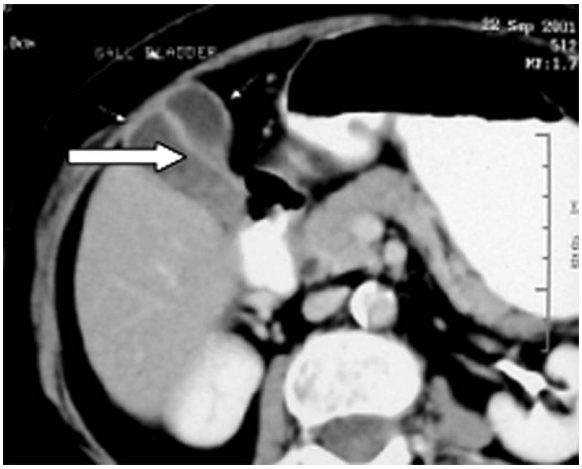

FIGURE 3.1: Axial CECT reveals a bilobed gallbladder. Note the complete septum between the two chambers (arrow).

Gallbladder Position

Gallbladder usually lies in a depression in the under surface of the liver between the left and right lobes. A long or loose mesentery increases the mobility of gallbladder and results in mobile or wandering, floating GB.

Intrahepatic gallbladder–gallbladder may some time be surrounded by liver, located in the interlobar plane, other rare vaients of gallbladder position include left sided GB, suprahepatic, retrohepatic, retroperitoneal or within the falciform ligament.

Gallbladder Shape

Shape of the gallbladder can be altered by folds and septae. The commonest type is the Phrygian cap (fold or septum in the fundus).

Transverse and longitudinal septae may also occur and may predispose to stone formation and cholecystitis.

Multiseptated and diverticulae are other rare anomalies.

GALLSTONES

Gallstones (cholelithiasis) are the most common cause of biliary tract disease in adults. Approximately 80% of patients with gallstones are asymptomatic and 20% have symptomatic biliary colic. About 1 to 2% of patients per year with asymptomatic gallstones develop biliary symptoms and once symptomatic these individuals have a 50% chance of having their next attack within 1 year. They also have a 1 to 2% per year risk of developing acute cholecystitis or other complication.

Two major types of gallstones exist.

1. *Cholesterol stones* are hard, crystalline stones that contain more than 50% cholesterol plus varying amounts of protein and calcium salts. They predominate (>85%) in the Western world.
2. *Pigment stones* consist of several insoluble calcium salts that are not normal constituents of bile.

The CT appearance of gallstones is variable, depending on their composition; pattern of calcification; and the presence of lamellation, fissuring, or gas. Stones with a high cholesterol content are difficult to see because they are isodense with the surrounding bile. Well-calcified stones are easily detected on CT. Stones that are denser than bile may be seen due to a rim or nidus of calcification. The CT attenuation of gallstones correlates more closely with the cholesterol content of the stones than with the calcium content. On CT, gallstones can be simulated by the enhancing mucosa of a contracted gallbladder wall or neck, which often fold upon themselves. CT is less sensitive in the detection of gallstones than is ultrasound: 75% compared with 98% (Figs 3.2 to 3.5).

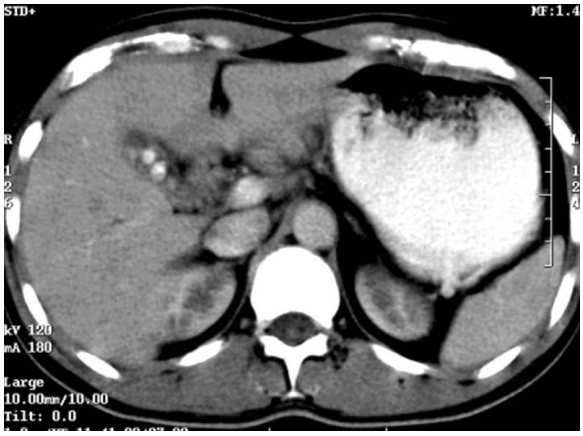

FIGURE 3.2: Axial CECT reveals contracted gallbladder with multiple calculi.

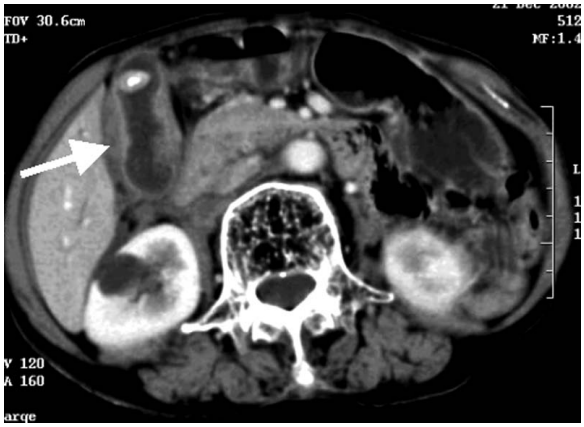

FIGURE 3.3: Axial CECT reveals laminated gallstone with distended gallbladder showing wall thickening with pericholecystic fluid (arrow).

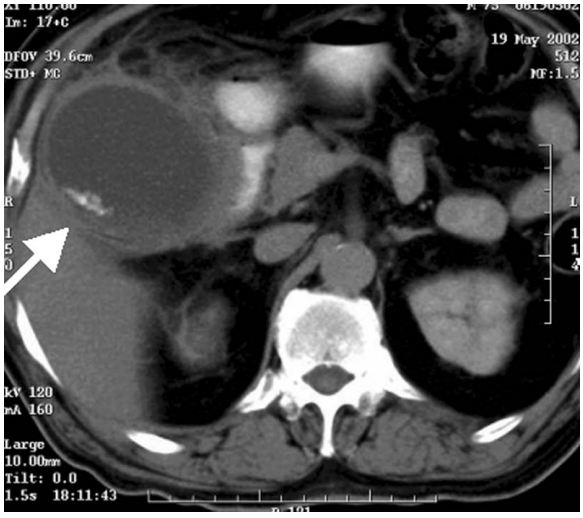

FIGURE 3.4: Axial CECT reveals thickened gallbladder wall with pericholecystic fluid, adjacent fat shows stranding. luminal calculus present (arrow).

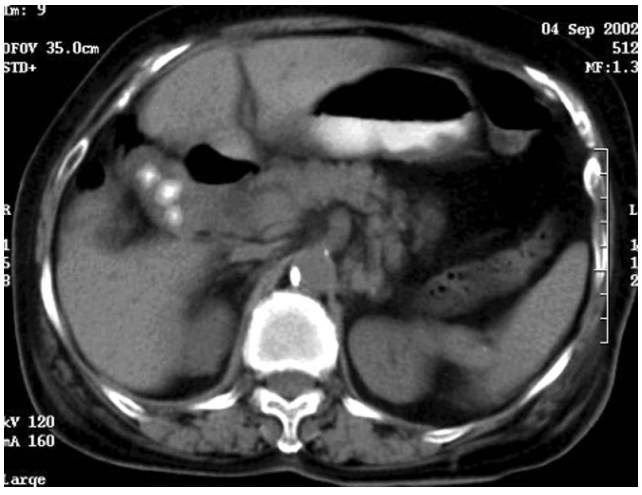

FIGURE 3.5: Axial CECT reveals contracted gallbladder with faceted luminal calculi.

Table 3.1: Complications of cholelithiasis

Complication	*Comments*
Biliary colic	Typically caused by transient obstruction of the cystic duct Pain lasts 13 hours, with or without nausea or vomiting Subsides when the stone falls back into the gallbladder or passes into the CBD
Choledocholithiasis	Persistent blockage at the level of the ampulla of Vater is a common cause of jaundice
Acute cholecystitis	A stone is impacted in the neck of the gallbladder or in the cystic duct in 95% of cases
Gallbladder perforation	Typically seen in the setting of acute cholecystitis A pericholecystic or, less commonly, intrahepatic abscess may result and may be amenable to percutaneous drainage in certain clinical settings; however, therapy almost invariably requires surgery
Pancreatitis	...
Biliary strictures	...
Cholangitis	...
Biliary fistula	Gallstone ileus Bouveret syndrome
Mirizzi syndrome	Obstruction of the CBD or hepatic duct Caused by a gallstone lodged in the cystic duct, with associated inflammation compressing adjacent ducts
Porcelain gallbladder	Associated with gallstones in 95% of cases Gallbladder carcinoma develops in 22% of cases

Milk of Calcium Bile

Milk of calcium bile or limey bile is an uncommon disorder characterized by puttylike, thickened bile composed of calcium carbonate. It is usually associated with cystic duct obstruction and chronic cholecystitis. CT and plain films show high-density material layering within the gallbladder lumen (Fig. 3.6).

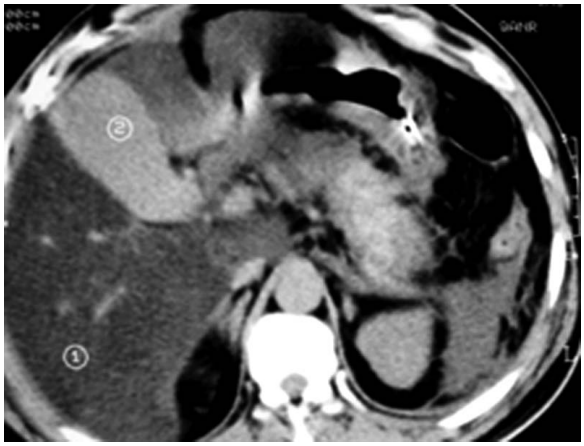

FIGURE 3.6: Axial plain CT shows a distended gallbladder with increased luminal attenuation.

CHOLECYSTITIS

Acute Cholecystitis

Most common clinical symptoms of acute chole cystitis are right upper quadrant or epigastric, nausea and vomiting.

The pathophysiology of acute cholecystitis is complex. Gallstones are present in 96% of cases and the stone causes cystic duct obstruction. The trapped bile concentrates and has an irritative effect on the gallbladder wall, which stimulates increased secretions. These secretions lead to wall edema, mural thickening, distention of the gallbladder lumen, and mural hypervascularity. The mural vessels become compressed as intraluminal pressure rises, which may produce thrombosis, ischemia, and subsequent necrosis of the gallbladder wall. This process may be complicated by bacterial colonization, perforation, or abscess formation.

The most common CT findings in acute cholecystitis include gallstones or stones in the cystic duct, gallbladder distention (>5 cm in transverse or anteroposterior [AP] diameter), mural thickening (>3 mm) and nodularity, pericholecystic fluid, poor definition of the gallbladder wall at the interface with the liver, a thin rim of pericholecystic fluid, inflammatory stranding in the pericholecystic fat, and increased density of bile (>20 HU). Hypervascularity of the gallbladder wall relates to the degree of inflammation and the duration of symptoms, but is a less reliable sign on CT when compared with power color Doppler ultrasound. The indistinctness of the interface between the liver and inflamed gallbladder relates to subserosal edema, inflammation, intramural hemorrhage, and inflammatory changes in the liver (Figs 3.7A and B).

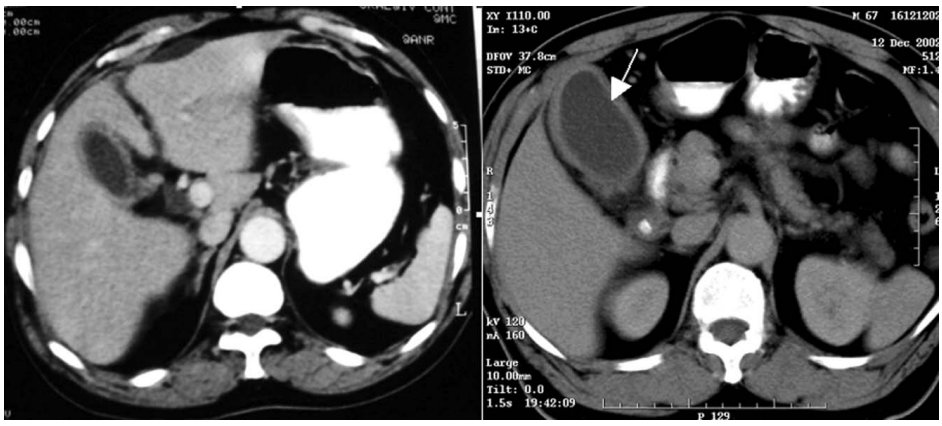

FIGURES 3.7A and B: Axial CECT reveals a distended gallbladder with thickened walls (arrow), impacted calculi seen in the proximal CBD.

Complications of Acute Cholecystitis

Complications develop in upto 40% of patients with acute cholecystitis. The major complications include empyema, perforation with pericholecystic abscess, emphysematous cholecystitis, gangrenous cholecystitis, hemorrhagic cholecystitis, and perforation with biliary–enteric fistula.

Empyema

Empyema of the gallbladder (suppurative cholecystitis) occurs when pus fills the distended, inflamed gallbladder. This complication typically occurs in diabetic patients and may behave like an intra-abdominal abscess with rapid progression of symptoms. Sonographically, pus within the gallbladder resembles sludge and the CT density of the lumen is high (>30 HU). The diagnosis can be established by imaging (usually sonographically) guided percutaneous needle aspiration of the gallbladder.

Gangrenous Cholecystitis

This major complication of acute cholecystitis is associated with intramural hemorrhage, necrosis microabscesses, mucosal ulcers, and intraluminal purulent debris, hemorrhage, and strands of fibrinous exudate. Gangrenous cholecystitis is associated with increased morbidity and mortality and requires emergency surgery. Clinical findings in this disorder are nonspecific and it may be difficult to identify gangrenous cholecystitis prospectively.

Intraluminal membranes relating to strands of fibrinous exudate and desquamated mucosa may cause coarse, nonlayering intraluminal echoes. Additionally, there may be marked asymmetry of the thickened gallbladder wall due to presence of intramural hemorrhage or microabscess formation. Complex pericholecystic fluid collections containing debris are usually the result of microperforations of the gallbladder.

Miyazaki score for gangrenous cholecystitis takes into account findings like intraluminal membranes, pericholecystic fluid, intraluminal debris, mural halo. The single most specific sign of high specificity is pericholecystic fluid (Figs 3.8A and B).

Emphysematous Cholecystitis

Emphysematous cholecystitis develops in less than 1% of cases of acute cholecystitis and is more common in patients with diabetes (38%) and splanchnic ischemia, and in men. This rapidly progressive and often fatal disease

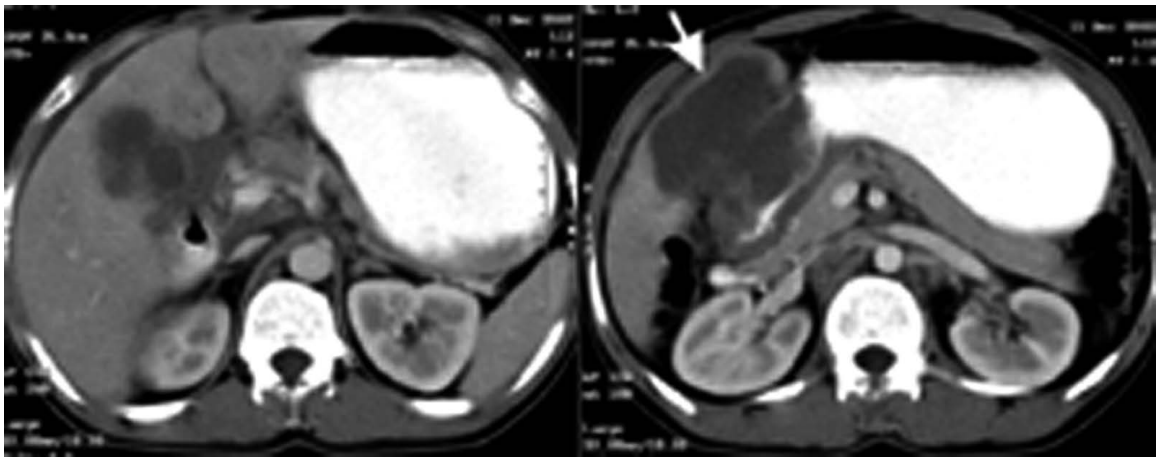

FIGURES 3.8A and B: Axial CECT reveals partially distended gallbladder with loss of normal contour of the wall with a large pericholecystic collection (arrow).

is characterized by the presence of gas within the wall or lumen of the gallbladder. *Clostridium perfringes, Clostridium welchii, Escherichia coli*, and *Klebsiella* are the most common gas-forming bacteria that cause this disease. Patients with emphysematous cholecystitis have a five-fold increased risk of perforation.

The CT and MR diagnosis of emphysematous cholecystitis is fairly straightforward: depiction of intraluminal or intramural air. The diagnosis may be more difficult sonographically. Intraluminal gas produces hyperechoic reflectors in the nondependent portion of the gallbladder, with "dirty" acoustic shadowing that contains "comet tail" or "ring-down" artifacts. These must be differentiated from the WES sign of a contracted gallbladder filled with stones. Intramural gas manifests as a hyperechoic ring around the fluid-filled gallbladder (Fig. 3.9).

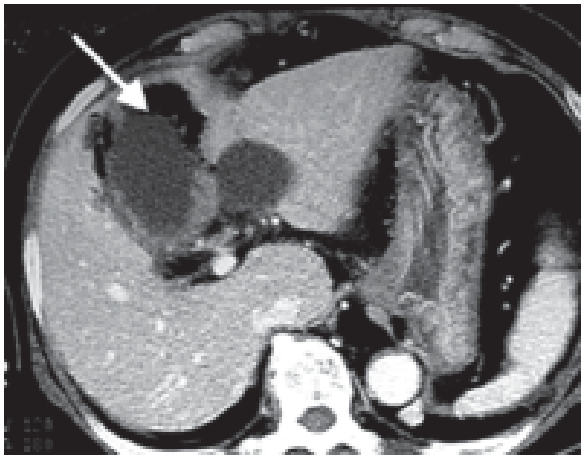

FIGUER 3.9: Axial CECT reveals distended gallbladder with thickened walls, multiple air pockets noted in the fundus and in the wall (arrow).

Gallbladder perforation and pericholecystic abscess: are life-threatening complications. They may lead to peritonitis and septic shock gallbladder perforation occurs in 5 to 10% of patients with acute cholecystitis. Diabetic and patients with acalculous cholecystitis have a higher incidence of gallbladder perforation.

Gallbladder perforation occurs most commonly in the setting of gangrenous cholecystitis with other risk factors including gallstones, impaired vascular supply, infection, malignancy, and steroid use. The fundus of the gallbladder is the most common site of perforation because of its poor blood supply. Perforation and abscess formation should

be suspected clinically in patients with acute cholecystitis who become toxic for unexplained reasons or whose clinical condition rapidly deteriorates. On CT and ultrasound, primary finding is a complex fluid collection is seen surrounding the gallbladder. The gallbladder wall may appear focally disrupted and the residual gallbladder lumen may be seen within or peripheral to the pericholecystic abscess (Figs 3.10 to 3.14).

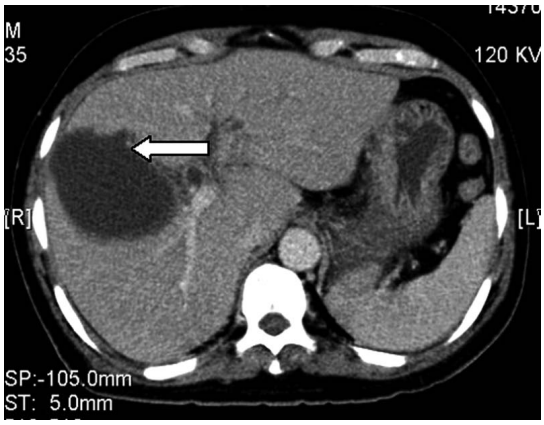

FIGURE 3.10: Axial CECT reveals distended gallbladder with thickened walls, focal defect suggestive of a contained perforation (arrow).

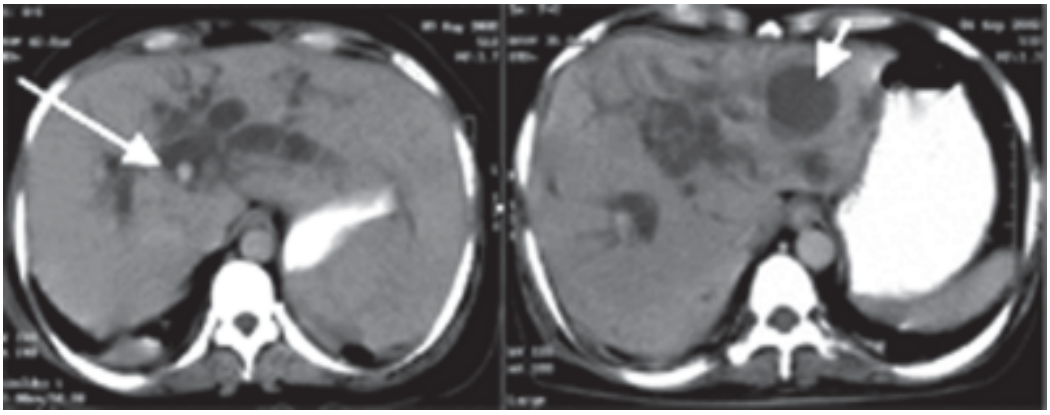

FIGURES 3.11A and B: Axial CECT (in a postoperative case) reveals dilated IHBR with a calculus in the CHD (arrow), left lobe liver shows a well marginated hypodense lesion suggestive of abscess (short arrow).

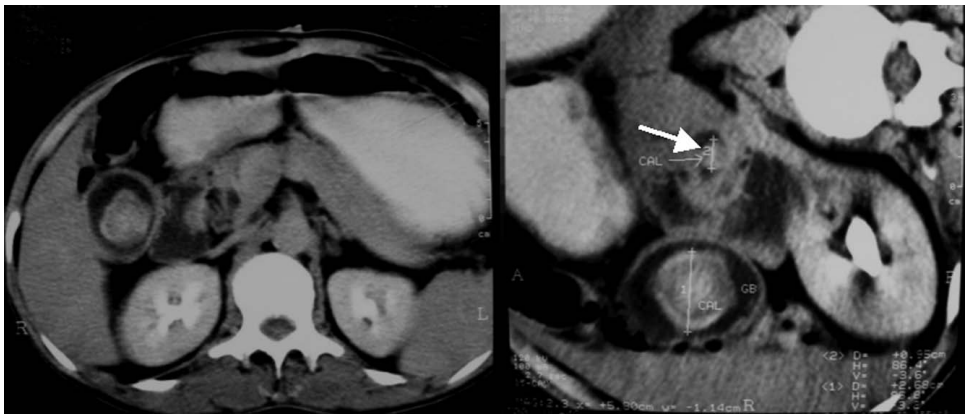

FIGURES 3.12A and B: Axial CECT shows a large laminated calculus in the gallbladder with thickening of the gallbladder wall. Decubitus CECT shows a distal CBD calculus showing a target sign (stone with rim of bile, arrow).

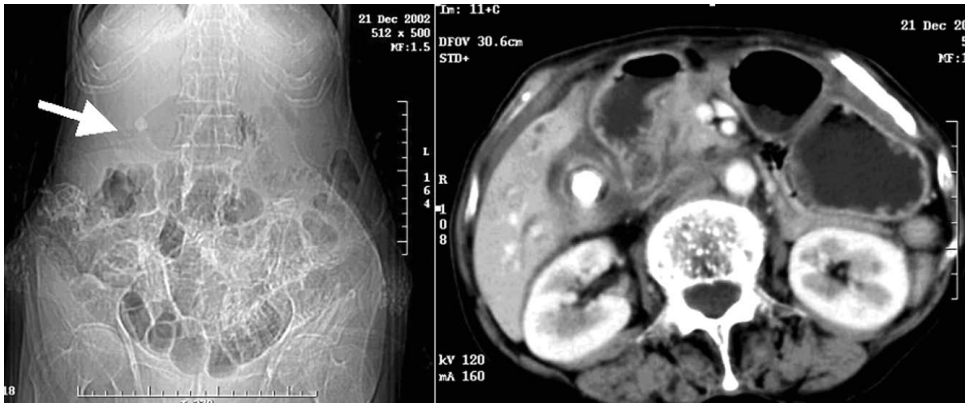

FIGURES 3.13A and B: Digital scanogram shows a radiopaque shadow in the right hypochondrium, axial CECT reveals a large gallstone in a contracted gallbladder.

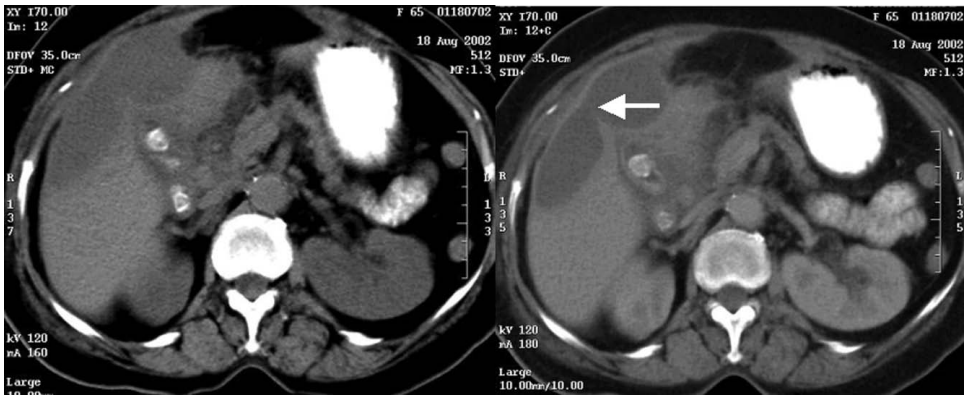

FIGURES 3.14A and B: Axial plain and CECT shows calculus cholecystitis with subcapsular abscess (arrow)

Takada classification of pericholecystic abscess is based on the anatomic location

1. Abscess within the gallbladder bed.
2. Intramural abscess
3. Intraperitoneal abscess.

Xanthogranulomatous Cholecystitis

Xanthogranulomatous cholecystitis (XGC) is an uncommon inflammatory condition in which the gallbladder wall is thickened by the infiltration of round cells, lipid-laden histiocytes, and multiple nucleated giant cells with fibroblast proliferation in the muscularis propria. XGC is found in 0.7 to 13% of cholecystectomy specimens. Imaging features may mimic gallbladder carcinoma. CT shows marked mural thickening of the gallbladder or a soft tissue mass in the gallbladder fossa. This inflammatory process may extend into the liver hilum or adjacent duodenum or colon.

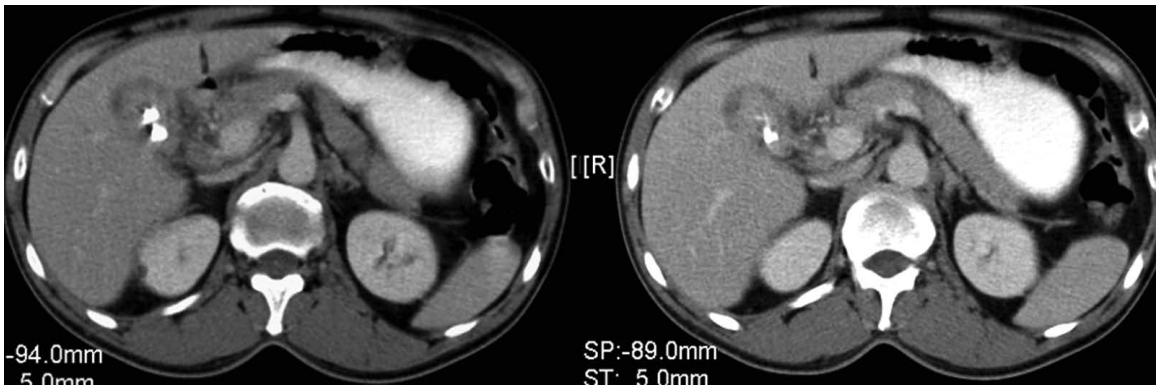

FIGURES 3.15A and B: Axial CECT reveals uniformly thickened enhancing gallbladder wall with central luminal calculus.

PORCELAIN GALLBLADDER

Porcelain gallbladder is an uncommon disorder in which chronic cholecystitis produces mural calcification of the gallbladder. The term derives from the blue discoloration and brittle consistency of the gallbladder. Porcelain gallbladder, seen in 0.06 to 0.8% of cholecystectomy specimens, presents with two types of histologic calcification: (1) a broad continuous band of calcification in the muscularis, and (2) multiple punctate calcifications scattered through the mucosa and submucosa. Only part of the wall or the entire wall of the gallbladder may be calcified. Porcelain gallbladder is five times more frequent in men than in women, with a mean age of 54 years at presentation. Patients often have few symptoms and the diagnosis is often marked by detecting a palpable right upper quadrant mass or finding typical calcifications on plain films.

Porcelain gallbladder is associated with carcinoma of the gallbladder.

CT nicely depicts the mural calcification and may directly visualize an associated carcinoma. The CT appearance of porcelain gallbladder can be simulated by a contracted gallbladder containing a large stone with a calcified rim and a bile attenuation center.

Cholesterolosis is due to the deposition of foamy, cholesterol-laden histiocytes in the lamina propria. There are two major morphologic types of cholesterolosis: diffuse, flat, and planar type and the larger polypoid type. The first type cannot be appreciated in imaging. The second type of cholesterolosis, cholesterol polyps, occurs in 20% of cases.

ADENOMYOMATOSIS

Adenomyomatosis is characterized by proliferation of the epithelium associated with muscular hypertrophy and mucosal–submucosal diverticula (Rokitansky-Aschoff sinuses). Adenomyomatosis manifests in three different ways: diffuse, segmental, and polypoid. The diffuse type is the least common and presents with diffuse mural thickening that can simulate other causes of diffuse thickening such as acute and chronic cholecystitis, gallbladder carcinoma, and hypoproteinemia. In the segmental form, there is mural thickening of the midportion or waist of the gallbladder, producing an "hourglass" appearance. The localized form of adenomyomatosis is the most common and is nearly always confined to the gallbladder fundus, where it is sometimes called an adenomyoma or myoepithelial abnormality. The localized thickening may appear as a solid mass and simulate carcinoma.

Rokitansky-Aschoff sinuses may appear sonographically as small, anechoic spaces within the thick wall when they contain bile. More commonly, they appear as echogenic foci within the gallbladder wall with ring-down or comet tail reverberation artifacts with or without wall thickening. These artifacts may simulate cholesterol polyps and intraluminal or intramural gas or stones. The echogenic foci are probably cholesterol crystals or tiny cholesterol stones within the intramural diverticula. The cholesterol crystals probably account for the reverberation artifacts as

well. Visualization of the Rokitansky-Aschoff sinuses is the only definite way to differentiate adenomyomatosis from other causes of gallbladder wall thickening.

Hemobilia

Biliary tract blood can be caused by blunt trauma, biliary tumors, inflammatory disease, traumatic venous or arterial-biliary fistulae, rupture of an aneurysm of the hepatic artery, hemorrhagic cholecystitis, and blood dyscrasias. Noncontrast CT may show high attenuation fluid (>30 HU) within the gallbladder (Fig. 3.16).

On CT, blood raises the attenuation of normal bile (0–20 HU) to a level generally greater than 50 HU. Initially, the entire gallbladder lumen may be diffusely increased in density. With clotting, the blood settles in the dependent portion of the gallbladder or bile ducts. This high attenuation can persist for several days. Other causes of increased attenuation of bile include vicarious excretion of contrast, sludge, debris, gallstones, hydrops, milk of calcium bile.

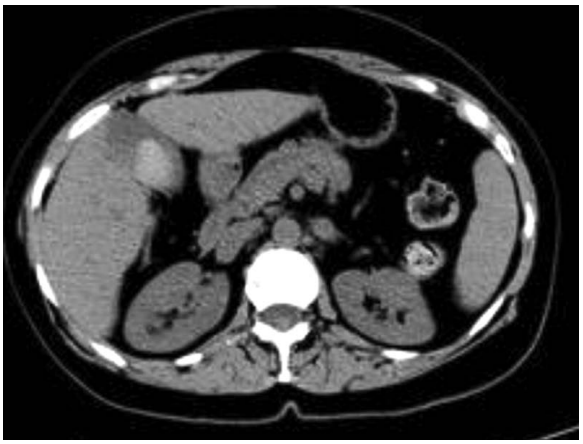

FIGURE 3.16: Axial plain CT reveals a hyperdense focus within the distended gallbladder in a patient who sustained a blunt injury abdomen.

ACUTE ACALCULOUS CHOLECYSTITIS

Acute gallbladder inflammation in the absence of stones is seen in 2 to 15% of patients undergoing cholecystectomy and accounts for 47% of cases of postoperative cholecystitis and 50% of children with acute cholecystitis. Acute acalculous cholecystitis (AAC) most commonly occurs in adults who are critically ill or have had trauma, burns, or major surgery. Other risk factors include hyperalimentation, mechanical ventilation, diabetes, sepsis, cardiac arrest, atherosclerosis, prolonged fasting, AIDS, and hepatic arterial chemotherapy. AAC most commonly results from a gradual increase of bile viscosity due to prolonged stasis that leads to functional obstruction of the cystic duct. Mural necrosis occurs in 60% of cases and gangrene and perforation are common. As result of difficulty in early diagnosis, acalculous cholecystitis has higher morbidity and mortality. In general the diagnostic accuracy of all modalities is lower than that with calculous cholecystitis. CT findings include asymmetric thickening of gallbladder wall and extensive inflammation in the pericholecystic space (Figs 3.17A and B).

One of the main advantages of CT is its ability to demonstrate edema and focal inflammatory changes in the pericholecystic fat.

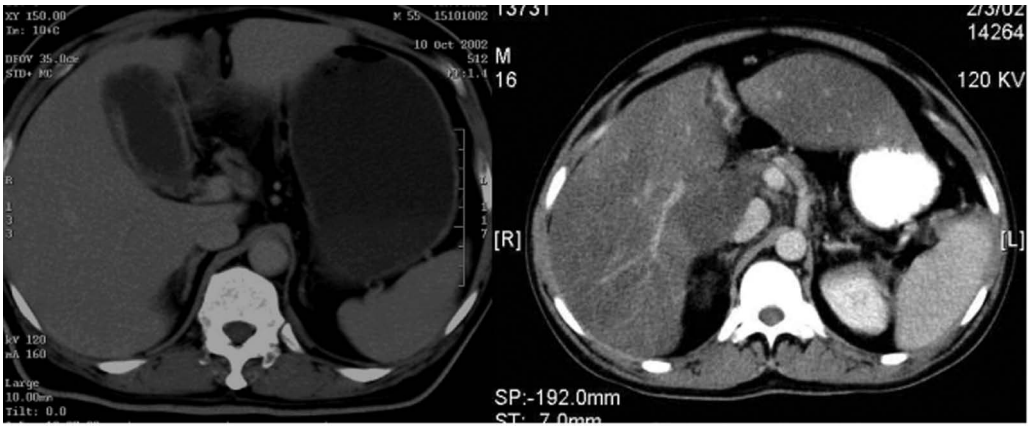

FIGURES 3.17A and B: Axial CECT reveals distended gallbladder with wall thickening and pericholecystic fluid no calculus. Axial CECT shows contracted gallbladder with intensely enhancing mucosa.

CHRONIC CALCULUS CHOLECYSTITIS

Chronic cholecystitis can have similar findings as acute cholecystitis, such as wall thickening, stones and wall enhancement. The gallbladder is, however, contracted rather than distended. Porcelain gallbladder is an uncommon manifestation of chronic cholecystitis where there is deposition of calcium in the gallbladder wall (Figs 3.18A and B).

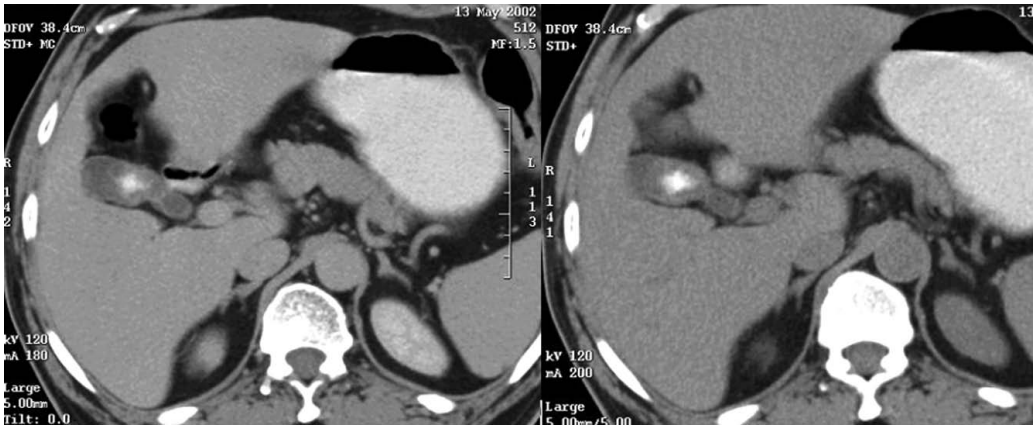

FIGURES 3.18A and B: Axial CECT showing features of chronic cholecystitis.

GALLBLADDER NEOPLASMS

Benign neoplasms: Common benign tumor of gallbladder is the adenoma. It appears as a small mass along the wall of gallbladder.

Others: Fibroma, lipoma, myxoma, leiomyoma, hemangioma, neurofibroma.

Table 3.2: Differential diagnosis of a gallbladder mass

Diagnosis	*Comments*
Stone	Echogenic mass with shadowing, usually mobile The mass is occasionally adherent (i.e. nonmobile)
Cholesterol polyp	Unifocal form of cholesterolosis Nonmobile, nonshadowing mass
Adenomyomatosis	May occur as focal mass(es), but most typically occurs as segmental mural thickening "Ring-down" artifacts may be seen and are attributable to debris and cholesterol crystals trapped in Rokitansky–Aschoff sinuses
Tumefactive sludge	Mobile echogenic mass without shadowing
Congenital fold or septum	...
Gallbladder carcinoma	May completely fill the gallbladder lumen 75% of patients have gallstones
Miscellaneous	Includes metastasis (e.g. from melanoma), adenoma (including adenomatous polyp, papilloma), ectopic pancreas, hematoma

Carcinoma of the Gallbladder

Clinical Features

Carcinoma of the gallbladder is the fifth most common malignancy of the gastrointestinal tract, responsible for nearly 7000 deaths annually in the United States. It is found incidentally in 1 to 3% of cholecystectomy specimens and 0.5 to 7.4% of autopsies. It is the most common malignancy of biliary tract. Gallbladder carcinoma has a peak

incidence in the sixth and seventh decades of life, with a female to male ratio of 4:1. Early diagnosis of gallbladder carcinoma is difficult because most patients present with nonspecific findings of right upper quadrant pain, malaise, weight loss, jaundice, anorexia, and vomiting. This presentation is often confused with symptomatic cholelithiasis or chronic cholecystitis. At the time of diagnosis, most patients are considered unresectable because of direct extension into adjacent organs, local lymph node metastases, or distant metastatic disease. The 5-year survival rate for this tumor is less than 5%.

Predisposing factors include gallstones (65-95%) and a history of chronic cholecystitis (40-50%), and an estimated 22% of patients with porcelain gallbladder will develop carcinoma. Patients with ulcerative colitis have increased risk of developing carcinoma.

Anomalous pancreaticobiliary ductal union is also associated with gallbladder carcinoma. Reflux of pancreatic and biliary juice may act as carcinogens.

Imaging Findings

Ultrasound, CT, and MR are the primary means of imaging gallbladder carcinoma. This neoplasm has three major patterns of presentation pathologically and on cross-sectional imaging: (1) focal or diffuse mural thickening; (2) an intraluminal polypoid mass, usually larger than 2 cm, originating in the gallbladder wall; and (3) most commonly (45-65%) a subhepatic mass replacing or obscuring the gallbladder, often invading adjacent liver.

Carcinoma with Mural Thickening

Gallbladder carcinoma presenting with focal or diffuse mural thickening is the least common presentation and the most difficult to diagnose The wall is usually 4-13 mm or greater in thickness, often asymmetrical and nodular. Normally the gallbladder wall is 3 mm or less in thickness and carcinomas that are confined to the mucosa or slightly raised lesions may not be visualized sonographically. The diagnosis may be difficult because of the small size of early masses and the subtle wall thickening associated with cancer can be obscured by gallstones. In addition, diffuse wall thickening is more commonly caused by acute and chronic cholecystitis, adenomyomatosis, inadequate gallbladder distention, hepatitis, low protein states, and other causes. Although CT is inferior to ultrasound in depicting mucosal irregularity, mural thickening, and cholelithiasis, it is superior for evaluating the thickness of portions of the gallbladder wall that are obscured by gallstones or mural calcification on ultrasound. CT may show focal or irregular mural thickening; in these cases, the images should be carefully inspected for bile duct dilation, local invasion, metastases, and adenopathy.

Carcinoma as a Polypoid Mass

Approximately 25% of gallbladder carcinomas present as intraluminal masses. It is important to recognize this appearance because these polypoid lesions tend to be well differentiated and confined by the muscularis propria and thus have a better prognosis at the time of diagnosis.

Sonographically, polypoid carcinoma typically have a homogeneous tissue texture, are fixed to the gallbladder wall at their base, and do not cast an acoustic shadow. Gallstones are often present and the gallbladder may be normal in size or expanded by the mass, which can be hyperechoic, isoechoic, or hypoechoic relative to the liver.

A small polypoid carcinoma can be difficult to differentiate from a cholesterol polyp, adenoma, or adherent stone. Benign polyps typically are less than 1 cm in size; if a polyp is greater than 1 cm in diameter and not clearly benign, a cholecystectomy should be considered. Tumefactive sludge or blood clot can simulate a polypoid carcinoma. Change in the appearance with positional maneuvers indicates blood or sludge, whereas color flow within the abnormality suggests a mass.

On CT, polypoid cancers enhance homogeneously after administration of contrast medium, and the adjacent gallbladder wall may be thickened. Polypoid gallbladder carcinomas does not usually show necrosis or calcification on CT.

Carcinoma as a Gallbladder Fossa Mass

This is the most common form of gallbladder cancer and presents as solid masses with variable echogenicity and may be homogeneous or inhomogeneous. The mass may be difficult to separate from the liver sonographically, especially when there is direct hepatic invasion. The absence of a gallbladder and the presence of gallstones can be helpful clues to the diagnosis. Infiltrating carcinomas that replace the gallbladder often show irregular contrast enhancement with scattered regions of internal necrosis on CT and MR (Figs 3.19A and B).

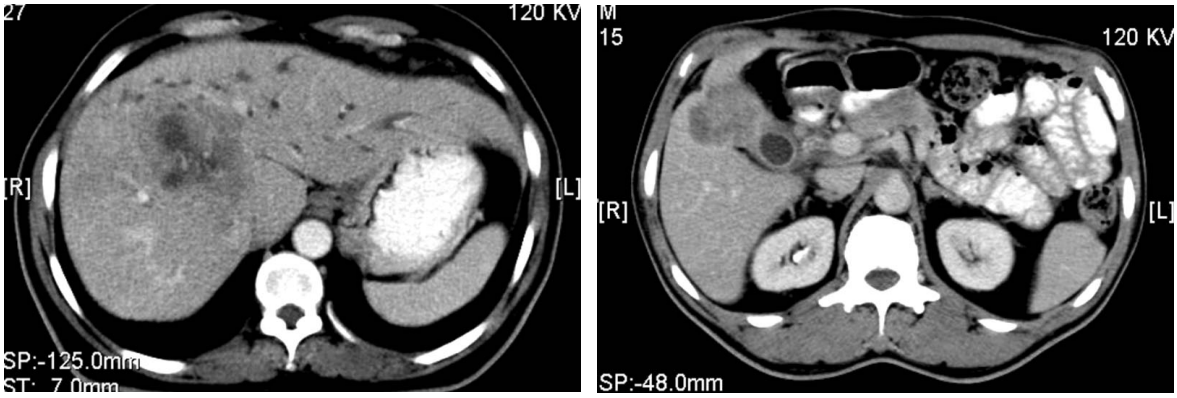

FIGURES 3.19A and B: Axial CECT reveals a heterogeneous mass involving the gallbladder fundus and proximal body infiltrating the adjacent liver parenchyma with segmental biliary dilatation CT features suggestive of gallbladder carcinoma.

Vicarious Contrast Excretion

Presence of contrast in the biliary tract after intravenous administration of contrast. This is due to increase in protein binding caused by prolonged intravascular contact in cases of acidosis. Seen in cases of uremia, acute unilateral obstruction, contrast extravasation.

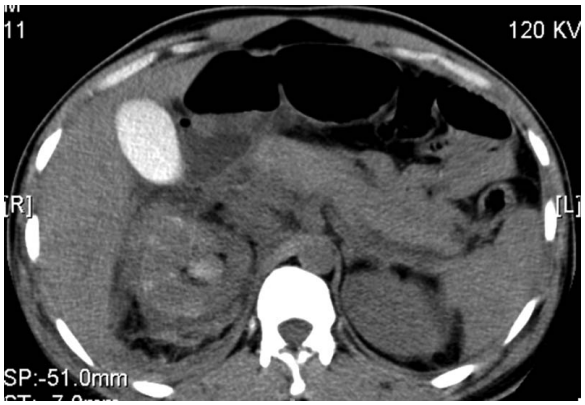

FIGURE 3.20: Delayed CT in a case of blunt injury abdomen shows opacified gallbladder suggestive of vicarious excretion.

Approach to Thick Walled Gallbladder on CT

On contrast enhanced CT, the normal gallbladder wall is usually perceptible as a thin enhancing rim of soft tissue density. Although its thickness depends upon the degree of gallbladder distention, 3 mm is regarded as the upper limit of normal and mural thickening is defined as a transverse wall measurement of 4 mm or greater. Gallbladder wall thickening is the most common finding in either acute calculus or acalculous cholecystitis. It is a non-specific finding that may be seen in gallbladder cancer and in a variety of extracholecystic benign conditions such as hepatitis, heart failure, hypoalbuminemia.

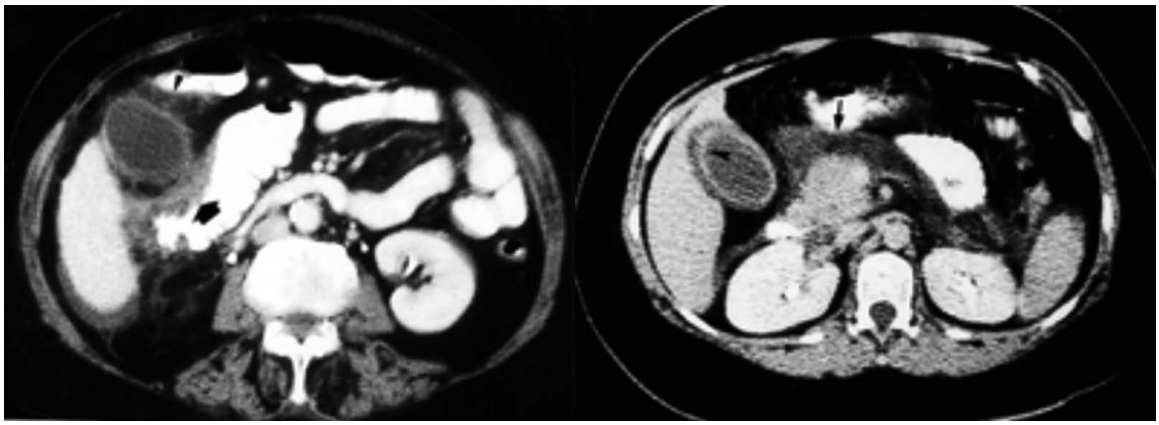

FIGURES 3.21A and B: Acute hepatitis, peritonitis, acute pancreatitis and acute pyelonephritis may cause gallbladder wall thickening.

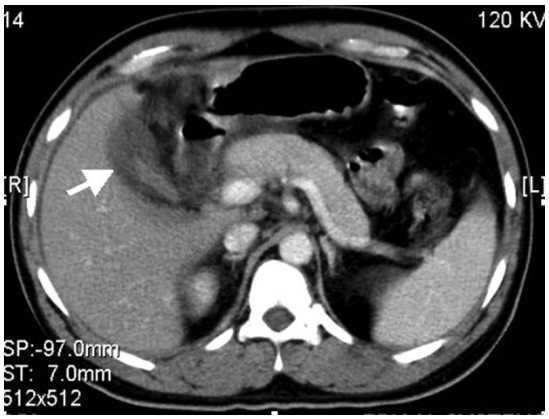

FIGURE 3.22: Axial CECT in a patient with fever and lab parameters suggestive of dengu fever reveals diffuse edematous gallbladder wall (arrow).

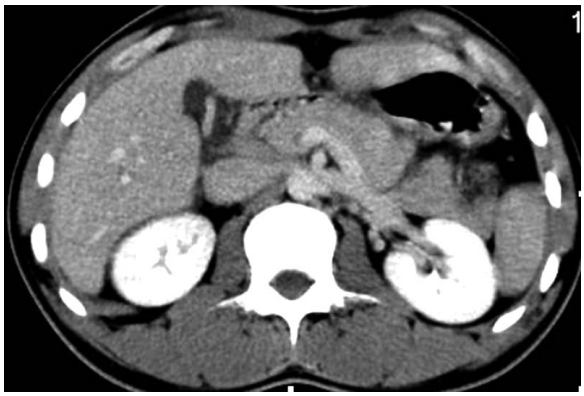

FIGURE 3.23: Axial CECT in a patient who sustained blunt injury abdomen reveals edematous gallbladder wall with hyperdense enhancing mucosa.

Thickening of the gallbladder wall is the most common finding of acute cholecystitis while gallstones may or may not be seen. In fact, 95% of patients with acute cholecystitis have gallstones, but only approximately 75% of these are detected on CT.

A thick-walled gallbladder is, however, a non-specific finding that may occur in a variety of extrabiliary conditions. The radiologist should, therefore, look for associated CT findings suggestive of acute cholecystitis including:

1. Transient focal hyperattenuation in the hepatic parenchyma adjacent to the inflamed gallbladder probably related to hepatic arterial hyperemia.
2. Indistinct interface of the gallbladder wall and the juxtaposed liver, regarded as highly suggestive of acute cholecystitis.
3. Pericholecystic stranding, which represents inflammatory changes within the fat surrounding the gallbladder. Extensive changes may cause reactive mural thickening and edema in the adjacent colon or duodenum irregular, discontinuous or absence of gallbladder wall enhancement on contrast-enhanced CT as well as pericholecystic abscess are specific signs of mural necrosis indicating gangrenous cholecystitis, a severe form of acute cholecystitis.

Hypoalbuminemic states and congestive right heart failure may cause thickening of the gallbladder wall. Additional findings of extravascular volume overload may be seen, such as pleural or pericardial effusions, ascites, dependent subcutaneous edema and distended IVC (Fig. 3.22).

Isolated penetrating trauma involving the gallbladder is a rare injury. Clinical symptoms may be minimal initially with gradual clinical deterioration related to spillage of bile into the peritoneal cavity. A high clinical index of suspicion is needed to avoid a diagnostic delay. As abdominal CT is often performed it may elicit findings of mural thickening and high-density fluid content within the gallbladder representing hemobilia as well as pericholecystic stranding (Fig. 3.23).

Diffuse gallbladder wall thickening secondary to tumor infiltration and inflammatory change is a common manifestation of advanced gallbladder carcinoma, which is often detected at a late stage due to lack of early clinical signs. Associated findings such as biliary dilatation, invasion of adjacent structures and liver and nodal metastases, may help in establishing the correct diagnosis and differentiating it from chronic cholecystitis.

Gallbladder wall thickening may be secondary to chronic cholecystitis, adenomyomatosis and polyps. Chronic cholecystitis may appear on CT with soft-tissue density wall thickening of, usually, a contracted gallbladder, often around gallstones. A "porcelain" gallbladder is an uncommon form of chronic cholecystitis with coarse mural calcification. Thickening of the gallbladder wall, either focal or diffuse, on CT is the common finding of adenomyomatosis.

BILIARY OBSTRUCTION

CT is usually performed as a correlative study to USG, the main goals of biliary CT is to determine (1) the presence of obstruction, (2) to determine the level and extent of obstruction, (3) determine the cause of obstruction.

The overall accuracy of CT in diagnosing biliary obstruction has been reported at 85 to 95%.

Hallmark of biliary obstruction in CT is biliary dilatation, it appears as confluent linear structures of water density that course with portal vein and gradually increase in size as they course towards the hilum. The dilated extrahepatic biliary ducts measure 8-10 mm in dimension. In post cholecystectomy patients ducts up to 10 mm may be considered normal in size. With high resolution, thin sections CT studies its normally possible to see non-dilated extrahepatic ducts.

Level and Extent of Obstruction

The dilated ducts can be traced on consecutive images to the transition point at which the caliber of ducts decrease or the duct disappears. The transition is best seen with thin collimation axial images along the course of the biliary tree, gallbladder dilatation is seen in more than 50% of distal duct obstruction. Pancreatic duct dilatation is seen in the distal common duct or ampullary obstruction.

Cause of Obstruction

The reported accuracy of CT for determining the cause of obstruction is 65-94%. Differential diagnosis is based at the level of obstruction. Intrahepatic duct obstruction can be caused by strictures secondary to sclerosing cholangitis, infection, neoplasm.

At hilum obstruction is commonly due to a cholangio or hepatic malignancy.

In the suprapancreatic portion stricture can be benign or malignant, distal pathologies include CBD calculi, tumor, pancreatic malignancy or ampullary tumor.

BILIARY TRACT DISEASES

Choledocholithiasis

USG is often the first step study in evaluating a patient with biliary colic, its reported sensitivity ranges from 80-84%, CT has a reported sensitivity in the range of 90%. The sensitivity of CT depends on a large extent to the type of stone and the technique used.

CT performed with thin collimation of 3-5 mm with overlapping reconstructions are found to be very helpful, oral administration of positive contrast may confuse the picture and its preferable to perform a plain study or use water as a negative contrast media. Even with good planning stones may elude detection because of their composition.

The primary sign of stone in the common duct is a radiopaque filling defect in the lumen, this sign may be seen even in a nondilated system, another sign to look for is the target sign which consists of higher central density of stone surrounded by the halo of bile. Rim sign is seen in some cases where there is central lucency surrounded by a thin rim of high attenuation, representing a peripheral calcified layer of the stone (Figs 3.24 to 3.26).

CHOLANGIOCARCINOMA (CCA)

Cholangiocarcinoma is an adenocarcinoma that arises from the bile duct epithelium. It is the second most prevalent liver cancer after hepatocellular carcinoma, comprising 5-1% of all malignancies, usually occurring 6-7th decade, with a slight male predominance.

The clinical manifestation depends on where the tumor arises, intrahepatic tumor usually presents with abdominal pain. Hilar and distal ductal tumors present early with painless jaundice.

Predisposing condition includes inflammatory bowel disease, sclerosing cholangitis, biliary enteric anastomosis, gallstone disease.

It is usually classified as either intrahepatic or extrahepatic. Intrahepatic cholangiocarcinoma is further classified as either peripheral or hilar. In the surgery literature, a tumor that arises peripheral to the secondary bifurcation of the left or right hepatic duct is considered to be peripheral cholangiocarcinoma, whereas a tumor that arises from one of the hepatic ducts or the bifurcation of the common hepatic duct is considered to be hilar cholangiocarcinoma (Klatskin tumor). These three types of cholangiocarcinoma—extrahepatic, peripheral intrahepatic, and hilar intrahepatic—are traditionally regarded as distinct disease entities clinically, therapeutically, and radiologically.

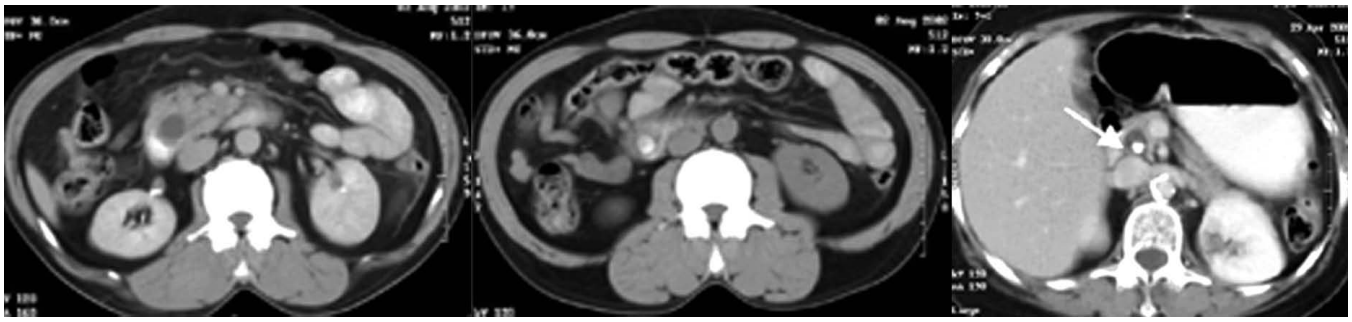

FIGURES 3.24A to C: Axial CECT shows meniscus sign of CBD calculus (crescent is formed by rim of low attenuation bile –arrow).

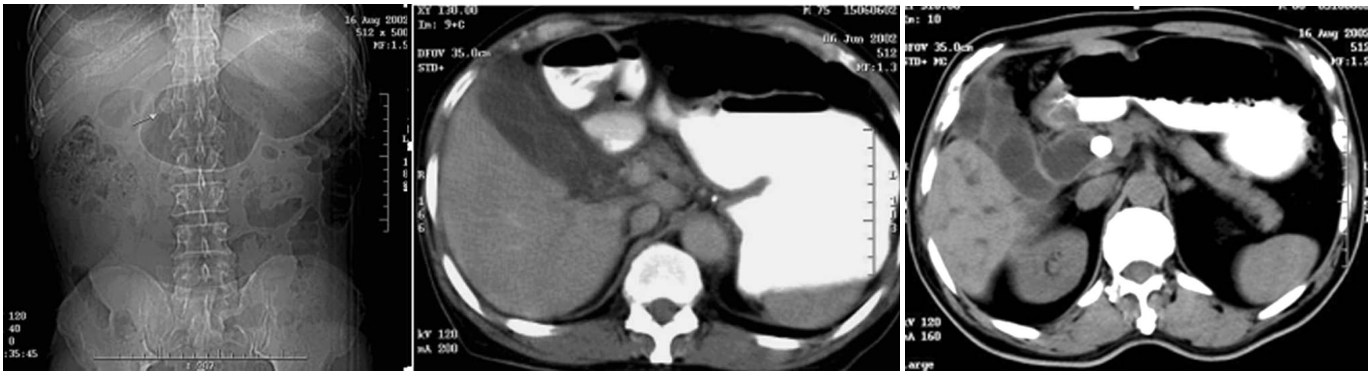

FIGURES 3.25A to C: Axial CECT reveals distended gallbladder with pericholecystic fluid and thickening of the wall with a impacted gallstone in the CBD.

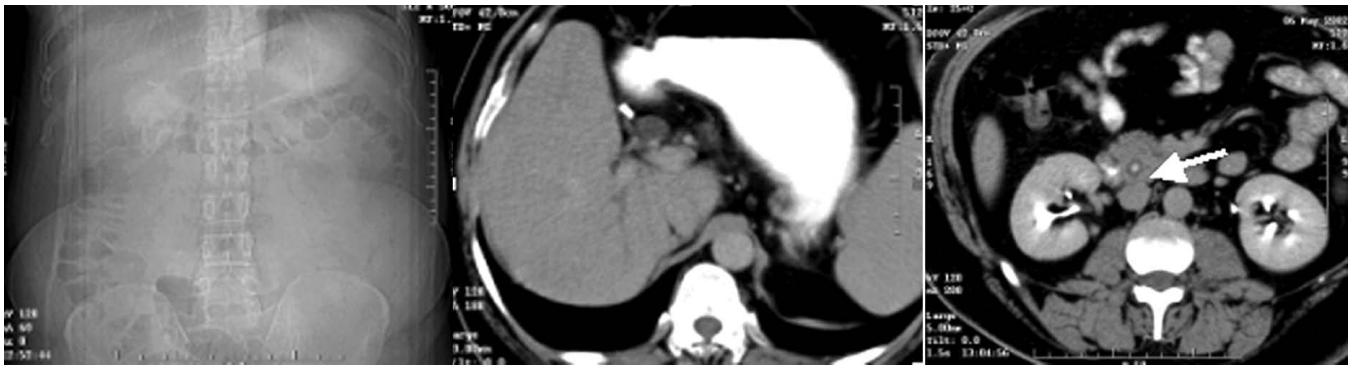

FIGURES 3.26A to C: Axial CECT (postcholecystectomy status) reveals a surgical clip in the gallbladder fossa, distal CBD calculus showing a target sign (Central high attenuation due to calculus with a circumferential rim of bile–arrow).

Intrahepatic Cholangiocarcinoma

Mass-forming intrahepatic cholangiocarcinoma: Mass-forming intrahepatic cholangiocarcinoma (peripheral cholangiocarcinoma) is the most common type of intrahepatic cholangiocarcinoma. At gross pathologic examination, peripheral cholangiocarcinoma typically manifests as a large, white tumor with dense fibrosis. Peripheral cholangiocarcinomas are usually large because they are rarely symptomatic early in their course. At CT, peripheral cholangiocarcinoma has been described as an irregular mass with markedly low attenuation, minimal peripheral enhancement, and focal dilatation of intrahepatic ducts around the tumor. At spiral CT, peripheral cholangiocarcinoma usually demonstrates thin, incomplete rim enhancement during both the arterial and portal venous phases. The central part of the tumor does not enhance during these phases, whereas there may be prolonged enhancement at delayed-phase CT. Frequently noted ancillary findings in peripheral cholangiocarcinoma include capsular retraction and dilatation and thickening of the peripheral intrahepatic ducts (especially when associated with clonorchiasis) (Fig. 3.27).

Differential diagnosis for this lesions include hcc, biliary cystadenoma and metastasis.

Intraductal intrahepatic cholangiocarcinoma: Intraductal intrahepatic cholangiocarcinoma has a better prognosis than other types of cholangiocarcinoma and, in some instances, a peculiar growth pattern characterized by superficial mucosal spreading. At CT, characteristic features include segmental or lobar dilatation of the intrahepatic bile duct

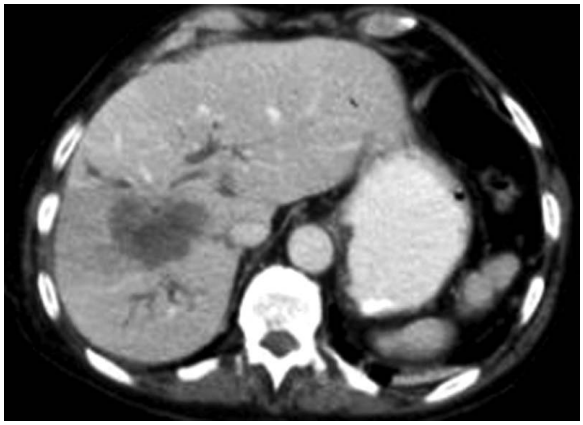

FIGURE 3.27: Axial CECT reveals a large hypodense lesion in the right lobe of liver with adjacent segmental intrahepatic biliary radicle dilatation.

with higher attenuation than that of bile. An obstructing mass is occasionally seen as a low-attenuation lesion when it is larger than 1 cm. Because of its peculiar growth patterns, this type of cholangiocarcinoma is thought to be a distinct entity rather than an early manifestation of the more typical mass-forming intrahepatic cholangiocarcinoma

Periductal infiltrating intrahepatic cholangiocarcinoma: Periductal infiltrating intrahepatic cholangiocarcinoma is radiologically and pathologically identical to infiltrating hilar cholangiocarcinoma (Klatskin tumor) but has a different location (i.e. peripheral to the secondary confluence). Very small fibrotic tumors cause segmental dilatation of the bile ducts. Unlike with intraductal intrahepatic cholangiocarcinoma, the bile ducts are isoattenuating relative to water, unless secondary biliary stones or sludge is formed. In the later stage, the tumor may invade the hepatic parenchyma and hepatic hilum.

Hilar cholangiocarcinoma: Hilar cholangiocarcinomas account for more than 50% of all large bile duct malignancies. The middle and distal portions of the common bile duct are affected in about 17% and 18% of these cases, respectively; Tumors originating from a large bile duct are in a critical location and are discovered early due to the presence of jaundice or cholangitis. Thus, these tumors are usually very small. Conversely, tumors originating from small bile ducts do not cause significant biliary obstruction until the late stage, when the tumor itself or metastatic hilar lymphadenopathy causes obstruction of the common hepatic duct. Therefore, most peripheral cholangiocarcinomas are large at the time of diagnosis.

Infiltrating hilar cholangiocarcinoma: Infiltrating hilar cholangiocarcinoma is the most common type of hilar cholangiocarcinoma (over 70% of cases). At contrast-enhanced CT, infiltrating tumors are seen as a focally thickened ductal wall obliterating the lumen. About 80% of these tumors are hyperattenuating relative to the liver.

Exophytic hilar cholangiocarcinoma: Exophytic hilar cholangiocarcinoma manifests as a large, low-attenuation mass with peripheral rim enhancement, findings that are similar to those in peripheral cholangiocarcinoma. The lesion may also represent infiltrating intrahepatic cholangiocarcinoma that involves the hepatic hilum by intraductal spreading and the hepatic parenchyma by direct invasion.

Polypoid hilar cholangiocarcinoma: Polypoid hilar cholangiocarcinoma manifests as an intraductal soft-tissue mass that is hypoattenuating relative to the hepatic parenchyma. The tumors are frequently multiple or disseminated within the biliary system and involve both the intrahepatic and extrahepatic bile ducts. Their site of origin determines the presenting symptoms.

Extrahepatic Cholangiocarcinoma

Infiltrating extrahepatic cholangiocarcinoma: Infiltrating extrahepatic cholangiocarcinoma is the most common type of cholangiocarcinoma involving the extrahepatic bile duct. It manifests as a high-attenuation mass or thickened wall at the site of biliary obstruction and has radiologic and pathologic features that are identical to those of hilar cholangiocarcinoma. On axial thin section CT scans, the dilated extrahepatic bile duct suddenly disappears and the lumen is replaced by a small, high-attenuation mass encircling the lumen.

*Polypoid extrahepatic cholangiocarcinoma***:** Polypoid extrahepatic cholangiocarcinoma manifests as a low-attenuation mass within the dilated bile duct and is identical to masses in the hilar area or intrahepatic ducts. This tumor frequently demonstrates extensive superficial spreading, resulting in diffuse involvement. The true extent of the tumor is difficult to determine. The benign counterpart of polypoid extrahepatic cholangiocarcinoma is known as papilloma or papillomatosis.

CCA arising from the extrahepatic ducts is the most common form of this tumor. Grossly these tumors are sclerosing and infiltrative, although it may be exophytic or polypoidal in some cases. Most common site for these tumors are the confluence of the right and left ducts with the common duct the so called Klatskin tumor which spreads along the ducts with fibrosis. The typical CT findings for these tumors is finding of dilated RT and left IHBR with non-union in the hilum or a hypodense mass in the hilum. Common site for nodal metastasis involve primarily the foramen of Winslow node, superior pancreaticoduodenal nodes, distal metastasis to liver, lung and bones have been documented (Figs 3.28 and 3.29).

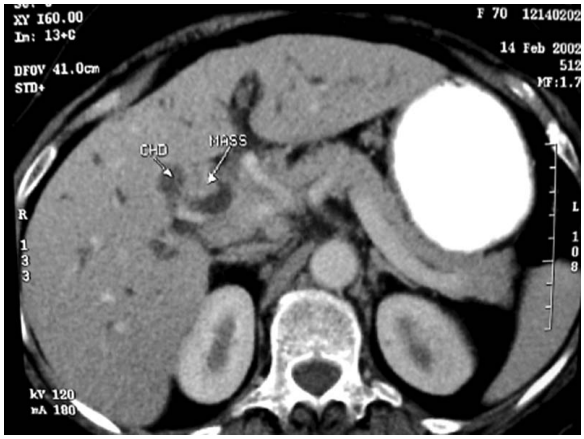

FIGURE 3.28: Axial CECT shows a polypoidal intraluminal mass (arrow).

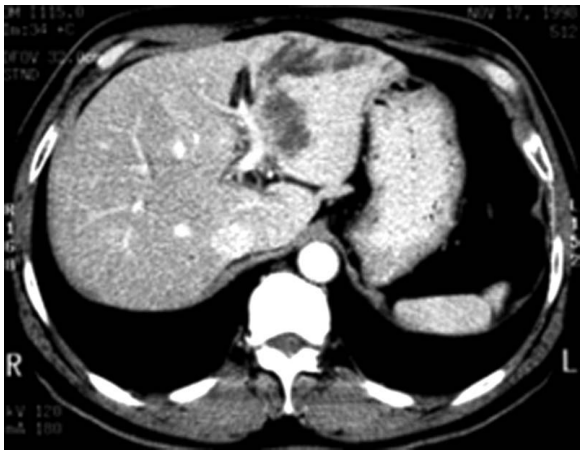

FIGURE 3.29: Axial CECT reveals a ill-defined infiltrative lesion involving the left lobe of liver with patchy enhancement. Lobar atrophy has been described with CCA particularly the hilar type, one of the causes postulated for atrophy includes biliary dilatation.

Choledochal Cyst

Choledochal cyst are congenital cystic dilatations of any portion of the bile duct, its postulated that this condition begins with an anomalous junction of CBD and pancreatic duct proximal to duodenal papillae, this anomalies is associated with anomalies of gallbladder. Complications include cholangitis, calculus formation, rupture and malignant transformation. Patient presents with a triad of right upper quadrant pain, intermittent jaundice and a palpable right upper quadrant mass (Figs 3.30 and 3.31).

Classification

Todanis

Type1—solitary fusiform dilatation of the extrahepatic duct
Type 2—extrahepatic supraduodenal diverticulum
Type 3—intraduodenal diverticulum – choledochocele.
Type 4
4a—multiple cysts involving intra- and extrahepatic bile ducts
4b—multiple extrahepatic ducts.
Type 5—multiple intrahepatic cysts – Carolis disease.

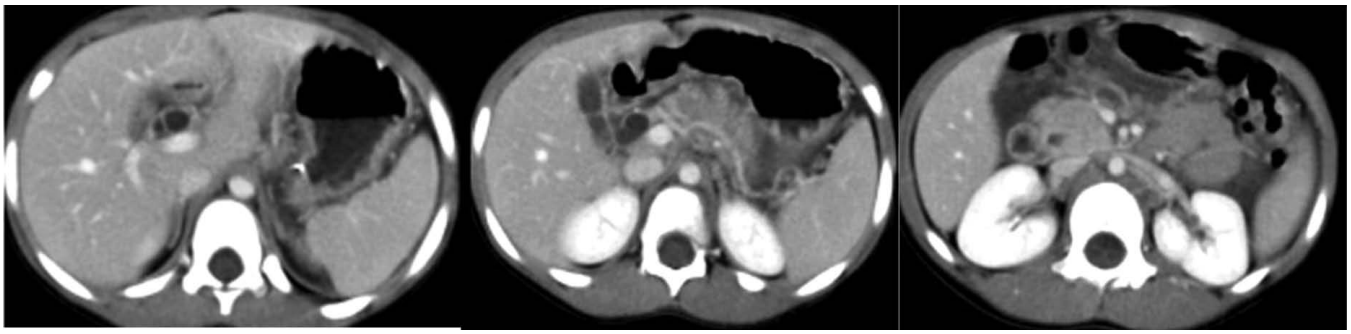

FIGURES 3.30A to C: Axial CECT reveals fusiform dilatation of the common bile duct in a 5-year-old female patient who presented with pancreatitis.

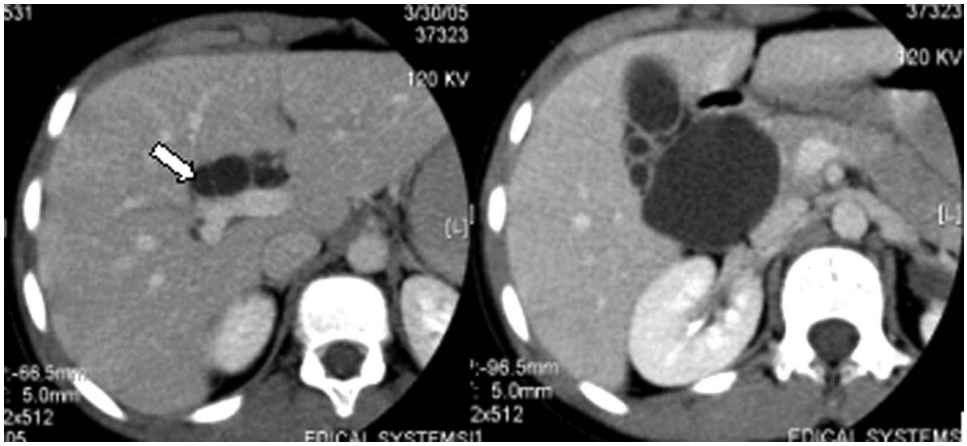

FIGURES 3.31A and B: Axial CECT reveals fusiform dilatation of CBD and the common hepatic ducts (arrow in A) in a 17-year old boy presenting with upper abdominal pain.

Pyogenic Cholangitis (Oriental Cholangitis)

Patients present with right upper quadrant pain, fever and chills with jaundice, the natural history is characterized by exacerbation and remission of cholangitis, parasitic infestation, malnutrition, and portal bacteremia are common predisposing etiologies. USG and CT reveal dilated ducts containing stones and sludge, all segments may be involved but the lateral segment of left lobe is commonly involved. Additional finding includes fatty metamorphosis, duct wall enhancement, hepatic abscess and pneumobilia. Bile duct wall thickening is mild ranging from 2-3 mm in an eccentric and diffuse distribution (Figs 3.32A and B).

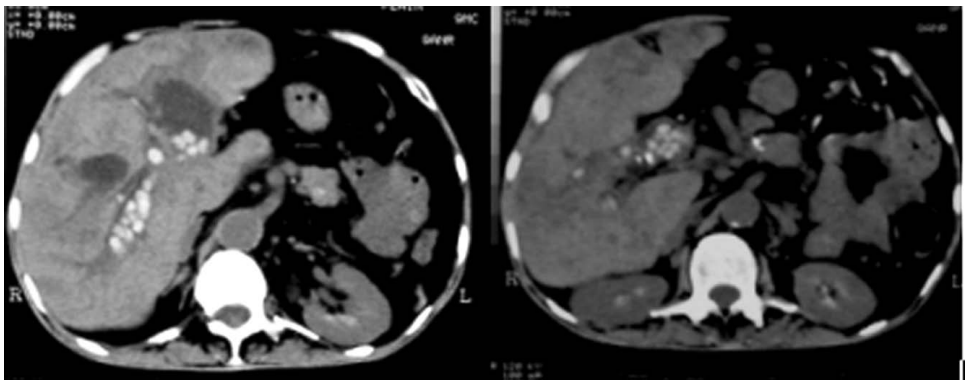

FIGURES 3.32A and B: Axial CECT in a 26-year-old male patient presenting with fever and right upper quadrant pain reveals dilated intrahepatic biliary radicles with multiple ductal calculi within.

Sclerosing Cholangitis

Primary sclerosing cholangitis is a chronic cholecystic disease of unknown etiology characterized by fibrosing inflammation of biliary tree. The term primary is used when it is associated with inflammatory bowel disease, retroperitoneal fibrosis and thyroditis, the term secondary is used when it is secondary to CBD stone, surgical trauma, chemicals and ischemia.

Clinical feature includes fatigue, pruritis, jaundice and right upper quadrant pain, USG and CT features include IHBR dilatation usually mild and focal, intrahepatic stenosis are depicted by presence of peripheral isolated ductal dilatation *termed as skip dilation,* their findings include pruning with feature of cirrhosis and wall thickening usually not exceeding 5 mm (> 5 mm wall thickness should raise the suspicion of malignancy).

Cholangiocarcinoma is a known complications with reported frequencies of 6 to 9%.

Pneumobilia

Air within the intrahepatic bile ducts seen as low density branching structures (Figs 3.33A and B).

Causes

- Incompetent sphincter of Oddi.
- Gallstone ileus.
- Trauma
- Postoperative
- Emphysematous inflammation.

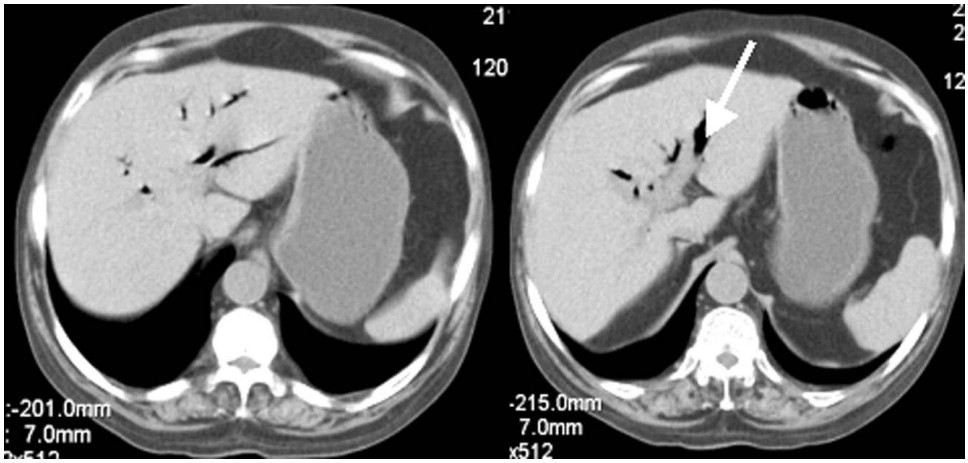

FIGURES 3.33A and B: Axial non-contrast enhanced CT reveals linear hypodensities suggestive of air within the biliary tree (arrow).

CHAPTER

4

Spleen

HELICAL CT

The helical CT appearance of the spleen largely depends on the timing of intravenous bolus administration of contrast material. Spleen may demonstrate heterogeneous enhancement during the first minute after initiation of intravenous administration of contrast material because of the different rates of flow through the cords of the red and white pulp. This heterogeneity is itself variable in appearance; patterns include arciform (alternating bands of high and low attenuation focal and diffuse heterogeneity). The frequency of these artifacts increases with increased injection rate. Familiarity with these enhancement characteristics minimizes the chance that artifacts will be mistaken for disease. In more than 95% of pediatric CT examinations, splenic heterogeneity is resolved within 70 seconds of the initiation of contrast material injection. Consequently, low-attenuation lesions that are seen after this time should raise suspicion for a disease process. Helical CT scans obtained during the portal venous phase usually demonstrate homogeneous attenuation throughout the spleen.

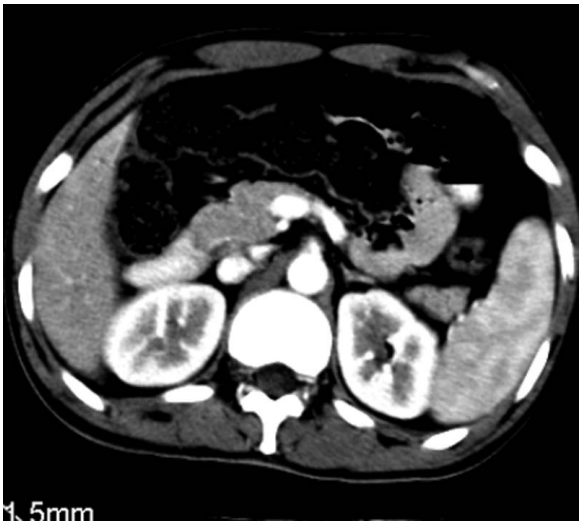

FIGURE 4.1: Axial CECT in early phase of IV contrast shows the alternating bands of high and low attenuation suggestive of the typical appearance of Moire spleen.

CT demonstrates the size, shape and location of the normal spleen as well as intrasplenic abnormalities.

Artifacts due to motion, beam hardening, or dynamic scanning can be done, important relationships to spleen with pancreatic tail, left lobe of liver, diaphragm, left adrenal gland, left kidney, stomach, splenic flexure and adjacent omental fat should be evaluated as pathologies in these regions can affect the spleen.

The spleen is commonly involved in a variety of pathologic processes. Some of these processes cause isolated splenic disease, whereas others involve the spleen as part of a systemic illness. Splenic anomalies are categorized as anomalies of splenic shape (clefts, notches, lobules).

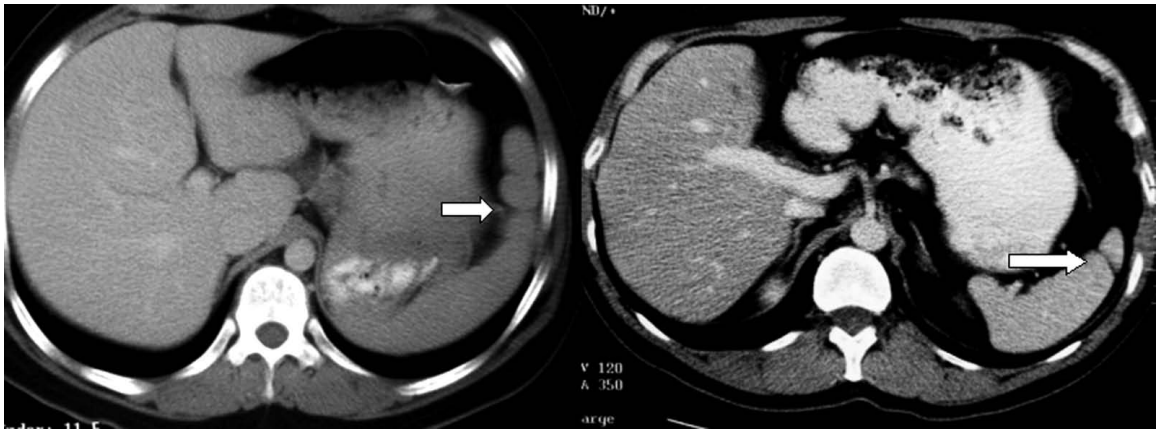

FIGURES 4.2A and B: Axial CECT in two different patients shows physiological cleft and notching (arrows).

Splenic clefts, notches, and lobules may persist into adult life as variations in normal shape. In addition, the spleen may be found in a variety of locations. Congenital diaphragmatic eventrations or hernias can lead to an intrathoracic location or a deep lateral peritoneal recess can leave the spleen lying posterior to the left kidney. Failure of the individual clumps of mesenchymal cells to fuse properly results in accessory spleens, which are found in upto 30% of autopsies. These spleens vary from a few millimeters to several centimeters in size. Accessory spleens range from one to six in number and are usually found near the splenic hilum, along the course of the splenic vessels, or within the layers of the omentum.

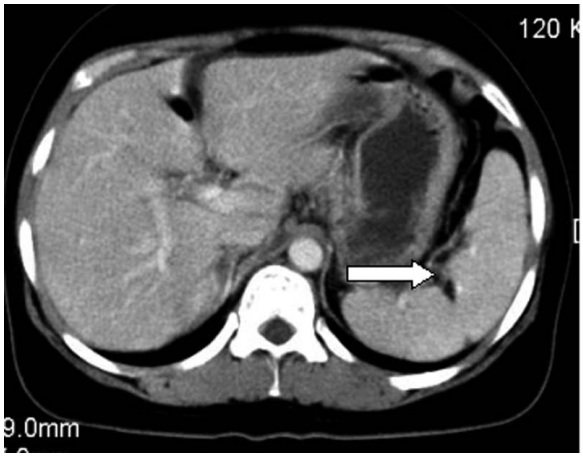

FIGURE 4.3: Axial CECT showing median splenic cleft (arrow).

WANDERING SPLEEN

Ligament laxity may result in splenic hypermobility, the entity is rare with a incidence 2%. Condition can be congenital due factors like abnormal fusion of the posterior mesogastrium, acquired causes may be due to hormonal effects and abdominal laxity associated with pregnancy, it has also been reported in cases of splenic enlargement due to malaria, Hodgkin's disease.

Most cases are diagnosed in adults, usually multiparus women 20-40 years. Diagnosis is made incidentally. Symptoms occur when there is torsion, torsion more than 180 degree leads to splenic infarction. Intermittent torsion may cause hypersplenism.

CT scans show change in shape and position, if torsion has occurred then there is change in the attenuation with areas of segmental infarction. Whorl sign may be present at the site of the torsion.

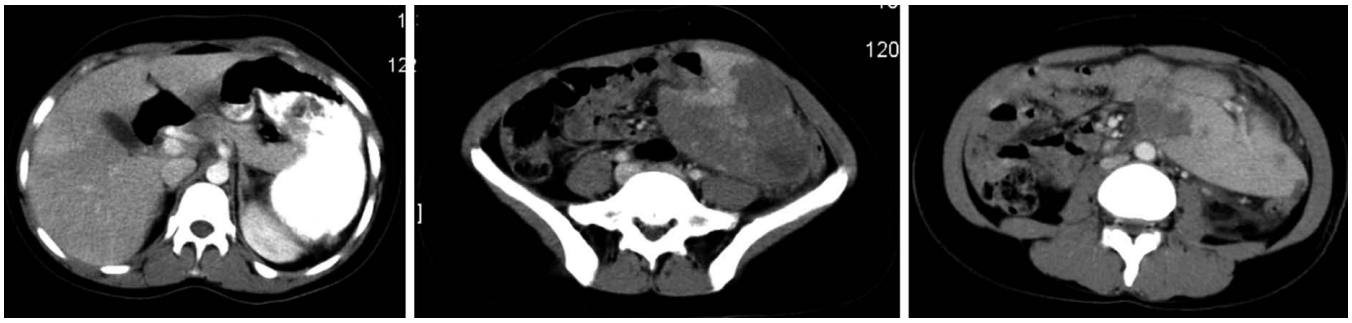

FIGURES 4.4A to C: Axial CECT reveals absent spleen in the left hypochondrium with posterior displaced fundus, left iliac fossa shows spleen with multiple areas of hypodensities – suggestive of wandering spleen with infarcts.

NUMBER (POLYSPLENIA, ASPLENIA)

Abnormalities in splenic size, number, and location can also accompany congenital heart disease. Either polysplenia or asplenia may be seen with abdominal situs ambiguous. Polysplenia is more common in females. In polysplenia, numerous small splenic masses can be seen predominantly in the right upper quadrant. Additional features of polysplenia syndrome include interruption of the infrahepatic portion of the inferior vena cava with azygous continuation and a tendency for bilateral distribution of left-sided viscera. Associated cardiac disease is usually amenable to surgery and commonly takes the form of acyanotic left-to-right shunts such as septal defects . Malrotation of the bowel and absence of the gallbladder have also been reported.

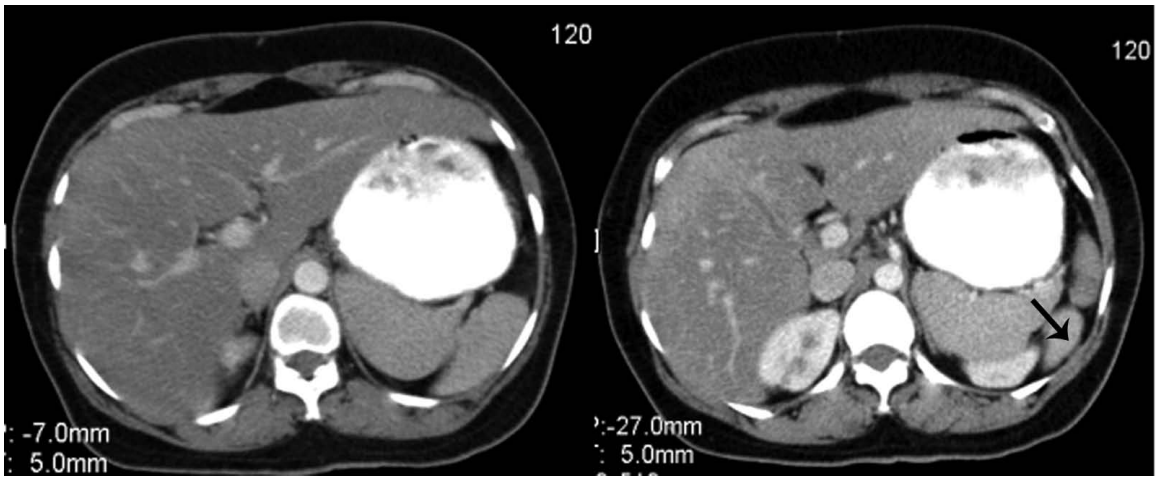

FIGURES 4.5A and B: CECT reveals multiple well marginated soft tissue in the left hypochondrium suggestive of splenenculi.

SIZE (SPLENOMEGALY, SPLENIC ATROPHY)

Splenomegaly is seen usually secondary to infiltrative diseases like leukemia, lymphoma, myelofibrosis, Gaucher's disease. Infective disease like malaria, vascular disorders like portal hypertension.

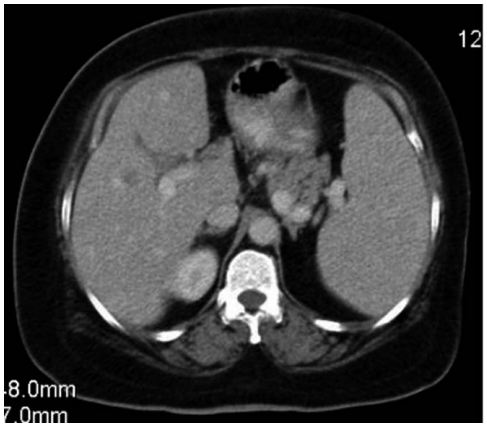

FIGURE 4.6: Axial NECT in a patient with malaria showing splenomegaly.

ATROPHY

Autosplenectomy noted in hemolytic anemia.

Autosplenectomy

End stage spleen – seen in patients with homozygous sickle cell anemia with extensive areas of fibrosis with deposition of calcium and hemosiderin. On CT spleen is small and calcified.

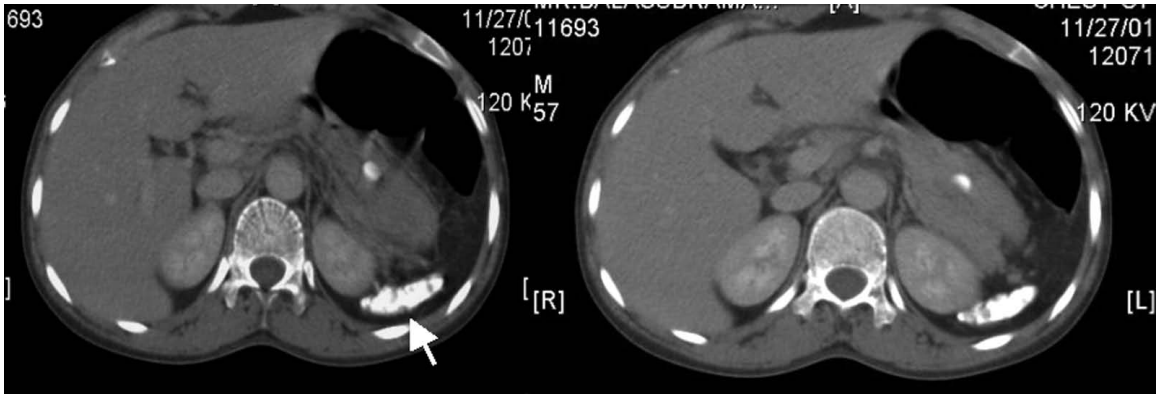

FIGURES 4.7A and B: Axial CECT reveals a shrunken calcified spleen (arrow)

SOLITARY LESIONS (E.G. CYSTS, LYMPHANGIOMAS, HEMANGIOMAS, HAMARTOMAS)

Cysts

Splenic cysts are classified as either true cysts (i.e. having an epithelial cell lining) or pseudocysts (i.e. lacking an epithelial cell lining). True cysts include congenital or epidermoid cysts and parasitic cysts secondary to ecchinococcal infection. Pseudocysts tend to follow trauma or infarction. Reliable differentiation between true cysts and pseudocysts is usually not possible at imaging. Complications of splenic cysts include infection and cystic rupture.

Epidermoid cysts account for 10% of all benign, nonparasitic splenic cysts worldwide. At US, epidermoid cysts manifest as well-defined, thin-walled anechoic lesions that do not change over time. Wall calcification has been reported in 10% of cases. Septations and cyst wall trabeculation may also be present. Intracystic fluid may have increased echogenicity due to cholesterol crystals, inflammatory debris, or hemorrhage. At CT, epidermoid cysts manifest as rounded, well-demarcated nonenhancing lesions with near water attenuation.

Lymphangiomas

Lymphangiomas are vascular lesions that may be single or multiple. When they are multiple, these lesions may form part of a generalized angiomatosis. At histopathologic analysis, lymphangiomas are made up of multiple endothelium-lined vascular channels filled with lymph. Capillary, cavernous, and cystic lymphangiomas have been identified, depending on the size of the channels CT may demonstrate splenomegaly with calcification in the dilated lymphatic vessels. CT imaging typically demonstrates septate, subcapsular cystic lesions. Curvilinear calcification can be seen at CT.

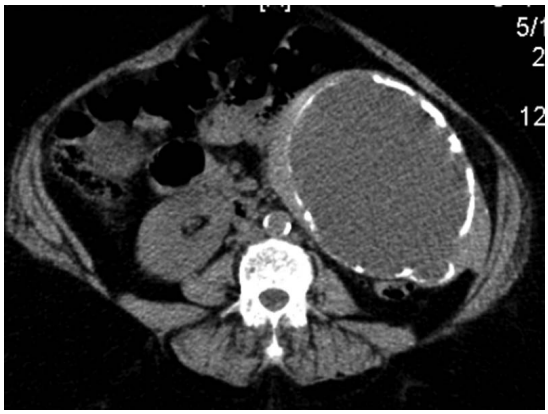

FIGURE 4.8: Axial CECT reveals a calcified hypodense lesion in the inferior pole of spleen suggestive of a splenic cyst with rim of calcification.

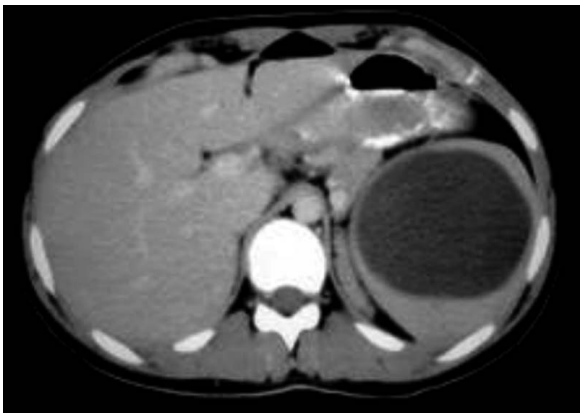

FIGURE 4.9: Axial CECT reveals a well marginated hypodense cyst note the smooth walls.

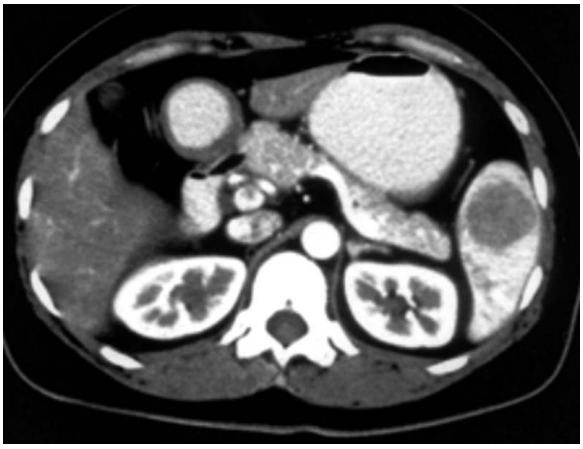

FIGURE 4.10: Axial CECT reveals a well marginated hypodense non-enhancing lesion in the anterior margin of spleen – proved to be a case of hamartoma.

Hemangiomas

Hemangiomas are the most common primary neoplasm of the spleen and are composed of endothelium-lined vascular channels filled with red blood cells. The lesions are divided into capillary and cavernous types, depending on the size of the channels. They may appear cystic, solid, or a combination of the two at imaging. Like lymphangiomas, hemangiomas may be multiple and form part of a generalized angiomatosis such as Klippel-Trénaunay-Weber syndrome. Hemangiomas have also been reported in association with Beckwith-Wiedemann syndrome and Turner syndrome. The lesions are usually asymptomatic but can cause portal hypertension, splenic rupture or Kasabach-Merritt syndrome. The latter can occur with large hemangiomas anywhere in the body secondary to platelet trapping, consumptive coagulopathy, or anemia.

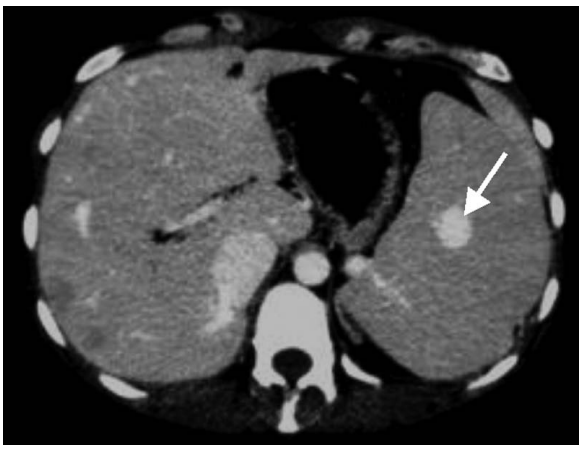

FIGURE 4.11: Axial CECT reveals a hyperdense well marginated enhancing lesion with features of hemangioma, (arrow).

Infection and Inflammation

The rarity of primary splenic abscesses is probably related to splenic phagocytic immune functions. A splenic abscess may be bacterial, fungal, or granulomatous. In infants and children, splenic abscesses occur most frequently in immunocompromised patients. Abscesses may be single or multiple. With fungal infections in an immunocompromised patient, abscesses are typically multiple.

Pyogenic abscesses can be secondary to underlying sepsis or spread by hematogenous seeding. Amebic dysentery, otitis media, mastoiditis, peritonsillar abscess, cutaneous infection, pneumonia, empyema, appendicitis, osteomyelitis, and intravenous drug abuse are all risk factors. Patients with hemoglobinopathies are also at risk for splenic abscess formation secondary to infarction and necrosis as well as functional asplenia.

Pyogenic abscesses manifest as ill-defined, hypoechoic lesions at US. Debris and internal septations may be present. In rare cases, gas bubbles may be seen. If present, intralesional gas is pathognomonic for pyogenic infection. At CT, pyogenic abscesses typically manifest as single, irregularly marginated lesions with low attenuation. Rim enhancement can be seen on contrast-enhanced scans.

Fungal abscesses are small lesions, typically only a few millimeters in diameter. The most common infecting organisms are *Candida albicans*, *Aspergillus fumigatus*, and *Cryptococcus neoformans*. *M. tuberculosis, M. avium intracellulare,* and *P. carinii* infection can have similar appearances. Fungal abscesses have a variable appearance at US. Typically, they manifest as rounded, hypoechoic lesions with a central area of increased echogenicity, creating a "target" or "bull's-eye" appearance. These findings correspond to fibrotic tissue surrounding a central inflammatory core at histopathologic analysis. The "wheel-in-a-wheel" appearance is seen when the central hyperechoic portion becomes necrotic and hypoechoic. Hepatosplenomegaly is usually associated with fungal abscesses. CT typically demonstrates multiple small, low-attenuation lesions. The lesions may be missed unless intravenously administered contrast material is used.

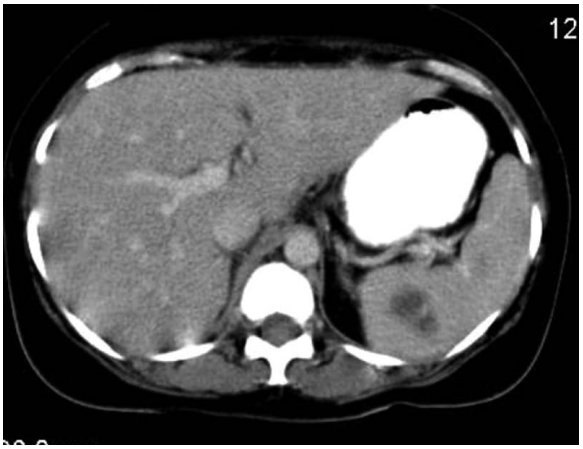

FIGURE 4.12: CT findings – bacterial abscess in CT is suggested by a thick irregular, dense rim surrounding a low density center of necrotic tissue.

Splenic abscess: The cause and root of infection have been classified into: (1) metastatic infection (sepsis), (2) contiguous infection (infected perinephric abscess, pancreatitis), (3) embolic noninfectious events with subsequent secondary infection, (4)immunodeficiency states.

Granulomatous Lesion

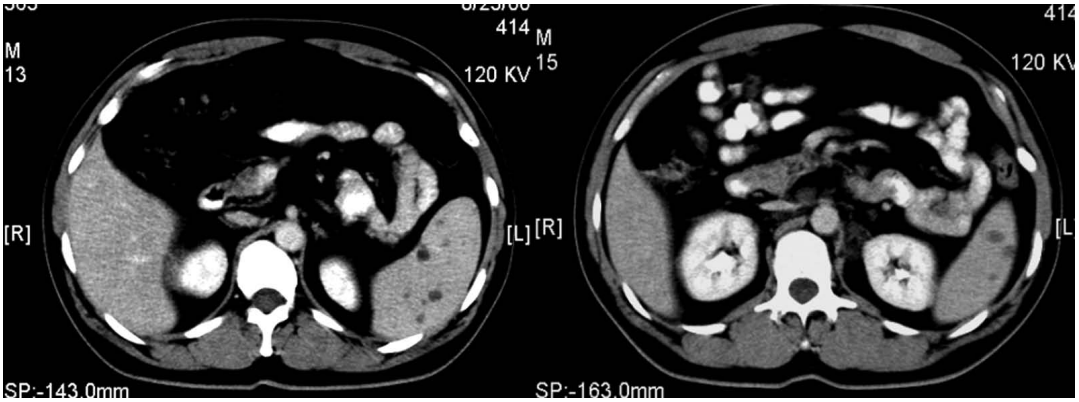

FIGURE 4.13: Axial CECT in a 20-year-old female patient who had features of military TB on CXR reveals multiple nodular hypodense lesions in the spleen.

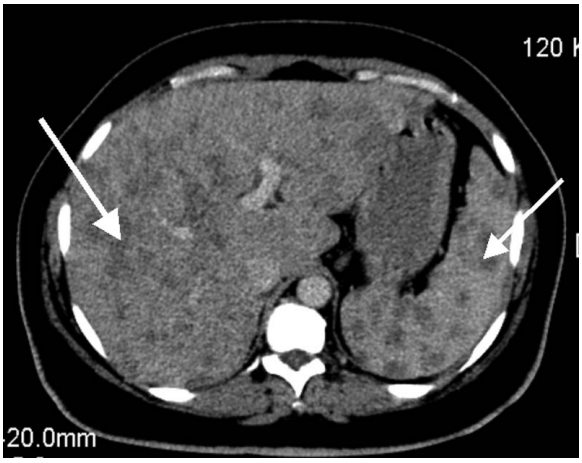

FIGURE 4.14: Axial CECT in an immunocompromised female patient reveals multiple hypodense lesion in both liver and spleen (arrows) case of candidiasis.

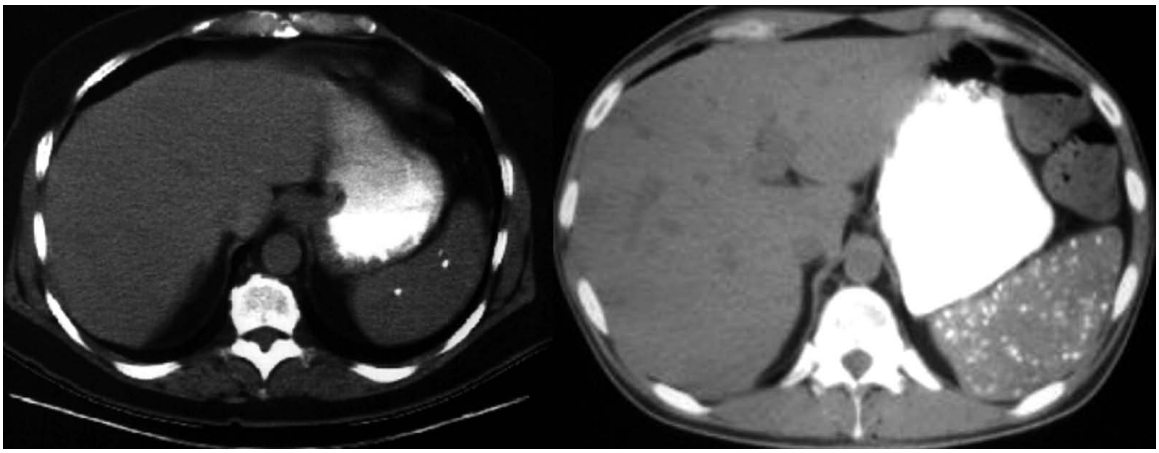

FIGURES 4.15A and B: Axial plain CT reveals multiple punctuate calcifications in the spleen in a patient with childhood military TB.

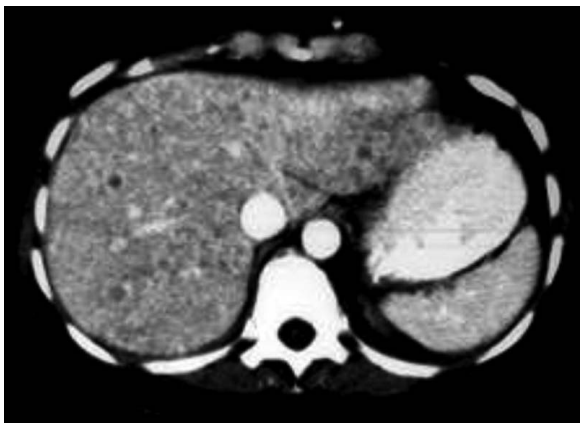

FIGURE 4.16: Axial CECT showing microabscess seen as non enhancing hypodense lesions typically smaller than 2 cm, more conspicuous in the liver

Splenic Calcifications

- Infections like tuberculosis, histoplasmosis, healed PCP
- Hematoma, hemangioma
- Infarct, congenital cyst, chronic abscess
- Hydatid cyst, sickle cell anemia

Fungal microabscess seen in persons with compromised host defense mechanism who are receiving multidrug chemotherapy candida is the most common organism countered in these patients.

CT findings on CT microabscess are seen as well-defined non-enhancing hypodense lesions typically smaller than 2 cm.

MALIGNANCY

The majority of splenic malignancies are due to leukemia or lymphoma. Both Hodgkin and non-Hodgkin lymphoma can involve the spleen. Lymphomatous involvement of the spleen may manifest as either focal lesions or diffuse disease. Primary lymphoma arising within the spleen can invade the capsule and extend beyond the spleen. Diffuse involvement usually manifests as splenomegaly with no discernible alterations in splenic echotexture. This finding corresponds to infiltrative disease or tiny miliary deposits of lymphomatous tissue seen at pathologic analysis. The majority of focal lesions seen at US are hypoechoic and lack acoustic enhancement. At CT, lesions typically have low attenuation. CT is also useful in assessing lymphadenopathy at the splenic hilum and along the supporting ligaments. Multiple inhomogeneous lesions of varying size may be seen at contrast-enhanced CT. These lesions represent larger deposits of lymphomatous tissue.

Chronic Myeloid Leukemia

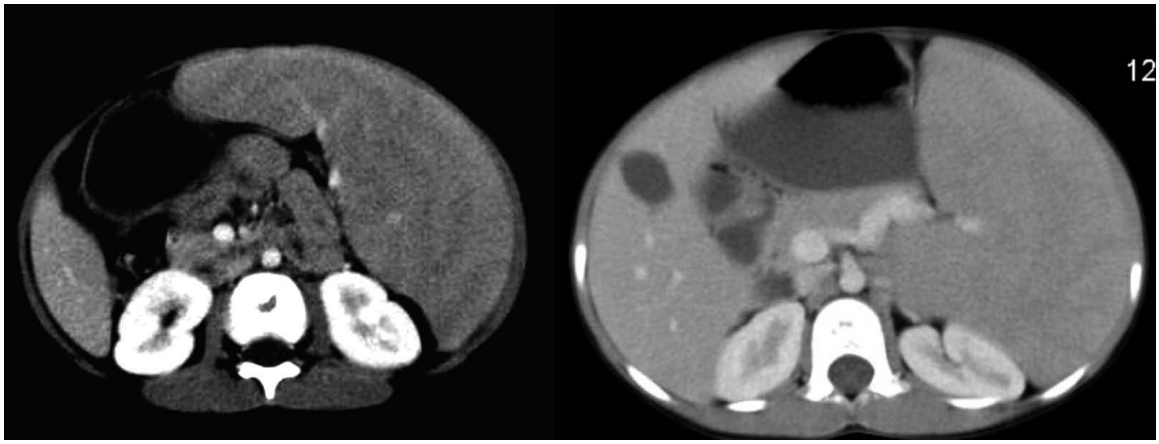

FIGURE 4.17: Axial CECT reveals a grossly enlarged spleen.

Hodgkin's Lymphoma

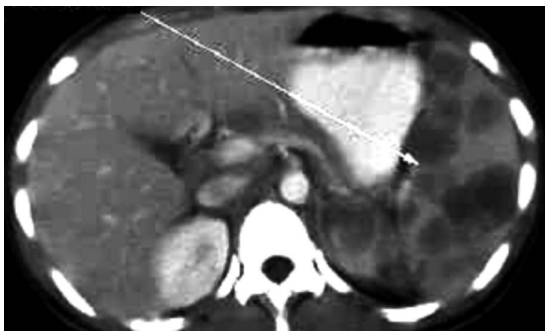

FIGURE 4.18: Axial CECT reveals a enlarged spleen with multiple hypodense lesions.

NonHodgkin's Lymphoma

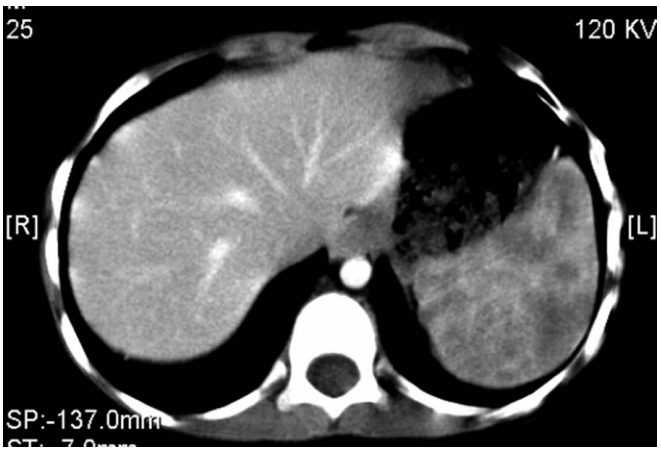

FIGURE 4.19: Axial CECT reveals a enlarged spleen with multiple hypodense lesions.

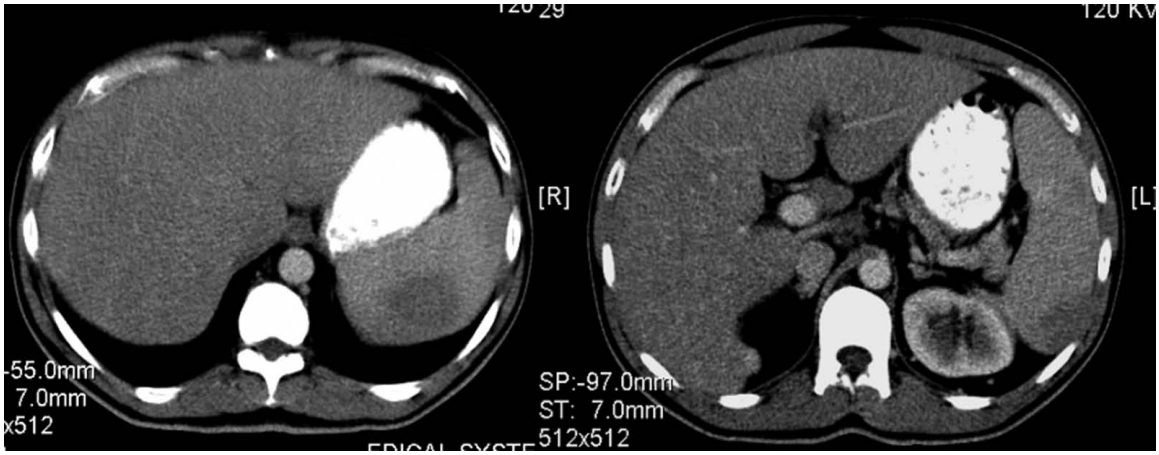

FIGURE 4.20: Axial CECT reveals a enlarged spleen with large hypodense lesions.

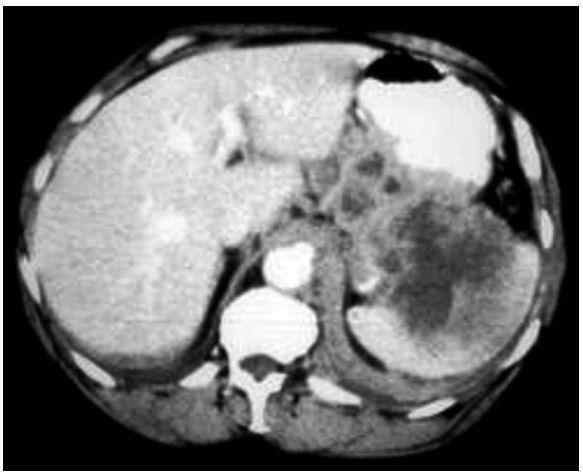

FIGURE 4.21: Axial CECT in a patient with carcinoma pancreas infiltrating the splenic hilum.

Diffuse Disease

Example: infarction, heavy metal deposition, hemangioendotheliomas, peliosis.

Infarction

Branches of the splenic artery are noncommunicating end arteries, and their occlusion leads to splenic infarction. In children, infarction usually occurs in the setting of sickle cell hemoglobinopathies and hematologic malignancies. Other recognized causes of infarction include cardiac emboli, torsion, collagen vascular disease, portal hypertension, and infiltrative disorders such as Gaucher disease. Complications of infarcts include acute febrile illness, abscess formation, splenic pseudocyst formation, splenic rupture, and hemorrhage. Splenic infarcts have a variable appearance at US. Initially, they appear as ill-defined, hypoechoic lesions. At histopathologic analysis, these findings are secondary to inflammation, edema, and necrosis. With organization and fibrosis, the lesions become increasingly well-defined and echogenic. The CT appearance of infarcts depends on the time elapsed since the insult. In the hyperacute phase, the spleen demonstrates a mottled echotexture secondary to hemorrhagic infarction with intravenous administration of contrast material. Over time, the lesions become better defined. Classically, they are peripheral and wedge-shaped, but they may have an irregular margin. With time, the anomalies may resolve completely, leaving only a cortical defect or a focus of calcification. In rare cases, the entire spleen may undergo infarction, leaving only a rim of enhancing capsule.

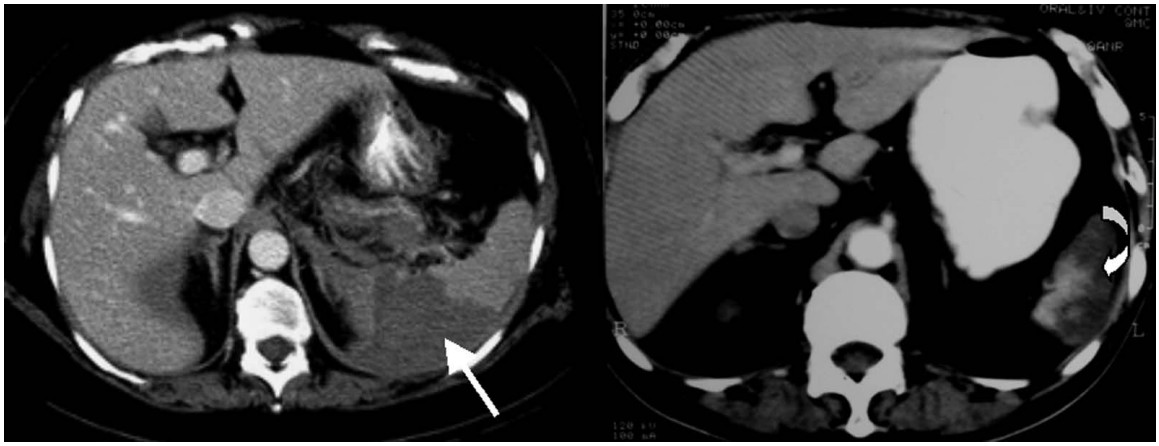

FIGURES 4.22A and B: Axial CECT reveals wedge shaped hypodensity in the spleen (arrow). Axial CECT reveals shrunken spleen with multiple peripheral hypodense areas suggestive of infarcts.

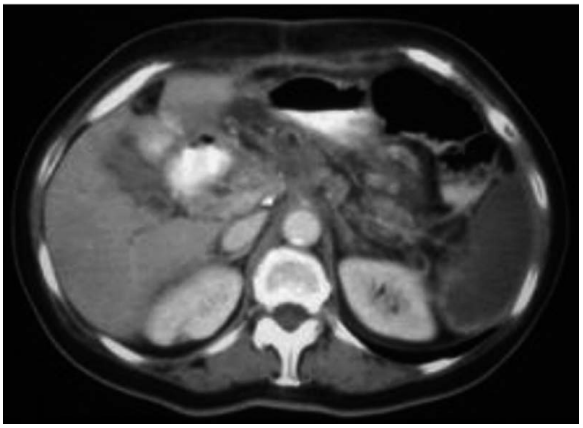

FIGURE 4.23: Axial CECT in a patient with subacute pancreatitis reveals hypodense pancreas suggestive of an infarct.

Splenic Hilar Collateral

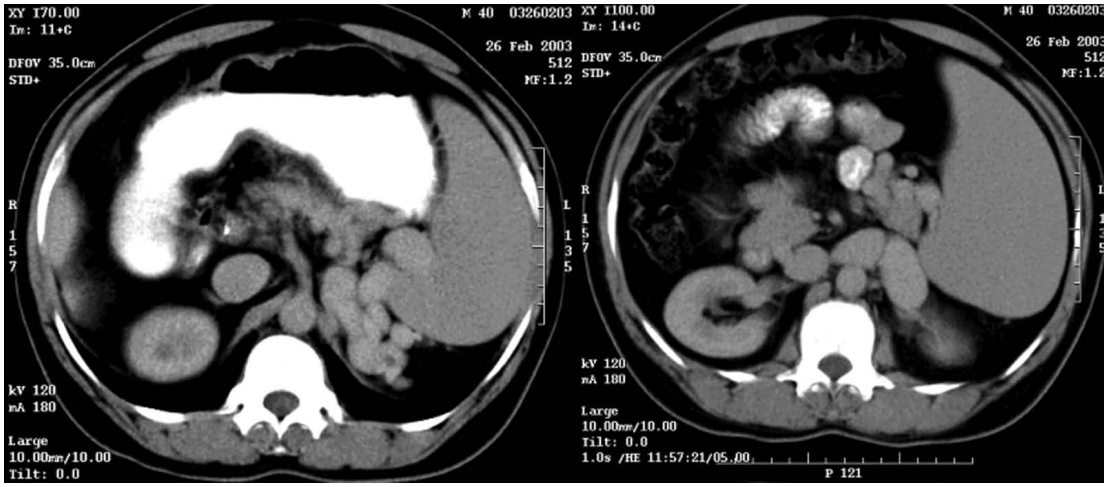

FIGURES 4.24A and B: Axial CECT reveals enlarged spleen with multiple tortous venous collaterals in the hilum and in the splenorenal areas.

Pseudoaneurysm

Discussion

Rupture of a pseudoaneurysm and bleeding into the abdominal cavity or gastrointestinal tract as a result of a different etiology, although with a different clinical presentation, is often associated with massive, life-threatening hemorrhage. The majority of pseudoaneurysms occur in pancreatitis, in association with or in close proximity to, pancreatic pseudocysts. In particular, although the natural history of pseudocyst in chronic pancreatitis is unpredictable, it can gradually erode the vascular wall of the adjacent vessels. This erosion has a double pathogenetic mechanism, enzymatic and mechanic. In the first case, the activated proteolytic enzymes in the liquid of the pancreatic pseudocyst cause necrotizing arthritis with a maceration of the vessel wall and bleeding inside the pseudocyst. The

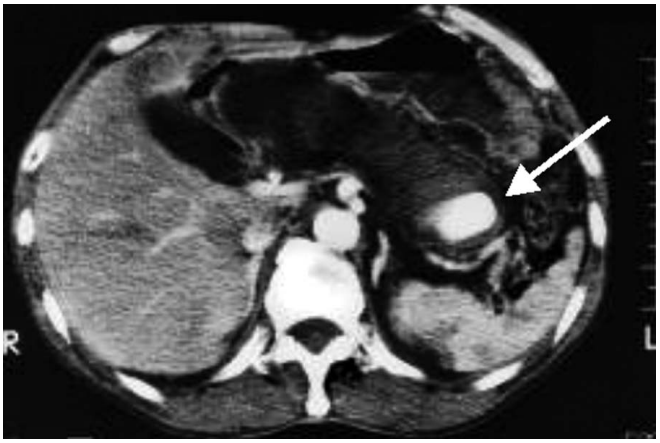

FIGURE 4.25: Axial CECT in a patient with pancreatitis reveals a focal hyperdense lesion in the region of pancreatic tail suggestive of a pseudoaneurysm (arrow).

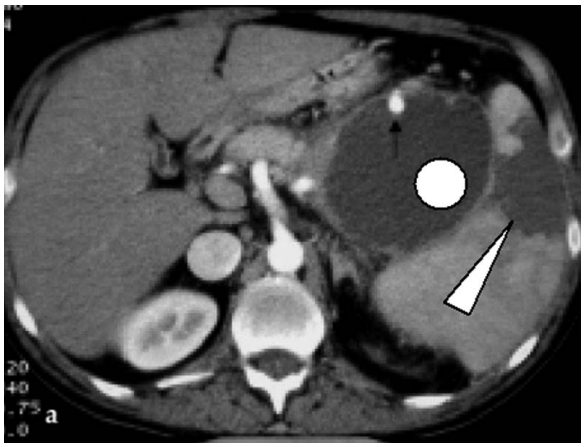

FIGURE 4.26: Axial CECT in apatient with pseudocyst (white circle), shows a intensely enhancing nodular lesion in the anterior wall of the pseudocyst (small black arrow) suggestive of a pseudoaneurysm, note the hypodense infarct in the spleen (arrowhead).

size of the pseudocyst is decisive in developing the type of the lesion: bleeding in a small pseudocyst is necessarily contained and more commonly ends up as a pseudoaneurysm; in case of a larger pseudocyst, rupture of the pseudoaneurysm and bleeding into the gastrointestinal tract or into the peritoneal and/or retroperitoneal spaces can occur.

Primary Splenic Artery Aneurysm

Primary splenic artery aneurysm is an uncommon vascular pathology, with incidence of 0.01 to 0.2% reported at autopsy series. It accounts for upto 60% of all visceral artery aneurysms. There is a female predominance, with the mean age of presentation at 52 years. They are usually saccular, and the majority of them are located in the mid to distal splenic artery. The pathogenesis of splenic artery aneurysm is not fully understood. However, there are close associations with medial fibrodysplasia, multiple pregnancies, portal hypertension, liver transplant, and splenomegaly. Atherosclerosis and inflammation are often seen histologically; although they are most commonly secondary events resulting from primary degeneration of the media. Most patients are asymptomatic, with aneurysm found incidentally on imaging studies. Upto 20% may present with epigastric or left upper quadrant abdominal pain. Occasionally, the aneurysm can erode into an adjacent viscus or into the pancreatic duct and presents as gastrointestinal hemorrhage. Rupture of the aneurysm causes severe abdominal pain and hypovolemic shock.

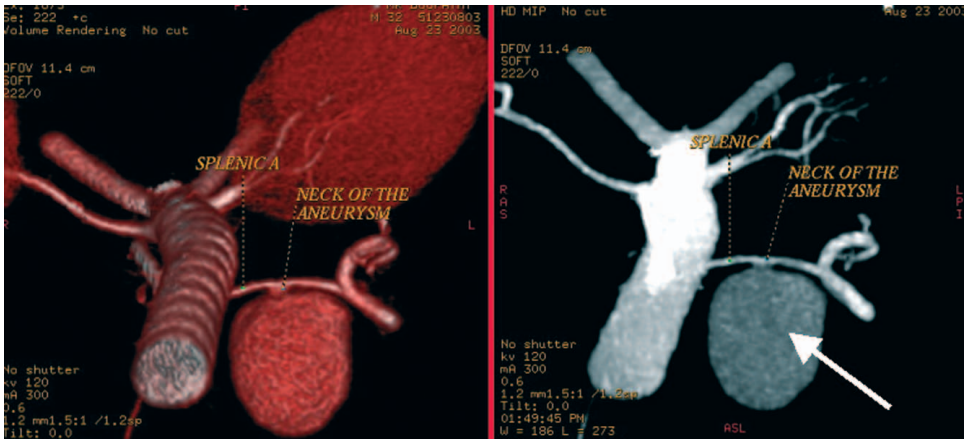

FIGURES 4.27A and B: 3D VR image and 3D MIP image showing a large aneurysm with a narrow neck arising from the splenic artery.

DIFFERENTIAL DIAGNOSIS IN SPLENIC PATHOLOGY

Primary Causes of Anomalies of Splenic Size

Splenomegaly

- Infection (bacterial, viral, protozoal, fungal; isolated splenomegaly with Epstein-Barr virus, malaria, *Mycobacterium* species, *Histoplasma* species)
- Lymphoma, leukemia
- Portal hypertension
- Acute splenic sequestration in sickle cell anemia
- Lymphoproliferative disease
- Collagen vascular disease
- Hemolytic anemia, extramedullary hematopoiesis

- Langerhans cell histiocytosis
- Storage disorders (Gaucher disease, Niemann-Pick disease, mucopolysaccharidoses)
- Sarcoidosis.

Small Spleen

- Infarction
- Congenital hypoplasia
- Celiac disease
- Fanconi anemia
- Partial splenectomy.

Patterns of Involvement in Splenic Parenchymal Disease

Solitary Lesions

- Cyst (true [epidermoid, *Echinococcus* species], false [secondary to infarct or trauma])
- Hemangioma, lymphangioma
- Hamartoma.

Multiple Focal Abnormalities

- Trauma (lacerations, fractures, intrasplenic and subcapsular hematomas)
- Splenic rupture (secondary to trauma, infarction, splenomegaly from any cause, hemangioma, epidermoid cyst, peliosis, pancreatitis).
- Abscess (bacterial, fungal, granulomatous)
- Calcified granuloma (*Histoplasma capsulatum*, *Mycobacterium* species, *Pneumocystis carinii*, cat-scratch fever, TORCH [*Toxoplasma gondii*, rubella virus, cytomegalovirus, herpes simplex virus] agents)
- Lymphoma, lymphoproliferative disorder
- Lymphangiomatosis, hemangiomatosis
- Langerhans cell histiocytosis
- Gaucher disease, Niemann-Pick disease
- Sarcoidosis.

Diffuse Disease Without Focal Lesion

- Lymphoma, leukemia
- Infarction (secondary to emboli, torsion, collagen vascular disease, portal hypertension, sickle cell anemia, splenic venous thrombosis, infiltration, Gaucher disease)
- Iron deposition disease (hemochromatosis, hemosiderosis)
- Hemangioma, hemangioendothelioma.

CHAPTER

5

Pancreas

CT is one of the single best techniques for noninvasive imaging of pancreas. The lobulated pancreas lies draped across the prevertebral aorta and inferior vena cava in the anterior pararenal space and is obliquely oriented superolaterally toward the splenic hilum. Although the pancreas lacks a serosa, it is invested with retroperitoneal parietal peritoneum, has the transverse mesocolon attached along its anterior surface, and lies just superior to the origin of the small bowel mesentery. The pancreas forms part of the floor of the lesser sac, and its tail lies within the splenorenal ligament, so that its position and shape are dictated in part by the splenic orientation.

The pancreas sits deep in the retroperitoneum and is richly invested with lymphovascular supply and drainage. It has a strategic relationship with the celiac axis and superior mesenteric artery and their branches, from which it receives most of its arterial supply. It lies in close relation to the confluence of the superior mesenteric, inferior mesenteric, splenic, and portal veins. Peripancreatic nodes of the celiac axis, porta hepatis, and portocaval region as well as the aortocaval and paraaortic chains are frequently involved by diseases of the gastrointestinal tract, liver, and pancreas.

The C loop of the duodenum abuts the head and uncinate process of the pancreas. The inferior pancreatic border is directly adjacent to the third portion of the duodenum and is closely related to the fourth portion, the ligament of Treitz, and the proximal jejunum. In some patients, the immediacy of the pancreas to the splenic or hepatic flexure may be noted as well. The stomach sits in close apposition to the anterior pancreas, being separated from it by the potential space of the lesser sac, and a redundant stomach fundus may lie adjacent to the pancreatic tail.

The extrahepatic biliary duct serves as a border to the foramen of Winslow, is closely apposed to the posterior pancreatic head, and meets the main pancreatic duct at the ampulla of Vater. A small accessory duct of Santorini may be seen superiorly and inferiorly.

EXAMINATION TECHNIQUES

Pancreas is best examined in supine position, for general survey we use 7/7 mm slices. For specific pancreatic evaluation 5/5 mm slices are obtained, plain study is done initially and is used to plan the contrast study.

For evaluation of pancreatic tumors, helical or MSCT is essential due to the ability to acquire thin section scans at narrow interscan increments and scanning during the phase of maximum vascular opacification by iodinated intravenous contrast material.

Optimal opacification of the pancreas is obtained at ± 35-40 sec after administration of 100 ml bolus injected at 2-3 ml/sec. Depending on the acquisition volume, collimation of 4 or 8 mm and pitch 1-1.5 are used. Double phase spiral CT scanning allows the pancreas to be visualized during the arterial phase and the liver during portal venous phase. Oral administration of diluted iodinated or barium sulphate contrast medium delineates the duodenum and small bowel.

Technique for Angiography

Accurate CT imaging of the pancreas requires careful attention to technique. First, when performing CT imaging for the evaluation of pancreatic cancer, high-density oral contrast agents should be avoided, especially if 3D imaging will be performed. We routinely administer water as oral contrast. The water is well tolerated, allows excellent visualization of the duodenum and small bowel, and does not requiring editing when performing CT angiography of the peripancreatic vessels. Second, a fast injection of nonionic intravenous contrast is essential. An injection rate of 3 to 5 mL/sec of IV contrast is optimal for visualization of the vasculature and enhancement of the pancreatic parenchyma. Third, fast data acquisition using thin collimation and an accurate timing protocol is crucial. The abdomen is scanned from the diaphragm to the iliac crest, in 15 to 20 seconds. Arterial phase images are acquired 25 seconds after the start of the injection. Venous phase images are acquired 50 seconds after the start of the injection. This allows for optimal visualization of both the mesenteric arteries and veins, and is essential for detecting vascular invasion. For detection and staging of adenocarcinoma of the pancreas, multiplanar reconstructions and 3D imaging is valuable. Real-time 3D volume-rendering systems are now widely available and affordable. These systems allow for real-time manipulation of the 3D volume data set, which can be manipulated using different orientations and cut planes to best demonstrate the pancreas and pathology. In addition to the use of cut planes, the radiologist has the ability to change the opacity, brightness, window width, and level.

CT angiography routinely uses a combination of both volume rendering and maximum intensity projection (MIP) for display of the vascular map. The use of alternative visualization techniques such as minimum intensity projection also may be useful in select cases.

Normal symmetry of the gland has to be observed with measurements for head (3 cm) body (2.2) tail (2.8) the thickness of the head should be less than transverse diameter of the adjacent vertebral body. Pancreas moves an average of 3.5 cm craniocaudally between phases of respiration.

Pancreatic duct should be no wider than 2-3 mm, the duct can be seen at least partially in 70% of normal patient, the duct is most frequently seen in the body as it arches over the spine and mesenteric vessels.

Oral contrast is mandatory for delineating the adjacent stomach, duodenum, and proximal small bowel gastric distention prevents pseudotumors additionally pancreas is oriented more transversely.

ANOMALIES AND ANATOMICAL VARIANTS

Pancreatic Divisum

Pancreatic divisum is a congenital anomaly of pancreatic development in which the dorsal and ventral pancreatic anlage fail to fuse, as a result pancreatic and uncinate process are drained by the duct of wirsung through the major papillae, the body and tail are drained by the duct of Santorini through the minor papillae.

CT scan can occasionally suggest the diagnosis when two distinct pancreatic moieties or two distinct ducts are seen separated by a cleft of fat or pancreatic tissue.

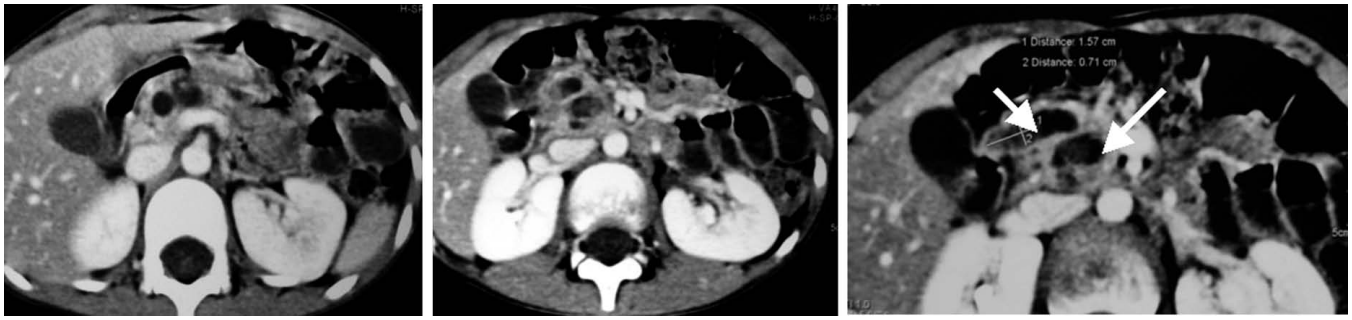

FIGURES 5.1A and B: Axial CECT in a 16-year-old girl with recurrent pancreatitis reveals heterogeneous pancreas with two dilated ducts (arrows).

Annular Pancreas

Annular pancreas is a uncommon condition in which a thin band of pancreatic tissue encircles the second portion of duodenum. ERCP is diagnostic in 85% of cases, in these cases a normally located main pancreatic duct is seen in the body and tail that communicates with the small duct of the pancreatic head, which encircles the duodenum, this latter duct is seen originating on the right anterior surface of the duodenum passing posteriorly around the duodenum and entering the main pancreatic or common bile duct near the ampulla.

The same findings have been shown in the post ERCP CT images below.

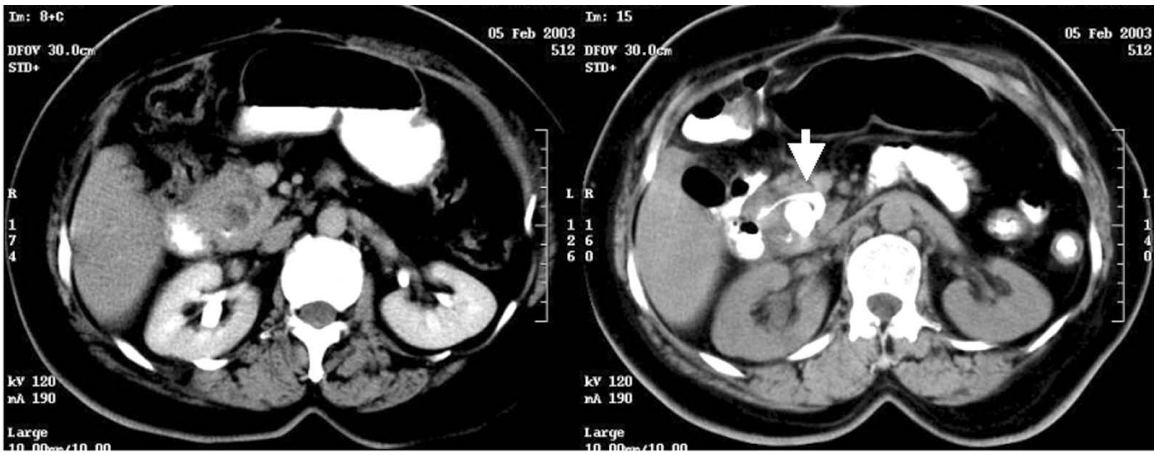

FIGURES 5.2A and B: Axial pre and post ERCP CT in a patient with annular pancreas reveals focally dilated proximal PD with the accessory duct curving anteriorly towards the duodenum (arrow).

Ectopic Pancreatic Tissue (see Fig. 8.41 page 255)

Ectopic rests of pancreatic tissue commonly lie in the gastric antrum or the proximal portion of duodenum, other ectopic sites include jejunum, Meckel's diverticulum, GB, appendix and colon. These lesions are usually submucosal when symptomatic it may simulate duodenal ulcer and gallbladder disease.

INFLAMMATORY CHANGES OF THE PANCREAS

Acute Pancreatitis

The most common causes for acute pancreatitis are alcoholism and biliary stone disease. The findings seen on CT reflect the changes caused by the retroperitoneal inflammatory process. Initially, the mild form of pancreatitis presents on CT as a normal pancreas or a slightly enlarged gland. Reports in the literature indicate that between 14-28% of patients with a mild clinical form of pancreatitis have normal CT findings but a more recent report from 1997 shows a false negative rate of only 11% that included all stages. This is most likely due to the superior resolution and improved bolus technique achieved with helical CT.

The initial injury leading to pancreatitis causes vasodilatation, increased blood flow to the pancreas and, therefore, increased parenchymal enhancement during and immediately after a bolus injection of contrast material. As the disease progresses, the pancreas appears mottled due to interstitial edema within the parenchyma. Also, hemorrhage may occur within the pancreas. At a later stage, the gland assumes a sausage-shaped configuration with low attenuation. This frequently is accompanied by extensive extrapancreatic inflammatory changes.

The typical radiographic appearance of mild pancreatitis is that of a pancreas which is diffusely enlarged with indistinct margins and a heterogeneous enhancement pattern.

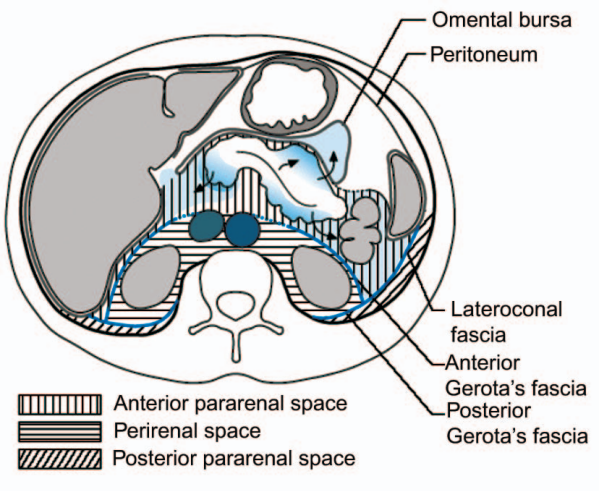

FIGURE 5.3: Schematic showing the relationship of pancreas to the retroperitoneal facial planes

Occasionally, only a portion of the pancreas is involved either exclusively or predominantly. In the case of segmental pancreatitis, the head is most frequently involved. Extravasation of pancreatic secretions occurs early due to the fact that the pancreas does not have a fibrous capsule. This process increases the density of the peripancreatic fat, which frequently appears "dirty" with multiple streaks of soft tissue density, and the adjacent fascial planes often are thickened. In traumatic pancreatitis, an actual fracture line or separation through the pancreatic parenchyma may be seen. Often, early signs of inflammatory changes can be seen only if an excellent bolus technique has been used.

CT is the modality of choice in acutely ill patients with the diagnostic dilemma of pancreatitis. Clinically severe pancreatitis in patients who fail to respond to conservative therapy in patients with suspected complications such as necrosis, infected pseudocyst.

CT features of acute severe pancreatitis include:

- Enlargement of the gland
- Changes in parenchymal enhancement pattern or attenuation,
- Indistinctness of gland margins,
- Inflammation with thickening of peripancreatic fascial planes, and
- One or more fluid collections.

TERMINOLOGIES

Pancreatic Necrosis

Pancreatic necrosis defined as diffuse or focal areas of non-viable pancreatic parenchyma seen in CT as well marginated zone of unenhanced parenchyma larger than 3 cm in diameter or larger than 30% area of pancreas.

Acute Fluid Collection

Collections of enzyme rich pancreatic juice that occur in about 40% of patients seen in CT as low attenuation poorly defined collection of fluid with no recognizable capsule.

Pseudocyst

Pseudocyst well marginated capsulated collections of pancreatic fluid which evolved from acute fluid collection in about 30% of patients with acute pancreatitis. This evolutionary process takes around 4 weeks. CT findings of the pseudocyst includes round or oval fluid collection with thin or thick capsule showing contrast enhancement.

Pancreatic Abscess

Circumscribed peripancreatic collection of pus arising as a sequela to limited necrosis with secondary infection. On CT they are seen as low attenuation thick walled with or without air pockets.

Hemorrhage and Pseudoaneurysm

One of the most feared complications of acute pancreatitis is severe and sudden retroperitoneal hemorrhage. Proteolytic enzymes extravasating from the pancreas can erode into peripancreatic vessels and result in bleeding or formation of a pseudoaneurysm. CT can identify bleeding into fluid collections or retroperitoneum by recognizing high-density fluid or fluid collections of high and low density in subacute hematomas.

A pseudoaneurysm is diagnosed as a rapidly enhancing mass with a washout effect similar to aorta and other larger arterial structures. These aneurysms can easily rupture and therefore, early interventional treatment is advised. CT may be useful for demonstrating the exact site of bleeding and thus shorten the time for angiographic identification of the bleeding and subsequent embolization. Based on a good bolus technique, CT also may be useful for demonstrating splenic or portal vein thrombosis that is diagnosed through absence of contrast enhancement during the contrast injection.

Table 5.1: CT classification of pancreatitis—Balthizar grading

Grade A:	Normal pancreas
Grade B:	Focal or diffuse enlargement of the pancreas with contour irregularity, inhomogeneity of gland dilatation of pancreatic duct, foci of small fluid collect ions in gland but no evidence of peripancreatic disease.
Grade C:	Intrinsic abnormalities of pancreas, haziness and streaky densities in peripancreatic fat.
Grade D	Single, ill-defined fluid collect ion or phlegmon.
Grade E:	2 or more ill-defined fluid collect ions or presence of gas in or adjacent to the pancreas.

CTSI (CT Severity Index)

CT Grade based on Balthazar score plus pancreatic necrosis with a maximum score of 10 points.
Grade A: 0 points
Grade B: 1 point
Grade C: 2 points
Grade D: 3 points
Grade E: 4 points

Points are given for necrosis with <30% being 2 points, 30-50% necrosis 4 points and >50% necrosis being 6 points.

Groove Pancreatitis

Groove pancreatitis is an uncommon type of chronic pancreatitis localized within the "groove" between the head of the pancreas, the duodenum, and the common bile duct. The pathogenesis remains unclear, although several factors, such as penetrating duodenal ulcers, trauma to the head of the pancreas after gastric resections, true duodenal wall or pancreatic cysts, pancreatic heterotopia in the duodenum, microscopic carcinoma obstructing Santorini's duct, and disturbance of flow of pancreatic juice in the Santorini duct, might be related to this condition. A long history of alcohol abuse is often found in patients presenting with groove pancreatitis.

Groove pancreatitis is classified into two types, the pure form and the segmental form. The pure form affects the groove only, while the pancreatic parenchyma is preserved; the pancreatic duct is intact and the condition is seldom detected. In segmental groove pancreatitis, scarring is found not only in the groove but also in the pancreatic parenchyma. The replacement of parenchyma by scar tissue is extended to the dorso-cranial portion of the pancreatic head. Segmental groove pancreatitis often shows stenosis or obstruction of Santorini's duct, while preserving Wirsung's duct.

On dynamic CT , the cicatricial "plate" in the "groove" may present as a mass lesion with poor enhancement and may resemble carcinoma of the head of the pancreas. Additional findings may consist of cysts in the duodenal wall and/or the groove, and duodenal wall thickening often accompanied by duodenal stenosis. In segmental groove pancreatitis a long, smooth stenosis of the distal common bile duct has also been reported.

Alcoholic Chronic Pancreatitis

In Western countries, alcohol abuse is responsible for approximately 70% of cases of CP. Substantial pancreatic fibrosis has been reported at autopsy in 50% of chronic alcoholics who did not have clinical CP. Despite that impressive number, only 5 to 15% of alcoholics develop clinical CP. These data suggest that alcohol produces pancreatic injury in many or most people who drink alcohol to the point of abuse. However, most do not pass the clinical threshold for the diagnosis of CP.

Classically, in alcoholic CP, the ducts are distorted and often contain calcifications. Pancreatic calcifications have been reported to occur more frequently in substantial pancreatic fibrosis while the absence of calcifications denotes less severe disease. In the initial phase of alcoholic CP, protein precipitates are deposited in the acini and pancreatic ducts, which subsequently undergo calcification to a variable extent. Therefore, not all patients with pancreatic fibrosis will have pancreatic calcifications. In hereditary pancreatitis, calcifications occur early in the course of the disease and tend to be large and to arrange themselves in a linear fashion within the main pancreatic duct. When alcoholic CP occurs in patients with pancreas divisum, isolated ductal alterations involving the ventral or dorsal pancreas may be seen as the first manifestation of a generalized pancreatic disease. This finding could be related to local ductal hypertension arising earlier either in the ventral or the dorsal duct. Finally, with further disease progression, involvement of both ducts is normally seen.

Autoimmune Pancreatitis

Autoimmune pancreatitis is defined as a special form of CP caused by an autoimmune mechanism. Associated autoimmune and related diseases have been reported in about 50% of cases and may be the key to a correct diagnosis. Associations with Sjögren's syndrome, primary sclerosing cholangitis, primary biliary cirrhosis, inflammatory bowel disease, and systemic lupus erythematosus have been described. Typical laboratory findings in autoimmune pancreatitis include increased serum gammaglobulin and IgG and the presence of autoantibodies. Clinical characteristics of autoimmune pancreatitis include mild symptoms without acute attacks of pancreatitis, no association with alcohol abuse, high incidence of obstructive jaundice and diabetes mellitus, and effective clinical response to steroid therapy. Specific histopathologic features of autoimmune pancreatitis include massive fibrosis, marked destruction of pancreatic islets and acini, and periductal lymphocytic infiltration causing narrowing and/or destruction of the main pancreatic duct and/or its side branches and fibrosis. Based on this histological aspect, the disease has also been called nonalcoholic duct destructive chronic pancreatitis.

Characteristic CT features of nonalcoholic duct-destructive CP include diffuse or focal pancreatic enlargement, narrowing of the main pancreatic duct. Additionally, contrast-enhanced imaging may show a capsular-like rim, decreased enhancement on the arterial-phase images, and normal enhancement on the delayed-phase images. On CT, this capsular-like rim is seen as a well-defined low-density band surrounding the pancreas. Recognition of autoimmune pancreatitis is clinically important because it is reversible when diagnosed and treated correctly.

Chronic Obstructive Pancreatitis

Chronic obstructive pancreatitis results from obstruction of the pancreatic ducts, most frequently occurring distally to a pancreatic neoplasm. Narrowing or obstruction of the main pancreatic duct involved by carcinoma of the

pancreatic head is characterized by dilatation of the distal main pancreatic duct and parenchymal atrophy, and seldom leads to dilatation of the duct of Santorini. The lesions are regularly spread in the occluded territory, protein plugs are rare, and calcifications are not observed.

Spectrum of Cases Depicting Various Stages of Acute Pancreatitis

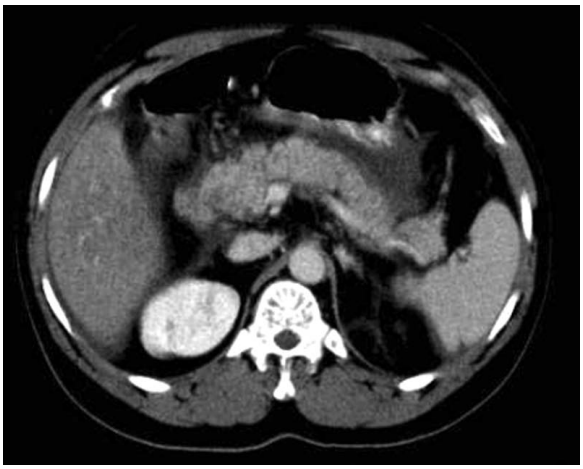

FIGURE 5.4: Axial CECT reveals mild alteration in the glandular architecture of pancreas with rim of peripancreatic fluid. Dimensions of the gland are normal.

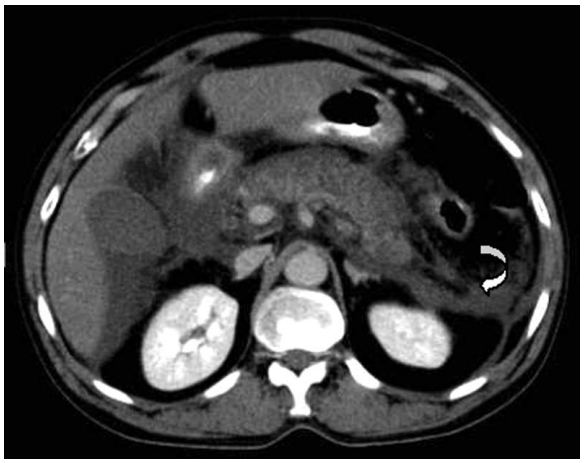

FIGURE 5.5: Axial CECT reveals hypodense edematous pancreatic parenchyma with rim of fluid, in the Morrisons pouch (arrow) with thickening of the left lateroconal and anterior gerotas fascia (curve arrow).

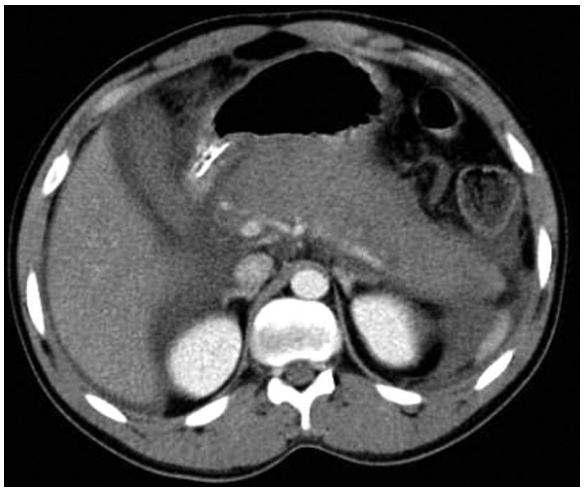

FIGURE 5.6: Axial CECT shows an enlarged edematous pancreas with peritoneal free fluid.

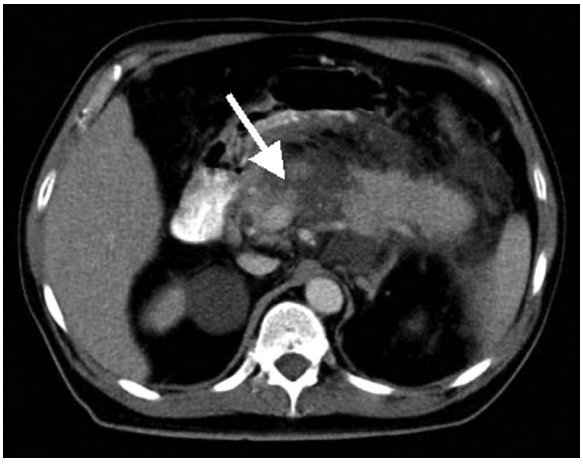

FIGURE 5.7: Axial CECT shows a focal hypodensity in the body of pancreas (arrow) with peripancreatic fluid.

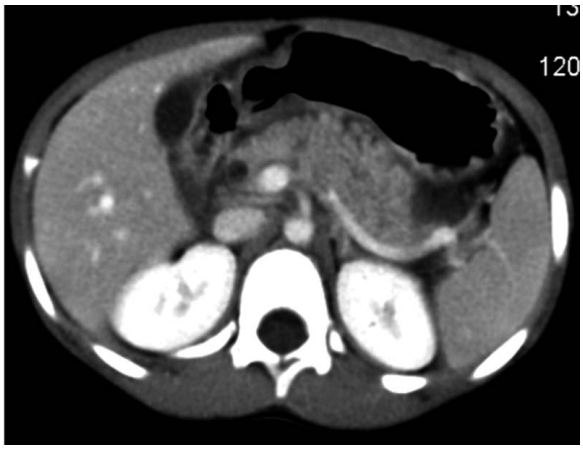

FIGURE 5.8: Axial CECT in a 6-year-old boy presenting with features of viral pancreatitis, pancreas shows diffuse enlargement.

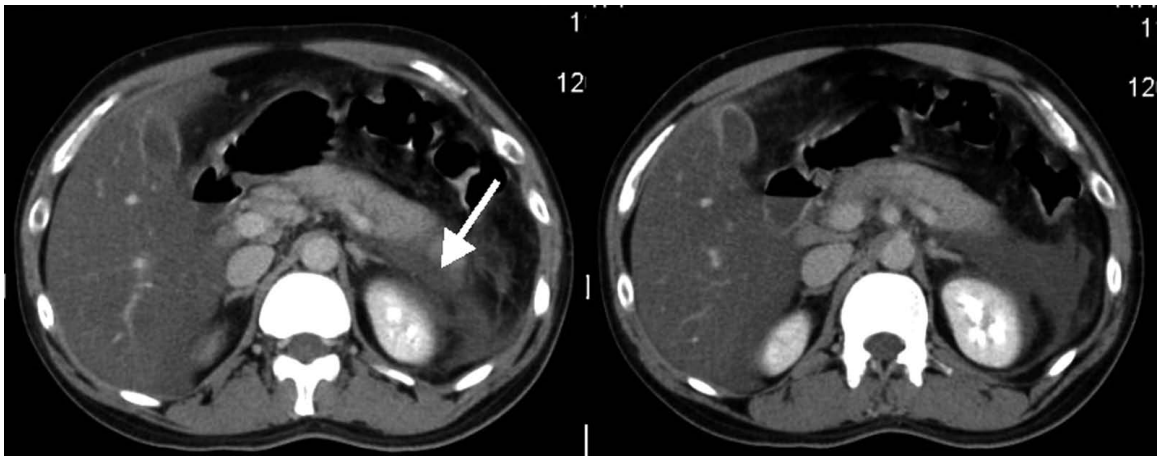

FIGURE 5.9: Axial CECT reveals focal thickening of the pancreatic tail with rim of fluid in the anterior pararenal fascial plane (arrow).

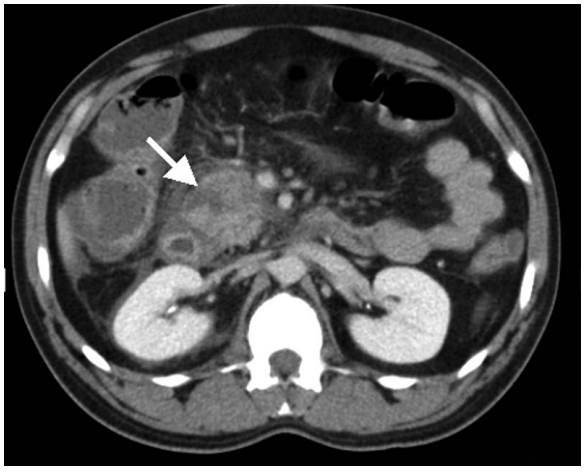

FIGURE 5.10: Axial CECT reveals heterogeneous edematous pancreatic head (arrow) suggestive of a focal pancreatitis.

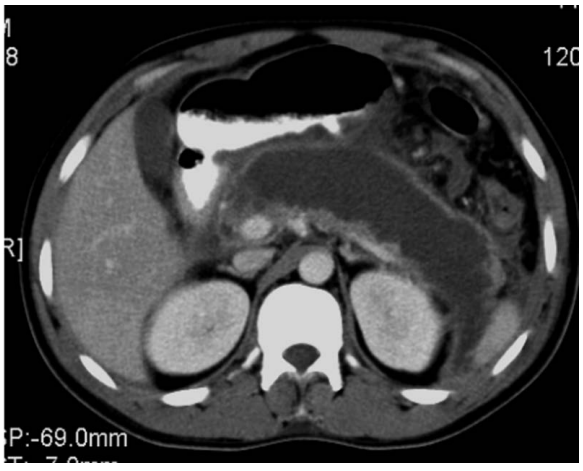

FIGURE 5.11: Axial CECT section reveals loss of normal pancreatic architecture with the entire pancreas appearing hypodense suggestive of necrosis with cyst formation.

PATTERN OF INFLAMMATORY CHANGES IN ACUTE PANCREATITIS

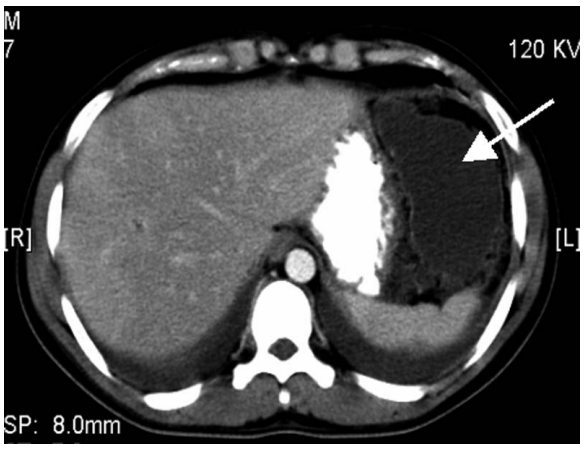

FIGURE 5.12: Axial CECT reveals a hypodense fluid collection in the greater omental region (arrow)

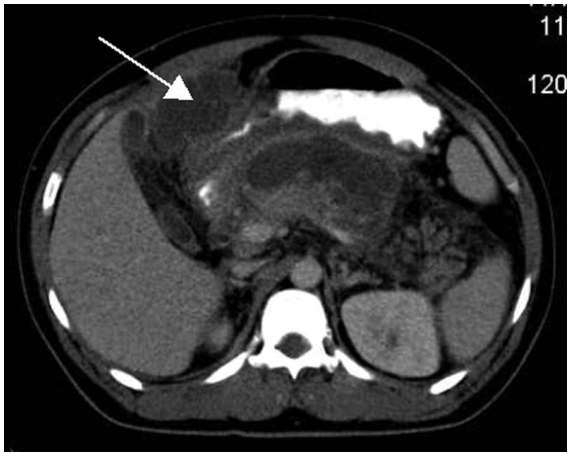

FIGURE 5.13: Axial CECT showing walled off fluid collection in the anterior subhepatic space indenting the antrum (arrow)

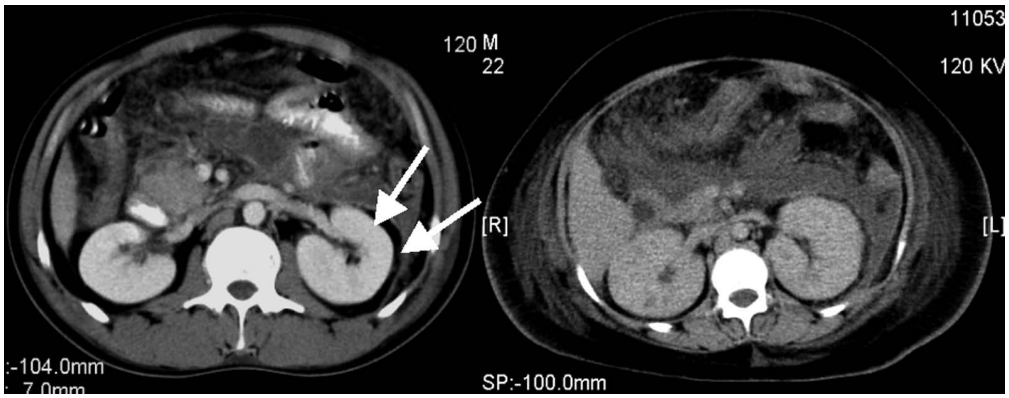

FIGURE 5.14: Axial CECT reveals thickening with fluid collection in the gerotas and lateroconal fascia (arrows)

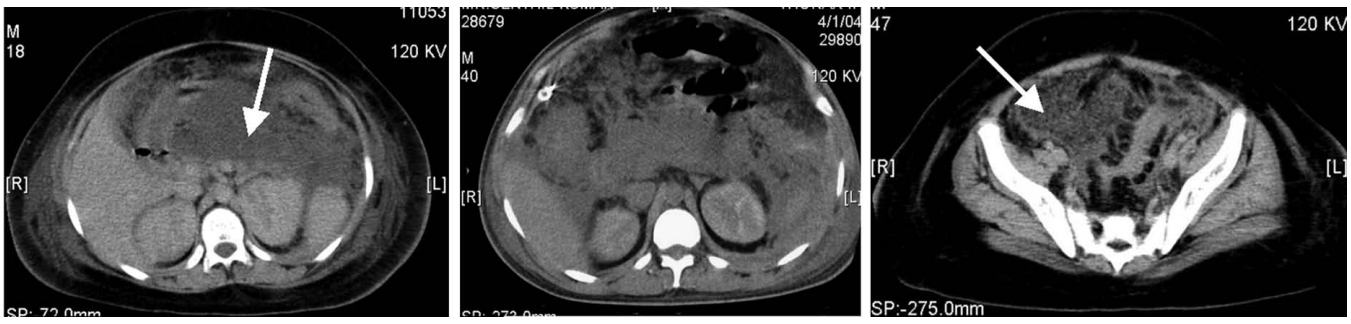

FIGURES 5.15A to C: Axial CECT (A) reveals a hypodense enlarged nonenhancing pancreas suggestive of necrosis (arrow). (B, C) reveals loss of normal peritoneal fat showing soft tissue stranding (arrows) reflecting process of saponification.

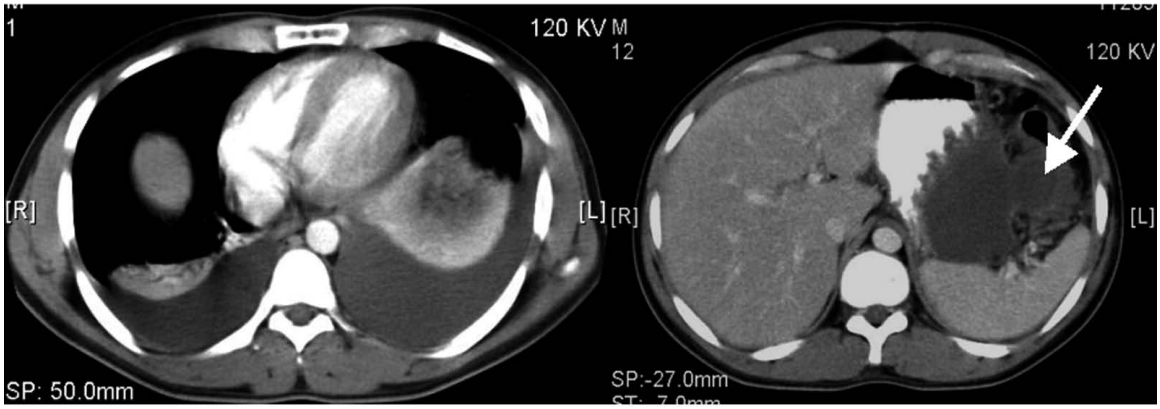

FIGURES 5.16A and B: Axial CECT (A) reveals bilateral pleural effusion, (B) fluid collection in the greater omentum (arrow).

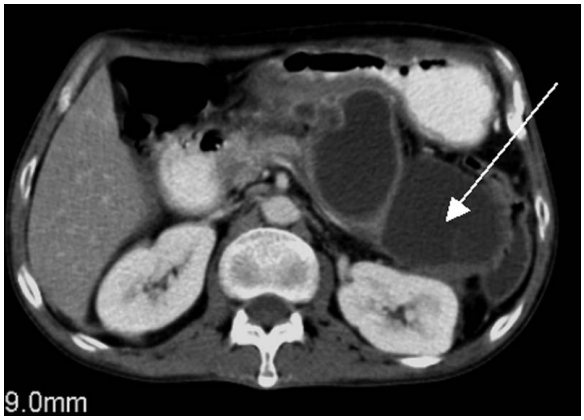

FIGURE 5.17: Axial CECT reveals intrapancreatic pseudocyst (arrow)

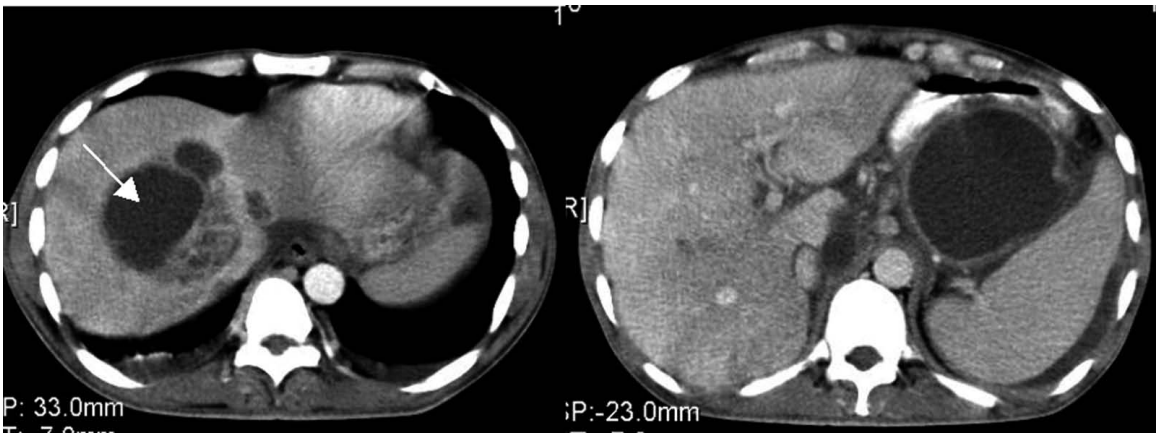

FIGURES 5.18A and B: (A) Axial CECT reveals intraparenchymal pseudo cyst (arrow), (B) Axial CECT reveals a well marginated cyst in the lesser sac.

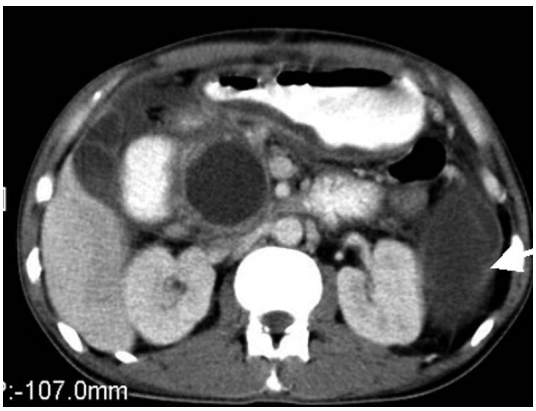

FIGURE 5.19: Axial CECT reveals a well marginated cyst in the pancreatic head within the c loop, walled of fluid collection in the left lateroconal fascia (arrow).

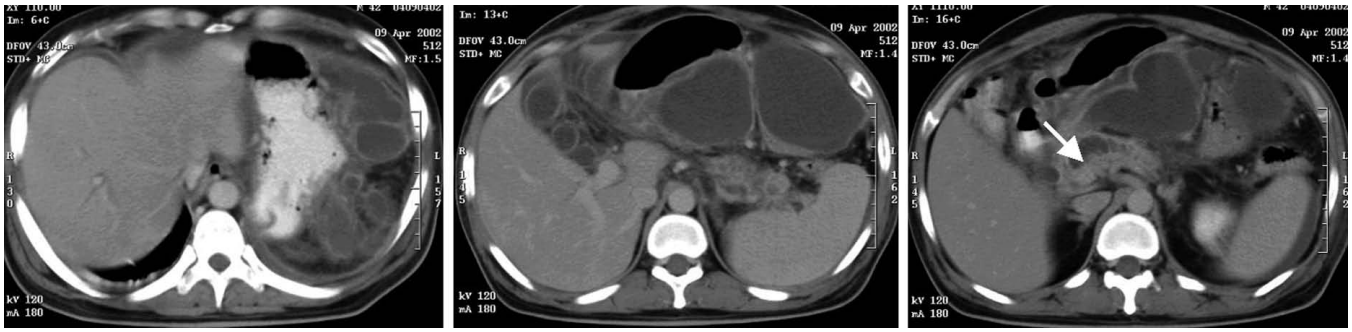

FIGURES 5.20A to C: Axial CECT reveals (A) multiseptated fluid collections in the greater omentum, (B) lesser sac region, (C) small linear fluid collection in the pancreatic head (arrow).

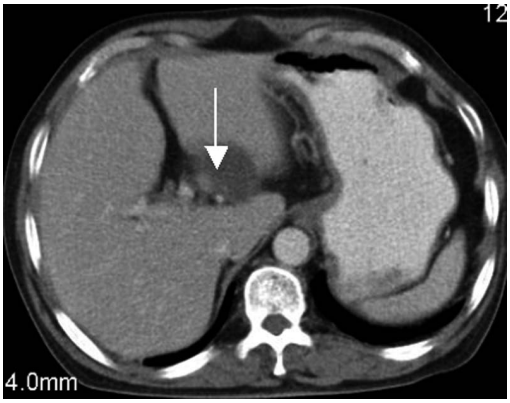

FIGURE 5.21: Axial CECT reveals a well marginated fluid collection in the porta (arrow).

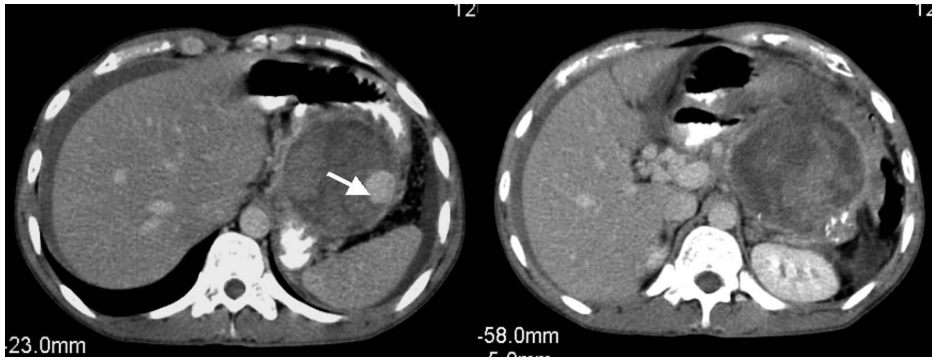

FIGURES 5.22A and B: Axial CECT reveals a complicated pseudocyst in the lesser sac region with a peripheral intense enhancing lesion suggestive of a pseudoaneurysm. (arrow).

Traumatic Pancreatitis

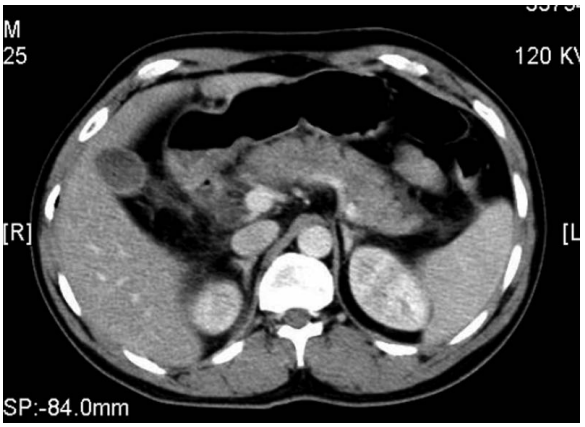

FIGURE 5.23: Axial CECT in a patient who sustained blunt injury abdomen reveals a heterogeneous pancreas with peripancreatic fluid

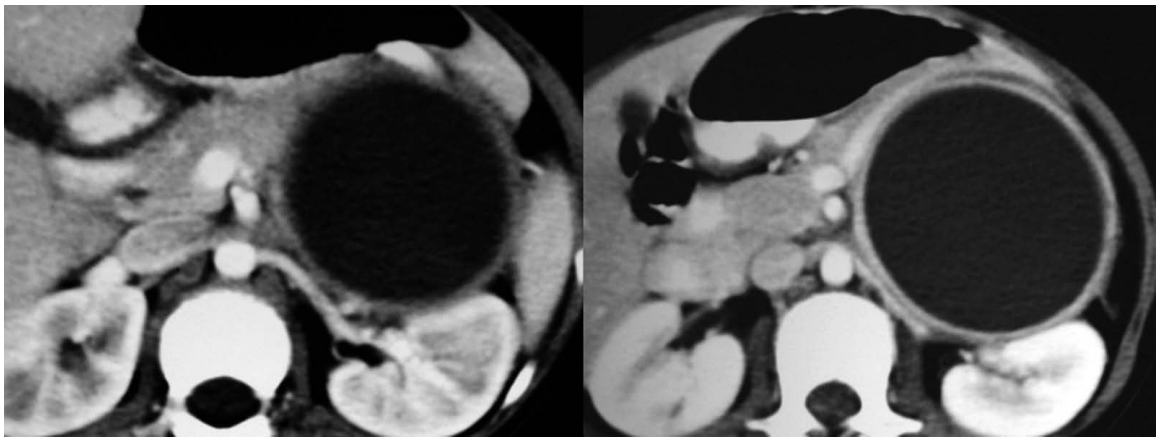

FIGURES 5.24A and B: Axial CECT in 4-year-old girl who had sustained a blunt injury 2 months prior reveals a well marginated lesion in the tail of pancreas suggestive of a pseudocyst.

Chronic Pancreatitis

Imaging has a role in both diagnosis and detection of complications in patients with chronic pancreatitis. The symptoms may mimic those associated with other diseases such as pancreatic carcinoma. Chronic pancreatitis predominantly is associated with alcoholism but may be hereditary in origin or caused by hyperparathyroidism, cystic fibrosis and hyperlipidemia.

The radiographic diagnosis of chronic pancreatitis is based on changes in the pancreatic duct and the parenchyma and on the detection of ductal calculi. Ultrasonography, CT, MRCP and ERCP can see these changes. MRCP offers the great advantage of superb delineation of the pancreatic changes without being invasive.

Radiographic Diagnosis

Findings consistent with chronic pancreatitis are pancreatic duct dilatation, pancreatic parenchymal texture alterations, parenchymal atrophy, and pancreatic calcifications. Size alone is not specific for pancreatitis. Additional but less common radiographic findings include biliary dilatation, pancreatic fluid collections, focal enlargement of pancreas (18%) and alterations in peripancreatic fat or renal fascia. Pancreatic duct dilation, beading of the pancreatic duct,

parenchymal atrophy and pancreatic calcifications can be detected easily by CT, chronic pancreatitis is strongly favored if there is gradual tapering of the CBD, malignant changes of ampulla or pancreatic head, the dilatation of the common bile duct usually ends abruptly.

Parenchymal atrophy and fatty replacement of the pancreas also can be seen easily by CT.

Calculi consisting of calcium carbonate, protein and polysaccharide are the third most common finding seen best by CT. Early in the stage of calculi formation, relatively radiolucent protein plugs are visible during ERCP which usually are not detected by CT.

In hereditary pancreatitis, calculi occur early in the course of the disease and tend to belarge and to arrange themselves in a linear fashion within the main pancreatic duct.

CT readily detects pseudocysts as areas of low attenuation in or next to the pancreas. If thin sections are obtained, even small pseudocysts measuring less than 1 cm in diameter can be visualized.

Extensive interlobular and periductal fibrous tissue proliferation and inflammatory infiltrates can produce mass lesions in the pancreas, which may mimic neoplasm. Distinction between a malignant and benign process is not possible based on morphology, and an aspiration biopsy is needed in these cases. This is particularly important to realize because in many patients with neoplasm, a history of acute and chronic obstructive pancreatitis may be obtained.

Role of Imaging in Chronic Pancreatitis

Chronic pancreatitis is a slowly progressive disease, which initially involves the pancreatic gland only focally, but diffuse abnormalities with various degrees of functional impairment are typical for the later stages. These morphological abnormalities can be detected by several imaging methods. The most sensitive method is ERCP, CT is superior for detecting calcifications and small cysts. For correlation of pancreatic function and morphology, ductal abnormalities must be assessed by ERCP and parenchymal changes by CT. Today, MRCP has shown excellent results in demonstrating ductal abnormalities as well as pseudocysts that may displace the main duct but not communicate with it.

Table 5.2: Cambridge classification of chronic pancreatitis

Changes	*ERCP*	*CT and US*
None	No abnormal LSB	Normal gland size and shape, homogeneous parenchyma
Equivocal	MPD normal	One of the following: < 3 abnormal LSB, MPD 2-4 mm, gland enlarged over 2 times normal size, heterogeneous parenchyma
Mild	MPD normal	Two ore more signs for diagnosis: > 3 abnormal LSB, MPD 2-4 mm, slight gland enlargement, heterogeneous parenchyma
Moderate	MPD changes LSB changes	Small cysts < 10 mm, MPD irregularity Focal acute pancreatitis (<1/3 of the gland), increased enhancement/echogenicity of MPD walls, gland countour irregularity
Severe	Any of the above changes plus one of the following: cyst > 10 mm, intraductal filling defects, calculi, MPD obstructive or stricture, severe MPD irregularity, or contiguous organ invasion	

LSB=lateral side branch ducts, MPD=main pancreatic duct

Differentiation Inflammatory Mass from Carcinoma

Areas of focal enlargement within the pancreas representing inflammatory masses may arise in both early and advanced stages of CP. Malignant masses arise relatively uncommonly in CP, but when present, differentiation with

these benign lesions may be very difficult. Both types of lesions occur most often in the pancreatic head, may cause bile duct obstruction, and may present in the absence of calcification or duct strictures and dilatation. However, patients with an inflammatory mass are likely to be younger at the time of presentation, have a history of alcoholism and have a history of previous episodes of acute or CP. Patients with biliary tract obstruction due to pancreatitis usually have a history of abdominal and back pain preceding the onset of jaundice. Jaundice due to pancreatitis often fluctuates in contrast to the continuously progressive jaundice found in patients with pancreatic carcinoma. The serum concentration of total bilirubin level is usually much higher in patients with pancreatic carcinoma than in those with chronic pancreatitis.

On unenhanced CT, both inflammatory masses and small carcinomas are usually iso-dense with normal pancreatic tissue and, when located in the pancreatic head, may cause upstream dilatation of the duct and atrophy of the tail. Carcinoma is typically hypovascular and seen as a low density mass surrounded by normal parenchyma. Sometimes, inflammatory tissue caused by obstructive pancreatitis may surround the tumor, resulting in peripheral enhancement. Tumor obstruction of the main pancreatic duct may lead to rupture of a side branch resulting in pseudocysts. Inflammatory masses may also show reduced contrast enhancement. However, this reduction is less marked than in the typical carcinoma.

Spectrum of Chronic Pancreatitis

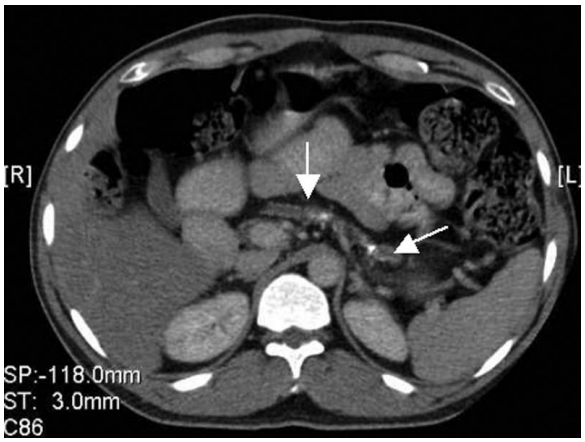

FIGURE 5.25: Axial CECT reveals complete atrophy of the pancreas, remnant duct seen with calcification (arrow).

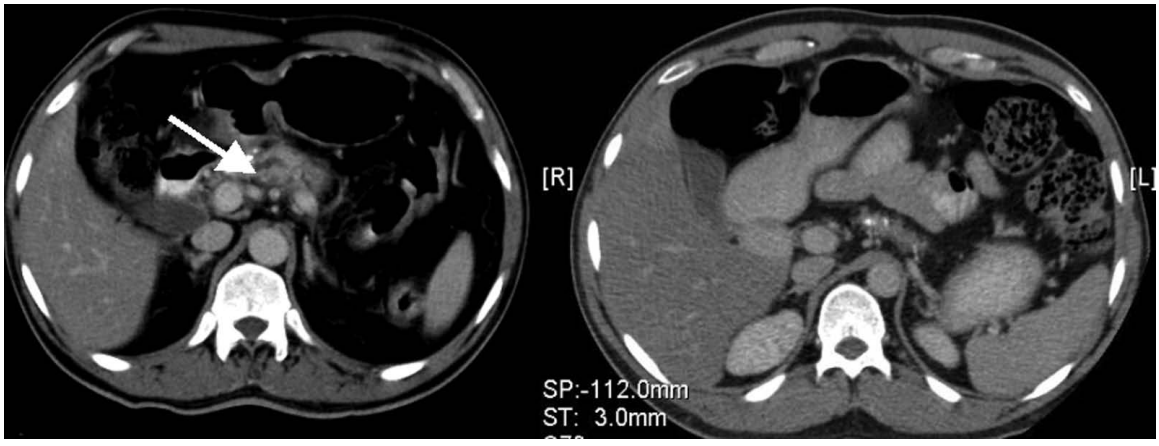

FIGURES 5.26A and B: Axial CECT reveals diffuse glandular atrophy of the gland with focal calcification in the head (arrow) with focal dilatation of the pancreatic duct.

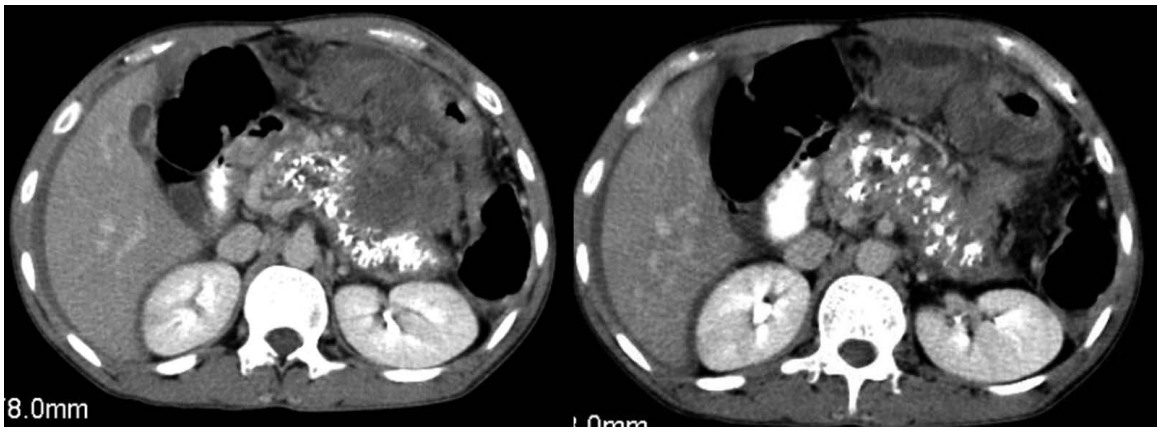

FIGURES 5.27A and B: Axial CECT reveals diffuse enlarged pancreas with multiple calcific specks involving the entire body with extensive peripancreatic inflammatory changes – features of chronic calcific pancreatitis with acute exacerbation.

Causes for Pancreatic Calcification

Chronic Pancreatitis

- Alcohol-related pancreatitis (20-50%)
- Biliary pancreatitis (20%)
- Hereditary pancreatitis (35-60%)
- Idiopathic pancreatitis
- Pseudocyst (12-20%)
- Kwashiorkor: tropical pancreatitis.

Tumor

- Microcystic adenoma (40%, stellate)
- Macrocystic adenoma (15%)
- Adenocarcinoma (2%)
- Cavernous hemangioma, lymphangioma (phleboliths)
- Metastases (e.g. from colon carcinoma).

Hyperparathyroidism

- Chronic pancreatitis in 10%, indistinguishable from alcohol-related pancreatitis.

Cystic Fibrosis

- Fine granular calcifications in advanced stage.

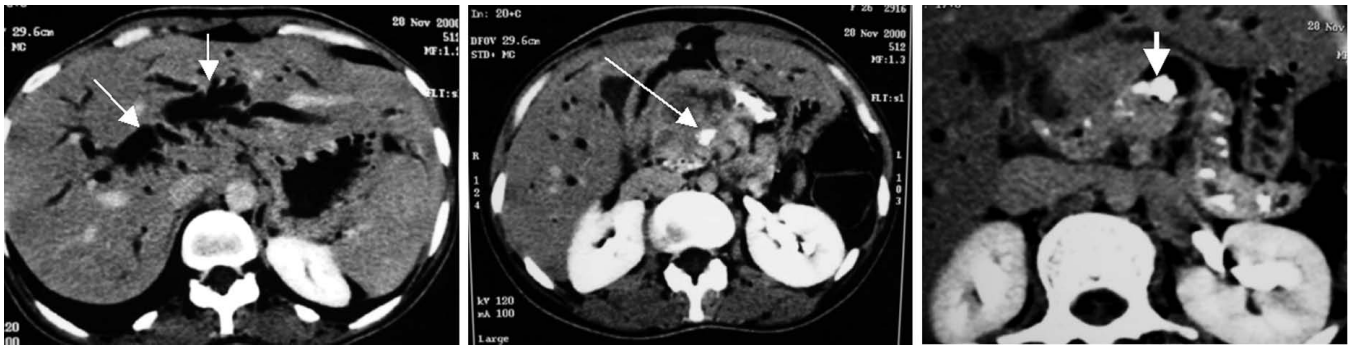

FIGURES 5.28A to C: Axial CECT (A) reveals bilateral intrahepatic biliary dilatation (arrow), (B) Axial CECT reveals a heterogeneous calcific mass in the pancreatic head with calcification (arrow). (C) Axial CECT reveals dilated pancreatic duct with multiple intraductal calculi (arrow).

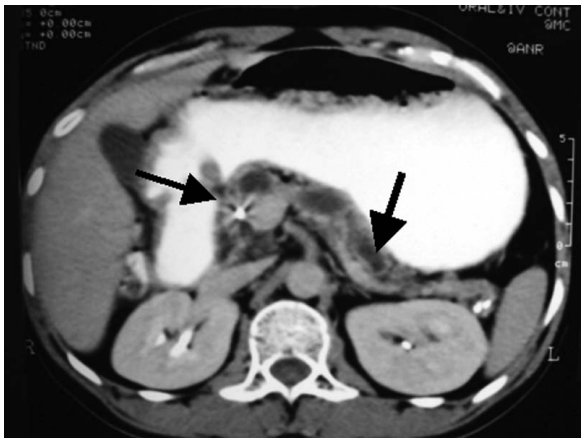

FIGURE 5.29: Axial CECT reveals dilated pancreatic duct through its entire course (arrow). Calcifications seen in the tail and in the proximal pancreatic duct.

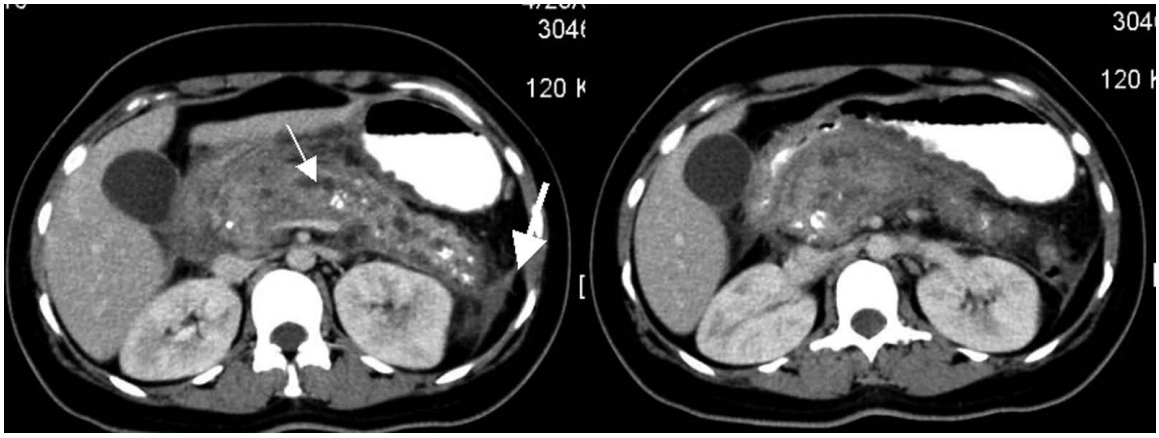

FIGURES 5.30A and B: Axial CECT reveals enlarged heterogeneous pancreas with multiple punctuate calcifications segmental dilated pancreatic ducts noted in the body and tail (arrow).

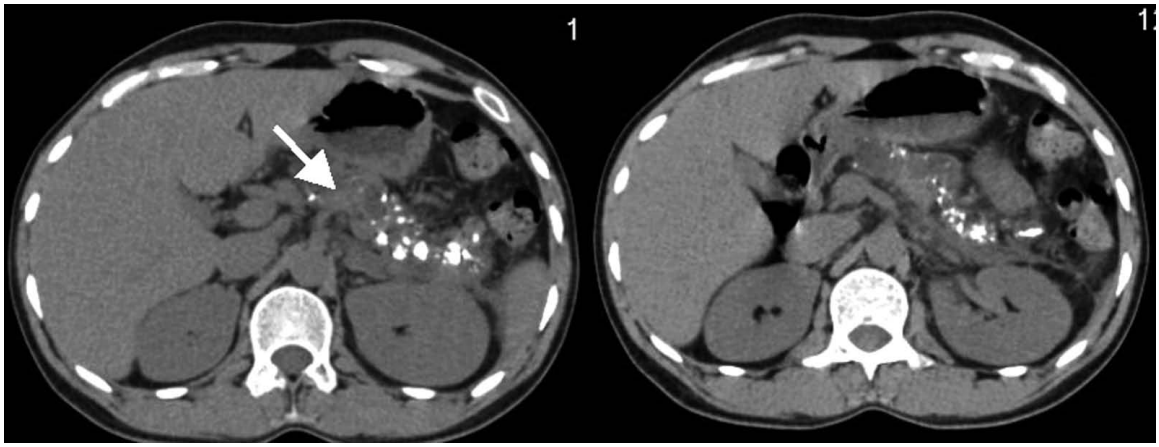

FIGURES 5.31A and B: Axial CECT reveals atrophic gland with dilated duct with multiple globular ductal and periductal calcification (arrow).

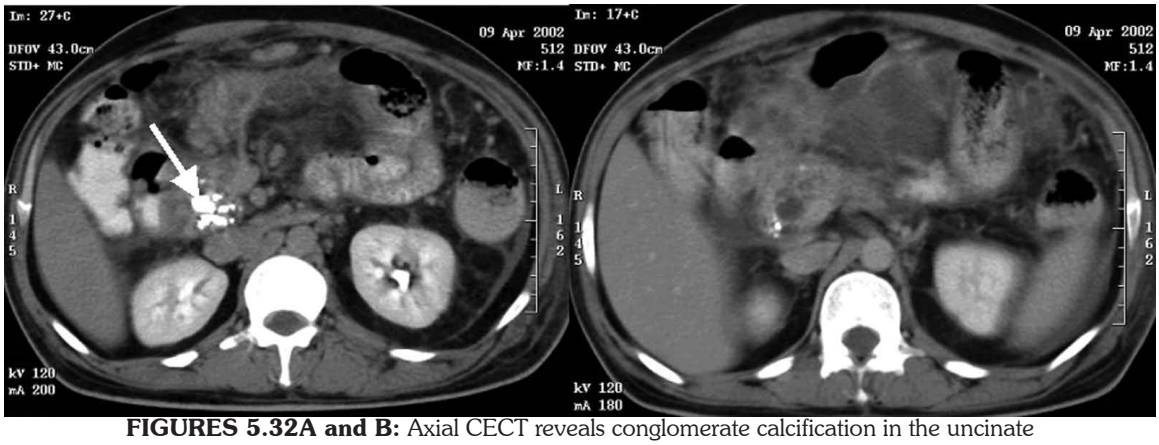

FIGURES 5.32A and B: Axial CECT reveals conglomerate calcification in the uncinate process of pancreas (arrow), with dilatation of the proximal PD.

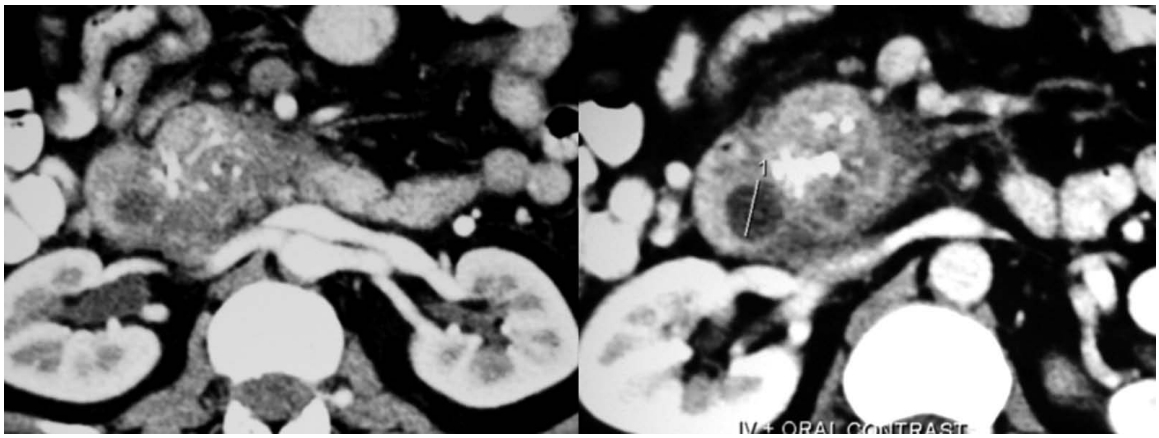

FIGURES 5.33A and B: Focal mixed dense mass in the head.

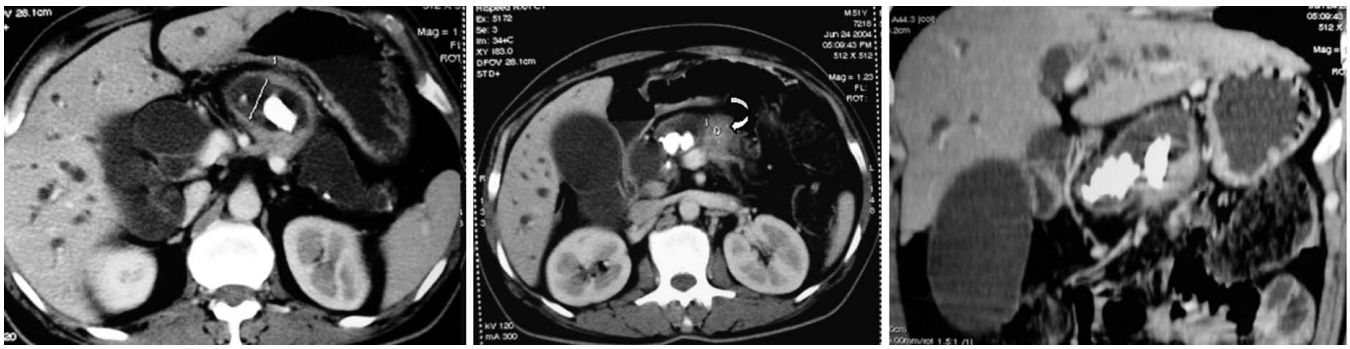

FIGURES 5.34A to C: Axial CECT Fig. A, B reveals grossly dilated pancreatic duct with large intraductal calcification (arrow), residual pancreatic tissue seen in the body (curved arrow)

Pancreatic Lipomatosis

Increased fat deposition in the pancreatic parenchyma may occur in the setting of obesity, senile atrophy, the end stage of chronic pancreatitis, cystic fibrosis, or following occlusion of the pancreatic duct. Lipomatous pancreatic atrophy in children is a rare disorder caused by a viral infection.

Differential diagnosis for fatty replacement of pancreas include steroid therapy, obesity cystic fibrosis, malnutrition, hemochromatosis, obstruction to the main pancreatic duct.

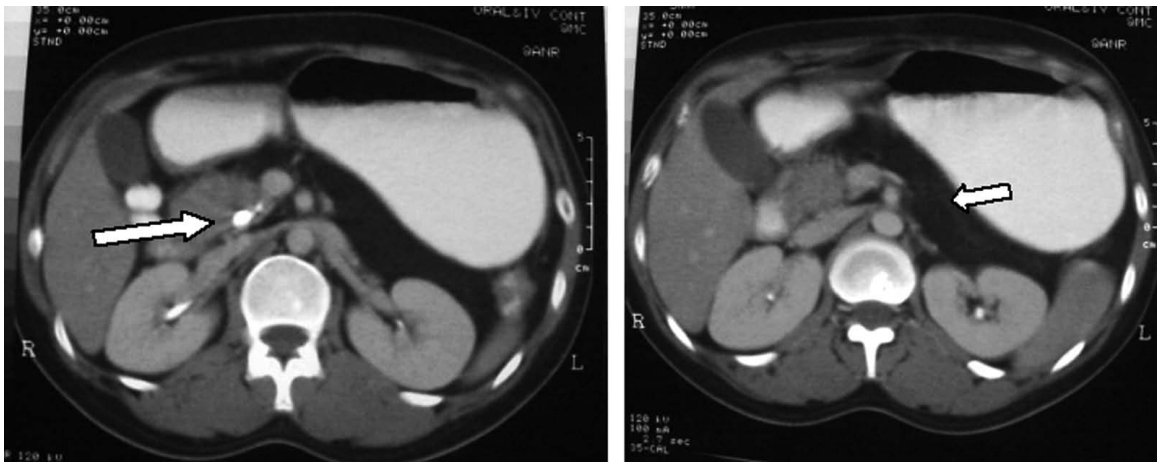

FIGURES 5.35A and B: Axial CECT reveals complete fatty replacement of body and tail (arrow in Fig. B) head and uncinate process shows normal attenuation with a speck of calcification.

Neoplasms of the Pancreas

Neoplasms of the pancreas may originate from both exocrine and endocrine cells, and they vary from benign to highly malignant. Two major groups of pancreatic neoplasms;adenocarcinoma and cystic lesions.

Clinically, 90% of pancreatic tumors are malignant ductal adenocarcinomas.

Types of Pancreatic Neoplasms

- Benign exocrine
  Serous cyst adenoma
  Mucinous cyst adenoma
- Malignant exocrine
  Ductal adenocarcinoma
  Mucinous cyst adenocarcinoma
- Endocrine
  Gastrinoma
  Insulinoma
  Other.

Incidence and Prognosis

Carcinoma of the pancreas has become more common in most Western countries over the past three decades, and although there is evidence of plateauing in some countries such as the United States, it still ranks as the sixth commonest cause of cancer death in the United Kingdom. Most patients are over the age of 60 years (80%) and many will have concurrent medical illnesses that complicate management decisions, particularly because the median survival from diagnosis is less than six months.

Clinical Presentation

Two-thirds of pancreatic cancers develop in the head of the pancreas, and most patients present with progressive, obstructive jaundice with dark urine and pale stools. Pruritus, occurring as a result of biliary obstruction, is often troublesome and rarely responds to antihistamines. Back pain is a poor prognostic sign, often being associated with

local invasion of tumors. Severe cachexia, as a result of increased energy expenditure mediated by the tumor, is also a poor prognostic indicator. Cachexia is the usual presenting symptom in patients with tumors of the body or tail of the pancreas.

Rarer Presentations of Pancreatic Carcinoma

- Recurrent or atypical venous thromboses (thrombophlebitis migrans)
- Acute pancreatitis
- Late onset diabetes mellitus
- Upper gastrointestinal bleeding.

CT EVALUATION OF PANCREATIC CANCER

Tumor Detection

Despite the development of other imaging technologies, such as magnetic resonance imaging and endoscopic ultrasound, CT continues to dominate radiologic imaging of the pancreas. Although overall 5-year survival rates for patients with adenocarcinoma of the pancreas are as low as 5%, studies have shown improved survival in patients with small tumors (<2 cm) with a reported survival of 30%. It is estimated that only 10 to 30% of patients with pancreatic cancer have resectable disease at the time of presentation; therefore, it is crucial to detect these small tumors and to identify patients eligible for surgical resection.

The overall accuracy of CT in the published literature for the detection of pancreatic tumors is approximately 80 to 91%. Most of the published studies, however, were done using older dynamic scanners or single-row spiral scanners and usually did not include 3D imaging. When scanning a patient for suspected pancreatic cancer, maximum enhancement of the pancreatic parenchyma is essential to increase tumor conspicuity. Because the normal pancreas enhances to a greater extent than do pancreatic adenocarcinomas, tumors will be easier to detect when the normal pancreas is optimally enhanced.

The rationale behind the use of dual-phase imaging is to obtain optimal pancreatic enhancement so that the tumors can be detected, and to obtain maximal vascular (arterial and venous) opacification to enable accurate assessment of vascular involvement. The optimal timing of the data acquisition, however, will depend on the scanner utilized, the rate of contrast administration, and the patient's cardiac output. There are bolus-tracking software packages available to help time the data acquisition. Some studies of dual-phase liver imaging suggest that the use of bolus tracking allows for optimized liver enhancement, reduces contrast dose requirements, and allows for more accurate timing of CT acquisition. Others advocate the use of a test bolus to determine the optimal scan delay in individual patients, and feel that this improves the timing of the acquisition when evaluating the pancreas.

The majority of pancreatic cancers occur in the head (60-65%), with only 20% occurring in the body, 10% occurring in the tail, and 5 to 10% involving the entire gland. On contrast-enhanced CT, most pancreatic adenocarcinomas will enhance less than the adjacent normal pancreatic parenchyma and will 'therefore' appear relatively lower in attenuation. Larger tumors will distort the normal contour of the pancreas and may infiltrate the adjacent fat, encase nearby vessels or obstruct the common or pancreatic duct. Smaller tumors may not distort the contour of the gland. In some patients, small masses may not be visualized directly. In these instances, helpful secondary signs are often visible that indicate the presence of a mass. For example, the presence of pancreatic ductal dilatation and common duct dilation in the absence of a stone is highly suspicious for either a small pancreatic or periampullary mass, even if the actual mass is not visible. Other secondary signs, such as pancreatic atrophy or pancreatitis, may be present in patients with pancreatic adenocarcinoma.

Issues in Pancreatic Tumor Imaging

Pancreatic Mass vs Inflammatory Mass

Distinguishing pancreatic cancer from pancreatitis at times can be challenging. A common cause of false-positive diagnosis of pancreatic cancer is a focal pancreatic mass or ductal dilatation resulting from chronic pancreatitis. The pancreatic duct can be dilated in both cancer and pancreatitis. Abrupt termination of the pancreatic or common duct favors the presence of malignant disease, however, even if no mass is visualized. The appearance of the dilated pancreatic duct also may help distinguish pancreatic cancer from chronic pancreatitis. For instance, the presence of smooth or beaded pancreatic ductal dilatation favors cancer over pancreatitis, whereas irregular ductal dilation is seen more commonly in pancreatitis. With the thinner collimation and improved resolution possible with MDCT, however, the reliance on secondary signs such as pancreatic ductal dilatation becomes less important, because the smaller masses can now be detected.

The following findings are in favor of pancreatitis:

a. Irregular dilatation of pancreatic duct;
b. Presence of dilated ducts and small pseudocysts within the mass;
c. Intraductal or parenchymal calcifications;
d. Less pronounced degree of atrophy of the pancreatic parenchyma;
e. Gradual (not abrupt) narrowing of the dilated pancreatic gland or bile duct.

Vascular Encasement

Due to the lack of a distinct pancreatic capsule, adenocarcinoma of the pancreas easily infiltrates adjacent tissues, including the peripancreatic fat and vessels. In the absence of obvious liver metastases, tumor resectability will depend on the presence of local extension or vascular involvement. Involvement of important arterial (i.e., celiac axis or superior mesenteric artery [SMA]) or venous (i.e., portal vein, splenic vein, or superior mesenteric vein [SMV]) structures will make surgical resection impossible. At some centers, isolated focal involvement of the portal vein or splenic vein is not always considered unresectable, because skilled surgeons may still opt for surgery with vascular reconstruction.

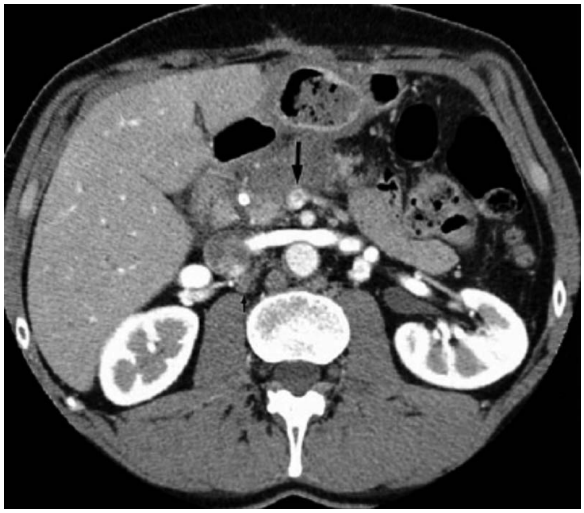

FIGURE 5.36: CECT image of a known pancreatic adenocarcinoma shows a hypodense, mildly enhancing mass seen in the pancreatic body encasing the proximal portal vein.

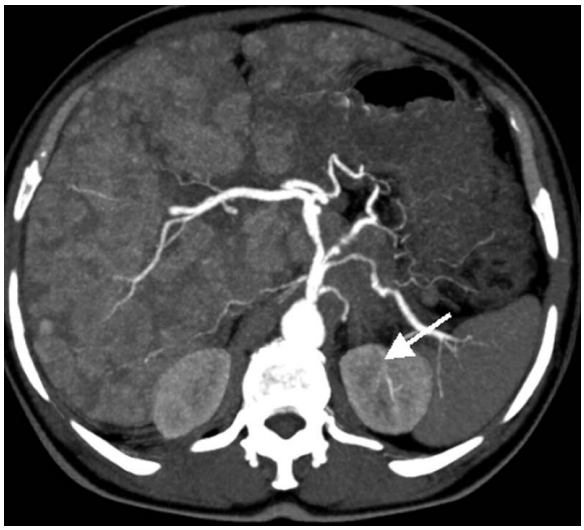

FIGURE 5.37: Axial CECT in the arterial phase showing tumoral encasement of proximal splenic artery due carcinoma body of pancreas.

To depict vascular involvement with CT, the arteries and veins must be well opacified. The faster scanning and thinner collimation that is possible with MDCT has greatly improved CT visualization of the mesenteric and peripancreatic artery and veins.

A CT grading system of vascular involvement has been reported by Lu et al. The authors prospectively graded vessel involvement using a 0 to 4 scale based on circumferential contiguity of tumor to vessel and found that when greater than 50% of the vessel circumference (grade 3-4) was in contact with a vessel, the tumor was not resectable. These criteria resulted in a sensitivity and specificity for unresectability of 84% and 98%, respectively.

Overall, the reported accuracy of CT for determining the presence of vascular involvement in patients with pancreatic cancer varies in the literature, largely due to differences in techniques and equipment.

Adenopathy

The CT detection of nodal metastases in patients with pancreatic cancer has always been limited. CT can suggest that there may be tumor involvement of nodes when they are enlarged. Large nodes do not necessarily contain tumor, however, and there may be tumor involvement of normal-sized nodes. Fortunately, in many patients, nodal involvement is not the only sign of advanced disease.

In addition, if there are no other signs of tumor extension (liver metastases or vascular invasion) the inability of CT to detect tumor in small nodes may not be that important because peripancreatic nodes are routinely resected and biopsied at the time of surgery.

Metastases

The detection of liver metastases is critical when evaluating patients with pancreatic cancer, because the liver is a common site of pancreatic metastases, and the presence of liver metastasis will make the patient ineligible for curative resection.

CT is considered the primary imaging modality for the detection of liver metastases. When performing CT for pancreatic cancer staging, liver metastases will usually appear as low-attenuation lesions compared with normally enhancing liver. These will be seen best during the portal venous phase of enhancement and may be missed if only arterial or pancreatic phase images are obtained. Small liver metastases (<1 cm) that are detected may be difficult to distinguish from small cysts or hemangiomas, even when dual-phase imaging is performed. In addition to liver metastases, to regional lymph nodes or the lungs are not uncommon.

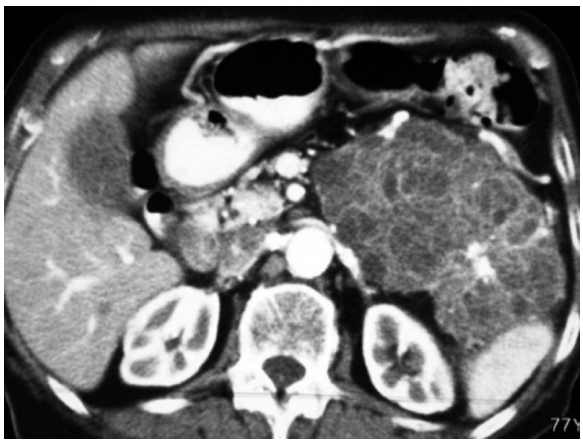

FIGURE 5.38: Axial CT showing a large multilocular well marginated lesion-case of macrocystic adenoma involving the body and tail of pancreas

Pancreatic Adenocarcinomas

Pancreatic adenocarcinomas appear, in most cases, as focal hypovascular masses. On CT , they are usually hypodense compared to enhanced parenchyma. Most patients present at a late stage in their disease, therefore it is not unusual to seem effects of extrapancreatic spread involving major peripancreatic arteries (celiac, SMA, splenic, hepatic). Tumor surrounding these vessels is indicative of extrapancreatic spread; these patients, while technically may be able to have the mass removed, generally will not benefit from surgical resection. Smaller lesions, which do not display obvious signs of extrapancreatic extension have become detectable. One must have a high index of suspicion when one encounters dilatation of the main pancreatic duct which cannot be followed to the ampulla of Vater. In these cases, a small intraparenchymal mass, which is non-contour deforming, must be suspected as the cause of this abnormality.

Associated findings are dilatation of the bile duct and/or pancreatic duct (double duct sign), obstructive pancreatitis, atrophy of the gland distal to the mass, and post-obstructive pseudocysts. Enlarged lymph nodes and metastatic lesions are also well demonstrated by CT.

Microcystic Cystadenoma (Fig. 5.40)

The microcystic cystadenoma is a well-encapsulated ovoid or multinodular mass. Its cystic portion is often multilocular, with (innumerable) cysts varying between 0.1 and 2 cm. It often has a solid portion with central septa. The solid portion may enhance in the late arterial phase after contrast administration. A stellar burst calcification is almost specific, though very rare. Demonstration on double phase spiral CT of a small cystic portion containing innumerable small cysts and a hypervascular solid portion is suggestive for serous cystadenoma.

Macrocystic Cystadenoma or Cystadenocarcinoma (Fig. 5.38)

The macrocystic cystadenoma or cystadenocarcinoma is a well-encapsulated round or lobular mass. Its cystic portion is more often unilocular or multilocular which frequently shows one large cyst with smaller daughter cysts. Its solid portion has a dominant fibrous wall which frequently shows papillary projections and/or convulsions. Calcification is occasionally seen.

Islet Cell Tumors

Islet cell tumors may be detected as small hypervascular lesions. Double phase spiral CT improves the detection of functioning endocrine tumors.

Intraductal Papillary Mucinous Tumor

Intraductal papillary mucinous tumor (IPMT) was recognised as a separate new subtype of cystic pancreatic neoplasms. In the past, this tumor has also been named mucinous ductal ectasia or ductectatic mucinous cystic tumor. It originates from proliferating mucin-secreting cells in the ductal wall that form papillary folds. There is an abundant secretion of viscous mucin leading to obstructive dilatation of the ducts. Unlike other mucinous tumors, the tumor is more frequent in men and presents in the seventh decade. The tumor can be either benign or (low grade) malignant. Its location affects the macroscopic features and several subtypes are recognised the *main duct type*, *branch duct type*, and *combined type*.

Solid Papillary Epithelial Tumor (Figs 5.52A and B)

The low-grade solid papillary epithelial tumor (papillary epithelial neoplasm, papillary cystic neoplasm) is a very rare neoplasm that almost exclusively affects women between 20 and 30 years of age. It is a separate histopathologic entity that shows little propensity for metastasis.

CT Morphology

The tumor most commonly involves the pancreatic tail and can reach considerable size (10 cm). It contains areas of cystic degeneration, necrosis, and solid material in varying proportions, and its CT morphology resembles that of macrocystic adenoma. It shows little or no contrast enhancement, and cystic lesions do not contain septations.

Table 5.3: Acute or chronic pancreatitis with focal mass

Acute or chronic pancreatitis with focal mass is the main pathological condition to be considered in the differential diagnosis. The following findings are in favor of pancreatitis: a. Irregular dilatation of pancreatic duct; b. Presence of dilated ducts and small pseudocysts within the mass; c. Intraductal or parenchymal calcifications; d. Less pronounced degree of atrophy of the pancreatic parenchyma; e. Gradual (not abrupt) narrowing of the dilated pancreatic gland or bile duct.

Differential Diagnosis of Cystic Lesions of the Pancreas

Dysontogenic cyst: Sharply circumscribed with a faint or invisible wall; septations are very rare; does not enhance after contrast administration.

Pancreatic pseudocyst: Thick granulating wall; rarely contains septations; frequently extrahepatic; history or direct evidence of pancreatitis.

Abscess: Gas collection (rare), granulating rim.

Cystic fibrosis: Small cysts may occur; no pancreatitis; history consistent with cystic fibrosis fatty involution of pancreas.

Lymphangioma: Malformation with cluster of small cysts; calcifications may occur; cysts contain lymphatic fluid.

Microcystic adenoma: Multiple (6) cysts 1-20 mm in diameter with hypervascular septa and central calcifications (40%); central scar; unilocular variant very rare.

Macrocystic adenoma: Unilocular or multilocular large cystic structure with irregularly thickened, hypervascular septa; calcifications (15%); no central scar.

Cystadenocarcinoma: Same as macrocystic adenoma (often indistinguishable); foci of infiltration; hypoattenuating soft-tissue components; lymph node enlargement; metastases.

IPMT—main duct type: Diffuse/segmental dilation of pancreatic duct; intraductal papillary soft tissue excrescences; bulging papilla; vague intraductal calcifications.

IPMT—branch duct type: Multilocular cystic lesion, usually in uncinate process, segmental pancreatic duct dilatation; communication of cystic lesion with main duct; bulging papilla.

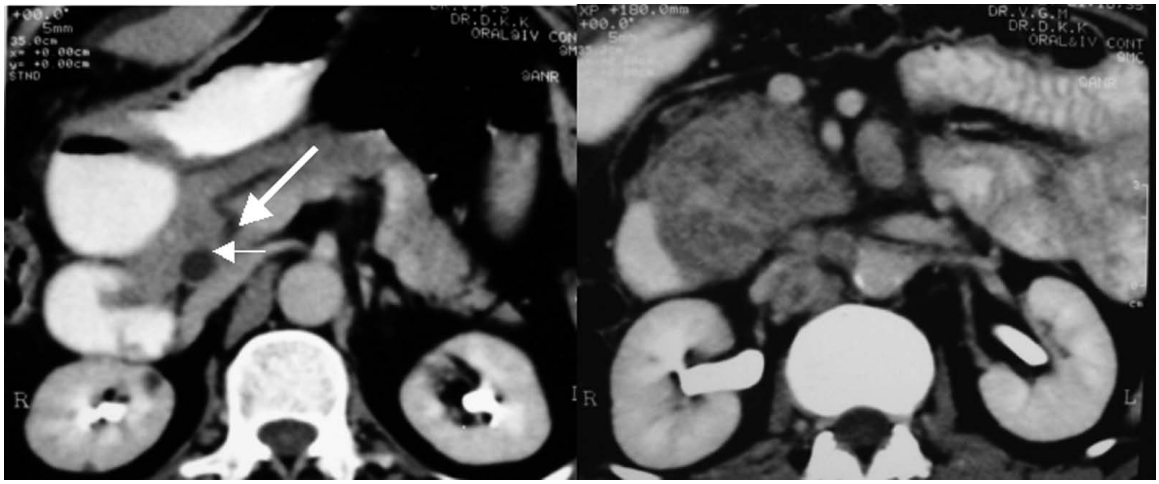

FIGURES 5.39A and B: Axial CECT reveals double duct sign (arrow showing both dilated pancreatic and common bile duct) Fig. B shows a large heterogeneously enhancing lesion in the pancreatic head.

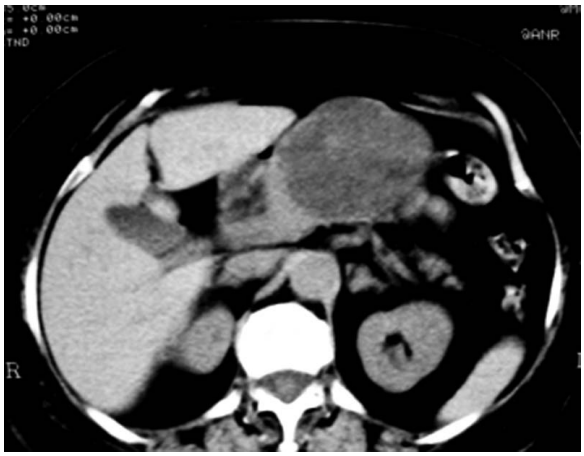

FIGURE 5.40: Axial CECT shows a large well capsulated lesion in the pancreatic body deforming the capsule—microcystic adenoma.

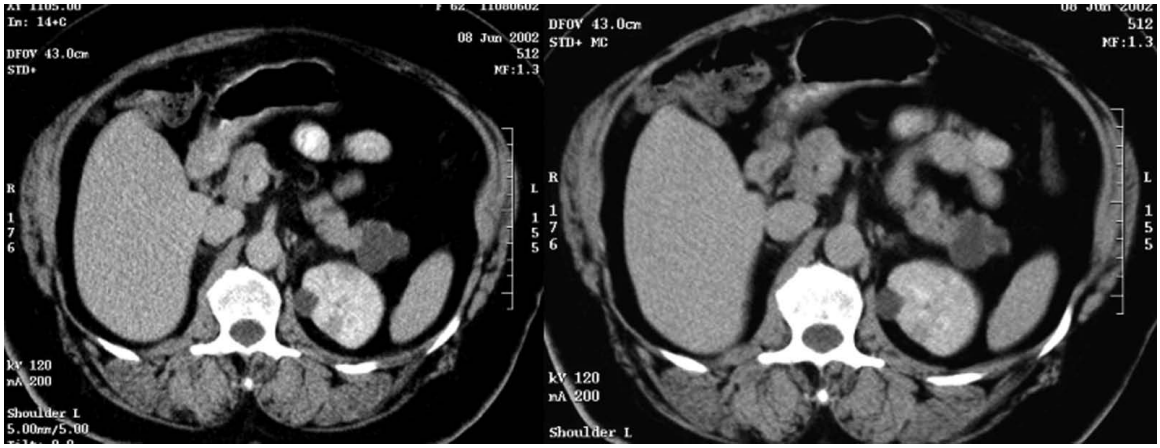

FIGURES 5.41A and B: Axial CECT reveals a well marginated hypodense non-enhancing lesion in the tail of pancreas suggestive of a mucinous cystadenoma.

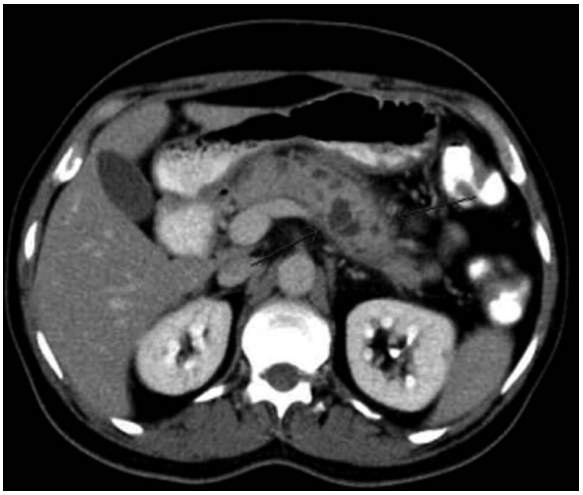

FIGURE 5.42: Axial CECT reveals nodular hypodense lesions in the body and tail of pancreas without deforming the contour – case of intrapancreatic mucinous tumor (IPMT).

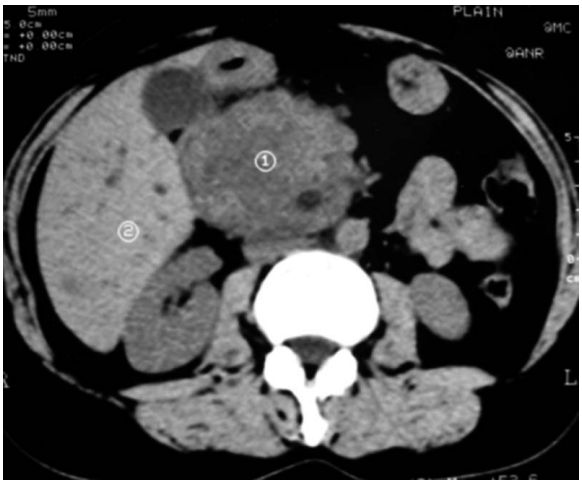

FIGURE 5.43: Axial plain CT reveals a large mass in the pancreatic head encasing the distal CBD.

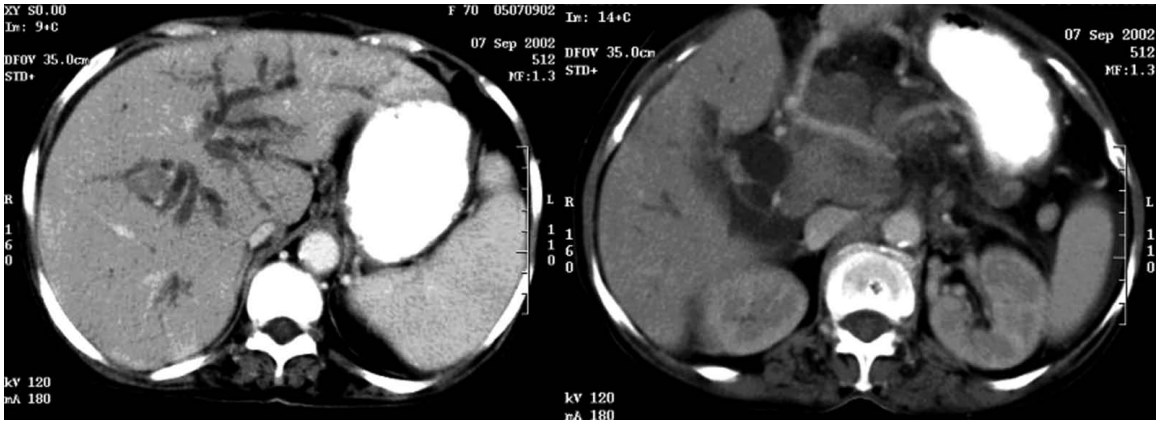

FIGURES 5.44A and B: (A) Axial CECT reveals dilatation of both intra- and extrahepatic biliary radicles. (B) Axial CECT reveals multiple lymph nodes encasing the celiac axis.

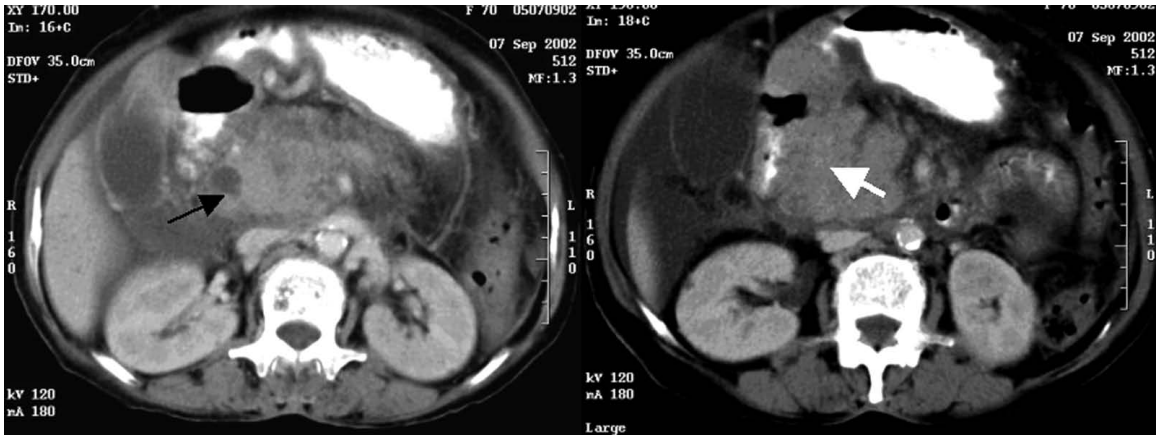

FIGURES 5.45A and B: Axial CECT reveals dilated distal CBD (arrow), axial CECT reveals circumferential thickening of the antrum with involvement of the pancreatic head (arrow).

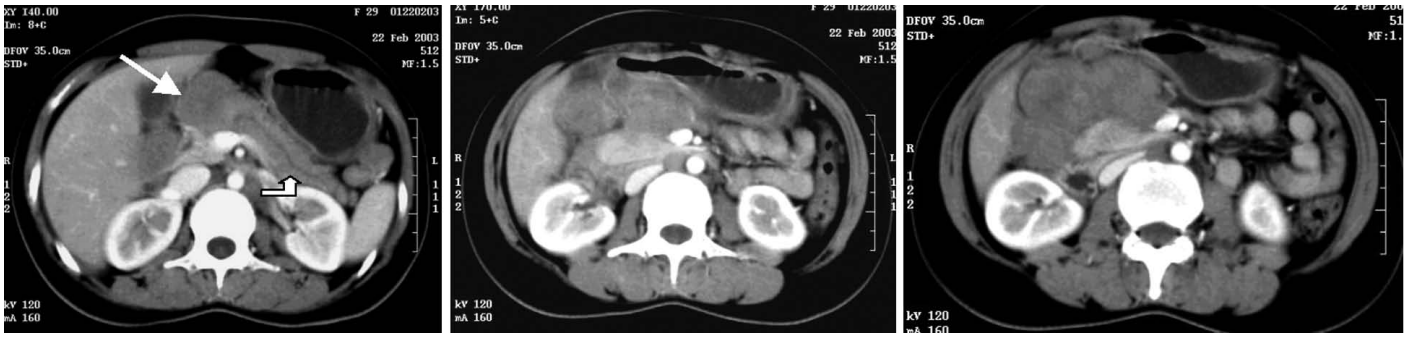

FIGURES 5.46A to C: Axial CECT reveals a hypodense lesion in the pancreatic head region (arrow) causing dilatation of the pancreatic duct (curved arrow), axial CECT reveals multiple hypodense lymph nodes (arrow in C).

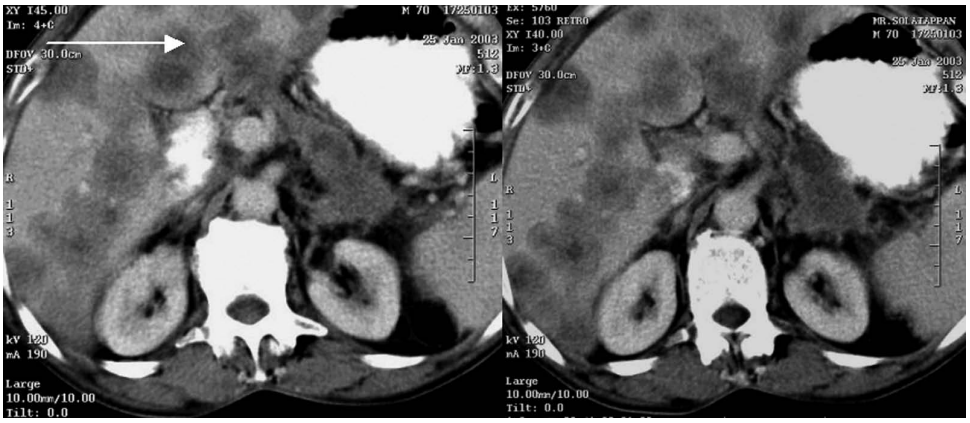

FIGURES 5.47A and B: Axial CECT reveals hypodense lesion in the body of pancreas (arrow) with multiple hypodense lesions in the liver suggestive of metastasis.

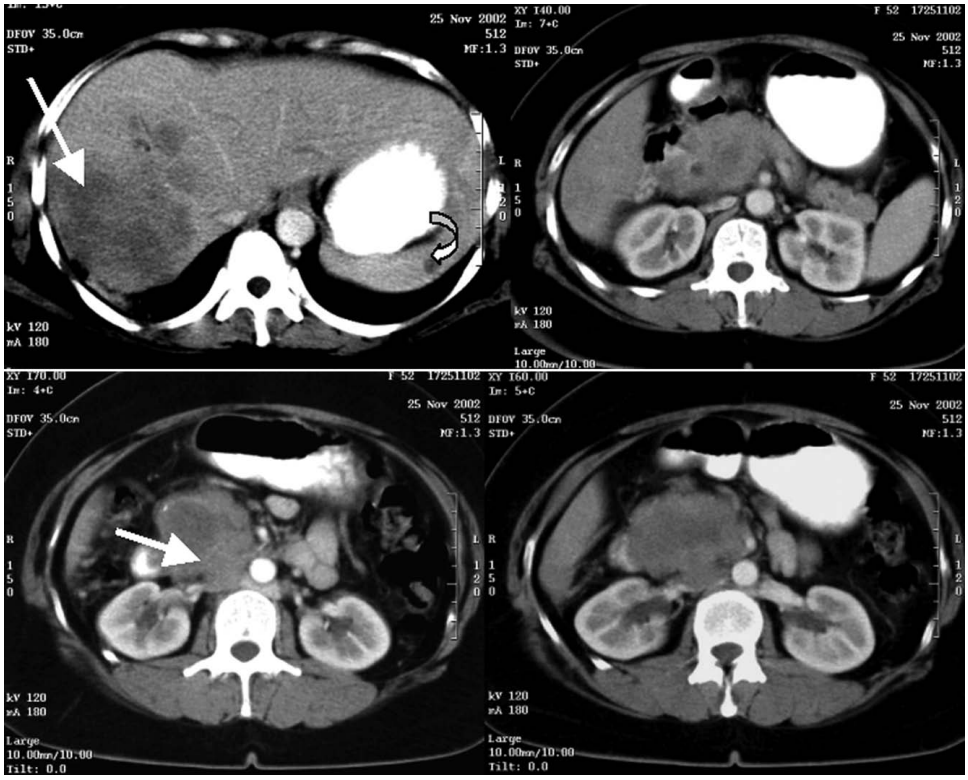

FIGURES 5.48A to D: Axial CECT reveals multiple hypodense lesion in the live (arrow), with a hypodense lesion in the spleen (curved arrow), axial CECT Figs B,C,D reveals a hypodense mass in the uncinate process of pancreas encasing the third part of duodenum with indentation on the right main renal artery (arrow in C).

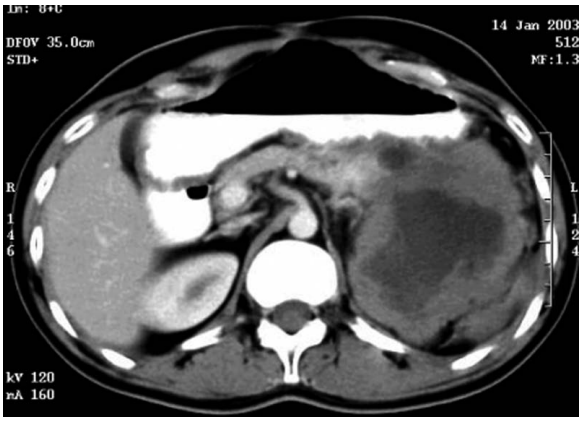

FIGURE 5.49: Axial CECT in a postoperative case of Ca pancreas involving the tail reveals a large heterogeneously enhancing mass in the tumor bed suggestive of recurrence.

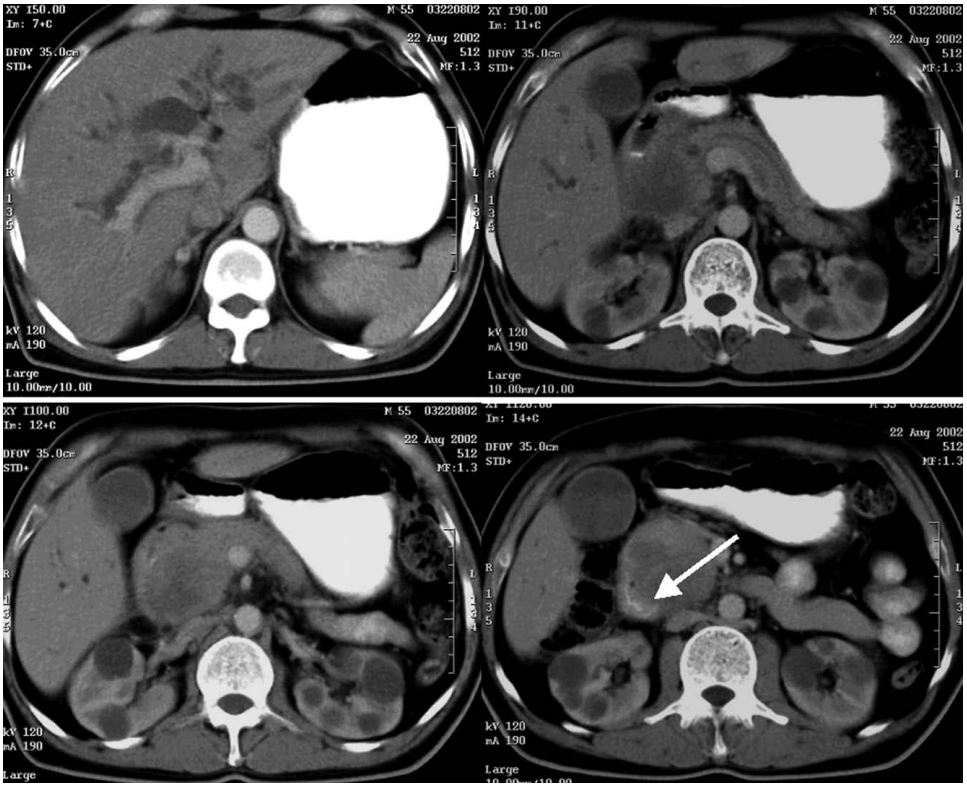

FIGURES 5.50A to D: Axial CECT (A) reveals IHBR dilatation, (B,C,D) reveals a hypodense lesion in the head of pancreas involving the medial duodenal wall (arrow in D) with pancreatic ductal dilatation.

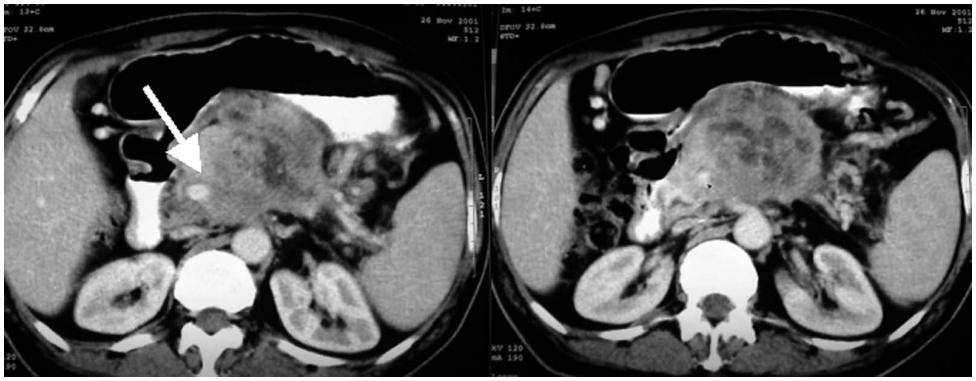

FIGURES 5.51A and B: Axial CECT reveals a heterogeneously enhancing lesion in the proximal body of pancreas encasing the SMA/SMV vessels (arrow) indenting the posterior stomach wall with loss of fat planes.

SOLID AND PAPILLARY EPITHELIAL NEOPLASM

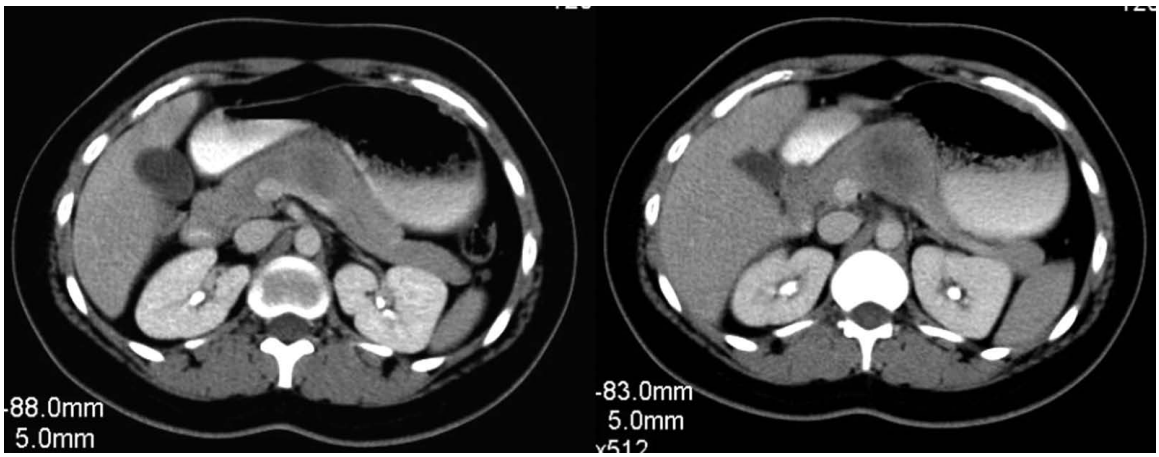

FIGURES 5.52A and B: Axial CECT reveals a hypodense lesion in the body of pancreas deforming the contour, indenting the posterior wall of stomach.

Pitfalls in Diagnosis of Pancreatic Masses

Stomach, Duodenum, and Proximal Jejunum

A normal redundant gastric fundus may lie posteroinferiorly and abut the pancreatic tail. The normal fourth portion of the duodenum or proximal jejunum abuts the pancreatic tail and may simulate a mass. Because small bowel will enhance to 110-120 HU after fast intravenous administration of a bolus of contrast material, it is not surprising that, in some cases, this phenomenon can result in a false-positive diagnosis of a pancreatic tail tumor.

The normal second portion of the duodenum and the pancreatic head tend to be displaced to the right posterolaterally after right nephrectomy and can be markedly distorted as a result. Doubts regarding bowel loops are best resolved with administration of additional positive oral contrast material.

Large tumors of the gastric fundus may displace it

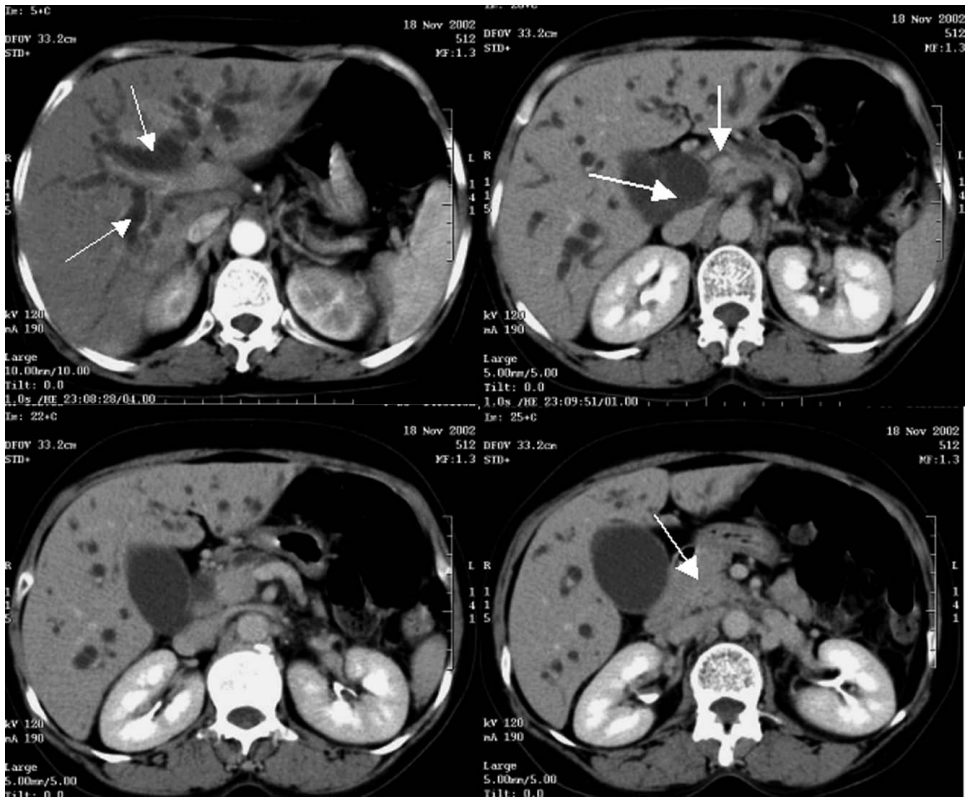

FIGURES 5.53A to D: Axial CECT (A) reveals dilated IHBR involving both lobes of liver (arrows), (B, C) positive double duct sign (dilated CBD, PD arrows) fig. (D) infiltrative soft tissue mass in the periampullary region (arrow).

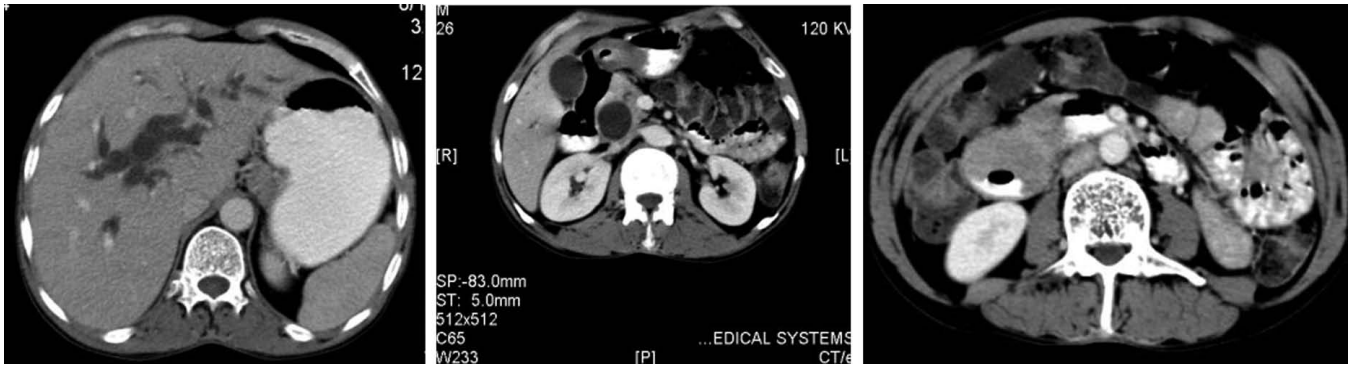

FIGURES 5.54A to C: Axial CECT (A) reveals IHBR dilatation, (B) shows dilated CBD, (C) shows a eccentric soft tissue mass involving the ampulla infiltrating the adjacent periampullary duodenum.

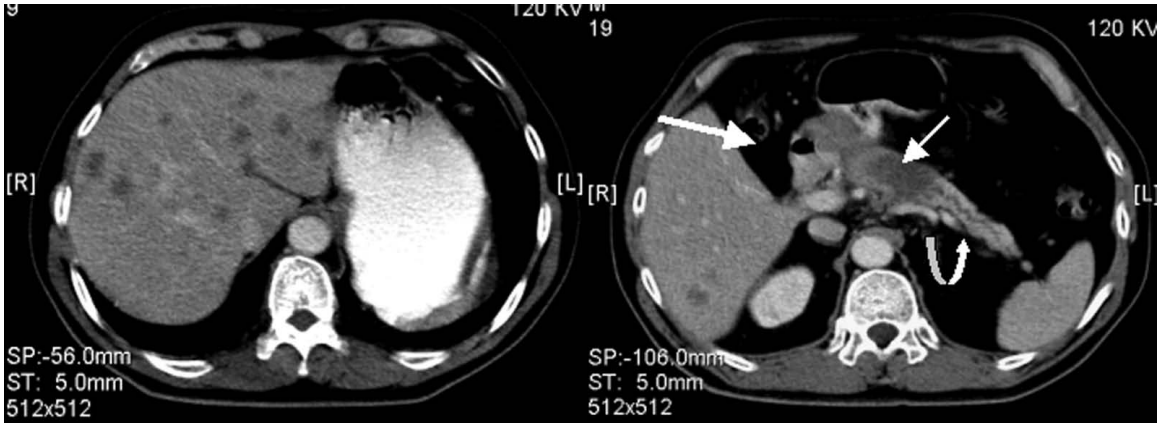

FIGURES 5.55A and B: (A) Axial CECT reveals multiple hypodense lesions in the liver, (B) axial CECT reveals a hypodense lesion in the body of pancreas with dilatation of the pancreatic duct distal to it (arrows).

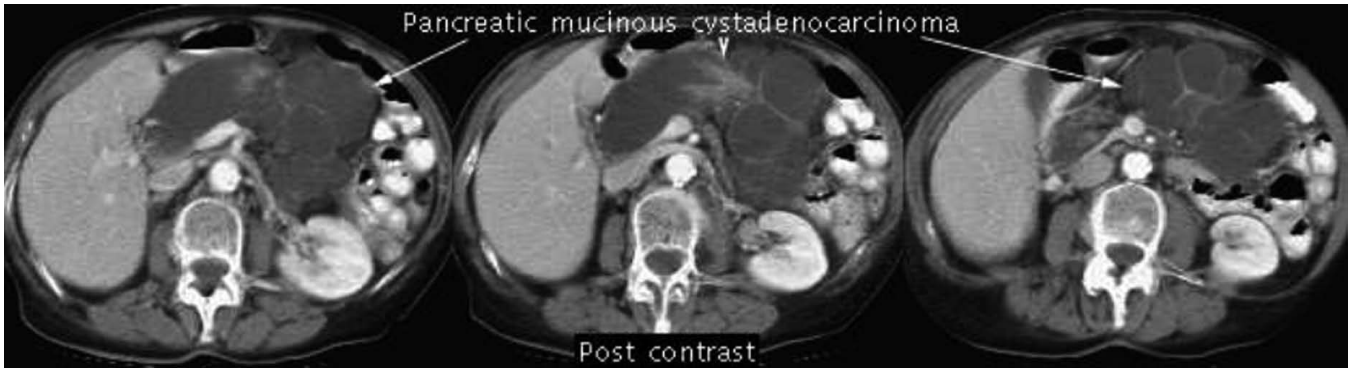

FIGURES 5.56A to C: Axial CECT reveals a multiseptated hypodense cystic lesion involving the body of pancreas.

inferiorly so that it abuts the pancreatic tail, and tumors of the posterior gastric wall may simulate a mass of the anterior pancreatic body. Most of the duodenum is directly apposed to the pancreas, so that there is no identifiable plane of delineation. Many duodenal lesions, both neoplastic and non-neoplastic have been confused with primary pancreatic disease. Extrinsic duodenal diverticulum or duplication cyst will simulate a necrotic mass or be confused with a pancreatic or peripancreatic abscess.

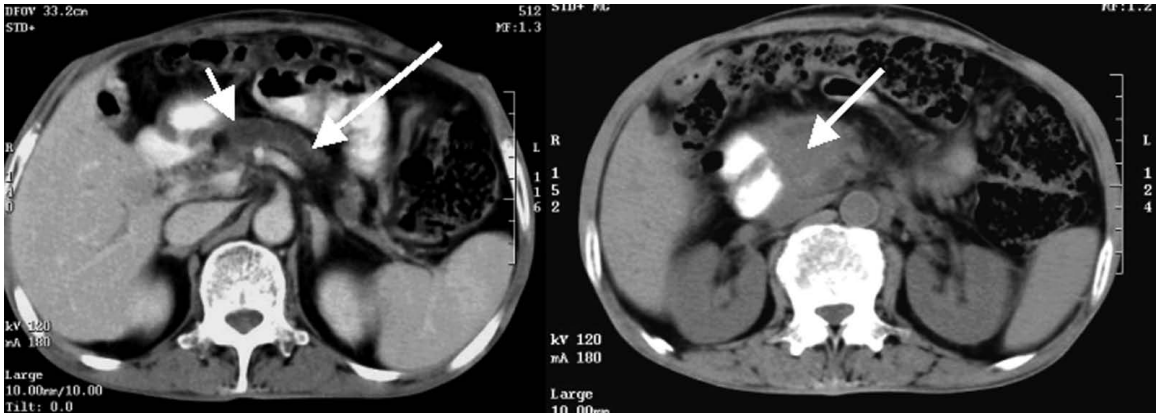

FIGURES 5.57A and B: (A) Axial CECT reveals atrophy of the body and tail with pancreatic ductal dilatation (arrow), (B) hypodense lesion in the uncinate process involving the medial duodenal wall (arrow).

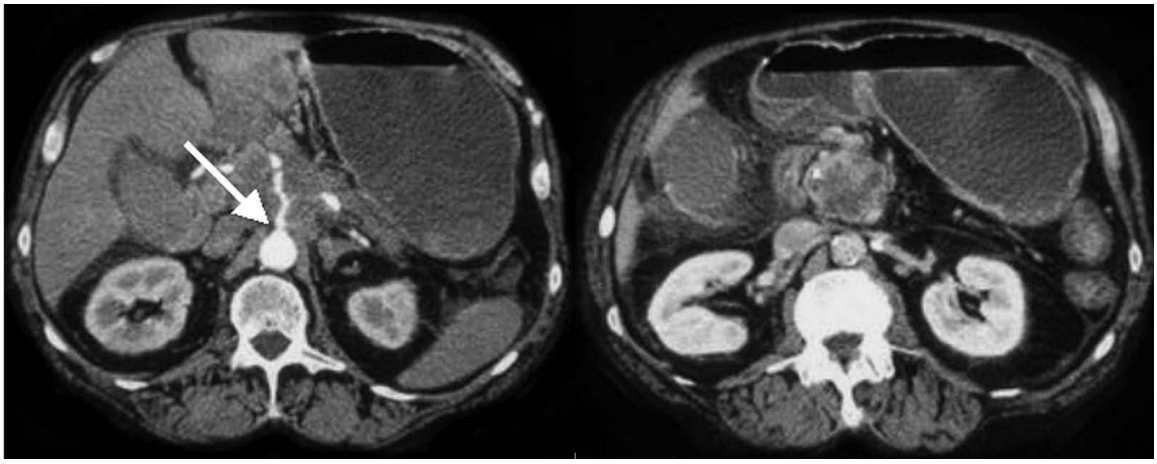

FIGURES 5.58A and B: Axial CECT reveals a heterogeneously enhancing mass in the head of pancreas encasing the celiac artery (arrow).

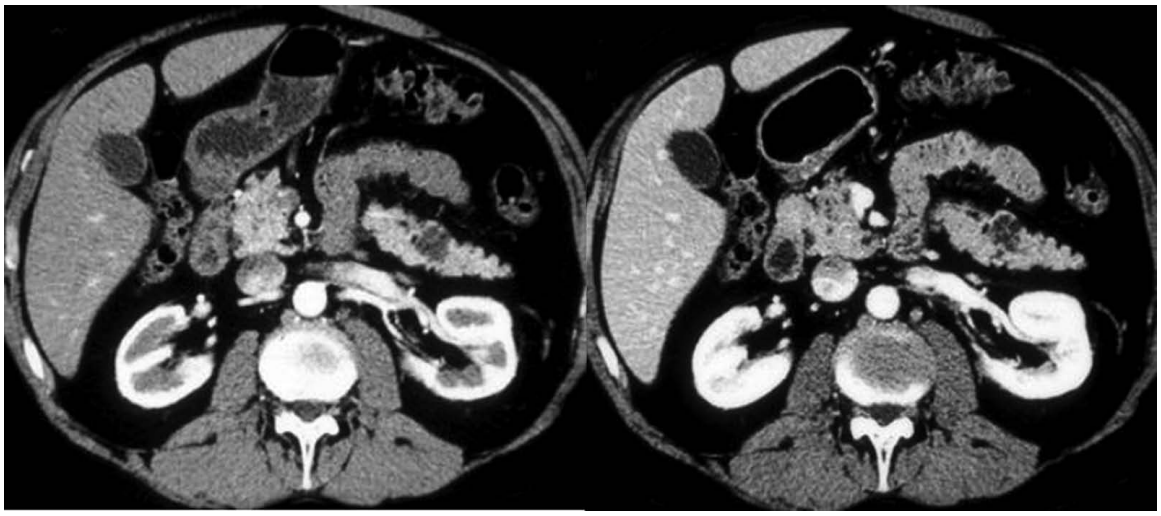

FIGURES 5.59A and B: Axial CECT reveals a well-defined nonenhancing hypodense lesion in the tail of pancreas suggestive of a focal mucinous tumor.

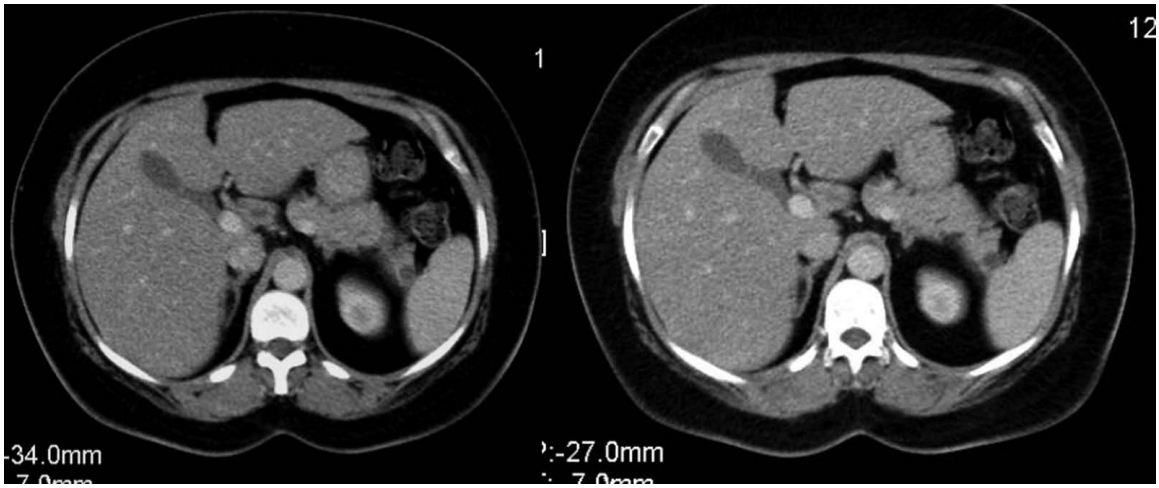

FIGURES 5.60A and B: Axial CECT reveals a small hypodense lesion in the tail of pancreas.

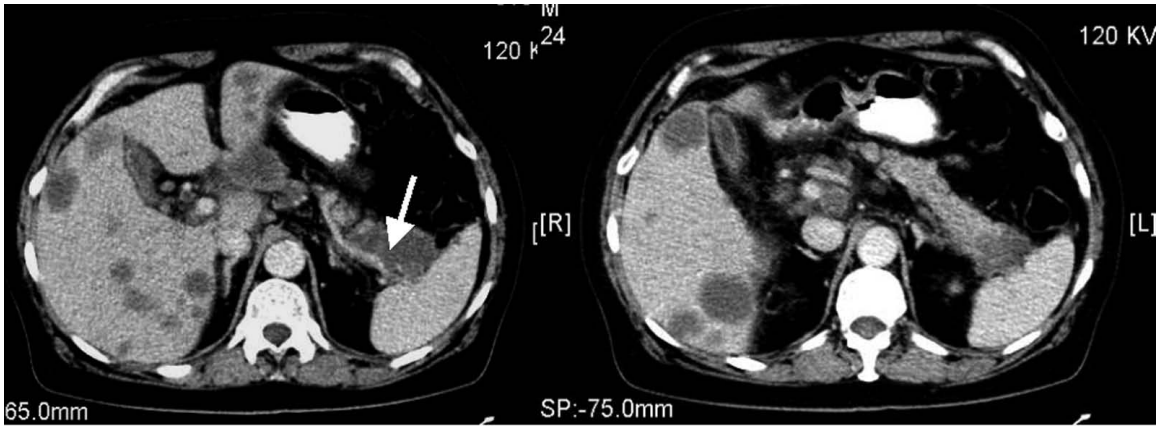

FIGURES 5.61A and B: Axial CECT reveals hypodense lesion in the tail of pancreas (arrow) with multiple hypodense lesions in the liver.

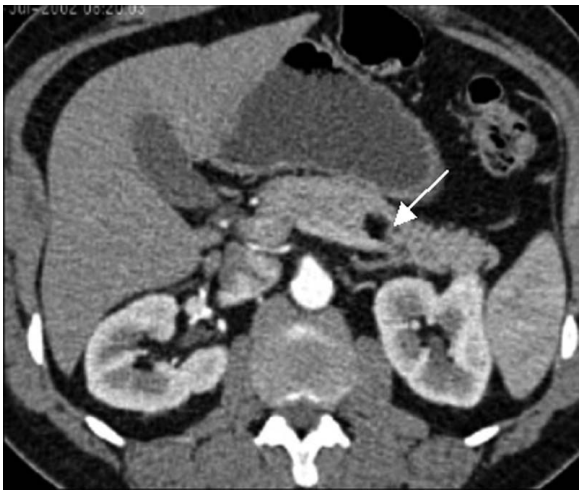

FIGURE 5.62: Axial CECT reveals a focal hypodense lesion in the body of pancreas with negative attenuation—features suggestive of a lipoma (arrow).

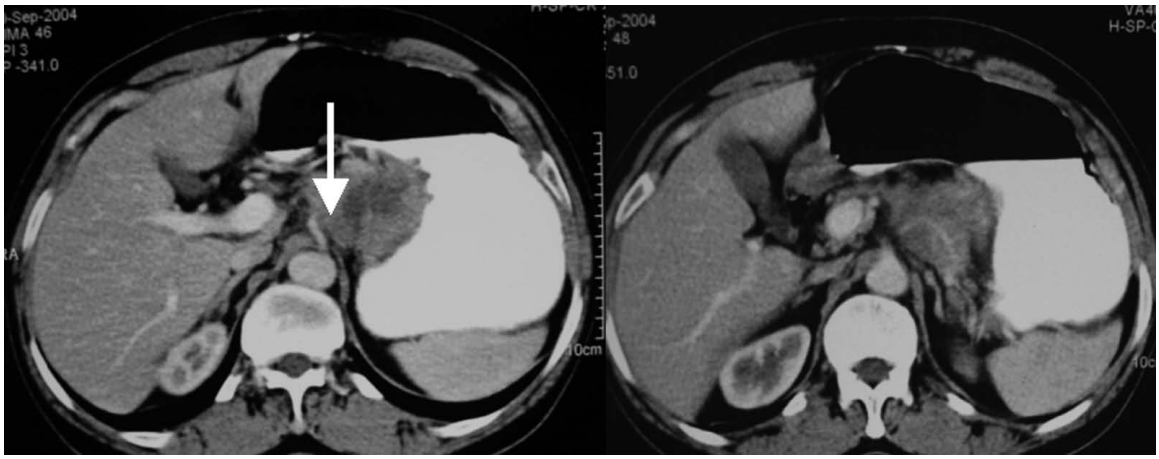

FIGURES 5.63A and B: Axial CECT reveals a heterogeneous moderately enhancing mass in the body of pancreas encasing distal celiac artery branches (arrow).

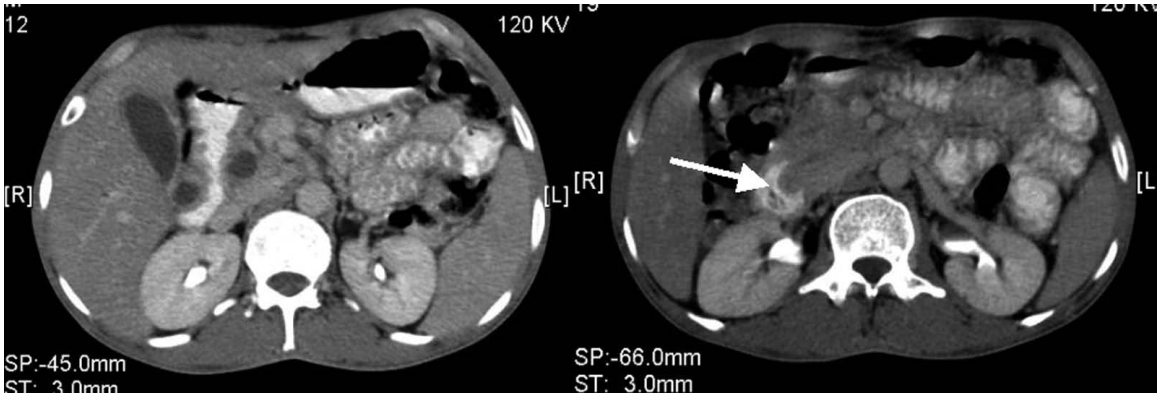

FIGURES 5.64A and B: Axial CECT (A) reveals positive double duct sign, (B) axial CECT reveals a well-defined mass in the ampullary region (arrow).

Adenopathy

Peripancreatic nodal enlargement can be due to a wide variety of pathologic processes ranging from lymphoma to gastrointestinal adenocarcinoma to granulomatous disease. Although at times these nodes may abut the pancreas, they are usually easy to distinguish because of their sharp borders, different enhancement patterns and textures, and known anatomic location. In other cases, especially in patients who are thin or have indistinct tissue planes or in the setting of bulky adenopathy, it may be difficult to distinguish nodes from the pancreas. The use of thin-section CT coupled with a properly timed contrast material injection usually makes this distinction clear by allowing optimal differentiation between the enhancing gland and the nonenhancing nodes.

Pancreatic Tuberculosis

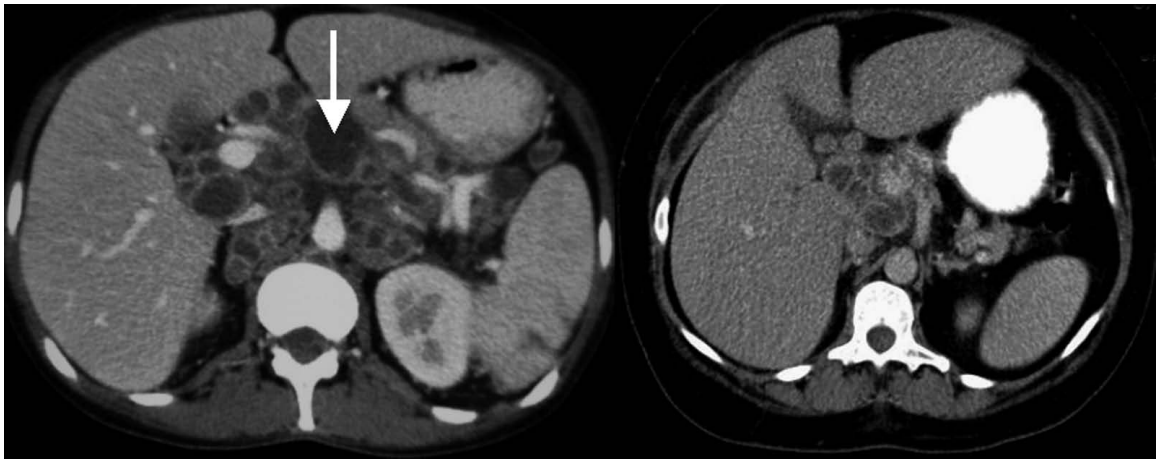

FIGURES 5.65A and B: Axial CECT in two different patients reveals multiple hypodense nodes in the peripancreatic region with hypodense lesion in the body (arrow).

Portocaval Nodes

Enlarged portocaval nodes are classically a site of recurrence in patients with right-sided colon cancer. Inflammatory processes such as tuberculosis, *Mycobacterium avium-intracellulare*, and sarcoidosis can involve this chain as well. Nonpathologic nodes at this site can exceed 1 cm in diameter.

Peripancreatic Nodes

Peripancreatic nodes are involved in a wide range of inflammatory and neoplastic diseases and can come into intimate contact with the pancreas. Many of these nodes lie near or around the second portion of the duodenum and between the duodenum and the pancreatic head. In most cases, these nodes are small (<1 cm) even in disease states, with lymphoma as a notable exception.

Nodes in the Root of the Mesentery

Nodal disease in the mesentery may be a result of inflammatory or neoplastic disease. When bulky, these nodes may extend up to or directly involve the lower aspects of the pancreas and encase the vasculature.

Adrenal Masses

Masses arising from the adrenal gland can typically be recognized as adrenal in origin, especially when they are 4 cm or less in diameter. As tumors get larger (especially when 8-10 cm or more in diameter), the normal gland is obscured and anatomic localization is difficult. Lesions of the right adrenal gland can occasionally be confused with a pancreatic lesion. On the left side, misdiagnosis may be more of an issue with larger tumors. This pitfall may also occur with a potentially benign adrenal lesion such as an adrenal cyst which can be confused with pancreatic pseudocyst, intraductal papillary mucinous tumor, cystadenoma, carcinoma, or cystic islet cell tumor.

Renal Masses

Larger renal tumors or masses that arise from the medial upper pole of the kidney may also be a source of confusion. Such tumors can displace or abut the pancreas and be confused with primary pancreatic disease. This problem is

more common with involvement of the upper pole of the left kidney, where larger masses may interface with the pancreatic tail through the lienorenal ligament or directly traverse the retroperitoneal layers.

Mesenteric Masses

Mesenteric masses (e.g. nodes) and tumors or tumor-like diseases (e.g. desmoid tumors, carcinoid tumors) may extend up to the base of the pancreas along the superior mesenteric vascular pedicle, large cancers of the colon can spread to the pancreas (and vice versa) along the transverse mesocolon. Mesenteric lesions tend to remain intimately related to the vasculature as they infiltrate inferiorly or anteriorly, often preserving a fat plane, whereas primary pancreatic lesions tend to spread within the anterior pararenal space.

DIFFERENTIAL DIAGNOSIS IN PANCREATIC DISEASE

Pancreatic Calcifications

- Chronic pancreatitis
- CBD stone
- Islet cell tumor
- Microcystic adenoma
- Organized pseudocyst
- Cystic fibrosis.

The discovery of pancreatic calcifications has long been used in the diagnosis of pancreatic disease, and for many years imaging of the pancreas was largely limited to the radiographic identification of these calcifications. Today, our ability to image the pancreas has greatly advanced with modalities including CT, sonography, endoscopic retrograde cholangiopancreatography, and MR imaging. This improved visualization of the pancreas allows better identification of pancreatic calcifications and their underlying cause.

Inflammatory Causes

Chronic alcoholic pancreatitis is the most common cause of pancreatic calcifications. The ducts become obstructed by proteinaceous plugs that can eventually accumulate calcium carbonate. This obstruction results in ductal ectasia and periductal fibrosis. The calculi occur in ducts of all sizes and vary from microscopic to greater than 1 cm in diameter.

The CT appearance is generally that of numerous irregular small calcifications throughout the pancreas. The head of the pancreas is usually involved more prominently than the tail.

Developmental

Hereditary pancreatitis has an autosomal dominant pattern of inheritance with an estimated 80% penetrance. It generally manifests itself during childhood with a peak incidence at 5 years old. However, a second peak at 17 years old may be attributable to the introduction of alcohol in the diet. Intraductal calcifications occur in approximately 50% of patients. These stones have a characteristic large, rounded appearance.

Neoplasms

The most common primary pancreatic tumor, ductal adenocarcinoma, characteristically does not calcify. However, pancreatic carcinoma may develop in a pancreas with underlying chronic calcific pancreatitis. Or, calcifications may develop in the setting of chronic pancreatitis from an obstructing ductal adenocarcinoma. A number of less common tumors have associated calcifications. Islet cell tumors are known for the presence of tumoral calcifications. Islet cell

tumors are classified as functional or nonhyperfunctional. Functional tumors are typically detected early because of their symptoms and thus are frequently less than 2 cm in diameter. Nonhyperfunctioning tumors tend to be larger at the time of diagnosis, measuring over 8 cm in diameter.

Serous cystadenomas are made up of numerous, small, thin-walled cysts. These characteristics give the tumor an overall nodular border with a honeycomb internal architecture. The tumors commonly calcify. The pattern of calcification is characteristic of a central calcified scar with calcified septations radiating outward, resulting in a sunburst pattern.

The mucinous cystic neoplasm consists of a thick outer capsule with its inner portion characteristically composed of ovarian stroma. Mucus fills the cyst, but septations and polypoid excrescences may also be present. Calcifications occur in the cyst wall or septa and tend to be curvilinear.

Focal Pancreatic Mass

Inflammatory

- Acute and chronic pancreatitis
- Pseudocyst
- Abscess
- Phlegmonus mass

Neoplastic

- Islet cell tumors
- Adenocarcinoma
- Mucinous cystadenoma
- IPMT (intra pancreatic mucinous tumor)
- Microcystic adenoma

Miscellaneous

- Pseudoaneurysm
- Complicated pseudocyst
- Lymphoma

Pancreatic Duct Dilatation

- Ductal calculi
- Chronic pancreatitis
- Ampullary mass
- Adenocarcinoma
- IPMT

Neoplastic duct dilatation has a smooth or lobulated appearance, duct occupies more than 50% of AP gland diameter.

Pancreatic and Peripancreatic Cystic Lesions

- Pseudocyst
- Cystic neoplasms
- Congenital—cystic ductal anomalies, polycystic disease, duplication cyst
- Echinococcal cyst
- Fluid collection in acute pancreatitis.

CHAPTER

6

Genitourinary System

The kidney can be excellently analyzed with computed tomography because of its typical enhacement characteristics, which allow for an optimal visualization of the renal parenchyma, renal lesions, and the renal vessels. Spiral CT has improved the detection and characterization of small renal neoplasms.

NONCONTRAST CT

A precontrast examination of the kidneys is appropriate for almost all investigations with primarily renal indications. Noncontrast scans are mandatory for detecting small calculi and are important for identifying hemorrhage and for measuring the density of fatty tumor components, e.g. in angiomyolipomas. Collimation should not exceed 5 mm, and smaller collimation will further improve the detection of small calculi.

Table 6.1: CT techniques for different renal CT indications

		Phases after contrast administration			
Scan delay	-	*25 sec*	*100 sec*	*> 5 min*	*> 15 min*
Clinical problem	*Noncontrast*	*Arterial*	*Parenchymal*	*Excretory*	*Delayed excretory*
Indeterminate lesion (suspicious for RCC)	+	+	+	-	-
Suspected RPC	+	-	+	+	-
Ureteral lesion	+	-	+	+	-
Pyelonephritis	-	-	+	-	+
Abscess	+	-	+	-	-
Urinary tract stone	+	-	-	+	-
Trauma	+	+	+	-	-
Vascular injury	+	+	+	-	-
Urinoma	+	-	+	-	+

RCC= renal cell carcinoma, RPC = renal pelvic carcinoma

Corticomedullary phase (delay 25-35 seconds) is a useful adjunct for demonstrating the vascular anatomy of the kidneys, especially in patients scheduled for nephron-sparing surgery. It may help distinguish small hypervascular tumors from pseudoenhancing cysts. In the vast majority of cases, hypervascularity suggests renal cell carcinoma. Arterial phase scanning alone may miss hypovascular lesions that are confined to the renal medulla.

Arterial phase scanning is therefore not mandatory, and imaging in the nephrographic phase in general will suffice for detection and staging of renal malignancies.

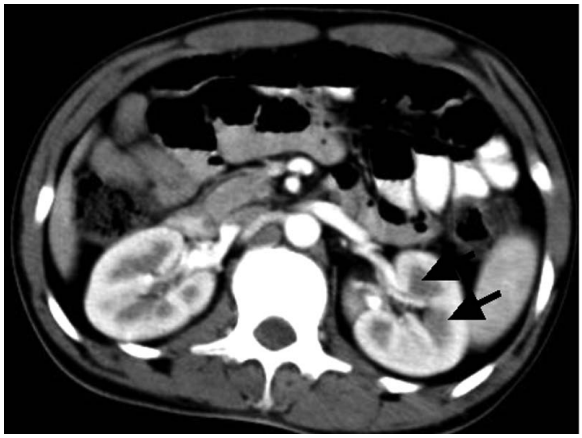

FIGURE 6.1: Axial CECT demonstrating the corticomedullary phase note the differential enhancement of cortex and medulla (arrow).

Parenchymal phase of enhancement (also called *nephrographic phase;* scan delay approximately 100-120 seconds).

During this phase the cortex and medulla show equal levels of enhancement while lesions appear markedly hypoattenuating to the renal parenchyma. For this reason, the rate of tumor detection is best in this phase.

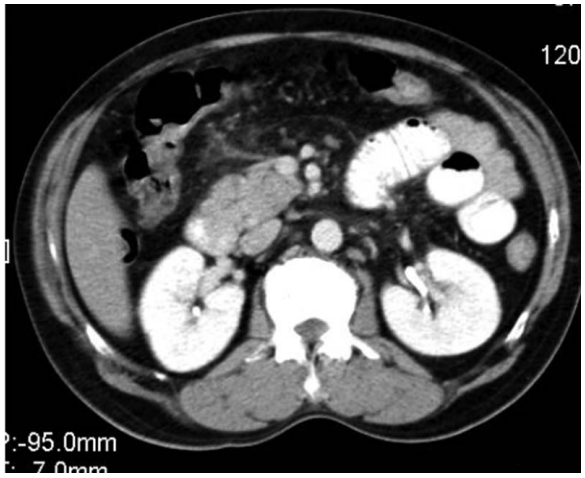

FIGURE 6.2: Axial CECT showing the uniform enhancement of the nephrographic phase, note the equal corticomedullary enhancement.

Excretory phase (*Pyelogram phase*) For studies focusing on the excretory portion of the urinary tract, images are acquried more than 6-10 minutes after the start of the contrast injection.

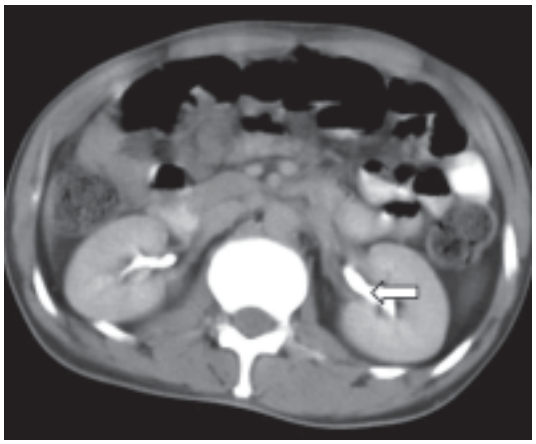

FIGURE 6.3: Axial CECT showing opacification of pelvis and ureter (arrow).

Hematuria

Hematuria can be well evaluated with a comprehensive contrast material–enhanced computed tomography protocol that combines unenhanced, nephrographic-phase, and excretory-phase imaging. Unenhanced images are obtained from the kidneys to the bladder and allow optimal detection of renal calculi, a common cause of hematuria. Renal parenchymal abnormalities, particularly masses, are best visualized on nephrographic-phase images, which also provide excellent evaluation of the other abdominal organs. Thin-section delayed images obtained from the kidneys to the bladder demonstrate the urinary tract distended with contrast material and are useful in detecting urothelial disease.

Hematuria can have a wide range of causes, including calculi, neoplasms, infection, trauma, drug toxicity, coagulopathy, and varices.

Calculi

Renal, ureteral, and bladder calculi are a common cause of hematuria. Twelve percent of people develop kidney stones at some point during their lifetime. The best imaging modality for evaluating calculi is unenhanced helical CT, which is commonly performed in patients with renal colic to detect obstructing calculi. In patients with hematuria, unenhanced CT is also helpful in detecting nonobstructing calculi.

Renal Masses

Renal masses frequently manifest with hematuria. Characterization of a renal mass as a simple cyst, a complex cyst, or a solid mass is essential. Simple cysts are benign and do not warrant further evaluation. Solid masses, with the exception of angiomyolipomas, are presumed to be malignant.

Papillary Necrosis

Papillary necrosis can have a wide range of causes, including diabetes, analgesic abuse, sickle cell disease, pyelonephritis, renal vein thrombosis, and obstructive uropathy. Excretory-phase CT may provide IVU-like visualization of the collecting system, allowing the diagnosis of papillary necrosis to be made.

Renal Pelvic and Ureteral Disease

A filling defect in the renal pelvis or ureter can be due to a neoplasm, calculus, blood clot, mycetoma, or vascular impression. Obstruction at the ureteropelvic junction (UPJ) may occur due to a short segment of nonfunctional smooth muscle and typically manifests with hydronephrosis. Other types of ureteral abnormalities include narrowing due to stricture or extrinsic disease.

Bladder Abnormalities

Bladder abnormalities are a common cause of hematuria and include neoplasms, usually transitional cell carcinoma, particularly in patients with exposure to aniline dyes, phenacetin, tobacco, and prior radiation therapy. Cystitis and diverticula are other types of bladder disease that may also cause hematuria. Bladder diverticula may be congenital, such as Hutch and urachal diverticula, or they may be acquired. Diverticula can predispose to carcinoma, calculi, or infections.

CLASSIFICATION OF CONGENITAL RENAL ABNORMALITIES

- Abnormalities of number
  - Renal agenesis
  - Supernumerary kidney

- Abnormalities of position
  - Rotational abnormalities—malrotation, nonrotation
  - Renal ectopia
- Abnormalities of renal fusion
  - Horse-shoe kidneys
  - Crossed fused ectopia
- Abnormalities of renal vasculature
  - Anomalous renal arteries and veins
- Abnormalities in structure
  - Fetal lobation
  - Renal pseudotumors
    - Column of Bertin
    - Hilar lips
    - Renal duplication
- Congenital cystic disease
  - Multicystic dysplastic Kidneys
    - Pelvoinfundibular type
    - Hydronephrotic type
  - Autosomal recessive polycystic kidney
    - Perinatal
    - Neonatal
    - Infantile
    - Juvenile
  - Medullary sponge kidney
  - Multilocular cystic nephroma
  - Calyceal diverticulum
- Congenital solid masses
  - Mesoblastic nephroma
  - Nephroblastomatosis
- Congenital ureteropelvic junction obstruction

Renal Agenesis

Failure of one or both kidneys to develop. Males are affected most often. Renal agenesis and dysplasia appear to be related disorders. Unilateral renal agenesis is sometimes associated with contralateral renal dysplasia.

Solitary Kidney

1 in 500-1000 livebirths, ipsilateral ureter, ureteral orifice and hemitrigone are absent in 80% of cases. Renal artery and vein are usually absent. Left sided renal agenesis is usally associated with presence of a left renal vein draining the left adrenal and gonadal veins. In males ipsilateral genital ducts may be absent with cyst in the seminal vesicle. Contralateral kidney is usually normal, dysplastic, malrotated, ectopic or hydronephrotic.

Bilateral Renal Agenesis

Most infants are born premature or stillborn, maternal oligohydramnios is a common feature. Renal arteries and ureters are generally absent. Trigone of the bladder is poorly defined.

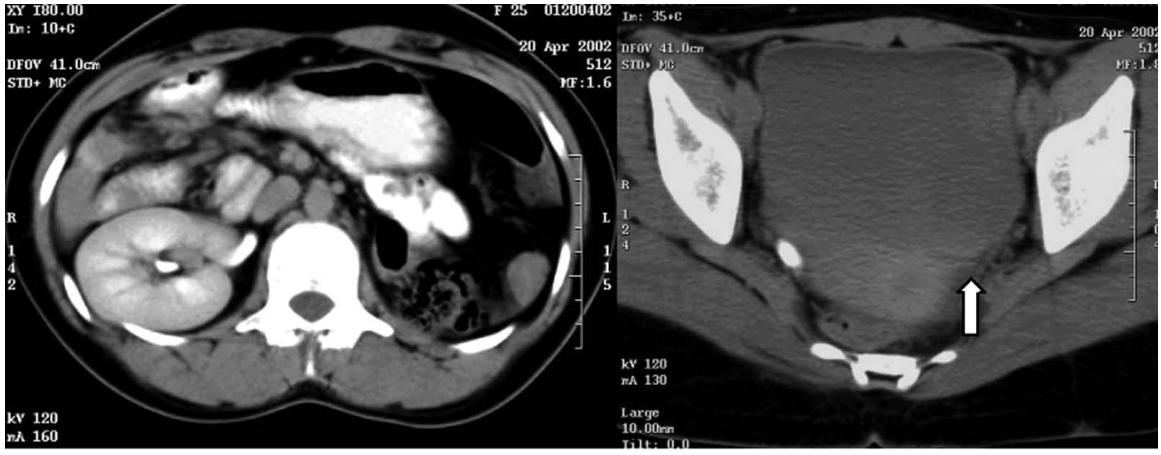

FIGURES 6.4A and B: Axial CECT showing absent left kidney, note the absence of the left ureterovesicle junction (arrow).

Simple Renal Hypoplasia

Dwarf or miniature kidney as its called is small but histologically and functionally normal kidney. Usually isolated in occurrence ureter, bladder and urethra normal. Main renal arteries and branches are small.

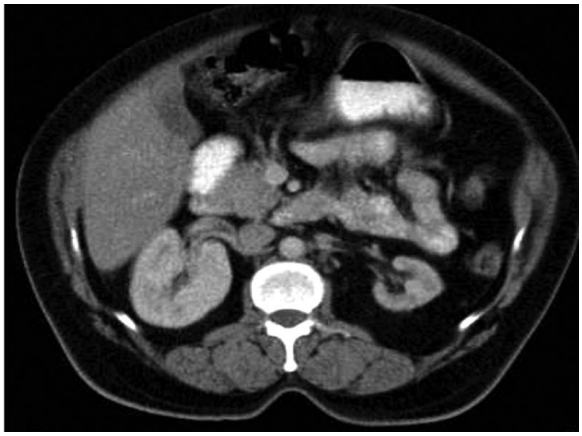

FIGURE 6.5: Axial CECT reveals a hypoplastic left kidney, note the smooth margins and simultaneous nephrogram when compared to the right kidney.

Ask Upmark Kidney

Segmental renal hypoplasia as its called is characterized by diminution in size and by presence of a transverse groove in the surface of kidney with clubbing of the underlying calyces. Commonly seen in adolescent females. Presently it is thought to be a form of chronic atrophic pyelonephritis due to vesicoureteric reflux.

Renal Aplasia

In this variant, the affected kidney is reduced to a nodule of tissue recognizible as kidney only histologically. Ureter ends blindly at the level of the aplastic kidney.

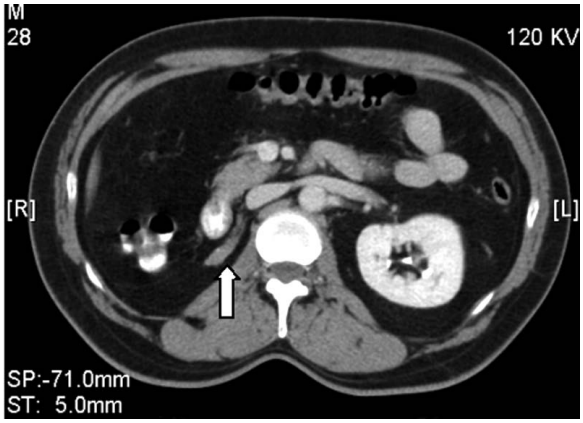

FIGURE 6.6: Axial CECT showing the right kidney replaced by a small nubbin of tissue (arrow).

Anomalies of Rotation

As the kidney ascends in fetal life from its origin in the pelvis to its fixed position opposite the second lumbar vertebrae, it undergoes a 90° inward rotation along its longitudinal axis so that the renal hilum is directed medially. In incomplete or deficient rotation or nonrotation the hilum faces anteriorly.

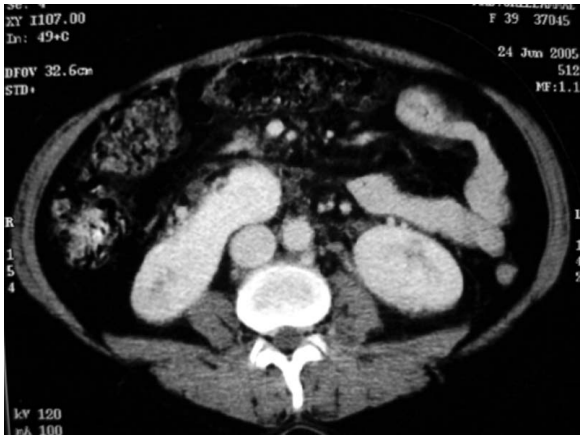

FIGURE 6.7: Axial CECT showing malrotated right kidney with anteriorly placed pelvis.

Renal Ectopia

Simple uncrossed renal ectopia – the affected kidney is in abnormal position, but without crossover to the opposite side or fusion with the opposite kidney. In low renal ectopia, the abnormal kidney lies in the lumbar, iliac or pelvic area and is frequently malrotated. The length of ureter is appropriate to the position of the kidney distinguishing true ectopia from nephroptosis. In high renal ectopia usually the left kidney is involved and is within the lower thorax posteriorly.

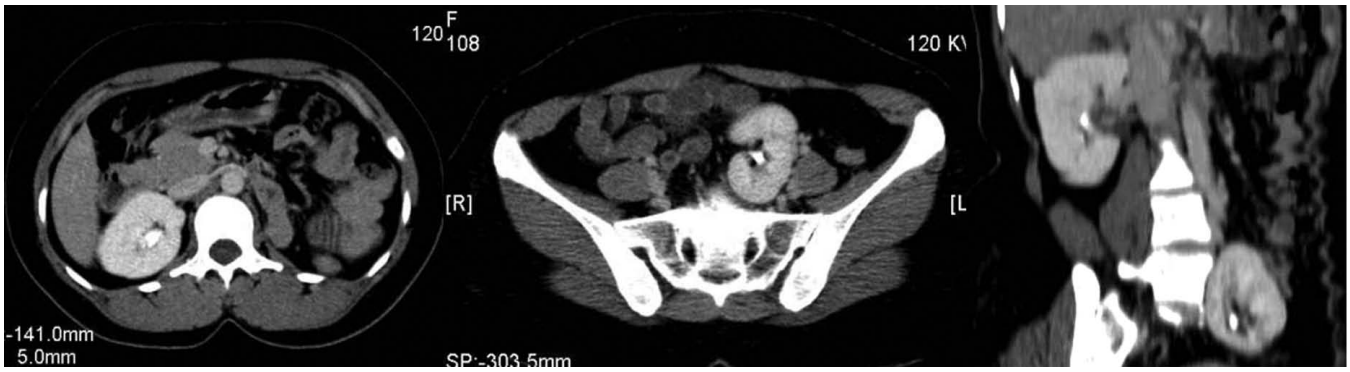

FIGURES 6.8A to C: Axial CECT with coronal reformation showing left pelvic kidney.

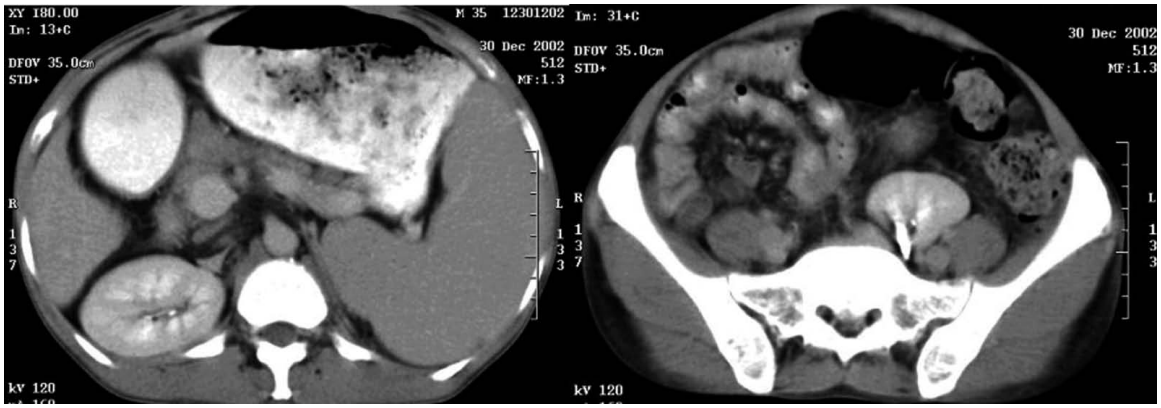

FIGURES 6.9A and B: Axial CECT showing left pelvic kidney with malrotation.

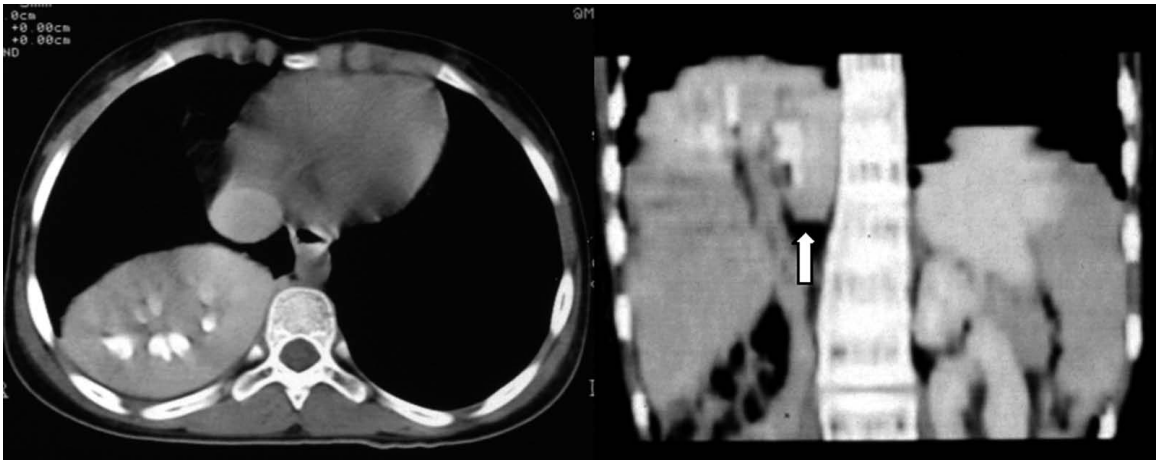

FIGURES 6.10A and B: Axial CECT with reformation studied showing right thoracic kidney, note the gap in the posterior diaphragmatic hiatus (arrow).

Crossed Renal Ectopia

Anomalous kidney lies below the orthotopic kidney. Usually ectopic kidney is vertically oriented and in most cases the fusion is between lower pole of orthotopic kidney and upper pole of the ectopic kidney. Malrotation of the ectopic kidney is the rule, it may be S-shaped or L-shaped.

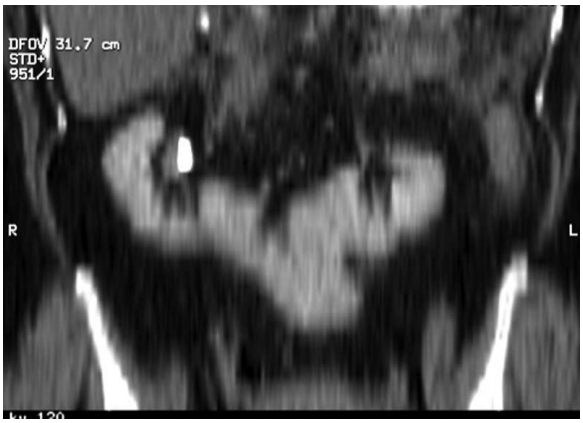

FIGURE 6.11: Coronal reformatted image showing supernumerary kidney with fusion.

Horse-shoe Kidney

Most common type of renal fusion anomalies, characterized by fusion of lower poles across the midline by an isthmus lying anterior to the aorta and IVC. Isthmus is usually composed of renal parenchyma but occasionally can be a fibrous band.

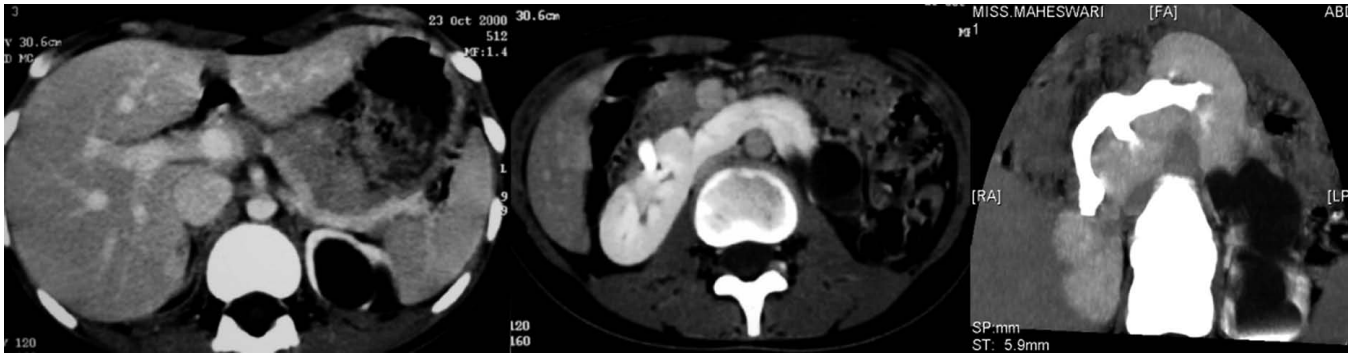

FIGURES 6.12A to C: Axial CECT with oblique reformation reveals horse-shoe kidney with a left renal upper pole duplicated system showing dilated collecting system.

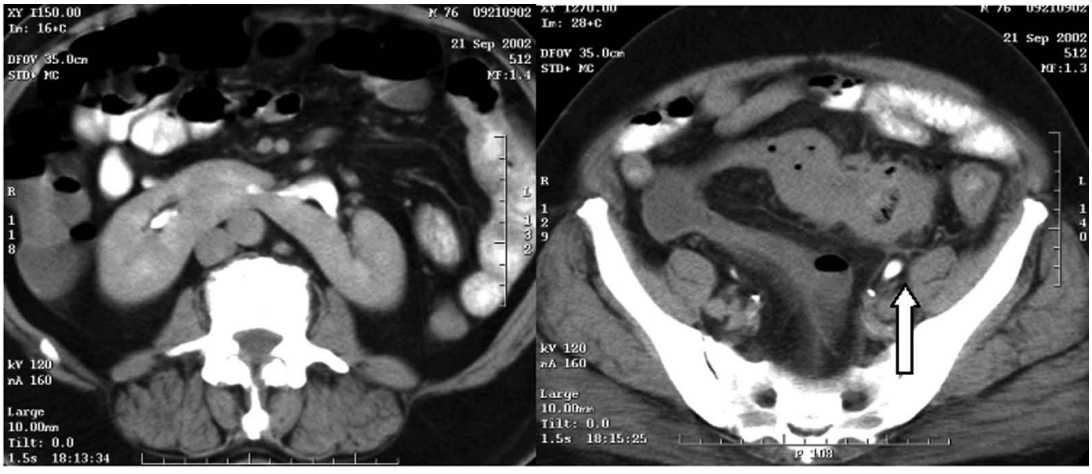

FIGURES 6.13A and B: Axial CECT showing horse-shoe kidney with a single left ureter (arrow).

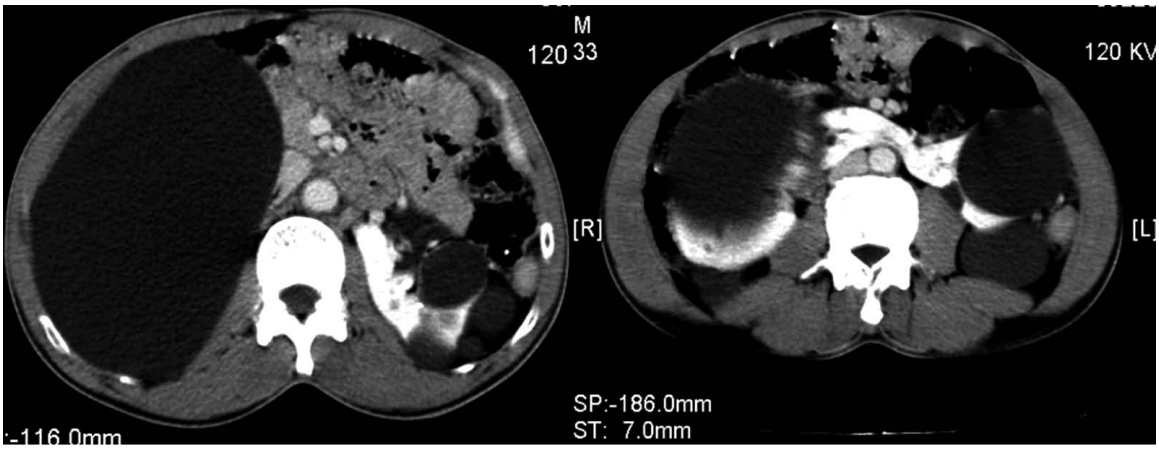

FIGURES 6.14A and B: Axial CECT showing horse-shoe kidney with multiple cysts suggestive of a polycystic renal disease.

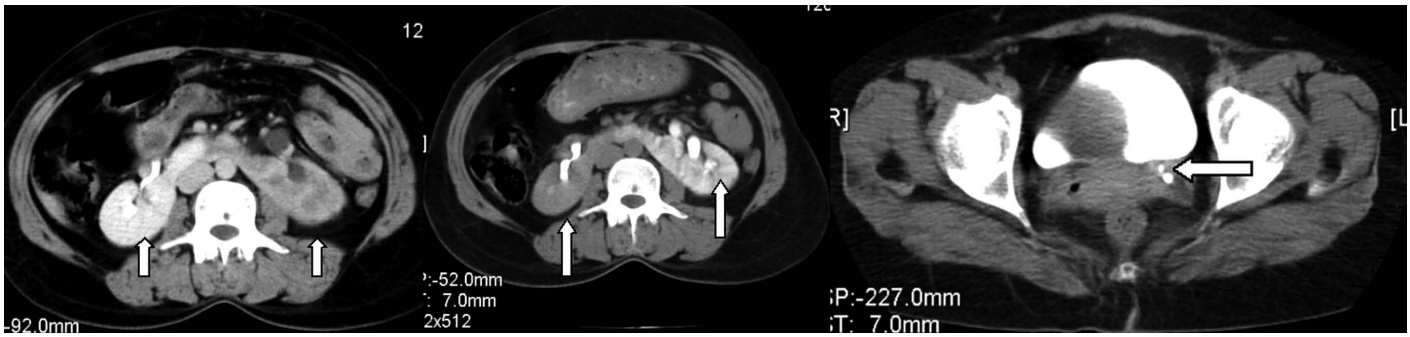

FIGURES 6.15A to C: Axial CECT showing delayed contrast excretion in the left kidney and the left segment of the isthmus of a horse-shoe kidney with dilated ureter suggestive of obstruction to the left ureter (arrow in Fig A). Note the typical differential excretory pattern which occurs in an obstructive system as shown in the Fig. B which shows the delayed nephrogram in the left side. Figure C at the level of UVJ showing narrowing suggestive of a stricture (arrow).

Cystic Disease

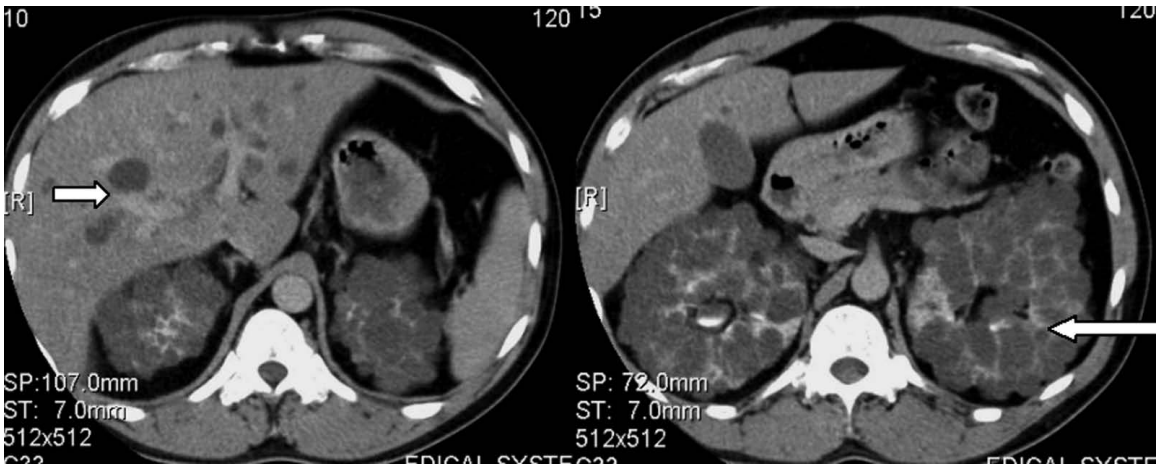

FIGURES 6.16A and B: Axial CECT showing bilateral enlarged kidneys showing multiple cysts (arrow in B), note the multiple cysts in the liver (arrow in A)—case of polycystic kidney disease (see page 170).

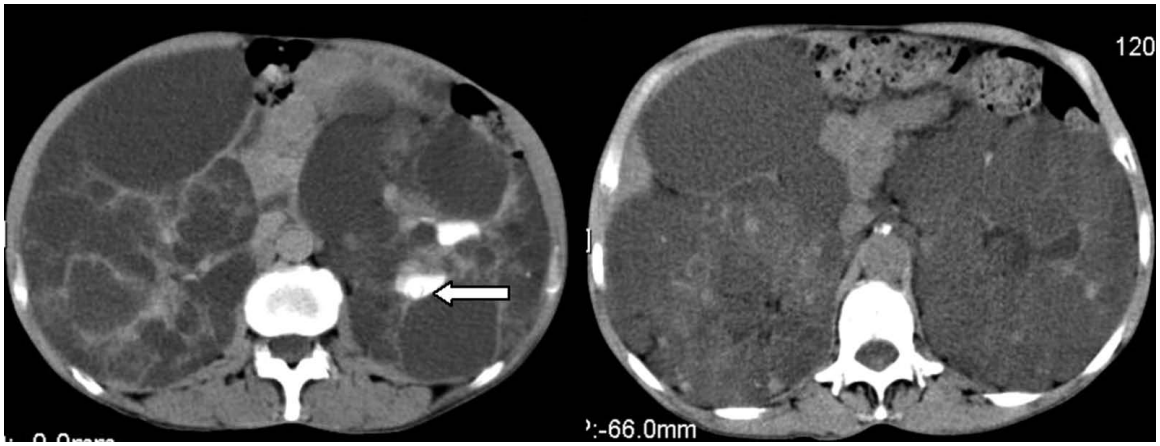

FIGURES 6.17A and B: Axial plain study showing grossly enlarged kidneys with calcification and calcium fluid level in few cysts (arrow)—Case of ADPKD.

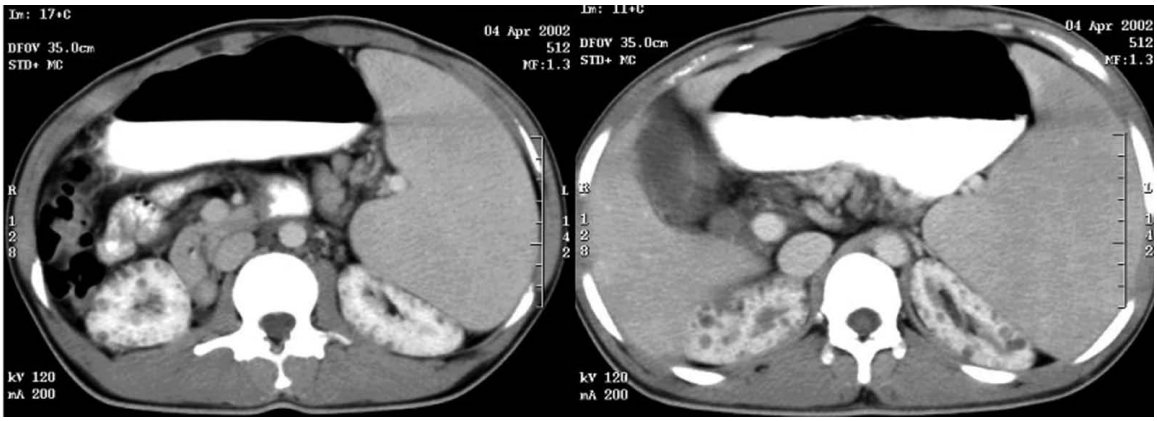

FIGURES 6.18A and B: Axial CECT showing multiple small cysts suggestive of cystic renal disease in a 17-year-old male. Patient associated splenomegaly due to portal hypertension.

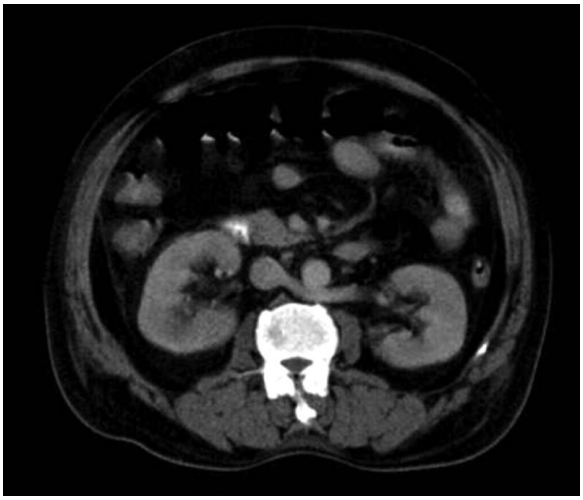

FIGURE 6.19: Axial CECT showing retroaortic left renal vein which is a common variant seen, especially important to note these variants in cases were renal surgeries have to be performed.

URINARY INFECTIONS

The normal urinary tract is sterile and very resistant to bacterial colonization. However, UTI is the most common bacterial infection in all age groups.

In neonates, UTIs are more common in males than in females and are often associated with bacteremia; this observation presumably relates to the greater frequency of congenital anomalies of the urinary tract in male infants. In children aged 1 to 5 year, the incidence of bacteriuria is about 0.03% in boys and 1 to 2% in girls; it rises to about 5% in girls > 10 year. Among patients aged 20 to 50 year, UTIs are about fifty fold greater in women. The incidence increases in men and women > 50 year; the female:male ratio decreases as a result of the increased frequency of prostate disease.

Etiology and Pathogenesis

Gram-negative aerobic bacteria cause most bacterial UTIs. A few UTIs are acquired hematogenously, but about 95% occur when bacteria ascend from a colonized vaginal introitus and urethra to the bladder and, in the case of acute uncomplicated pyelonephritis, up the ureter to the kidney. *Escherichia coli* is the most common bacterium isolated and accounts for about 80% of community-acquired infections, and *Staphylococcus saprophyticus* for about 10%. In hospitalized patients, *E. coli* accounts for about 50% of cases; the gram-negative species *Klebsiella, Proteus, Enterobacter,* and *Serratia* for about 40%; and the gram-positive bacterial cocci *Enterococcus faecalis* and *Staphylococcus* sp (*saprophyticus, aureus*) for the remainder.

Complicated UTIs occur in the setting of urologic impairment, usually due to instrumentation or obstruction (anatomic abnormalities, neurogenic dysfunction, calculi, catheterization). Although obstruction alone does not cause UTI, its presence predisposes to UTI and makes UTI more difficult to eradicate with medical therapy.

Bacteriuria is more common in elderly men because of abnormal micturition and significant residual bladder urine; poor emptying of the bladder due to uterine prolapse and cystocele formation and soiling of the perineum from fecal incontinence in women; and neuromuscular diseases and increased use of instrumentation and bladder catheters in both sexes. Diabetics who have neurogenic bladders or who have been catheterized have an increased incidence and severity of infections. Because pregnancy may induce urinary stasis due to functional and anatomic obstruction of ureters and bladder, UTI during pregnancy should be regarded as complicated.

Urethritis

Bacterial infection of the urethra occurs when organisms that gain access to it acutely or chronically colonize the numerous periurethral glands in the bulbous and pendulous portions of the male urethra and the entire female urethra.

The sexually transmitted pathogens *Chlamydia trachomatis, Neisseria gonorrhoeae,* and herpes simplex are common causes of dysuria in men and women.

Cystitis

Bacterial infection of the bladder in men is usually complicated and generally results from ascending infection of the urethra or prostate or occurs secondary to urethral instrumentation. In women, sexual intercourse usually precedes uncomplicated cystitis.

Prostatitis

Chronic bacterial prostate infection is the most common cause of recurrent UTI in men due to reintroduction of infection into the bladder.

Acute Pyelonephritis

The term pyelonephritis refers to bacterial infection of the kidney parenchyma and should not be used to describe any tubulointerstitial nephropathy unless UTI is documented. About 20% of community-acquired bacteremias in women are attributed to pyelonephritis. Pyelonephritis is uncommon in men with a normal urinary tract. In patients who have recurrent infections and no structural abnormalities, the normal host defense mechanisms may be decreased.

In 30 to 50% of women with a normal urinary tract, pyelonephritis occurs by the ascending route despite the dynamics of urine flow and the interference of the vesicoureteral junction. Cystitis alone or anatomic defects may produce reflux. This tendency is greatly enhanced when peristalsis is inhibited (e.g. during pregnancy, by obstruction, by endotoxins of gram-negative bacteria). Although obstruction (strictures, calculi, tumors, prostatic hypertrophy, neurogenic bladder, VUR) predisposes to infection, most women with pyelonephritis have no demonstrable functional or anatomic defects of the urinary tract. Pyelonephritis or focal abscess may be due to hematogenous UTI, which is infrequent and usually results from bacteremia with virulent bacilli (e.g. *Salmonella* organisms, *S. aureus*). Pyelonephritis is very common in girls or in pregnant women after instrumentation or bladder catheterization.

The kidney is usually enlarged due to inflammatory PMNs and edema. Infection is focal and patchy beginning in the pelvis and medulla and extending into the cortex as an enlarging wedge. Chronic inflammatory cells appear within a few days, and medullary and subcortical abscesses may develop. Parenchymal tissue between foci of infection is common. Arteries, arterioles, and glomeruli are considerably resistant to infection. Papillary necrosis may be evident in acute pyelonephritis associated with diabetes, obstruction, sickle cell disease, or analgesic nephropathy. Although acute pyelonephritis is frequently associated with renal scarring in children, similar scarring in adults is not detectable in the absence of reflux or obstruction.

On CECT pyelonephritis may be focal or diffuse. Focal lesions are characterized by sharply marginated wedge shaped zones of decreased attenuation radiating from the collecting system to the renal capsule. There is poor contrast nephrogram followed by delayed pelvicalyceal opacification, severe focal lesions may progress to focal areas of decreased or increased cortical echogenicity. Severe untreated lesions may progress to focal abscess formation.

Chronic Pyelonephritis (Chronic Infective Tubulointerstitial Nephritis)

This chronic patchy, often bilateral, pyogenic infection of the kidney produces atrophy and calyceal deformity with overlying parenchymal scarring. It causes end-stage renal failure in about 2 to 3% of patients treated by dialysis or transplantation. Chronic pyelonephritis occurs only in patients with major anatomic abnormalities, such as obstructive uropathy, struvite calculi, or, most commonly, VUR (in 30 to 45% of young children with symptomatic UTI). VUR is usually a congenital defect that results in incompetence of the ureterovesical valve, most often due to a short intramural segment. VUR can be acquired in patients with a flaccid bladder due to spinal cord injury.

Xanthogranulomatous Pyelonephritis

Xanthogranulomatous pyelonephritis is an unusual variant of chronic pyelonephritis that typically occurs in middle-aged women with a history of recurrent UTIs. It is a complication of obstruction due to renal calculi and is typically associated with *Proteus* infections. The kidney is enlarged, and perirenal fibrosis and adhesions to adjacent retroperitoneal structures are common. The disease is almost always unilateral and appears to represent an abnormal immune response to infection with giant cells, lipid-laden macrophages, and cholesterol clefts, which accounts for the yellow color of the infected tissue. Two presentations occur in children. The most common affects boys and girls equally and involves the entire kidney. The other form, which is more common in girls, is localized and may mimic a tumor.

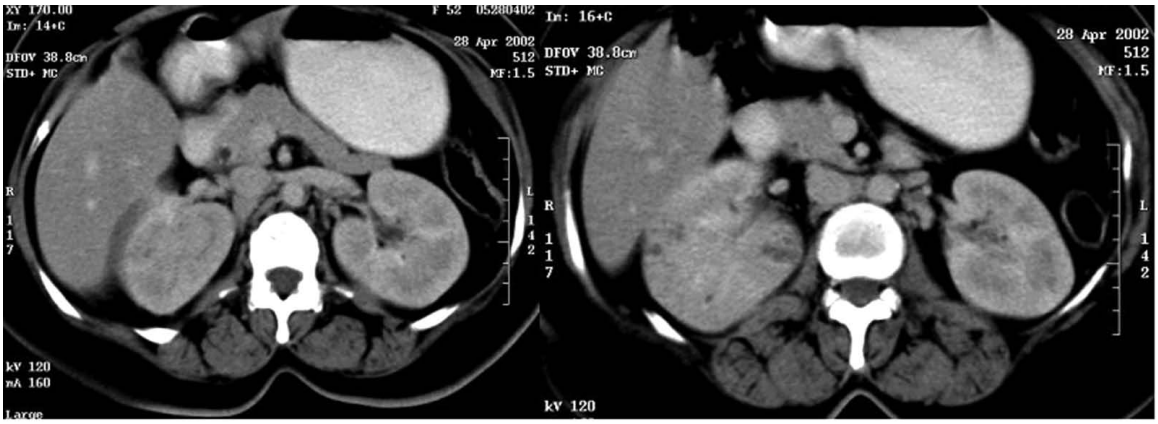

FIGURES 6.20A and B: Axial CECT reveals enlarged right kidney with loss of normal corticomedullary differentiation, with few low attenuation foci – features of pyelonephritis.

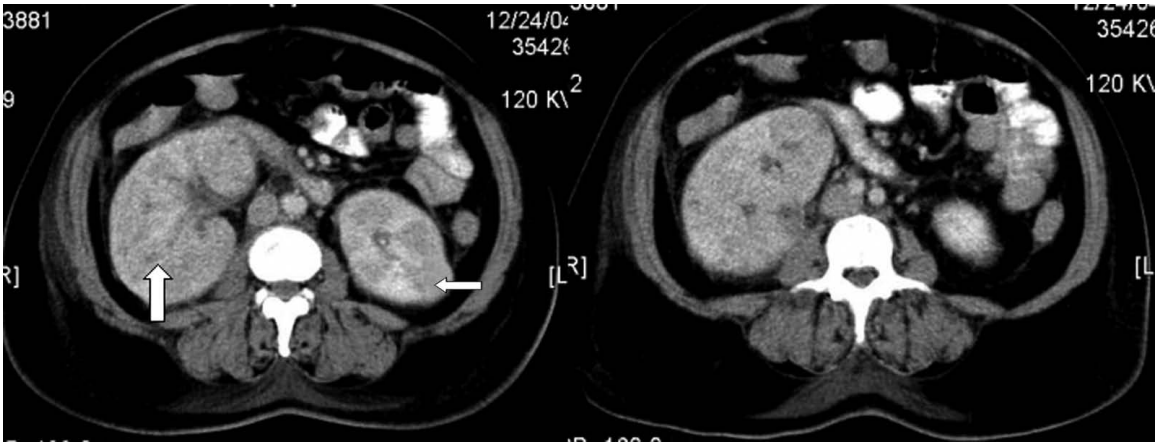

FIGURES 6.21A and B: Axial CECT in a diabetic patient with fever and bilateral loin pain shows enlarged right kidney with multiple ill-defined hypodense areas (arrow in A). Left kidney shows normal dimension but altered contrast enhancement pattern (small arrow).

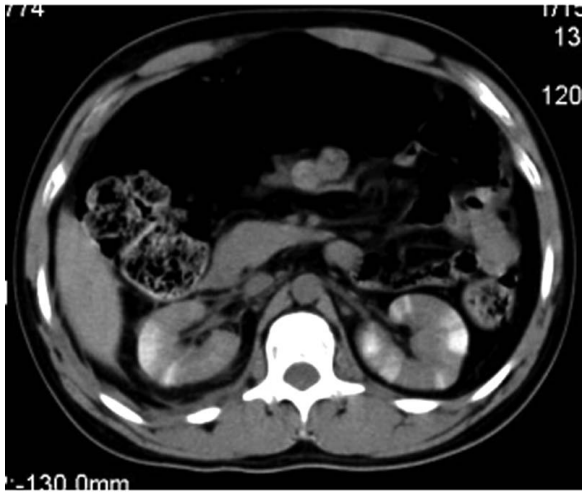

FIGURE 6.22: Axial CECT delayed image showing striated nephrogram with wedge shaped hyperdense areas alternating with hypodense nonenhancing regions suggestive of pyelonephritis.

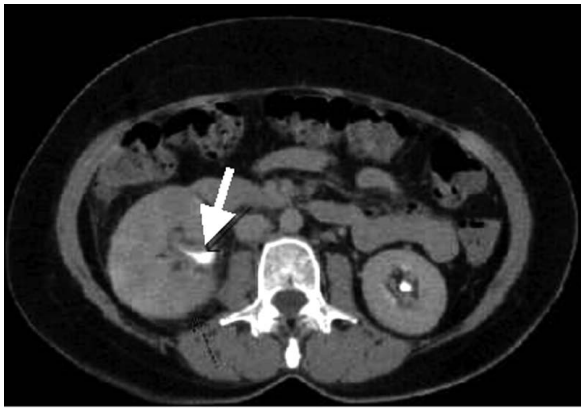

FIGURES 6.23: Axial CECT reveals a enlarged kidney with perinephric stranding, renal pelvis shows thickening (arrow).

Emphysematous Pyelonephritis

Renal and Perirenal Gas

Emphysematous pyelonephritis is an acute, severe, necrotizing, renal infection characterized by spontaneous generation of gas within the renal parenchyma and surrounding tissues. Since 1898 when it was originally described by Kelly and MacCallum, it has become apparent that the spectrum of renal and perirenal gas includes several distinct clinical entities. These include:

- emphysematous pyelonephritis, a severe bacterial infection associated with gas formation within the renal parenchyma.
- emphysematous pyelitis, in which gas is confined to the renal pelvis and calyces; and
- perinephric gas, which may represent an outward extension of advanced emphysematous pyelo-nephritis or an inward extension of a gas-forming retroperitoneal infection (such as that from perforated retrocecal appendicitis) or a renal or perirenal abscess with gas formation.

Emphysematous pyelonephritis: This condition is associated with diabetes in 90% of patients, but it also occurs in nondiabetic patients with urinary obstruction or altered immunity. Women are affected twice as often as men, and the condition may be seen in a wide range of ages (19-18 years). Emphysematous pyelonephritis has been reported bilaterally in polycystic as well as in transplanted kidneys. It can be seen in nondiabetic patients with calculous disease or obstruction and it can be associated with xanthogranulomatous pyelonephritis. *Escherichia coli* is the most common pathogen, responsible for 68% of cases, but *Klebsiella, Proteus, Pseudomonas, Aerobacter,* and *Candida* have also been cited as causative agents. Clostridial infection is an exceedingly rare etiology.

Emphysematous pyelitis, renal abscess, and other conditions associated with intrarenal air or gas: In emphysematous pyelitis, the presence of gas is limited to the renal collecting system. The prognostic significance of emphysematous pyelitis is less grave than that of emphysematous pyelonephritis because most patients usually respond to medical treatment alone or combined with relief of obstruction, if present. Women are affected 3 times more often than men. Fifty percent of the patients have diabetes mellitus. Pyuria is almost always evident on urinalysis, and *E coli* is the most common infecting organism.

Gas-forming renal abscesses are exceedingly rare, especially in the absence of diabetes mellitus, urinary calculi, and obstructive uropathy—the usual predisposing factors. Gas formation after therapeutic embolization of renal tumors is a well recognized and usually benign occurrence. Rarely, spontaneous gas abscess transformation can be seen in large renal cell carcinomas and is probably related to massive infarction of the tumor.

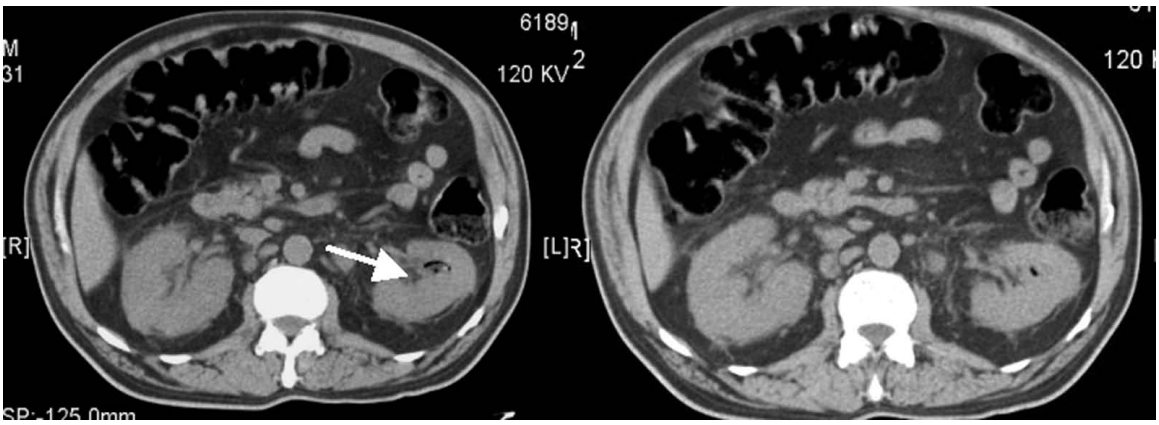

FIGURES 6.24A and B: Axial plain CT reveals left perinephric fat scarring, focal hypodense air pocket seen in the anterior renal pelvis (arrow).

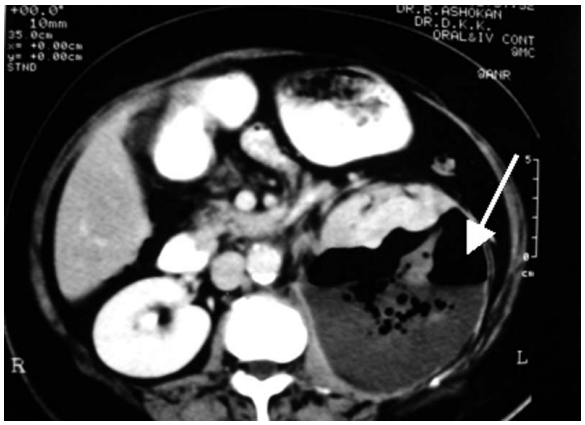

FIGURE 6.25: Axial CECT reveals a left renal subcapsular collection with an air fluid level displacing the kidney anteriorly (arrow).

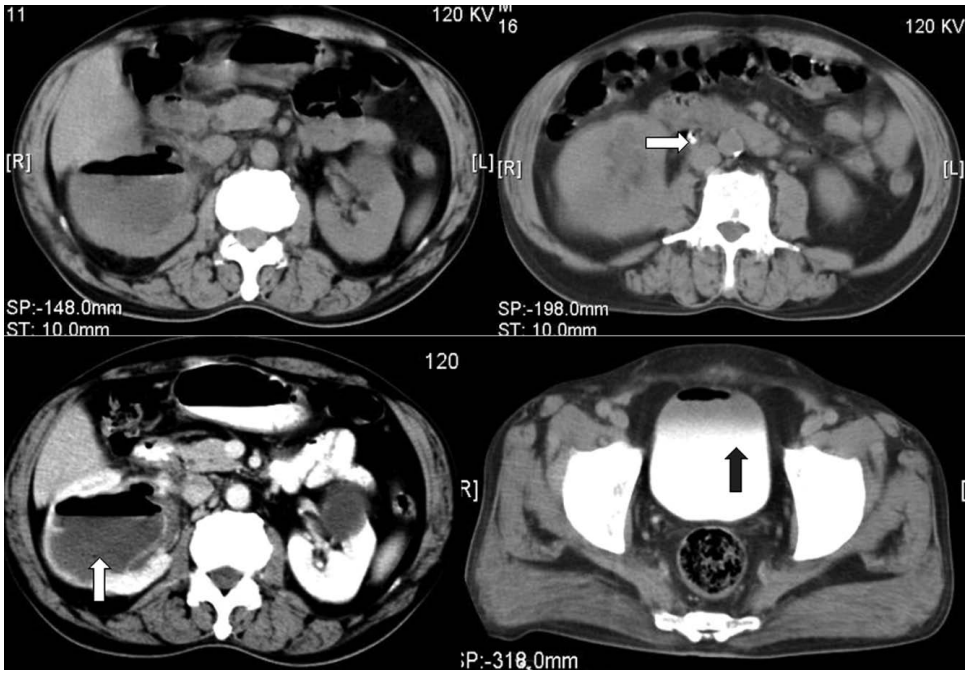

FIGURES 6.26A to D: Axial CECT showing a infected pelvic cyst with air fluid (arrow in C), note the air pockets in the proximal ureter with a small calculus (arrow in B). Air is seen in the urinary bladder (arrow in D) patient was a known diabetic who had proximal ureteric calculus with mild hydronephrosis, USG scan done 1 week prior did not show any air in the pelvic cyst.

Perinephric abscess with gas formation: Gas in the perinephric space may signify the presence of a gas-containing primary perirenal abscess, may be secondary to extension from a diverticular or appendiceal abscess, may be an outside extension of emphysematous pyelonephritis, or may be due to renoalimentary fistula or penetrating trauma. Percutaneous drainage of gas-forming perinephric abscesses is commonly performed using CT or US guidance, with frequent salvage of the kidney and preservation of significant residual renal function.

Table 6.2: Causes of gas in the genitourinary tract

Infections	*Scrotum, testicle, and prostate*
(gas-forming organisms)	Abscess
	Fournier's gangrene
Kidney	*Iatrogenic causes*
Emphysematous pyelonephritis	Surgery
Emphysematous pyelitis	Radiologic procedure
Abscess	Infarction of renal carcinoma (therapeutic or spontaneous)
Perinephric emphysema	
Bladder	*Penetrating trauma*
Emphysematous cystitis	
Uterus and ovaries	*Renogastrointestinal tract fistula*
Endometritis	Inflammatory
	Neoplastic etiology

Pyonephrosis

Pyonephrosis is accumulation of pus in an obstructed pelvi calyceal system, CT usually cannot reliably differentiate between an infected and uninfected system, although the presence of gas strongly suggest infection. CT shows the site and cause of infection in most cases serving as a problem solving tool when USG is equivocal.

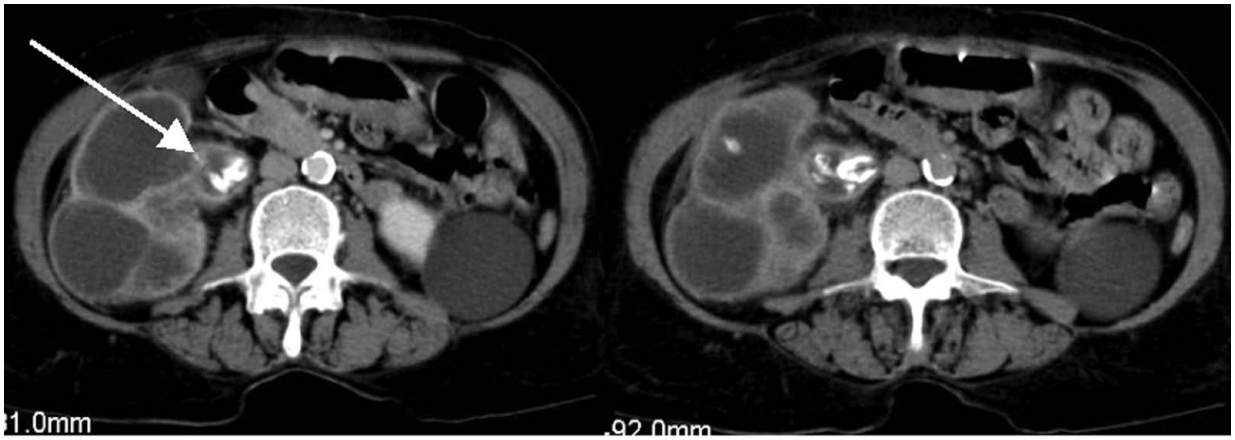

FIGURES 6.27A and B: Axial CECT reveals grossly hydronephrotic kidney with multiple calcifications within the renal pelvis (arrow) – feature of post-obstructive pyonephrosis.

Renal and Perirenal Abscesses

Early in evolution abscess may be ill-defined on CT and surrounded by zones of decreased parenchymal enhancement, representing enhancement that has not yet become necrosis. The borders become increasingly well-defined as the abscess encapsulates. They have a low HU 20-30 and do not enhance after contrast. Gas is seen ocassionaly, focal thickening of the adjacent renal fascia and stranding in the adjacent fat is common. A perinephric abscess may finally result if the infection spreads through the renal capsule.

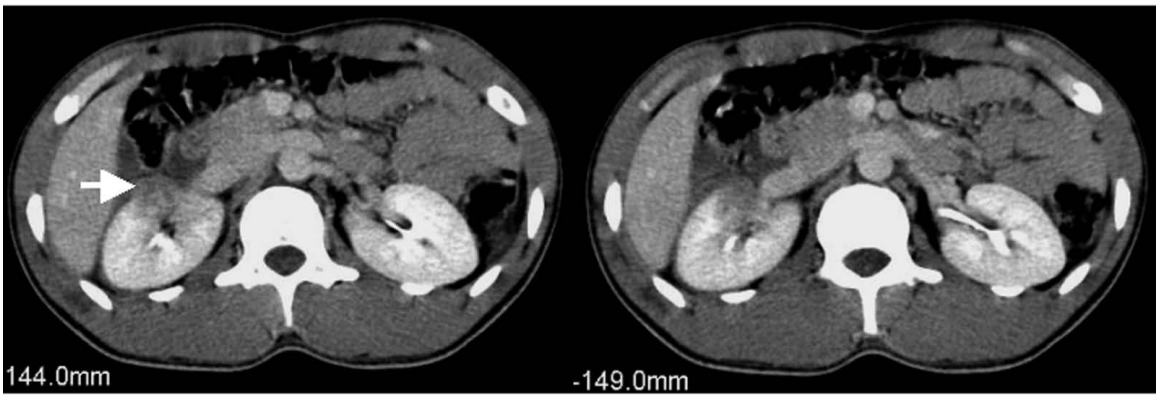

FIGURES 6.28A and B: Axial CECT in a diabetic patient with right loin pain reveals a focal low attenuation in the anterior margin of the right kidney with adjacent rim of perinephric fluid (arrow).

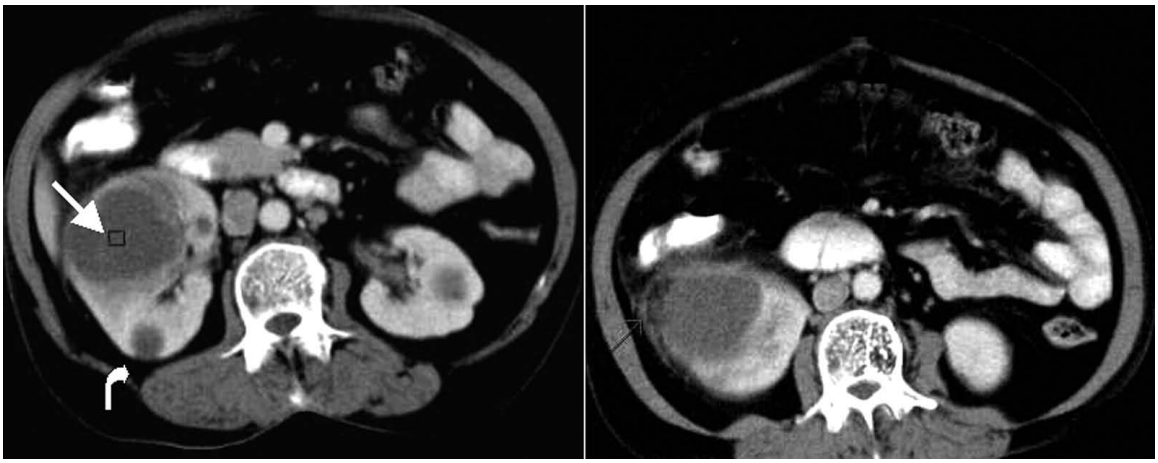

FIGURES 6.29A and B: Axial CECT reveals a hypodense lesion in the anterior margin of the left kidney with rim enhancement in a patient with diabetes (arrow). Curved arrow shows presence of cortical cysts.

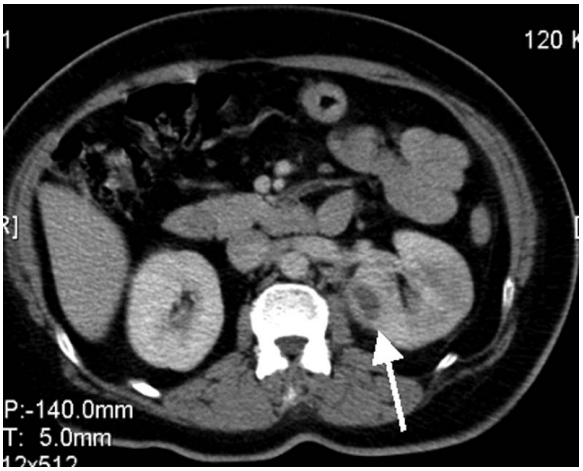

FIGURE 6.30: Axial CECT in a diabetic patient with PUO reveals a focal hypodense lesion in the medial interpolar region of left kidney (arrow).

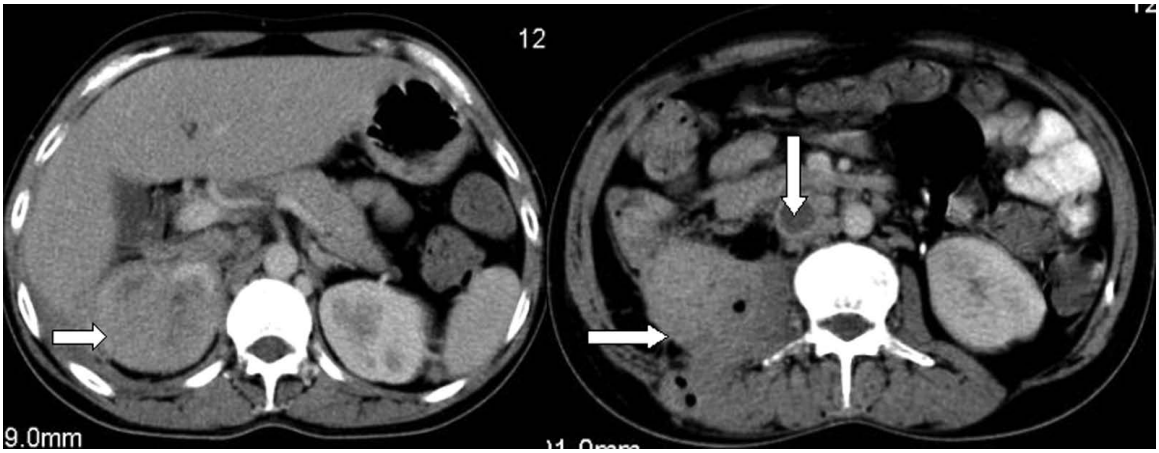

FIGURES 6.31A and B: Axial CECT showing hypodense lesion effacing the renal pelvis and cortex in a infiltrating pattern (arrow in A), lower pole region shows a perinephric soft tissue with air pockets involving the posterior paraspinal muscle planes, secondary IVC thrombus is also seen (arrows) patient was a diabetic on irregular medication.

Tuberculosis

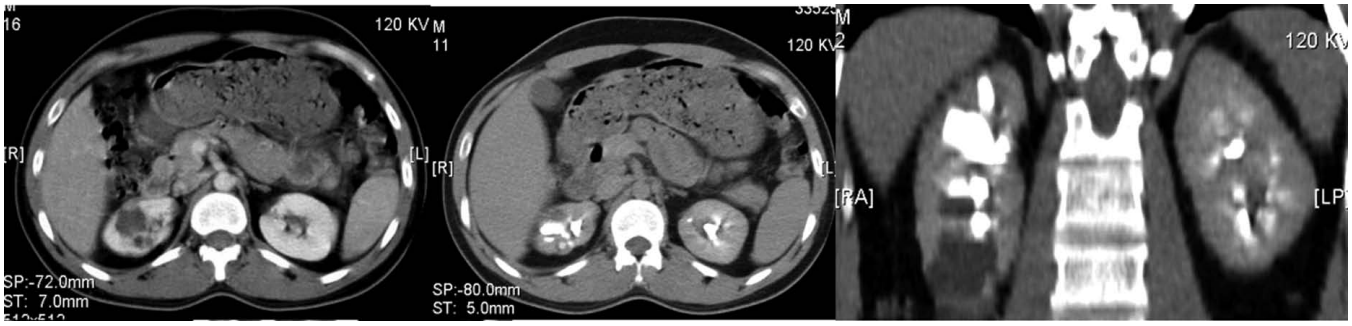

FIGURES 6.32A to C: Axial CECT with delayed phase imaging showing irregular right upper pole calyces with dilatation suggestive of calyectasis in a patient with known urinary tuberculosis. Fig. C is a coronal reformation showing the same findings.

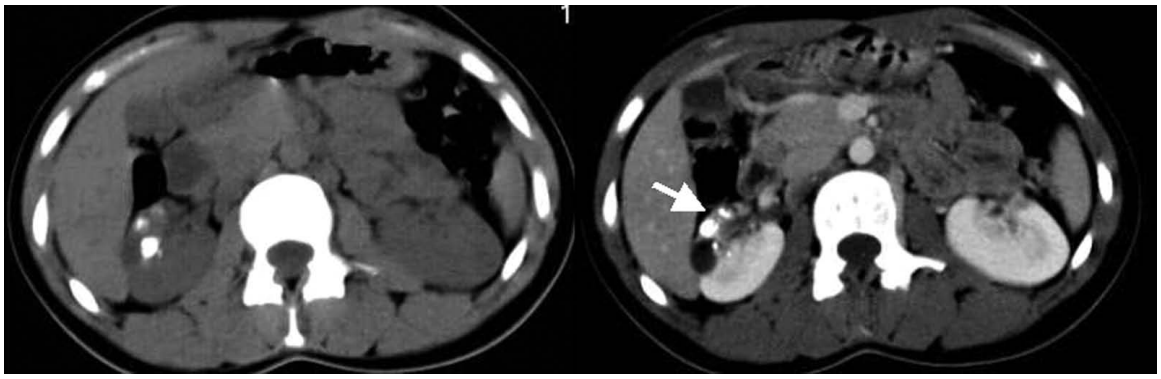

FIGURES 6.33A and B: Axial plain CT (known case of renal TB on follow-up) reveals focal hypodensity with calcific foci in the anterior margin of the midpole (arrow).

Tuberculosis

The genitourinary tract is the second most common site for tuberculous infection after the lungs. The spread to the kidneys usually is hematogenous from the lungs, bone, or a GI tract focus. The true incidence of renal tuberculosis may be underestimated since radiologic findings may be absent and diagnosis is made by urine culture.

The initial renal focus is usually a small tubercle in the glandular and cortical arterioles. With the passage of time, these lesions progress to form necrotizing lesions. The disease spreads to the renal tubules and renal medulla in which further tubercles develop, usually at the turn of the loop of Henle, coalescing into larger necrotic irregular cavities. The cavities usually communicate with the renal collecting system, generally a calyx, with formation of fistulae and stricturing. Eventually, the kidney may become fibrotic and scarred.

Ureteric involvement occurs as a descending infection secondary to kidney infection. Tubercles may involve the transitional epithelium, causing mucosal granulomas that project into the ureteric lumen. Eventually, fibrosis occurs in the ureter. These pathologic processes can be demonstrated radiologically by the appearance of a beaded, saw-toothed, crokscrew, or pipestem ureter depending on the stage of disease. Usually, the upper and/or lower third of the ureters are involved. The vesicoureteric junction may become fixed and patulous, allowing vesicoureteric reflux. The kidneys are always involved when ureteric tuberculosis is present.

Bladder tuberculous infection is almost always secondary to renal involvement. Initially, interstitial cystitis occurs, eventually causing bladder mucosal ulceration and thickening of the bladder wall. End-stage disease causes scarring and bladder fibrosis, resulting in diminished capacity of the urinary bladder. Bladder wall calcification is uncommon.

RENAL MASSES

Classification

Non-neoplastic

1. Cysts
   - Simple
   - Complicated
   - Parapelvic
   - Polycystic kidney
   - Multicystic dysplastic kidney
   - Multilocular cystic nephroma
2. Inflammatory
   - Renal abscess
   - Focal pyelonephritis—lobar nephronia
   - XGP
   - Malacoplakia
3. Vascular
   - Hematoma
   - Aneurysms, AVMs
   - Angiomyolipoma
4. Hydronephrosis

Neoplastic

1. Renal parenchymal tumors
   - Renal cell carcinoma
   - Adenoma

- Wilms
- Oncocytoma
- Nephroblastomatosis
- Mesoblastic nephroma

2. Mesenchymal tumors
   - Angiomyolipoma
   - Hemangioma
   - Sarcoma
3. Renal pelvis tumors
   - Transitional cell carcinoma
   - Papilloma
   - Squamous cell carcinoma
   - Fibroma
   - Angioma
4. Secondary tumors
   - Lymphoma
   - Metastasis

Approach to Renal Masses

- Cystic/solid lesions
- Infiltrative/expansile lesions
- Fatty/soft tissue lesion
- Solitary/multiple lesion.

Pattern of Growth

- Expansile—ball-like lesion, spherical exophytic frequently encapsulated.
- Malignant—adenocarcinoma, metastasis, lymphoma.
- Benign—cyst, angiomyolipoma, oncocytoma.

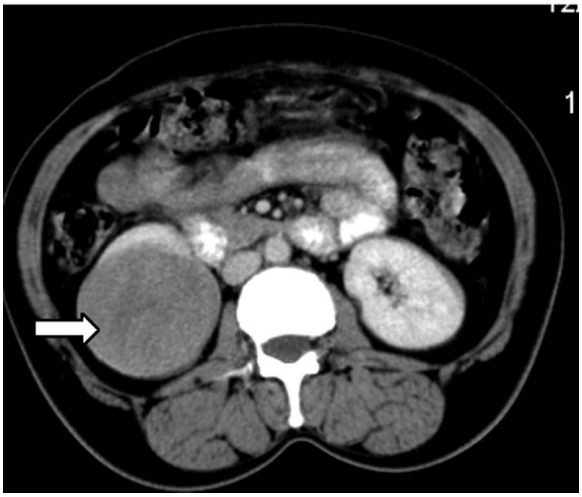

FIGURE 6.34: Axial CECT showing ball-like expansile lesion in the right renal lower pole-renal cell carcinoma.

- Infiltrative—invades renal parenchyma, preserves renal contour.
- Benign—xanthogranulomatous pyelonephritis, TB, pyelonephritis.
- Malignant—transitional cell carcinoma, squamous cell Ca, lymphoma.

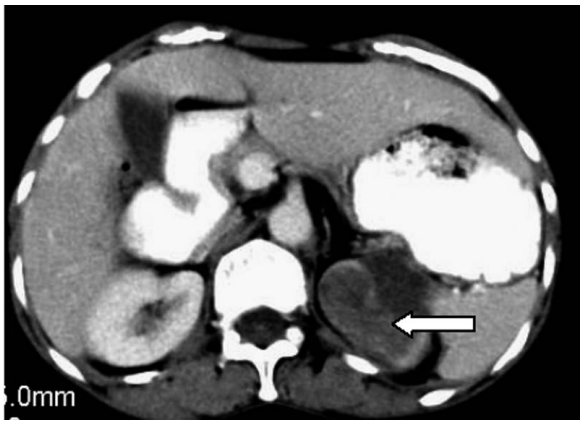

FIGURE 6.35: Axial CECT shows an infiltrative lesion in the left renal upper pole – transitional cell tumor.

- *Calcification*—seen in 20-30 % of renal cell carcinoma and 1-2% of benign cases. Central calcification is seen in more than 80% of malignant cases. Benign lesions in more than 80% of cases show rim calcification.

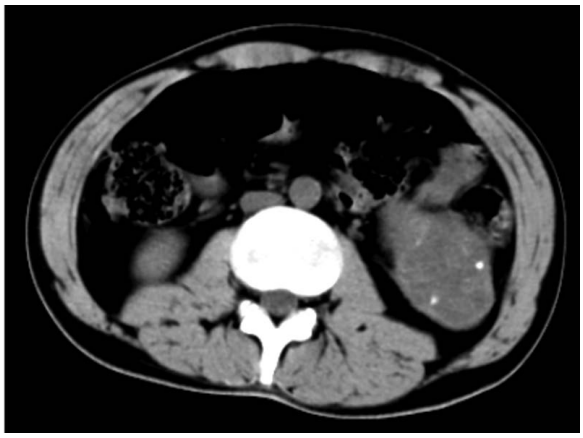

FIGURE 6.36: Axial CECT showing left renal lower pole RCC showing calcific specks.

- *Surgical lesions*—enhancing lesions having nodularity with thick wall and enhancing septa having central calcification.

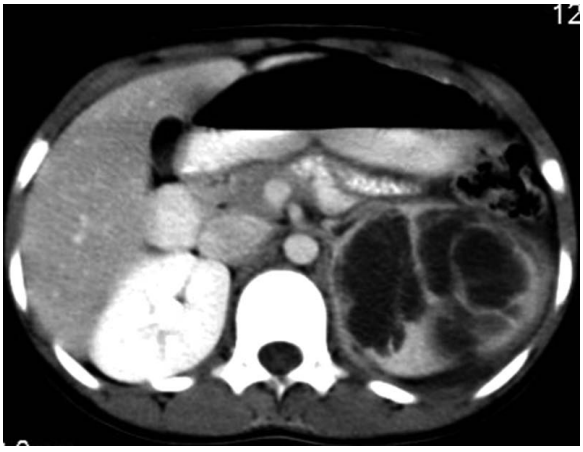

FIGURE 6.37: Axial CECT showing a left renal upper polar septated cystic mass.

Renal Cell Carcinoma (*also known as adenocarcinoma, Gravitz's tumor, hypernephroma)*

- It is the most common primary renal malignancy. Commonly presents between 50 and 70 years.
- It originates from renal tubular epithelium and develops in the cortex of the kidney. Common in males.
- Three to five percent of neoplasms occur bilaterally.

With the widespread use of cross-sectional imaging, many tumors are detected incidentally. Single- and multidetector computed tomography (CT) have helped refine the diagnostic work-up of renal masses by allowing image acquisition in various phases of renal enhancement after intravenous administration of a single bolus of contrast material. The scanning protocol should include unenhanced CT followed by imaging during the corticomedullary and nephrographic phases of enhancement. The nephrographic phase is the most sensitive for tumoral detection, while the corticomedullary phase is essential for imaging the renal veins for possible tumoral extension and the parenchymal organs for potential metastases. Knowledge of the tumoral stage at the time of diagnosis is essential for prognosis and surgical planning.

Unenhanced CT

An initial series of unenhanced scans through the kidneys should be part of every protocol for evaluation of a suspected renal mass; it provides a baseline from which to measure the enhancement within the lesion after the administration of intravenous contrast material. This enhancement characteristic is important in distinguishing hyperdense cysts from solid tumors. Because most renal cell carcinomas have a rich vascular supply, they enhance significantly after administration of contrast material. Enhancement values of more than 12 HU are considered suspicious for malignancy.

Most renal cell carcinomas are solid lesions with attenuation values of 20 HU or greater at unenhanced CT. Small (3-cm-diameter) tumors usually have a homogeneous appearance while larger lesions tend to be more heterogeneous owing to hemorrhage or necrosis. Calcifications are detected in upto 30% of cases of renal cell carcinoma.

Corticomedullary Phase

The corticomedullary phase is the first phase of contrast enhancement. It occurs between 25 and 70 seconds after the start of injection. In this phase, the contrast material is primarily within the cortical capillaries, peritubular spaces, and cortical tubular lamina and has not yet filtered through the more distal renal tubules. The renal cortex enhances brightly and is easily differentiated from the minimally enhancing renal medulla.

Pitfalls, the corticomedullary phase small, hypervascular renal masses may enhance to the same degree as the renal cortex and may be mistaken for normal parenchyma at the corticomedullary phase. A more common source of error (false-negative) occurs when a centrally located tumor is mistaken for the normal, hypoattenuating medulla.

Advantages

Maximal opacification of the renal arteries and veins occurs, allowing confident diagnosis of venous extension of tumoral tissue. Accurate delineation of the arterial anatomy is helpful in selected cases to plan nephron-sparing surgery. Hypervascular metastases to the liver, spleen, and pancreas are most conspicuous on the corticomedullary-phase scans, when these organs are imaged during the arterial phase of enhancement.

Nephrographic phase: As contrast material filters through the glomeruli into the loops of Henle and the collecting tubules, the nephrographic phase of contrast enhancement begins. This phase is best imaged after a scanning delay of at least 80 seconds and lasts up to 180 seconds after the start of injection. The renal parenchyma enhances homogeneously, allowing the best opportunity for discrimination between the normal renal medulla and masses.

Enhancement of solid renal tumors is time-dependent, being greater during the nephrographic phase than during the corticomedullary phase. The nephrographic phase is the most valuable for detecting renal masses and characterizing indeterminate lesions.

Excretory phase: The excretory phase begins approximately 180 seconds after the initiation of injection of iodinated contrast material. The contrast material is excreted into the collecting system. Delayed scanning can also be used in lieu of unenhanced scanning to characterize an incidental renal lesion detected on a routine contrast-enhanced CT scan.

Delayed De-enhancement

It has been shown that measurement of the washout of contrast material from a lesion at 15 minutes allows differentiation between hyperdense cysts and renal neoplasms. There was no change in the attenuation of high-density cysts between the initial contrast-enhanced CT scan and the 15-minute-delayed images. In comparison, all lesions that proved to be neoplasms at surgery or follow-up studies showed a decrease in attenuation or "de-enhancement" of at least 15 HU at delayed CT, which was attributed to the washout of contrast material from the vascular bed of the tumor.

CT Findings

NECT: Soft tissue renal mass, can be iso-, hypo- or hyperdense to the normal renal parenchyma. Lesion may have lobulated irregular margins.

CECT: Hypodense compared to the kidney, or inhomogenous enhancement due to tumor necrosis or hemorrhage.

Tumor extension into renal vein/IVC may be seen as low attenuation mass within the lumen of the vessel.

Spontaneous renal or perirenal hemorrhage is not an infrequent finding.

CT is important in staging, in detecting retroperitoneal lymphadenopathy and metastasis to liver, bone, contralateral kidney, adrenal glands, lungs. Metastasis from renal cell carcinoma are hyperdense (hypervascular).

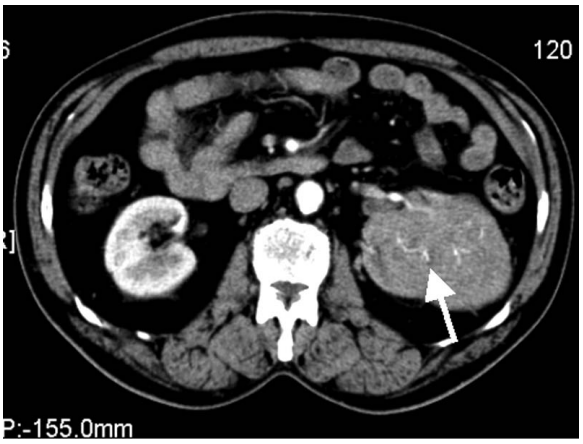

FIGURE 6.38: Axial CECT showing a left renal lower pole mass with serpiginous areas of enhancement (arrow) suggestive of tumor vessels.

ROBSON CT STAGING OF RENAL CELL CARCINOMA

STAGE I : Tumor within renal capsule

STAGE II : Tumor spread to perinephric fat

STAGE III A : Venous extension of tumor
STAGE III B : Regional lymph node metastasis
STAGE III C : Venous extension and regional node metastasis.
STAGE IV A : Invasion beyond Gerota's fascia (involves adrenals)
STAGE IV B : Distant metastasis.

Perinephric invasion is suggested by perinephric soft tissue mass of at least 1 cm, perinephric stranding, cobwebbing, fat plane obliteration, fascial thickening.

Oncocytoma

Oncocytomas, are composed of large epithelial cells with abundant granular eosinophilic cytoplasm. It can occur in thyroid, parathyroid, salivary glands and kidneys. Peak incidence is in 6th-7th decades and is more common in males.

CT Findings

Well-defined masses with smooth margins, shows homogenous enhancement following IV contrast. Has a pseudo capsule at the periphery of the mass formed from renal parenchyma compressed around the edge of the mass.

Central stellate scar (typical of oncocytoma, but also seen in renal cell carcinoma).

Benign renal lesions	*Noninvasive, no extracapsular extension*
Pseudotumor	Same enhancement pattern as renal cortex (renal columns, fetal lobulation, parenchymal scars)
Angiomyolipoma	Fatty areas (<-20 HU) accompanied by areas of soft-tissue attenuation
Lipoma	Fat attenuation only (<-80 HU)
Oncocytoma	Stellate central scar, nonhomogeneous enhancement pattern; differential diagnosis: renal cell carcinoma
Adenoma	< 3 cm, nonspecific enhancement pattern; differential diagnosis, renal cell carcinoma, lesions 3 cm or larger are potentially malignant
Fibroma, hemangioma, etc	< 3 cm nonspecific
Papilloma	Like renal pelvic carcinoma, but noninvasive, often multifocal (differential diagnosis, renal pelvic carcinoma)

Malignant renal lesions	*Invasive, possible extracapsular extension (grade T3 or higher)*
Renal cell carcinoma	Usually hypervascular, rarely hypovascular, tends to infiltrate the renal vein
Nephroblastoma (Wilms tumor)	Children, nonhomogeneous hypervascularity, often very large, tends to infiltrate the renal vein
Sarcomas	May be hypervascular, liposarcoma contains nonhomogeneous fatty components
Metastases	Usually hypovascular, often bilateral, multifocal, primary tumor?
Renal pelvic carcinoma	Located in renal sinus, frequent pyelocaliceal obstruction; drop metastases
Lymphoma	Bilateral > unilateral, diffuse infiltration is common, abdominal lymphadenopathy, hypovascular

Pseudotumors

Fetal lobulation—key to identification is the presence of normal parenchymal thickness, calyces are centered between the indentations.

Prominent columns of Bertin—invagination of renal cortical tissue extending from cortex to renal sinus. Its a normal functioning tissue and commonly occurs in the junction of upper and mid third of renal parenchyma. averages 3-4 cm in size, its bilateral in 60% of cases.

Dromedary Hump

Hilar lip—prominent collection of normal renal tissue, that occur in the areas of renal parenchyma surrounding the renal sinus. usually occurring in the upper pole of left kidney.

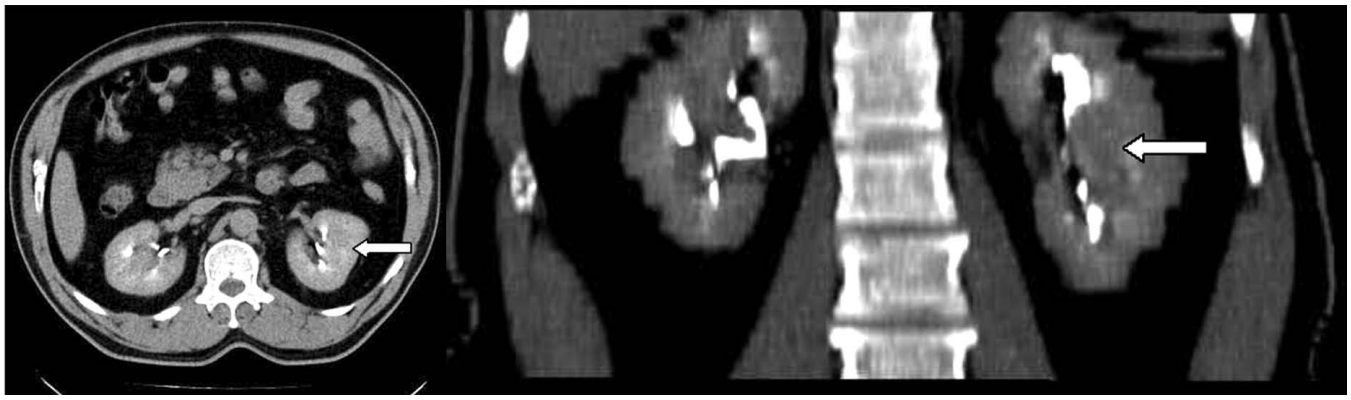

FIGURE 6.39: Axial CECT showing a prominent column of Bertin (arrow).

Angiomyolipoma

It is a fairly common benign tumor usually classified as a hamartoma and is composed of various proportion of smooth muscle, blood vessels, and fat. It occurs in two subgroups 40-70% of patients with tuberous sclerosis have AML, in these patients tumors are small, bilateral and incidentally discovered has a equal distribution.

In patients without tuberous sclerosis these lesions are large, symptomatic and have a female preponderence.

AML expands slowly are nonencapsulated, tend to enlarge in a expansile pattern, distort the collecting system without destroying it. CT appearance is dignostic with HU values ranging from –150 to + 160.

In lesions containing predominant vascular tissue or muscle or in those in which recent hemorrhage has occurred the majority of tumor may have CT density values greater than 20 HU with regions of contrast enhancement.

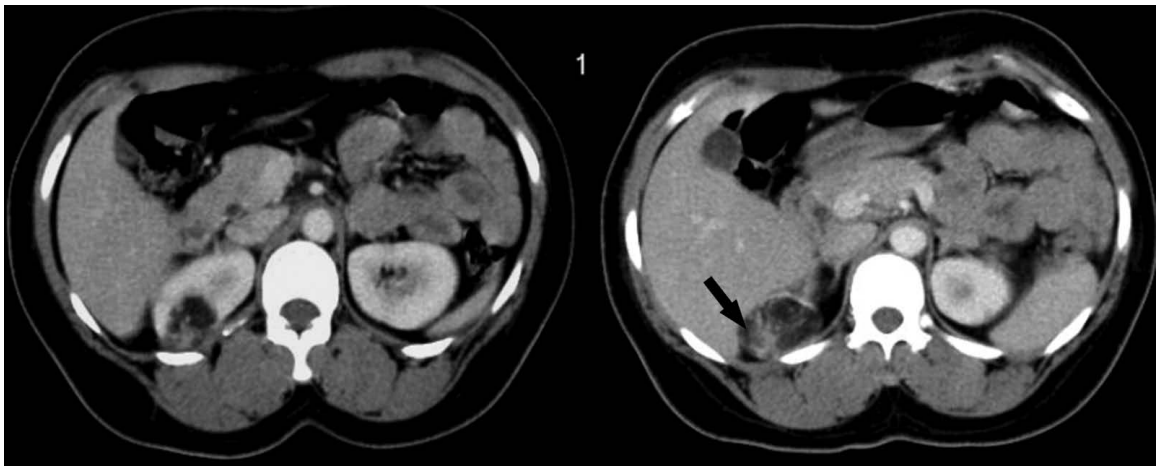

FIGURES 6.40A and B: Axial CECT reveals a right renal hypodense lesion involving the upper pole showing a predominant fat attenuation (arrow).

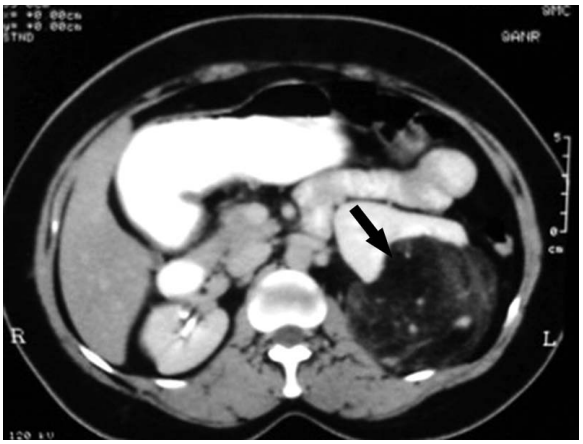

FIGURE 6.41: Axial CECT reveals a large exophytic fatty lesions arising from the left renal interpole.

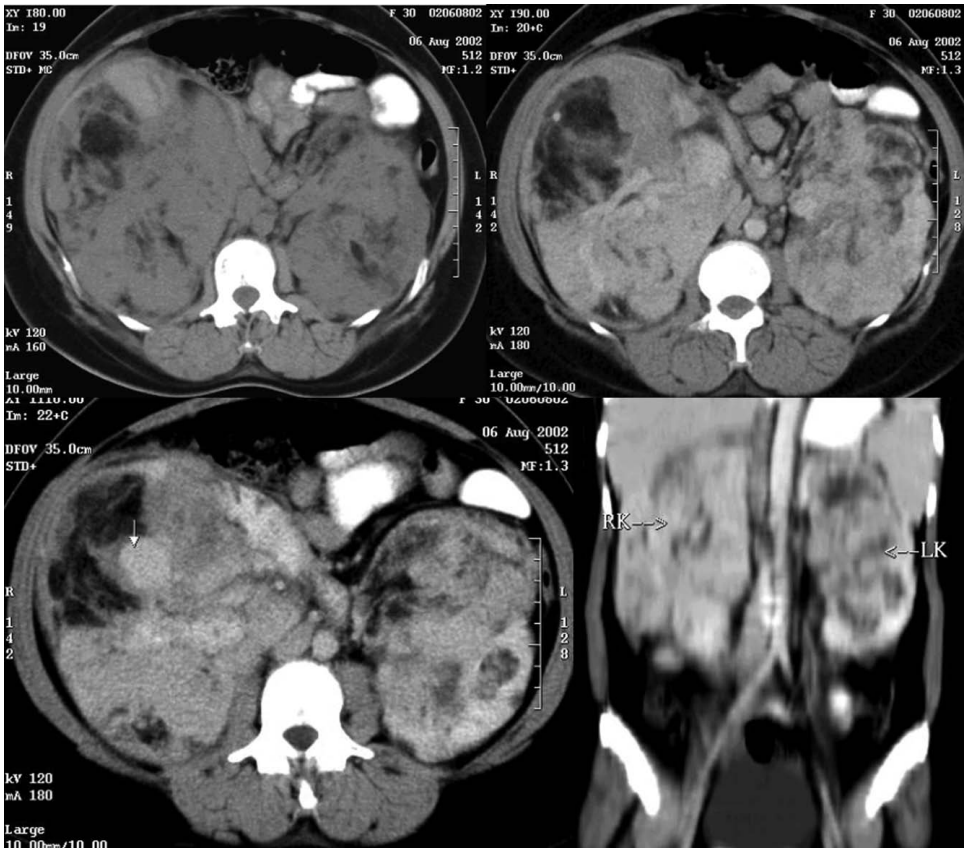

FIGURES 6.42A to D: Axial NECT and CECT shows bilateral enlarged kidney showing fatty and soft tissue components with prominent vascular channels. Features suggestive of hemorrhage within the AML in a female patient with features of tuberous sclerosis.

Lymphoma

The most common manifestation of renal lymphoma is multiple parenchymal nodules (61%). Invasion from perirenal disease (11%), solitary nodules (7%), large single lesions (6%) and diffuse infiltration (6%) are less frequent features. Bilateral involvement is three times more common than unilateral involvement.

The CT manifestation of lymphomatous involvement are varied and include:

1. Bilateral enlarged kidneys without demonstrable masses.
2. Enlarged or normal sized kidneys with multiple focal, nodular solid masses of variable size with decreased density post-contrast.
3. Solitary, irregular solid intrarenal masses.
4. Infiltrative pattern maintaing the reniform shape
5. Nonfunctioning kidney due to a large retroperitoneal mass.

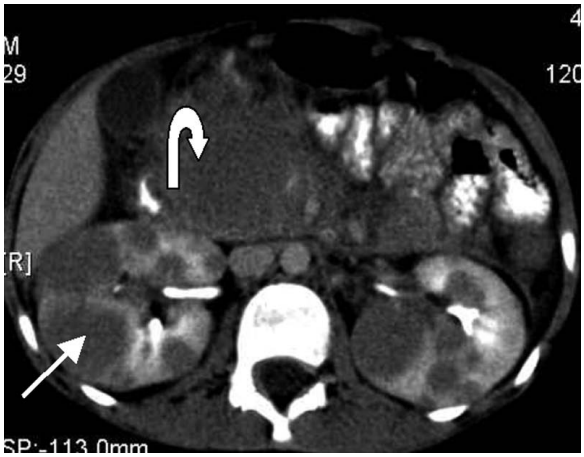

FIGURE 6.43: Axial CECT reveals bilateral multiple hypodense nonenhancing lesions involving the kidneys (arrow), hypodense lesion involving the pancreatic head (curved arrow).

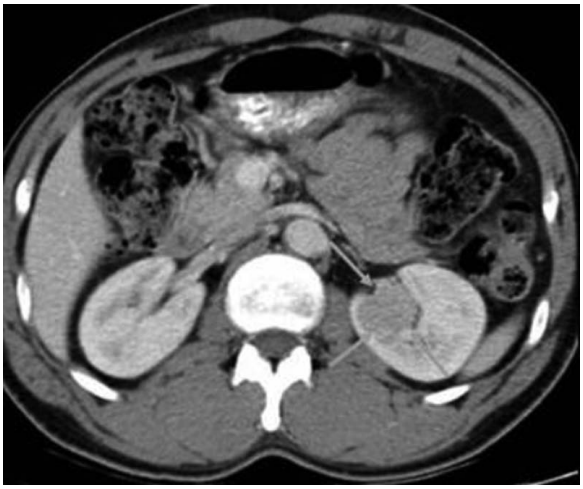

FIGURE 6.44: Axial CECT showing a left interpolar hypodense well marginated lesion—lymphomatous masses are typically homogeneous, hypovascular and with minimal enhancement.

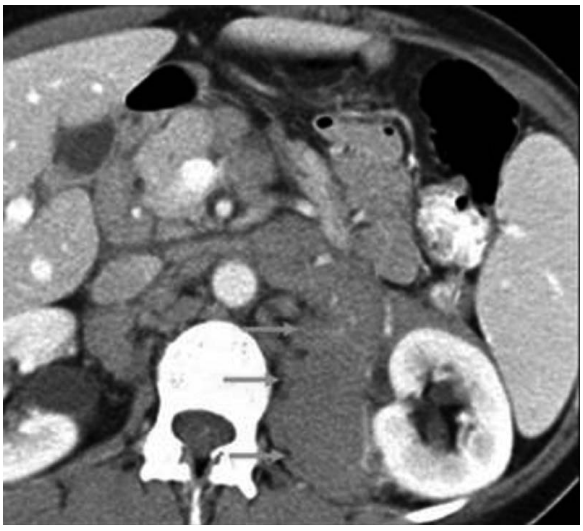

FIGURE 6.45: Contrast enhanced CT images show a large perirenal soft tissue mass (arrows) causing lateral displacement of the left kidney.

PATTERNS OF RENAL CELL CARCINOMA

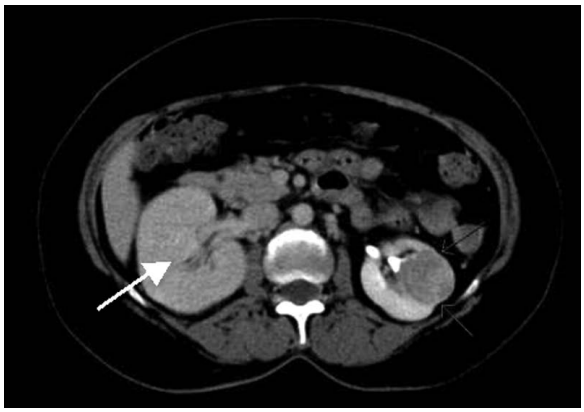

FIGURE 6.46: Axial CECT reveals enlarged right kidney with mild alteration of architecture (arrow), left renal interpole shows a well marginated lesion effacing the pelvis.

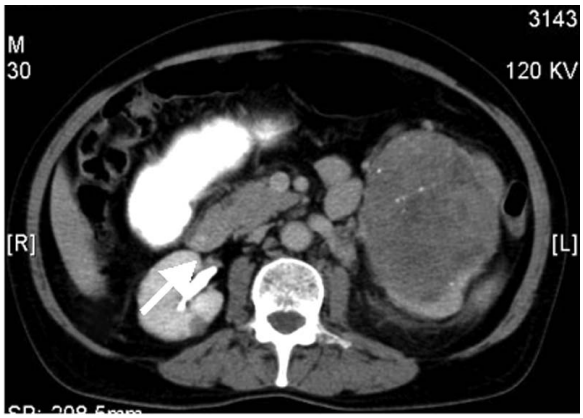

FIGURE 6.47: Axial CECT reveals a large heterogeneous relatively hypovascular mass involving the lower pole of left kidney with mild perinephric fat stranding. Right kidney shows a medial interpolar cortical cyst (arrow).

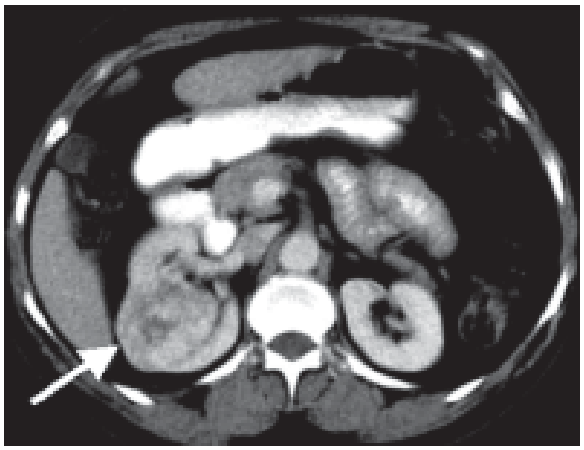

FIGURE 6.48: Axial CECT reveals a heterogeneously enhancing mass in the right interpolar region involving the pelvis, perinephric fat planes preserved (arrow).

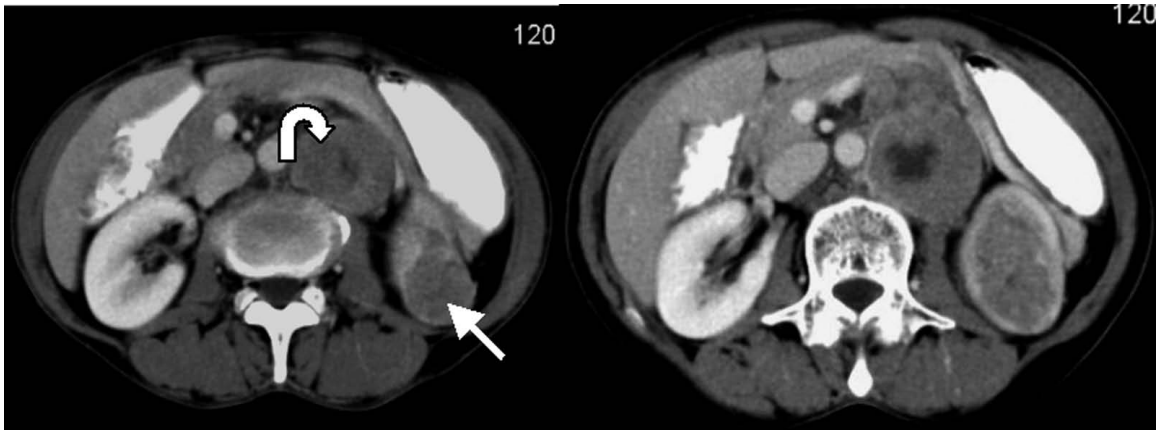

FIGURE 6.49: Axial CECT reveals a hypodense variably enhancing exophytic mass in the lower pole (arrow) infiltrating the renal pelvis with large hypodense lymph nodes seen in the para-aortic region (curved arrow)—note the morphology of the node is similar to the primary lesion.

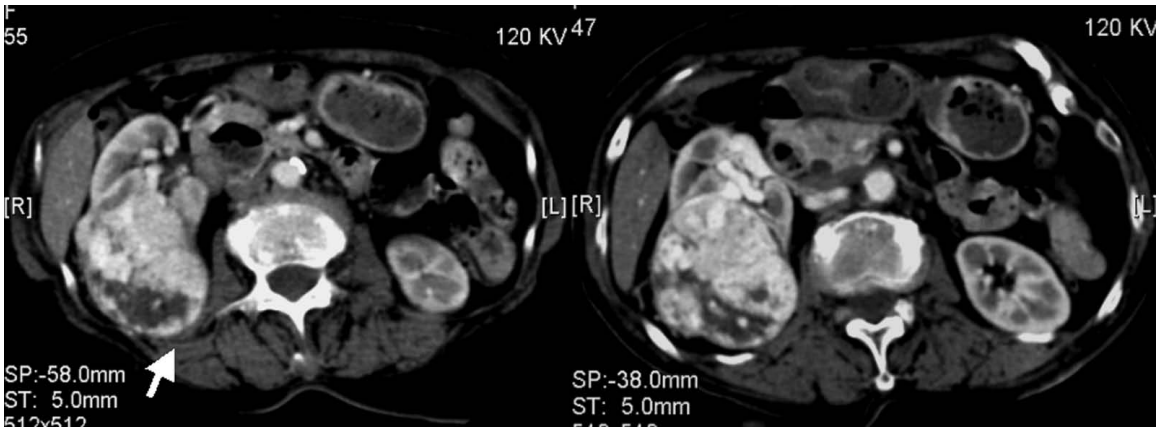

FIGURE 6.50: Axial CECT reveals a large hypervascular lesion involving the inter and lower pole of the right kidney displacing the kidney anteromedially. Note the focal loss of fat planes between the mass and the posterior abdominal wall (arrow).

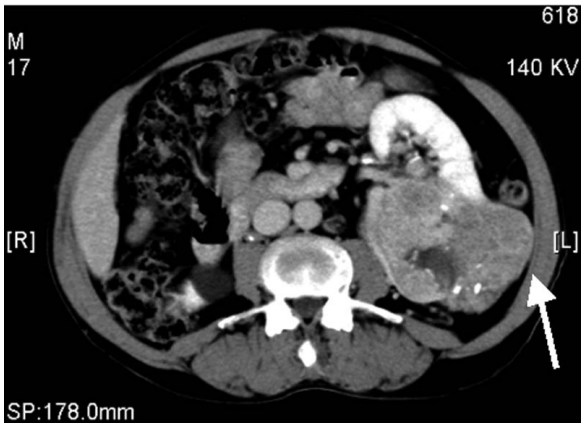

FIGURE 6.51: Axial CECT reveals a large mass replacing the left renal lower pole infiltrating into the renal pelvis. Note focal loss of fat plane between the lesion and the lateral abdominal wall (arrow).

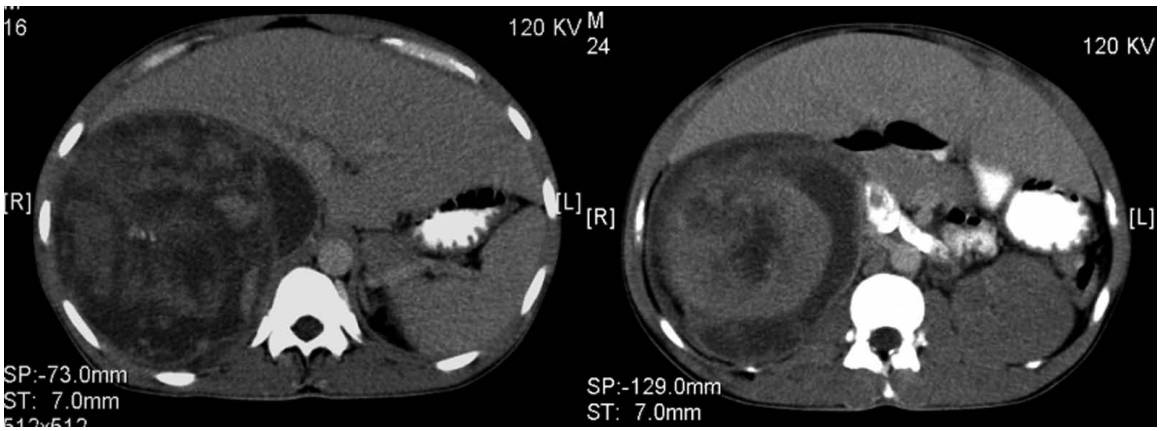

FIGURE 6.52: Axial CECT reveals a large heterogeneous lesion replacing the upper pole of right kidney with a medial subcapsular collection (arrow). IVC and left renal vein show stasis of contrast due to the mass effect over the IVC by the right renal mass (arrow).

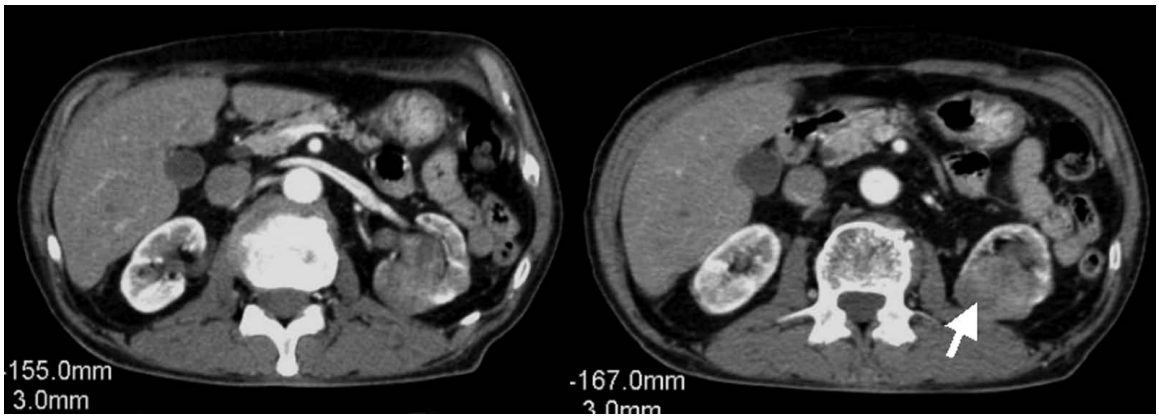

FIGURE 6.53: Axial CECT reveals a well marginated posterior left interpolar mass involving the renal pelvis, note the focal loss of fat planes between the mass and the left psoas muscle plane.

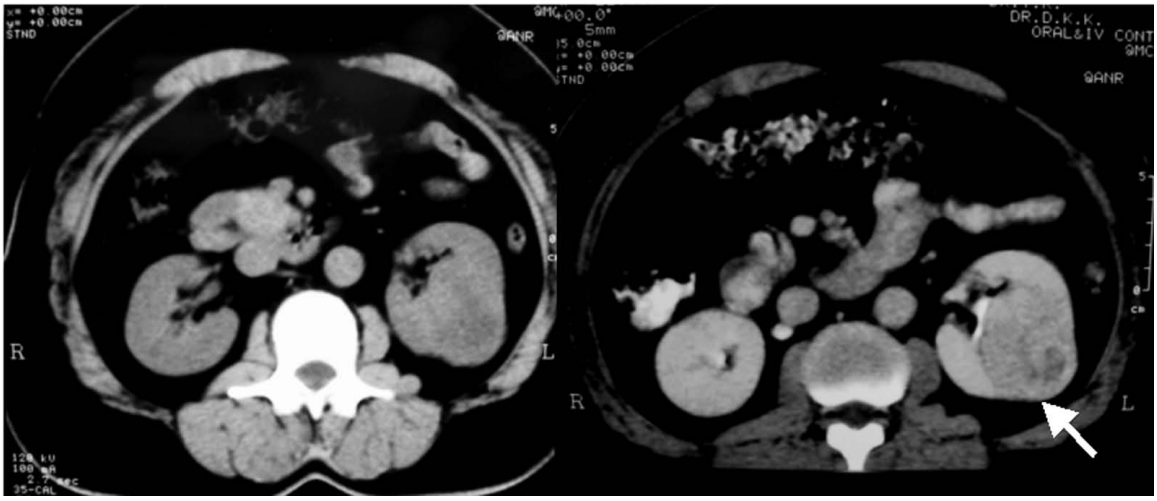

FIGURE 6.54: Axial CECT reveals a left interpolar mixed dense lesion indenting the renal pelvis.

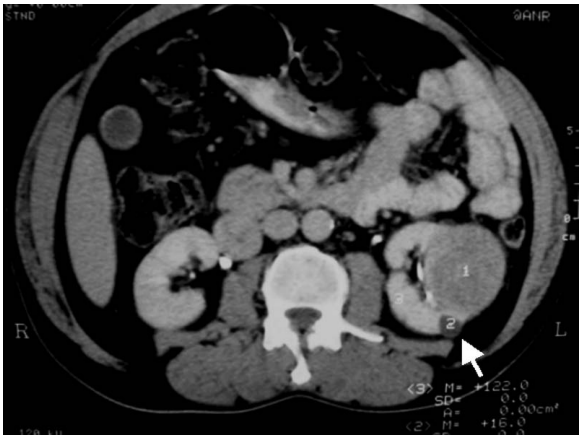

FIGURE 6.55: Axial CECT reveals a left renal interpolar lesion, note the adjoining cortical cyst (arrow).

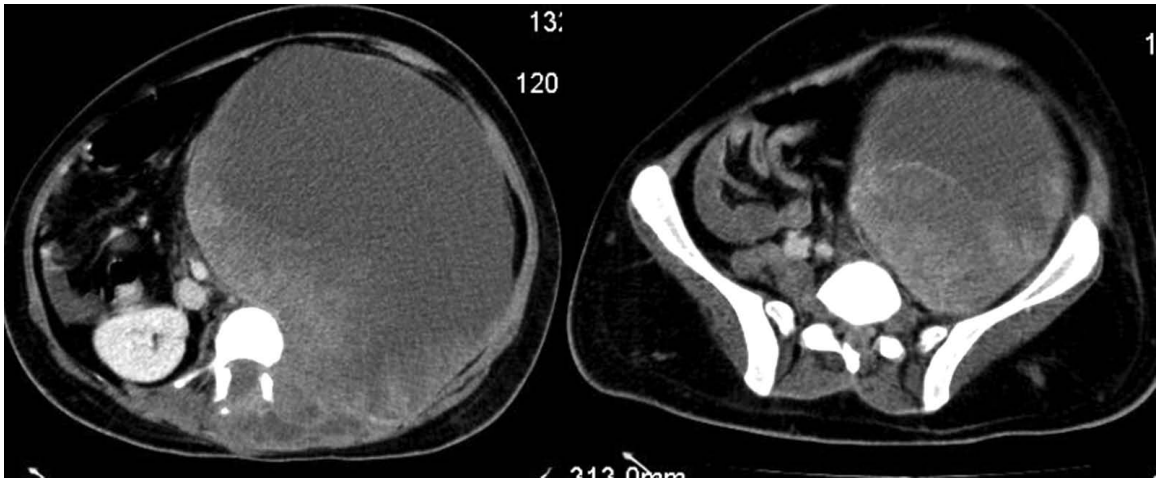

FIGURE 6.56: Axial CECT in a patient with neurofibrosarcoma reveals a large mixed dense predominantly cystic lesion replacing the left kidney infiltrating the adjacent psoas and posterior para-spinal muscles.

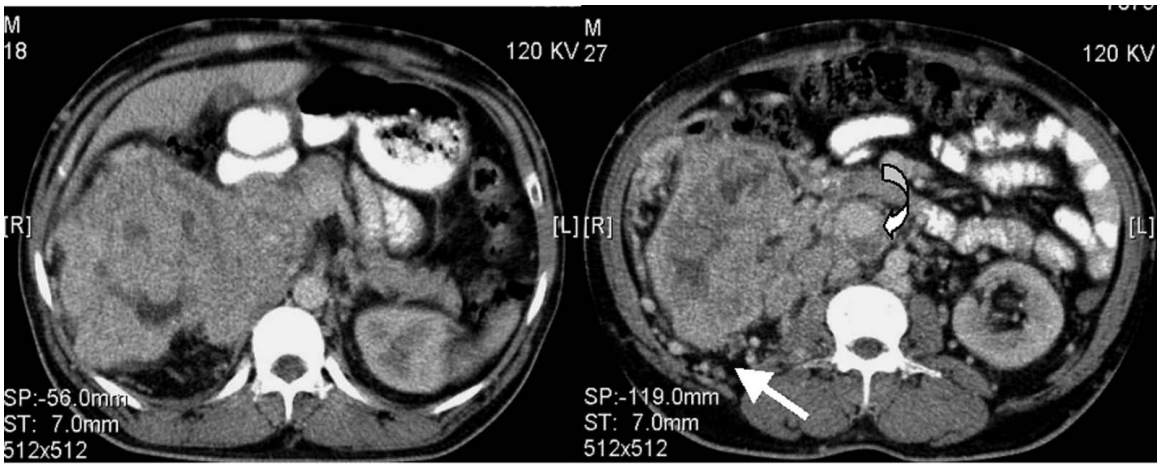

FIGURE 6.57: Axial CECT reveals a large heterogeneous mass replacing the upper and interpole of right kidney with multiple retroperitoneal collaterals secondary to vascular involvement of the left renal vein and IVC (note the eccentric thrombus in the IVC curved arrow).

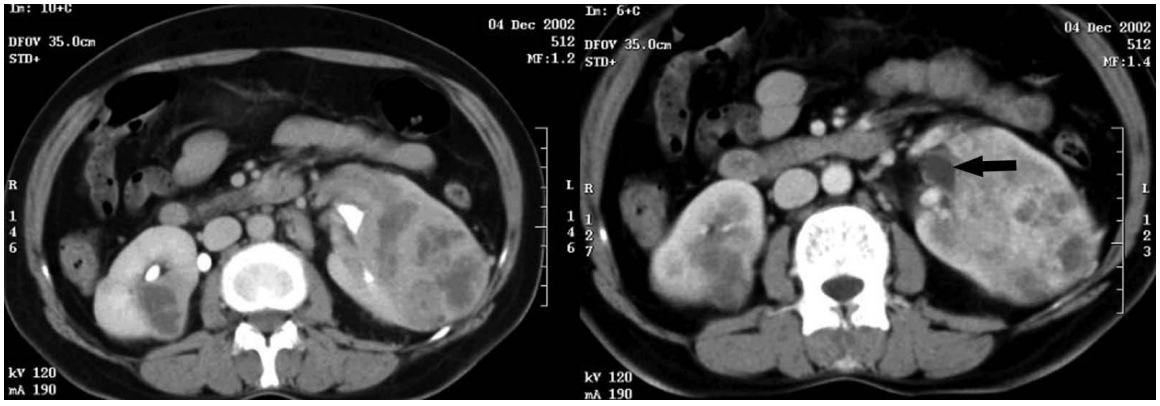

FIGURE 6.58: Axial CECT shows a large heterogeneously enhancing mass in the left renal interpole infiltrating into the renal pelvis (arrow). Right interpole posteromedial cortex hypodense lesion indenting the pelvis—case of bilateral synchronous malignancy.

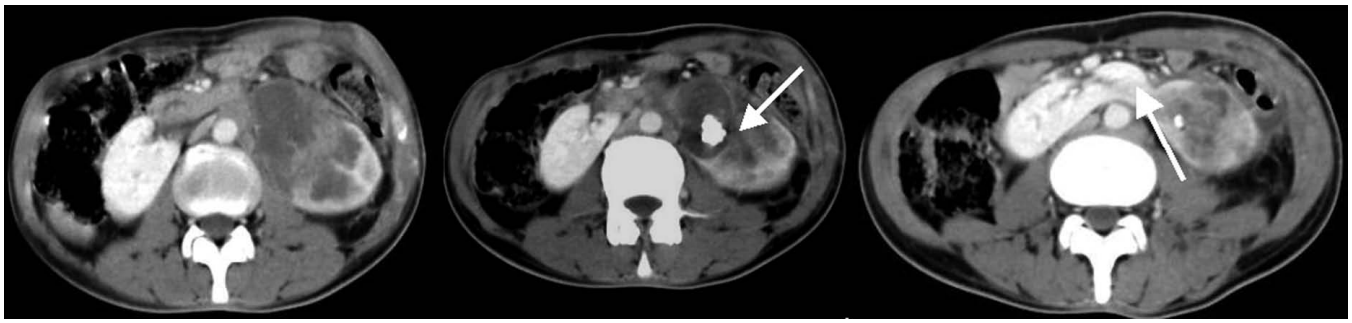

FIGURES 6.59A to C: Axial CECT showing horse-shoe kidney (arrow in C), with a mixed dense mass with a cystic component showing calcification (arrow in B).

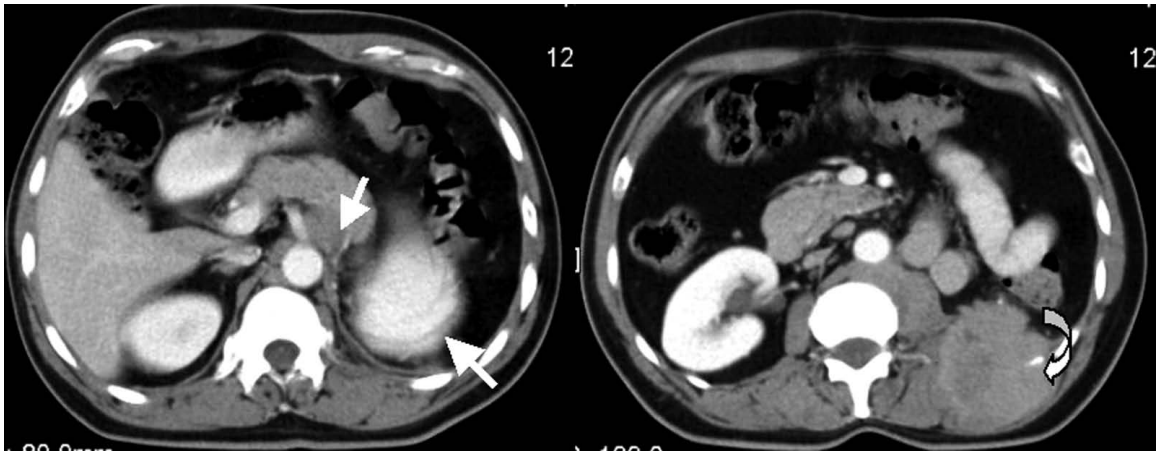

FIGURE 6.60: Axial CECT in a postoperative case of left renal tumor shows a posteriorly placed fundus of stomach (arrow) lymph node seen in the left para-aortic region (arrow). Soft tissue mass seen in the tumor bed infiltrating the posterior abdominal wall (curved arrow) suggestive of recurrence.

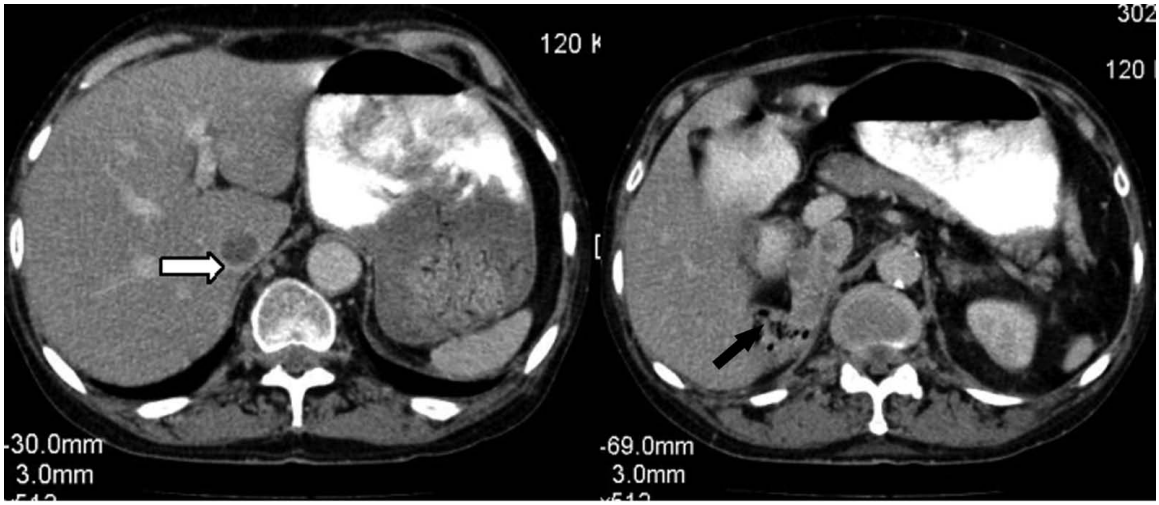

FIGURES 6.61A and B: Axial CECT in a postoperative right nephrectomy patient (case of RCC) on follow-up shows IVC thrombosis (arrow in A). Note the soft tissue in the right renal fossa suggestive of recurrence (arrow in B).

Renal Pelvic Tumors

Transitional cell Ca is the most common (80-90%) epithelial tumor of renal pelvis, in upto 40% of cases these lesions are multiple. Most of the TCC are of the papillary type that are slow to grow and follow a benign course. Nonpapillary form is more aggressive. They are 3-4 times more common in males more than 60 years of age.

Squamous cell carcinoma constitutes about 15% of pelvic tumors and is associated with chronic leukoplakia. More than 50% of tumors have associated calculi and extrarenal spread is the rule at the time of diagnosis. Hematuria and flank pain are common presenting symptoms.

CT appearances are varied small lesions are seen in the excretory phase as filling defects that can have a smooth, irregular or lobulated margins. CT values range from 15-40 HU and do not change dramatically after CECT.

Nonopaque calculi have a higher CT value, blood clots tend to be round, smooth, and dependently positioned within the renal pelvis. Where as tumors are usually irregular nondependent masses. In these cases the entire urinary tract has to be screened.

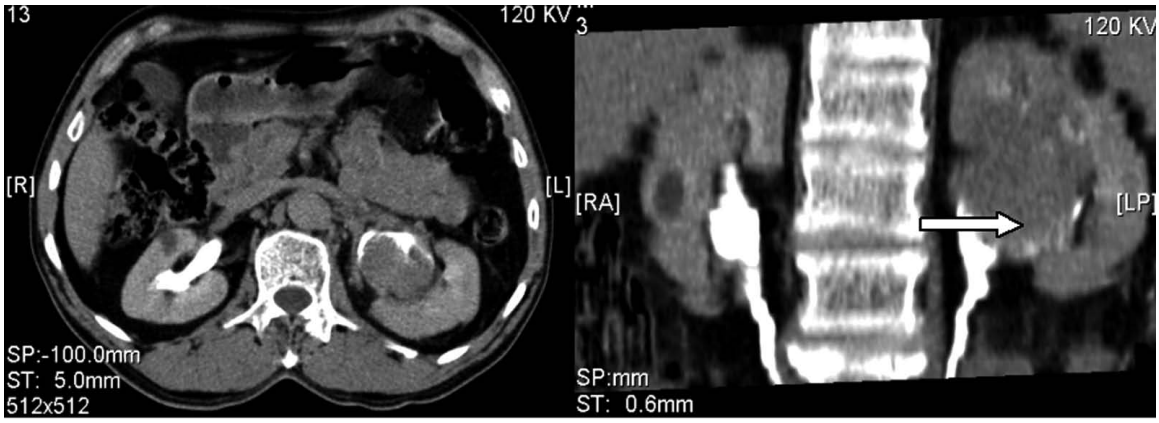

FIGURES 6.62A and B: Axial CECT during the excretory phase shows a hypodense pelvic mass. Fig. B is coronal MPR showing the intrapelvic mass (arrow).

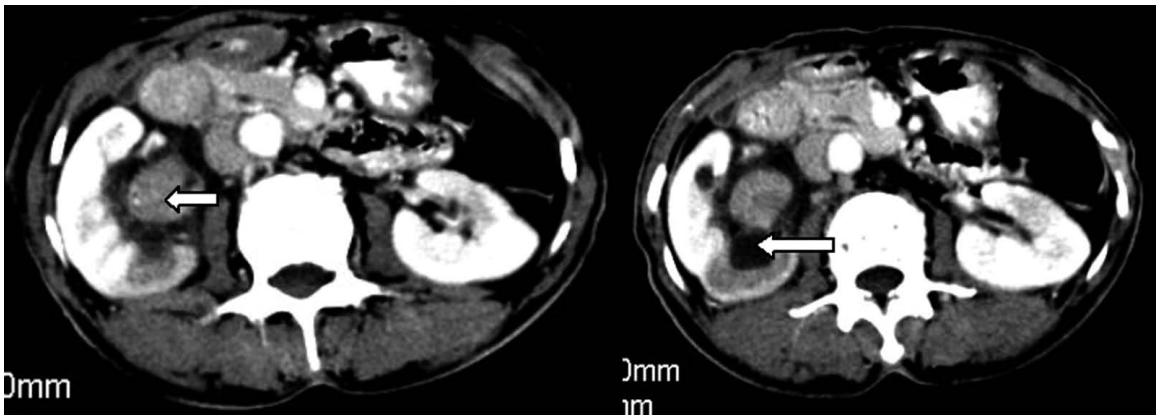

FIGURES 6.63A and B: Axial CECT showing right renal pelvic hypovascular mass (arrow in A) causing posterior calyceal cutoff (arrow in B).

Cystic Renal Masses

Renal cysts may be intraparenchymal or parapelvic, and they can reach considerable size. Complicated cysts result from secondary infection or hemorrhage into the cyst. While the majority of uncomplicated renal cysts are easily diagnosed, complicated cysts can be very difficult to distinguish from tumors.

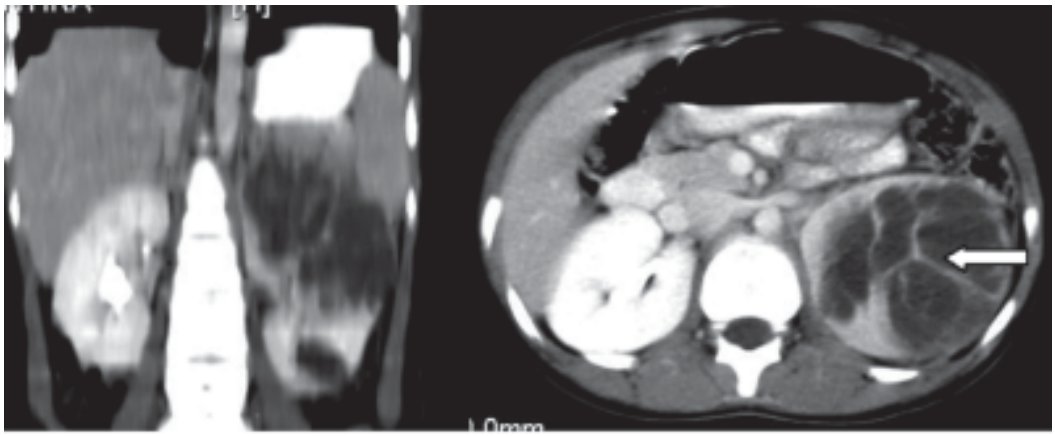

FIGURES 6.64A and B: Coronal MPR and axial CECT showing left renal upper polar cystic septated mass (arrow), lower pole calyceal dilatation seen.

Bosniack Classification of Renal Cyst

Category I: Uncomplicated cyst

Category II: Probable benign cyst follow-up at 3, 6, and 12 months

- Homogeneous attenuation before contrast administration (narrow window setting)
- No enhancement with contrast medium (narrow window setting, <10 HU attenuation difference) and <3 cm diameter
- Less than 1/3 of the cyst extends outside the kidney and has smooth margins
- Less than 3 cm in diameter.

Category III: Possible malignancy

- Thick, irregular septal or wall calcification
- Thick > 1 mm septa
- Nodular wall thickening.

Category IV: Typical malignant lesion

- Detection of a solid component (no matter how small) that enhances with contrast medium
  or
- Irregular, ill-defined margins.

APPROACH TO RENAL CYST EVALUATION

Cystic Renal Disease—Classification

Nongenetic Disease

Developmental

- Multicystic dysplastic kidney
- Medullary sponge

Acquired

- Simple cyst
- Inflammatory cyst
- Neoplastic cyst
- Cysts in hemodialysis patient

GENETIC

- *POLYCYSTIC*
  - Autosomal recessive
  - Autosomal dominant
- *MEDULLARY CYSTIC*
  - Autosomal recessive (juvenile nephronophthisis)
  - Autosomal dominant
- *GLOMERULOCYSTIC DISEASE*
- *CYSTS IN MALFORMATION SYNDROMES*

Glossary of Terms in Cystic Kidney

- Renal cyst—Is an enclosed epithelial lined sac.
- Cystic kidney—Kidney with 3 or more cysts.
- Polycystic kidney—Autosomal recessive/dominant kidney disease.
- Multicystic kidney—Non-specific term for a kidney with multiple cysts.

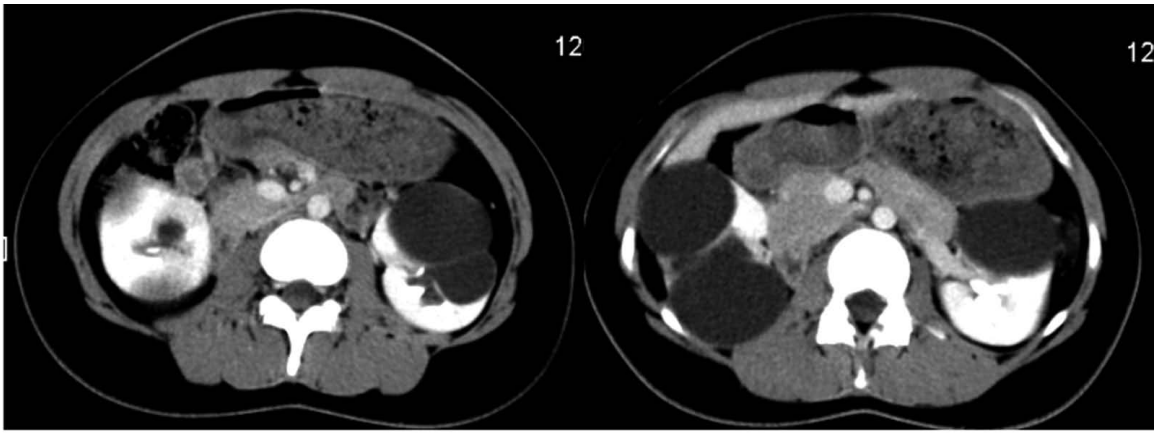

FIGURES 6.65A and B: Axial CECT reveals multiple cortical cysts in both kidneys.

The pathologic and imaging features of the renal cyst have been well described. A fluid-filled lesion is considered a cystic mass (i.e. not a simple cyst) when it has any of the following features: calcification, high attenuation (>20 HU) at computed tomography, septations, multiple locules, enhancement, wall thickening, or nodularity. There are two important causes of a cystic renal mass: a complicated simple cyst (e.g. one with hemorrhage, infection, or ischemia) and cystic renal cell carcinoma.

Computed Tomography

CT remains the major method of imaging and characterizing cystic renal lesions. Enhancement at CT is caused by the presence of tumor microvasculature, which can vary from very hypervascular in the case of renal cell carcinoma to hypovascular in the case of papillary renal cancer. Enhancement is dependent on the dose and rate of administration of iodinated contrast material as well as the timing of the imaging. A precontrast image is usually needed to establish enhancement, although "deenhancement" is an equally valid indicator of vascularity. A change of less than 10 HU from pre- to postcontrast images is usually considered typical of a benign cyst. This criterion was suggested by Bosniak. In contradistinction, a change within the solid portion of a cystic renal lesion of more than 15 HU is almost always indicative of a pathologic process although not always a malignancy, as cystic angiomyolipomas, oncocytomas, and infections may enhance.

A change in attenuation between 10 and 15 HU after intravenous administration of contrast material is considered suspicious but not diagnostic for a neoplasm.

Calcification

Calcification has been reported in 1-3% of cases of renal cysts. In all calcified cystic masses, it is important to obtain nonenhanced and contrast-enhanced CT.

Benign Calcification

A calcified cystic mass can be considered benign when there is a small amount of calcium smoothly deposited in the wall or septum of an otherwise simple cyst. Milk of calcium in the dependent portion of a cystic mass can also be considered benign.

Mitotic Lesion with Calcification

A calcified cystic mass is considered malignant if there is associated enhancement, nodularity, or wall thickening within the mass.

High Attenuation

A mass is considered hyperattenuating if it measures greater than 20 HU at unenhanced CT. A hyperattenuating can be considered a benign hyperattenuating cyst if it is sharply marginated or homogeneous or demonstrates a hematocrit effect on nonenhanced and contrast-enhanced scans and demonstrates no significant enhancement.

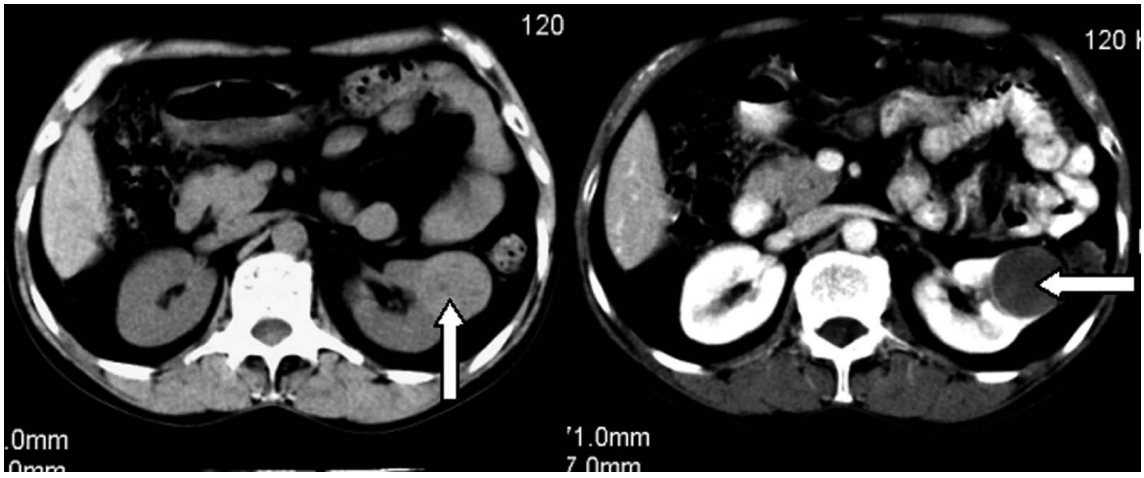

FIGURES 6.66A and B: Axial plain and CECT showing a left renal upper pole hyperdense cortical cyst, note the hypodense cystic nature of the cyst well seen in the contrast CT (arrows).

Septations

Septations may result from healing or organization of a cyst that has hemorrhaged or been infected. Septations also may result from two adjacent cysts that share a common wall. Septations are often partial. Calcification may be deposited in the septations in a fine curvilinear pattern that is best evaluated with CT.

Benign Septations

Benign septations are thin (1 mm or less) and smooth and attach to the walls of the cyst without associated nodularity, septations may be calcified.

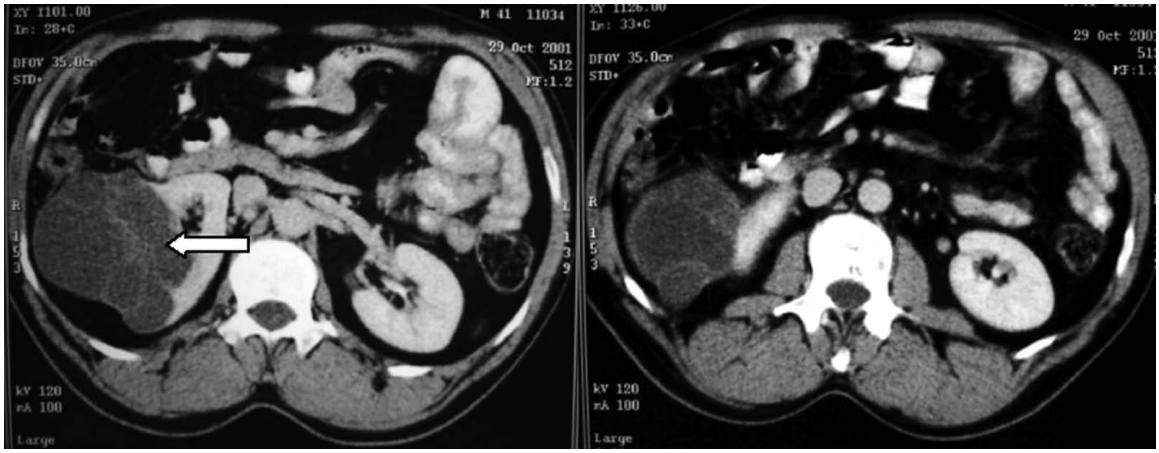

FIGURES 6.67A and B: Axial CECT showing a multiseptated right renal cyst.

Multiple Locules

Although the exact number is arbitrary, when a mass has more than three or four septations, it should be considered multiloculated. The multilocular cystic nephroma is an uncommon, nonhereditary cystic neoplasm. It is characterized by a well-developed capsule, fibrous stroma, and septa that separate multiple epithelium-lined, noncommunicating cysts. Although the vast majority of multilocular cystic nephromas are benign, metastases have been reported.

Wall Thickening, Nodularity and Enhancement

The simple, uncomplicated cyst is characterized by an extremely thin cyst wall without nodularity. As it does not enhance, the wall of a simple cyst is barely perceptible.

Cystic renal cell carcinoma often has thickening or nodularity in a portion of its wall. The finding of wall thickening can be quite subtle as the wall may measure only 2-3 mm in thickness. The recognition of wall thickening in a small cystic lesion is especially challenging.

Discrete nodularity within a cystic mass is another feature that may be seen in cystic renal cell carcinoma. Asymmetric wall thickening or septations seen en face can resemble nodules.

Enhancement within a cystic lesion often makes areas of wall thickening and nodularity more conspicuous. Wall thickening and enhancement must not be confused with the normal renal parenchyma that at least partially surrounds a cystic lesion.

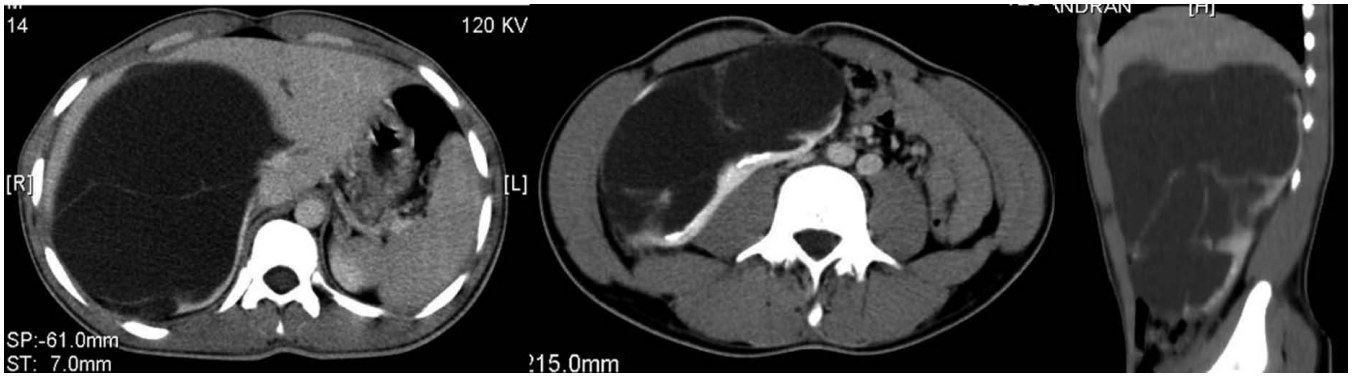

FIGURES 6.68A to C: Axial CECT with sagittal reformats showing a large septated cyst replacing most of the renal parenchyma.

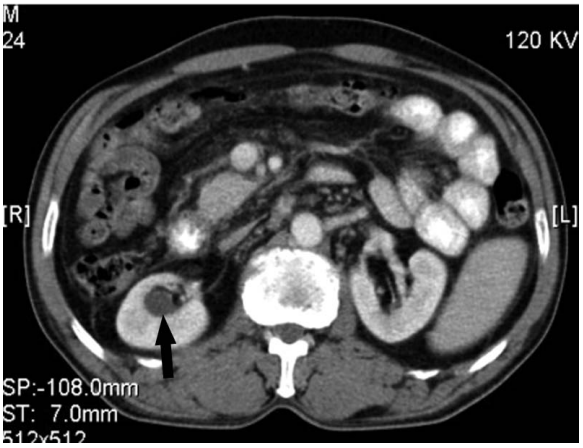

FIGURE 6.69: Axial CECT showing a small pelvic cyst.

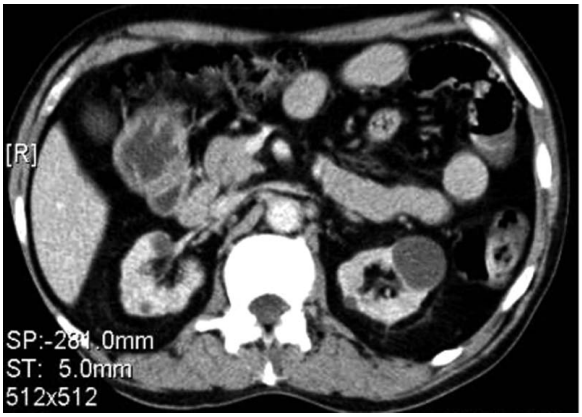

FIGURE 6.70: Axial CECT showing cortical cysts of varying sizes involving both kidneys. Contrast CT especially in the nephrographic phase shows cysts not evident in plain study or in USG.

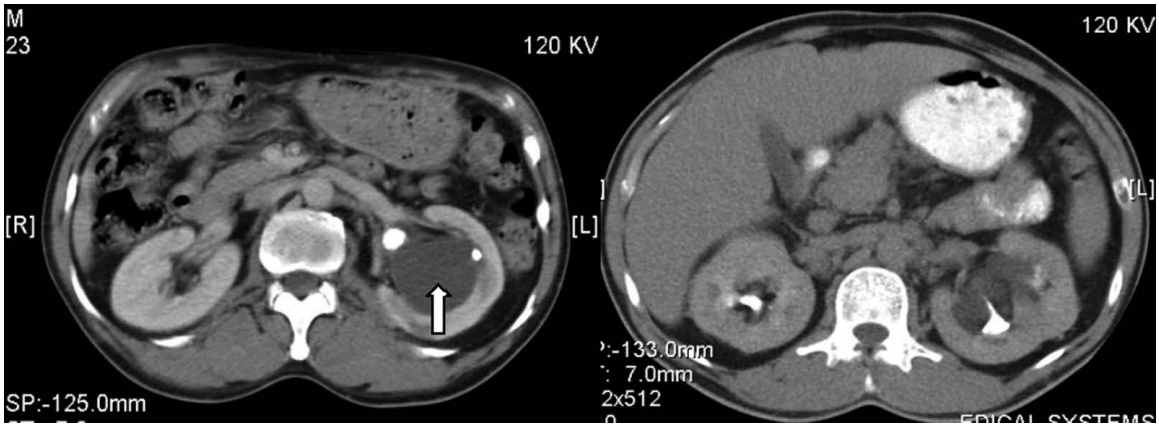

FIGURES 6.71A and B: Axial CECT in two different patients showing left renal pelvic cyst. Note the displacement of the pelvis and calyces (arrow).

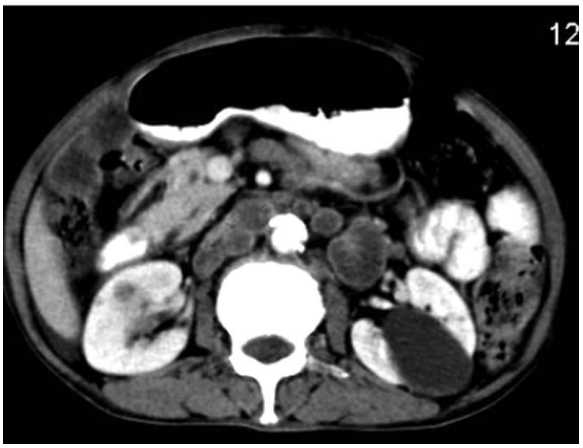

FIGURE 6.72: Axial CECT showing a exophytic pelvic cyst.

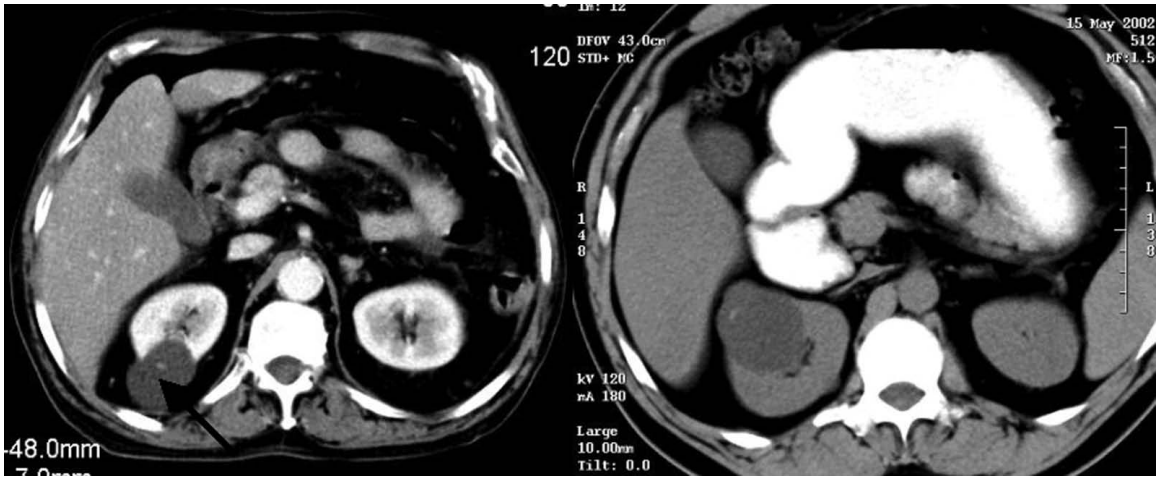

FIGURES 6.73A and B: Axial CECT and NECT in two different patients showing subtle linear calcification.

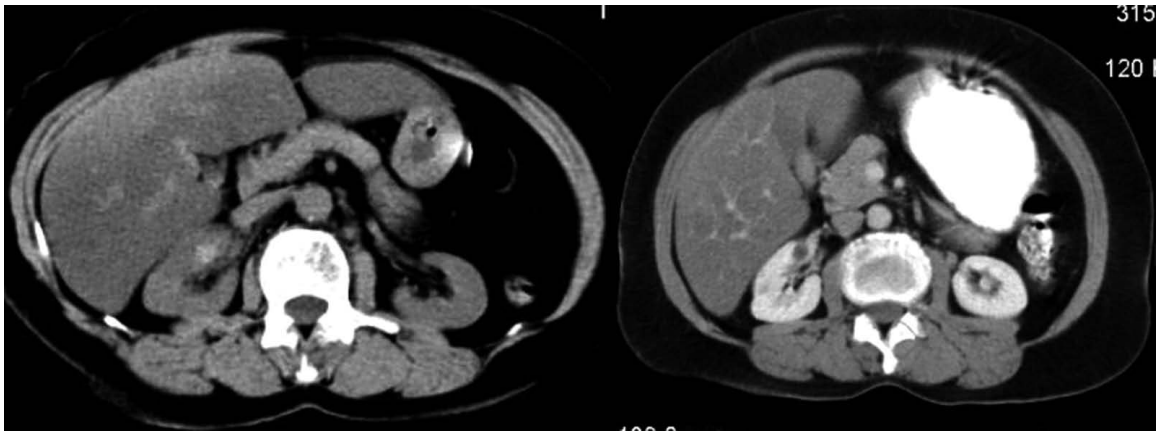

FIGURES 6.74A and B: Axial CECT showing a small hyperdense anterior interpolar cyst.

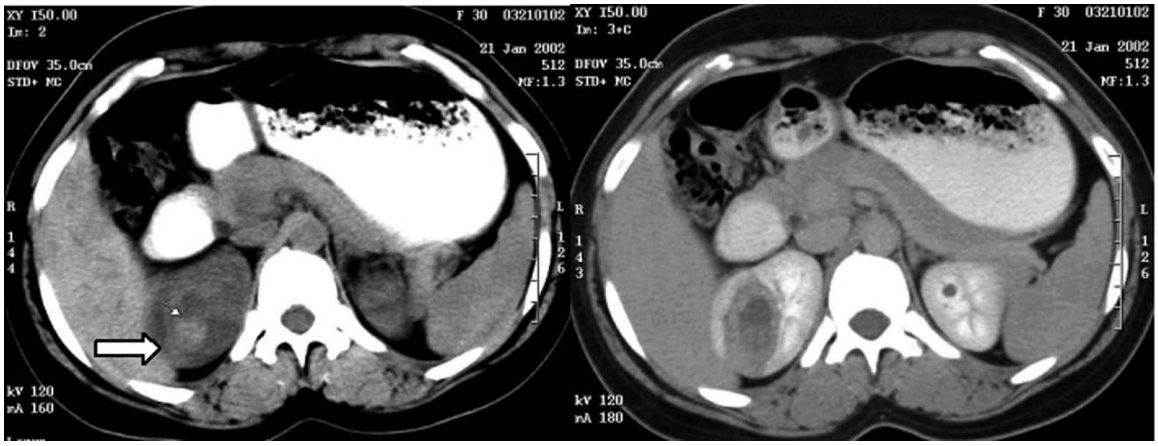

FIGURES 6.75A and B: Axial CECT showing a complex cyst with areas of layering, note the central high attenuation (arrow in Fig A) reflecting a proteinacious content.

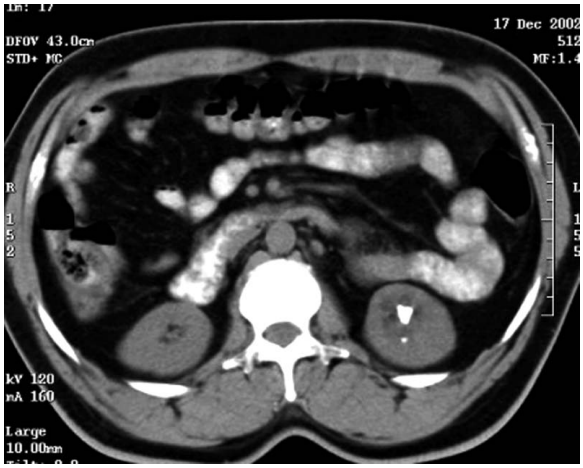

FIGURE 6.76: Axial NECT showing a calcium fluid level in the left renal interpole reflecting milk of calcium in the cyst.

Hereditary Renal Cancer

Hereditary renal cancer syndromes can lead to multiple bilateral kidney tumors that occur at a younger age than do nonhereditary renal cancers. Imaging plays an important role in the diagnosis and management of these syndromes. von Hippel–Lindau disease tuberous sclerosis, hereditary papillary renal cancer, Birt-Hogg-Dubé syndrome, hereditary leiomyoma renal cell **carcinoma**, familial renal oncocytoma, hereditary nonpolyposis colon cancer, and medullary **carcinoma** of the kidney.

Table 6.3: Staging of renal malignancy

Tumor position	*Robson stage*	*TNM class*	*CT findings*	*CT pitfalls*
Confined within renal capsule	I	…	Soft-tissue mass enhances less than normal renal Parenchyma; central Necrosis in large renal cell carcinoma	…
Small (<7 cm diameter)	…	T1	..	…
Large (>7 cm diameter)	…	T2	…	…

Contd...

Contd...

Tumor position	*Robson stage*	*TNM class*	*CT findings*	*CT pitfalls*
Spread to perinephric fat	II	T3a	Perinephric stranding: Perinephric collateral vessels	Not reliable or specific; found in 50% of T1 and T2 tumors; false-negative if Spread is microscopic
			Soft-tissue mass in Perinephric space	Specific, not sensitive in 45-50% of cases
Venous thrombus	IIIA	…	Filling defect within a distended vein; direct continuity of thrombus with primary mass; IV contrast enhancement indicates tumor thrombus; collateral veins	False-negative: right renal vein and ivc obscured by large renal cell carcinoma; false-negative: enhancing thrombus obscured; false-positive: venous enlargement due to Increased flow; false-Positive: streaming of Unopacified blood in IVC (perform delayed scanning)
Renal vein only	…	T3b	…	…
IVC infradiaphragmatic	…	T3c	…	…
IVC supradiaphragmatic	…	T4b	…	…
Regional lymph node metastases	IIIB	N1-N3	Lymph nodes 1 cm in diameter or larger	False-negative rate: 4% false-positive: enlarged Inflammatory nodes
Direct invasion of adjacent organs	IVA	T4a	Obliteration of normal soft-tissue planes between tumor and adjacent organs	False-positive: partial volume averaging: false-positive: tumor adherent but not directly invading
Distant metastases	IVB	Mia-d	Metastases enhance with IV contrast material; hepatic metastases best in arterial phase	Hypervascular metastases may be obscured in portal venous phase
	…	N4	…	…

Small Renal Mass

The small renal mass is defined as a geographic renal lesion that measures 3 cm or less in diameter. Small renal masses are commonly detected during imaging of the kidneys. The sensitivity is 67% for excretory urography, 79% for sonography, and 94% for conventional nonhelical CT. The most cost-effective approach is to go directly to renal sonography. With this technique 80% of detected renal masses are characterized as simple cysts, thus ending their diagnostic evaluation. The remaining 20% of renal masses require further study with CT or MR imaging. Any mass detected initially on sonography or evaluated with sonography after detection with another imaging technique that does not meet the strict sonographic criteria for a simple cyst should be further evaluated with CT or MR imaging of the kidneys. For diagnosis of a simple renal cyst based on sonographic findings, a renal mass must be anechoic with a sharply defined back wall and enhancement of through sound transmission. One or two thin septations may also be visible sonographically in simple renal cysts. Because these findings are diagnostic, no further imaging or follow-up is needed in the evaluation of these lesions. However, other atypical features—sonographically detected calcifications, more than two septations, septal thickening or nodularity and the presence of solid components—indicate that sonography alone will not be adequate for complete evaluation (i.e. diagnosis and possible staging) of these renal masses. Whereas renal masses 0-5 mm in diameter can be particularly enigmatic on CT or MR imaging, masses of this size are rarely problematic for sonography because they are almost universally undetectable with current sonography techniques.

CT is the standard imaging technique for the evaluation of small renal masses. Helical CT has led to further improvements in renal mass imaging, such as rapid multiphase imaging of the kidneys without misregistration artifacts attributable to patient breathing and the capability for high-quality multiplanar (three-dimensional) postprocessing of images. With helical CT, the kidneys can be rapidly scanned before injection of contrast material and during different phases of opacification of the kidneys. Multidetector helical CT scanners allow rapid scanning of the kidneys with narrow collimation that can be completed during a single breath-hold. Helical CT may improve not only the characterization of lesions but also their detection. Two recent studies analyzed the detection of surgically resected small renal masses and showed discrepancies between results obtained with helical CT and those obtained with standard incremental CT. Incremental CT revealed 153 (75%) of 205 renal masses identified at surgery: 47% of masses less than 5 mm in diameter, 60% of masses 5-10 mm in diameter, 75% of masses 10-15 mm in diameter, and 100% of masses 15 mm and larger. Another study in which helical CT was used to scan the kidneys during both the corticomedullary phase and the nephrographic phase of contrast enhancement reported better detection of small renal masses than with incremental CT; 97 (95%) of 102 renal masses 8-15 mm in diameter were detectable. All renal masses larger than 15 mm were also detectable with helical CT.

When a renal mass is suspected, the unenhanced scan should be obtained to serve as the baseline for measurements of enhancement on images obtained after contrast material administration. For the accurate detection of renal masses, the nephrographic phase obtained approximately 3 min after the initiation of contrast material injection is optimal. The corticomedullary phase should also be included not for detection or diagnosis but for staging information. Commencing approximately 70 sec after the initiation of contrast material injection, this is the optimal phase for evaluation of the renal vein and the other solid abdominal viscera, including the liver, which is a common site of metastatic spread.

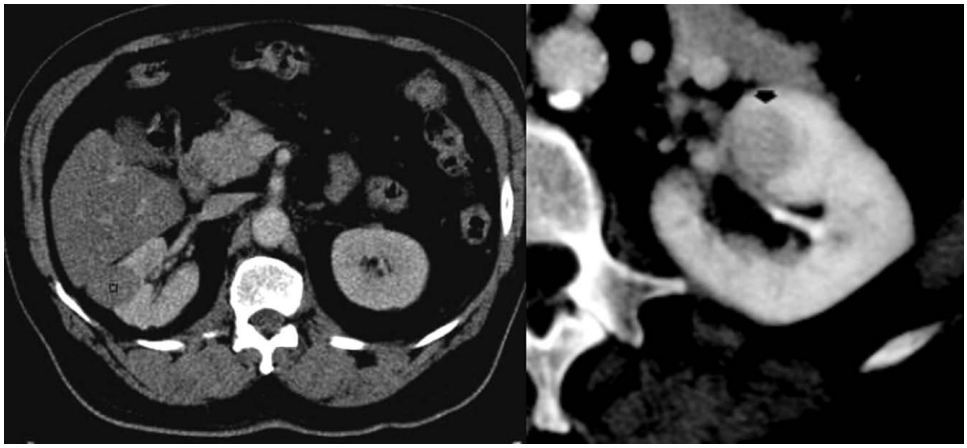

FIGURES 6.77A and B: Axial CECT in two different patients showing well marginated solid lesions.

PEDIATRIC RENAL TUMOR

Primary Renal Tumors of Infancy

- Wilms tumor
- Nephroblastomatosis
- Multilocular cystic renal tumor
- Clear cell sarcoma of kidney
- Rhabdoid tumor of kidney
- Mesoblastic nephroma

Primary Renal Tumors in Older Children

- Angiomyolipoma
- Renal cell carcinoma
- Renal medullary carcinoma
- Lymphoma

Nephrogenic Rests — GLOSSARY

Nephrogenic rests – persistent fetal renal blastoma beyond 36 weeks.
Seen in 1% of normal infants.

Perilobar nephrogenic rests

Superficial cortical location, associated with Beckwith-Wiedman syndrome.

Intralobar

Deep cortical
Associated with Wagr and Drash syndrome.

Nephroblastomatosis

Multifocal nephrogenic rests.

Imaging Findings

Multifocal discrete or confluent homogeneous solid cortical nodules, lobular nephromegaly scalloping and compression of central renal tissue. They appear as poorly enhancing low attenuation peripheral nodules.

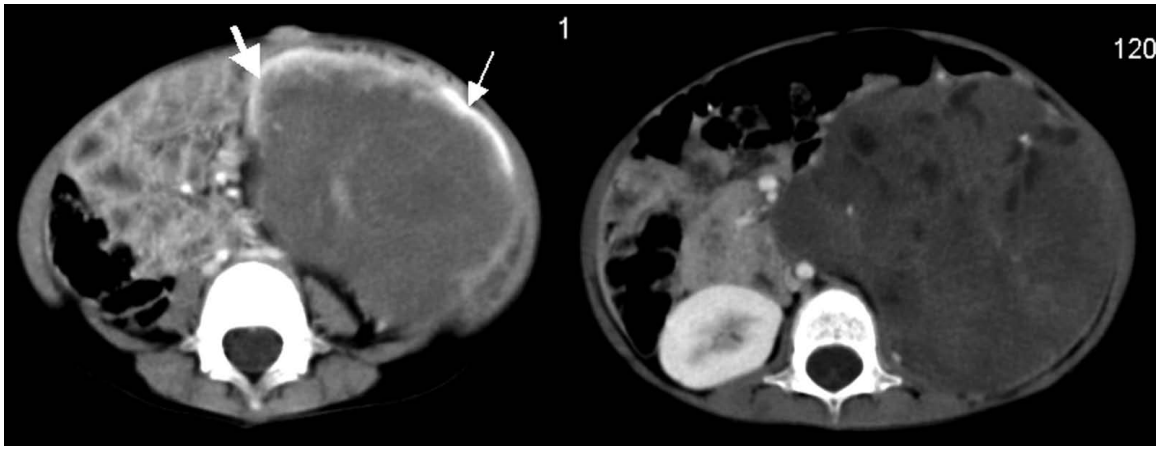

FIGURES 6.78A and B: Axial CECT reveals a large upper pole lesion of the left kidney involving the interpole replacing most of the normal renal parenchyma with a thin peripheral rim of enhancing renal tissue (arrow).

CT TECHNIQUE FOR PELVIS AND URINARY BLADDER

Adequate opacification of small and large bowel by oral contrast is essential. Oral contrast can be administered 3-4 hours prior to the study or alternatively 100-150 ml of contrast can be instilled via rectum. In cases where gynecological malignancy is suspected a vaginal tampon may be useful.

IV contrast is essential for differentiating nodes and vessels, and also to delineate enhancing component of mass lesion. 80-100 ml of 300 mg/ ml nonionic contrast agents is used at the rate of 3 ml/sec. Scanning the pelvis at approximately 35-40 seconds after commencement of injection allows enhancement of bladder wall prior to the filling of bladder with contrast. Ideally the ureteric jets have to opacified. Delayed scans after 10-15 minutes allow ureteric and bladder opacification.

The urinary bladder consists of an apex, superior surface, two inferolateral surface, a base, or posterior surface and a neck, the apex of bladder ends as the medial umbilical ligament, the superior surface is covered by peritoneum. The base of bladder contains the trigone, and the bladder neck is pierced by the internal urethral orifice.

Diffuse Thickening of Bladder Wall

Common causes

Non-distention, trabeculation, pancystitis

Uncommon causes

Hemorrhage, edema

Infiltration, carcinoma

Trabeculation

Trabeculation of the bladder wall is observed most commonly in patients with bladder outlet obstruction or neurogenic bladder, imaging reveals generalized trabeculation of the inner wall of bladder associated findings include primary causes of outlet obstruction like enlarged prostate (both neoplastic and non-neoplastic causes).

Cystitis

Cystitis is inflammation of part or all of the urinary bladder wall, acute cystitis refers to bladder inflammation of recent symptomatic onset, imaging-wise the bladder may appear normal even in the presence of cystoscopic abnormalities.

Chronic cystitis refers an inflammatory process of longer duration resulting in a bladder with thickened walls and small capacity. Focal lesions which can be seen include bullous edema, polypoidal pseudotumor, cystitis cystica, malacoplakia.

Bacterial cystitis is the most common form of infectious cystitis often occurring in sexually active and is thought to be due to retrograde bacterial deposition. In men cystitis usually occurs as a consequence of bladder outlet obstruction. Milder forms may appear normal on CT severe forms can present as irregular or nodular mural thickening, an unusual manifestation of recurrent infection is malakoplakia, a granulomatous inflammation of lower ureter and bladder. TB cystitis follows hematogenous dissemination from lungs, cystitis follows infection of kidneys and ureter. Focal irregular mural filling defects may be seen early in the diseases. If infection proceeds transmural involvement occurs resulting in reduced bladder capacity, VUR and ureteral obstruction frequently occurs with reduced vesicle compliance.

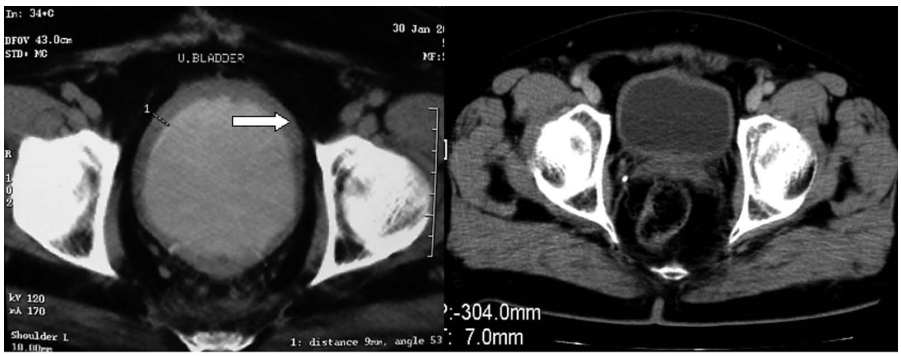

FIGURES 6.79A and B: Axial CECT with distended urinary bladder shows diffuse mural thickening in two different patients with clinical features of UTI. It is important to have a distended bladder. In patients with atypical findings it is advisible to undergo cystoscopy to rule out mitotic lesions.

Non-infectious causes for cystitis include mechanical, toxic, drug induced, radiation induced and allergic causes. Common irritants include indewelling catheter, bladder stone, suture material, paravesicle disease like diverticulitis, pelvic abscess and gynecological malignancy. Fulminant cystitis can be caused by cyclophosphamide resulting in hematuria with nodular bladder wall thickening. Interstitial cystitis can be caused by rheumatoid arthritis, SLE, polyarteritis nodosa.

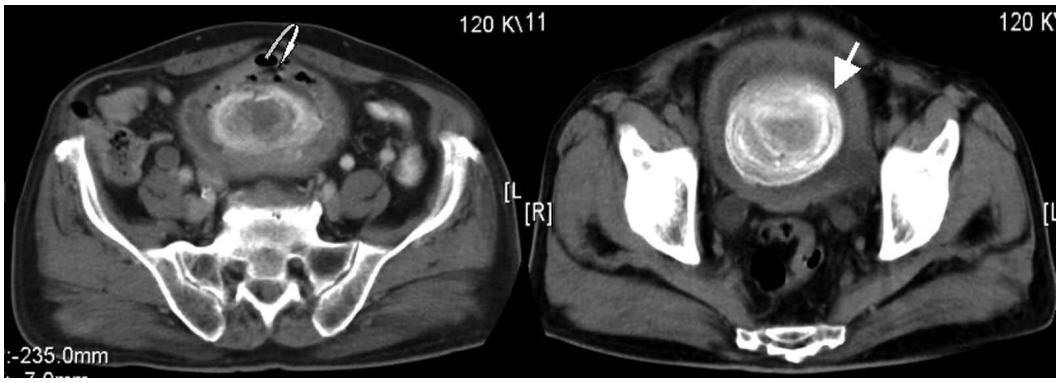

FIGURES 6.80A and B: Axial CECT reveals a laminated vesicle calculus (arrow) diffusely thickened bladder wall with small airpockets in the anterior vesicle wall (curved arrow) –feature of emphysematous cystitis.

Outpouching from Bladder

Outpouching of bladder wall
Common—diverticulum and saccule, cystocele
Uncommon—urachal diverticulum.

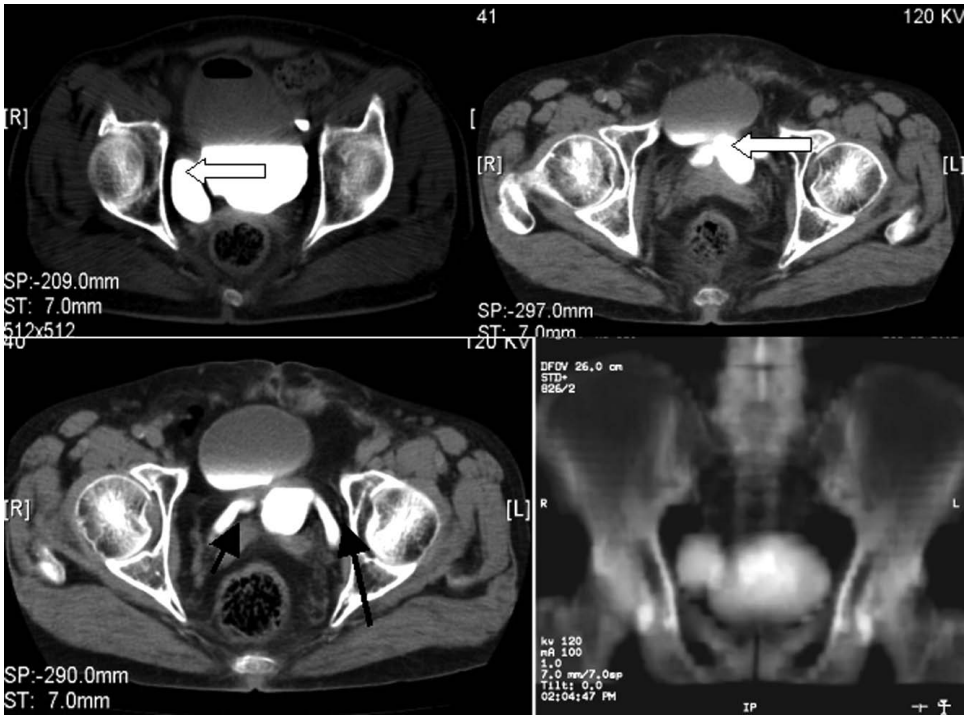

FIGURES 6.81A to D: Axial CECT shows distended urinary bladder with right lateral wall and bladder base diverticula (arrows), note the ectopic insertion of both ureters into the basal diverticulum (arrow in C).

Diverticula

Diverticula are focal herniation of urothelium and submucosa through naturally weak sites in the bladder. When acquired diverticula are a result of chronic elevation of intravesicle pressure. These herniations tend to occur next to the ureteral orifice. They are important causes for urinary stasis causing infection, VUR, ureteral obstruction. Large lesions may cause mass effect over the bladder and displace them lateral deviation of the ureter can occur because of the diverticula. Outpouching of less than 2 cm area are referred as saccules. Filling defects seen within the diverticulae can be caused by stone or tumor.

Bladder Herniation

Herniation of bladder through a pelvic or abdominal opening is an unusual cause of a small or asymmetrically shaped bladder associated with focal area of outpouching. Herniation through inguinal or femoral canal occur in more than 95% of all patients.

In infants less than 1 year transient small inguinal herniations can be seen in upto 10% of cases undergoing VCUR these are called bladder ears and are normal variants in children without any pathological significance.

Bladder hernias usually are less than 2-2.5 cm in size, the wall of the hernias are smooth unless they are complicated by infection or stone. The lateral and inferior portion of bladder herniates anteriorly and inferiorly in patients with inguinal canal herniation.

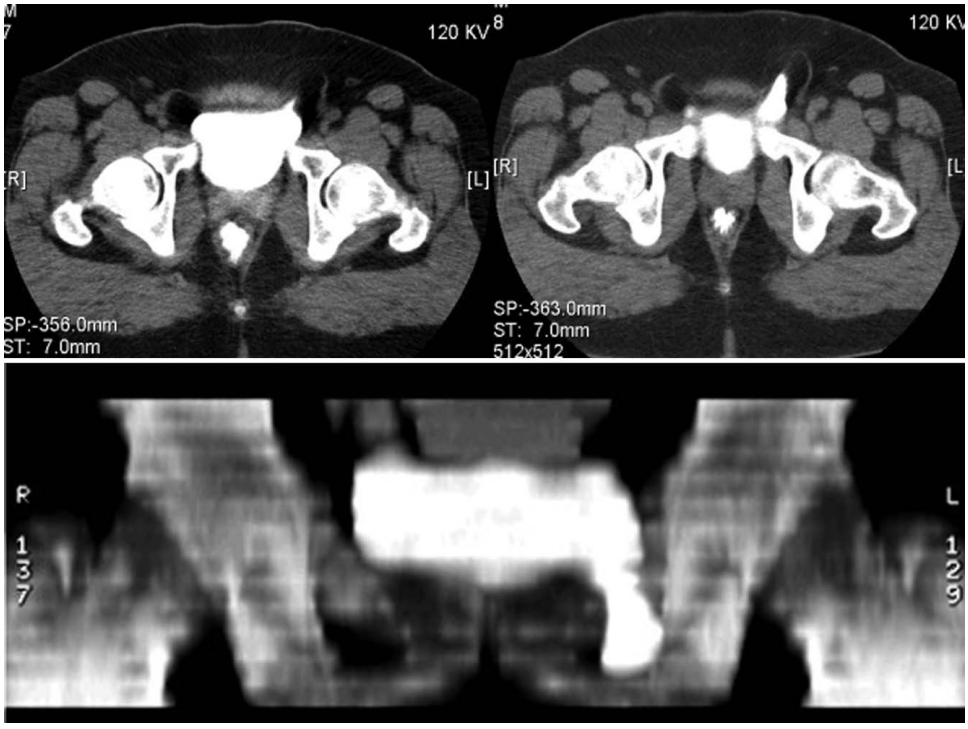

FIGURES 6.82A to C: Axial CECT with reformation studied reveals a elongated outpouching of the urinary bladder in the distended state herniating into the inguinal ring.

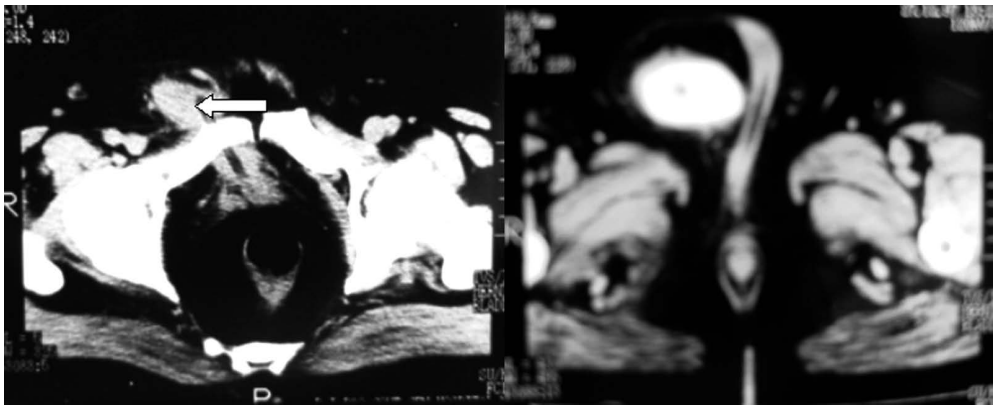

FIGURES 6.83A and B: Axial CECT showing right inguino scrotal herniation of the urinary bladder, note the Foley's bulb in situ (arrow).

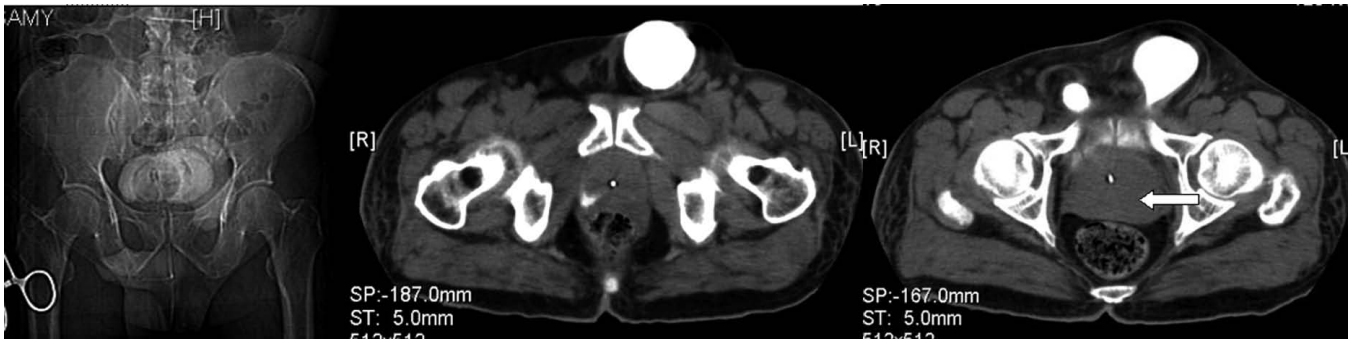

FIGURES 6.84A to C: Axial CECT showing distended urinary bladder with herniation within both the inguinal rings. Note the enlarged prostrate causing bladder outlet obstruction (arrow).

Bladder Stones (Fig. 6.85)

Bladder stones have a propensity to form when urinary stasis and infection are present, uric acid stones predominate in the setting of bladder outlet obstruction. Magnesium ammonium phosphate and apatite stones are seen in patient with UTI particularly with proteus species. Patients may present with microscopic hematuria, pain, interruption of stream with bladder neck obstruction. Important complication to look out for is squamous cell Ca.

- Mural or luminal bladder calcification.
- Common—bladder stone, TCC, cystitis.
- Uncommon—foreign body, amyloid encrustation.

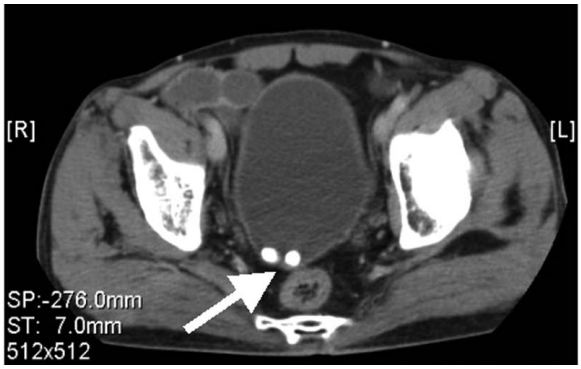

FIGURE 6.85: Axial CECT reveals two hyperdense well marginated vesicle calculus (arrow)

Extrinsic Bladder Compression

Pelvic Hematoma or Urinoma

Pelvic hematomas usually occur as a result of trauma to the internal iliac artery or perivesicle venous plexuses causing compression or displacement of the urinary bladder. Other common causes include pelvic mass lesions, bladder diverticulum, lymphadenopathy pelvic lipomatosis and iliopsoas hypertrophy.

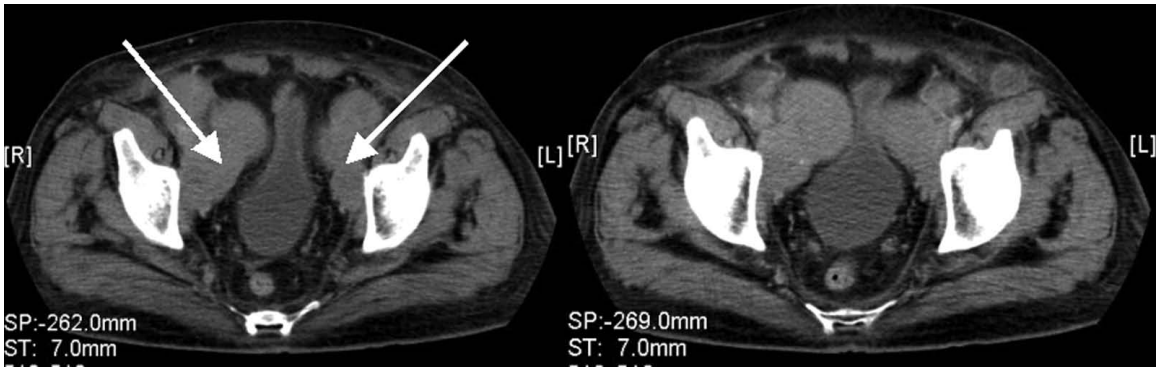

FIGURES 6.86A and B: Axial CT in a patient with testicular tumor reveals multiple iliac lymph nodes compressing the urinary bladder causing a pear shaped bladder (arrow).

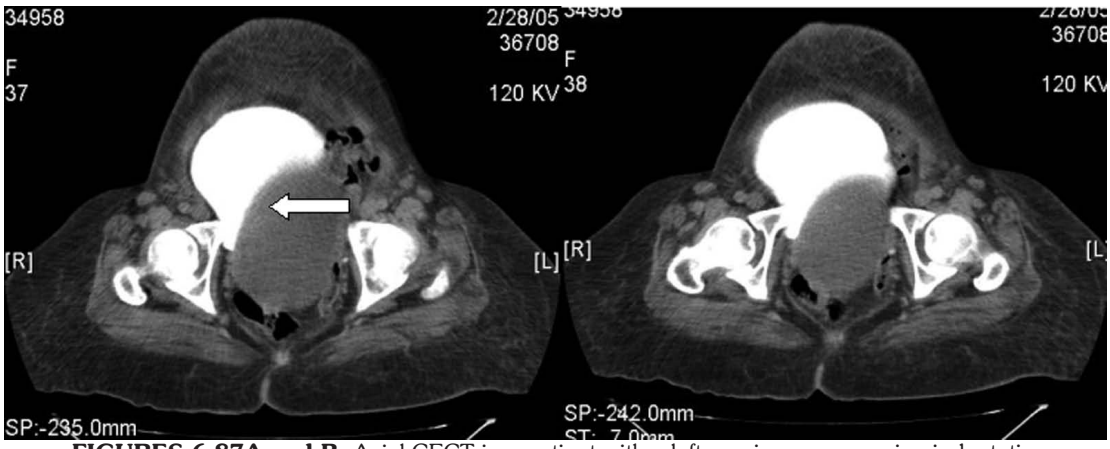

FIGURES 6.87A and B: Axial CECT in a patient with a left ovarian mass causing indentation with displacement of the urinary bladder (arrow).

Neoplasms of Bladder

Bladder neoplasms account for 4% of all malignancies with a peak incidence in the 6th decade with a male preponderance. Tumors can be classified into two categories: (1) epithelial and (2) non-epithelial malignancies.

Approximately 95% of tumors are epithelial, these lesions can be papillary, sessile or invasive in growth pattern. Rhabdomyosarcoma of the bladder is more common in children aged 2-6 years. Malignant tumors of the neighboring organs can involve the bladder secondarly. Local malignancies involving the bladder include prostate, cervix, rectum. Common primary tumors metastasizing to the bladder include stomach and breast.

- **Malignant**—TCC, SCC, adenocarcinoma.
- **Benign**—Leiomyoma, fibroepithelial polyp, adenoma.

Table 6.4: TNM classification for the staging of cancer of the urinary bladder

Stage	*Characteristics of TNM classification system*
Primary tumor (T)	
Tis	Carcinoma in situ: "flat tumor"
Ta	Noninvasive papillary carcinoma
T 1	Tumor invades subepithelial connective tissue
T 2	Tumor invades muscle
T 2 a	Tumor invades superficial muscle (inner half)
T 2 b	Tumor invades deep muscle (outer half)
T 3	Tumor invades perivesical tissue
T 3 a	Tumor invades perivesical tissue microscopically
T 3 b	Tumor invades perivesical tissue macroscopically (extravesical mass)
T 4	Tumor invades any of the following adjacent organs: prostate, uterus, vagina, pelvic wall, and abdominal wall
T 4 a	Tumor invades prostate, uterus, or vagina
T 4 b	Tumor invades pelvic wall or abdominal wall
Lymph nodes (N)	
N 0	No regional lymph node metastasis
N 1	Metastasis in a single lymph node 2 cm in greatest dimension
N 2	Metastasis in a single lymph node > 2 cm but 5 cm in greatest dimension or metastasis in multiple lymph nodes, none > 5 cm in greatest dimension
N 3	Metastasis in a lymph node > 5 cm in greatest dimension
Distant metastasis (M)	
M 0	No distant metastasis
M 1	Distant metastasis

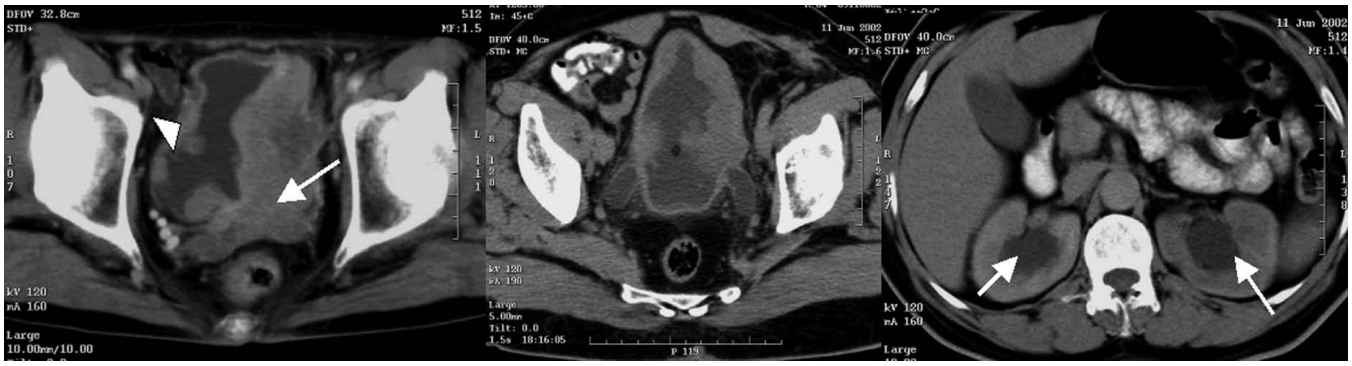

FIGURES 6.88A to C: Axial CECT reveals large mass involving the left lateral wall and base of bladder (arrow) infiltrating the seminal vesicle, note multiple satellite lesion involving the right lateral wall (arrowhead) with infiltration of both UV junctions causing bilateral obstructive uropathy (arrows in Fig. C).

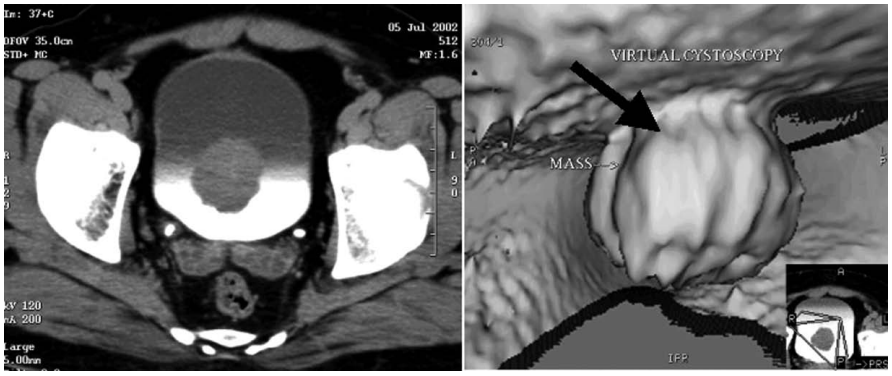

FIGURES 6.89A and B: Axial CECT reveals a hypodense mass arising from the anterior bladder wall, virtual cystoscopy shows the mass (arrows) arising from the vesicle wall.

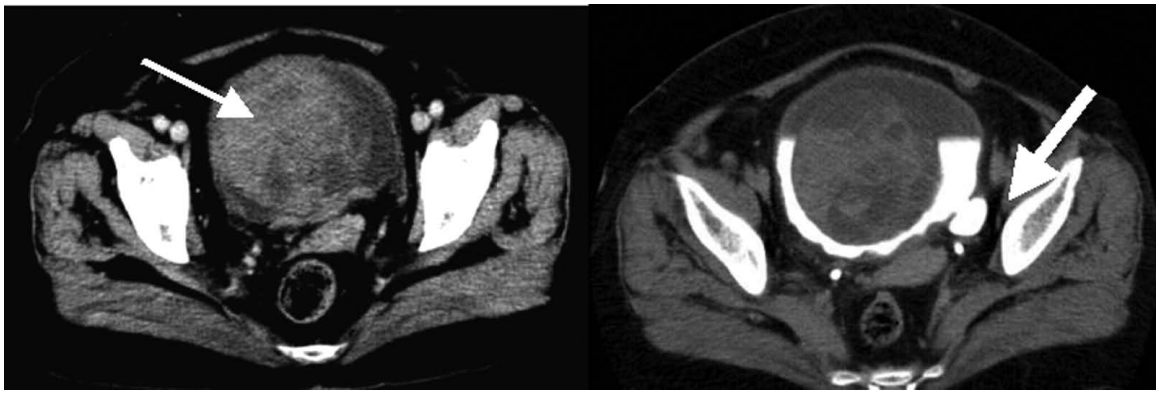

FIGURES 6.90A and B: Axial CECT reveals a large heterogenous moderately enhancing mass arising from the anterosuperior bladder wall (arrow), note the small paraureteric diverticulum (thick arrow in Fig. B).

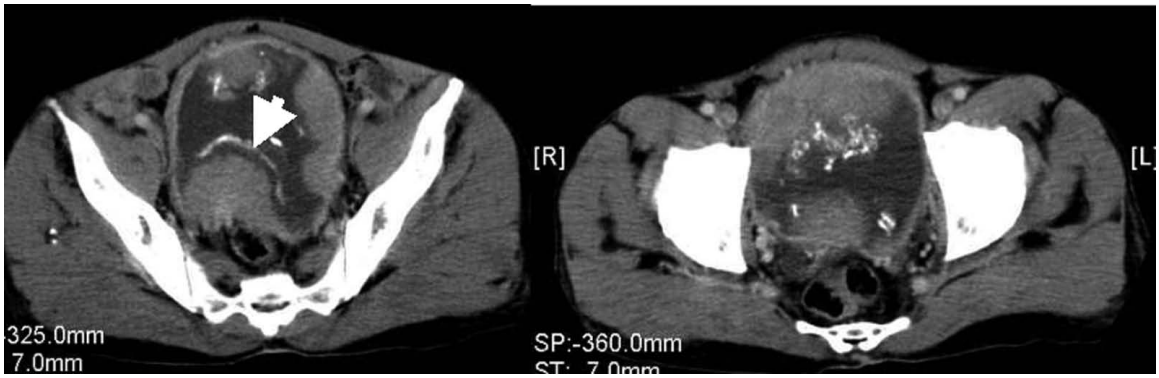

FIGURES 6.91A and B: Axial CECT reveals multiple soft tissue masses arising from the bladder dome, base and lateral walls, note the surface rim calcifications (arrow).

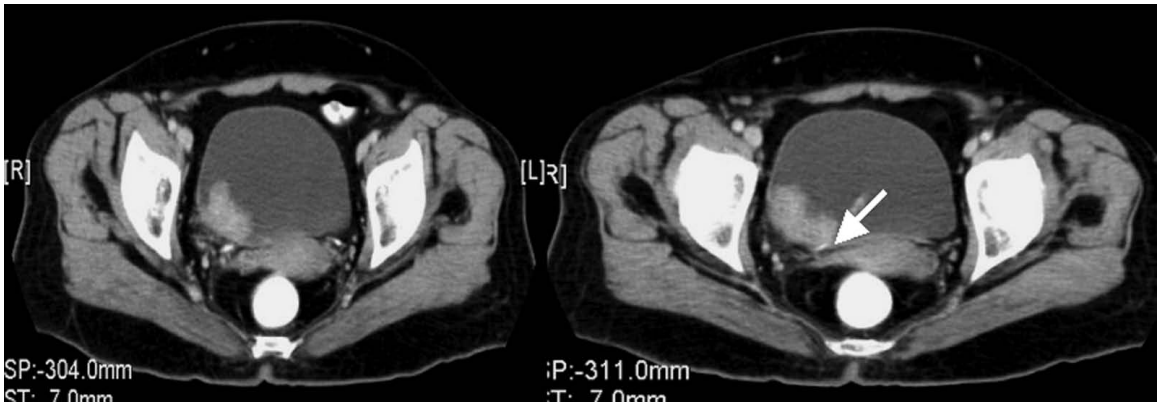

FIGURES 6.92A and B: Axial CECT reveals a lobulated enhancing mass in the right lateral wall adjoining the right UV junction, note the ureteric jet (arrow).

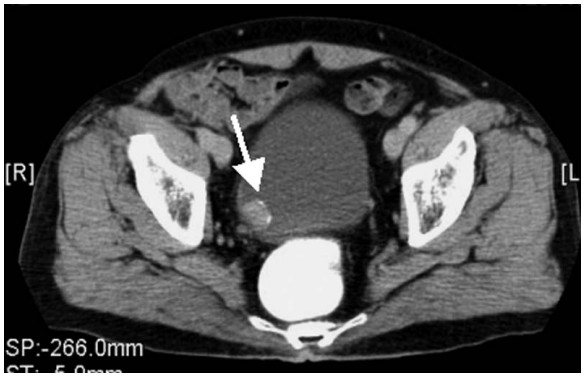

FIGURE 6.93: Axial CECT reveals a well marginated lesion in the right lateral vesicle wall indenting the right UV junction, note the fine surface calcification.

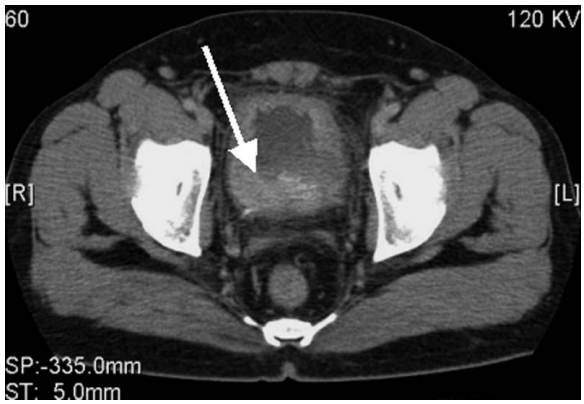

FIGURE 6.94: Axial CECT reveals diffusely thickened bladder mucosa showing areas of ulceration (arrow).

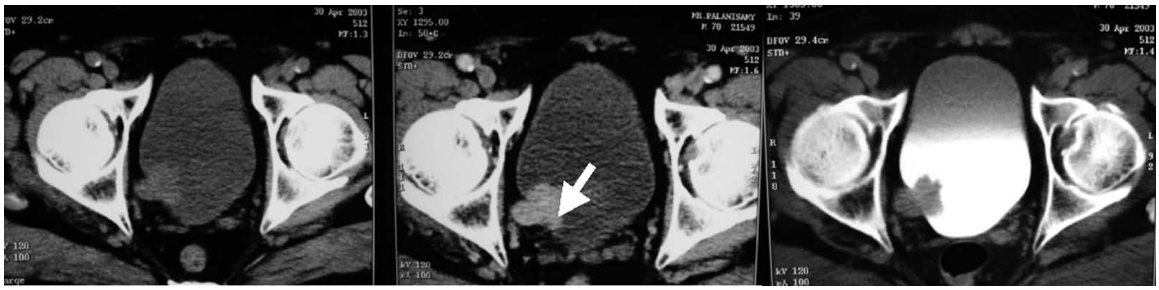

FIGURES 6.95A to C: Axial plain and CECT reveals a lobulated mass involving the right distal ureter protruding into the vesicle lumen through the right UV junction.

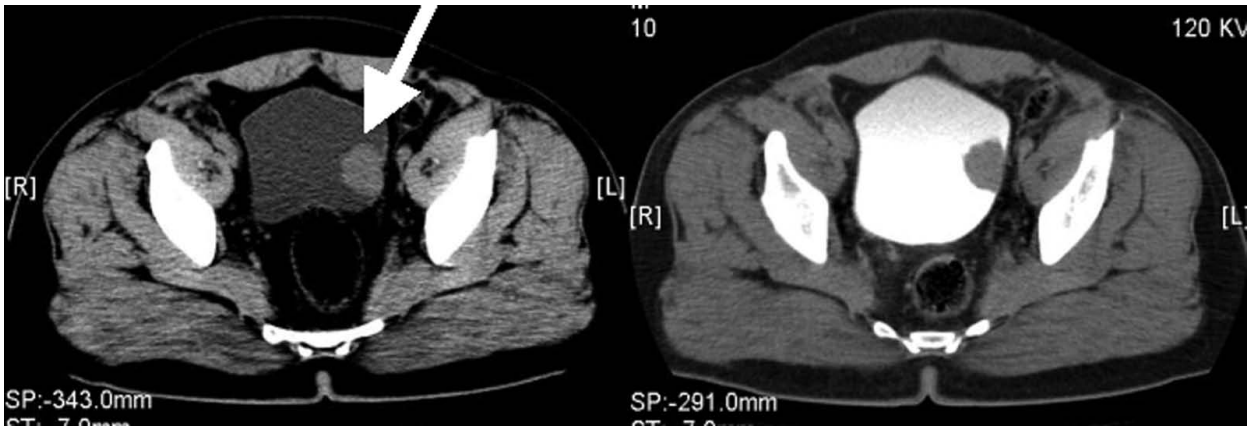

FIGURES 6.96A and B: Axial plain and CECT reveals a lobulated mass in the right lateral vesicle wall, the perivesicle fat planes are preserved.

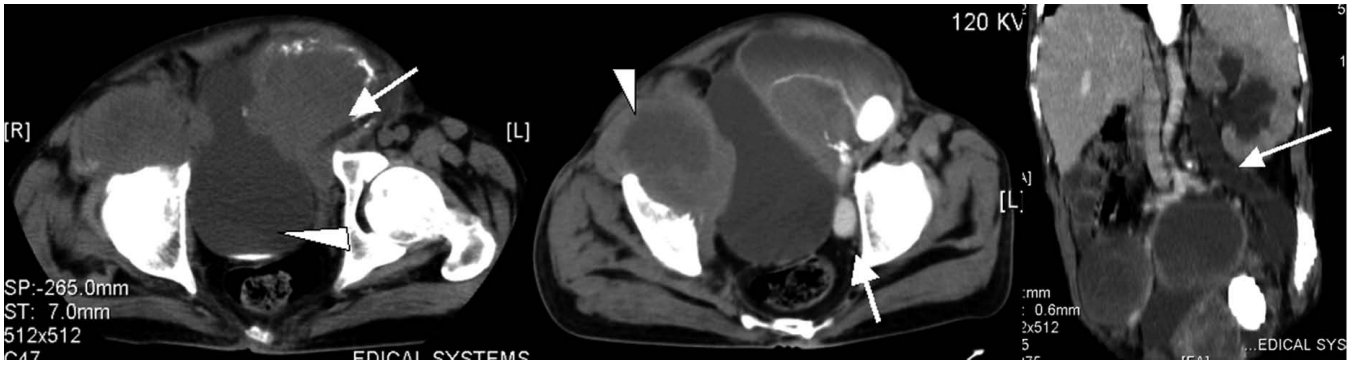

FIGURES 6.97A to C: Axial CECT with coronal reformation reveals a large mass arising from the bladder base (arrow in Fig. A, note the left ureter entering the bladder (arrow in Fig. B). The unopacified cystic structure (arrow head in Fig. A) represents a diverticulum. Reformatted image shows hydroureteronephrosis (arrow in Fig. C). Note the presence of a right iliopsoas metastatic deposit (arrowhead in B). Also note the agenesis of the right kidney in the reformatted images.

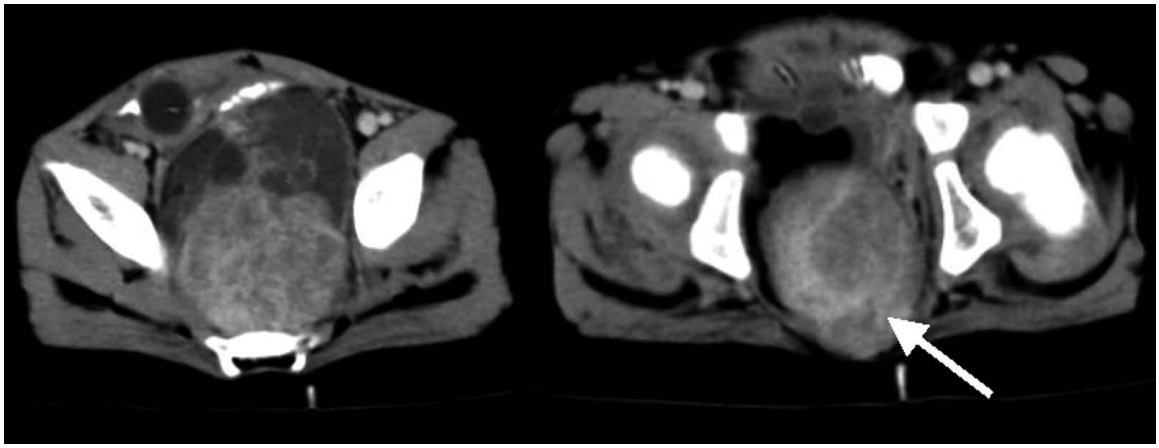

FIGURES 6.98A and B: Axial CECT reveals a large heterogeneous mass showing moderate enhancement arising from the bladder base displacing the bladder superiorly, case of rhabdomyosarcoma.

Urachal Disease

The urachus is a musculofibrous band that is an extension of the urogenital sinus. This band extends from the bladder dome to the umbilicus; in the fetus, it is contiguous with the allantois. The urachus lies in the space of Retzius, between the transversalis fascia anteriorly and the peritoneum posteriorly. In 70% of adults, a small lumen lined by transitional epithelium remains in the urachus. The persistence of a urachal lumen can lead to a urachal fistula, urachal cyst, or urachal sinus.

In vesicourachal diverticulum, the urachus communicates only with the bladder dome. This condition results when the vesical end of the urachus fails to close. Vesicourachal diverticulum is asymptomatic in most cases and is usually discovered incidentally at axial CT performed for unrelated reasons, appearing as a midline cystic lesion just above the anterosuperior aspect of the bladder.

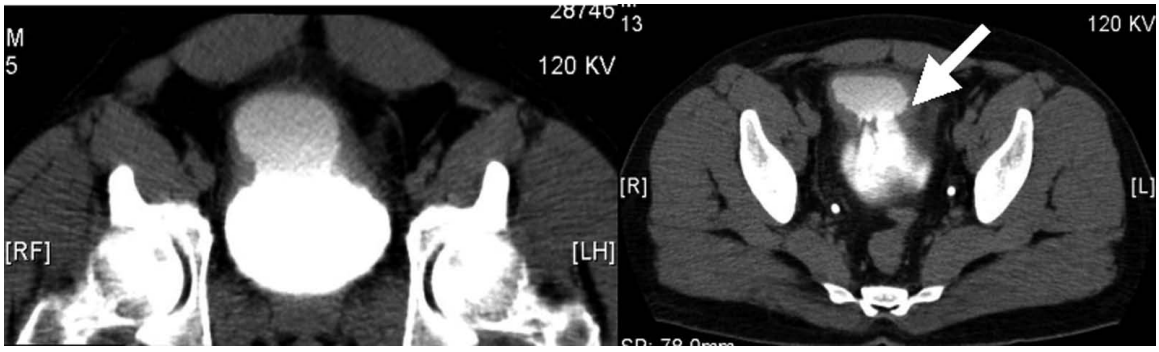

FIGURES 6.99A and B: Axial CECT reveals a diverticular outpouching from the dome with irregularity of the mucosa (arrow).

Benign urachal neoplasms include adenomas, fibromas, fibroadenomas, fibromyomas, and hamartomas are extremely rare; however, they are important in that they mimic urachal malignancy. Malignant urachal neoplasms are also rare, representing less than 0.5% of all bladder cancers. Although the normal urachus is most commonly lined by the transitional epithelium, urachal carcinoma predominantly manifests as adenocarcinoma (90% of cases), probably due to the metaplasia of the urachal mucosa into columnar epithelium followed by malignant transformation. Most (90%) urachal carcinomas are juxtavesical, specifically supravesical, anterior to the bladder, or in its midline.

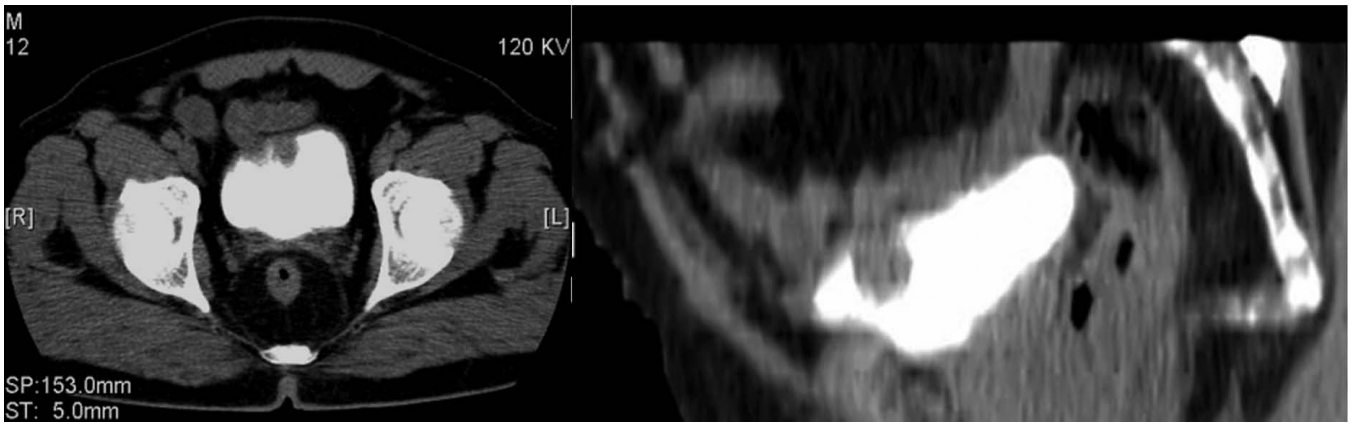

FIGURES 6.100A and B: Axial CECT with sagittal reformats reveals a well-defined lesion in the bladder dome (arrow).

These tumors are most commonly seen in patients 40-70 years of age, two-thirds of whom are men.

PELVICALYCEAL SYSTEM AND URETER

Normally approximately 8-15 calyces subtend each kidney. A simple calyx is a concave structure applied to the papillae of renal medulla. When seen enface the calyx appears circular, when viewed in profile the simple calyx is concave and has sharp forniceal angles. Single or multiple simple calyces are drained by infundibulum also known as major calyx which empties into the renal pelvis.

The renal pelvis is generally a triangular structure and it tapers smoothly to its junction with the ureter, the UPJ is a ill-defined area where the renal pelvis joins the ureter. The ureter also is narrowed when it is crossed by the iliac vessel at the pelvis. Proximal to this junction it shows a focal bulge were its called a spindle. It enters the bladder at the UV junction were it tunnels the bladder. The ureter normally extends along the ventral surface of the psoas muscle. It lies anterior to the transverse process of the lumbar spine less than 1 cm lateral, and not medial to the pedicle.

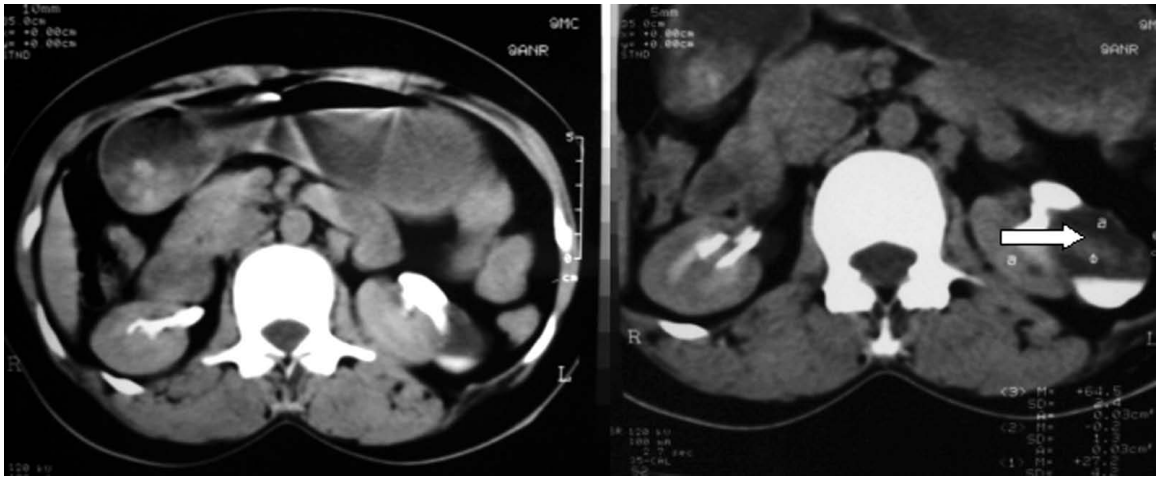

FIGURES 6.101A and B: Axial CECT in excretory phase showing a well marginated cyst showing a fluid contrast level in the left renal interpole communicating with calyx (arrow)—calyceal diverticulum.

Congenital Anomalies

Congenital variants of the pelvicalyceal system and ureter are common. Duplication anomalies are represented by a spectrum of findings. Mild anomalies include bifid renal pelvis, and incomplete ureteral duplication.

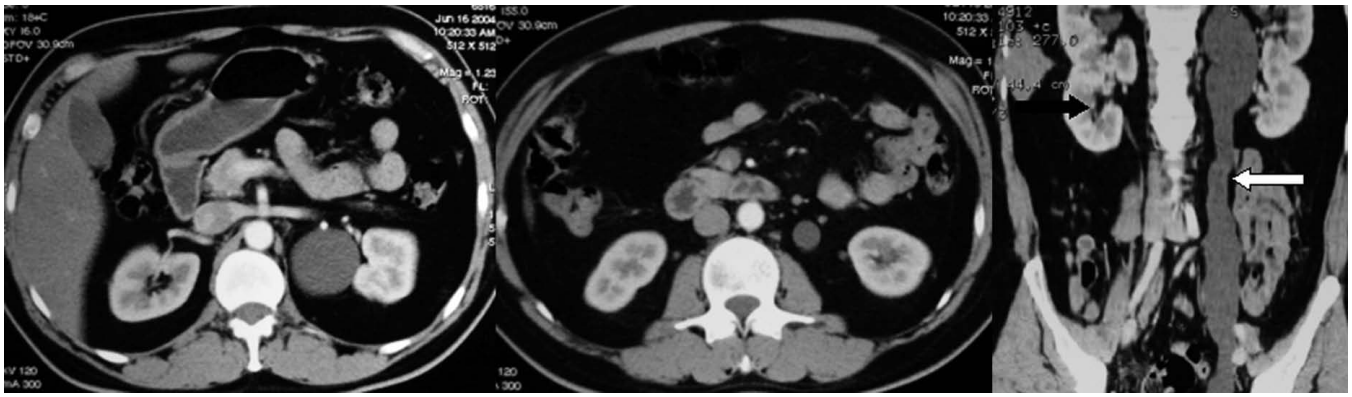

FIGURES 6.102A to C: Axial CECT with reformation shows a blind ending tubular fluid-filled structure along the left kidney and ureter suggestive of a complete duplication system (arrow in C), the apparent presence of double kidneys in Figure C (black arrow) is due to reconstruction artifact.

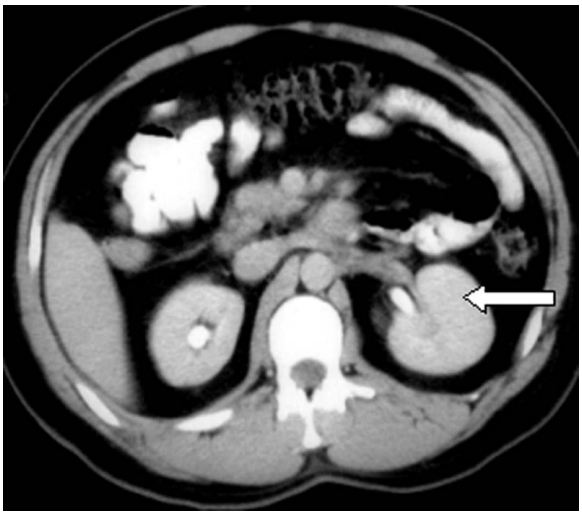

FIGURE 6.103: Axial CECT showing faceless kidney which is a feature of duplicating collecting system (arrow).

Complete urethral duplications are also seen occasionally in this context its important to remember the Weigert-Meyer rule, which states that the upper pole of kidney drains via the ureter which inserts inferior and medial to the normal expected ureteral insertion point. This ectopic insertion can have a ureterocele. The lower moiety of the completely duplicated system generally is normal.

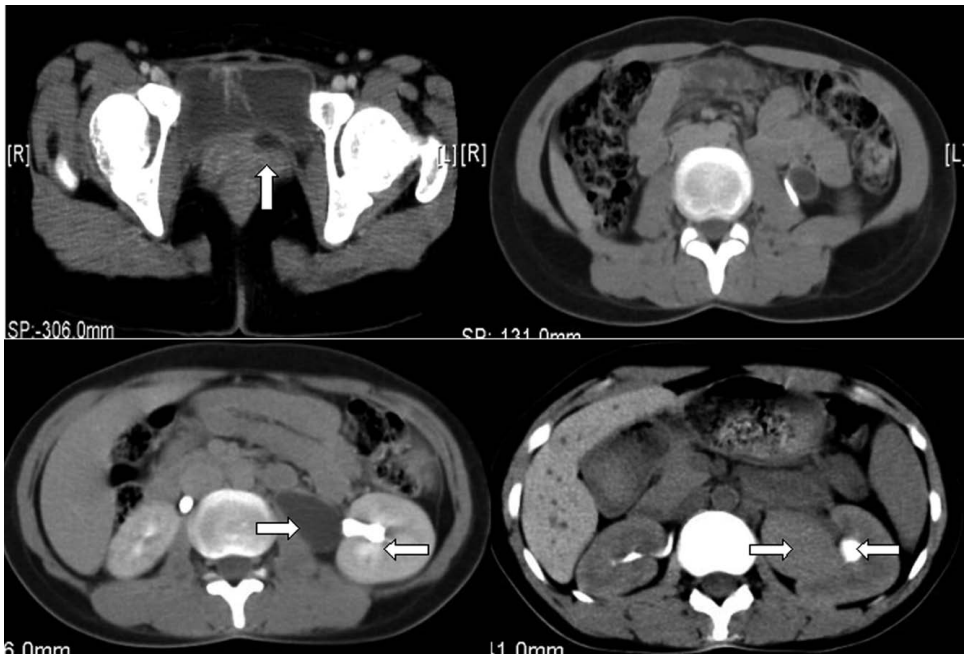

FIGURES 6.104A to D: Axial CECT in the excretory phase shows a double moiety (arrow in C,D) note the delayed functioning of the dilated upper moiety. Fig. A at the level of UV junction shows the ureterocele as a focal dilatation (arrow).

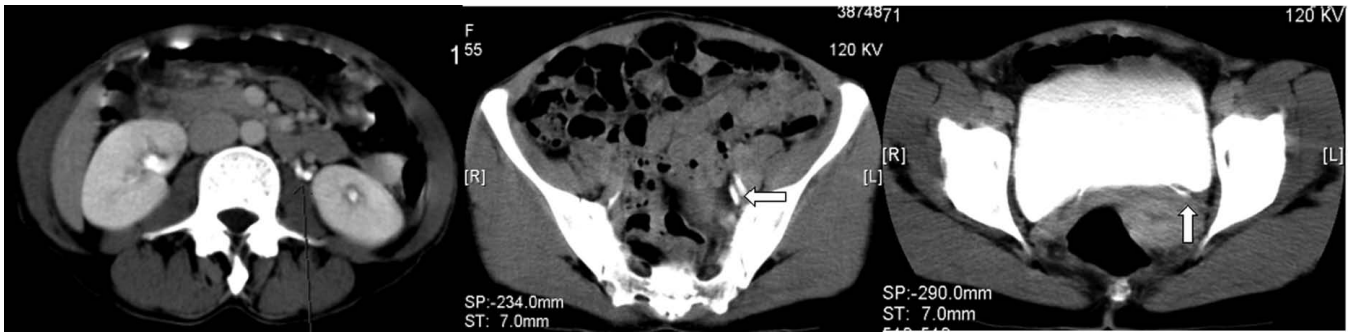

FIGURES 6.105A to C: Axial CECT shows double ureter (arrow in B), Figure C shows single UVJ (arrow) suggesting fusion of the ureters proximal to UVJ.

DEVIATIONS OF URETER

The ureter may deviate medially or laterally, deviation can occur as a whole or segmentally, abnormalities of ureteric course is usually secondary to extrinsic disease.

MEDIAL DEVIATION OF THE URETER

Upper Ureter

- Lower pole renal mass
- Psoas enlargement, retrocaval ureters, retroperitoneal fibrosis.

Lower Ureter

- Lymphadenopathy
- Pelvic lipomatosis
- Iliopsoas enlargement
- Pelvic mass
- Cystocele

LATERAL DEVIATION OF THE URETER

Upper Ureter

- Malrotated or horse-shoe kidney
- Lymphadenopathy
- Psoas hypertrophy
- Aortic aneurysm
- Retroperitoneal mass

Lower Ureter

- Central pelvic mass of pelvic fluid collection.

Abnormalities of Ureteric Caliber

Caliber abnormalities include dilatation and narrowing.

Dilatation in the Absence of Intrinsic Obstruction

Entire Ureter

- Bilateral—primary megaureter, bladder outlet obstruction, bladder neoplasms, inflammation, diabetes insipidus, prune belly syndrome.
- Unilateral—VUR, primary megaureter, bacterial infection, ectopic ureteric insertion.

Lower Ureter

- Primary megaureter, VUR.

Upper Ureter

Retrocaval ureter, enlarged uterus, postpartum ectasia.

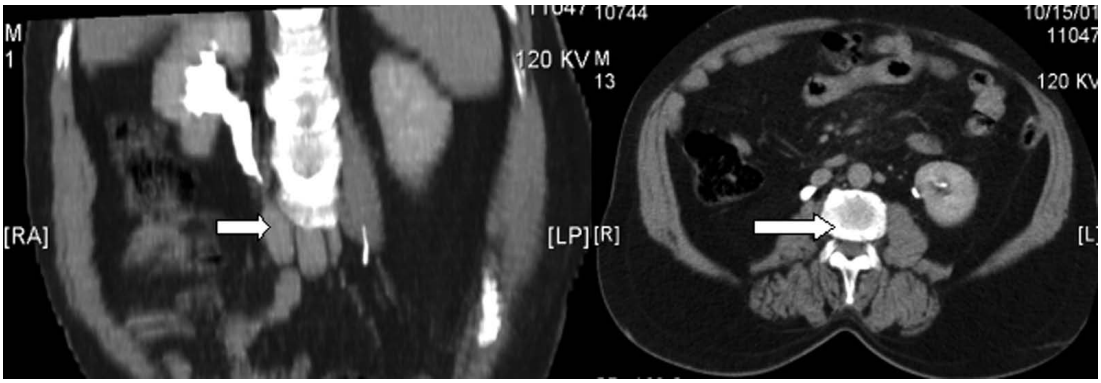

FIGURES 6.106A and B: Axial CECT with coronal reformation shows medially deviated right ureter going posterior to IVC suggestive of a retrocaval ureter (arrow in B), Figure A shows abrupt termination of the ureter suggestive of a stricture (arrow).

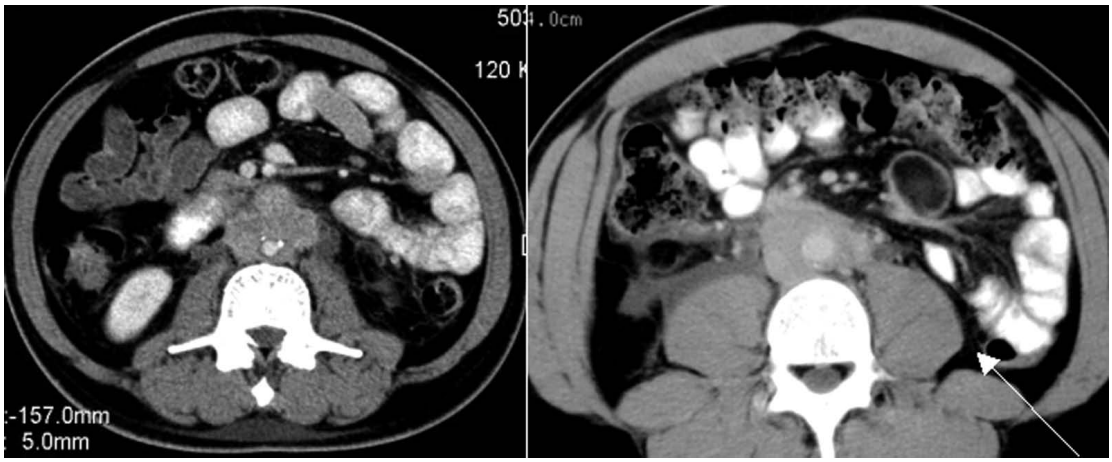

FIGURES 6.107A and B: Axial CECT in two different patients with periaortic soft tissue, Figure A was due to primary retroperitoneal fibrosis, Figure B was a case of para-aortic lymphadenopathy causing medial deviation of the ureter (arrows).

Nonobstructive Ureteral Dilatation

- Increased intraluminal volume like VUR, primary megaureter, polydipsia, diabetes.
- Flaccid ureteric musculature—prune belly syndrome, bacterial infection, residual dilatation from remote obstruction.

Approach to Suspected Ureteric Obstruction

Unenhanced helical computed tomography (CT) has proved to be an accurate, safe, and rapid examination used to diagnose and treat patients presenting with acute flank pain. Secondary signs of urinary tract obstruction and other signs such as the soft-tissue rim sign have been described that aid in interpretation of the CT examination.

CT is more sensitive than other imaging modalities for detecting urinary calculi. It can even detect small noncalcified stones that are radiolucent on abdominal radiographs, as their attenuation values are always greater than 100 HU.

Calcium-containing stones (90% of all stones) and cystine stones have attenuation values of 450 to 1500 HU, while xanthine stones are in the range of 100 to 600 HU.

Papillary calcifications and arterial calcifications are usually distinguished by their location from stones in the collecting system.

Noncontrast spiral CT is more effective than intravenous urography in identifying ureteral stones and as effective as intravenous urography in determining whether there is renal obstruction.

Secondary Signs of Urinary Tract Obstruction

Interpretation of the CT scans begins with inspection for secondary signs of urinary tract obstruction. The secondary signs of obstruction first described include asymmetric stranding of the perinephric fat, dilatation of the intrarenal collecting system, hydroureter, and unilateral renal enlargement. Subsequently, unilateral absence of the white pyramid was described as an additional secondary sign.

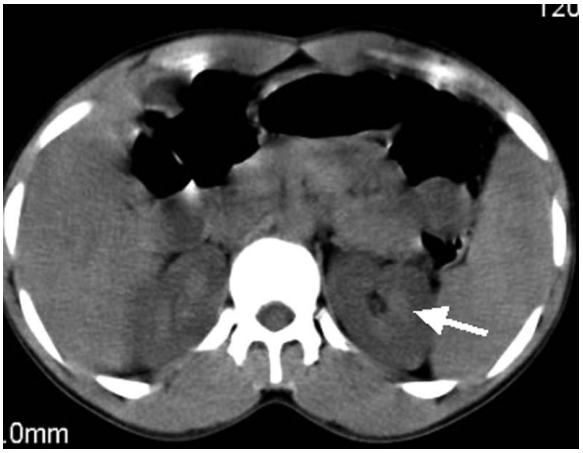

FIGURE 6.108: Axial plain CT reveals the white pyramid in a normal patient (arrow)

Stranding of the perinephric fat is a common finding. The stranding likely represents fluid that collects within the bridging septa of the perinephric fat as a result of increased lymphatic pressure. Focal, nonlinear perinephric fluid collections associated with obstruction likely represent extravasated urine as a result of forniceal rupture.

Although unilateral or asymmetric perinephric stranding is often obvious the findings may be difficult to discern. When the difference in stranding is subtle, it may be apparent only at the upper or lower poles of the kidneys. Asymmetric stranding of the perinephric fat may be seen as a loss of definition of the fat-kidney interface or a very fine linear stranding compared with that of a well-defined interface around the contralateral kidney.

Evaluation for collecting system dilatation should focus on the renal sinus in the upper and lower poles. Because the presence of an extrarenal pelvis may lead to an erroneous diagnosis of urinary tract obstruction, apparent dilatation of the central portions of the renal collecting system must be viewed with caution. Collecting system dilatation is best identified in the upper and lower poles. Dilated calices and infundibula appear as rounded fluid-filled structures that partially obliterate the renal sinus fat compared with the contralateral kidney.

Recently, unilateral absence of the white pyramid was described as an additional secondary sign of urinary tract obstruction. Ureteral obstruction may result in tubular hydronephrosis, decreasing the attenuation of the medullary pyramid on the obstructed side so that the pyramids have high attenuation on only the unobstructed side. Although the sensitivity and specificity of this sign are yet to be proved, the finding of high-attenuation medullary pyramids in only one kidney suggests the presence of obstruction in the contralateral kidney.

After the evaluation for signs of obstruction, the ureters are inspected for calcifications. This evaluation should begin by following the course of each ureter from the renal pelvis to the bladder. One of the most common difficulties is distinguishing distal ureteral stones from phleboliths. It is helpful in identifying the ureter on each image from the renal pelvis to the ureteropelvic junction. The soft-tissue rim sign can be used when the ureter cannot be confidently identified by any of the above methods. Although not all ureteral stones have this sign, approximately 77% of them are surrounded by a rim of soft tissue. Less than 10% of phleboliths have a soft-tissue rim. Therefore, the absence of the rim sign does not have a high negative predictive value, but its presence is highly predictive of a ureteral stone.

Signs of acute obstruction due to urolithiasis:

- Hyperattenuating focus (>120 HU) in the collecting system
- Dilation of the intrarenal collecting system
- Hydroureter (ureteral obstruction)
- Stranding of the perinephric fat (unilateral)
- Perinephric fluid (markely more pronounced on one side)
- Unilateral increase in renal cortical thickness
- Unilaterally reduced cortical enhancement.

Ureter stone:

- Tissue rim sign
- Periureteral stranding

SPECTRUM OF URETERIC CALCULI

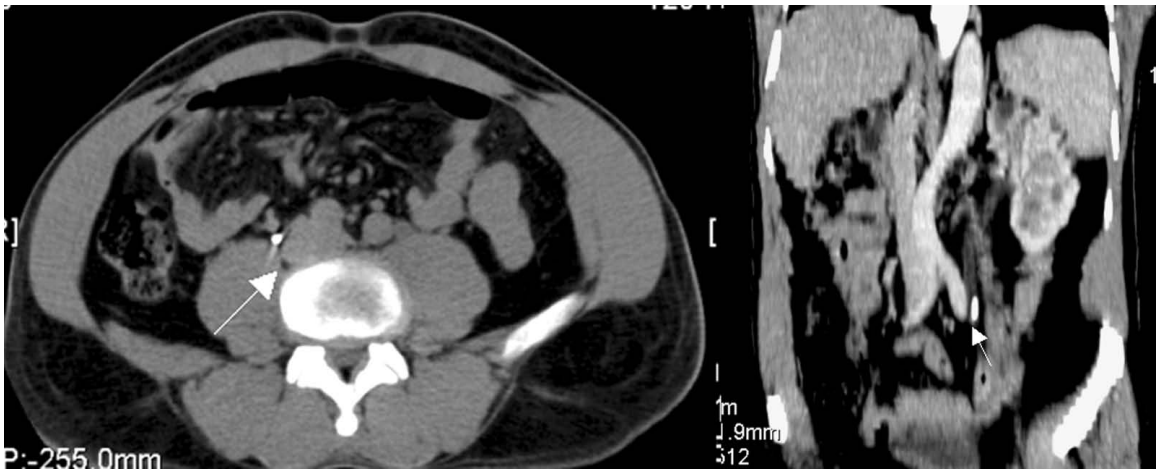

FIGURES 6.109A and B: Axial plain CT showing a right mid ureteric calculus as a high attenuation focus (arrow). Coronal MPR image in another patient showing left mid ureteric calculus (arrow) with proximal dilated ureter.

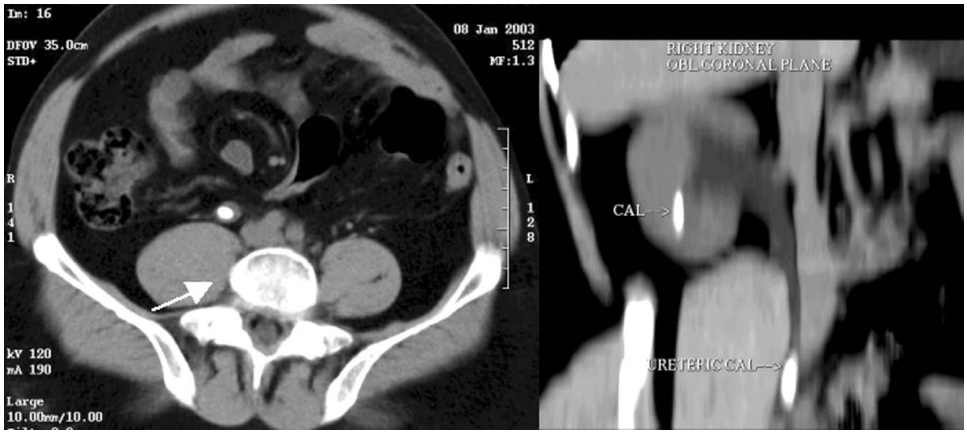

FIGURES 6.110A and B: (A) Axial plain CT showing a mid ureteric calculus causing a cresent of fluid—case of partial ureteric obstruction (arrow). (B) Oblique coronal MPR showing a lower pole parenchymal calculus.

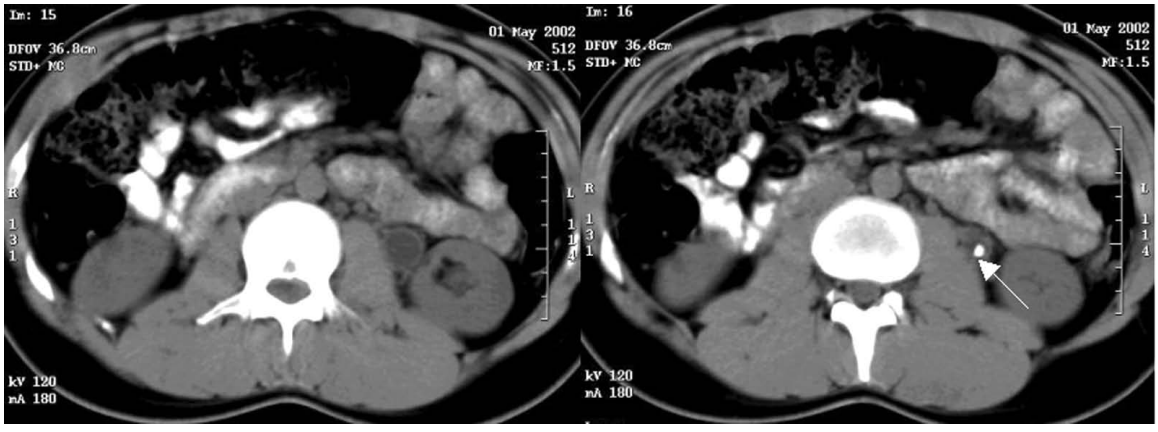

FIGURES 16.111A and B: Axial plain CT showing proximal ureteric calculus (arrow).

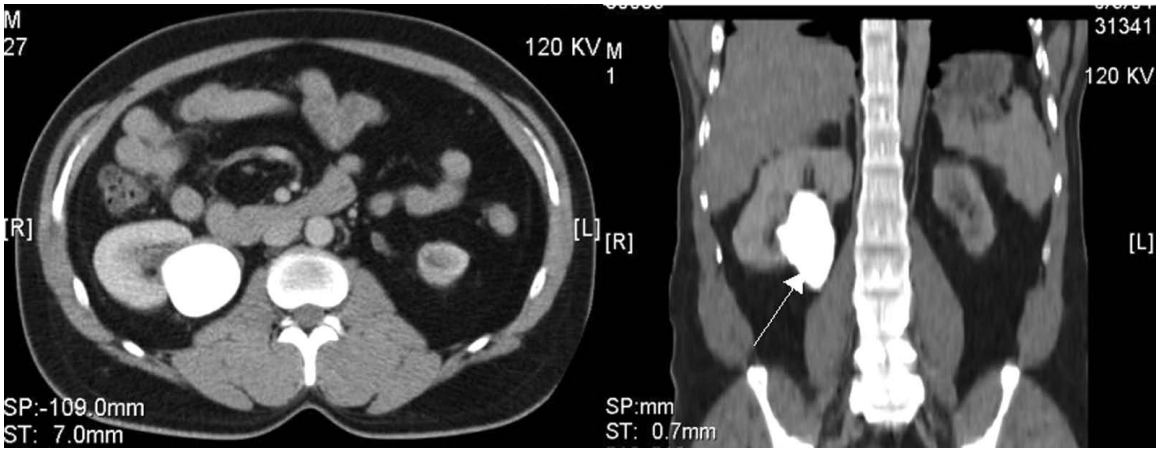

FIGURES 16.112A and B: Axial and coronal MIP images show a large pelvic calculus, note in the reformatted image the calculus takes the shape of the renal pelvis (arrow).

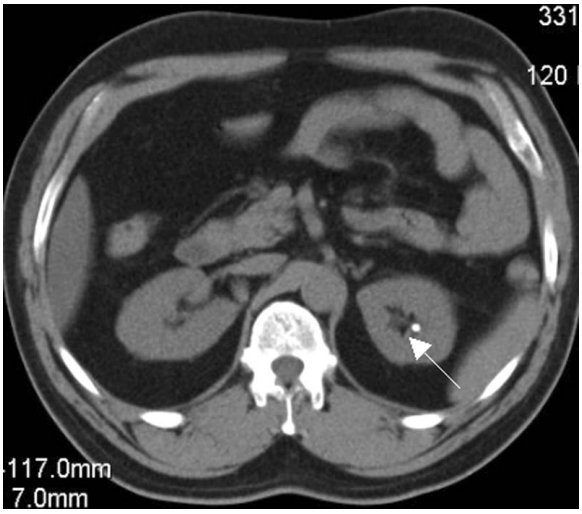

FIGURE 16.113: Axial NECT showing left renal interpolar non-obstructive calculi.

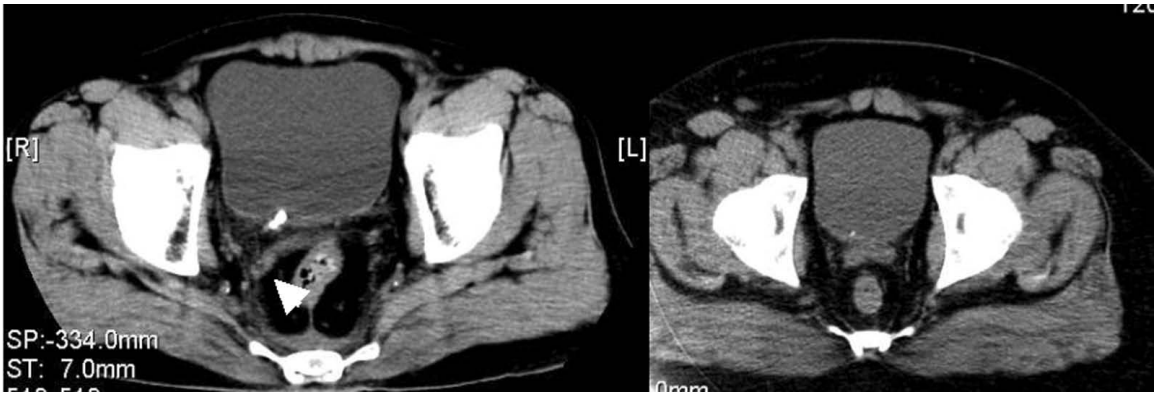

FIGURES 6.114A and B: (A) Axial plain study showing extruding right UVJ calculus.

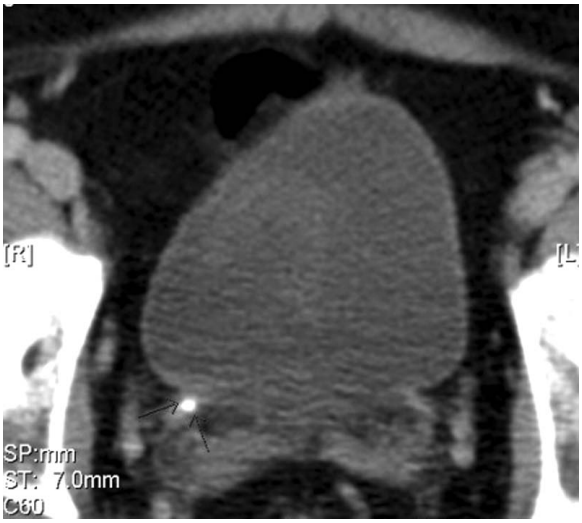

FIGURE 16.115: Axial NECT shows a juxtavesicle right sided calculi.

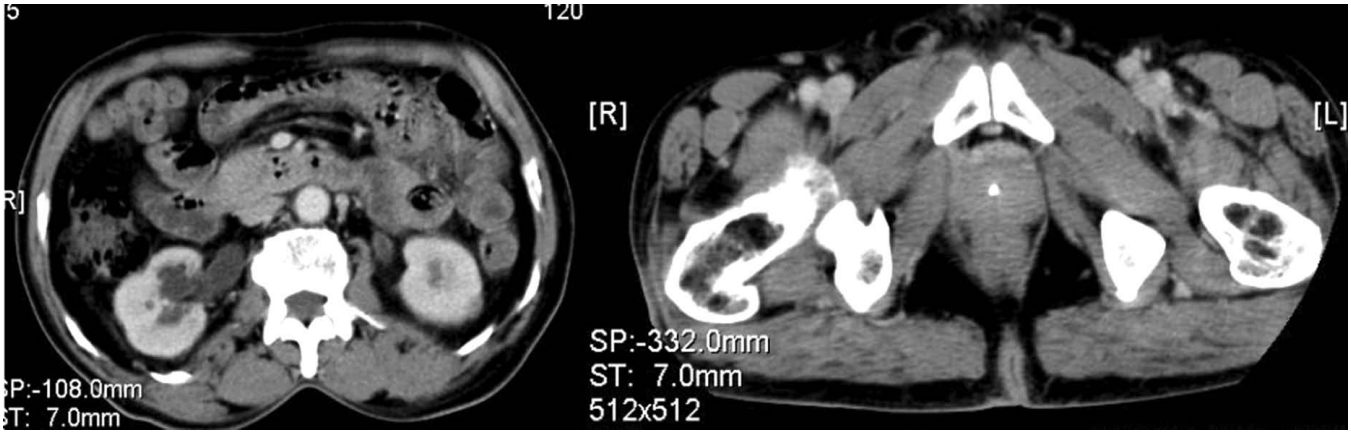

FIGURES 6.116A and B: Axial NECT showing bilateral hydroureteronephrosis more evident on the right side due to a impacted prostatic ureteric calculus.

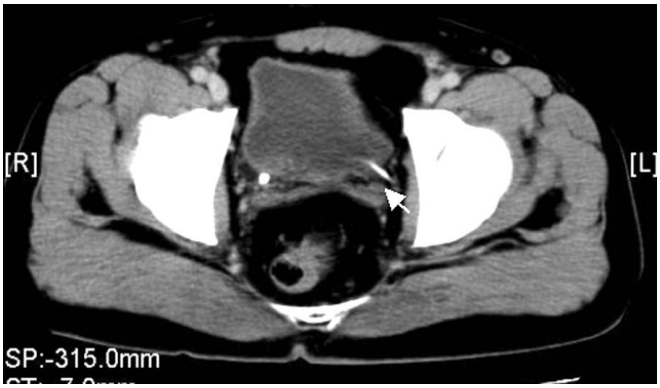

FIGURE 6.117: Axial CECT showing the right UVJ calculus and the normal ureteric jet on the left side.

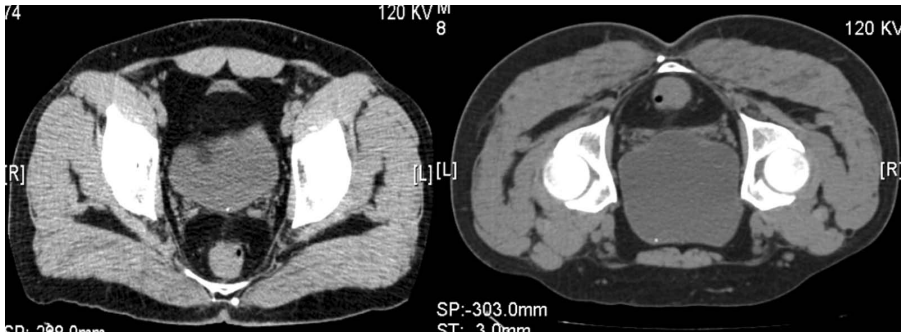

FIGURES 6.118A and B: Axial supine and prone images show an extruded vesicle calculus showing shifting in position. This is an easy way of delineating a very small vesicle calculus.

URETERAL NARROWING

The causes of ureteric narrowing are numerous. The first step in assessment of obstruction is to differentiate an intrinsic from extrinsic cause. Intrinsic lesions such as TCC causes abrupt caliber change with irregularity of the mucosa. Benign strictures are caused by recurrent UTI, stone disease and iatrogenic causes including radiation therapy.

Radiation-induced strictures develop when a segment of ureter is involved in the field of irradiation of pelvis neoplasms, imaging findings are that of abrupt narrowing, these strictures develop classically after a time lag of about 12 months. Infective strictures are usually secondary to tuberculosis and renal parenchyma. Multifocal areas of ureteral narrowing suggests TCC, TB, metastatic disease or lymphoma. Segmental strictures can occur secondary to Crohn's disease or diverticulitis.

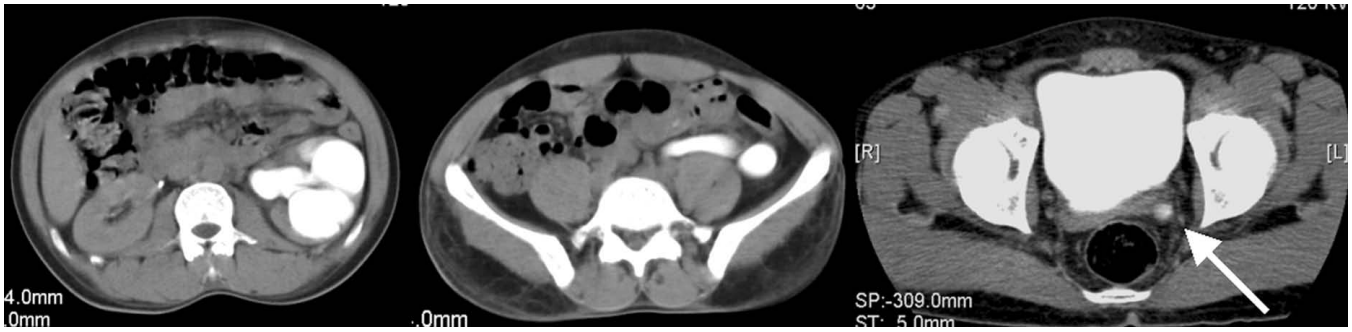

FIGURES 6.119A to C: Axial CECT reveals gross left hydroureteronephrosis with abrupt termination of juxta vesicle portion of the distal ureter (arrow) due to stricture.

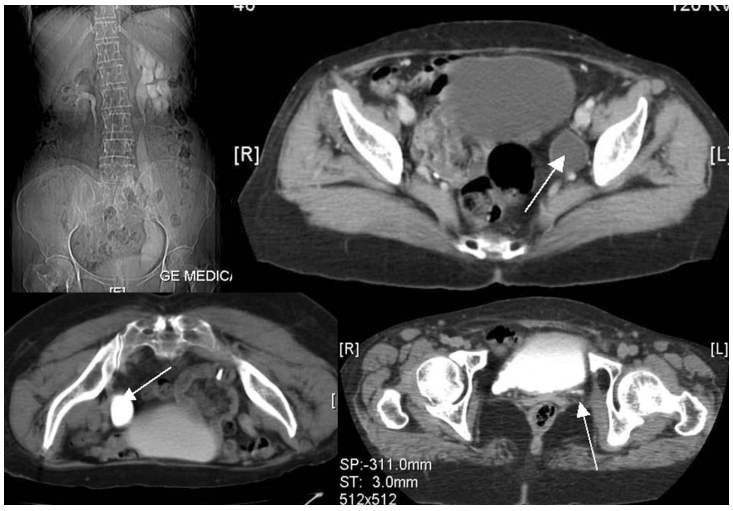

FIGURES 6.120A to D: (A) Digital scanogram showing moderate hydroureteronephrosis on the left side, (B, C, D) Supine plain and prone postcontrast views showing the tapering ureter at UVJ level suggestive of a mega ureter secondary to a ureteric stricture (arrows).

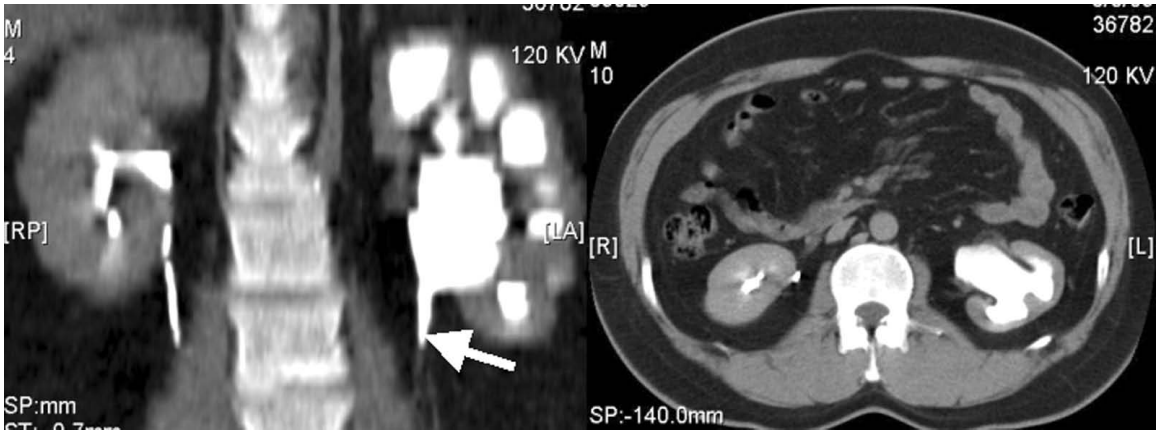

FIGURES 6.121A and B: Coronal MIP and axial delayed CECT shows an upper ureteric stricture causing moderate proximal pelvicalyceal dilatation (arrow).

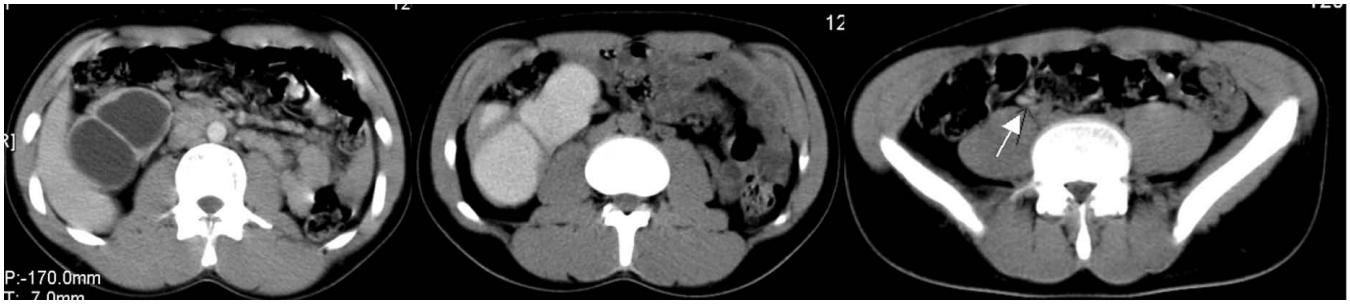

FIGURES 6.122A to C: Axial CECT with delayed phase imaging studied shows an right distal ureteric stricture causing severe hydroureteronephrosis (arrows).

Ureteric Tumors

Ureteral tumors are of same cell types as pelvic or bladder tumors, common presenting symptoms would be hematuria, pain, and flank mass.

CT typically shows hydroureteronephrosis with delayed renal excretion of contrast they usually appear as soft tissue filling defect within the ureter or as thickening of the ureteral wall.

Periureteral metastatic masses cannot be differentiated from primary ureteric neoplasms in the absence of other features of the primary malignancy.

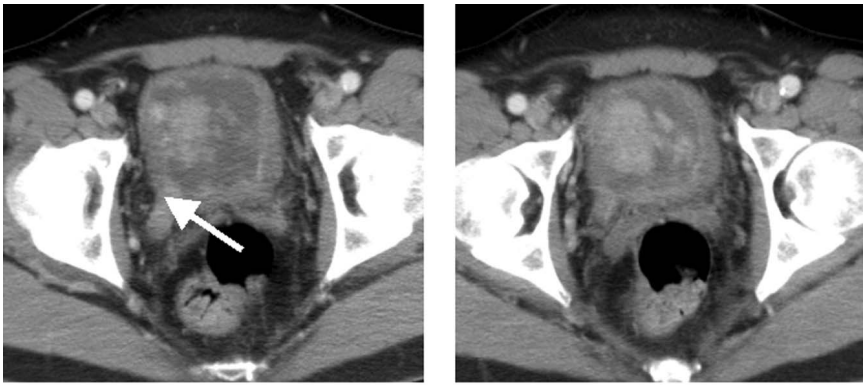

FIGURES 6.123A and B: Axial CECT showing the right distal juxta vesicle and UVJ mass with a large intravesicle mass involving the right lateral wall – case of contiguous spread (arrow).

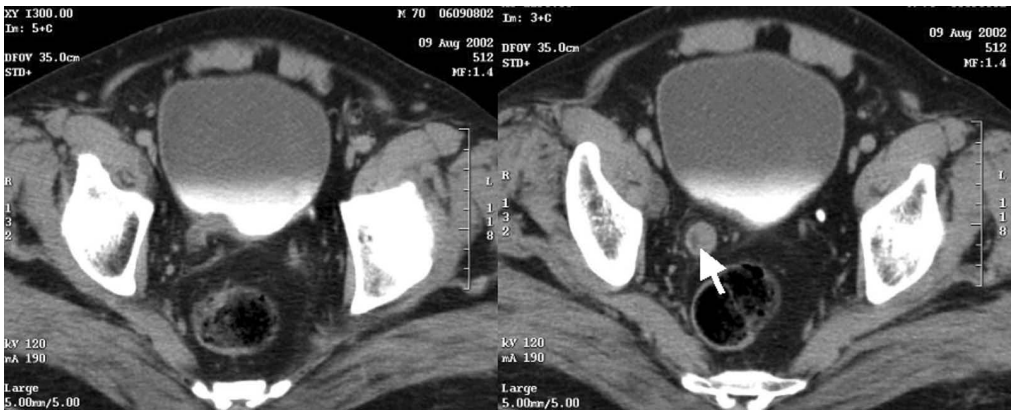

FIGURES 6.124A and B: Axial CECT showing right distal and UVJ polypoidal mass (arrow).

Ureteral Narrowing

Malignancy—Urothelial, lymphoma, metastasis.
Infectious—Tuberculosis, schistosomiasis.
Gynecological—Endometriosis.
Trauma—Pelvic lipomatosis, retroperitoneal fibrosis.

- Solitary transitional cell lesions frequently demonstrate slight dilatation distal to lesion (Bergman's sign), which helps to differentiate them from calculi or blood clots.

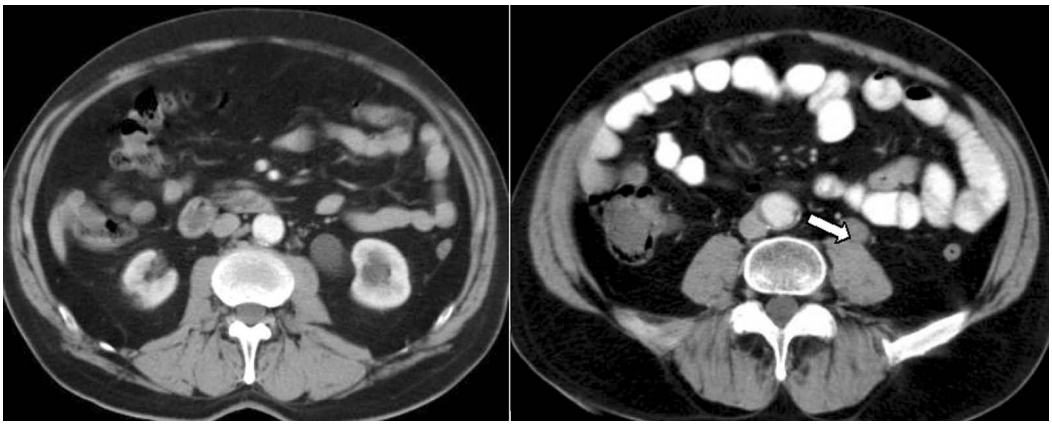

FIGURES 6.125A and B: Axial CECT showing left mid ureteric luminal soft tissue (arrow).

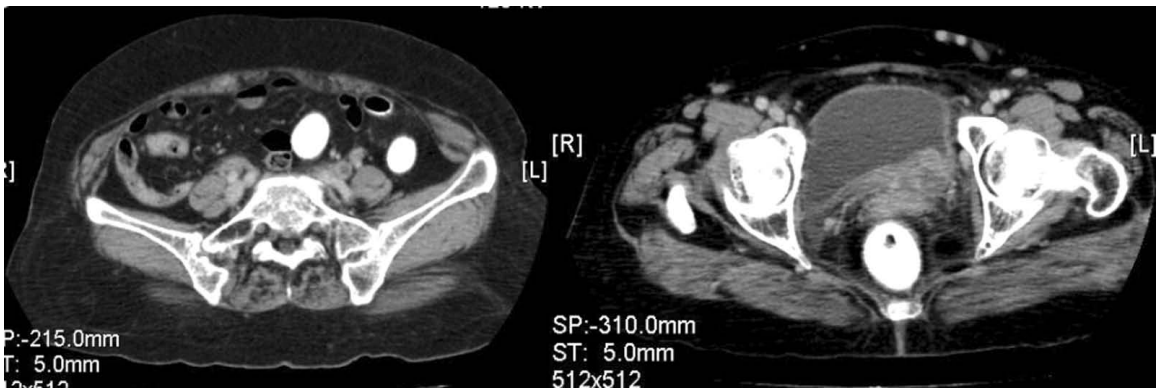

FIGURES 6.126A and B: Axial CECT showing left ureteric dilatation due to a left perivesicle mass infiltrating the left UVJ and adjacent bladder base – case of Ca cervix post surgery recurrence.

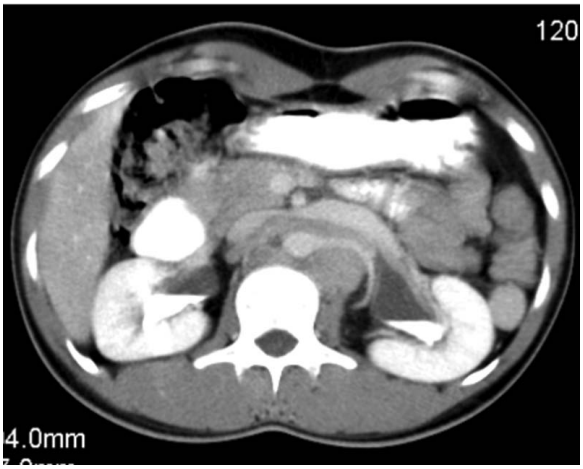

FIGURE 6.127: Axial CECT showing conglomerate para aortic nodes causing proximal left pelvi ureteric junction obstruction.

Urine Leaks

Urine leaks from the kidney, ureter, bladder, and urethra most commonly result from trauma. Urinomas may be occult initially and may lead to complications such as abscess formation and electrolyte imbalances if not promptly diagnosed and appropriately managed. Radiologists play a key role in diagnosing urine leaks and determining their cause and extent. Contrast material-enhanced computed tomography (CT) with delayed imaging, CT cystography, and retrograde urethrography are the diagnostic imaging studies of choice.

Urine leaks and urinomas result from disruption of the urinary collecting system at any level from the calix to the urethra. Persistent urine leakage is common following injury. Urinomas may initially be clinically occult and may manifest with delayed complications such as hydronephrosis, paralytic ileus, electrolyte imbalances, and abscess formation. Urine leaks and urinomas have a variety of appearances and may be misdiagnosed as ordinary ascites, abdominal or pelvic abscesses or hematomas, cystic masses, or pancreatic pseudocysts.

Causes

Renal urine leaks result from disruption of the calices, infundibula, or renal pelvis. Most commonly, renal urine leaks result from blunt or penetrating renal trauma. They may accompany any form of renal trauma, ranging from a simple renal laceration to a renal vascular pedicle injury. Renal urine leaks may also be the result of transmitted back pressure caused by obstruction of the **genitourinary** system due to a ureteral stone or pelvic mass, pregnancy, retroperitoneal fibrosis, posterior urethral valves, or bladder outlet obstruction. Iatrogenic injury during surgical or percutaneous procedures is an uncommon cause of renal injury.

Diagnosis and Imaging Features

Computed tomography (CT) is the study of choice in the diagnosis of renal urine leaks and urinomas. CT protocols in patients with a suspected urine leak involve scanning the abdomen and pelvis prior to and following the intravenous administration of 100-150 mL of contrast material. Delayed phase images (obtained 5-20 minutes after contrast material injection) are the key for demonstrating a urine leak because iodinated urine increases the attenuation of the urinoma over time. Coronal and sagittal three-dimensional reformatted CT images can help further define the extent of injuries to the collecting system. Even if a urine leak or urinoma is not suspected at the time the CT protocol is prescribed, it may still be diagnosed following CT if the location and pattern of spread of the fluid

collection is recognized. Urinomas may be confined, encapsulated fluid collections or may manifest as free fluid. However, most urinomas leak into a subcapsular location or into the perirenal space within the Gerota fascia. If extensive, a urine leak may cross the midline within the perirenal space anterior to the aorta and inferior vena cava and extend into the contralateral perirenal space. A urine leak may extend superiorly through the aortic hiatus into the mediastinum and through the diaphragm into the pleural space. Urine may also travel through lymphatic vessels from a urinoma to the pleural and mediastinal space, or it may extend inferiorly along the iliopsoas compartment below the inguinal ligament to the soft tissues of the thigh, pelvis, buttocks, or scrotum or into the perineum. A urine leak may extend into the intraperitoneal cavity and surround bowel loops, causing urinary ascites. Intraperitoneal urine leaks are usually a result of penetrating or iatrogenic injury.

Ureteral Urine Leaks

Causes

Like renal urine leaks, ureteral urine leaks may result from blunt or penetrating trauma, iatrogenic injury, or transmitted back pressure caused by downstream obstruction due to a ureteral stone, surgical ligature, or abdominal or pelvic mass. Unlike renal urine leaks, ureteral urine leaks most commonly occur as a result of iatrogenic injury following **genitourinary**, retroperitoneal, pelvic, or gynecologic surgery. Ureteral perforations resulting in urine leakage may also occur following ureteral antegrade or retrograde manipulation during endourologic procedures. Ureteral anastomotic dehiscence may occur following renal transplantation or ureteral diversion procedures.

Diagnosis and Imaging Features

The diagnosis of ureteral injuries may readily be accomplished with retrograde or antegrade pyelography or with CT that includes unenhanced, corticomedullary, and delayed imaging. CT with delayed imaging is the least invasive and most readily available of these three options. Delayed phase CT scans (obtained 5-20 minutes after contrast material injection) are optimal for demonstrating ureteral urine leaks. Coronal and sagittal three-dimensional reformatted CT images can help further define the extent of injury to the ureter. In patients who are not candidates for imaging with intravenous contrast material, scintigraphy plays a vital role in the diagnosis of ureteral urine leaks. The reported sensitivity of intravenous pyelography in the diagnosis of ureteral injury is 33%.

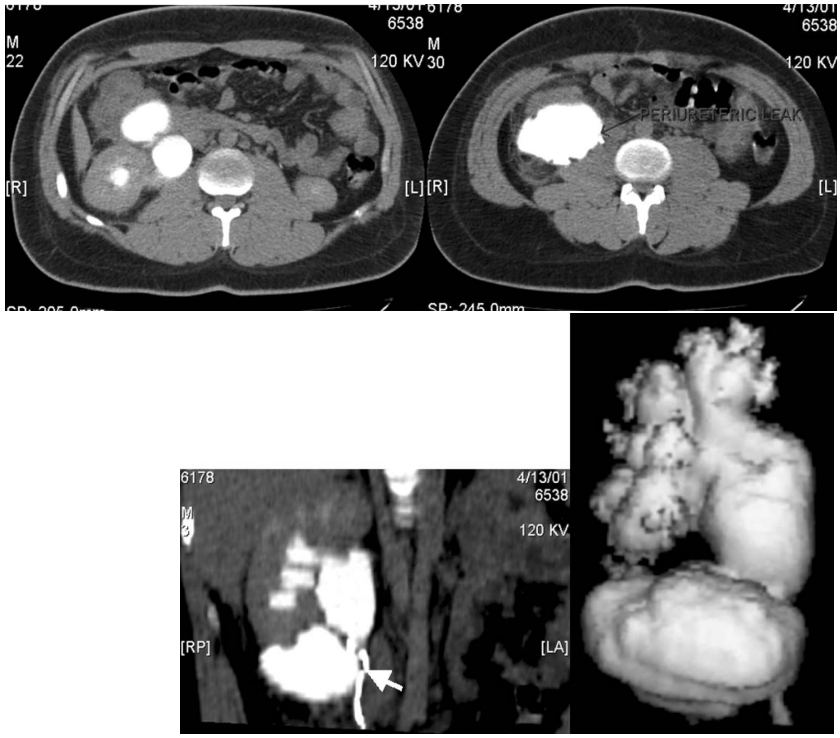

FIGURES 6.128A to D: Axial and coronal MPR with 3D SSD images in a case of penetrating injury shows a large proximal ureteric collection of contrast due to a ureteric injury (arrow).

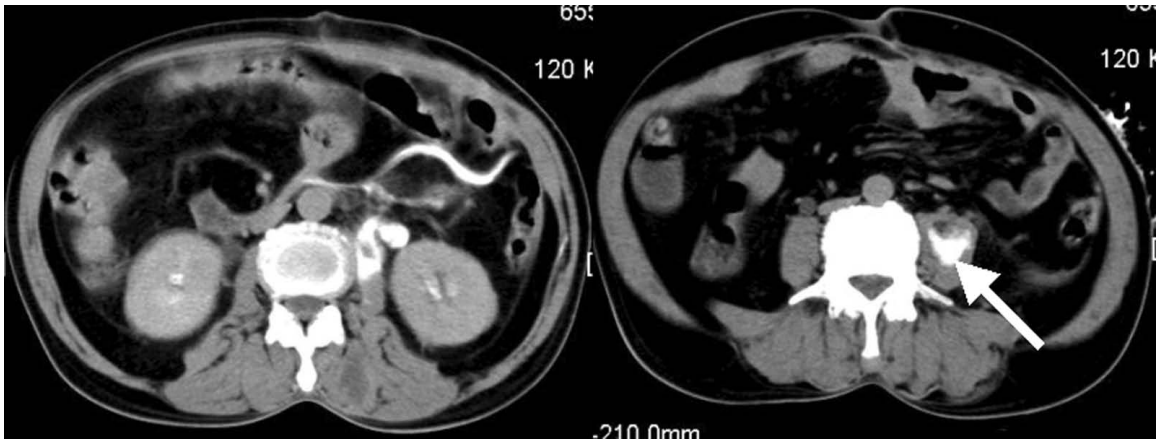

FIGURES 6.129A and B: Axial CECT showing proximal left ureteric fistula with pooling of contrast within the left psoas muscle (arrow). Note the hypodense area in the right erector spinae muscle, which is the site of the penetrating stab injury.

Ureteroceles

Its been postulated ureteroceles develop as a result of failure of normal epithelial membrane to recanalise, between the bladder and ureter (chwallas membrane). The ectopic ureterocele represents marked submucosal dilatation of the intravesicle portion of the ureter at the UV junction.

Ectopic ureteroceles are seen predominantly in females they generally cause obstruction of the proximal ureter, another cause of obstruction in these patients is the extravesicle insertion of the ureter. In male patients the ureter never inserts inferior to the external sphincter so its protected from infection, and incontinence is rarely a symptom.

Another type of ureterocele is the orthotopic ureterocele which occurs in the adults seen incidentally characterized by a cystic dilatation of the intramural portion of the ureter.

Extravesical insertion of ureter in females is frequently associated with chronic incontinence.

Congenital anomalies of ureter which result in hydronephrosis or ureteral dilatation include congenital strictures, retrocaval ureter, primary megaureter, vesicoureteral reflux.

When hydronephrosis is detected, attention is to be given to try and define the transition point from dilated ureter to the normal ureter. Congenital strictures are common, and may develop at any site along the course of ureter. Majority develop at the site of PUJ.

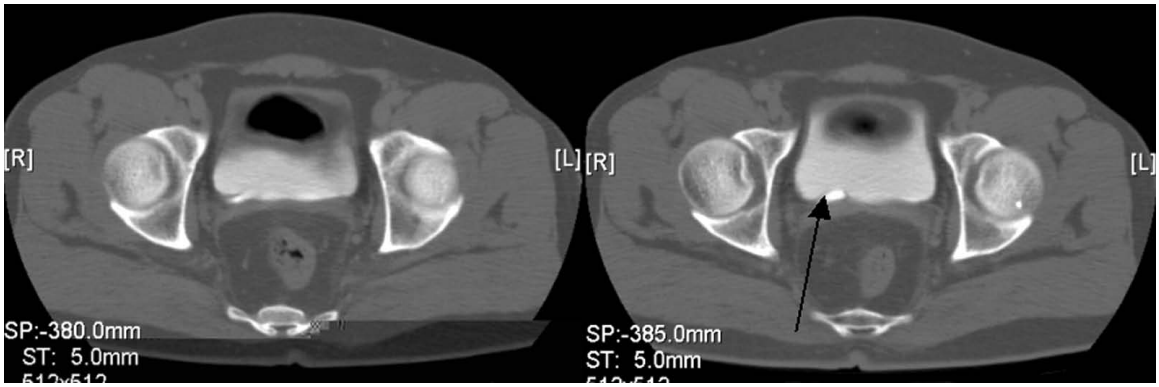

FIGURES 6.130A and B: Axial CECT reveals a focal dilatation of the rigt UV junction suggestive of a ureterocele.

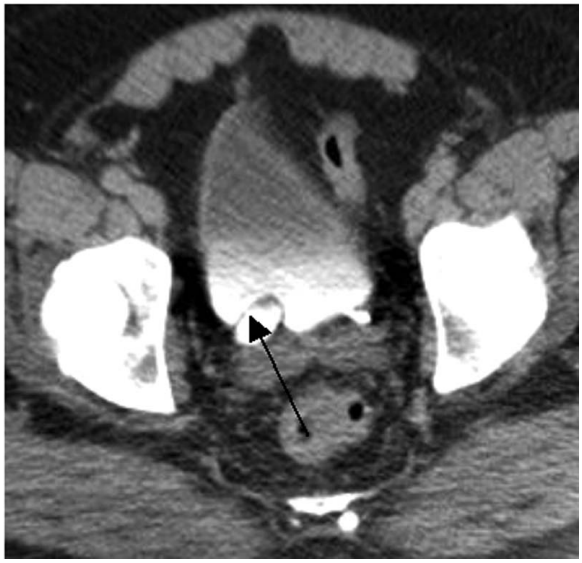

FIGURE 6.131: Axial CECT showing a large juxta vesicle ureterocele on the right side (arrow).

Primary Mega Ureter

Primary mega ureter results from inadequate musculature inhibiting peristalsis along a short segment of ureter near the UV junction. This segment of ureter appears normally on imaging without any stenosis or filling defect. However inhibition of peristalsis along this segment leads to a transient hold up of urine above the segment, eventually resulting in ureteral dilatation, typically gross dilatation of lower ureter is seen. In long-standing cases the entire ureter is dilated. In majority of cases the calyx retains its sharp non-dilated appearance in contrast to calyceal blunting and cupping seen in other obstructive causes. Primary mega ureter is unilateral in 75% of cases more common on the right side, common in men complications include recurrent UTI, calculus disease.

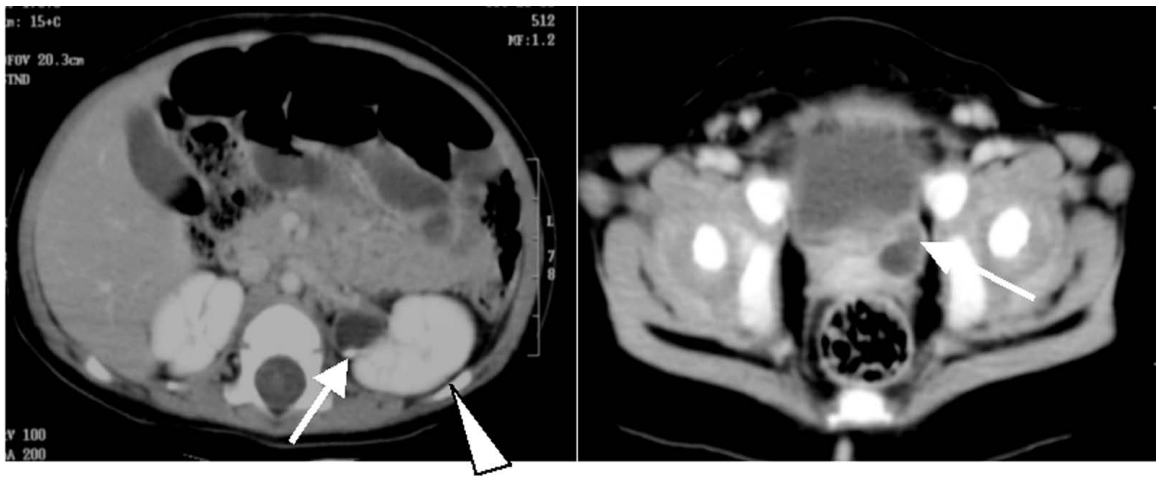

FIGURES 6.132A and B: Axial CECT in a 7-year-old child reveals dilated ureter traced till the UV junction, (arrows in Figs A,B), note the absence of pelvicalyceal dilatation (arrowhead).

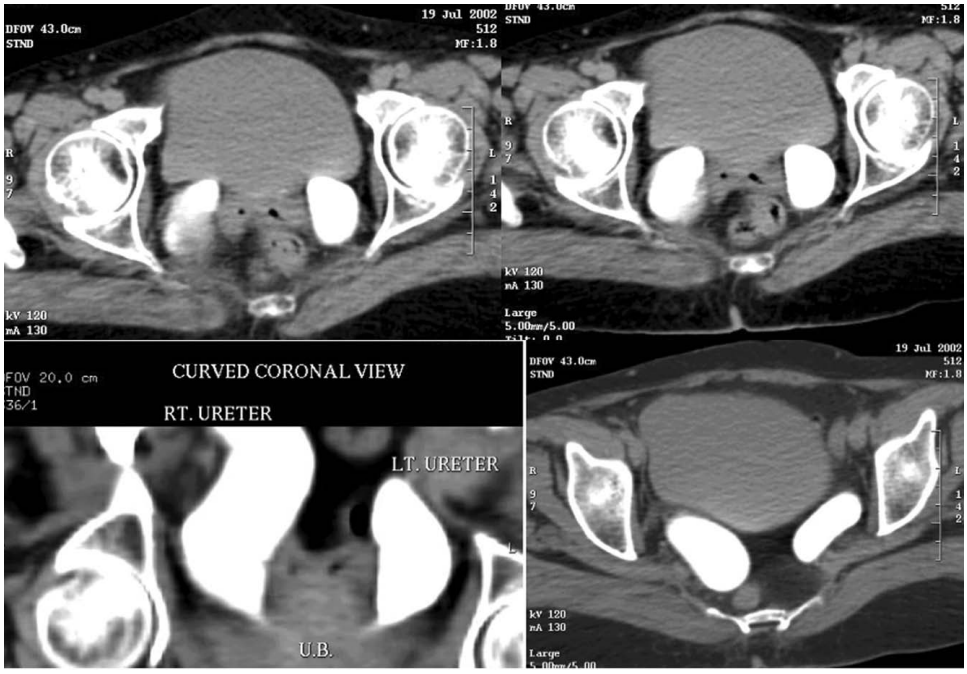

FIGURES 6.133A to D: Axial and coronal MIP projection showing bilateral dilated ureters showing abrupt funneling at the PUJ levels.

Pelviureteric Junction Obstruction

Common cause for PUJ obstruction is due to congenital stricture, the etiology of these strictures are unclear, the extreme form of these strictures result in a nonfunctioning hydronephrotic form of multicystic dysplastic kidney. Milder forms are not noticed till adulthood.

Typical symptoms include flankpain, hematuria, stone disease and recurrent UTI. Approximately 5% of cases are due to aberrant renal vessel crossing and compressing the PUJ. If the narrowed segment of ureter curves smoothly laterally with a concave medial margin an aberrant vessel crossing should be suspected. The diagnosis can be made with contrast helical or MDCT. Up to 25% of patients with congenital PUJ obstruction will have associated anomalies on the contralateral side such as multicystic dysplastic kidney, and contralateral PUJ obstruction.

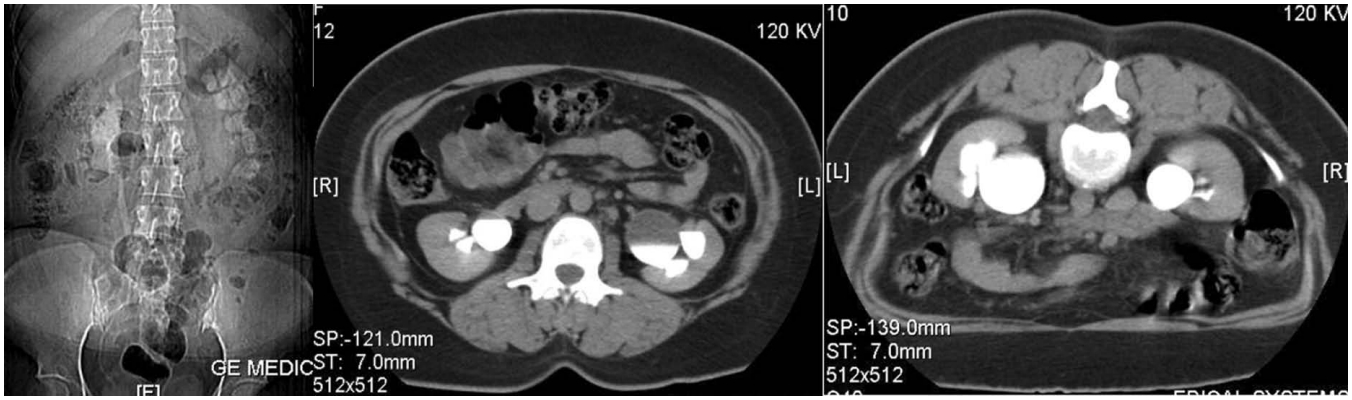

FIGURES 6.134A to C: Digital scanogram showing moderate left pelvicalyceal dilatation with extrarenal opacified pelvis –note the inverted tear drop shaped pelvis without ureteric opacification. Axial supine and prone views show opacification of pelvis.

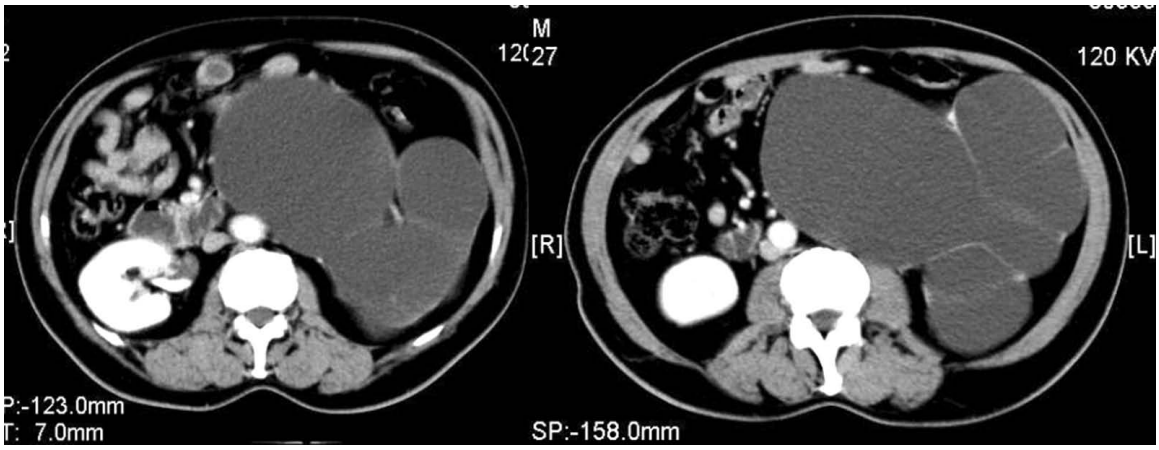

FIGURES 6.135A and B: Axial CECT showing the grossly ballooned out pelvis with thinned out parenchyma typical of long-standing PUJ obstruction.

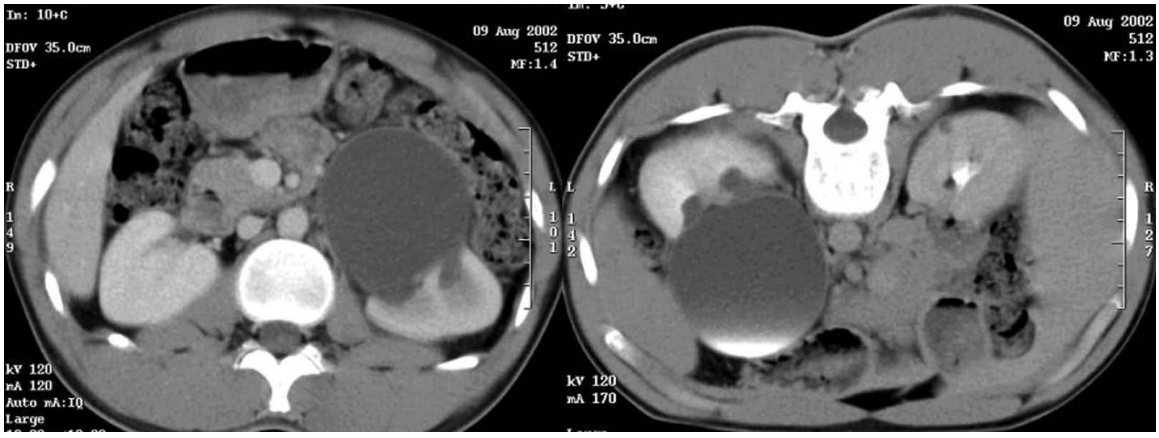

FIGURES 6.136A and B: Axial supine and prone CT showing dilated left renal pelvis with layering of contrast. We routinely obtain prone views to differentiate cases of complete obstruction from ones due to dysfunction.

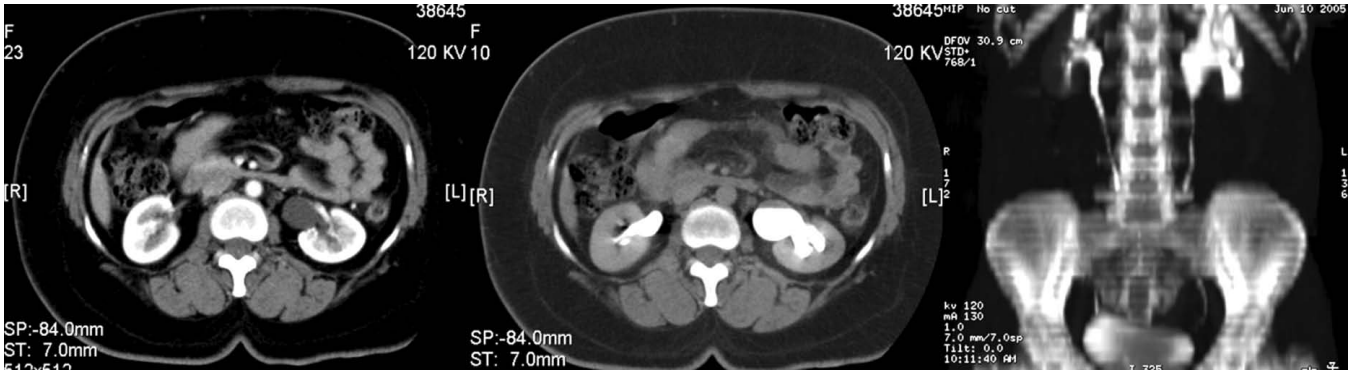

FIGURES 6.137A to C: (A, B) Axial CECT and coronal MIP (C) Showing left extrarenal pelvis with dilatation showing opacification of the distal ureter following prone positioning for 5 minutes—typical finding in cases with PU dysfunction.

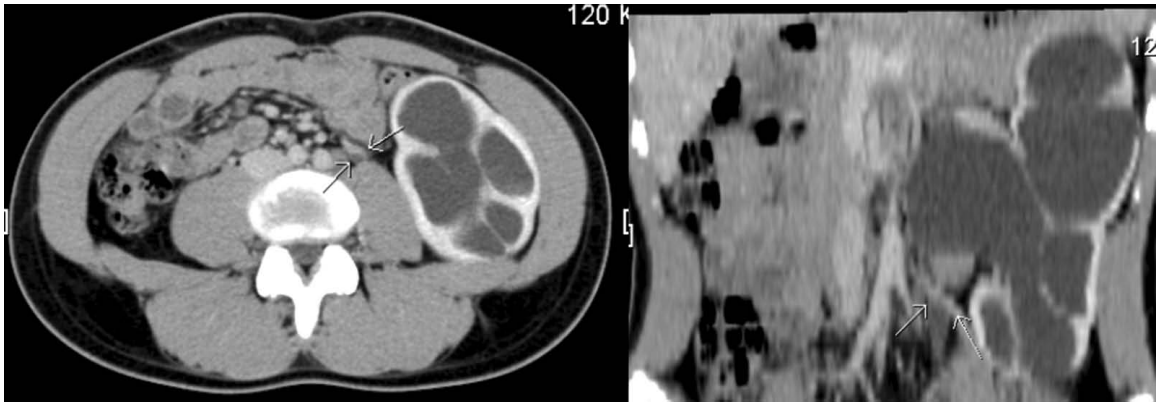

FIGURES 6.138A and B: Axial and coronal CT showing an aberrent vessel crossing.

Neobladder

The use of orthotopic bladder substitution and urinary diversion has increased markedly over the last 15 years and this trend is expected to continue. Up to 50% of patients with invasive bladder cancer may be suitable candidates for orthotopic reconstruction. Medium and long-term follow-up data indicate that the use of orthotopic bladder substitution can result in superior quality of life for patients compared with other forms of urinary diversion.

Noncontinent Urinary Diversion

Diversion into a noncontinent conduit is considered less technically demanding and is associated with the fewest postoperative complications; therefore, this technique is the criterion standard. Noncontinent urinary diversion is performed by either directly anastomosing the ureters to the anterior body wall (i.e. cutaneous ureterostomy) or using a segment of bowel to anastomose in a similar manner to the anterior wall for ostomy bag drainage.

The bowels most commonly used for noncontinent conduit diversion are 15-25 cm of ileum, colon, and, least often, jejunum bowel segments. These segments usually lend themselves to easy mobilization on a vascular pedicle, which allows for ureter anastomosis at the proximal end and stoma formation on the abdominal wall (most often in the right lower quadrant) at the distal end.

Direct ureter anastomosis with the skin is the only form of diversion that does not require use of the gastrointestinal tract. In pediatric patients, a cutaneous ureterostomy often is performed as a temporizing measure prior to a future and more definitive procedure. In adults, cutaneous ureterostomy is rarely performed currently.

Continent Urinary Diversion

The most commonly used bowel segments for continent urinary diversion are either ileum or a combination of terminal ileum and ascending colon. Ensuring that all continent diversions store and empty urine at low pressures is paramount. High storage and voiding pressures ultimately cause high-pressure reflux nephropathy and may result in renal failure; therefore, all bowel segments used for continent diversion, with the exception of their use in a retrosigmoidostomy procedure, initially are detubularized. The bowel segments then are refashioned in a more spherical shape, which increases capacity and decreases luminal pressure by a magnitude of 3- to 4-times lower than the original segmental pressure.

Continent diversion may be further categorized into 3 types:

1. Orthotopic or neobladder diversion,
2. Continent catheterizable diversion,
3. Ureterosigmoidostomy.

Etiology

The most common indications for urinary system diversion are as follows:

- Bladder cancer requiring cystectomy
- Neurogenic bladder conditions that threaten renal function
- Severe radiation injury to the bladder
- Intractable incontinence in females.

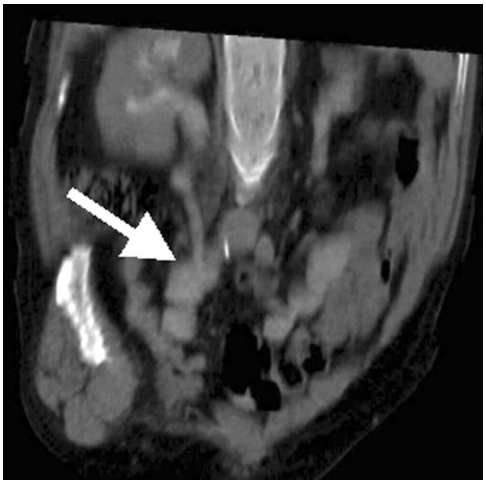

FIGURE 6.139: CECT in coronal reformat shows an ileal conduit, note the right ureter draining into the ileal loop (arrow)

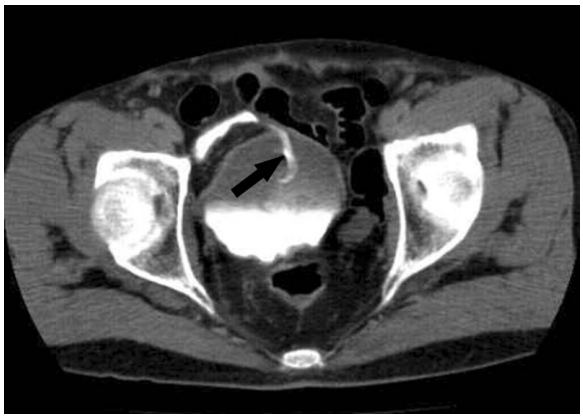

FIGURE 6.140: Axial CECT showing an ureter implanted into a sigmoid bowel loop (arrow).

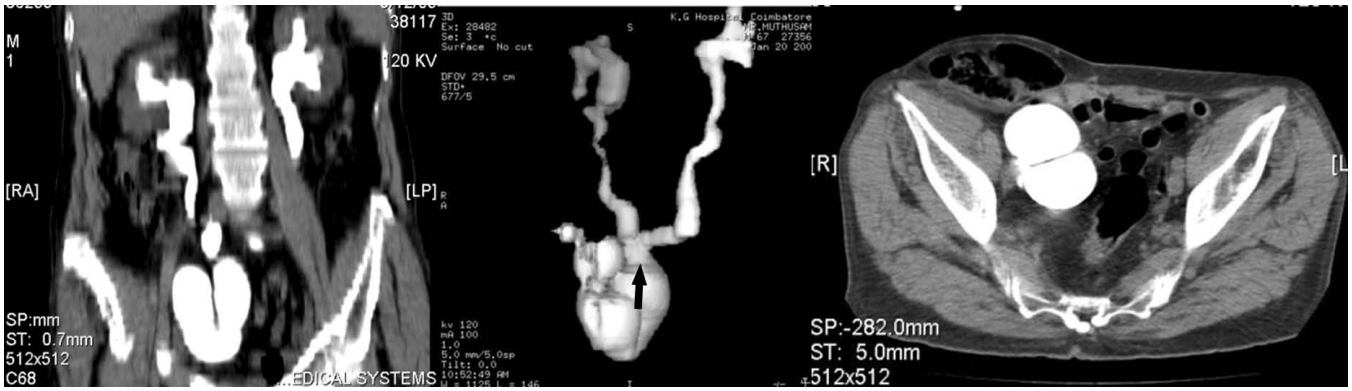

FIGURES 6.141A to C: Coronal CECT, 3D and axial images show a continent diversion-note the implanted ureters (arrow B)

RENAL VASCULAR DISORDERS

Computed tomography (CT) plays an important role in evaluation and management of both primary renovascular disease and the secondary manifestations of renovascular disease.

CT protocol for initial evaluation of the kidneys consists of both nonenhanced and contrast material–enhanced CT scans. A contrast-enhanced study is essential for evaluating patients with suspected renovascular disease. Nonenhanced CT is useful for demonstrating renal hemorrhage, renal parenchymal or vascular calcifications and masses.

A contrast-enhanced study can allow direct visualization of the renal vessels and identification of nephrographic abnormalities due to a renovascular process. A renal infarct can be accurately demonstrated following intravenous administration of contrast material. Delayed CT scans of the kidneys are necessary when a mass, infarct, or urinary obstruction is suspected on the early-phase scans.

Identification of global or regional nephrographic abnormalities during a particular phase of enhancement is valuable in assessing renal perfusion and function. Renal vascularity is evaluated during the vascular phase, which occurs approximately 15-25 seconds after the start of intravenous contrast material administration. CT protocol for a dedicated kidney study includes an initial axial or helical nonenhanced scan of the kidneys with contiguous 5-mm-thick sections following a scout scan. Contrast-enhanced helical CT studies of the abdomen are performed within 30 seconds for the cortical nephrographic phase. Helical scans for the diffuse nephrographic phase are obtained approximately 100 seconds after the start of intravenous contrast material administration. Rapid injection of a 100 mL bolus of 60% nonionic iodinated contrast material can be performed at a rate of 2.0-3.0 mL/sec via the antecubital fossa by using a mechanical power injector and an 18-20-gauge angiographic catheter. The scanning parameters include a collimation of 5 mm, a pitch of 1.5, and an image reconstruction increment of 5 mm.

Typical acquisition parameters for CT angiography of the renal artery include a collimation of 3 mm, a pitch of 1.5-2.0, a reconstruction interval of 1-2 mm, a scan delay of 25 seconds after the start of intravenous contrast material administration, and an injection rate of 3 mL/sec or greater.

When the timing of the scan is optimized to the peak of intravascular enhancement (the vascular phase), helical CT can be used as a minimally invasive modality for vascular imaging that serves as an alternative to conventional angiography. Image postprocessing including multiplanar two-dimensional and three-dimensional reconstruction techniques on an independent workstation can then be used to directly image the proximal renal arteries and allows assessment of primary vascular disease. In most cases, threshold-based shaded-surface display or maximum-intensity projection images are generated from the data set of the original axial images for the three-dimensional presentation. A volume-rendered image on a workstation can be viewed in an interactive fashion, and overlying anatomic structures can be removed or highlighted for optimal morphologic demonstration.

Arteriovenous Communications

Arteriovenous communications can be congenital or acquired. They are direct communications from an artery to a vein without an intervening capillary bed.

Arteriovenous malformations (AVMs) are usually asymptomatic and are found more often in women than in men. Cirsoid AVMs consist of multiple small arteriovenous communications that are supplied by multiple segmental or interlobar arterial branches of normal caliber and tend to be located adjacent to the collecting system. Patients with AVMs often present with gross hematuria. An AVM is a rare cause of subcapsular or perinephric hematoma.

Arteriovenous fistulas can result from trauma, surgery, tumors, inflammation, or erosion of an aneurysm directly into a vein (idiopathic arteriovenous fistula). Arteriovenous fistulas typically have a single feeding artery and a single draining vein, both of which are markedly enlarged. Arteriovenous fistulas are seen more often in men than in women because penetrating trauma is the most common cause. The most common clinical manifestation of a renal arteriovenous fistula is an abnormal bruit. Persistent or delayed hematuria is also common. Ischemia in the renal parenchyma distal to the arteriovenous fistula may induce renin-mediated hypertension and impaired renal function.

CT Findings

The CT appearance of arteriovenous communications depends on the timing of image acquisition relative to intravenous contrast material administration, the amount of contrast material, and the injection rate. Contrast-

enhanced helical CT performed during the vascular and early cortical nephrographic phases is valuable in detection of an intrarenal vascular mass with feeding and draining vessels, which are usually engorged. There is prompt filling of the draining veins as well as the renal vein and IVC immediately after enhancement of the arteries.

Aneurysms of the Renal Artery

The most common cause of aneurysms of the renal artery is atherosclerosis. Less common causes include medial fibroplasia, pregnancy, and mesenchymal diseases such as neurofibromatosis and Ehlers-Danlos syndrome. Renal pseudoaneurysms are usually posttraumatic or inflammatory (e.g., Behçet's disease, mycotic aneurysm). The prevalence of renal artery aneurysms is reported to be 0.01-0.1%. Renal artery aneurysms account for 22% of visceral aneurysms. Renal artery aneurysms often contain mural thrombus and may give rise to emboli of the kidney. The risk of rupture is small, particularly when rim-like calcification is present in the wall of the aneurysm.

Renal artery aneurysms can be classified into four types: saccular, fusiform, dissecting, and intrarenal. Saccular aneurysms are usually present in the main renal branch near the first bifurcation and are associated with medial fibroplasia and atherosclerosis. Fusiform aneurysms are usually found in medial fibroplasia and are not calcified. Dissecting aneurysms, which may involve the main renal artery with or without extension to the segmental branches, may be classified according to cause as traumatic, spontaneous (e.g., atherosclerosis, intimal fibroplasia, perimedial, fibroplasia), and iatrogenic (e.g., catheterization). Intrarenal aneurysms are frequently associated with arteritis (e.g., polyarteritis nodosa, Wegener granulomatosis) but can also be caused by atherosclerosis, fibroplasia, trauma, vascular malformations, syphilis, tuberculosis, or tumors.

CT Findings

Most aneurysms are extrarenal. If calcified, a renal artery aneurysm can be recognized on plain abdominal radiographs. At CT, calcification is readily evident along the wall of the aneurysm and typically appears as an incomplete or complete ring of calcification or as a series of rings. After administration of contrast material, variable enhancement occurs, depending on the amount of mural thrombus within the aneurysm. Contrast-enhanced helical CT performed with thin sections can show an intimal flap in the main renal artery, a finding consistent with dissection.

Vasculitis

Characteristic CT findings can be found in some of the diseases associated with vasculitis, although it is often difficult to distinguish between the various causative conditions.

Polyarteritis Nodosa

Renal involvement occurs in 90% of patients with polyarteritis nodosa. Patients with polyarteritis nodosa often present with hematuria. Renal ischemia occurs as a result of involvement of medium-sized vessels, and renin-mediated hypertension is common.

CT Findings

Occasionally, the "microaneurysms" in patients with polyarteritis nodosa may be seen at dynamic contrast-enhanced CT.

Contrast-enhanced CT can demonstrate areas of infarction of different ages. The kidneys may appear lobulated with irregular thinning of the parenchyma due to prior cortical infarcts. The collecting system is usually preserved. Multiple linear bands of low attenuation may be present in the kidneys and are attributed to occlusion of intrarenal arteries.

Systemic Lupus Erythematosus

Renal disease occurs in 30-50% of patients with systemic lupus erythematosus (SLE) and encompasses the entire spectrum of glomerular, tubular, or vascular disease. Patients with SLE have a high-risk of developing a thrombus in the renal vein.

CT Findings

The larger lobular arteries are usually unaffected renal vein thrombosis is seen as a filling defect in a thick-walled renal vein with or without extension into the IVC on contrast-enhanced CT scans. Collateral vessels may be present along the proximal to middle ureter and at the renal hilum.

The kidney may be enlarged or diminutive depending on the stage of lupus nephritis. Multiple linear bands of a decreased nephrogram may be present as a result of associated vasculitis.

Spontaneous (nontraumatic) renal hematoma may occur as a result of rupture of a renal tumor, vasculitis, hemorrhage from an aneurysm, hemorrhagic diathesis due to anticoagulant therapy or coagulopathy, infection, and acute or chronic nephritis.

Renal Neoplasms that Cause Renal Hemorrhage

Twenty-five percent of cases of spontaneous renal hemorrhage are due to benign renal tumors, with angiomyolipoma being the most common type. Tuberous sclerosis is typically associated with bilateral renal angiomyolipomas. Sporadic angiomyolipomas are usually solitary. Among angiomyolipomas 4 cm or larger in diameter, 82-94% are symptomatic and 50-60% bleed spontaneously. Angiomyolipomas smaller than 4 cm in diameter are seldom symptomatic and less likely to bleed.

Renal cell carcinoma is also a cause of spontaneous renal hemorrhage. Because CT is highly sensitive in detection of renal cell carcinoma, absence of a renal mass virtually excludes this diagnosis. Renal cell carcinoma may be found in at least 50% of cases of spontaneous renal hemorrhage.

CT Findings

If the cause of a perinephric hematoma (e.g. trauma, vasculitis, anticoagulant therapy, clotting disorder) is not apparent and initial CT does not show a cause, repeat tailored thin-section helical CT performed with and without intravenously administered contrast material is required to exclude a small renal cell carcinoma.

Selective renal angiography may be necessary to exclude vascular lesions, including vasculitis, arteriovenous communications, and aneurysms, when a dedicated CT study does not demonstrate the source of the bleeding. If the cause of a perinephric hemorrhage remains indeterminate, follow-up CT at 3 and 6 months may be indicated.

Renal Artery Stenosis

Renovascular hypertension accounts for 1-4% of all patients with hypertension. Renovascular hypertension is renin-mediated and occurs as a response to renal ischemia. Atherosclerosis accounts for approximately two-thirds of patients with significant narrowing of the main renal artery. Atherosclerotic lesions usually occur at the origin of the renal artery or within the proximal 2 cm. Fibrous lesions of the renal artery account for the remaining one-third of cases. Medial fibroplasia is often referred to as "fibrous dysplasia" or "fibromuscular dysplasia". The latter term is a misnomer because hyperplasia of the smooth muscle is not present. Medial fibroplasia constitutes 75-80% of all fibrous lesions and typically affects women 20-50 years of age. Fibromuscular hyperplasia, which consists of true hyperplasia of the smooth muscle and fibrous tissue, is rare, comprising only 2-3% of fibrous lesions. Intimal hyperplasia occurs in children and young adults and accounts for 10-15% of fibrous lesions. The lesion is progressive and may be complicated by dissection. Perimedial (subadventitial) fibroplasia accounts for up to 15% of fibrous lesions. Young females are affected, and the right renal artery is frequently involved. Less common causes are Takayasu aortitis neurofibromatosis, and irradiation.

CT Findings

Stenosis of the main renal artery is best demonstrated with CT angiographic techniques. Lesions of atherosclerosis are either eccentric or concentric with respect to the artery. Poststenotic dilatation of the artery may be present. Helical CT angiography can be used as a screening procedure for renal artery stenosis.

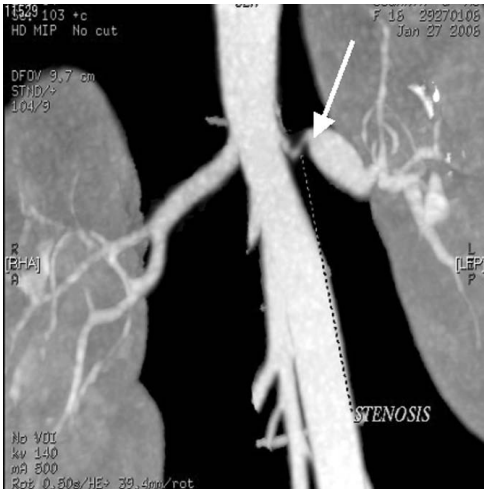

FIGURE 6.142: Coronal MIP in a young girl with hypertension shows a very tight osteoproximal stenosis of the left renal artery.

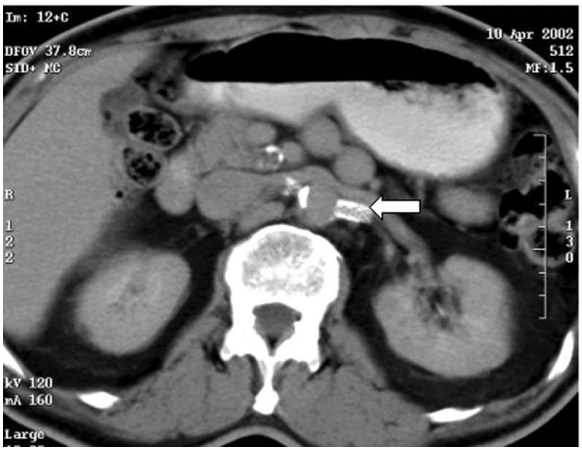

FIGURE 6.143: Axial plain CT in a case of left renal artery stenosis who underwent a stent insertion (arrow).

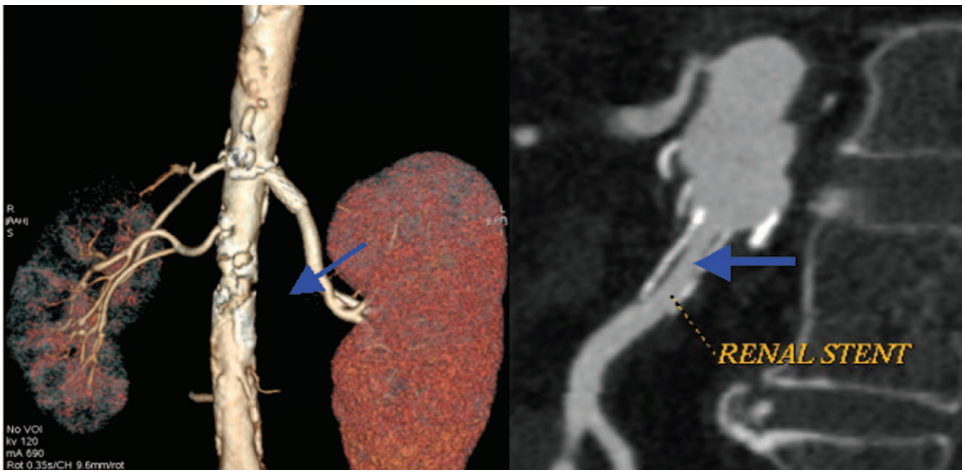

FIGURES 6.144A and B: Axial 3D MIP projection showing left osteoproximal renal artery stent (arrow), curved MPR showing neointimal hyperplasia within the stent (arrow in B).

Renal Infarction

Renal infarction occurs in a variety of clinical settings. The most common cause is thromboembolism from cardiovascular disease. The most common clinical manifestation is sudden onset of flank or back pain. Hematuria, proteinuria, fever, and leukocytosis may be present. Although it is more common for venous thrombosis to be associated with malignancy (paraneoplastic syndrome), arterial thrombosis is also occasionally associated with malignancy.

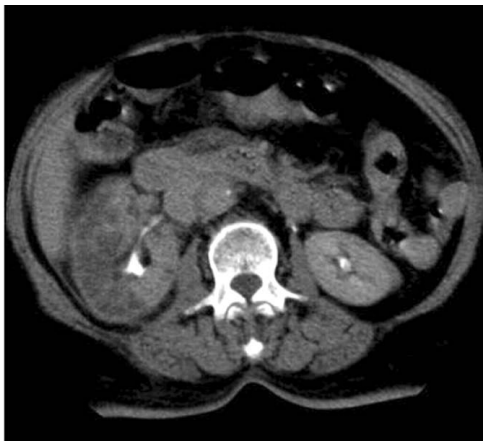

FIGURE 6.145: Axial CECT in a patient with right loin pain (patient underwent thrombolysis for acute myocardial infarction 12 days ago) reveals hypodense nonenhancing regions at upper and interpolar cortex suggestive of infarcts.

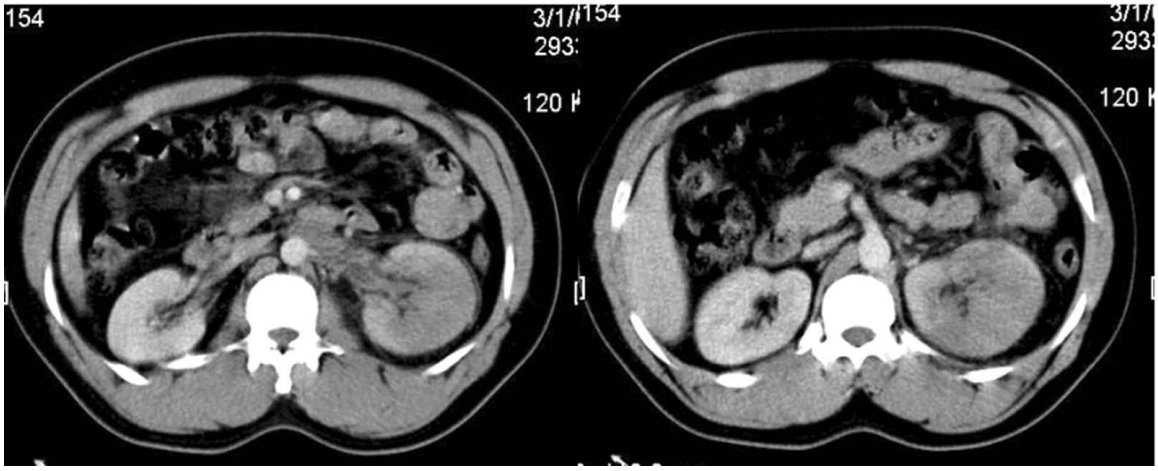

FIGURES 6.146A and B: Axial CECT in a patient with left loin pain (case of infective endocarditis) reveals left renal inter and lower polar parenchymal hypodensity suggestive of infarcts.

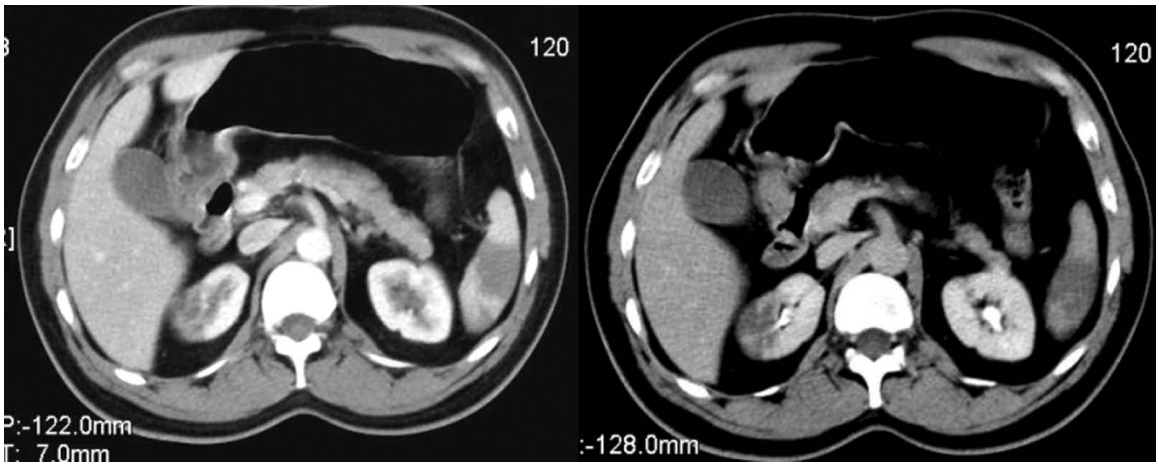

FIGUERS 6.147A and B: Axial CECT reveals focal wedge shaped hypodensity in the spleen and right renal upper pole suggestive of infarcts.

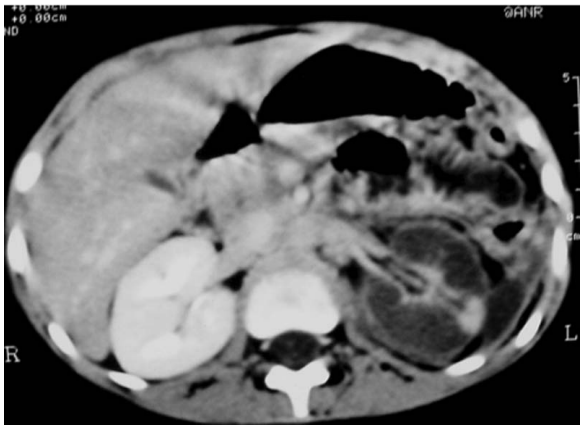

FIGURE 6.148: Axial CECT reveals hypodense non-enhancing left kidney (history of blunt injury abdomen 2 weeks prior to CT study) suggestive of infarcted kidney.

Causes of Renal Infarction

- Thromboembolism
- Thrombus in the left side of the heart or aorta
- Aneurysm of the aorta or renal artery
- Atherosclerosis
- Subacute bacterial endocarditis (septic emboli)
- Transcatheter embolization and other endovascular procedures
- Dissection of the aorta or renal artery
- Vasculitis
- Polyarteritis nodosa
- SLE
- Drug-induced vasculitis
- Trauma
- Avulsion of the renal artery
- Occlusion of the renal artery
- Penetrating vascular injury
- Paraneoplastic syndrome
- Hypercoagulable state
- Acute venous occlusion.

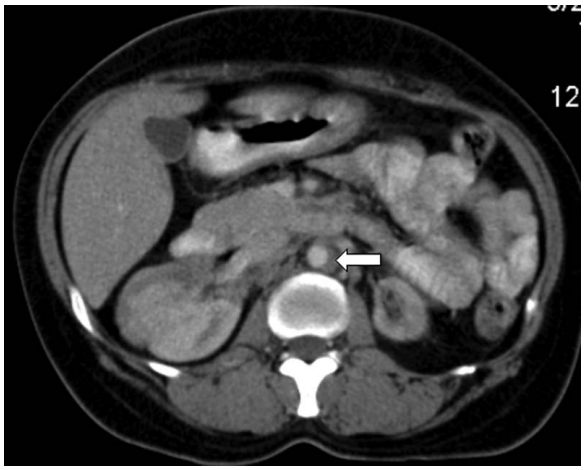

FIGURE 6.149: Axial CECT in a case of aortoarteritis involving both renal arteries (arrow showing the ring of periaortic soft tissue). Note the small left kidney and the variable enhancement of the right kidney.

Renal Vein Thrombosis

Thrombosis of the renal vein is usually caused by an underlying abnormality of the clotting system or the kidney itself or, in infants, dehydration. Renal vein thrombosis is more common on the left side, presumably because of the longer left renal vein. The clinical manifestations of renal vein thrombosis depend on the age of the patient, the specific disease process, and the speed with which it occurs. A classic acute presentation includes gross hematuria, flank pain, and loss of renal function. Renal vein thrombosis is a complication of the nephrotic syndrome and hypercoagulable state in patients with SLE. Renal vein thrombosis associated with tumor is frequently caused by direct tumor extension and occurs most commonly in cases of renal cell carcinoma and occasionally in cases of transitional cell carcinoma or Wilms' tumor. Tumor thrombus in the renal vein may also result from a left adrenal tumor. Left ovarian vein thrombosis may extend into the left renal vein.

CT Findings

Contrast-enhanced CT shows thrombus in a thick-walled renal vein with or without extension into the IVC. In the chronic phase of renal vein thrombosis, the affected renal vein becomes attenuated due to retraction of the clot along with development of extensive collateral vessels along the proximal to middle ureter and around the kidney. The presence of inhomogeneous enhancement in the thrombus is indicative of tumor involvement. Accurate demonstration of extension of tumor thrombus into the IVC may be problematic because the IVC above the renal veins frequently appears inhomogeneous on early-phase contrast-enhanced helical scans due to mixing of enhanced blood flow from the renal veins and nonenhanced blood flow from the IVC. Delayed scans may also improve visualization of the IVC. If the CT findings are still indeterminate, MR imaging is suggested for evaluation of tumor thrombus.

Causes of Renal Vein Thrombosis

- Hypercoagulable state
  - Nephrotic syndrome
    - Membranous glomerulonephritis
    - Membranoproliferative glomerulonephritis
    - Lupoid nephrosis
  - SLE
  - Inherited hypercoagulable state
    - Antithrombin III deficiency
    - Protein C deficiency
    - Protein S deficiency
- Dehydration
- Mechanical process
  - Trauma
  - Neoplasm
    - Renal cell carcinoma
    - Transitional cell carcinoma
    - Wilms' tumor
    - Left adrenal carcinoma
  - Abscess
  - Aneurysm
  - Adrenal hematoma
- Left ovarian vein thrombosis

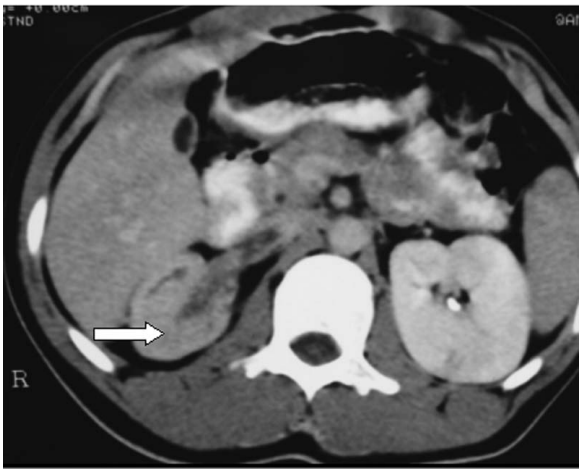

FIGURE 6.150: Axial CECT shows contracted right kidney with delayed faint nephrogram, note the enlarged right renal vein with a non-enhancing area within suggestive of a thrombus (arrow) case of chronic renal vein thrombus.

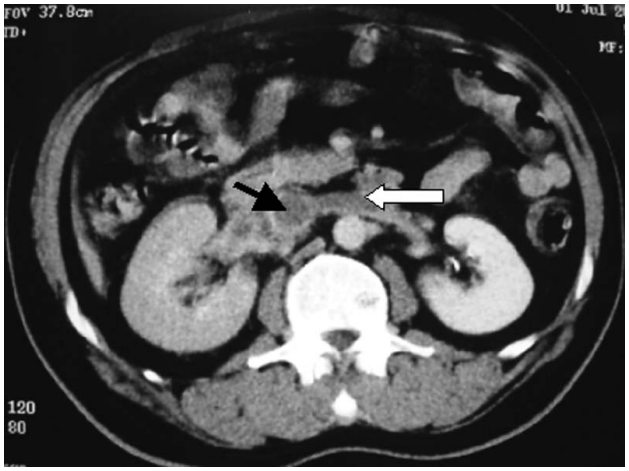

FIGURE 6.151: Axial CECT shows thrombus within the IVC and left renal vein (arrow). Thrombus is seen in the proximal right renal vein causing delayed contrast excretion of the right kidney.

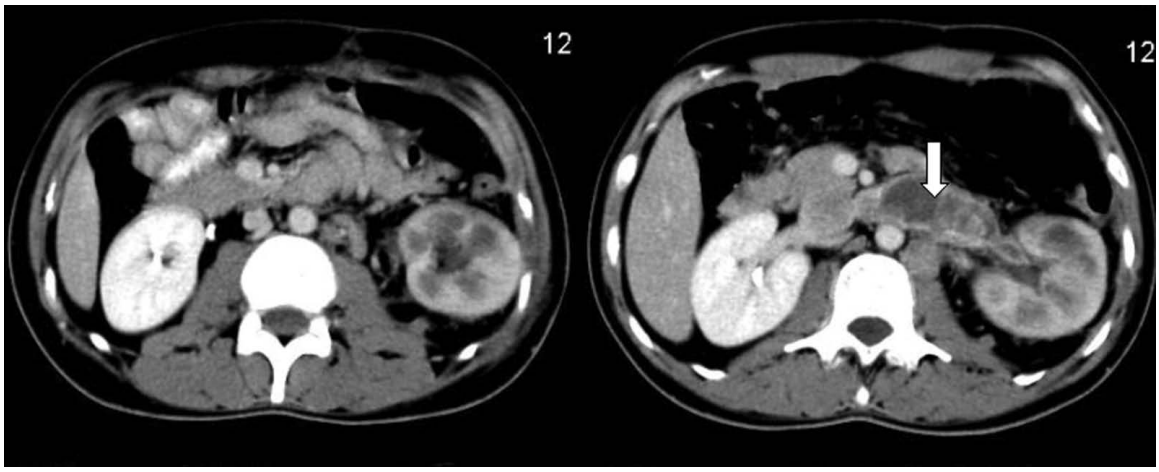

FIGURES 6.152A and B: Axial CECT showing a large enhancing thrombus in the left renal vein causing delayed left renal nephrogram. Patient is a postoperative case of left adrenal carcinoma, enhancement of thrombus indicates the malignant nature of thrombus (arrow).

Renal Hemorrhage

CT is the best technique for evaluating patients who are suspected of having acute renal hemorrhage as it depicts the presence and location of the bleed and often shows the underlying cause, its characterized by high attenuation blood (60-90) HU. Best seen in unenhanced CT scans.

Renal hemorrhage may be suburothelial, intraparenchymal, subcapsular, perinephric, or pararenal in location. Suburothelial bleed is characterized on CT by mural thickening in pelvis and upper ureter, usually associated with anticoagulants or coagulation disorders. Subcapsular bleed is characterized by flattening of adjacent renal parenchyma, elevation of renal capsule, and medial displacement of the renal collecting system.

The configuration of perinephric hematoma is determined largely by the bridging septa of the perinephric fat.

When the hematoma is confined by the posterior renorenal bridging septum, it may compress and indent the renal surface and because its separated from the renal fascia, it may simulate a subcapsular hematoma. While the subcapsular hematoma are confined to the kidney by the renal capsule, perinephric hematomas often extend caudally below the kidney into the cone of renal fascia.

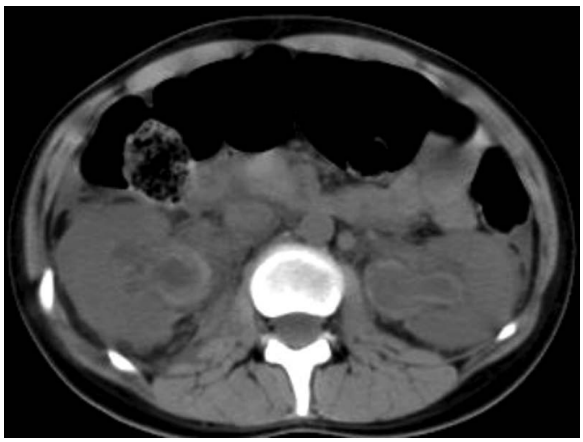

FIGURE 6.153: Axial NECT in a 67-year-old female patient on anticoagulants for stroke who presented with bilateral flank pain shows hyperdense edematous ureteric walls suggestive of periureteric hemorrhage.

Causes of Subcapsular Renal or Perinephric Hemorrhage

- Trauma
- Renal laceration
- Avulsion of the renal artery
- Neoplasm
- Malignant (renal cell carcinoma)
- Benign (angiomyolipoma)
- Vasculitis
- Polyarteritis nodosa
- AVM
- Aneurysm
- Anticoagulant therapy
- Acute infection
- Acute or chronic nephritis.

RENAL TRANSPLANT

Noninvasive imaging techniques allow improved detection of vascular and nonvascular diseases in renal transplantation. Ultrasonography (US) and nuclear medicine examinations make up the vast majority of radiologic procedures used to study these diseases. The helical or MDCT computed tomographic (CT) techniques and less nephrotoxic nonionic iodine contrast material allow low-risk, accurate evaluation of renal transplantation diseases at a lower cost and with greater availability than is possible with magnetic resonance (MR) imaging.

Helical CT can depict parenchymal, perirenal, renal sinus, pyeloureteral, and vascular diseases in renal transplantation in great detail.

Posttransplantation complications are characterized as either early or late. Early complications appear in the first weeks after transplantation and are usually attributable to surgical difficulties. Late complications appear some

weeks after the procedure and are usually due to medical problems such as those related to immunosuppression and toxicity. Early complications include acute rejection, acute tubular necrosis, hematoma, pyelonephritis, abscess, urinoma, ureteral obstruction, vascular complications (e.g. arterial stenosis and thrombosis, arteriovenous fistula and arterial pseudoaneurysm, renal vein thrombosis, graft torsion).

Late complications include chronic rejection, other causes of ureteral obstruction, lymphocele, cyst, renal cell carcinoma and transitional cell carcinoma of the graft, complications due to immunosuppression (e.g. lymphoma, Kaposi's sarcoma, opportunistic infections involving the transplanted kidney.

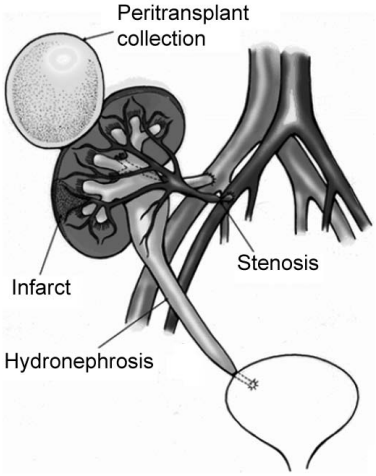

FIGURE 6.154: Schematic showing complications of renal transplant

Parenchyma

In adults, most kidney allografts are placed in an extraperitoneal location in the iliac fossa. At unenhanced CT, the renal parenchyma demonstrates homogeneous soft-tissue attenuation. Contrast material-enhanced arterial-phase CT is used to evaluate the renal graft artery and vein and the iliac arterial system. In this phase, the cortex appears hyperattenuating and the medulla remains hypoattenuating because contrast material has not yet reached it. Venous-phase (tubular nephrogram–phase) CT, at which the normal parenchyma is uniformly enhanced, is useful for demonstrating parenchymal masses. Late excretory-phase (pyelogram–phase) CT is used to evaluate the pyeloureteral system and demonstrates hypoattenuating, heterogeneous renal parenchyma and contrast material filling of the collecting system.

Vasculature

The most common technique for anastomosing the renal graft arterial supply in adults is the end-to-side technique using the renal artery and the external or common iliac artery. Some surgeons choose an end-to-end anastomosis involving the renal artery and the internal iliac artery. Multiple renal arteries can be anastomosed together using an aortic patch (Carrel patch) or anastomosed separately.

Venous anastomoses are almost always performed end-to-side to the recipient external iliac vein. When there are no abnormalities, the left donor kidney is preferred because the longer left renal vein facilitates venous anastomosis. A venous patch may be used in cases involving a short right renal vein.

Pyeloureter

The most frequently used technique for ureteral anastomosis is the intravesical anastomosis which involves creation of a submucosal vesical tunnel near the trigone to avoid reflux and of a nippled ureteral anastomosis through the

inside of the bladder. Postoperative fluid collections are common following transplantation and include hematomas, lymphoceles, seromas, abscesses, and urinomas. The majority of these collections can be detected at US. However, CT often delineates fluid collections and their anatomic relationship to adjacent structures better than US, particularly in obese patients.

Perirenal Hematoma

CT shows acute hematoma as a fluid collection with hyperattenuating areas prior to intravenous contrast material administration, a finding that is consistent with fresh blood. Immediate postoperative hematoma can be secondary to graft rupture or injury to the vascular pedicle. The presence of an asymptomatic, hyperattenuating perirenal collection after surgery is common and can be treated conservatively if it does not increase in size.

Perirenal Lymphocele

Lymphocele formation is a late complication of renal transplantation caused by lymphatic obstruction or leak. It is usually asymptomatic but sometimes compresses adjacent structures and may cause hydronephrosis. It can occur in upto 15% of renal transplantations. At CT, lymphocele is seen as a round, hypoattenuating collection that appears similar to seroma. The key to differentiation is that seroma appears immediately after surgery and decreases spontaneously, whereas lymphocele develops later and tends to grow.

Perirenal Abscess

Perirenal abscess is an uncommon early complication of renal transplantation. When a patient presents with fever and CT demonstrates a hypoattenuating perirenal collection with air, the diagnosis of perirenal abscess is clear. In cases with noninfectious clinical findings and a perirenal collection without air, diagnostic puncture is required.

Parenchymal Abscess

Urinary tract infection, the most common infection in renal transplant recipients, has a benign course and usually improves with antibiotic therapy. However, bacterial pyelonephritis often accompanies renal failure. Graft kidneys are less responsive to antibiotic therapy for acute pyelonephritis than are native kidneys. Abdominal CT should be performed in patients who respond poorly to antibiotic therapy to detect acute focal bacterial nephritis or renal abscess. Abscess manifests as a nonenhancing, hypoattenuating collection in the kidney.

Renal Artery Stenosis

Stenosis, the most common vascular complication of renal transplantation, occurs in 1-12% of transplanted renal arteries and represents a potentially curable cause of hypertension following transplantation. The stenosis usually occurs near the anastomosis site and is related to the surgical technique used.

Renal Artery Thrombosis

Renal artery thrombosis appears immediately after transplantation. It is most often caused by hyperacute or acute rejection but may also be caused by inadequate surgical technique, hypotension, hypercoagulable state, cyclosporine therapy, and atherosclerotic embolism. Renal infarct appears as a nonenhancing kidney with an enhancing capsule. Thrombosis of the main renal artery usually results in loss of the renal allograft.

Intrarenal Arteriovenous Fistula and Pseudoaneurysm

Intrarenal arteriovenous fistulas and pseudoaneurysms are caused by trauma during percutaneous needle biopsy. They occur in 1-18% of renal biopsies. Arteriovenous fistulas may form when an artery and vein are lacerated;

pseudoaneurysms result when only the artery is lacerated. Small lesions may resolve spontaneously; if they do not, they can be successfully treated with percutaneous transcatheter embolization. They are usually asymptomatic but can manifest with hypertension, hematuria, and deterioration of renal function. Helical CT is a good alternative when US cannot define the nature of the lesion. Visualization of a round abnormality in the renal parenchyma that enhances similar to the aorta at arterial-phase CT indicates the vascular nature of the lesion.

Renal Graft Torsion

Torsion of the renal graft is a rare surgical complication that usually occurs in children with intraperitoneal transplants. Torsion occurs when the kidney rotates around the vascular pedicle, leading to vascular occlusion and parenchymal infarction. Renal torsion can be an early or late complication. Prompt diagnosis permits graft detorsion and possible salvage. The most suggestive imaging finding is a change in the axis of the transplanted kidney. CT and MR imaging can show changes in renal graft orientation and vascular pedicle kinking, or secondary changes such as swelling or abnormal enhancement of the graft, hydronephrosis, and sinusal and perirenal fat infiltration.

Renal Vein Thrombosis

Renal vein thrombosis is an early complication of renal transplantation and is usually related to inadequate surgical technique, hypovolemia, renal vein compression, and iliac vein thrombosis. Renal vein thrombosis occurs in upto 4% of transplant recipients. Doppler US is used for quick diagnosis because the pathologic condition must be treated with thrombectomy as soon as possible. Delayed renal and iliac vein thrombosis has been described in chronic rejection and treated successfully with anticoagulation therapy. Stenosis of the renal vein is another infrequent venous complication secondary to inadequate surgical technique and perivenous diseases such as fibrosis or mass compression. Helical CT allows direct visualization of the stenosis and perivascular causes in these cases.

Urinoma

The prevalence of urologic complications following renal transplantation is 2.6-13%. Ureteral extravasation producing urinoma can be caused by graft rejection, ureteral necrosis due to ischemia, or inadequate surgical technique. At unenhanced CT, urinoma manifests as a hypoattenuating collection; after contrast material administration, direct visualization of the passage of ureteral contrast material to the collection is the clue to diagnosis.

GRAFT RENAL ARTERY THROMBUS

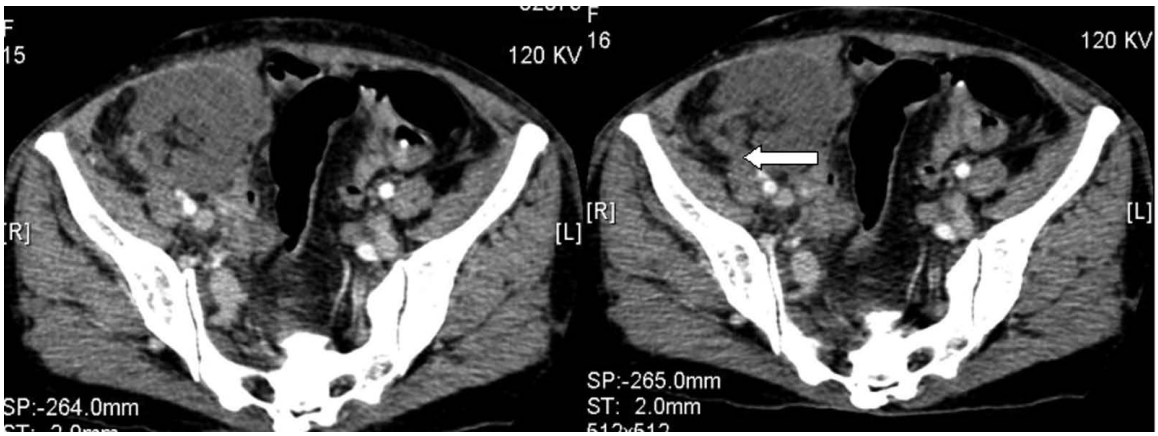

FIGURES 6.155A and B: Axial CECT in a post-transplant patient with graft dysfunction shows nonenhancing graft, there is abrupt termination of the renal artery (arrow in A) suggestive of occlusion, note the distal non-opacified artery (arrow in B).

Post-transplant Lymphocele

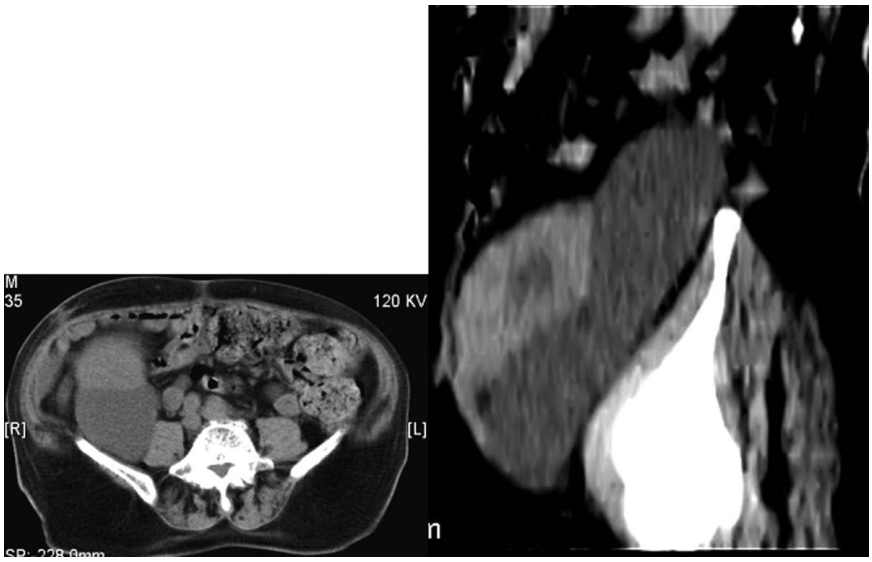

FIGURES 6.156A and B: Axial NECT in a patient with perigraft fluid collection showing an oblong walled of fluid collection posterior to the graft – aspiration of the graft was suggestive of lymphocele.

Post-transplant Renal Artery Stenosis

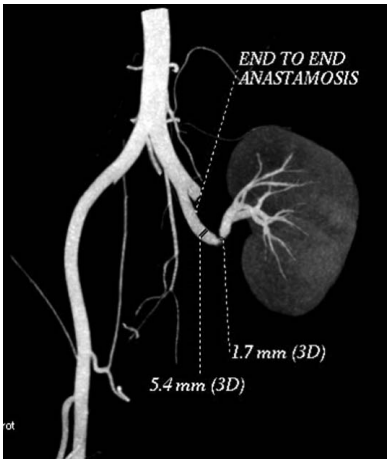

FIGURE 6.157: Coronal MIP showing left transplant kidney with a tight stenosis of the mid-transplant renal artery.

CHAPTER

7

Adrenal Gland

INTRODUCTION

The adrenal gland is a common site of disease, and detection of adrenal masses has increased with the expanding use of cross-sectional imaging. Radiology is playing a critical role in not only the detection of adrenal abnormalities but also in characterizing them as benign or malignant.

CT has been shown to be able to localize and define the appearance of the adrenal gland in 100% of patients with thin collimation (3 mm or less). CT is not only able to define the size of the gland but also helps to identify changes in tissue attenuation. The most common lesion of the adrenal gland is referred to as an incidentaloma and is an adenoma of the adrenal which can occur in upto 10% of patients. By understanding the various appearances of the adrenal gland on non-contrast, contrast and delayed CT scans, one is able to not only detect the presence of adrenal disease but be very specific as to its etiology in most cases.

The work-up of a suspected adrenal mass should start with appropriate biochemical screening tests followed by thin-collimation computed tomography (CT). If results of CT are not diagnostic, magnetic resonance (MR) and nuclear medicine imaging examinations should be performed. CT has become the study of choice to differentiate a benign adenoma from a metastasis in the oncology patient. If the attenuation of the adrenal gland is over 10 HU at nonenhanced CT, contrast material–enhanced CT should be performed and washout calculated. Over 50% washout of contrast material on a 10-minute delayed CT scan is diagnostic of an adenoma. For adrenal lesions that are indeterminate at CT in the oncology patient, chemical shift MR imaging or adrenal biopsy should be performed.

Abnormalities of the adrenal gland include primary neoplasm, metastases, hemorrhage, or enlargement of the adrenal gland from external hormonal stimulation. Adrenal masses can be divided into two physiologic categories based on whether they hypersecrete a hormone. Hyperfunctioning adrenal masses produce a hormone that results in a chemical imbalance and include pheochromocytomas, aldosteronomas, and cortisol or androgen-producing tumors. Nonfunctioning adrenal masses cause enlargement of the adrenal gland but no significant increased hormone production. Adrenal adenomas and metastases are the most common nonfunctioning adrenal masses.

Hyperfunctioning diseases of the adrenal gland originate from either the adrenal medulla (pheochromocytoma) or the adrenal cortex (Cushing syndrome, Conn syndrome, or hyperandrogenism).

ADRENAL PSEUDOMASSES

- Prominent lobation of the hepatic lobe, or hepatic tumor
- Gastric diverticulum and redundant gastric fundus
- Fluid filled duodenum/colon
- Splenic lobulation

- Tortuous or dilated splenic arteries and veins
- Pancreatic tail in an unusual location, or pancreas tail mass
- Exophytic upper pole renal mass
- Abundant suprarenal fat
- Focal thickening of adjacent diaphragmatic crus
- Retroperitoneal tumor localized in the area of adrenal gland.

Hyperfunctioning Adrenal Medullary Neoplasms

Pheochromocytoma is a neoplasm of the adrenal medulla. Although they are typically unilateral and benign, pheochromocytomas may be bilateral and malignant in 10% of patients. The tumor secretes catecholamines that can result in hypertension and palpitations. The clinical diagnosis is suspected in a younger patient with hypertension. The first-line tests for evaluating a patient with suspected pheochromocytoma are plasma catecholamine levels and 24-hour urine vanillylmandelic acid and metanephrine levels. These tests have sensitivities ranging from 89 to 100%, although false-negative values may result from exogenous drugs or episodic catecholamine production. Although hypertension is one of the most common symptoms of pheochromocytoma, pheochromocytomas are the cause of hypertension in less than 1% of hypertensive patients.

Hyperfunctioning Adrenal Cortical Neoplasms

The adrenal cortex is composed of three separate zones: the zona fasciculata, the zona glomerulosa, and the zona reticularis. The zona fasciculata produces cortisol, the zona glomerulosa produces aldosterone, and the zona reticularis produces androgens. All three are produced in response to adrenocorticotropic hormone (ACTH) produced by the pituitary gland; however, only cortisol has negative feedback on ACTH production. Hyperfunctioning tumors of the adrenal cortex can produce Cushing syndrome from cortisol overproduction, Conn syndrome from production of aldosterone, or hyperandrogenism from overproduction of androgens.

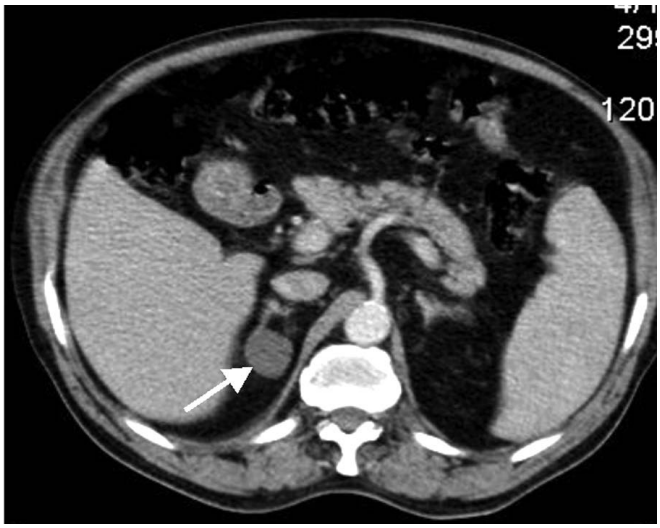

FIGURE 7.1: Axial CECT showing a well marginated low density right adrenal lesion arising from the lateral limb, with CT attenuation characteristics of an adenoma, lesion was incidentally picked up in a patient who was screened for interstitial lung disease.

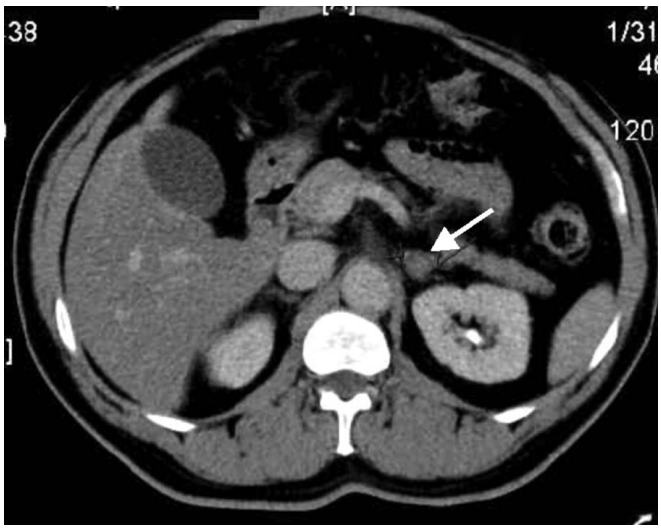

FIGURE 7.2: Axial CECT in a 34-year-old male patient who presented with uncontrolled hypertension and lab parameters suggesting an adrenal lesion reveals a focal marginally enhancing lesion in the left adrenal with feature of a functioning adenoma.

CT in Differentiating Benign from Malignant Adrenal Masses

At CT, certain imaging findings are helpful in differentiating benign from malignant lesions. Larger lesions have a greater likelihood of being malignant. In particular, lesions greater than 4 cm in diameter tend to be either metastasis or a primary adrenal carcinoma. The shape of the adrenal gland can also be helpful in predicting malignancy. Adenomas tend to have smooth margins and a homogeneous density, whereas metastases can be heterogeneous and have an irregular shape. However, although these findings are helpful in differentiating a benign from a malignant adrenal mass, they are not specific.

Currently, there are two main CT criteria used to differentiate benign adenomas from malignant adrenal masses. Intracellular lipid content of the adrenal mass represents the anatomic difference between adenomas and metastases, and differences in vascular enhancement patterns represent the physiologic difference. Adenomas have abundant intracytoplasmic fat in the adrenal cortex and thus have low attenuation at CT (lesion measuring less than 10 HU on non-contrast CT is a benign adenoma).

Conversely, metastases have little intracytoplasmic fat and thus do not have low attenuation at nonenhanced CT.

Two features can be measured at delayed CT: the attenuation value of the adrenal gland and the washout of contrast media. A Hounsfield unit of less than approximately 30 at 10 minutes after injection has been shown to be diagnostic of a lipid-rich adenoma; however, most adenomas have an attenuation value higher than 30, and thus it is a specific but not a sensitive test. A more useful parameter is the percentage of washout of contrast material in which the attenuation of the adrenal gland at delayed CT is compared with its attenuation at dynamic CT. Loss of 50% of the attenuation value of the adrenal mass at delayed CT is specific for an adenoma; less than 50% washout is indicative of either a metastasis or an atypical adenoma. Percentage of washout is typically calculated by the following formula: (1 - delayed enhanced HU value/initial enhanced HU value) × 100.

Although an attenuation value of less than 10 HU at nonenhanced CT is diagnostic of an adenoma, an attenuation value of greater than 10 HU is not diagnostic of a metastasis. A lesion greater than 10 HU at nonenhanced CT may be either an adenoma or metastasis.

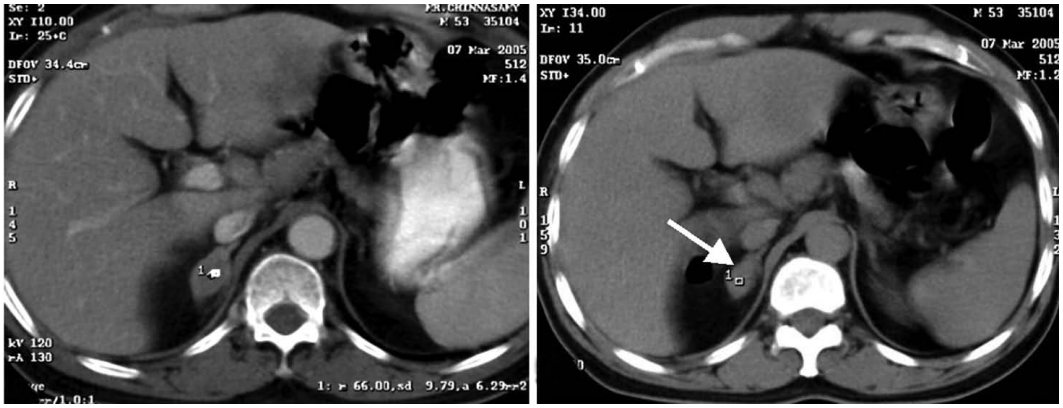

FIGURES 7.3A and B: Axial CECT with delayed imaging reveals persistent increased attenuation of the right adrenal lesion suggesting a metastatic lesion (arrow in B).

It is important to stress that if a lesion in an oncology patient cannot be definitively called an adenoma after CT examination, the patient should undergo further evaluation with MR imaging or an adrenal biopsy to confirm a benign or malignant adrenal lesion.

METASTASIS

Adrenals are the fourth most common site for blood-borne metastatic disease, common primaries to involve adrenal gland include carcinoma lung, breast, thyroid, and colon carcinoma. In up 15% of patients the adrenal is the only site of metastasis in patients with ca lung. Metastasis more often produces bilateral masses with soft tissue attenuation.

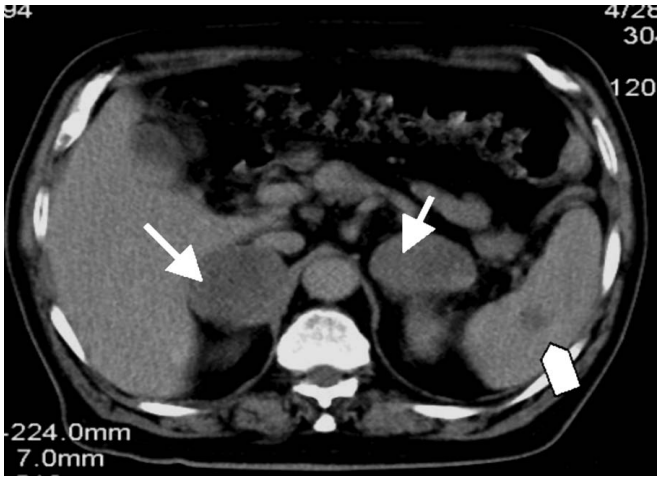

FIGURE 7.4: Axial CECT in a patient with right upper lobe lung carcinoma showing bilateral nodular adrenal masses (arrows). Note the hypodense metastasis in the spleen (arrowhead).

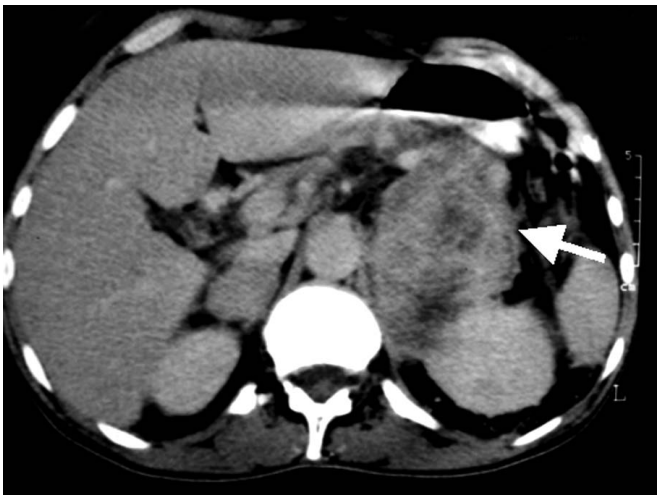

FIGURE 7.5: Axial CECT in a patient on radiation therapy for a central bronchogenic tumor in the right lung reveals bilateral adrenal lesion with the left adrenal lesion showing heterogenous enhancement with central necrosis.

ADRENAL MASS

- Large mass favors carcinoma
- Mass between 2-6 cm, pheochromocytoma/hyperfunctioning adenoma
- Calcification—old bleed, granuloma, carcinoma
- Small, hypodense homogenous lesion—adenoma.

Myelolipomas

Adrenal myelolipomas is a benign adrenal tumor consisting of mature fat interspersed with hematopoietic elements. These lesions most commonly occur in the adrenal gland as an incidental finding. CT is the study of choice as it demonstrates the presence of fat within these lesions making the diagnosis fairly straightforward. Please note that the amount of fat in an individual myelolipoma will vary from being nearly 100% fat to having only foci of fat. These lesions can bleed and if they do the fat will be difficult if not impossible to define. Myelolipomas are typically unilateral although bilateral myelolipomas have been reported in the literature. The key differential diagnosis point with myelolipomas is that when they are large they can be confused with retroperitoneal lipomas or liposarcomas. Practically, these lesions are typically discovered in older patients often as part of malignancy work-up. It is, therefore, important to recognize these lesions for their benign nature and that no biopsy or further evaluation is needed. In select cases, MR may be helpful but typically the diagnosis can easily be made on CT scan once one is familiar with the appearance of myelolipomas.

Myelolipomas as noted can bleed but this typically occurs in lesions that were larger and contained extensive fat. Average lesion size was over 10 cm in lesions that bleed.

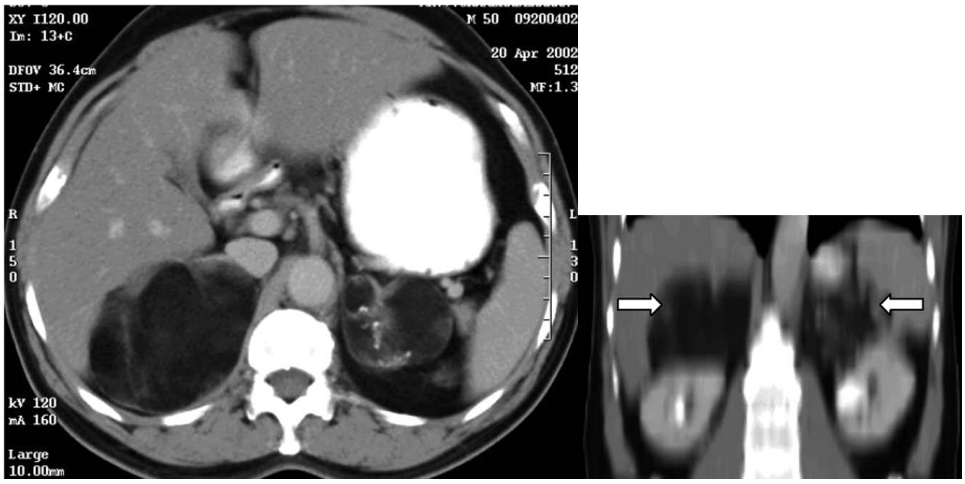

FIGURES 7.6A and B: Axial CECT reveals bilateral lobulated hypodense fat containing lesion involving both adrenal glands suggestive of myelolipomas.

Although one typically considers myelolipomas to be fatty tumors, it is important to recognize that the presence of calcification is not uncommon. The calcification in the lesions are punctate in nature and typically the presence of calcification is also accompanied by fat.

Miscellaneous

Adrenal hemorrhage is another a benign adrenal lesion that has a specific appearance in most cases. Adrenal hemorrhage can be seen due to a number of processes including stress, trauma, and anticoagulant therapy. Adrenal hemorrhage can be unilateral or bilateral with bilateral disease leading to an Addisonian crisis. The appearance of adrenal hemorrhage is an enlarged adrenal gland of high CT attenuation. The CT diagnosis is critical as the clinical diagnosis of adrenal hemorrhage is rarely even suggested by the referring physician.

Finally, another benign adrenal lesion is a lymphangioma. This is an uncommon lesion which is of low CT attenuation and usually measures between 3-5 cm in size.

There are other categories of benign adrenal lesions including old adrenal hematomas and adrenal cysts. There are true adrenal cysts, which are epithelial, or endothelial in nature and range in size from several centimeters to

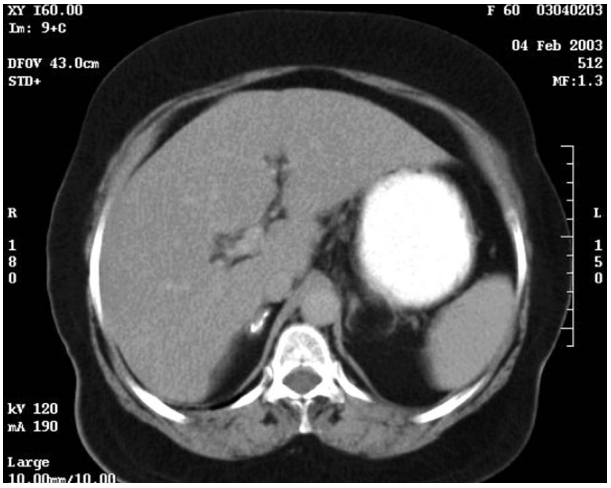

FIGURE 7.7: Axial CECT in a patient with healed left apical lung TB reveals right adrenal calcification.

15-20 cm in size. In our experience these are uncommon. Adrenal hematomas when chronic may look similar to adrenal cysts although a key differential diagnosis point is that they typically have thin calcifications of the cyst wall. This is very helpful in making the diagnosis.

Please note that other adrenal lesions can calcify. Calcification can be seen in unusual infectious diseases like hydatid disease as well as in TB and histoplasmosis. Adrenal hemorrhage, cystic neuroblastoma, lymphangioma, or true cysts may contain some degree of calcification though typically not along the border of the lesion.

Adrenocortical Carcinoma

Adrenocortical carcinomas are malignant tumors of the adrenal cortex that account for less than 0.2% of all cancers in the United States. They can occur at any age group but classically have a bimodal age distribution with the first peak occurring before age 5 and the second peak in the 4th and 5th decade of life. Interestingly, women comprise 65-90% of reported cases. Although most adrenal cortical malignant tumors are unilateral upto 10% may be bilateral.

The most common syndrome associated with adrenocortical tumors are hyperaldosteronism and Cushing syndrome. Cushing syndrome is present in 40% of patients with adrenocortical cancer. Feminization occurs less frequently in adults than Cushing's but is the most common hormonal syndrome in children with adrenocortical cancer. Although one often associates adrenocortical neoplasms with abnormal adrenal function, in over half of cases of adult patients there is no recognizable endocrine syndrome. These patients typically present with a large mass or with symptoms due to abdominal pain, palpable mass, weight loss or distant metastases.

Staging for adrenocortical carcinomas is based on tumor size, nodal involvement, invasion of adjacent organs and presence of distant metastasis. Only Stage 1 and Stage 2 lesions are curable surgically and unfortunately most patients are at Stage 3 or Stage 4 at time of diagnosis. The 5-year survival for Stage 3 disease is under 30%. Common sites of metastases from adrenal carcinoma are to the lymph nodes, the lung parenchyma, liver and skeletal system.

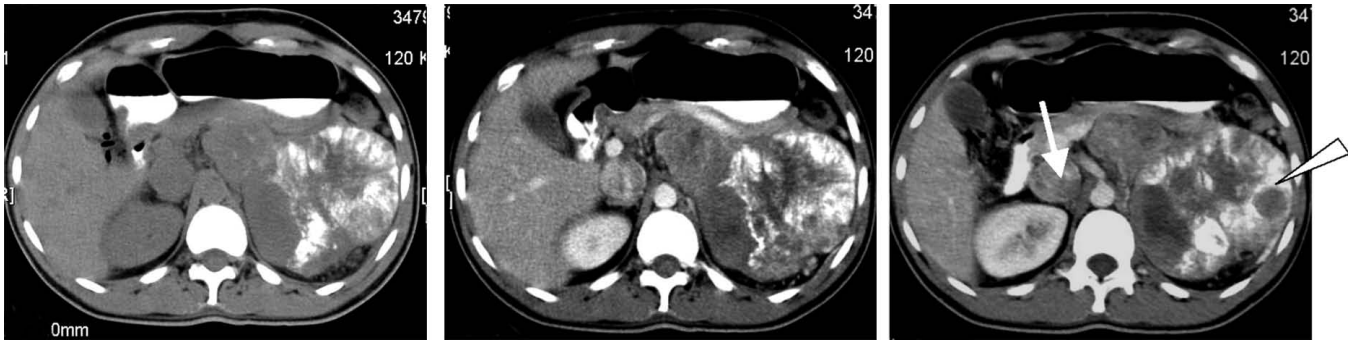

FIGURES 7.8A to C: Axial plain and CECT showing a large left adrenal lesion showing heterogeneous enhancement with confluent calcifications (arrowhead), note the enhancing luminal thrombus in the IVC (arrow).

CT staging as well as definition of the tumor bed is helpful in determining the best approach for the individual patient.

Pheochromocytoma

Pheochromocytomas are one of the few curable cause of hypertension although they are found in far less than 1% of all hypertensive patients. The prevalence of pheochromocytoma ranges from 3 to 95% in autopsy and so we will discover incidental pheochromocytomas in clinical practice. Radiographically and clinically, there is no way to determine and distinguish benign from malignant pheochromocytomas.

Ninety percent of pheochromocytomas arise in the adrenal medulla and 97% arise below the diaphragm. Roughly 2-3% of all pheochromocytomas are thoracic in location. Pheochromocytomas commonly follow the rule of 10, in that 10% are bilateral, malignant, multifocal, extrarenal or found in children or associated with the familial syndrome. Interestingly, upto 30% of extra-adrenal pheochromocytomas are malignant in contrast to about 2.5% of intra-adrenal pheochromocytoma which are malignant pheochromocytomas. Pheochromocytomas can be diagnosed because of their excess catecholamines although in some cases the tumors will secrete ACTH. Other causes of ectopic ACTH production include small cell cancer of the lung, and medullary thyroid cancer.

Although CT or MR to be the study of choice for the evaluation of pheochromocytoma, it is important to recognize that biochemical screening for pheochromocytoma can be 100% sensitive and specific. The measurement of catecholamines and their metabolites in 24-hour urine collections approaches 100% sensitivity and specificity. Once laboratory test or biochemical screening focuses on the diagnosis of pheochromocytoma, radiologic imaging studies are done for evaluation. CT and MR are commonly used. CT classically will show 3-5 cm mass which is hypervascular with contrast material. When we scan a patient for pheochromocytoma, we obviously will carefully scan the adrenal gland. If no evidence of adrenal lesion is seen, then needs to scan the length from the diaphragm through the aortic bifurcation with specific emphasis on the most common site of extra-adrenal pheochromocytoma which is the organ of Zuckerkandl.

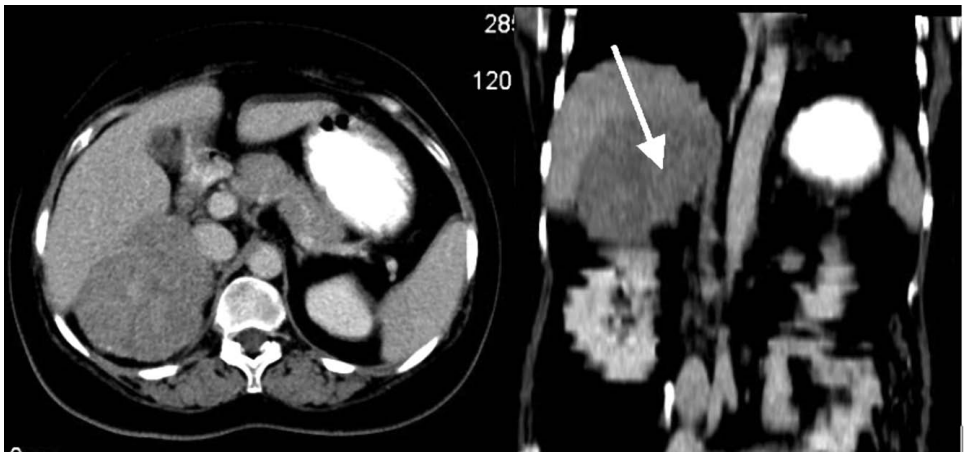

FIGURES 7.9A and B: Axial CECT with coronal reformation reveals a large hypodense mass in the right adrenal (arrow) in Figure B—case of pheochromocytoma.

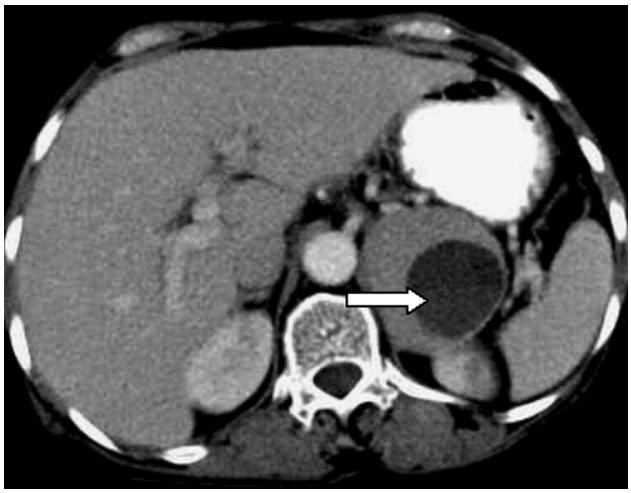

FIGURE 7.10: Axial CECT in a patient with hypertension reveals a left adrenal well marginated lesion with a central fluid–fluid level (arrow) a specific feature of pheochromocytoma.

NEUROBLASTOMA

It is the most common extracranial, solid malignant neoplasm of chidhood accounting for approximately 10% of all pediatric neoplasm. More than 80% of cases are diagnosed below 3 years of age and more than 50% have metastasis at the time of diagnosis.

They arise from adrenal medulla and the sympathetic ganglia as well, they commonly occur on the left side of the body. On CT they appear as irregular shaped, solid masses of predominantly soft tissue density that have areas of necrosis, hemorrhage and calcification.

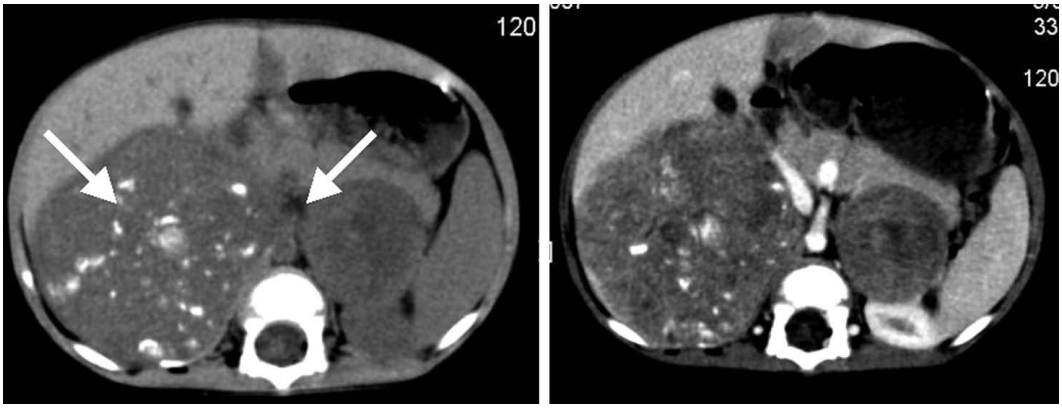

FIGURES 7.11A and B: Axial plain and CECT in a 3-year-old girl reveals large heterogeneous well marginated hypodense mass in both the adrenals (arrows), note multiple calcifications in the right adrenal lesions—case of neuroblastoma

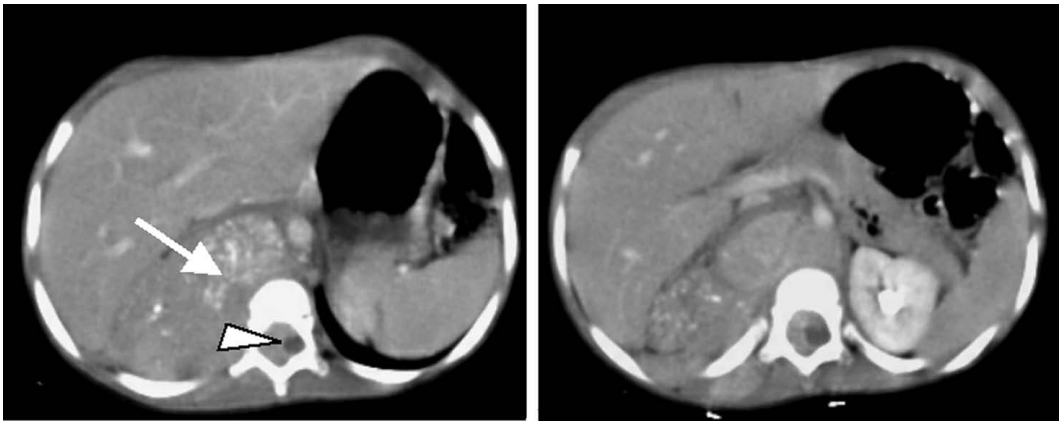

FIGURES 7.12A and B: Axial CECT in a 2-year-old female reveals a heterogeneous right adrenal mass with punctuate calcification (arrow). Note the epidural extension causing mass effect over the thecal column (arrowhead).

ADRENAL HYPERPLASIA

Adrenal hyperplasia is seen in 8-10% of cases of Cushing's syndrome and 15-20% of cases of hyperaldosteronism. Most cases are corticotropin-dependent due to pituitary causes. Most cases are seen in adults. Enlargement may be a smooth hyperplasia or cortical nodular hyperplasia.

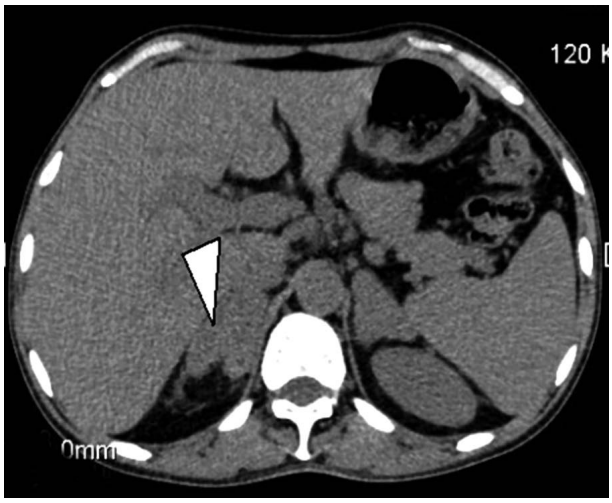

FIGURE 7.13: Axial CT reveals bilateral adrenal enlargement, note the preservation of the shape suggestive of hyperplasia.

ADRENAL CYST

Adrenal cysts are classified into parasitic, epithelial, endothelial (lymphangitic, angiomatous, and hamartomatous) and pseudocystic (due to necrosis or hemorrhagic). Adrenal cysts typically produce rounded, low density masses with a smooth well-defined contour.

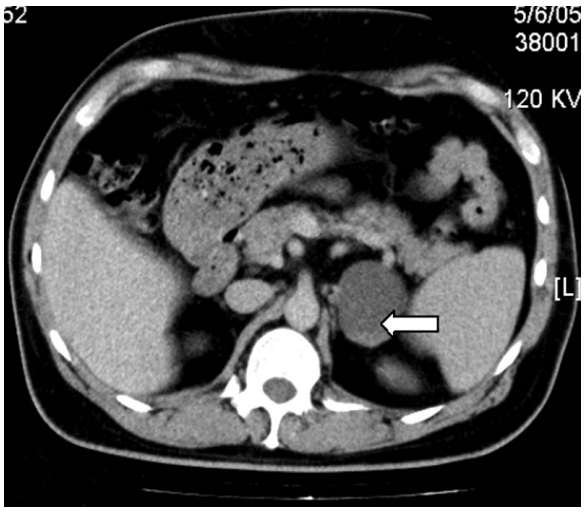

FIGURE 7.14: Axial CECT in a 49-year-old male patient with vague left flank pain of 1 week duration reveals a well marginated cyst in the left adrenal replacing the gland with a thin hyperdense fuid-fluid level (arrow) suggesting hemorrhage.

CONGENITAL ADRENAL CORTICAL HYPERPLASIA

Results due to block of adrenal cortical steroid synthesis, the absence of steroid synthesis induces chronic overproduction of ACTH by the pituitary gland causing adrenal hyperplasia. CT demonstrates large hyperplastic gland which may have areas of calcification, necrosis, and hemorrhage.

ADDISON'S DISEASE

At least 90% gland has to be destroyed before hypoadrenalism can become evident, most common documented cause has been tuberculosis. Hemorrhage or idiopathic atropy, lymphoma, metastasis hemochromatosis, can also cause hypoadrenalism.

CT findings show calcification with atropic adrenals.

INFECTIONS

Tuberculosis, histoplasmosis, are the most frequent infectious agents affecting the adrenal gland. Infection can result in adrenal calcification or solid or cystic masses may be unilateral or bilateral. Adrenal TB involvement can be present without lung lesions and pulmonary cultures may be negative.

Adrenal abscesses caused by hematogenous infections are more common in neonates.

Differential Diagnosis for Adrenal Lesion

Adrenal Malignancies

- Neuroblastoma
- Ganglioneuroma
- Ganglioneuroblastoma
- Pheochromocytoma
- Adrenal cortical carcinoma

Nonmalignant Adrenal Disease

- Cushing's syndrome
- Conn's syndrome
- Adrenogenital syndrome
- Adrenal hyperplasia

Unilateral Adrenal Lesions

- Adrenal adenoma (incidentaloma)
- Functioning adrenal adenoma
- Metastases
- Hyperplasia
- Infectious disease
- Myelolipoma
- Pheochromocytoma
- Metastases
- Primary adrenal carcinoma
- Hemorrhage

Calcific Adrenal Lesions

- Tumoral calcification
- Chronic hematoma
- Tuberculosis, histoplasmosis
- Wolman's disease.

CHAPTER

8

Gastrointestinal System

CT INDICATION FOR EVALUATING THE GUT

1. Diagnosing or suggesting the presence of primary gut disease.
2. Evaluating the nature and extent of a known gut disease.
3. Determining the presence, location, and severity of secondary lesions such as phlegmons, abscess, and perforations.

Advantage of CT in evaluating the gut is that it provides a direct imaging of serosal, mural, and intraluminal abnormalities as well as information regarding the extravisceral structures. Because bowel wall thickening is the single most important indicator of GI abnormality on CT, adequate CT examination of gut requires bowel discrimination and distention best achieved by administration of oral and IV contrast.

As a general rule before the start of the scan the radiologist should determine whether IV or oral contrast has to be given for the particular indication.

Technical Considerations

1. Luminal opacification with oral contrast is very essential to deliniate the wall thickness and the mucosa (800 ml of 2% barium or gastro graafian in water one hour before scan). Additional 100-200 ml can be given 5 minutes before the scan.
2. If the region of interest is in the distal large bowel gastrograafian enema can be given.
3. Subtle lesions can be detected by obtaining scans in the decubitus position or in prone position based on the need.
4. Intravenous contrast should be used to evaluate the pattern of enhancement and the nature of thickening.

Points to be Evaluated

1. Identification of areas of bowel thickening or inhomogeneity.
2. Evaluation of luminal and serosal surface.
3. Inspection of adjacent peritoneal and mesenteric and perivisceral retroperitoneal fat planes.
4. Evaluation of lymphadenopathy and blood vessels.
5. General inspection of abdominal cavity for mural and extramural gas, abscess, fistulae, sinus tract.
6. Evaluation of parenchymal organs for focal or diffuse diseases.
7. Visualization of skeletal structures.

Pitfalls

1. Empty or fluid filled bowels may mimic soft tissue lesions,

2. Non-distended loops if evenly thickened and homogenously enhancing should not be falsely diagnosed as tumoral thickening. Bowel in a distended state rarely exceeds 2 mm in thickness.

Regimens for Abdominal Survey

First step is to determine whether oral or IV contrast has to be given, based on patients history and previous imaging findings.

Additional contrast usage like rectal contrast, prone or decubitus scans to be decided.

Planning of scanning sequence like arterial phase/portal phase studies.

Consideration for Specific Areas

Esophagus

Technique: To obtain good distention continuous sipping of oral contrast can be tried in cooperative patient. In uncooperative patients the air they swallow can be used as negative contrast.

Distended esophagus measures less than 3 mm, thickening over 5 mm has to be considered abnormal.

If nondistended the air in the lumen has to be present centrally.

Anatomy: The esophagus extends from pharynx to the cardia of stomach. It is 20-25 cm in length and distends upto 30 mm in width. It is grossly divided into three parts:

1. Cervical segment—located near the midline and is posterior to the trachea in the neck.
2. Thoracic segment—lies behind the trachea till the bifurcation.
3. Retrocardiac segment—lies behind the heart.
4. Abdominal segment—shortest segment, reaches the cardia of stomach via the hiatus.

On CT esophagus appears as well delineated circle of soft tissue, wall thickness should not exceed 3 mm in size, a small amount of air is usually seen, but a airfluid level, fluid-filled lumen, lumen caliber more than 1cm usually indicate obstruction or dysfunction.

Stomach

Technique: For adequate gastric distention oral contrast has to be ingested just before scan. As much as 750-1000 ml of oral contrast is to be used based on the patient's habitus.

Normal gastric wall except for the fundus should measure 2-5 mm. Right decubitus is used for visualizing the antrum. And left decubitus for distending the fundus.

The normal go junction can produce a smooth bulge along the medial border of the cardia, the perigastric ligament contain major vascular structures and nodes, and are important pathway for metastasis, the gastrohepatic ligament is the most superior portion of the lesser omentum and contains the left gastric artery and vein.

Duodenum

Technique: Usually inadequately opacified because of vigorous peristalsis, decubitus position can be used.

Anatomy: Apart from the duodenal bulb and a short segment distal to the ligament of Treitz, the duodenum is a retroperitoneal structure, with adequate distention the wall should measure a maximum of 10 mm.

Small Intestine

If primary indication for CT is for small bowel evaluation adequate distention is needed with at least 1500 ml of oral

contrast. Metaclopromide can be used sometimes to promote motility. The contrast has to be diluted well to avoid artifacts and must be administered 25-30 minutes prior to the study.

On CT normal small bowel is 2-3 mm in thickness and more than 4 mm is considered abnormal. The thickness of valvulae should not exceed 3 mm.

Colon

Antegrade filling can be achieved by administering oral contrast 3 to 7 hours prior to the procedure, retrograde filling can be produced by enema. Patients with suspected enterovesicle fistula should have pelvic imaging first with oral or rectal contrast prior to IV contrast injection.

Alternative techniques include ingestion of 500 ml of oral contrast followed by ingestion a tablet of metaclopromide, which hastens the transit of oral contrast material.

On CT colon is visualized by its anatomic location, and its typical haustral morphology, recognition of caecum is facilitated by visualization of the terminal ileum, the ascending and descending colons are within the anterior pararenal space. The transverse colon is seen suspended within the peritoneal cavity by the mesocolon.

The rectum is about 12-15 cm in length, the peritoneum covers the anterior surface of the upper rectum. The lower two thirds is enveloped by a extraperitoneal connective tissue. The wall of colon measure 3 mm when the colon is distended.

Computed tomography demonstrates intestinal wall abnormalities that can be analyzed by categorizing attenuation changes in the intestinal wall. These attenuation patterns include white, gray, water halo sign, fat halo sign, and black.

The **white pattern** represents avid contrast material enhancement that uniformly affects most of the thickened bowel wall. If the bowel wall is enhanced to a degree equal to or greater than that of venous opacification in the same scan, it should be classified in the white attenuation, also look for dilated periintestinal vessels. Common diagnoses with this sign include idiopathic inflammatory bowel diseases, vascular disorders, infectious diseases, and radiation damage.

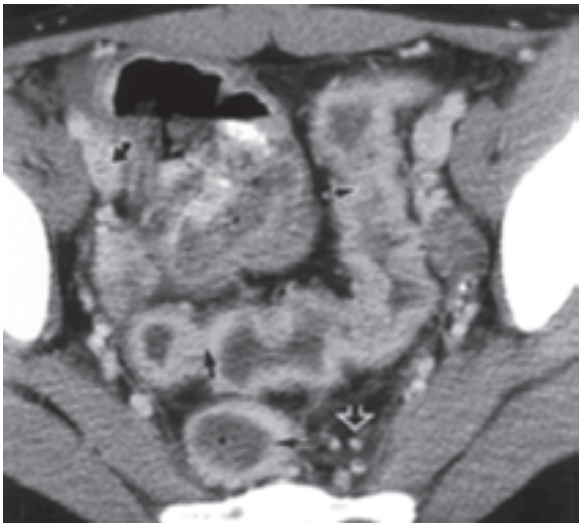

FIGURE 8.1: Suspected ulcerative colitis showing intensely enhancing mucosa.

The **fat halo** sign refers to a three-layered pattern. Common diagnoses with this pattern include idiopathic inflammatory bowel diseases (Fig. 8.2).

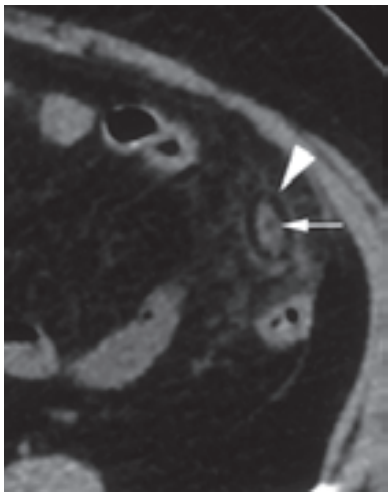

FIGURE 8.2: Axial CT showing the fat halo sign.

Pitfalls—Intramural fat may exist in both the distal ileum and colon as a "normal" variant in patients without gastrointestinal symptoms or a history of gastrointestinal disease. In the small intestine, normal intramural fat is seen most commonly in the terminal ileum. In the colon, it is found most often in the descending colon. The normal intramural fat layer is generally very thin, usually thinner than the fat stratum seen with idiopathic inflammatory bowel diseases.

The **gray pattern** is defined as a thickened bowel wall with limited enhancement whose homogeneous attenuation is comparable with that of enhanced muscle. This pattern is used to differentiate between benign and malignant disease, but it is the least specific of the patterns and should be combined with morphologic observations (Fig. 8.3A).

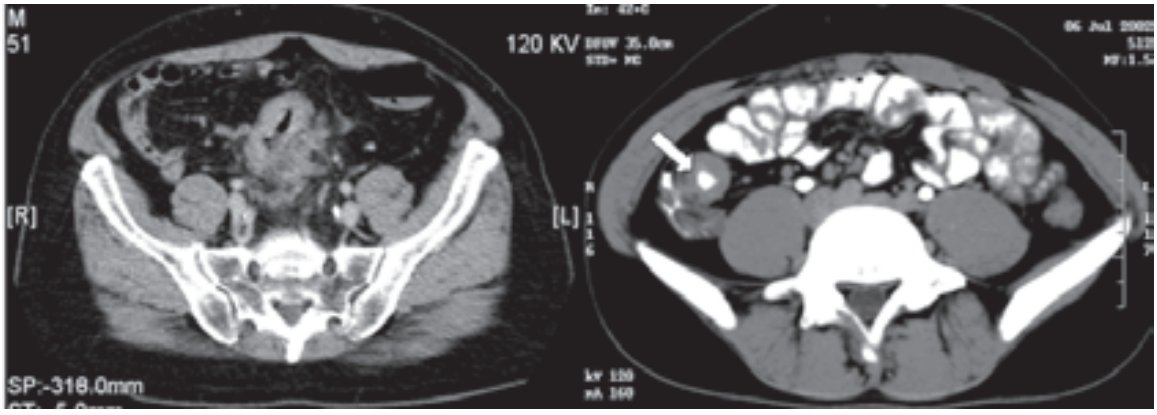

FIGURES 8.3A and B: Axial CT showing the gray pattern.

Pitfalls—A common cause of false-positive diagnosis in either the small intestine or colon is incomplete luminal distention.

The gray attenuation pattern is the least specific of the five attenuation categories for diagnosis, and it is common in both benign and malignant diseases. Macari and Balthazar noted that bowel wall thickening of less than 2 cm was more characteristic of benign conditions, whereas thickening greater than 3 cm was usually present in neoplastic cases.

The **water halo** sign indicates stratification within a thickened bowel wall that consists of either target sign of thickened bowel in which the middle or "submucosal" layer has a fatty attenuation. Common diagnoses with this sign include Crohn disease in the small intestine and idiopathic inflammatory bowel diseases in the colon (Fig. 8.4).

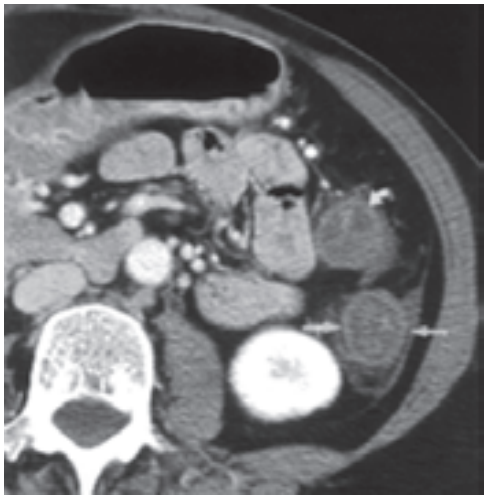

FIGURE 8.4: Axial CT showing water halo sign.

Pitfalls—Hounsfield unit measurement and histologic correlation suggest that the pathophysiologic underpinning of the water halo sign is most likely edema. The finding is therefore categorized as the water halo sign to distinguish it from the fat halo sign of category 4. Although eyeball differentiation of the two signs is usually sufficient, a positive Hounsfield unit value rather than the negative Hounsfield unit value of fat helps confirm the finding.

Black attenuation is the equivalent of pneumatosis, and this pattern is commonly seen in ischemia, infection, and trauma.

Pitfalls—The challenge is not only to detect small collections of intramural gas but to avoid confusing them with intraluminal gas collections that cling to the mucosa. Initial positive detection is made by recognizing gas bubbles within the dependent bowel wall, some of which have a geometric rather than round configuration (Fig. 8.5).

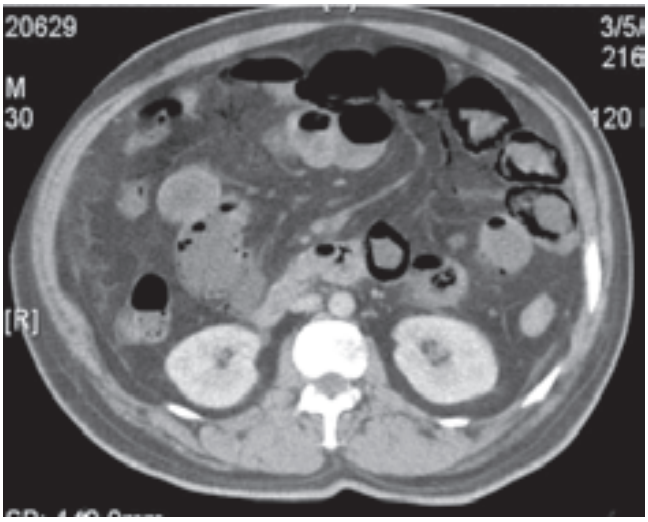

FIGURE 8.5: Axial CT showing the black pattern.

TECHNIQUE FOR GASTRIC CT

Oral Contrast Agent

For dedicated imaging of the stomach, adequate distention is essential. If the stomach is not well distended, disease may be overlooked or, conversely, the collapsed gastric wall may mimic disease.

Traditionally, high-attenuation contrast agents have been administered to enhance and distend the stomach and gastrointestinal tract. These agents can be categorized as positive contrast agents because they have a CT attenuation greater than that of water.

Although these agents are safe, well tolerated, and result in good gastric distention, they may not be optimal when CT angiography is done. The contrast agent may obscure enhanced vessels, thereby necessitating extensive editing.

Occasionally, positive oral contrast material may not mix uniformly with gastric contents, and pseudotumors can be created, on both axial and endoluminal images. Because the wall of the gastrointestinal tract can enhance upto 120 HU after the intravenous administration of contrast material, the high-attenuation intraluminal contrast material may mask subtle disease.

Whole milk has been proposed as a possible CT oral contrast agent and is routinely used for CT angiography. Milk is emptied from the stomach relatively slowly and has a slower small bowel transit time than water.

Water as an oral contrast agent in patients with suspected gastric disease. It distends the stomach wall, allows good visualization of the enhancing wall. When CT is performed specifically to evaluate the stomach, the patient is given 750 mL of water approximately 15 minutes before scanning. An additional 250 mL is given immediately prior to the study.

One disadvantage of using water as an oral contrast agent is that it results in suboptimal distention of the distal small bowel. Some authors have advocated administering positive contrast material initially, followed by water. The positive contrast material will fill the distal small bowel loops, and the water will distend the stomach and proximal small bowel.

Inflammatory Conditions

Gastritis

The most common CT finding in patients with gastritis is thickening of the gastric folds and wall. In severe cases, the gastric wall will demonstrate low attenuation compatible with submucosal edema and inflammation. At the same time, the mucosa may enhance due to hyperemia. This enhancement may give the wall a layered appearance, which is most pronounced at arterial phase imaging. This layering or "halo" will help distinguish gastritis from other conditions that cause gastric wall thickening (e.g. neoplasms). Neoplasms will not penetrate the layers of the gastrointestinal tract wall and therefore will not create this striated or halo appearance.

Emphysematous Gastritis

Emphysematous gastritis is an uncommon entity that is usually caused by invasion of the gastric wall by a gas-producing organism, typically *Escherichia coli*. At CT, the stomach is thickened and there is air within the layers of the wall. Air within the gastric wall may rarely occur after caustic ingestion or gastric infarction. The CT appearance of these two entities can be identical. However, patients with benign gastric emphysema are asymptomatic, and the condition tends to resolve spontaneously.

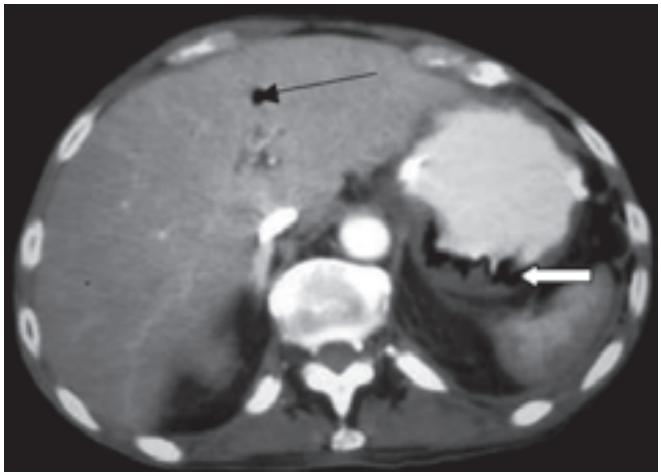

FIGURE 8.6: Axial CECT in a patient with caustic ingestion reveals linear hypodensity in the gastric wall suggestive of air, note the speck of air in the left portal vein branch (thin arrow).

Gastric Neoplasms

Gastric Adenocarcinoma

Gastric adenocarcinoma comprises 95% of primary gastric malignancies.

It is well known that there is a difference in the prevalence of gastric cancer between the East and the West. There is also difference in the rate of detection of early gastric cancer in different countries. Western literature has reported the detection of Early Gastric Cancer (EGC) in 10 to 20% of all resections for gastric carcinoma. The reported detection of EGC in surgical specimens in Japan has been 40% or more. The differences in the rate of early gastric cancer is probably the result of screening endoscopy practiced in Japan since the 1960s.

Early gastric cancer (EGC, also called superficial spreading carcinoma)is defined as adenocarcinoma limited to the gastric mucosa and submucosa regardless of whether regional lymph nodes are involved or not.

Pathogenesis

Environmental factors appear to play a significant role in the pathogenesis of gastric cancer. Dietary nitrites used prominently in food preservation in higher risk regions have received a great deal of attention and may play an important role in the pathogenesis of this cancer. Several definite risk factors have been identified, some to such a degree that surveillance is advised by some. Gastric mucosa with high-grade dysplasia, familial adenomatous polyposis, gastric adenomas and Barrett's esophagus (for Ca of GE junction and gastric cardia) are factors with the highest known risk for gastric cancer. Other risk factors considered to have definitely higher risk are mucosa with intestinal metaplasia, chronic atrophic gastritis including patients with pernicious anemia, *Helicobacter pylori* infection, and hereditary non-polyposis colorectal cancer (Lynch II) syndrome. Patients over 20-years removed from undergoing subtotal/ near-total gastrectomy are also probably at higher risk.

Clinical Features and Diagnosis

1. *Early gastric cancer:* Observational studies have shown that approximately 70% of patients with EGC have symptoms of uncomplicated dyspepsia and are not complicated by anemia, dysphagia, or weight loss. A high level of suspicion needs to be kept in mind to consider an endoscopic examination especially in groups in which incidence are higher.
2. *Advanced gastric cancer:* The majority of patients present with advanced disease with symptoms such as weight loss, vomiting, anorexia, early satiety, abdominal pain, and anemia. These symptoms often mimic peptic ulcer disease or other gastrointestinal conditions.

Advanced gastric cancer is the much more common form of gastric cancer at the time of diagnosis, even in Japan with its long-standing screening program. The location of the cancer is in the antrum 50% of the time and in the body 25% of the time. The remainder is in the cardia or comprises the entire stomach. Advanced carcinoma may be fungating, polypoid, flat (superficial), ulcerated, or diffusely infiltrating (linitis plastica). 60-70% of gastric cancers are ulcerating or fungating. Ulcerating types may mimic benign ulcers, but are usually larger, have more heaped up edges (rather that appearing "punched out"), and have a more irregular or "shaggy" base. Linitis plastica or "leather bottle" stomach makes up 10% of cases. There is no luminal mass, but the stomach wall is diffusely infiltrated and usually markedly thickened. There are two basic pattern of gastric adenocarcinoma histologically: intestinal (expanding) type and diffuse (infiltrating) type. The former presents a picture of a fairly cohesive mass of relatively well-differentiated glands or cords of tumor cells tending to push as a broad front onto the gastric wall. This type is often associated with adjacent intestinal metaplasia of the gastric mucosa. This histologic pattern seems to be decreasing in frequency. The diffuse type involves individual tumor cells permeating into the gastric wall diffusely. Frequently, the cytoplasmic mucin is found to push aside the nucleus, forming a "signet ring cell" appearance. This is seen more commonly in women and has not changed in frequency.

Regional lymph nodes and liver are the most common sites for metastasis. Occasionally, spread to ovaries, supraclavicular (Virchow's) nodes, or peritoneal cul-de-sac may be the first sign of the disease. Ovarian tumors that contain signet-ring cells, metastatic from a gastric carcinoma primary, are called Krukenberg tumors. These are typically bilateral. Rarely, they may originate from cancers of other sites, such as colon or appendix.

Gastric Lymphomas

These are almost always of the non-Hodgkin's type, and usually are secondary foci of widely disseminated lymphoma. Primary gastrointestinal lymphoma is most commonly gastric and comprises only 3-5% of all gastric malignancies. These lymphomas have no systemic involvement until very late in their course, by definition. Patients with AIDS have a five-fold increased risk for GI lymphomas. One of the types of gastric lymphoma is the *mucosa associated lymphoma tumor* (MALT), which has gained much attention in recent years because of its association with *Helicobacter pylori*. *H. pylori* has been implicated as a potential etiologic factor in the pathogenesis of gastric lymphoma, particularly MALT lymphomas. More that 90% of low-grade MALT lymphomas are positive for *H. pylori* infection. Additionally, *eradication of H. pylori has resulted in the regression of gastric MALT lymphoma* in several case reports.

Stromal Tumors

These were formerly called leiomyomas and leiomyosarcomas, as it was thought that gastric smooth muscle was the origin of these tumors. More recently it has become apparent that other tissues such as neural (Interstitial cells of Cajal) and vascular endothelial tissue may be the tissues of origin. The term gastrointestinal stromal tumor (GIST) has been adopted and denotes tumors arising from stromal tissue with no definite cell line of origin and varying in patterns of differentiation.

Gastric Carcinoid

Most GI carcinoids are found within the small bowel, and only 2% are found within the stomach.

Carcinoid syndrome does not develop until hepatic metastasis has occurred. Further discussion of the carcinoids is given below.

Post Gastrojejunostomy CT

In addition to assessing for routine postoperative complications such as abscess, hematoma, or pancreatitis, CT aids in assessing the structural and functional integrity of the billroth 2 anastomosis, in patients with poor gastric transit CT can help differentiate anatomic causes of anastomotic compromise such as peristomal edema, or perianastomotic abscess, afferent loop syndromes can be identified.

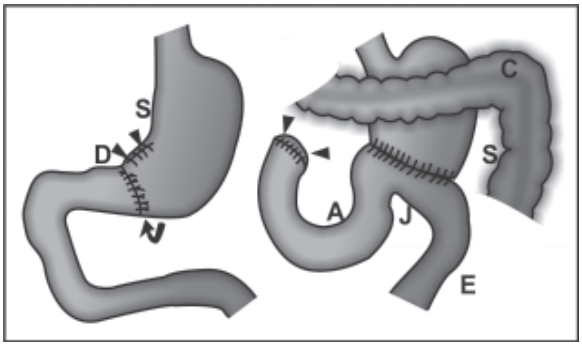

FIGURES 8.7A and B: (A) Gastroduodenostomy (B) gastrojejunostomy.

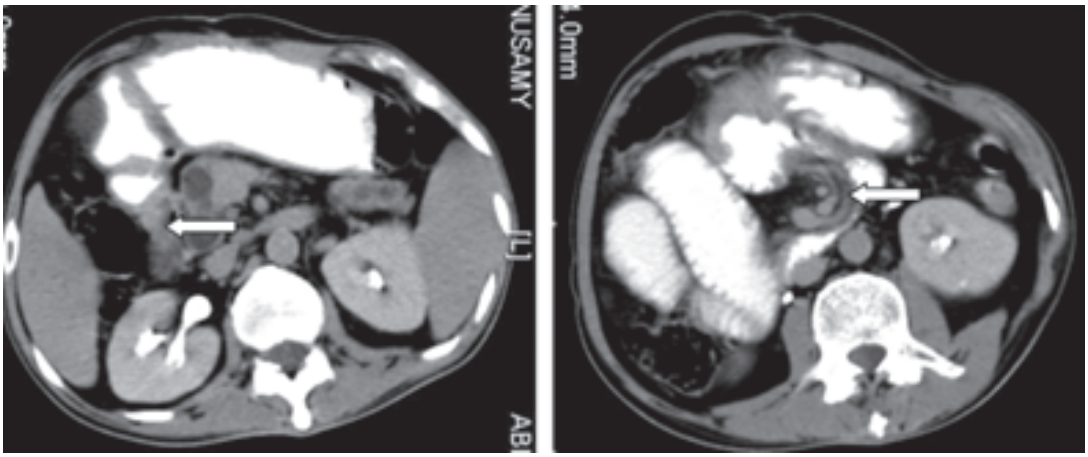

FIGURES 8.8A and B: Axial CECT in a patient with duodenal ulcer reveals gastrojejunostomy (arrow in B), note the contracted duodenum causing CBD dilatation (arrow in A).

Miscellaneous Cause of Gastric Wall Thickening

A wide range of pathological entities produce gastric wall thickening on CT apart from malignancy they include Menietrier's disease were thick folds upto 3 cm are seen predominantly in the fundus and body.

Gastritis

Antrum is involved in Crohn's disease, antral thickening is also seen in chronic granulomatous disease of childhood and also in HIV, gas is seen in patients with emphysematous gastritis. Fold or wall thickening is also seen in Zollinger-Ellison syndrome and eosinophilic.

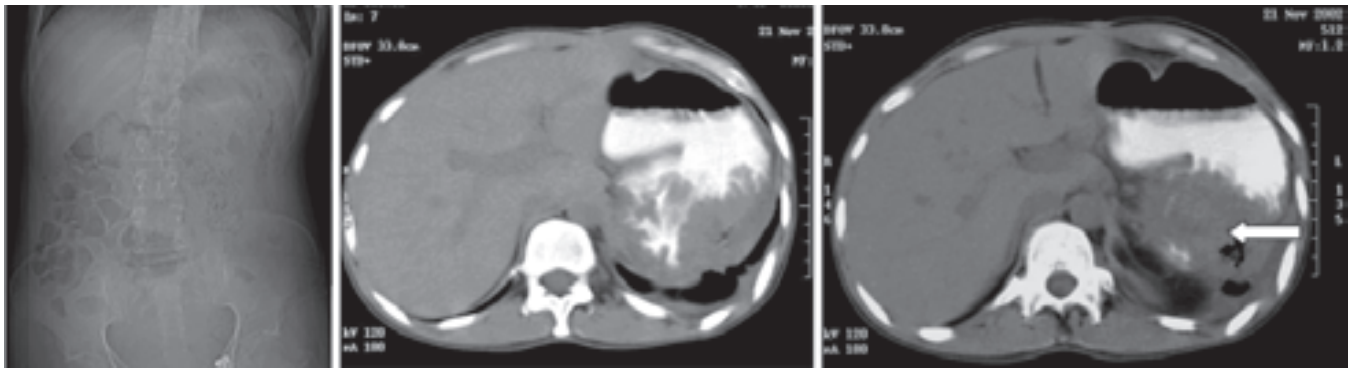

FIGURES 8.9A to C: Axial CECT in a patient with long-standing documented gastric ulcer showing perigastric abscess with air pockets and deep ulcer (arrow in C).

CT of Malignant Gastric Masses

Adenocarcinoma is the commonest primary tumor of the stomach with antrum being the most common site, patterns of involvement include focal ulcerative mass, diffuse infiltrative pattern, focal area of thickening.

CT Staging of Gastric Adenocarcinoma

Stage 1—luminal mass without wall thickening, no evidence of local or distal spread of disease.
Stage 2—thickened gastric wall (>1cm) without invasion of adjacent organs or distant metastasis.

Stage 3—thickened gastric wall with direct extension into adjacent organs, no distant metastasis.
Stage 4—any tumor stage with distant metastatic disease.

CT findings	*Lymphoma*	*Carcinoma*
Wall thickness	4 cm	1.5
Average	2-7 cm	1.2-3
Range		
Extent	Diffuse	Focal
Lymphadenopathy above and below renal hilum.	40%	0%

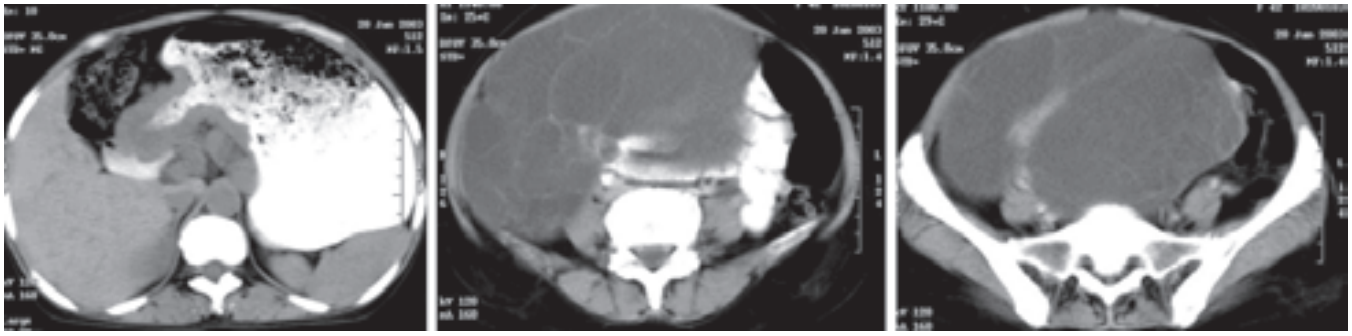

FIGURES 8.10A to C: CECT Fig. A reveals circumferential mural thickening of the gastric antrum causing luminal narrowing, peritoneal and pelvic cavity shows exudative septated fluid collection suggestive of carcinomatosis.

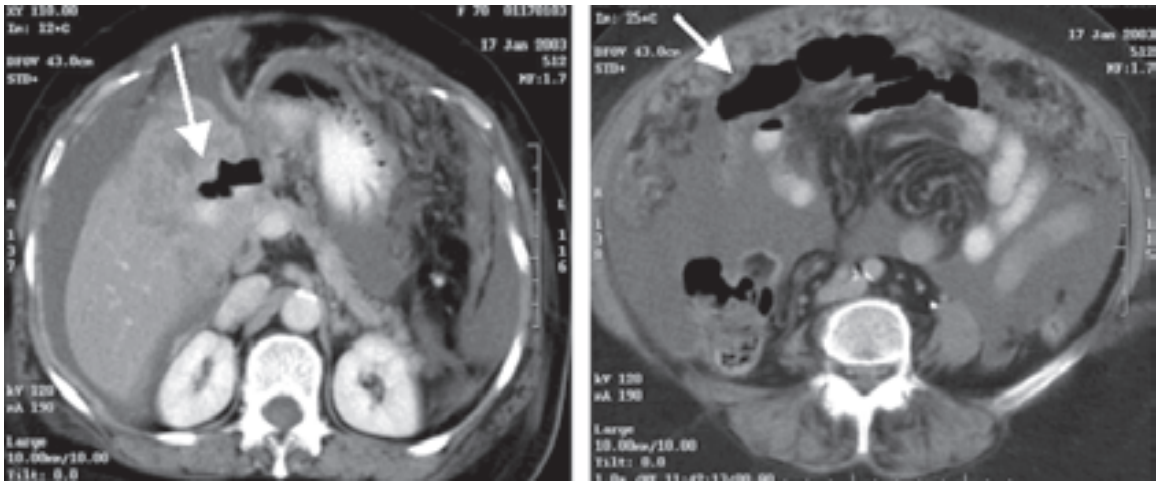

FIGURES 8.11A and B: Axial CECT in a patient with antral malignancy (arrow note the infiltration into liver) shows extensive peritoneal thickening (arrow in Fig. B) with free fluid.

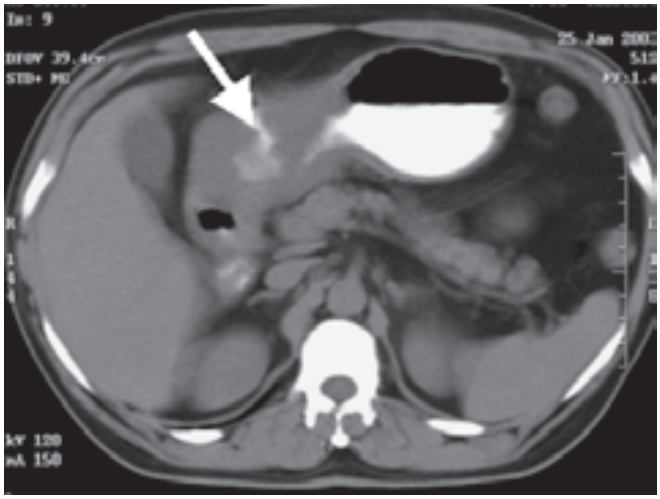

FIGURE 8.12: Axial CECT reveals circumferential mural thickening involving the antrum with ulceration (arrow), note the preservation of periserosal fat.

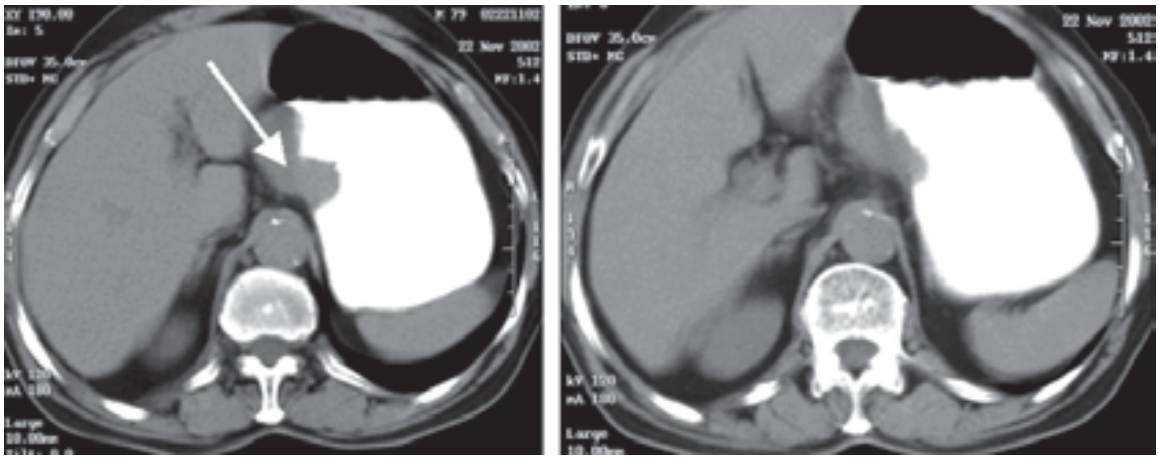

FIGURES 8.13A and B: Axial CECT reveals a focal thickening with mucosal irregularity (arrow) in the gastric fundus adjoining the GO junction.

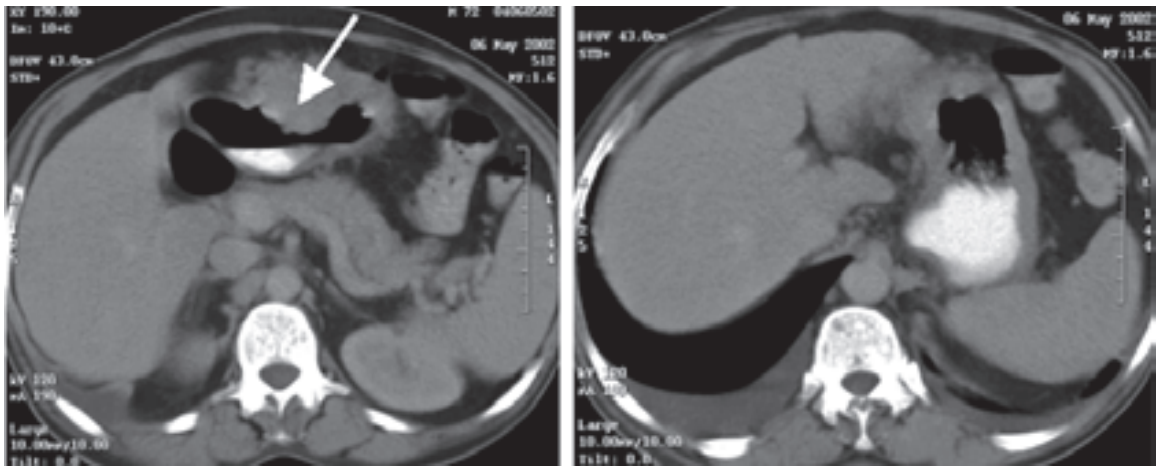

FIGURES 8.14A and B: Axial CECT reveals focal thickening in the anterior gastric wall causing a luminal impression.

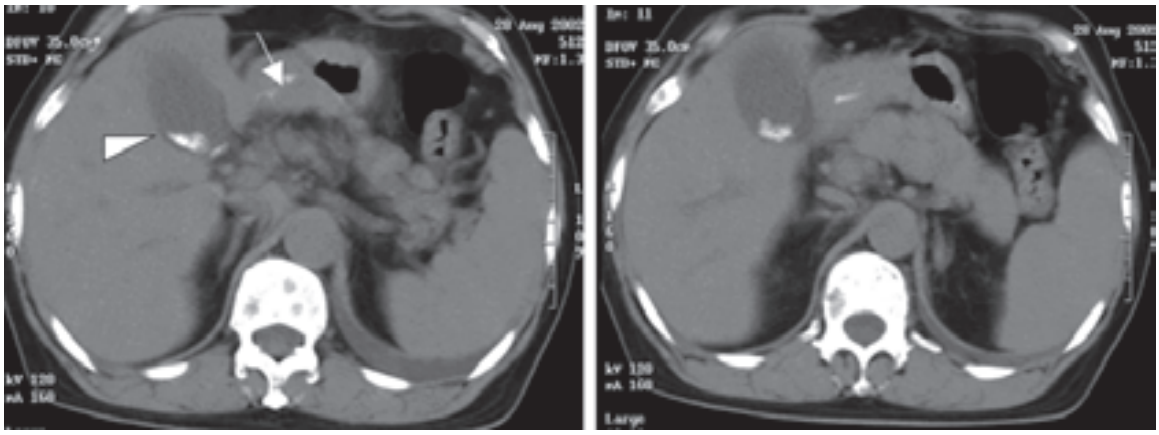

FIGURES 8.15A and B: Axial CECT without oral contrast shows focal circumferential thickening in the antral region with specks of calcification (arrow). Note cholelithiasis (arrowhead) with left pleural effusion.

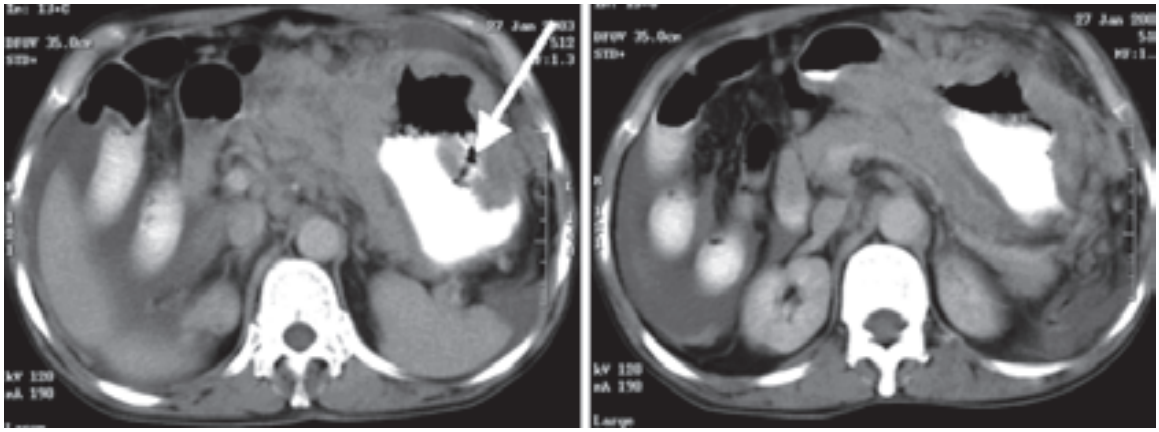

FIGURES 8.16A and B: Axial CECT reveals diffuse thickening of the body of stomach with ulceration along the greater curvature (arrow).

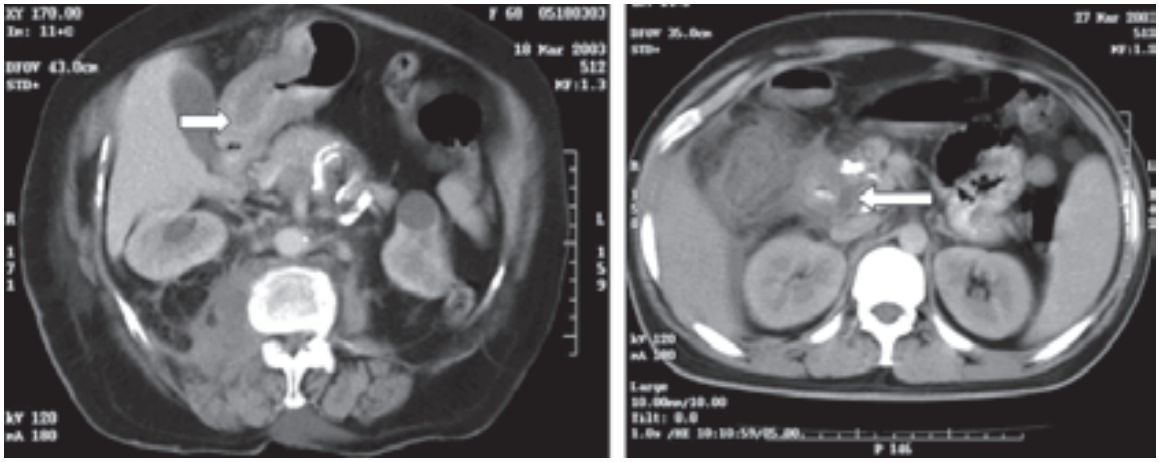

FIGURES 8.17A and B: Axial CECT reveals circumferential antral duodenal thickening with shouldering (arrow in A), note the periampullary thickening with pancreatic duct dilatation (arrow in B).

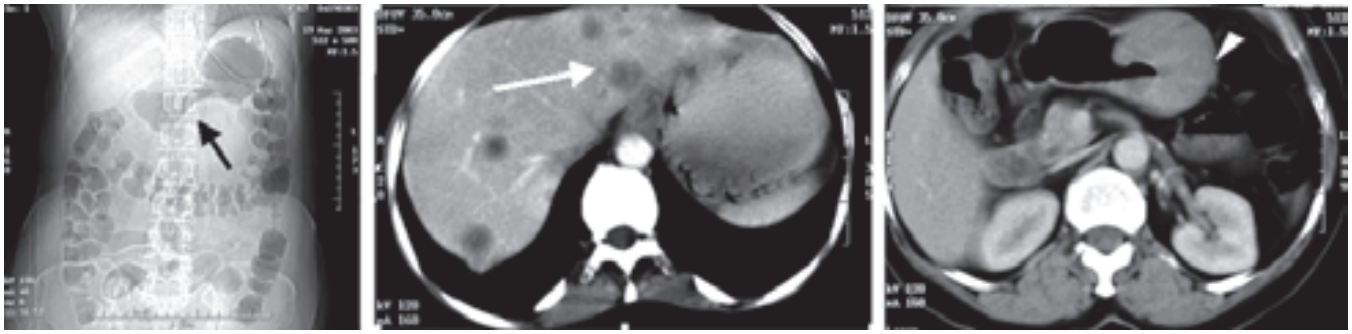

FIGURES 8.18A to C: Scanogram showing focal filling defect in the stomach wall along the greater curvature (arrow), axial CECT reveals multiple hypodense lesion in the liver suggestive of metastasis (arrow in Fig. B), axial CECT reveals eccentric thickening of the gastric wall (arrowhead).

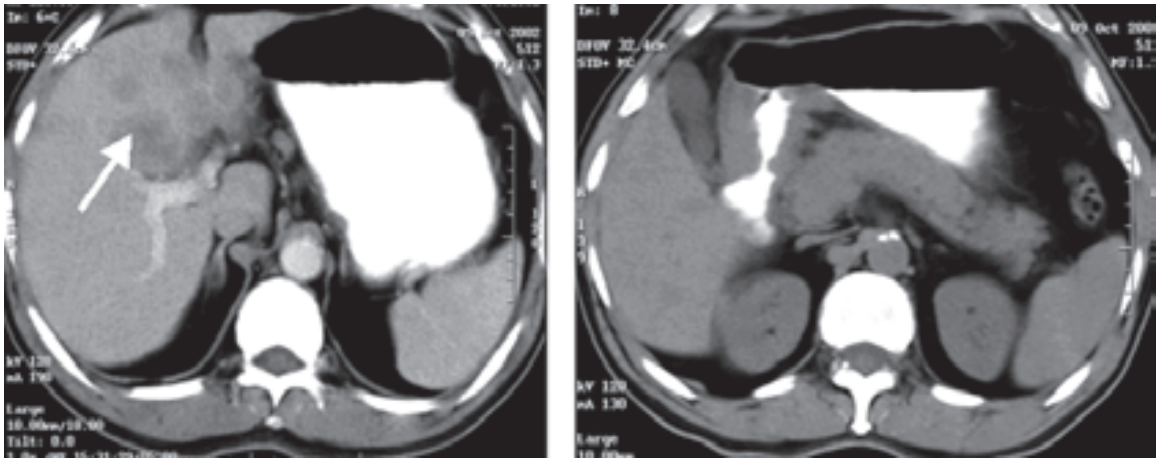

FIGURES 8.19A and B: Axial CECT reveals antral thickening with multiple hepatic lesions (arrow).

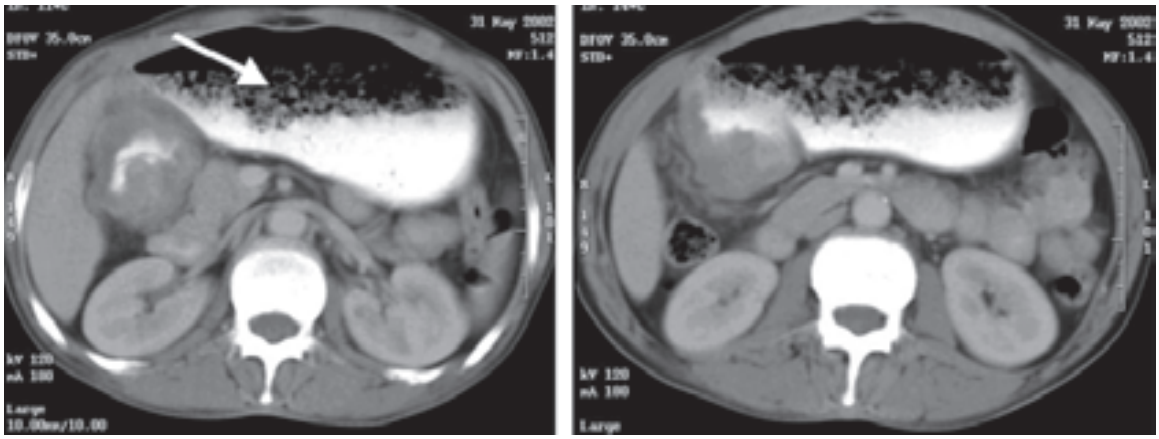

FIGURES 8.20A and B: Axial CECT reveals a dilated stomach with antral thickening, note the residual food materials due to outlet obstruction.

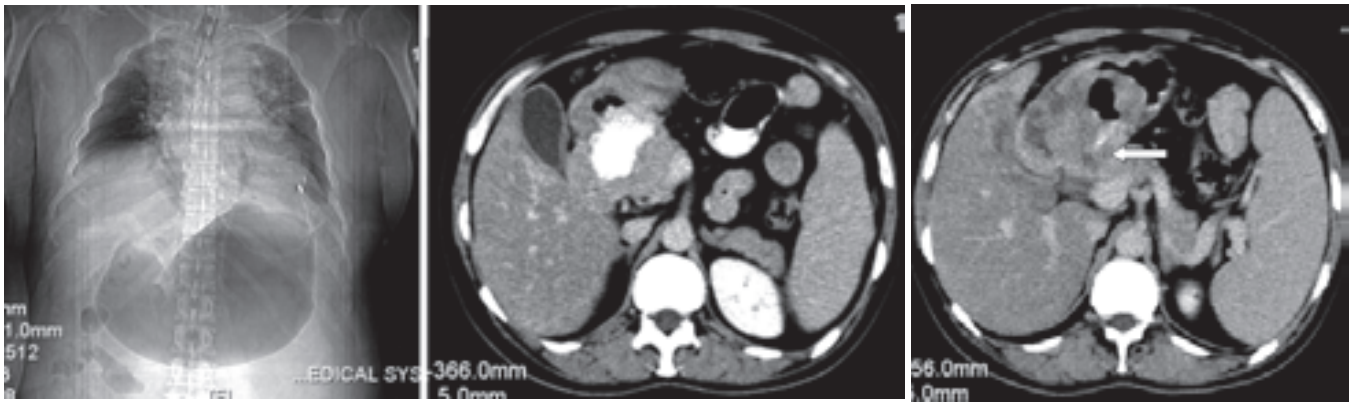

FIGURES 8.21A to C: Scanogram shows grossly dilated stomach. Axial CECT reveals mural thickening in the gastric antrum showing variable heterogeneous enhancement. Note the focal loss of fat planes between the mass and pancreatic head (arrow).

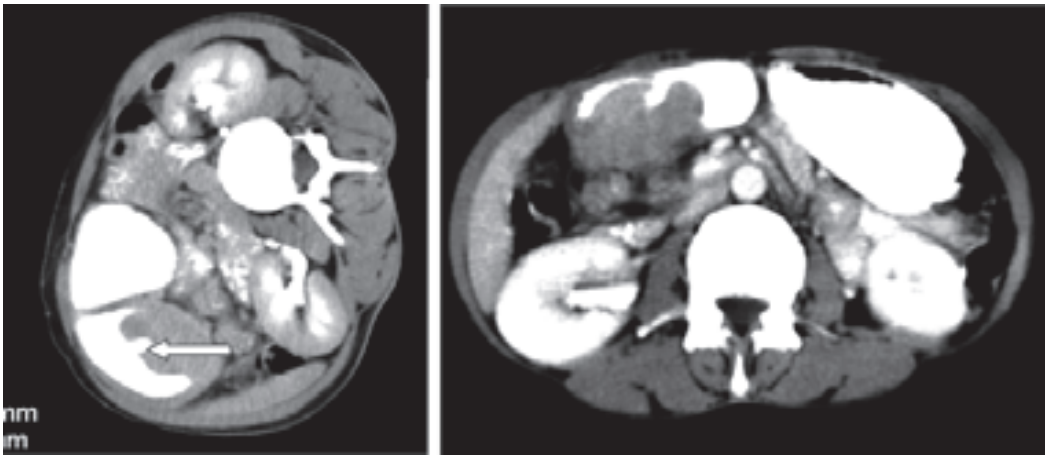

FIGURES 8.22A and B: Axial right lateral decubitus and axial CECT reveals an eccentric mass in the antrum showing central ulceration (arrow). Note the significance of decubitus positioning.

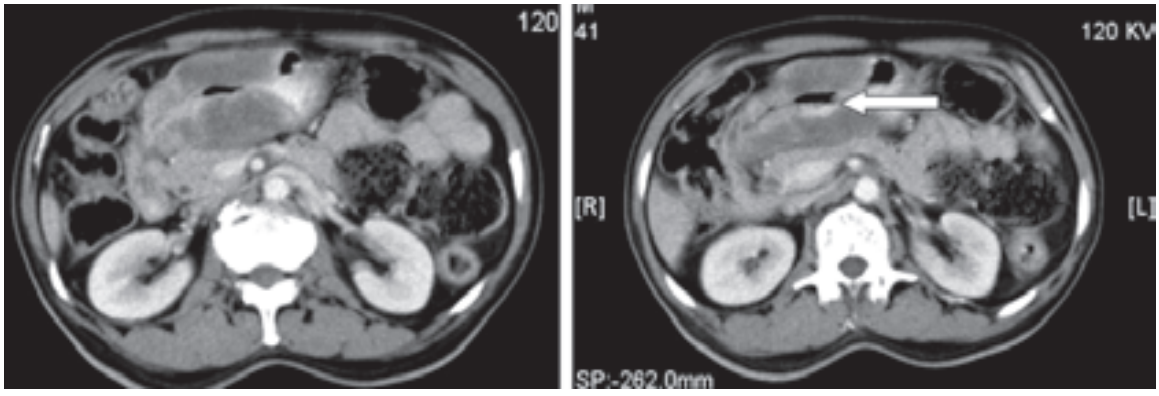

FIGURES 8.23A and B: Axial CECT showing a circumferential hypodense thickening of the distal body and antrum causing luminal narrowing (arrow). This pattern is usually seen in mucinous tumors.

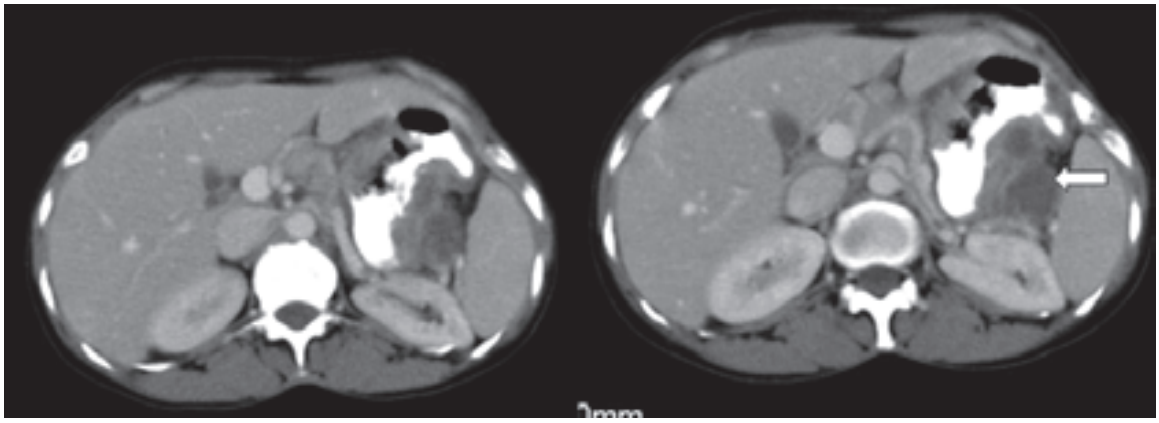

FIGURES 8.24A and B: Axial CECT showing an irregular mural thickening involving the greater curvature with nodular periserosal soft tissue suggestive of transmural spread.

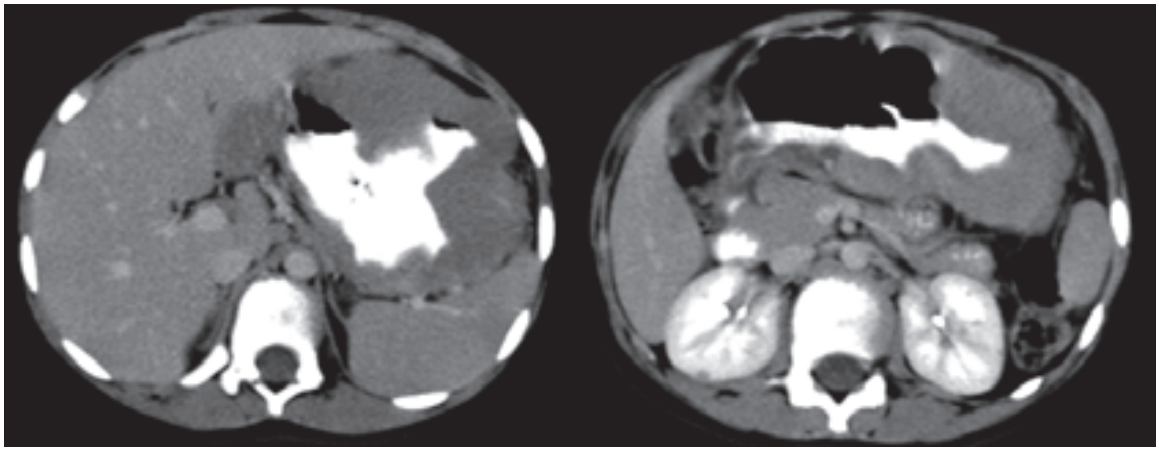

FIGURES 8.25A and B: Axial CECT in a 4-year-old male reveals a diffuse thickening involving the body and fundus with ulceration (HPE–mucinous adenocarcinoma).

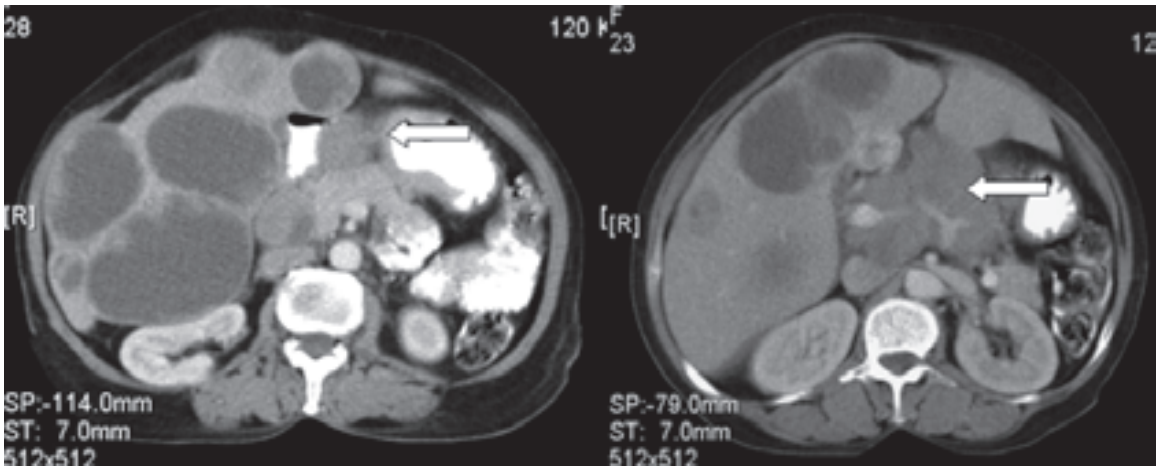

FIGURES 8.26A and B: Axial CECT reveals a focal mural thickening in the distal body causing luminal thickening (arrow), note multiple hepatic metastatic lesions with celiac and superior mesenteric lymphadenopathy encasing the vessels (arrow).

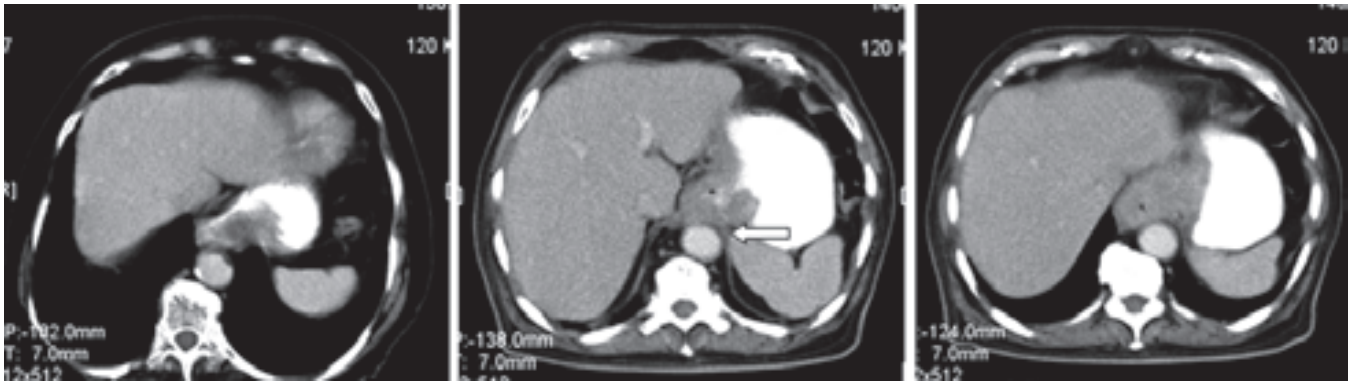

FIGURES 8.27A to C: Axial CECT showing circumferential GO junction growth, note focal loss of fat planes between the lesion and the diaphragmatic crus (arrow in Fig. B).

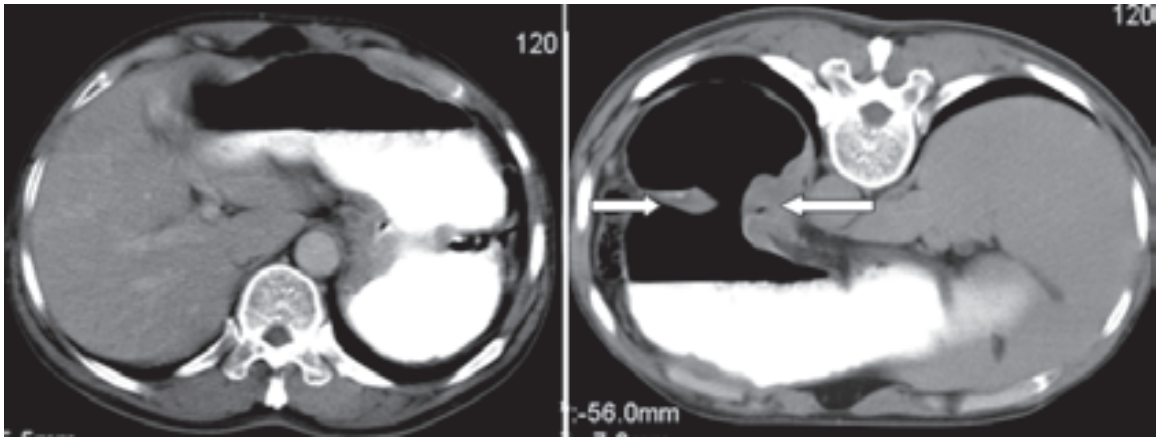

FIGURES 8.28A and B: Axial supine and prone CECT reveals an exophytic ulcerated lesion in the proximal body, note the inward infolding along the greater curvature corresponding to a niche and notch phenomenon (arrows).

Stromal Cell Lesion

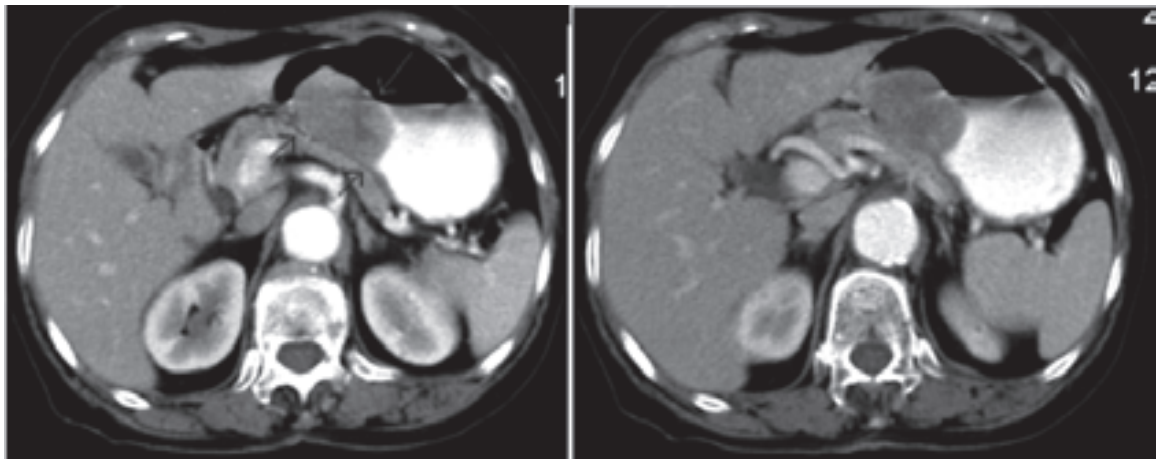

FIGURES 8.29A and B: Axial CECT reveals a focal mass with variable enhancement involving the posterior gastric wall in the distal body (arrow), note the smooth indentation of body of pancreas without loss of fat planes – case of leiomyoma.

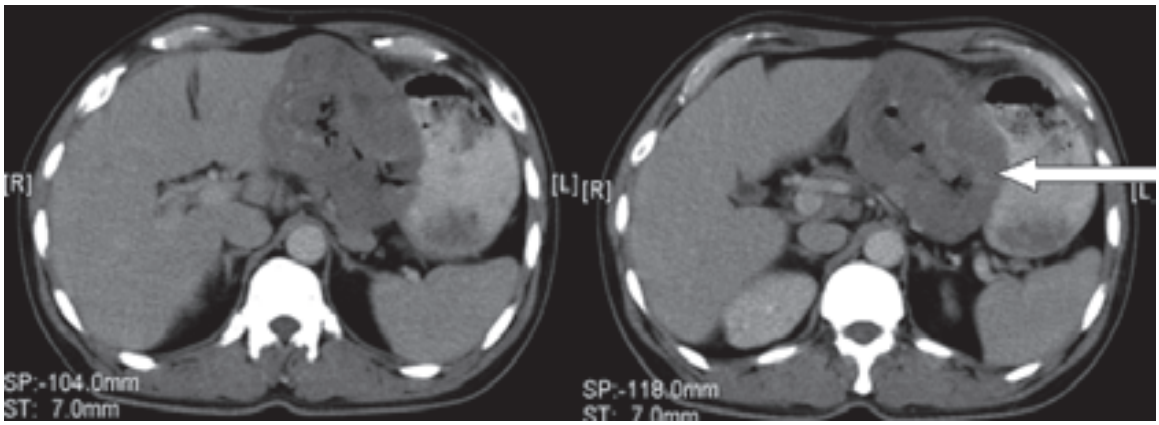

FIGURES 8.30A and B: Axial CECT reveals a large exophytic mass with central ulceration displacing the distal body of stomach along the lesser curvature.

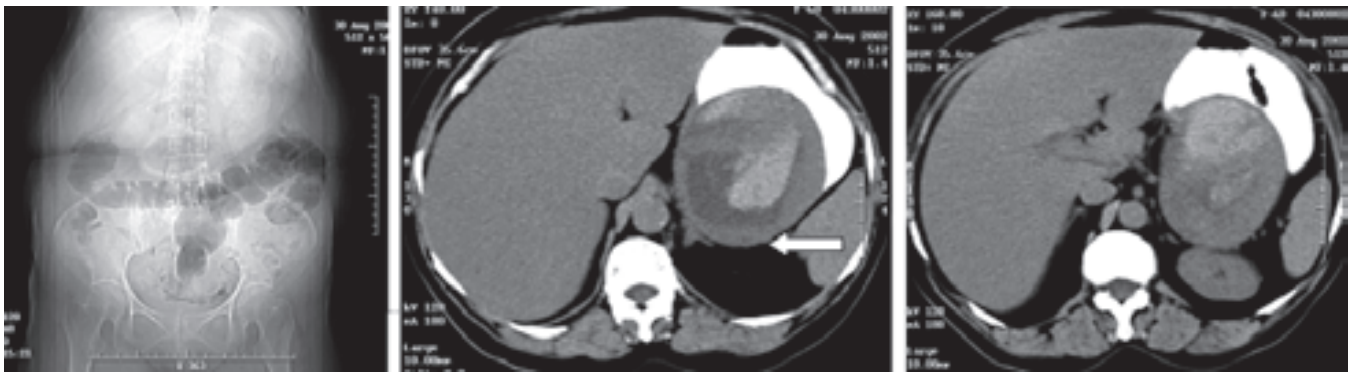

FIGURES 8.31A and B: Axial CECT in a patient with acute abdominal pain and hematemesis reveals a large exophytic mass in the lesser sac with areas of acute hemorrhage within (arrow).

Gastric Volvulus

Dilatation of stomach is seen in four major conditions:

1. Gastric outlet obstruction.
2. Paralytic ileus
3. Volvulus
4. Air swallowing.

Volvulus is an uncommon condition and may result from the stomach twisting around the longitudinal or mesenteric axis. Most of these cases are associated with diaphragmatic hernia or eventration.

Primary:
1. Occurs spontaneously without any diaphragmatic hernia or other intra-abdominal abnormality.
2. 30% of cases of volvulus
3. More common in adults than in children.
4. Has been described in children with absence of the gastrocolic ligament and congenital gastric bands.

Secondary:
1. Most common form
2. Most patients have diaphragmatic defects and derangements.
3. Paraesophageal hernias most common cause in adults.

Type 1—organoaxial (59%) – most common form.
Type 2—mesenteroaxial (29%).
Type 3—combined or mixed (2%).
Type 4—unclassified (10%).

In organoaxial type the stomach twists either anteriorly or posteriorly around its longitudinal axis with two points of luminal obstruction, one at the GO junction and other at the antrum. Usually cause obstruction but rarely cause strangulation. Usually occurs with hiatal hernia.

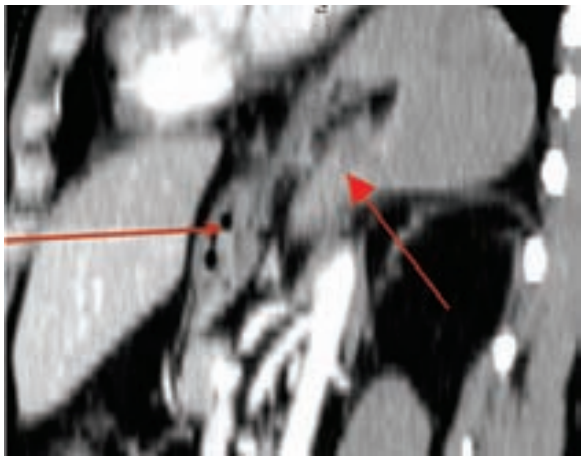

FIGURE 8.32: Sagittal CECT showing the typical disposition of a organoaxial gastric volvulus.

Mesenteroaxial volvulus results when the stomach twists around the mesentery so that the antrum and pylorus lie above the gastric fundus. This can cause complete obstruction, occlude the gastric vessels and lead to strangulation.

Pylorus rotates superiorly and anteriorly.

Upside-down stomach with the posterior surface lying anteriorly and antrum lying superiorly and extending to the right of fundus.

Frequently exists without diaphragmatic defect.

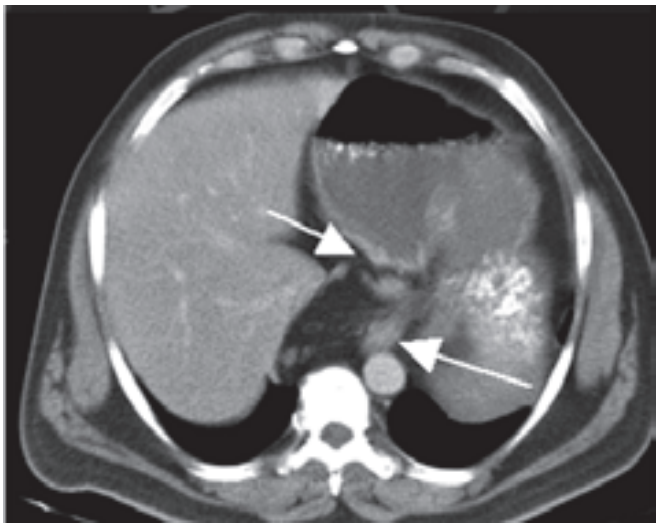

FIGURE 8.33: Axial CECT showing GO junction and pylorus at the same level (arrow).

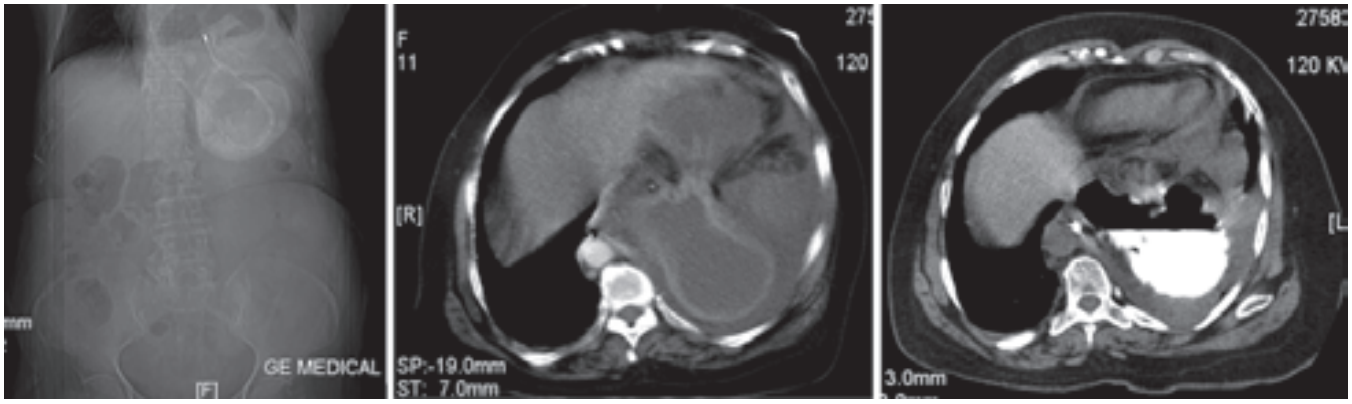

FIGURES 8.34A to C: Axial CECT in a patient with severe chest pain reveals hiatus hernia with secondary mesentricoaxial volvulus.

CT of Duodenum

The name *duodenum,* meaning "two plus ten", originated because the length of this part of the small bowel was thought to be equal to 12 fingers' breadth. It is the widest portion of the small bowel, has no mesentery, and is only partially covered by the peritoneum. The duodenum is 25-30 cm long and is divided into four sections. The first (superior) portion of the duodenum extends from the pylorus to the neck of the gallbladder and is primarily composed of the duodenal bulb. The second (descending) portion extends from the neck of the gallbladder to the genu, usually at the level of the fourth lumbar vertebra, and abnormalities in this portion are mainly due to pathologic conditions in adjacent structures, including the pancreas and biliary system. The third (horizontal) portion of the duodenum extends from the fourth lumbar vertebra to the level of the aorta and is often affected by trauma, given its retroperitoneal location and proximity to the spine. The fourth (ascending) portion extends from the aorta to the ligament of Treitz.

CT Technique

Most conventional abdominal CT scans are obtained with the use of radiopaque oral contrast material to delineate the gastrointestinal tract. When there is suspicion of a duodenal lesion, several techniques can be used to optimize imaging of this commonly overlooked structure. Large amounts of oral contrast material are helpful in opacifying the duodenum, and bicarbonate granules, through the release of carbon dioxide, can distend the stomach and duodenum. If a mucosal abnormality is suspected, low-attenuation oral contrast agents, such as water or whole milk, can be used. These agents create excellent contrast with the duodenal wall, particularly when intravenous contrast material is injected at 4 mL/sec during a dynamic helical acquisition. For routine imaging, a pitch of 1.0 mm with a collimation of 5 mm is typically chosen, although thinner-collimation images (3.0 mm) can be obtained if greater anatomic resolution is needed. Multiplanar reconstructions, including planes oblique and coronal to the plane of the duodenum, are now possible with the thin-collimation, helical acquisition techniques. Dynamic administration of intravenous contrast material with helical thin collimation is useful in the identification of vascular structures and the enhancement pattern of lesions within and adjacent to the duodenum. Placement of the patient in the right posterior oblique position to maximize opacification is also helpful to image the first and second portions of the duodenum, and the left posterior oblique position is helpful when carbon dioxide is used to distend the duodenum.

Duplications and Diverticula

The duodenum arises from the embryonic midgut and is composed of both endodermal and mesodermal tissue. At 8 weeks of gestation, the duodenal mucosa proliferates and occludes the lumen, with recanalization occurring by

the 10th week. True duodenal diverticula and duplications are believed to be due to abnormalities of recanalization of the duodenal lumen. The most frequent location of the more common duodenal pseudodiverticula is along the medial wall of the second and third portions of the duodenum, usually within 2.0 cm of the ampulla of Vater (hepatopancreatic ampulla). Most patients are asymptomatic, and the diagnosis can be performed easily at CT.

While duplications are rare in the gastrointestinal tract, approximately 12% occur in the gastroduodenal region. Duodenal duplication arises most often in the medial wall of the second and third portions of the duodenum and typically appears as a well-circumscribed cystic mass with fluid attenuation. The duplications typically do not communicate with the duodenal lumen and are often incidental findings at abdominal CT. On rare occasions, carcinoma can arise inside a duplication cyst, and the presence of vegetation or mural nodules should raise concern.

Malrotation

During the 6th week of intrauterine gestation, differential growth rates of the anterior and posterior sides of the duodenum result in a rotation of the duodenum across the midline, with the ligament of Treitz lying in the left upper quadrant. If there is abnormal rotation, the duodenum does not cross the midline but remains in the right side of the abdomen. Malrotation is reliably imaged at CT when the duodenum is not visible between the aorta and the superior mesenteric artery, an anatomic relationship that is consistently seen on all abdominal CT scans with normal findings. Secondary findings of malrotation include reversed location of the superior mesenteric artery and vein and presence of the colon in the left side of the abdomen and the small bowel in the right side. Patients with malrotation can present with small bowel volvulus and ischemia secondary to torsion of the small bowel on its abnormally short mesentery. Duodenal obstruction can also occur on the basis of congenital peritoneal bands.

Annular Pancreas

The pancreas develops from dorsal and ventral buds. In normal development, the ventral bud is typically bifid, with atrophy of one of the buds followed by fusion with the dorsal component. Theories of annular pancreas development suggest that either the two ventral buds persist, with encircling of the duodenum, or the remaining ventral bud adheres to the duodenum early in development, with a portion of ventral pancreatic tissue failing to rotate completely, resulting in annular obstruction. Patients with annular pancreas can present in the 1st decade of life with duodenal stenosis and vomiting, although in approximately 50% of cases, the diagnosis is not made until adulthood. Diagnosis of the entity prospectively at CT is difficult owing to the paucity of intra-abdominal fat in pediatric patients and the narrow width of the pancreatic band. The use of low-attenuation oral contrast material and imaging in the arterial phase to view the enhancing pancreatic tissue are sometimes helpful, but ERCP allows for accurate delineation of the pancreatic ductal anatomy.

Duodenal Trauma

Duodenal trauma may result from penetrating or blunt injury. During blunt trauma, the duodenum may be crushed against the vertebral body, causing contusion or transection. Rapid deceleration in motor vehicle accidents can also result in duodenal trauma. Detection of blunt traumatic injury to the duodenum is difficult at physical examination, and the choice of treatment is dependent on whether there is a contusion or a perforation. Intramural hematoma without perforation is usually managed conservatively, but traumatic duodenal perforation is a surgical emergency. These diagnoses are extremely difficult to determine clinically, since peritoneal signs are frequently absent because of the retroperitoneal location of the pancreas and duodenum. In addition, high morbidity and mortality are associated with missed duodenal injuries. The combination of high mortality and difficulty in establishing the clinical diagnosis increases the importance of the radiologist in detection of this injury. CT is the primary imaging modality for assessment of abdominal trauma, and the diagnosis of duodenal injury should be suspected when any of the following findings

are observed: (a) air adjacent to the duodenum in the retroperitoneum, (b) extravasation of oral contrast material in the retroperitoneum, (c) fluid in the retroperitoneum, (d) edema in the duodenal wall, (e) stranding of the peripancreatic fat, and (f) pancreatic transection.

Iatrogenic duodenal perforation is a rare complication of endoscopy and is usually suspected at the time of endoscopic examination. Perforation may be due to rupture from the endoscope or from an extended sphincterotomy. Typical CT findings include retroperitoneal air and fluid adjacent to the duodenum. Most patients undergo nonoperative treatment, surgery being reserved for those with persistent pain, signs of infection, or large perforations of the lateral duodenal wall.

Inflammatory Process

The most common inflammatory process to affect the duodenum is secondary involvement from pancreatitis. Pancreatic inflammation and release of exocrine enzymes cause mild to severe duodenal edema that obstructs the gastric outlet. In addition, severe pancreatitis can cause an intramural hematoma from disruption of the intramural vasculature by the elastase present in pancreatic enzymes.

The reported prevalence of Crohn disease that involves the duodenum ranges from 0.5 to 4%, although this range is based primarily on findings of barium studies, and series based on findings of routine endoscopy have suggested a higher incidence, ranging from 5 to 60%. Primary involvement tends to manifest as ulcer or stricture formation, while secondary involvement typically occurs as a fistulous communication from an adjacent affected loop of small bowel or colon.

Duodenal ulcers are common pathologic entities that occur most frequently in the duodenal bulb. Perforated duodenal ulcers can be diagnosed at CT from the presence of (a) wall thickening, (b) periduodenal fluid, (c) retroperitoneal air, or (d) free intraperitoneal air. Duodenitis from inflammation without ulcer formation is manifested by thickening of the duodenal bulb wall. Inflammation of the duodenal papillae can occur in patients with acquired immunodeficiency syndrome or who are undergoing radiation therapy. On rare occasions, severe duodenal ulcers can result in strictures and obstruction of the gastric outlet. Postbulbar ulcers are rare, and when they occur, alternate causes such as Crohn disease and Zollinger-Ellison syndrome should be considered.

Infectious Processes

Infectious processes in the duodenum are rarely diagnosed prospectively from CT scans. Most infectious processes result in inflammation of the duodenum and secondary duodenal wall edema. The most common infectious cause of duodenitis is *Helicobacter pylori*. Less common infections include giardiasis and tropical sprue. The findings tend to be nonspecific, such as wall thickening and luminal dilatation. Correlation with clinical history is helpful in diagnosis.

Hematologic Abnormalities

Henoch-Schönlein purpura is a systemic hypersensitivity disease of unknown pathogenesis. Deposition of immune complexes within small vessels throughout the body results in abnormal permeability of small blood vessels. This altered permeability can result in a purpuric rash, glomerulonephritis, and hemorrhage in the gastrointestinal tract. At abdominal CT, one can see multifocal areas of bowel wall thickening and mesenteric edema. The diagnosis of Henoch-Schönlein purpura should be considered when these findings are seen in young patients with abdominal pain.

Neoplastic Processes

Small bowel malignancies are 50 times less common than colonic neoplasms, but the duodenum is a common site of tumors in the small bowel, accounting for approximately 20% of these neoplasms. Neoplastic processes in the

duodenum can be separated into benign and malignant pathogeneses. The most common symptomatic benign neoplasm of the duodenum is a benign gastrointestinal stromal tumor (leiomyoma). Patients with these tumors often present with gastrointestinal bleeding and, occasionally, abdominal pain. At CT, the neoplasm may be seen as a heterogeneous mass with moderate enhancement and an annular narrowing of the lumen with abrupt concentric or irregular edges. Duodenal lipomas are benign lesions that can be reliably diagnosed on CT scans as a smooth-margined mass with a low Hounsfield unit measurement. They usually produce no symptoms and most often occur in men in their 7th decade. There are three types of duodenal adenomas: tubular type, villous adenoma, and Brunner gland adenoma. Villous adenomas have a malignant potential and are treated with surgical resection, while tubular adenomas and Brunner gland adenomas are typically resected for symptomatic reasons.

While the small bowel can be involved in various polyposis syndromes, Peutz-Jeghers syndrome is the only one that affects it primarily. This syndrome of mucocutaneous melanin pigmentation and associated hamartomatous gastrointestinal polyps is an autosomal-dominant abnormality. Presenting symptoms are bleeding and obstruction from intussusception. At CT, one may see intraluminal polyps, and the multiplicity of these lesions should suggest a polyposis syndrome.

Malignant primary neoplasms of the duodenum are rare. Adenocarcinoma is the most common primary malignant neoplasm of the duodenum, with 50-70% of small bowel adenocarcinomas occurring either in the duodenum or proximal jejunum. The peak prevalence is in the 7th decade, and patients present with signs of bleeding, jaundice, or obstruction. Patients with this neoplasm tend to present at an advanced stage, with more than 50% of them having metastases at the time of diagnosis. At CT, one sees a polypoid or intramural mass. Rare tumors such as paragangliomas can also occur in the duodenum. These neoplasms can occur in external, intramural, or intraluminal locations, typically in the second or third portions of the duodenum. At CT imaging, these tumors are soft-tissue-attenuation masses with homogeneous enhancement and have a characteristic smoothly margined "dumbbell" appearance.

Lymphomatous involvement of the duodenum can occur with both primary duodenal lymphoma and involvement from systemic disease. Associations exist with immunodeficiency states, notably infection with the human immunodeficiency virus, celiac disease, and parasitic infestation. Most often, CT shows large, segmental nodular wall thickening, with a gradual junction with normal mucosa. Alternatively, a large eccentric mass with extension into adjacent tissues can be seen.

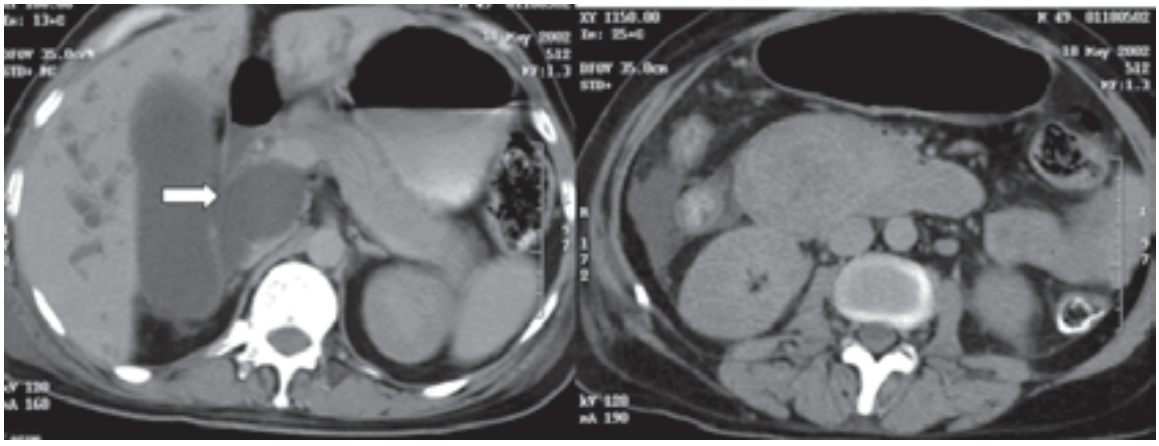

FIGURES 8.35A and B: Axial CECT in a patient with features of obstructive jaundice reveals distended gallbladder and dilated CBD (arrow). Note the circumferential thickening with luminal narrowing of the third part of duodenum (arrow in B).

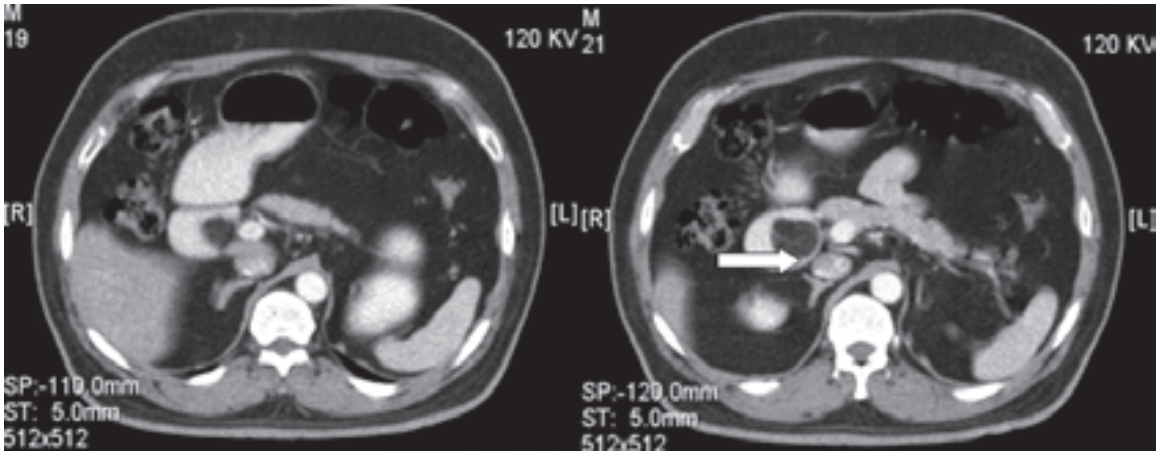

FIGURES 8.36A and B: Axial CECT reveals a well-defined hypodense lesion in the second part of duodenum having a fat attenuation suggestive of lipoma.

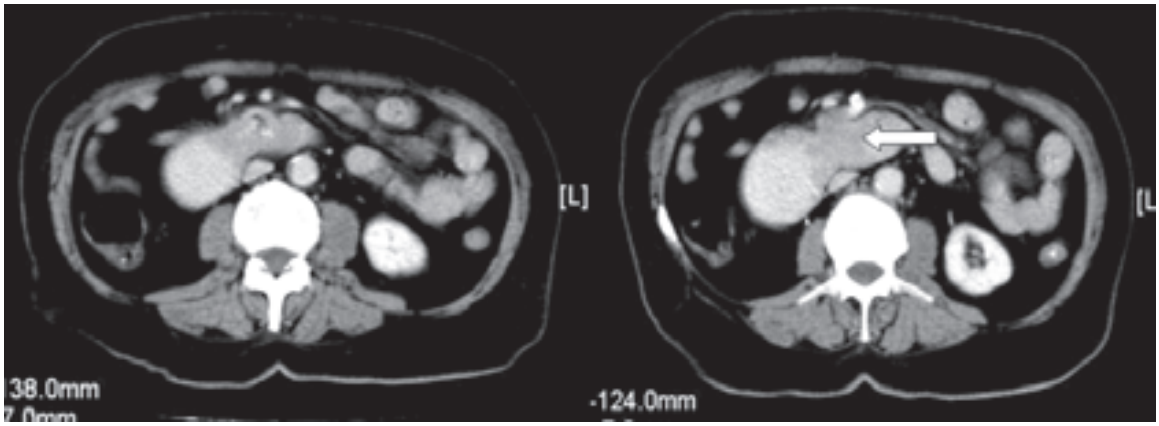

FIGURES 8.37A and B: Axial CECT in a patient with weight loss reveals a circumferential mural thickening of the third part of duodenum with luminal narrowing (arrow).

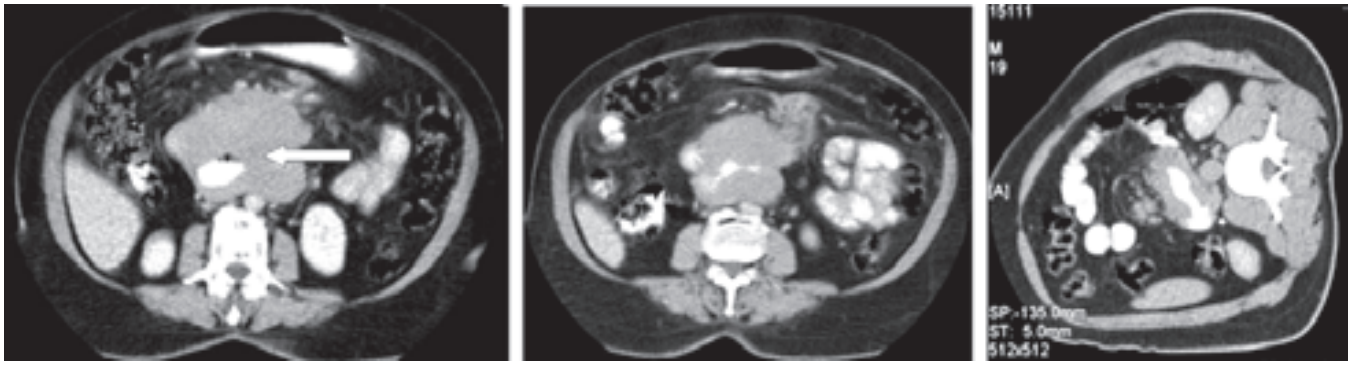

FIGURES 8.38A to C: Axial CECT in a patient with weight loss and vomiting reveals a circumferential thickening (arrow) of the fourth part of duodenum (case of non-Hodgkin's lymphoma).

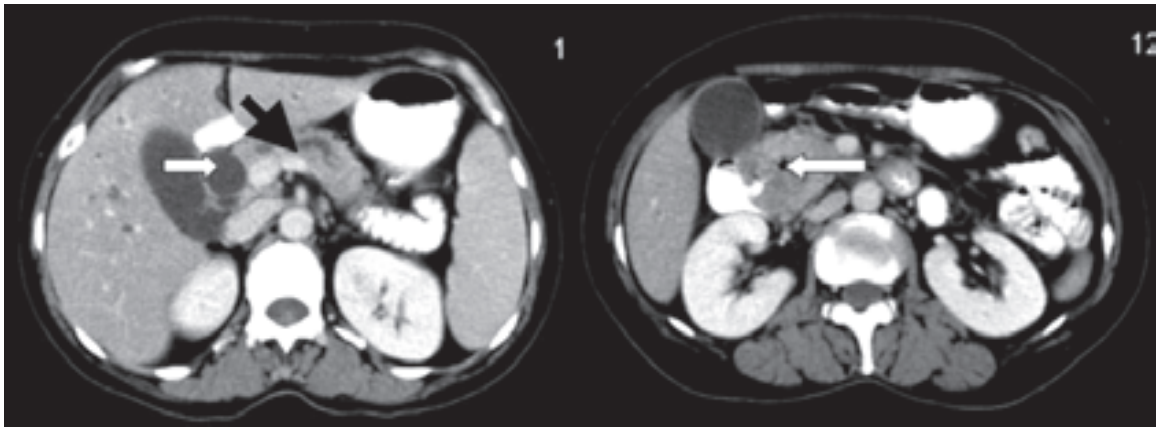

FIGURES 8.39A and B: Axial CECT in a patient with obstructive jaundice reveals double duct sign (arrows in Fig. A), ulcerated periampullary mass lesion causing CBD and PD obstruction (arrow).

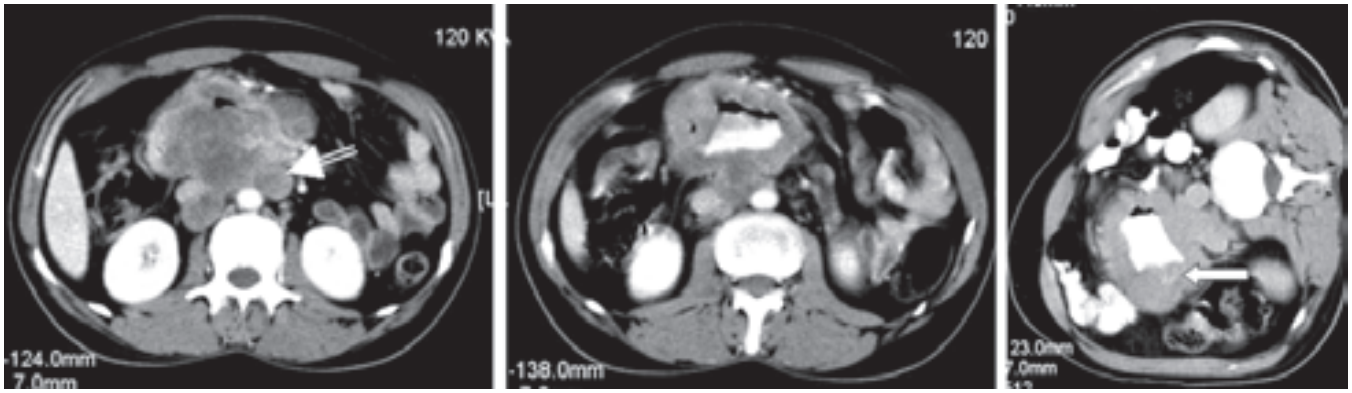

FIGURES 8.40A to C: Axial and decubitus CECT in a patient with upper GI obstructive symptoms reveals a circumferential transmural thickening with an eccentric soft tissue component involving the third and fourth part of duodenum (arrow in C). Note the periserosal lymph nodes (arrow in A) (adenocarcinoma).

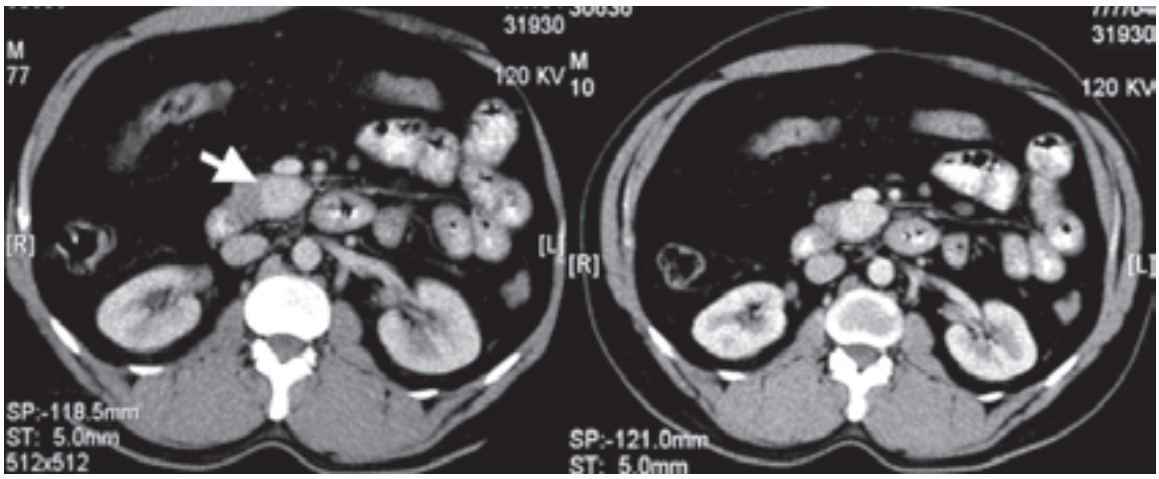

FIGURES 8.41A and B: Axial CECT in a patient with suspected insulinoma showing a well marginated enhancing lesion in the fourth part of duodenum.

Secondary involvement of the duodenum with other primary malignancies can occur by means of local extension or metastases from distant sites. Pancreatic adenocarcinomas can be locally aggressive, and extension to the duodenum can be seen at CT. Colon carcinoma can cause local mass effect or invasion, occasionally with formation of a coloduodenal fistula. Ovarian carcinoma typically produces peritoneal disease but can occasionally manifest with metastatic disease to the duodenum. In addition, periduodenal lymph nodes are a common site of metastasis, and differentiating involved nodes from a primary duodenal mass can be difficult at CT. MR imaging can be a useful adjunct in the differentiation of primary duodenal pathologic conditions from periduodenal lymphadenopathy when CT findings are equivocal. Metastatic disease from melanoma to the small bowel is a common finding in autopsy series and can cause single or multiple intraluminal masses. Alternatively, it can manifest with lymphadenopathy or peritoneal implants.

Diaphragms and Webs

Antral mucosal diaphragms are thin membranous septa that are usually located within 3 cm of the pyloric canal and are oriented perpendicular to the long axis of the stomach. Presentation is with symptoms of partial gastric obstruction, depending on the size of the aperture.

Congenital duodenal webs are membranous projection that occlude the lumen to varying degrees most often occur in the second portion of the duodenum near the ampulla. Imaging features are that of a thin lucent line extending across the lumen with proximal duodenal dilatation.

Other Causes of Outlet Obstruction

1. Adult hypertrophic pyloric stenosis.
2. Gastric outlet obstruction due to peptic ulcer, carcinoma.
   Duodenal obstruction to mesenteric root syndrome, hematoma, diverticulum.

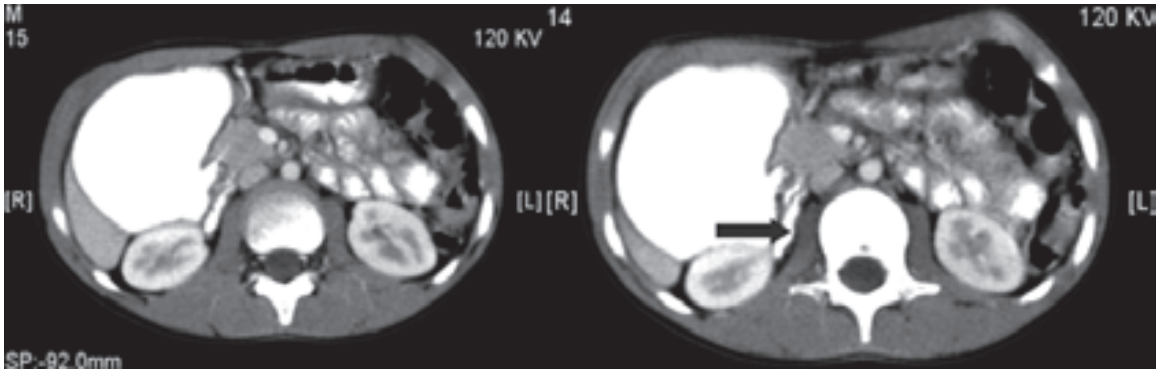

FIGURES 8.42A and B: Axial CECT reveals a grossly distended first part of duodenum. Note the thin membrane extending all round the lumen (arrow) causing symptoms of outlet obstruction.

IMAGING OF SMALL BOWEL

A wide variety of small bowel abnormalities have been seen on CT. Spiral CT of the small bowel is performed by using scan parameters of 7 mm slice thickness, 7 mm/s table speed (pitch of 1), 3 mm interval reconstruction is done when needed, meticulous opacification of bowel is required, so as to avoid misinterpretation of nondistended bowel loops for pathology. 800-1000 ml of 2-3% gastrograafian is used to opacify the bowel. Intravenous contrast (100 to 120 cc of non-ionic contrast 300) is injected at a rate of 2 to 3 cc/sec. Scanning is started approximately 30-40 seconds after initiation of contrast injection.

Normal Findings and Interpretation of Small Bowel CT

The normal small bowel, when imaged axially on CT scans, should have a wall thickness of less than 4 mm. The wall should be symmetric and have a homogeneous attenuation. Valvulae conniventes are commonly seen in the jejunum and are not visualized in the ileum. The surrounding mensentery should have a fat density (excluding lymph nodes and blood vessels).

Mural thickening on a CT scan is the hallmark of small bowel disease. Neoplastic, inflammatory, and vascular disorders of the small bowel are recognized on CT scans by thickening of the bowel wall. It is important to characterize the lesion as to its location and to determine the degree of mural thickening, symmetry of involvement, pattern of contrast enhancement, and smooth versus irregular or lobulated inner or outer contour.

To further narrow the differential diagnosis, associated findings such as abscess, lymphadenopathy, metastases, and adjacent inflammatory response in the mesentery should be sought. Transition of luminal diameter and pattern of folds also are helpful for detecting bowel pathology.

Small Bowel Malignancies

Malignancies involving the small intestine are rare. Although the small intestine represents 75 percent of the length and 90 percent of the surface area of the alimentary tract, small bowel malignancies account for only 1 to 2 percent of all gastrointestinal (GI) neoplasms.

Small bowel malignancies may be associated with several heritable conditions that affect the GI tract.

Predisposing Conditions

A number of disease states are associated with an increased incidence of small bowel neoplasms. These include: Peutz-Jeghers syndrome (hamartomatous polyps occurring primarily in the jejunum and ileum); Crohn's disease (adenocarcinoma); Gardner's syndrome (adenoma); familial colonic polyposis (adenoma); celiac disease (lymphoma, carcinoma); immunodeficiency states; and autoimmune disorders (lymphoma).

The most common presenting symptoms are intermittent obstruction, intussusception, occult bleeding, palpable abdominal mass, and abdominal pain. Perforation and gross bleeding are rare.

Patients with malignant small bowel neoplasms more often have GI symptoms, compared to those with benign tumors. However, the clinical presentation alone does not permit the distinction between benign and malignant lesions.

The often vague and nonspecific nature of the symptoms may make diagnosis difficult.

Types of Tumors

The small bowel can be affected by both malignant and benign lesions.

- Adenocarcinoma — 45 percent
- Carcinoid — 29 percent
- Lymphoma — 15 percent
- Sarcoma — 10 percent

Adenocarcinomas

Adenocarcinomas represent from 25 to 50 percent of small bowel cancers. They usually present between the ages of 50 to 70, with a male predominance. The risk of adenocarcinoma may be higher in patients who have had colorectal cancer, suggesting a possible common etiology. The incidence of adenocarcinoma is highest in the duodenum, and decreases progressively through the rest of the small intestine; 65 percent are periampullary. Small intestinal adenocarcinomas occur with high incidence in patients with adult celiac disease.

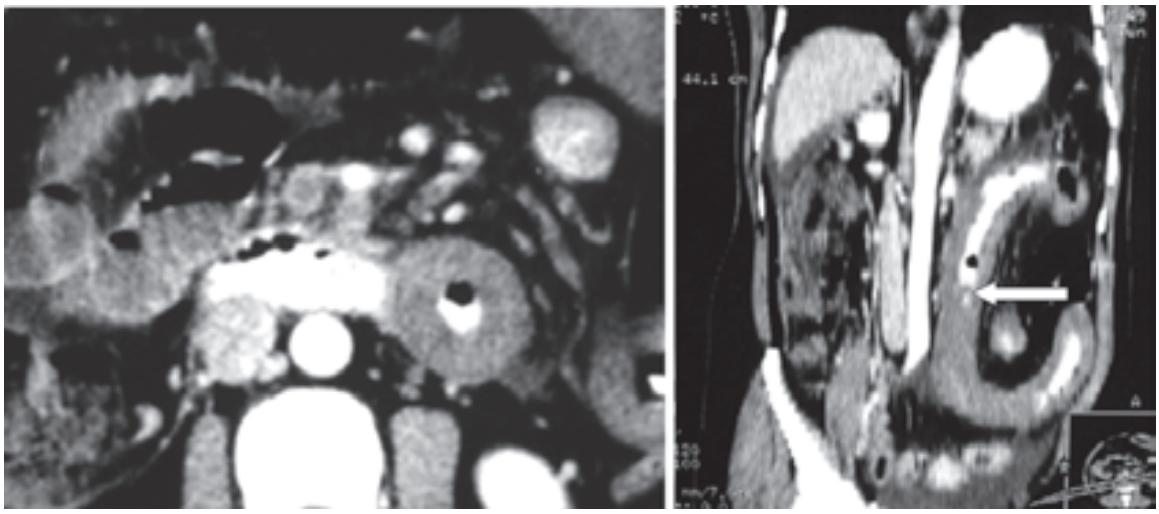

FIGURES 8.43A and B: Axial CECT with reformation reveals a long segment circumferential mural thickening of jejunum (adenocarcinoma).

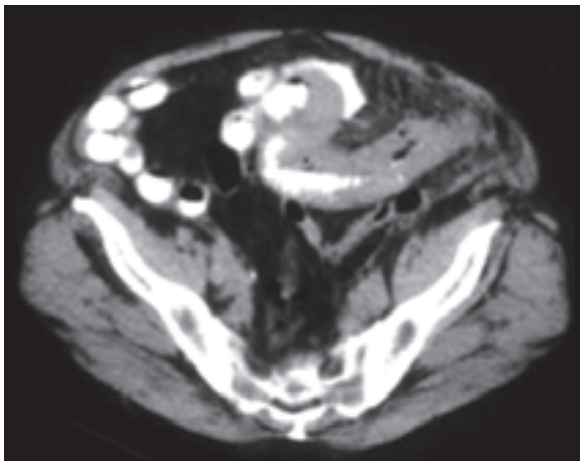

FIGURE 8.44: Axial CECT reveals a long segment thickening with ulceration of the proximal ileum (adeno Ca).

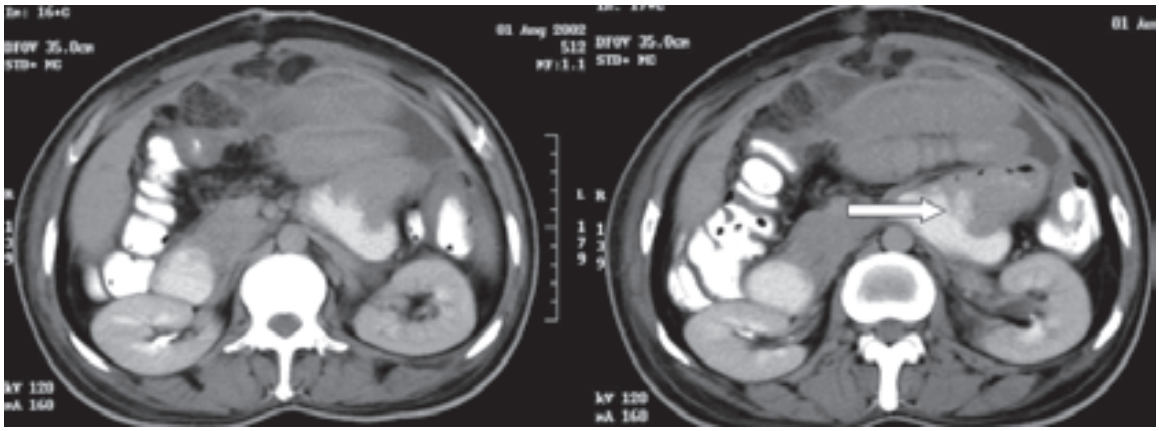

FIGURES 8.45A and B: Axial CECT reveals a short segment proximal jejunal lesion with shouldering (arrow) (case of adenocarcinoma).

An exception to the proximal location occurs in patients with Crohn's disease; 70 percent of such lesions are in the ileum. Bowel adenocarcinomas tend to infiltrate into the muscularis propria, and may extend through the serosa into adjacent tissues. Ulceration is common, and may result in occult GI bleeding or chronic anemia. Intestinal obstruction can be caused by progression of an apple core lesion or by a large intraluminal polypoid mass.

CT shows circumferential thickening of bowel wall, tumor mass may be typically 3-6 cm in diameter, thickening may be of uniform attenuation or have low attenuation areas, enlargement of regional mesenteric lymph nodes is seen in most of the patients. Prestenotic dilatation can be marked.

Carcinoid Tumors

Carcinoid tumors are rare, indolent neuroendocrine tumors that are mainly located in the bowel, stomach and lung. Carcinoid tumors represent upto 40 percent of primary small intestinal malignancies. They have been reported in patients from 20 to 80 years old, with the highest incidence between 50 and 60.

Carcinoids originate from the Kulchitsky cell, an enterochromaffin cell located in the crypts of Lieberkuhn. These tumors are classified according to their embryological origin into foregut (bronchus, stomach, duodenum, and pancreas), midgut (jejunum, ileum, and proximal colon), and hindgut (distal colon, rectum, and genitourinary tract) types.

Small bowel carcinoids are most commonly found in the ileum, within 60 cm of the ileocecal valve. The presence of multiple synchronous nodules in 30 percent of patients mandates careful inspection of the entire small intestine to exclude other sites of disease.

Grossly, carcinoid tumors appear as firm intramucosal or submucosal nodules, with a yellow cut surface due to their high lipid content. The tumor tends to infiltrate the bowel wall, and may extend through the serosa, causing shortening and thickening of the mesentery due to an intense associated desmoplastic reaction.

Intermittent obstruction occurs in 25 percent of all small intestinal carcinoids. Obstruction may be caused by intraluminal tumor, but often results from mesenteric kinking and distortion brought on by tumor invasion and a secondary desmoplastic response.

Small bowel carcinoids do not produce carcinoid syndrome because the serotonin released by the tumor into the mesenteric veins is metabolized on passage through the liver. The presence of syndrome is, therefore, a good indicator of metastatic spread of small intestinal tumor to the liver.

CT is very helpful in detecting the carcinoid tumor of the small intestine and their extent of spread, mesenteric spread, metastatic deposits in the liver and retroperitoneal nodes are frequently detectable. Typically the carcinoid tumor appear as a mass in the root of mesentery. The tumor may contain specks of calcification but is other wise homogenous in attenuation, fibrous strands radiate from the mass and produce a stellate pattern.

Primary GI Tract Lymphoma

Lymphoma may arise as a primary neoplasm or as a component of systemic disease with GI involvement. The diagnosis of a primary GI lymphoma requires the following:

- No peripheral or mediastinal lymphadenopathy
- A normal white blood cell count and differential on the peripheral blood smear
- Tumor involvement must be predominantly in the GI tract
- No evidence of liver or spleen involvement

Primary GI lymphoma is the most common extranodal form of lymphoma; the stomach and small bowel are most often involved.

- Stomach — 75 percent
- Small bowel (including duodenum) — 9 percent

- Ileocecal region — 7 percent
- More than one GI site — 6 percent
- Rectum — 2 percent
- Diffuse colonic involvement — 1 percent

Some of the predisposing conditions include:

- Autoimmune disease
- Immunodeficiency syndromes (e.g. AIDS)
- Long-standing immuno suppressive therapy (e.g. post-transplantation).
- Crohn's disease
- Radiation therapy
- Nodular lymphoid hyperplasia.

CT is useful in detecting, characterizing and staging of small bowel lymphomas, they are five patterns of involvement (1) multiple nodules, (2) infiltrating tumor, (3) polypoidal mass, (4) endoexoenteric form with excavation, fistula formation, (5) mesenteric involvement with extraluminal mass.

Focal or diffuse thickening of bowel wall, long segment thickening (8-12 cm, longer than involved segments in adenocarcinomas), effacement of mucosal folds, nodularity, ulceration, luminal caliber may be narrowed, normal or widened (aneurysmal dilatation) separation of adjacent bowel loops due to mural thickening is also noted in some cases. Conglomerate nodal masses seen indenting the mesenteric border of small intestine in a scalloped manner is characteristic on CT scans.

Enlargement of regional mesenteric nodes and the finding of a large mass without mechanical obstruction are frequently seen in non-Hodgkin's lymphoma.

Sarcomas

Sarcomas represent approximately 10 percent of small bowel neoplasms, and are most common in the jejunum, ileum, and in Meckel's diverticulae. The most common type is a leiomyosarcoma (75%) followed by fibrosarcoma, liposarcoma, and angiosarcoma.

Neuroendocrine Tumors

Neuroendocrine tumors of the small bowel include duodenal gastrinoma and somatostatinoma, neuroendocrine carcinomas, and paraganglionomas.

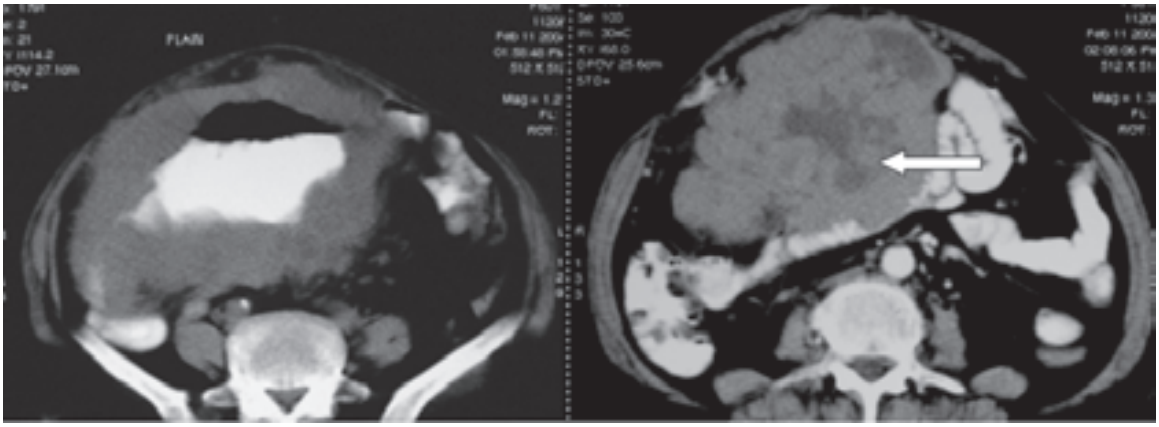

FIGURES 8.46A and B: Axial CECT showing a large distal ileal exoendophytic mass, note the large extraluminal soft tissue mass (arrow).

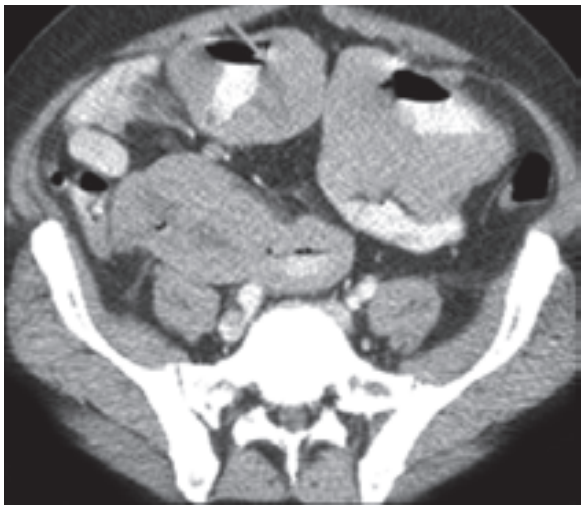

FIGURE 8.47: NHL. Diffuse, circumferential, homogeneous thickening of jejunal and ileal wall.

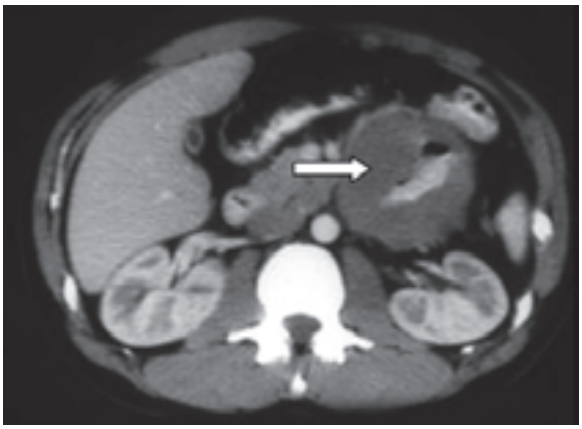

FIGURE 8.48: Axial CECT showing gross circumferential mural thickening involving the DJ flexure (case of non-Hodgkin's lymphoma).

Metastatic Lesions

The small bowel is the most common site of gastrointestinal metastatic melanoma. Primaries from breast, lung, and kidney also have metastasized to small bowel by hematogenous spread. In comparison, cervical, ovarian, and colon cancers can involve the small bowel by direct extension.

Benign Lesions

Benign lesions include adenomas, leiomyomas, fibromas, and lipomas.

Adenomas

There are three major types of benign small bowel adenomas: simple villous; tubular; and Brunner's gland adenomas. Villous adenomas carry a significant potential for malignant transformation. The superficial part of the tumor may appear benign with areas of adenocarcinoma in the deeper parts. The usual presentation is with bleeding or obstruction of the small bowel.

Tubular adenomas have a lower malignant potential. They are most common in the duodenum, are usually asymptomatic, but may present with bleeding or obstruction.

A Brunner's gland adenoma is a rare small bowel neoplasm. It is caused by hyperplasia of the exocrine glands within the proximal duodenal mucosa.

Leiomyomas

Leiomyomas are single, firm, gray or white, well-defined masses that arise in the submucosal layer of the wall of the small intestine. They are seen more frequently in jejunum. These tumors usually enlarge extraluminally and therefore are not detected until they outgrow their blood supply causing central necrosis, ulceration, and bleeding into the bowel lumen. These average 5 cm in diameter and are smoothly marginated and are spherical or ovoid. The characteristic eccentric growth pattern is more obvious on CT than on barium. The tumor may be uniform or may show areas of low attenuation, there may be specks of calcification, they are hypervascular on contrast.

Lipomas

Lipomas occur mostly in the ileum and duodenum. They arise from either submucosal adipose tissue or serosal fat, and may present with obstruction or as an incidental finding. Lipomas are submucosal lesions with homogeneous fatty tissue on a cut surface. They have a diagnostic low attenuation appearance on CT scan.

Other Benign Lesions

Among other benign small bowel tumors, desmoid tumors may grow intraluminally, causing obstruction, or extraluminally, presenting as a palpable abdominal mass.

Polyposis Syndromes

Peutz-Jeghers Syndrome

It is an autosomal dominant syndrome, consisting of hamartomatous polyps of GI tract, brown pigmented lesions of skin and mucous membrane of lips. Patients are in their 2nd decade. Usually asymptomatic but intussusception and anemia due to GI bleed are common.

Polyps affect the small bowel predominantly they vary in size from very small lesions to lesions as large as 4 cm. Polyps are seen in CT as intraluminal soft tissue filling defects.

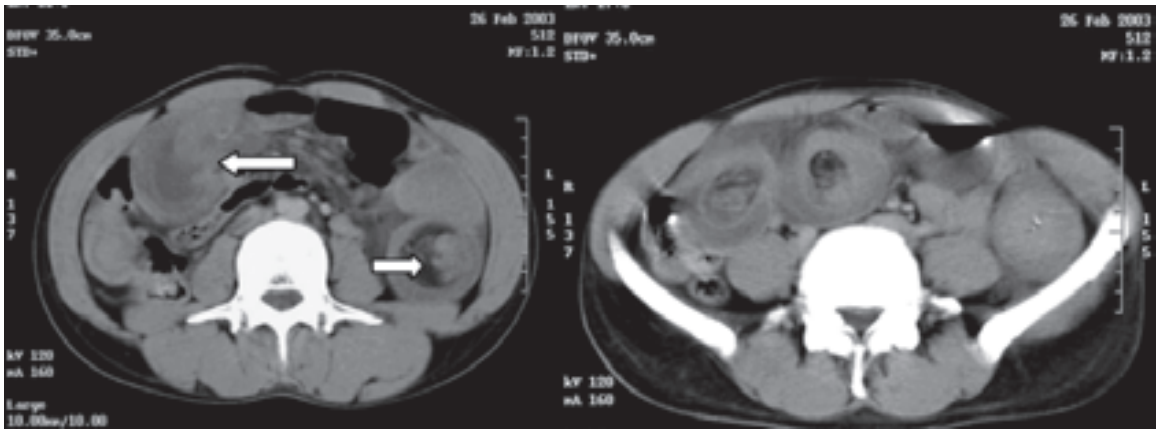

FIGURE 8.49: Axial CECT in a patient with recurrent abdominal pain reveals multiple intussusception with polyps (arrows).

Cronkhite Canada Syndrome

A rare polyposis syndrome that involves the small bowel, they usually develop after the age of 40 years, associated ectodermal changes include alopecia, brownish pigmentation of skin, dystrophic changes of skin, patients present with features of malabsorption, diarrhea.

The Solitary Polyp

There are numerous different types of small bowel polyps; the more common are as follows:

- Carcinoid
- Adenoma
- Brunner gland hamartoma
- Gastrointestinal stromal tumor
- Lipoma
- Ectopic gastric mucosa

- Ectopic pancreas
- Hemangioma
- Hamartoma
- Nerve cell tumors
  - Gangliocytic paraganglioma
  - Neurofibroma
  - Ganglioneuroma
  - Neurilemoma
- Inflammatory fibroid polyp (fibroepithelial polyp).
- Inverted Meckel's diverticulum.

Multiple Polypoid Lesions

- Common
  - Hematogenous metastases
  - Carcinoid
  - Lymphoma
- Uncommon
  - Neurofibromas
  - Kaposi's sarcoma
  - Peutz-Jeghers hamartomas
  - Multiple myeloma
  - Amyloid deposits
  - Adenomas in familial adenomatous polyposis syndrome
  - Hamartomas in Cowden disease.

The polyposis syndromes involving the small intestine have relatively distinct radiologic features. Small bowel adenomas arising in patients with familial adenomatous polyposis syndrome occur primarily in the duodenum. Numerous small, sessile, hemispheric polyps line the duodenum. Patients with familial adenomatous polyposis syndrome have a high incidence for the development of adenocarcinoma of the papilla of Vater. In patients with Cowden disease, the hamartomatous polyps are more frequently found in the colon than small intestine.

NON-NEOPLASTIC SMALL BOWEL DISEASES

Ischemic Bowel Disorders

Mesenteric Ischemia and Infarction

Acute mesenteric ischemia (AMI) is the clinical syndrome resulting from a decrease in blood flow to the small intestine, usually involving the circulation of the superior mesenteric artery (SMA). Emboli to the SMA are responsible for almost half of all cases of AMI. Emboli result from disruption of a thrombus in the left ventricle or atrium in the setting of atrial fibrillation, myocardial infarction, cardioversion, or cardiac catheterization. The middle colic artery is the vessel obstructed most frequently.

Causes of Acute Bowel Ischemia and/or Ischemic Colitis

Cause Mechanism

1. **Mesenteric arterial occlusion (proximal or distal)**
   - Thrombosis, thromboembolism
   - Atherosclerosis, dissection

- Cholesterol embolization
- Aortic surgery, stent placement, etc
- Therapeutic embolization for gastrointestinal hemorrhage
- Fibromuscular dysplasia (rare)
- Various types of vasculitides
- Thrombotic microangiopathies
- Small vessel diseases

2. Mesenteric venous occlusion (proximal or distal)

- Venous thrombosis (primary and secondary)
- Phlebitis of intramural veins (rare)

Mechanical Strangulation with or without mesenteric venous thrombosis
Pronounced overdistention (prestenotic, distention colitis).

Inflammation Pancreatitis, appendicitis, diverticulitis, peritonitis, etc.

3. Low flow or vasospasm Hemorrhagic, cardiogenic, septic shock

- Cardiac failure, cardiac arrhythmia
- Nonpulsatile cardiopulmonary bypass
- Dehydration, stress (high-endurance athletes)
- Chronic renal failure requiring hemodialysis
- Use of various legal and "illegal" drugs
- Pheochromocytoma.

Clinical suspicion for acute mesenteric infarction was no primary indication for CT scanning but used to be urgently evaluated by arterial angiography. Arterial angiography remains the gold standard especially in the light of potential interventional therapeutic procedures. However, the excellent imaging properties of CT angiography, which could be further improved by multislice scanning, make CT an ideal non-invasive diagnostic tool for excluding arterial occlusion down to the first segmental branches and or exclude manifest signs of bowel ischemia.

The majority of ***emboli*** lodge approximately 3 to 10 cm from the ostium of the SMA, just distal to the origin of the middle colic artery. The arterial embolus may be identified as contrast filling defect or abrupt cutoff of vascular opacification. Frequently the arterial occlusion is followed by secondary venous thrombosis due to stasis. In these cases, there is a lack of opacification of the mesenteric veins after injection of contrast media also in the portal venous phase (at least 60 seconds delay).

CT reveals moderate (< 15 mm) bowel wall thickening. Submucosal hemorrhage leads to asymmetric high attenuation areas. The bowel segments may be dilated and are mostly completely atonic with fluid-air levels (paralytic ileus). Scans may also show intramural air inclusions and air collections in the portal and mesenteric veins indicating (although not absolutely conclusive) bowel gangrene. While in the early evolution of ischemic injury there is intense mucosal enhancement after administration of intravenous contrast (due to slower transit of blood through capillaries) in later phases the hypoperfusion of affected bowel segments may be seen.

Table 8.1: Comparison of mesenteric ischemia syndromes

	Acute mesenteric ischemia	*Mesenteric angina*	*Ischemic colitis*
Presentation	Severe abdominal pain disproportionate to clinical findings	Postprandial pain, fear of eating, weight loss	Hematochezia; diarrhea; lower abdominal pain
Suggested diagnostic tests	Angiography, CT scan	CT scan. Angiography in the appropriate clinical setting	Colonoscopy, CT scan

Nonocclusive mesenteric ischemia (NOMI), or mesenteric vasospasm in the absence of vascular occlusion, causes AMI in 20 to 30% of cases. As a result of systemic hypoperfusion, mesenteric vasospasm occurs to preserve cardiac and cerebral blood flow. The vasospasm may persist after the hypotension resolves, leading to ongoing intestinal ischemia. Causes of NOMI include myocardial infarction, aortic insufficiency, congestive heart failure, renal insufficiency, cardiac or intra-abdominal surgery, cardiopulmonary bypass, treatment with vasoconstrictive drugs such as digitalis, diuretics, and alpha-adrenergic agents, and use of cocaine.

Superior mesenteric venous thrombosis (SMVT) accounts for 5% of cases of AMI. The thrombosis results from a combination of low flow through the mesenteric vessels and a hypercoagulable state. Although some patients do not have an identifiable cause for the SMVT, many others have a definite precipitating etiology. Causes of mesenteric venous thrombosis include: primary hypercoagulable syndromes such as factor V Leiden mutation, protein C deficiency, antithrombin III deficiency, protein S deficiency, and anticardiolipin antibodies; hematologic disorders associated with thrombosis, such as polycythemia vera, thrombocytosis, and paroxysmal nocturnal hemoglobinuria; intra-abdominal inflammation as in pancreatitis, peritonitis, or inflammatory bowel disease; intra-abdominal surgery; and cirrhosis with portal hypertension.

In cases of ***mesenteric venous thrombosis***, a prominent intraluminal filling defect in the mesenteric vein can be identified. Care has to be taken not to misinterpret inhomogeneous contrast filling of the mesenteric vein as thrombotic filling defect if the scan is performed too early.

In spiral CT scans acquired during the late arterial or early portal phase after intravenous contrast administration, differences in the timing of contrast arrival in the splenic and mesenteric veins can produce pseudothrombus artifacts that mimic mesenteric vein thrombosis.

CT Manifestations of Bowel Ischemia

Bowel ischemia represents a process of insufficient blood supply of the small or large bowel with the consequences ranging from a transient, totally reversible attack to a lethally catastrophic event. The severity of the ischemic attack depends on the acuteness, duration, degree, and state of the collateral circulation; extent of the involved area; and promptness in correcting the underlying pathologic process. The damage starts with the mucosa, which is most vulnerable to the ischemic insult, extends outward through the submucosa and the proper muscular layer, and ends at the serosa. The extent of the injury may range from mucosal, to mural, to transmural necrosis.

Mesenteric ischemia can result in changes in the affected bowel loops, which may be detected on CT. The most common reported CT finding is bowel wall thickening, which is a result of submucosal edema/inflammation and usually does not exceed 1.5 cm in thickness.

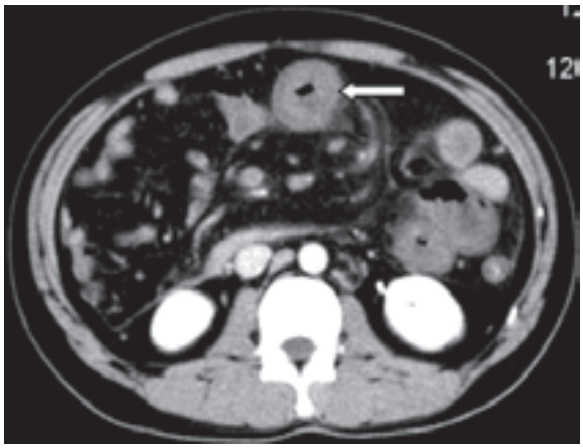

Target Sign

Bowel wall edema presents as circumferential thickening of the affected bowel loop demonstrating a hyperdense serosa, relatively hypoattenuating submucosa and mucosal hyperemia. This has been termed as the target appearance.

FIGURE 8.50: Axial CECT in a case with SMA thrombus showing the typical pattern of enhancement in a ischemic bowel (target sign arrow).

The loops are typically circumferentially thickened. The bowel wall may appear low in density reflecting edema and inflammation or in patients with submucosal hemorrhage, the wall may appear high in density due to the blood or persistent enhancement. Intramural hemorrhage, however, is not specific for ischemia, as it can occur as a result of condition including trauma, anticoagulation therapy or radiation. Although the bowel wall thickening is usually homogeneous, a halo appearance to the bowel wall has also been described in patients with ischemia. Associated stranding and fluid in the mesentery may also be present. Although bowel wall thickening is a common findings in patients with ischemic bowel, it is very nonspecific, as it occurs in many inflammatory, infectious, or neoplastic conditions.

Thickened small bowel loops may demonstrate absence of enhancement or in some cases, delay in enhancement when compared to unaffected loops. Visualization of the bowel wall and its enhancement may be improved if a low density oral contrast agent is administered. Low attenuation oral agents offer two major advantages over traditional CT oral contrast agents when evaluating for mesenteric ischemia. First, low attenuation contrast agents do not interfere with manipulation of 3D volume sets and therefore the mesenteric vessels and their branches and be readily visualized without the need for extensive editing. Second, a low attenuation intraluminal agent allows better visualization of the enhancing bowel wall and therefore allows functional information to be acquired. Low attenuation contrast agents coupled with spiral CT and rapid intravenous contrast administration makes it possible to quantify small bowel enhancement. Thus, low density oral contrast agents (water) along with the faster scanning obtainable with spiral and now MDCT allows better visualization of the enhancing bowel wall and can be utilized to obtain functional as well as anatomic information. Luminal dilatation of affected bowel loops is another common finding on CT scans, probably resulting from disruption of the normal peristaltic activity. The dilated bowel loops are often filled with fluid, which is most likely due to fluid and blood, which has seeped from the ischemic bowel wall. However, as with bowel wall thickening, small bowel dilatation is certainly not specific for ischemia.

Pneumatosis is a less common finding in patients with ischemia bowel, but is a much more specific finding. It occurs when intraluminal gas dissects into the friable ischemic bowel wall. Although pneumatosis has been reported in benign condition such as collagen vascular disease, steroid use, pulmonary disease, etc. the clinical presentation and history usually will allow differentiation. On CT pneumatosis appears as air within both the bowel wall. In some patients the intramural air may then dissect from the bowel wall into the mesenteric vein or portal vein branches in the liver which can be easily detected with CT. Also, free intraperitoneal air has been reported, and as with pneumatosis is an ominous sign, usually signifying transmural infarction of the bowel.

- Reduced enhancement of bowel wall
- Thickening of bowel wall
- Thickening of bowel wall with target sign
- Abnormal enhancement of bowel wall (reduced enhancement, target sign, or both.
- Mesenteric fluid
- Mesenteric congestion
- Ascites.

Persistent Arterial Insufficiency without Reperfusion

Sometimes, the ischemic event persists long enough without reperfusion and becomes destined to its final outcome: necrosis of the whole bowel wall. The intramural arteriocapillaries first lose part of their volume as the earlier entered blood flows out from the veins, even though some blood may seep back from the veins. At this moment, the CT shows a thin, poorly or suboptimally enhanced bowel wall. Occasionally, detailed ischemic mucosal folds can be seen. Poor enhancement along the antimesenteric side is suggestive of nonocclusive ischemia. The intestinal fluid is decreased because the enterocytes cannot produce a normal amount of secretions if the arterial supply is

blocked. The bowel wall is first pale and then turns to black and becomes thinned as a result of intravascular volume loss and collapse of necrotic tissue. Not uncommonly, the infarcted bowel is described as grossly dark red or purple and filled with bloody fluid. In fact, this description represents a reperfused instead of a nonreperfused ischemic bowel because there should not be a lot of erythrocytes or plasma extravasating through the damaged and ruptured microvascular wall into the mucosa, submucosa, or bowel lumen if the arterial supply is severely reduced, either occlusively or nonocclusively, without a subsequent reperfusion taking place. Microscopically, inflammatory cell infiltration in response to bacterial invasion is much more prominent than RBC extravasation in the nonreperfused attenuated wall. The evolution of bloody diarrhea or bloody intraluminal fluid is most likely due to an outpouring of the reperfused blood from the infarcted mucosa or submucosa into the lumen. Even though the residual blood in the capillaries that flows back from the venules may cause extravasation of RBC in the mucosa (lamina propria of the villi) or scattered hemorrhagic foci in the submucosa or subserosa, it is unlikely for this small amount of hemorrhage to cause considerable wall thickening. As bacteria proliferate and more gas is produced, the intraluminal gas may dissect into the necrotic wall (pneumatosis intestinalis), spread through the mesenteric veins, and finally flow into the portal veins.

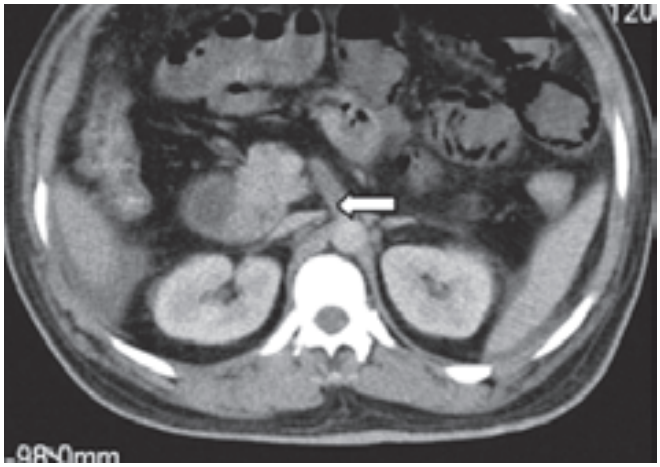

FIGURE 8.51: Axial CECT showing superior mesenteric artery thrombus, note the non-enhancing hypodensity (arrow).

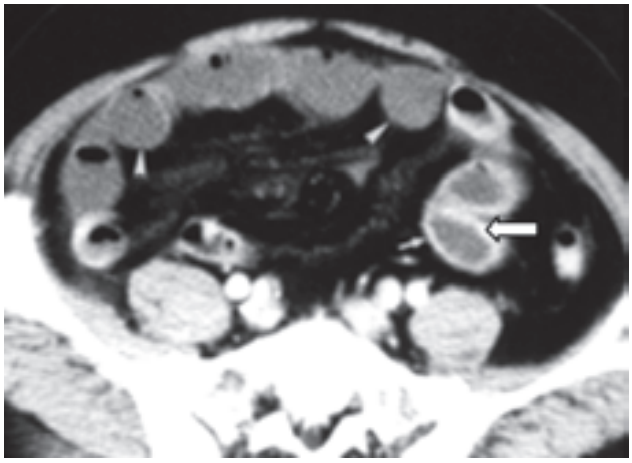

FIGURE 8.52: Axial CECT show segments of nonenhancing bowel walls (arrowheads), note enhancing adjacent bowel loops (arrow).

Transient Arterial Insufficiency with Subsequent Reperfusion

If the pathologic processes were corrected (by lysis of the embolus, reestablishment of blood pressure, release of external compression, or prompt development of collateral circulation), the reentered blood might cause different CT appearances, depending on the degree of disruption of the vascular wall integrity. The intestinal microvessel derives its oxygen supply through direct diffusion from the blood. When the arterial supply is insufficient for a certain period and returns later, the microvascular endothelium and the mucosal epithelium become damaged, and the permeability increases proportionately to the duration of oxygen deprivation and the degree of the reperfusion injury. If the degree is mild, only water molecules leak into the extravascular space and cause a mucosal or submucosal edema appearance on CT. When the damage becomes more severe, the molecules of contrast medium follow the previously escaped fluid and cause various degrees of mucosal or submucosal enhancement. As the ruptures between the damaged endothelial cells further enlarge, the RBC also leak, resulting in a thickened soft-tissue-density bowel wall with or without mucosal enhancement. The thickened mucosal folds or thumbprinting appearance seen

radiologically are caused by submucosal edema or hemorrhage. The mucosa may remain intact or become necrotic. In the case of reperfusion, the bowel is grossly dark red, the wall is thickened, and the lumen is largely filled with bloody fluid in contrast with appearances of the nonreperfused condition.

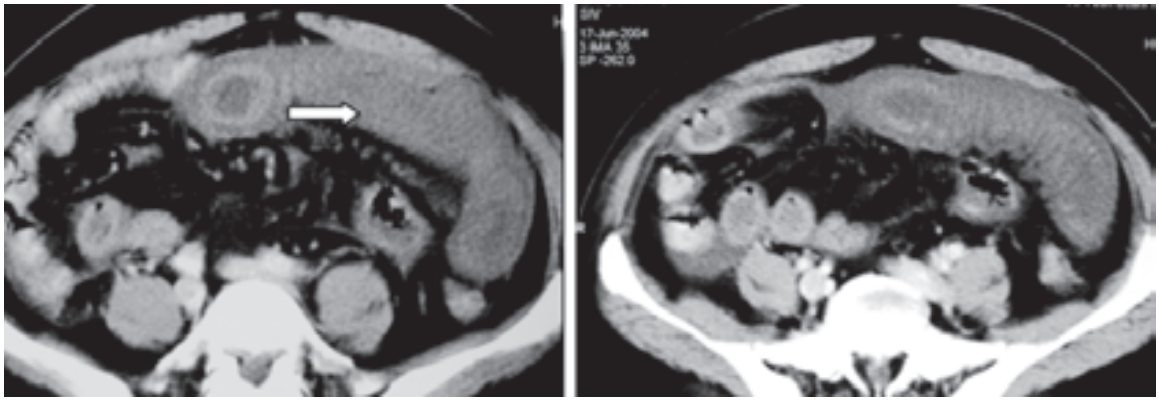

FIGURES 8.53A and B: Axial CECT showing long segment of ischemic bowel with thickened walls and mucosal enhancement (arrow in A).

Impaired Venous Drainage

When the mesenteric venous drainage is impaired, the intravascular volume increases, and the hydrostatic pressure rises as the arterial blood continues flowing into the capillary bed and venules of the bowel and mesentery. The elevated hydrostatic pressure causes the molecules of water or contrast material, or even the erythrocytes, to escape through the enlarged fenestrations of the stretched arteriocapillary endothelium into the submucosa, appearing as submucosal and mesenteric edema or hemorrhage on CT. These appearances are similar to those of reperfused ischemia previously described. However, the mechanism is different from that of a directly arterial origin, which is caused by oxygen-deprived and free radical-induced disruption of vascular wall integrity and resultant increased permeability. As the tissue tension in the extravascular compartment of the submucosa increases, the arterial supply may be compromised and the mucosal enhancement decreased. Tissue tension may reach an extent sufficient to cause a complete failure of the arterial supply because of stasis of blood flow or thrombosis of small arterioles and subsequent bowel necrosis. The mesenteric veins are usually engorged during this condition.

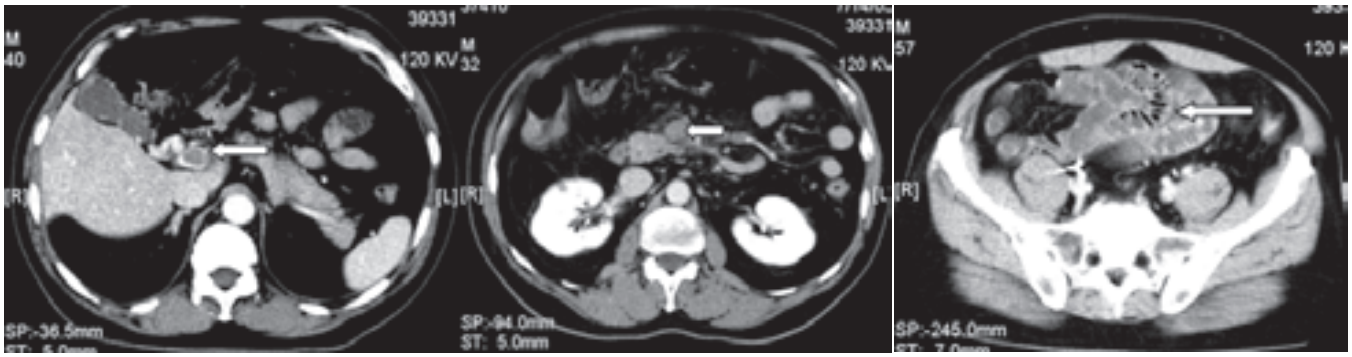

FIGURES 8.54A and B: Axial CECT showing acute thrombus in the portal and mesenteric vein (arrows in A,B). Note the dilated small bowel loops with enhancement and mural air pockets (arrow in C).

Ischemia due to Closed-loop Small-Bowel Obstruction

Closed loop small-bowel obstruction is caused by adhesion, incarcerated hernia, or volvulus. Both the artery and vein are compressed. Because the arterial pressure is higher than the venous pressure, the arterial inflow is usually

more than the venous outflow. Thus, the CT appearances are similar to those of impaired venous drainage. The relatively rich arterial supply may contribute to increased intestinal secretions and rapid fluid-filling of the lumen of the closed bowel loop, which is occluded at both ends. Theoretically, the arterial supply is still adequate if the mucosal enhancement is normal. If the artery were compressed more tightly, the wall enhancement might be suboptimal, and the thickness would not be increased. If the compression is tight enough from the beginning of the obstruction, the wall might be thin and totally unenhanced, similar to that of nonreperfused ischemia.

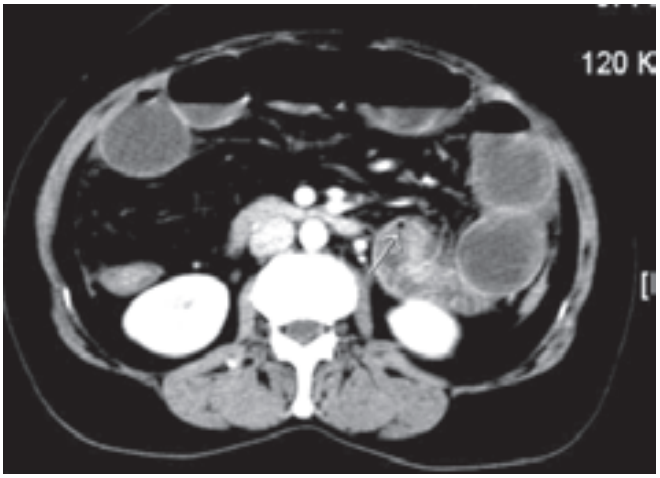

FIGURE 8.55: Axial CECT in a patient with small bowel obstruction showing proximal jejunal thickening with mural air pocket (segmental gangrene was found at surgery).

Portomesenteric Vein Gas

Portomesenteric vein gas is a rare condition whose pathogenesis is not fully understood. Portomesenteric vein gas is most commonly caused by mesenteric ischemia but may have a variety of other causes. The primary factors that favor the development of this pathologic entity are intestinal wall alterations, bowel distention, and sepsis. Portomesenteric vein gas is idiopathic in approximately 15% of cases. Advanced imaging techniques such as computed tomography (CT) have increased the sensitivity for detection of portomesenteric vein gas. At CT, portal vein gas appears as tubular areas of decreased attenuation in the liver, predominantly in the left lobe. Gas in the great mesenteric veins can easily be demonstrated with contrast material–enhanced CT, whereas gas in the small mesenteric veins appears as tubular or branched areas of decreased attenuation in the mesenteric border of the bowel. Findings of portomesenteric vein gas at CT should be carefully evaluated in the context of clinical findings. In the majority of cases, the prognosis is favorable and surgery is not required. However, when CT demonstrates portomesenteric vein gas and clinical findings suggest the presence of mesenteric ischemia, surgery is mandatory.

Mesenteric Vein Gas

Gas from the intestinal lumen can pass through the intestinal wall and travel via the small mesenteric veins and the superior or inferior mesenteric vein to the portal vein and into the liver. The presence of gas in the superior or inferior mesenteric vein depends on the vascular supply to the affected intestine. Gas in the great mesenteric veins can easily be demonstrated with contrast-enhanced CT. Gas in the small mesenteric veins appears as tubular or branched areas of decreased attenuation in the mesenteric border of the bowel. Mesenteric vein gas should not be confused with pneumoperitoneum or air in the appendix. Pneumoperitoneum does not have a tubular or branched appearance and can be found in the interface between the antimesenteric border of the bowel and the parietal peritoneum (peritoneal cavity).

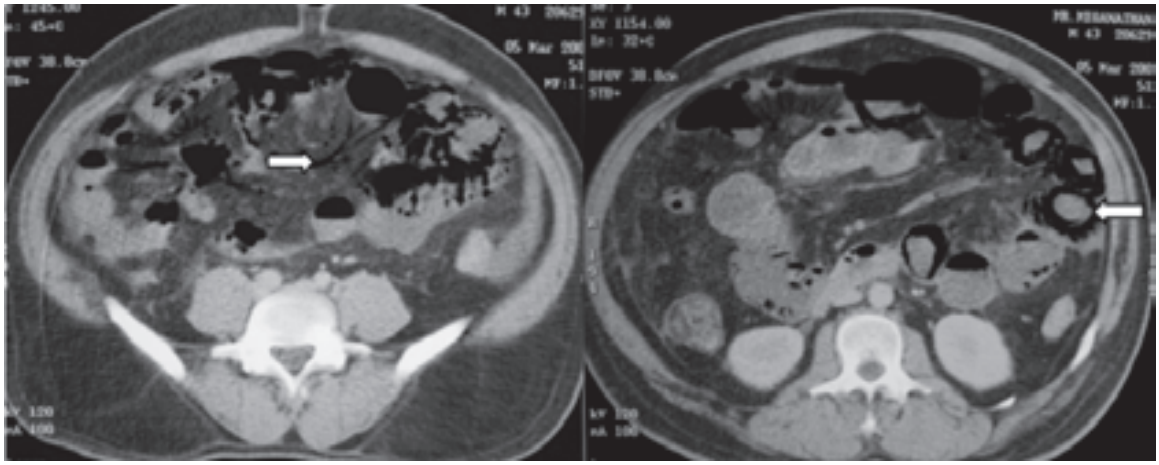

FIGURES 8.56A and B: Axial CECT in a patient with SMA thrombus showing pneumatosis of the distal small bowels (arrow in B), note the air within the mesenteric vessels (arrow in A).

GI Vasculitis

Vasculitis

Vasculitis can affect blood vessels of all sizes, resulting in necrosis and inflammation. The extent and clinical course of disease depends on the size and location of the affected vessel. With larger vessels, abdominal manifestations of vasculitis may be indistinguishable from those of mesenteric ischemia caused by emboli or thrombosis unless there is associated evidence of systemic disease. Inflammation of medium-sized arteries may lead to the formation of aneurysms, which commonly occurs in polyarteritis nodosa. Rupture of these aneurysms may cause gastrointestinal or intra-abdominal hemorrhage. With small-vessel involvement, ulceration and stricture formation are common but perforation is seen less frequently. The vasa recta and intramural arteries and arterioles may be affected in virtually all disorders associated with systemic vasculitis.

Major Categories of Noninfectious Vasculitis

- Large-vessel vasculitis
  - Giant cell arteritis
  - Takayasu arteritis
- Medium-sized-vessel vasculitis
  - Polyarteritis nodosa
  - Kawasaki disease
  - Primary granulomatous central nervous system vasculitis
- Small-vessel vasculitis
  - Antineutrophil cytoplasmic autoantibody (ANCA)–associated small-vessel vasculitis
  - Microscopic polyangiitis
  - Wegener granulomatosis
  - Churg-Strauss syndrome
  - Drug-induced ANCA-associated vasculitis
- Immune complex small-vessel vasculitis
  - Henoch-Schönlein purpura
  - Cryoglobulinemic vasculitis

  - Lupus vasculitis
  - Rheumatoid vasculitis
  - Sjögren syndrome vasculitis
  - Hypocomplementemic urticarial vasculitis
  - Behçet syndrome
  - Goodpasture syndrome
  - Serum sickness vasculitis
  - Drug-induced immune complex vasculitis
  - Infection-induced immune complex vasculitis
- Paraneoplastic small-vessel vasculitis
  - Lymphoproliferative neoplasm induced vasculitis
  - Myeloproliferative neoplasm-induced vasculitis
  - Carcinoma-induced vasculitis
  - Inflammatory bowel disease vasculitis.

Systemic Lupus Erythematosus

Systemic lupus erythematosus is an autoimmune disorder that affects the musculoskeletal system, kidneys, gastrointestinal tract, or skin. Local deposition of antigen-antibody complexes or antibodies inducing necrotizing vasculitis is presumed to be the cause of this disease. Most patients are between 16 and 41 years old, with the disease occurring most commonly in women during the child-bearing years. A diagnosis of systemic lupus erythematosus can be made with 98% specificity and 97% sensitivity if at least four of 11 diagnostic criteria are present at any time during the course of the disease. These criteria include malar rash, discoid rash, photosensitivity, oral ulcers, arthritis, serositis, antinuclear antibodies, and renal, neurologic, hematologic, and immunologic disorders. Inflammation of the small blood vessels of the gut produces a variety of complications including intestinal ischemia, hemorrhage, ileus, ulceration, infarction, and perforation. Systemic lupus erythematosus may involve any part of the gastrointestinal tract from the esophagus to the colon including the stomach, duodenum, colon, and rectum. However, the territory of the superior mesenteric artery is most commonly affected.

Vasculitis involving the gastrointestinal tract is part of a systemic process although the signs and symptoms may initially be limited.

The signs and symptoms of systemic vasculitis involving the gastrointestinal tract result from mesenteric ischemia.

- Abdominal pain — 25 percent
- Gastrointestinal bleeding — 7 percent
- Peritonitis — 4 percent

Specific Disorders

Polyarteritis Nodosa

Polyarteritis nodosa affects small and medium sized arteries and can cause a variety of gastrointestinal symptoms as noted above. The more severe manifestations include intestinal infarction or perforation, pneumatosis intestinalis, and pseudomembranous colitis.

Churg-Strauss Syndrome

The Churg-Strauss syndrome (also called allergic granulomatosis and angiitis) is a multisystem disease similar to PAN except for the characteristic triad of allergic rhinitis, asthma, and prominent peripheral blood eosinophilia.

Henoch-Schönlein Purpura

Henoch-Schönlein purpura (HSP) is a small vessel vasculitis that typically occurs in children although all ages can be affected. Patients classically exhibit lower extremity purpura, arthritis, and hematuria. The gastrointestinal tract is affected in upto 50 percent of patients. Gastrointestinal symptoms include colicky abdominal pain, nausea, vomiting, diarrhea, constipation, and occult or overt intestinal bleeding. The course can wax and wane over several weeks and often resolves spontaneously.

Systemic Lupus Erythematosus

The vasculitis associated with systemic lupus erythematosus (SLE) involves small- and medium-sized vessels, and involves the gastrointestinal tract in upto 50 percent of patients. Lower abdominal pain secondary to mesenteric vasculitis is generally an insidious symptom that may be intermittent for months prior to the development of an acute abdomen with nausea, vomiting, diarrhea, GI bleeding, and fever.

Antiphospholipid Antibody Syndrome

The antiphospholipid antibody syndrome (APS) can occur in patients with SLE or as an isolated disorder. It represents a hypercoagulable state which can be associated with a variety of clinical features including arterial and venous thrombosis, livedoreticularis, and spontaneous abortions. Gastrointestinal manifestations of APS are due to ischemia involving the esophagus, stomach, duodenum, jejunoileum, or colon, resulting in gastrointestinal bleeding, abdominal pain, an acute abdomen, esophageal necrosis with perforation, or giant gastric ulceration.

Inflammatory Bowel Disease Associated Vasculitis

Vasculitis is often considered in the differential diagnosis of inflammatory bowel disease (IBD), especially Crohn's disease.

Imaging studies: Imaging studies, such as CT scanning or barium studies, are frequently normal in patients with symptomatic intestinal vasculitis and, when abnormal, have nonspecific abnormalities such as a thickened edematous bowel wall unless mesenteric infarction has occurred. Angiography may be useful in diagnosing small and medium vessel vasculitis, such as PAN.

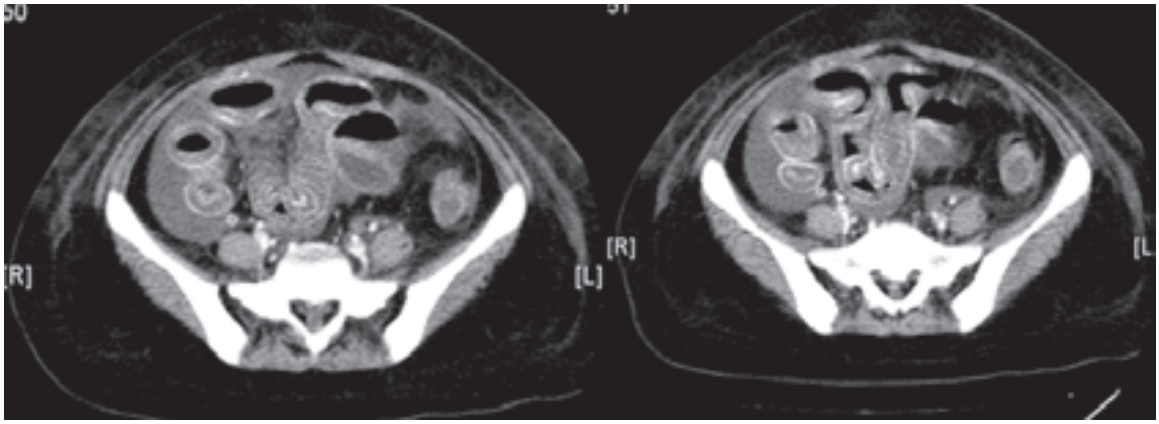

FIGURES 8.57A and B: Axial CECT in a patient with SLE presenting with diffuse abdominal pain reveals peritoneal free fluid with diffuse serosal enhancement of the small bowel which are thickened, findings resolved subsequently after conservative treatment.

Henoch-Schönlein Syndrome

Henoch-Schönlein syndrome is one of the subgroups of hypersensitivity-related acute small-vessel vasculitis. Although its cause is unknown, immunization, insect bites, medications, infections, and certain foods may play a role in its development. Henoch-Schönlein syndrome occurs most commonly in children between 3 and 10 years of age, but in some series, 30% of affected patients have been reported to be over 20 years old. The diagnosis is based on characteristic clinical signs and symptoms such as skin rash, arthritis involving the large joints, colicky abdominal pain, gastrointestinal bleeding, and hematuria. The gastrointestinal manifestations are thought to be related to edema and intramural hemorrhage. When gastrointestinal symptoms predominate or precede the appearance of skin lesions, the syndrome may mimic a number of acute abdominal diseases, resulting in unnecessary laparotomies. Gastrointestinal hemorrhage is mostly confined to the mucosa and submucosa, and full-thickness necrosis and perforation of a bowel loop is rare. Therefore, most gastrointestinal manifestations are self-limited and without residua: Only 3-5% of patients develop bowel infarct, perforation, or irreducible intussusception. No characteristic radiologic findings are seen, although multifocal bowel wall thickening with unaffected areas along with clinical findings are important in establishing a diagnosis.

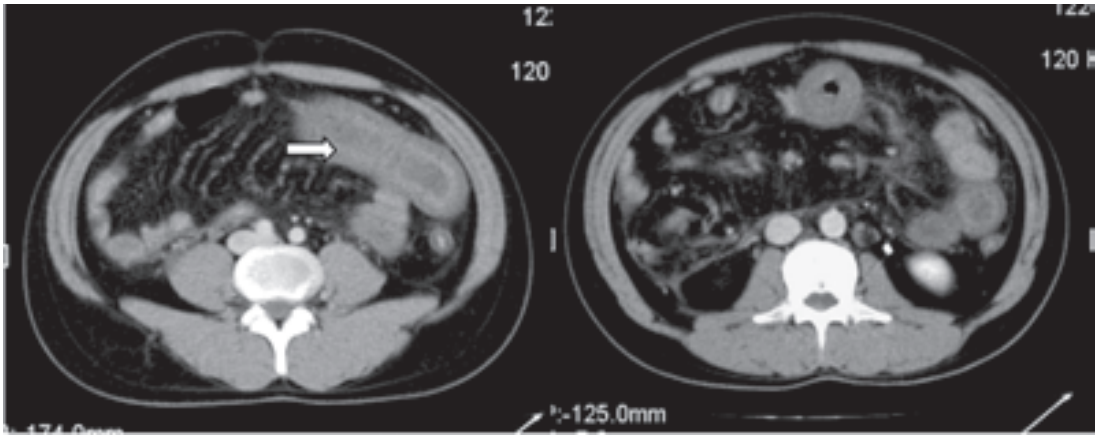

FIGURES 8.58A and B: Axial CECT in a patient with known Henoch-Schönlein purpura presenting with abdominal pain showing thickening of distal jejunum showing mucosal enhancement (arrow).

Malabsorption

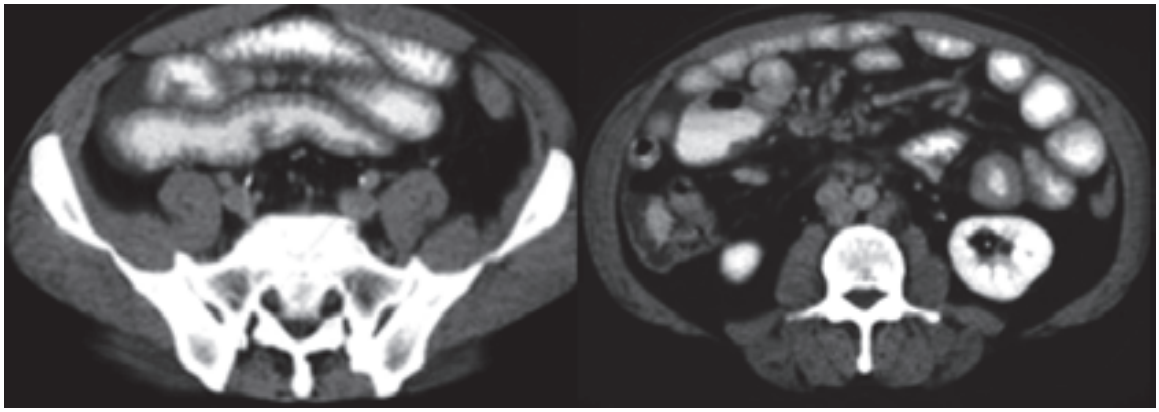

FIGURES 8.59A and B: Axial CECT in a patient with nonspecific abdominal symptoms showing nonspecific mucosal thickening.

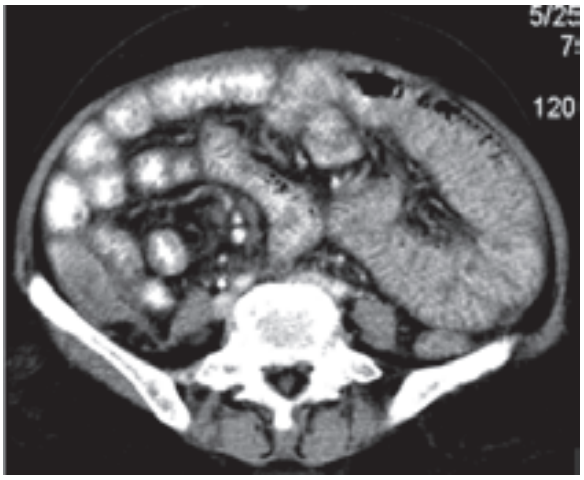

FIGURE 8.60: Axial CECT in a patient with tuberculosis reveals diffuse jejunal mucosal thickening with nodularity.

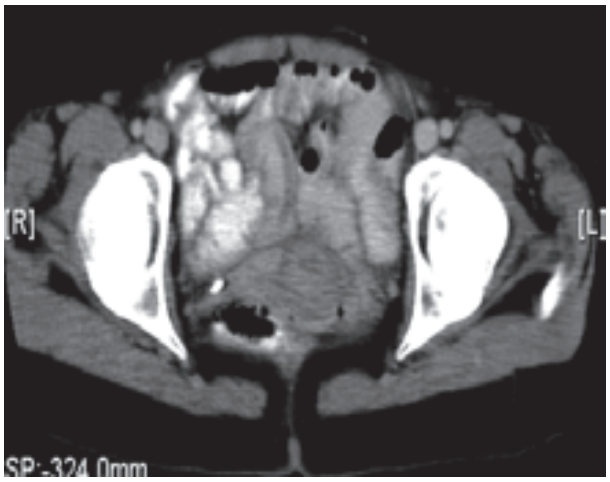

FIGURE 8.61: Axial CECT in a patient with abdominal cramps and distention showing a linear luminal opacity in the distal small bowel suggesting an ascariasis worm.

Adult Intussusception

Intussusception is defined as the telescoping of one segment of GIT into an adjacent one, in adults it accounts for 5% of mechanical. Various extrinsic, intrinsic, or intraluminal processes may result in small bowel intussusception. The final common pathway is invagination of an entire proximal small bowel loop and part of its mesentery into the lumen of the distal small bowel. Polypoid tumors, benign or malignant, are the most common cause of small bowel intussusception in adults. Intussusception may occur in extrinsic disorders such as adhesions or duplications. Although a histologic diagnosis cannot be made with CT, a guarded differential diagnosis can be made based on clinical history, tumor location, and specific imaging features. At CT, intussusception displays one of three patterns depending on the severity and duration of the disease: the target sign, a sausage-shaped mass with alternating layers of low and high attenuation, and a reniform mass. In a small percentage of patients with metastatic melanoma, small bowel obstruction with intussusception is the initial manifestation of disease.

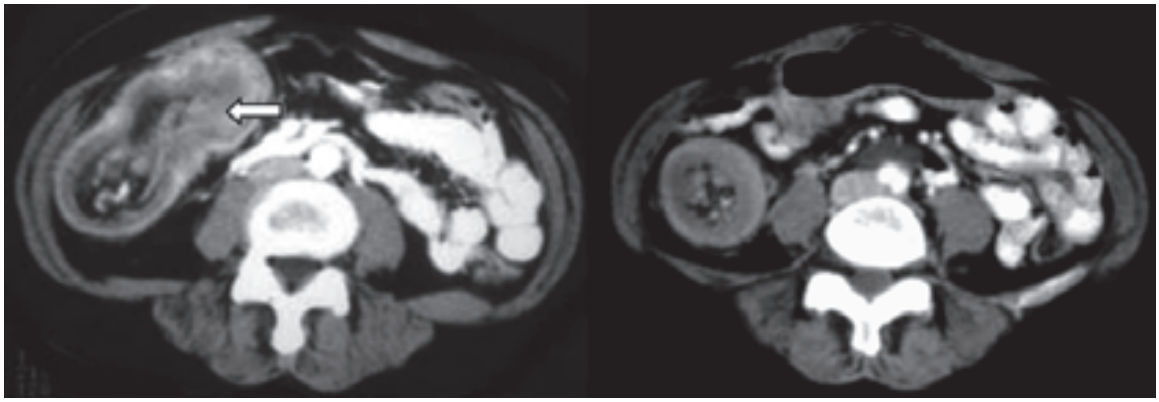

FIGURES 8.62A and B: Axial CECT showing a sausage shaped mass in the right iliac fossa with typical features of intussusception. Note the luminal fat attenuation (arrow).

Small Bowel Obstruction

There is a growing importance of CT for the diagnosis of SBO for a variety of reasons: (1) it does not rely on peristaltic propulsion and can be also used in cases of complete obstruction or paralytic ileus, (2) it provides global assessment of the abdomen, (3) it does not require oral administration of contrast media, and (4) it can readily assess strangulation.

A *non-obstructive paralytic ileus* is characterized by uniformly dilated loops of small and large bowel with gas-fluid levels and no demonstrable lesion causing the obstruction.

In *mechanical bowel obstruction*, dilated bowel loops with gas-fluid levels are seen proximal to the obstruction. The site of obstruction ('transition zone of obstruction') is characterized by an abrupt caliber change. CT usually provides more detailed information on the cause and location of the obstruction. If perforation occurs, extraluminal air is seen in the abdominal cavity and ascites is sometimes observed. A simple obstruction usually shows no mesenteric changes such as vascular engorgement.

Strangulation usually shows a moderately dilated, fluid filled bowel segment that has a radial or U-shaped configuration. Converging and engorged, edematous vascular bundles represent congested mesenteric vessels. Venous strangulation of the bowel wall is suggested when CT shows circumferential thickening of the bowel wall with increased attenuation, hazy mesenteric vessels and increased enhancement after intravenous contrast administration (target sign). Arterial strangulation may be directly assumed when there is delayed or reduced opacification of the bowel wall within the closed loop after administration of intravenous contrast medium or even a total lack of opacification. The latter is frequently associated with the presence of intramural or extraluminal air.

The whirl sign, convergence of mesenteric vessels toward the twisted site or a reversed position of the mesenteric artery and vein are CT signs indicative of a ***volvulus*** or a ***closed bowel loop***. However, the whirl sign is also seen in asymptomatic subjects (approximately 7% of asymptomatic patients), especially at the anatomic level just below the inferior pole of the right kidney. This sign can also be seen in patients after previous abdominal surgery (e.g. gastrectomy). Therefore, it is necessary to combine the presence of the whirl sign with a suggestive abdominal symptoms or other morphological findings such as dilated bowel loops.

A scan across an ***intussusception*** demonstrates three concentric rings formed by (1) the canal and wall of the intussusceptum (inner layer), (2) the mesenteric fat (middle layer), and (3) the intussuscipiens (outer layer). Proximal to the intussusception is an obstruction with dilated bowel loops.

Classification of Hernias

External Hernias

- Inguinal
- Femoral
- Obturator
- Sciatic
- Umbilical
- Ventral
- Spigelian
- Lumbar
- Incisional

Internal Hernias

- Right paraduodenal
- Left paraduodenal
- Foramen of Winslow
- Pericecal
- Intersigmoid
- Transmesenteric
- Transmesocolic
- Retroanastomotic

Causes of Small Bowel Obstruction in Adults

Extrinsic Lesions

- Adhesions
- External hernias
- Internal hernias
- Extrinsic tumors
- Abscess
- Aneurysm
- Hematoma
- Endometriosis

Intrinsic Lesions

- Tumors
  - Adenocarcinoma
  - Carcinoid tumor
  - Lymphoma
  - Gastrointestinal stromal tumor
- Inflammatory lesions
  - Crohn's disease
  - Tuberculosis
  - Eosinophilic gastroenteritis
- Vascular lesions
  - Radiation enteropathy
  - Ischemia
- Hematoma
  - Trauma
  - Anticaogulants
  - Thrombocytopenia

Intussusception

- Adhesions
- Tumors

Intraluminal Lesions

- Gallstones
- Bezoars
- Foreign bodies

Peritoneal Carcinomatosis

Ovarian carcinoma is the most frequent cause of metastatic disease of the omentum. Other tumors that frequently spread to the omentum include carcinoma of the colon, stomach, pancreas, breast, and endometrium. CT findings in small bowel obstruction secondary to peritoneal carcinomatosis include an omental mass in the transition zone causing obstruction.

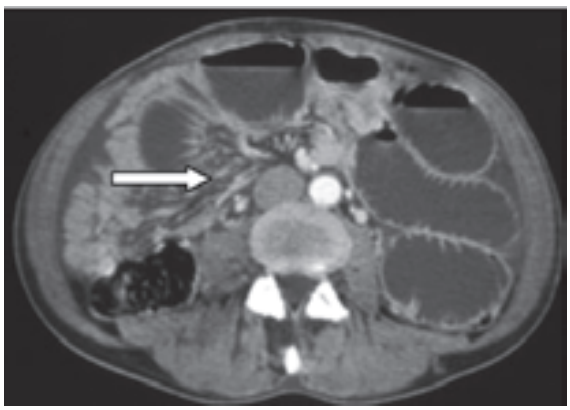

FIGURE 8.63: Axial CECT reveals dilated proximal small bowels with collapsed distal bowel loops in a patient with gastric carcinoma. Note the mesenteric infiltrations with stranding.

Appendicitis and Diverticulitis

CT is accurate in the diagnosis of appendicitis and the detection of complications such as phlegmon, abscess, and peritonitis. Less commonly, small bowel obstruction may be secondary to appendicitis.

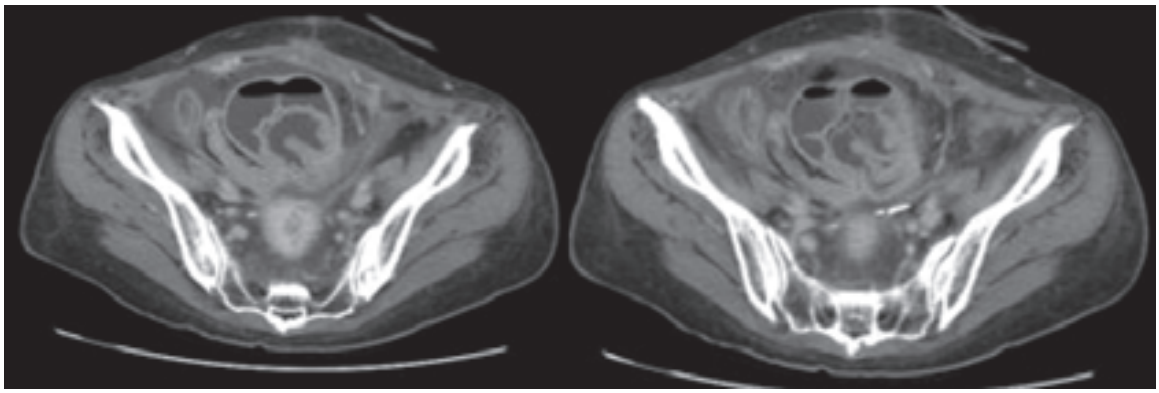

FIGURES 8.64A and B: Axial CECT showing dilated ileal loops with interloop and right iliac fluid in a patient with perforated appendix (postop finding).

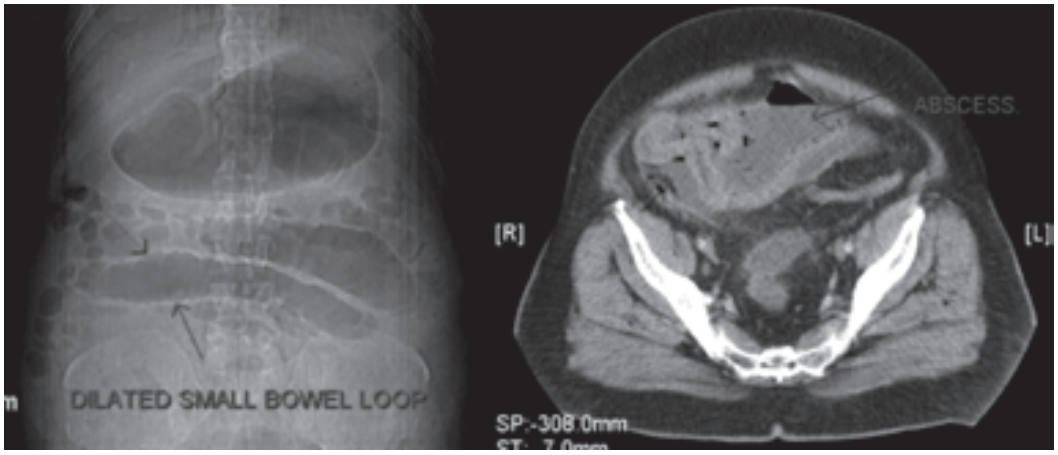

FIGURES 8.65A and B: Axial CECT in a patient with interloop abscess and dilated small bowel loops.

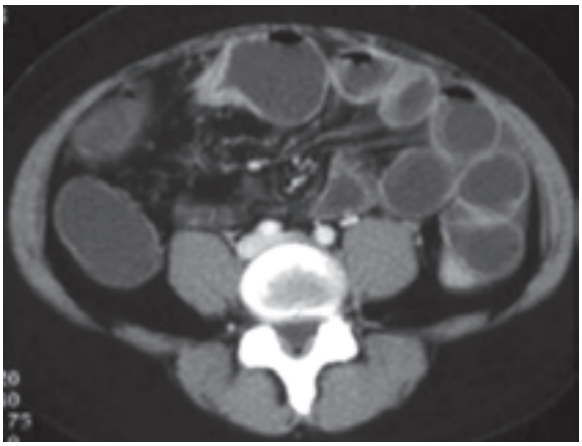

FIGURE 8.66: Axial CECT showing a short segment ileal lesion causing abrupt shouldering and proximal bowel dilatation.

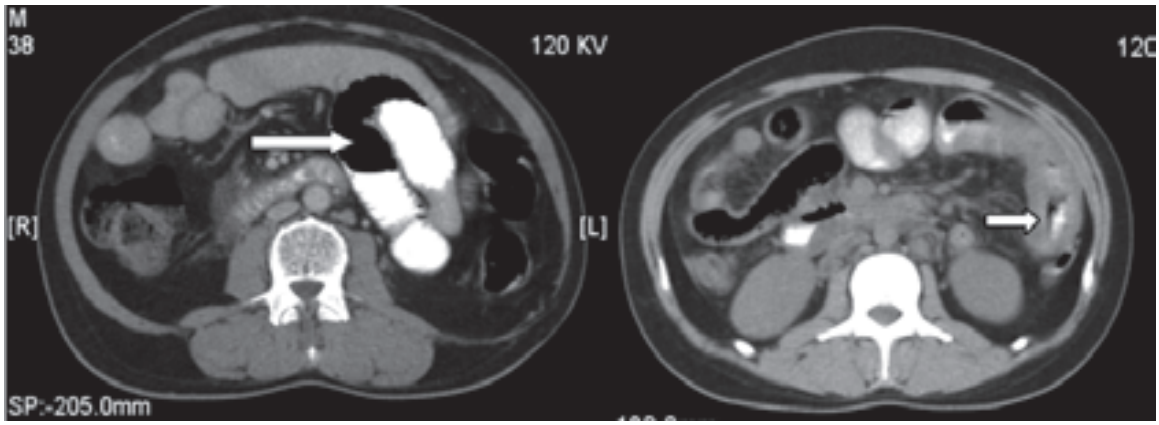

FIGURES 8.67A and B: Axial CECT showing proximal U-shaped bowel dilatation seen in patients with distal bowel obstruction, note the distal bowel lesion (arrow in B).

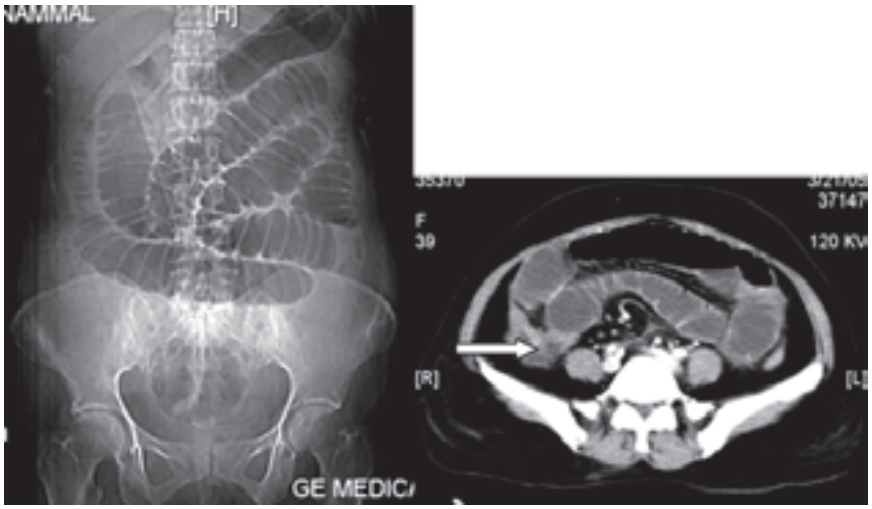

FIGURES 8.68A and B: Digital scanogram showing grossly dilated small bowel loops (arrow). Axial CECT showing a short segment ileal stricture (arrow) causing proximal bowel loop dilatation.

Hernia

Indirect inguinal hernias are the most common abdominal wall hernias. In cases of strangulated hernia, compromise of the blood supply is present, resulting in thickening of bowel loops. Adjacent inflammatory changes can be seen at CT in association with small bowel obstruction.

Extrinsic Causes

The diagnosis of small bowel obstruction due to adhesions is made when all other causes of obstruction have been ruled out at CT. Bowel obstruction is considered to be present at CT when distended bowel loops are seen proximal to collapsed loops. When a point of transition from dilated small bowel to normal-caliber bowel without apparent cause is identified, adhesions are the presumed cause.

CT findings in closed-loop obstruction depend on the length, degree of distention, and orientation of the closed loop in the abdomen. When a closed small bowel loop is horizontally oriented, it has a U- or C-shaped configuration at cross-sectional imaging. A radial configuration with stretched mesenteric vessels converging toward the site of

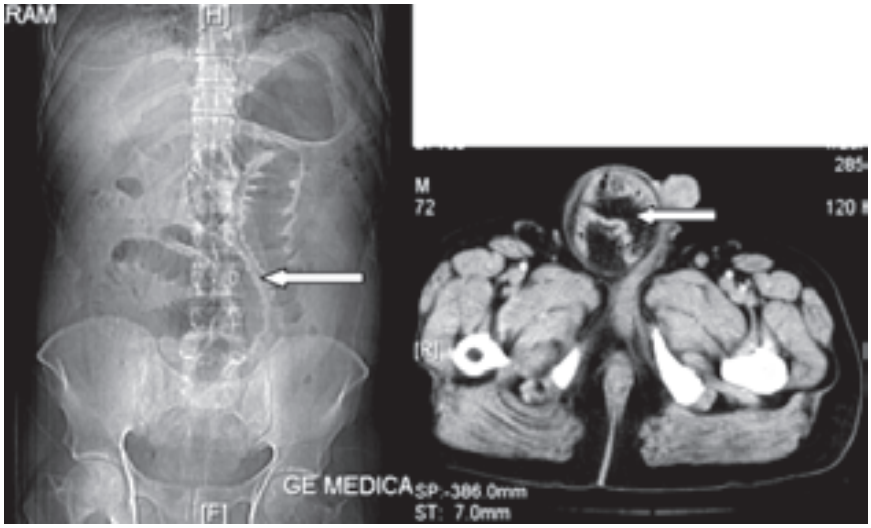

FIGURES 8.69A and B: Axial CECT showing a right inguinoscrotal hernia with bowel loops and mesenteric fat (arrow in B) causing proximal bowel dilatation as seen in the scanogram (arrow).

torsion may be detected depending on the orientation of different small bowel loops within the incarcerated bowel segment. At the site of obstruction, the collapsed loops are round, oval, or triangular. The "beak sign" seen at the site of torsion appears as a fusiform tapering at longitudinal bowel imaging.

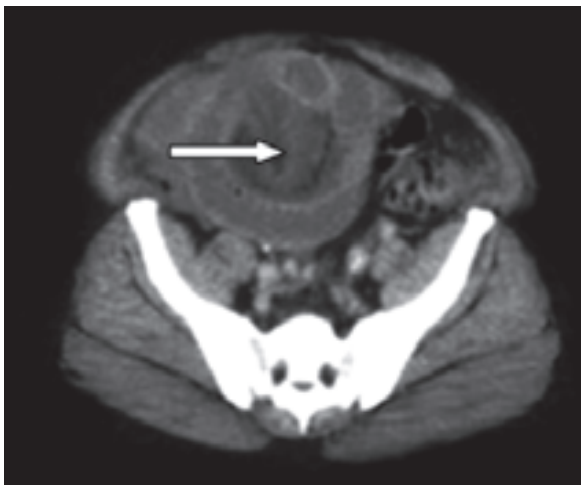

FIGURE 8.70: Axial CECT showing dilated distal ileal loops with abrupt transition (arrow), focal adhesive band was seen at surgery.

Strangulation

CT findings include evidence of small bowel obstruction, a circumferentially thickened loop with high attenuation within the wall, the "target sign", and congestion or hemorrhage in the mesentery attached to the closed loop. In advanced cases, pneumatosis intestinalis may develop.

Volvulus

Small bowel obstruction is a common cause of emergency surgical admission. The most frequent causes are well known and may often be safely treated conservatively in the first instance. However, some of the rarer causes of small bowel obstruction require prompt diagnosis and treatment if they are not to progress rapidly to gangrene. One such cause is small bowel volvulus (SBV).

Table 8.2: Common causes of small bowel obstruction (SBO)

Age group	Intraluminal causes	Intramural causes	Extramural causes (Extrinsic Compression)
Neonates and infants <24 mo	Meconium ileus, milk curd obstruction, foreign bodies	Congenital atresias, stenoses, and diaphragms; duplication cysts; intussusception; Henoch-Schönlein purpura	Inguinal hernia, congenial bands, midgut volvulus, postoperative adhesions
Children and young adults	Foreign bodies, *A lumbricoides*	Crohn disease, tuberculosis, benign neoplasms, primary and secondary malignant neoplasms	Inguinal hernia, congenital and postoperative adhesions, midgut volvulus, complications of appendicitis
Elderly persons	Foreign bodies, gallstones, food bolus	Crohn disease, tuberculosis, primary and secondary neoplasia, potassium strictures, radiation strictures, complications of surgical anastomosis	Postoperative adhesions; femoral, inguinal, umbilical, or incisional hernia; colonic and ovarian neoplasia; adhesion to an inflammatory process (e.g. appendicitis or diverticulitis).

Epidemiology

SBV is uncommon in Western countries but is more common in Africa and Asia. In Western societies its annual occurrence varies from 1.7 to 5.7/100 000 of the population, compared with 24 to 60/100 000 per population in Africa or Asia. The prevalence of SBV varies considerably and accounts for 3.5 to 6.2% of small bowel obstruction in the Western world, compared with 18.5 to 51.5% of small bowel obstruction in Africa and Asia. The rarity and consequent delayed diagnosis accounts for the higher incidence of gangrenous SBV in the Western world.

Etiology and Pathogenesis

The causes of SBV may be classified as either primary or secondary.

Primary Small Bowel Volvulus

This occurs in an otherwise normal abdominal cavity and is much more common in Africa and Asia. Although the etiology is still poorly understood, several etiological factors have been proposed.

Diet: Duke and Yar reported a ten-fold increase in the incidence of SBV among Muslims in Afghanistan during the Ramadam festival. They suggested that diet may be a factor as their patients had eaten large quantities of fiber after prolonged fasting. In the largely Hindu population of Nepal the marked seasonal variation of SBV peaks during the monsoon, a season marked with feasts and festivals.

Gut motility: Several studies have suggested that increased intrinsic gut motility has a role in the etiology of SBV. Parasitic infestation is known to alter small bowel motility, and there is a close correlation between regions where parasitism is endemic and the geographic areas where primary SBV is most prevalent. Desouza reported 12 cases from Uganda where primary SBV had developed a few hours after consumption of local beer containing high concentrations of 5 hydroxy-tryptamine (5HT), a known stimulant of gut motility. It has also been hypothesized that altered bowel tone and peristaltic activity resulting from diabetic automatic neuropathy may contribute to some cases of SBV.

The suggested mechanism(s) underlying primary SBV is that a bulky bolus of food enters the proximal jejunum, causing the loop to descend into the pelvis. This displaces empty small bowel loops upwards, initiating rotation of the mesentery and leading to volvulus. For this to occur, there must be a combination of a long small bowel attached to a broad-based, fat-free mesentery (which splints the bowel), very firm abdominal muscles (restricting bowel movement to the coronal plane) and a diet with an exceptionally high bulk, eaten rapidly on an empty stomach.

Secondary Small Bowel Volvulus

Volvulus of the small bowel may develop as a result of various, often acquired, predisposing factors. It is relatively more common in Western countries where it accounts for 70-90% of cases in SBV. The most frequently related conditions are bands, adhesions, Meckel's diverticulum, internal hernia, Ascariasis, and pregnancy. Other associations that have been reported include ileal atresia, meconium ileus, enteroenterostomy, leiomyoma of the mesentery, and following operations, particularly gastrostomy, gastrectomy, and total hip replacement. The suggested mechanism(s) of secondary volvulus involves obstruction of a small bowel loop at two fixed points by one of these predisposing conditions. As the loop fills with liquid, peristalsis causes it to twist around its mesentery.

Age and Sex Distribution

SBV may occur at any age, although the primary variety mainly occurs in children and young adults. In contrast, secondary SBV is uncommon in those under 40 years of age, with a peak incidence in the 6th to 8th decades. Males predominate in both primary and secondary SBV. In pregnant females, volvulus is the second most common cause of intestinal obstruction, yet rarely is the small bowel involved (colonic volvulus being most common) and even less frequently is the volvulus complete.

Clinical Features

SBV presents with the classical features of intestinal obstruction. The outstanding symptom is central abdominal pain, the severity of which may be out of proportion to the apparent degree of obstruction. The diagnosis should be particularly considered if the pain does not respond to narcotic analgesia, although in such cases frank gangrene

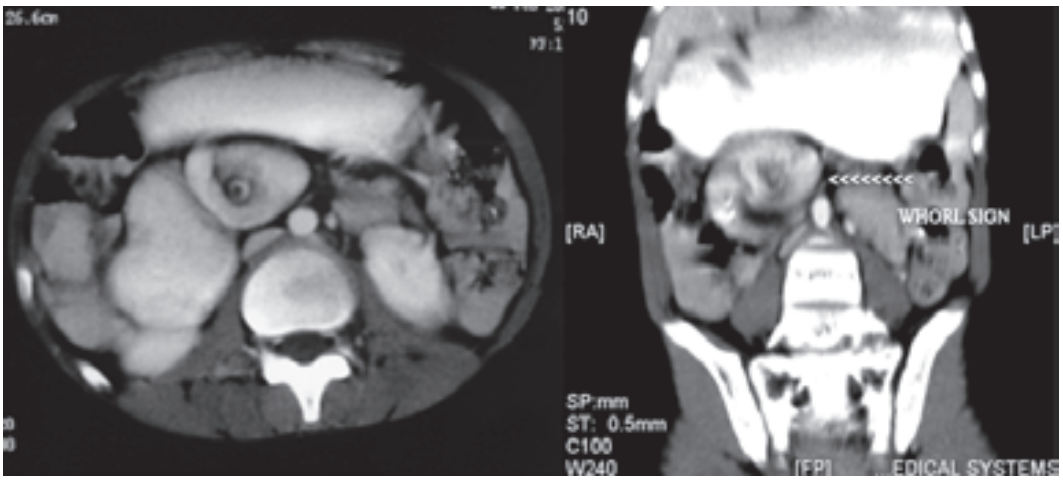

FIGURES 8.71A and B: CT whirl sign – is constituted by the afferent and efferent limbs leading into the volvulus. Tightly twisted mesentery and bowel compose the central portion of the whirl.

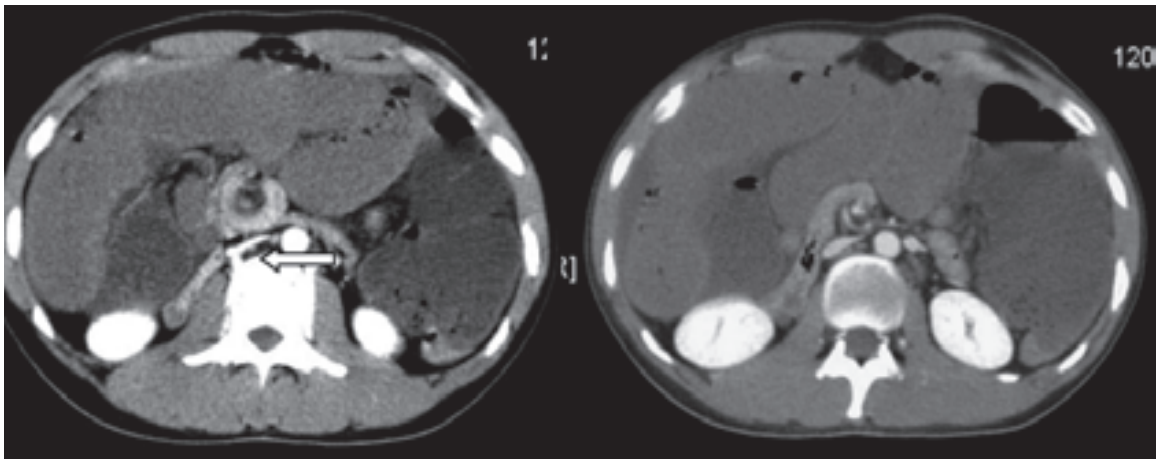

FIGURES 8.72A and B: Axial CECT showing a partial whirling (arrow) with dilated bowel loops due bowel to obstruction.

is often already present. Of the 35 cases that presented to the Massachusetts General Hospital over a ten-year period, severe abdominal pain was the principal symptom in 94% of patients. Three quarters of the patients had not any previous abdominal pain. Associated symptoms included nausea (83%), vomiting (100%) and abdominal distention (55%), with one quarter of patients having clinically detectable peritonism on admission. Although preoperative peritoneal irritation is an indication of the need for laparotomy and possible small bowel resection, no single diagnostic clinical sign consistently identifies the presence of infarcted bowel. In a review of 238 cases of small bowel obstruction from various causes, 90% of those with gangrenous small bowel had a combination of fever, tachycardia and peritoneal irritation. In a computer-assisted analysis of 197 patients with small bowel obstruction, Pain and colleagues correctly identified 97% of cases of gangrenous small bowel and 85% of those with nongangrenous obstruction (the main diagnostic features being continuous pain, vomiting, distention, tenderness, peritonism, absent bowel sounds, elevated temperature, tachycardia, and leukocytosis).

Internal Hernias

Internal hernia is a rare cause of small-bowel obstruction, with a reported incidence of 0.2–0.9%. These hernias may be either congenital or acquired. This condition involves herniation of a viscus, usually the small bowel, through a normal or abnormal aperture within the peritoneal cavity. This herniation may be persistent or intermittent. Because of the risk of strangulation of the hernia contents, even small internal hernias are dangerous and may be lethal.

More than 50% of internal hernias reported in the radiology and surgery literature have been paraduodenal. The other types of internal hernia that have been described include transmesenteric, supra- and/or perivesical, intersigmoid, foramen of Winslow, and rarely, omental hernias.

Paraduodenal Hernia

Left-sided paraduodenal hernias have a characteristic appearance of a cluster of dilated small-bowel loops seemingly encased in a sac and lying between the pancreatic body and/or tail and the stomach to the left of the ligament of Treitz. There is usually a mass effect causing displacement of the posterior wall of the stomach, duodenojejunal flexure (inferiorly), and transverse colon (inferiorly).

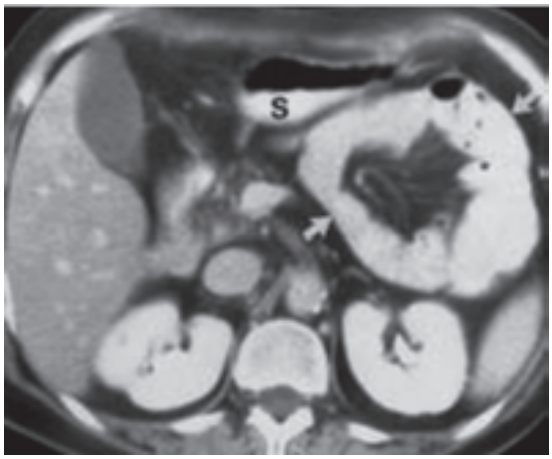

FIGURE 8.73: Axial CECT reveals a loop of bowel loops in the lesser sac region indenting the greater curvature of stomach.

The mesenteric vessels that supply the herniated small-bowel segments are crowded together at the entrance of the hernia sac, and the vessels are often engorged. Several of these signs were demonstrated in all of our patients with left-sided paraduodenal hernias who underwent CT and/or SBFT studies. Therefore, for patients with left-sided paraduodenal hernias who are examined during symptomatic periods, we believe that results of both CT and SBFT are likely to be diagnostic.

Transmesenteric Hernias

When the small bowel herniates through a defect in the mesentery or omentum, the herniated bowel is compressed against the abdominal wall, with no overlying omental fat in most cases and at most levels of anatomic section through the herniated bowel. The herniated bowel tends to appear clustered and lies outside the colon, a reversal of the normal anatomic arrangement. As a result, the adjacent colon is displaced centrally (e.g., transverse colon displaced dorsally, ascending colon displaced medially). There will be some degree of compression, crowding, displacement, and obstruction of both the bowel and blood vessels. The herniated bowel may also twist within the hernia sac, which results in volvulus and a predisposition to bowel ischemia. Twisting of the mesenteric vessels or the whirl sign, or twisting of the bowel itself is diagnostic of volvulus, and engorged blood vessels, mesenteric ascites, and bowel wall thickening suggest bowel ischemia.

What is Malrotation?

Malrotation of the intestines results when the intestinal rotation and fixation that occurs during pregnancy fails to occur. This normally happens in the 4th and 12th weeks of fetal life. In the 4th fetal week, the entire bowel is basically a straight tube with the superior mesenteric artery (SMA). During the course of pregnancy, the bowel rotates in place to the left of the SMA at the ligament of Treitz.

Normal fixation of the bowel in place looks like this: Malrotation of the bowel may look like this:

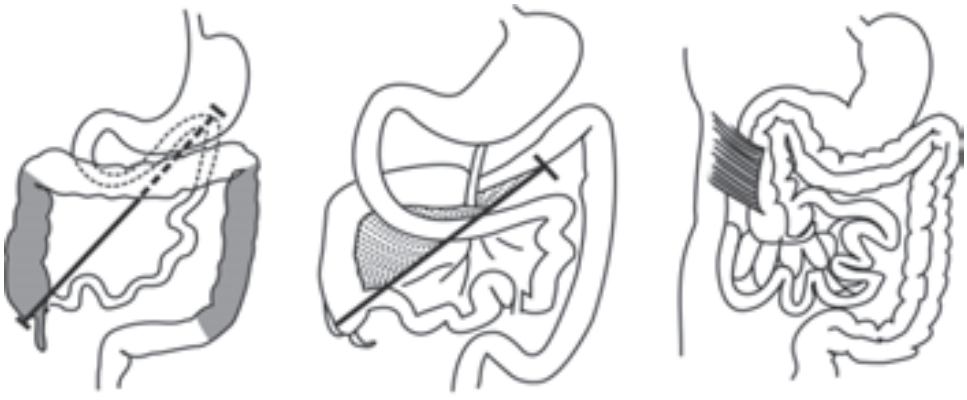

FIGURE 8.74: Schematic showing normal midgut rotation

Why is Malrotation of Concern?

In normal rotation and fixation of the intestines, the bowel has plenty of room to function normally. In malrotation, the primary concern becomes volvulus, or twisting of the intestine that causes obstruction and death to that part of the gut (Fig. 8.75). Accidental bodily movements, unusual effort, abnormal peristaltic movement or distention of the intestine can bring on this volvulus.

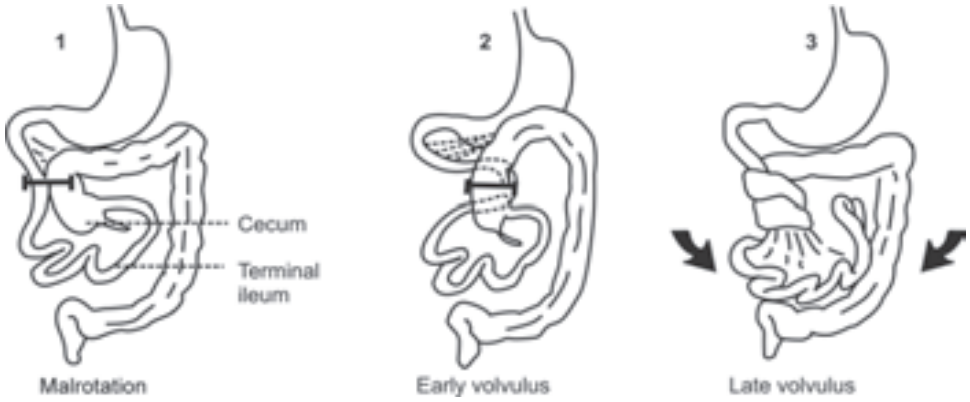

FIGURE 8.75: Schematic showing types of malrotation

Diagrams showing how volvulus occurs in a case of **malrotation**. The first diagram shows the non-fixed terminal ileum and cecum. The second diagram shows **early volvulus** as this area begins to twist on itself. The twisting continues until, as shown in the third diagram (**late volvulus**), the intestines are obstructed and the blood supply to this area is constricted (shut-off).

How is Malrotation Diagnosed?

The major symptoms of malrotation are bilious vomiting, abdominal pain and abdominal distention. All of these are signs of the intestinal obstruction that has occurred. The bowel twists causing pain; becomes distended (enlarged) because of the pressure and the child will vomit the bile that is released for normal digestion.

X-rays of the abdomen will show air in the stomach and lower in the intestine past the obstruction without air being present anywhere else. Further testing that can occur is a barium swallow that will show the barium coming to a stop at the point of the obstruction. A barium enema will show the location of obstruction and, more clearly, the malrotation as the colon is visualized. A contrast CT is very sensitive in delineating the type of malrotation.

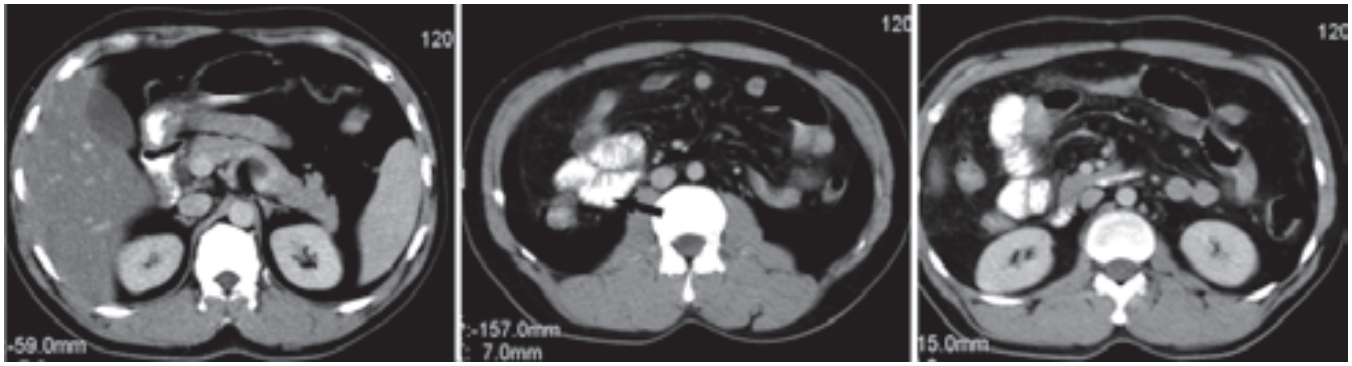

FIGURES 8.76A to C: Axial CECT in a 34-year-old male patient with nonspecific abdominal symptoms and abdominal pain reveals DJ flexure in right (arrow).

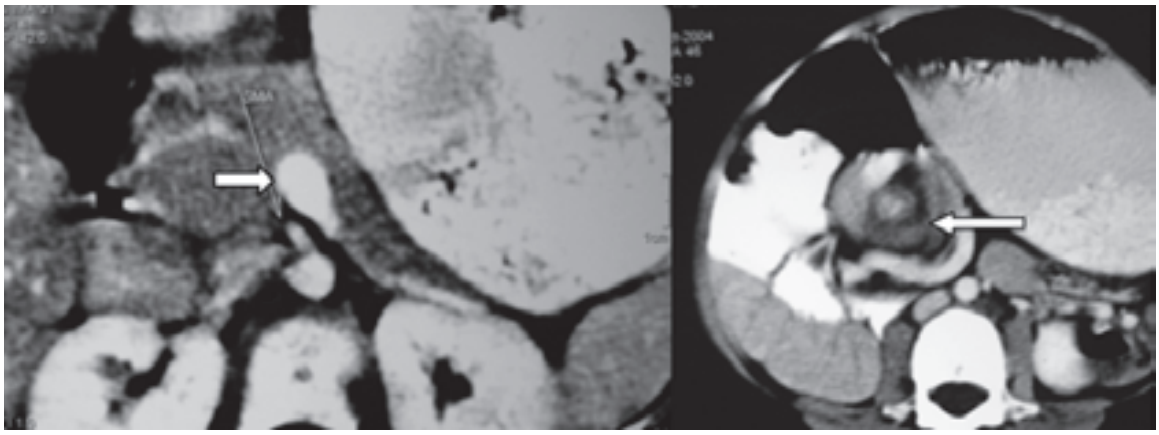

FIGURES 8.77A and B: Axial CECT in a patient with features of subacute intestinal obstruction reveals the altered SMA/SMV relationship (Note the SMA is to the right of SMV arrow). Figure B shows the whirling of the small bowel mesentery (arrow).

Approach to the Diseased Small Bowel—Summary

Most benign intestinal lesions cause circumferential and symmetric mural thickening, usually of less than 1 cm. The bowel wall will show either a homogeneous soft-tissue density or alternate rings of high and low density, known as the "double halo" or target sign.

These different densities are secondary to submucosal edema and/or fat deposition and are best appreciated during the arterial phase of enhancement using spiral CT. They can be found in some physiologic and diseased states such as Crohn's disease, ischemic enteritis, infectious enteritis, radiation enteritis, eosinophilic gastroenteritis, Henoch-Schönlein purpura, and bowel edema associated with portal hypertension. In mural hemorrhage, the wall is thickened with areas of high density on the precontrast image.

In benign disease, the involvement of the small bowel is usually segmental and the adjacent mesenteric fat is often thickened, with a streaky, higher-density appearance. With progressive disease, the bowel wall may become thicker (1 to 2 cm), but the symmetric, circumferential involvement and segmental distribution are maintained.

When inflammatory disease is suspected, the fat of the adjacent mesentery should be carefully examined. The involved fat usually will show a hazy density and linear stranding. Additionally, phlegmons or frank abscesses may develop.

The extramucosal complications of Crohn's disease, such as "creeping fat" of the mesentery, phlegmon, abscess, and fistula, are well depicted on CT scans.

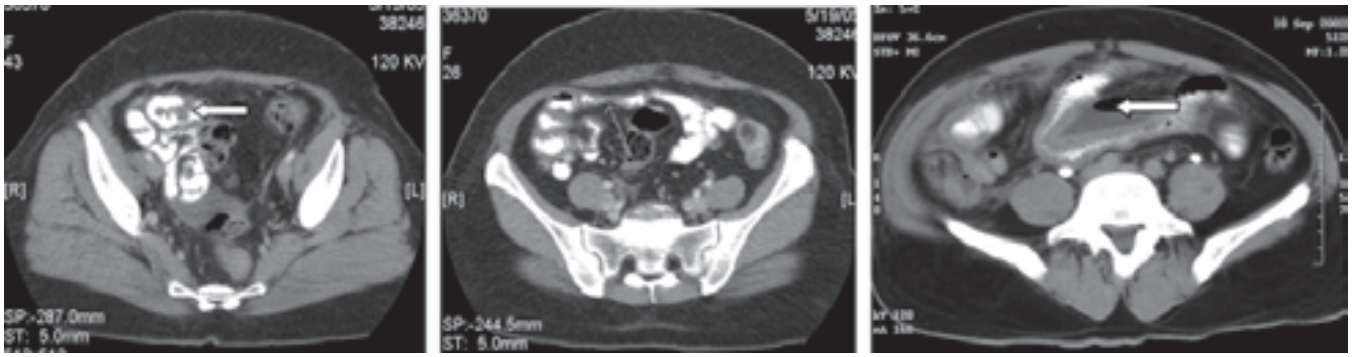

FIGURES 8.78A to C: Axial CECT in three different patients showing spectrum of inflammatory changes. Figure A shows clumped up small bowel loops with small mucosal polyps (arrow). Figure B shows a short segment stricture with mucosal thickening of adjacent bowel loops. Figure C shows a long segment bowel thickening with adjacent fluid–air level suggestive of abscess (arrow).

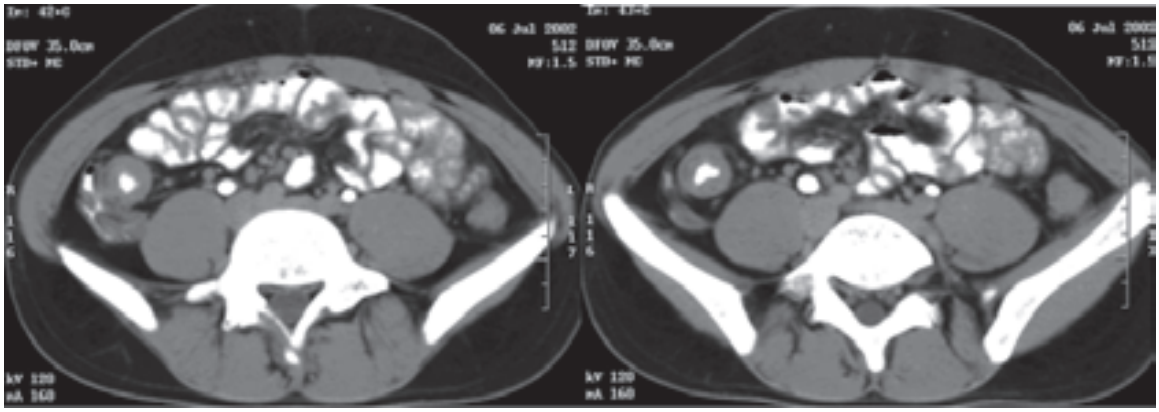

FIGURES 8.79A and B: Axial CECT reveals circumferential ileal thickening of ileal loop at ileocecal junction (case of tuberculosis).

Mesenteric ischemia is a devastating disease which demands a prompt diagnosis and quick decisions for treatment. Ischemic bowel disease typically produces mild (5 to 10 mm), circumferential, and symmetric mural thickening with segmental distribution. The wall may have a homogeneous or double halo density. Using proper intravenous contrast techniques and rapid scanning with spiral CT may add some valuable information in detecting small bowel ischemia. With contrast enhancement, thrombus may be visible in the superior mesenteric and portal vein and, rarely, superior mesenteric artery.

CT scans are increasingly used as screening tests in patients with acute abdominal pain. Bowel dilatation and abnormal gas in the bowel wall or the portal system are clues for predicting irreversibility of bowel ischemia. If bowel dilatation is extensive, or if it exceeds 35 mm in the maximum diameter, the chance of having reversible ischemia lessens.

Obstruction

The diagnosis of bowel obstruction is traditionally made on the basis of clinical findings, history, plain films of the abdomen, and contrast studies of the gut. Dilatation of the small bowel is a common finding in patients with various systemic or regional processes.

CT findings of obstruction vary with the cause of the obstruction. Intussusception is almost invariably associated with either acute intestinal obstruction or partial and recurrent obstruction, air-fluid levels, and proximal bowel distention. Closed loop obstruction is indicated on CT scans by a characteristic "u" shaped configuration of a distended loop of bowel, with collapsed bowel distal to the obstruction; mural edema and hemorrhage also may be present.

Neoplasms

The hallmarks of a neoplastic small bowel lesion are eccentric or asymmetric mural thickening, a lobulated inner and outer contour, and/or a focal soft-tissue mass exceeding 2 cm from the lumen to the serosal surface. The lumen is narrowed, the outer contour of the mass is often spiculated, and there is abrupt transition between normal and abnormal gut wall. The presence of mesenteric, retroperitoneal, and liver metastases; regional adenopathy; and/or malignant-appearing ascites confirms the presence of a malignant neoplasm.

Small bowel tumors often show relatively specific morphologic features on CT. Adenocarcinomas typically manifest as solitary soft-tissue masses which cause lumen narrowing and obstruction. Leiomyomas and leiomyosarcomas share a characteristic pattern of a bulky lesion that grows eccentrically and sometimes calcifies. When larger that 4 cm, these lesions may have a low-attenuation center. Carcinoids present with radiating soft-

tissue strands in the mesentery, along with displacement of small bowel loops and a small mesenteric mass. Lymphomas present with homogeneous mural thickening of greater than 2 cm and frequently are associated with a normal-sized or enlarged lumen. Lipoma appears on CT as a well-circumscribed, intraluminal homogeneous mass with fat attenuation.

CT has a detection rate of 80% for small bowel tumors and has been found to provide accurate preoperative staging. With the increased use of spiral CT for the evaluation of small bowel pathology, it has become accepted that the ability to scan at the optimal vascular enhancement of spiral CT may be important in detecting and defining the extent of tumor involvement, thus resulting in more accurate staging.

Bowel and mesenteric injuries—CT can detect small bowel and mesenteric injuries, intraperitoneal fluid and/or free air, and associated organ injury. CT is able to accurately visualize the entire bowel wall, as well as local extra-enteric and distant changes. In certain clinical situations (e.g. ischemia, abscess, obstruction, Crohn's disease), CT should be the initial diagnostic modality.

Cavitary Masses

Cavities may form in large polypoid masses when ulcers extend deeply into the tumor's tissue or the center of the tumor undergoes necrosis when the blood supply is destroyed. Cavitary masses include the following:

- Common
  - Primary non-Hodgkin's lymphoma
  - Metastatic melanoma
  - Gastrointestinal stromal tumor
- Uncommon
  - Crohn's disease
  - Diverticulitis
  - Ectopic pancreas with pancreatitis
  - Primary adenocarcinoma

The most common causes of these bulky, cavitary lesions are primary non-Hodgkin's lymphoma, metastatic melanoma, and malignant gastrointestinal stromal tumor. Sometimes, an abscess in the small mesentery adjacent to an inflammatory process mimics a cavitary tumor. Jejunal diverticulitis with abscess formation or an abscess adjacent to an area of Crohn's disease superficially mimics a cavitary mass. Demonstration of the tumor in the small bowel differentiates a cavity related to tumor, rather than an inflammatory process in the small bowel mesentery.

Annular Lesions

Primary adenocarcinoma of the small bowel usually arises in the duodenum or proximal jejunum. These tumors usually appear as short circumferential narrowing with abrupt shelf-like margins and nodular or ulcerated mucosa. Rarely, however, a primary adenocarcinoma appears as a polypoid or cavitary mass. Primary small bowel lymphoma may be a circumferential lesion, but it is usually longer than the typical adenocarcinoma. Primary small bowel lymphoma is a soft cellular tumor that does not incite desmoplasia similar to adenocarcinoma. Primary small bowel lymphoma only mildly, if any, narrows the lumen. In fact, circumferential extension of lymphoma may weaken the small bowel wall resulting in dilatation of the lumen (aneurysmal dilatation). Intraperitoneal metastases may cause circumferential narrowing, but the valvulae conniventes are preserved, although tethered. The desmoplastic reaction caused by intraperitoneal metastasis in the small bowel mesentery leads to angulation of loops and obstruction. When the submucosal mass of a carcinoid tumor begins to extend circumferentially around the bowel, a lesion that resembles a saddle is produced. When a saddle lesion is seen en face it appears as an annular lesion as follows:

- Narrowing and shouldered margin
  - Primary adenocarcinoma

  - Carcinoid
  - Metastasis
  - Primary small bowel lymphoma
  - Crohn's disease
  - Anastomotic stricture
  - Nonsteroidal anti-inflammatory agent
- Narrowing and tapered margin
  - Crohn's stricture
  - Adhesion
  - Radiation
  - Ischemia
  - Trauma

Benign lesions can also appear as abrupt circumferential lesions. The transition zone of an adhesive band may appear as a sharp radiolucent band crossing the bowel. Proximally, the bowel is dilated, with the lumen abruptly coming to a beak-like or shelf-like narrowing. Distally the bowel is collapsed. The key to the diagnosis of an adhesive band rather than an adenocarcinoma is that the mucosa is smooth and the folds are preserved. Strictures related to nonsteroidal anti-inflammatory agents may cause multiple thick, ring-like narrowing. These thick webs result in low-grade obstruction. An end-to-end anastomotic stricture may also appear as a smooth, ring-like narrowing. The clinical history of prior surgery or the demonstration of a staple line results in the correct diagnosis.

Some strictures have tapered margins. The narrowing related to Crohn's disease usually has smooth tapered margins, associated with nodular mucosa or a mesenteric border ulcer. Ischemic strictures are tapered and may cause low-grade obstruction. Ischemic strictures related to radiation therapy are associated with changes of radiation serositis. The small bowel loops are angulated and the mucosal folds are tethered by radiation-induced adhesions in the serosa and adjacent small bowel mesentery.

Contour Distortions of Extrinsic Origin

Tethering of Folds

When small bowel is distended, most valvulae conniventes lie perpendicular or only slightly angled in relation to the longitudinal axis of the lumen. When a desmoplastic process in the small bowel mesentery or serosa pulls on the outside of the small bowel loop, the pliable loop may become angulated or kinked and the mucosal folds are pulled toward the area of extrinsic abnormality. Adhesions are by far the most common cause of tethering of mucosal folds and angulation of bowel loops. Endometriosis implants in the serosa of the ileum may cause pelvic ileal loops to be angulated. The desmoplastic process of metastatic carcinoid tumor in the small bowel mesentery may be manifest only by tethering of folds and angulation of loops, without the mass effect of tumor on the mesenteric border of the bowel.

Extrinsic Mass Effect and Tethering

Broad-based impression on a bowel loop associated with tethering of the folds or spiculation of the luminal contour implies that there is a mass in the small bowel mesentery or on the peritoneal surface that involves the serosa of the bowel. Some of the causes of tethering of mucosal folds and mass effect includes the following:

- Left upper quadrant
  - Pancreatitis
  - Metastasis to root of small bowel mesentery

- Right lower quadrant and mid abdomen
  - Intraperitoneal metastasis
  - Carcinoid tumor
  - Endometriosis
  - Retractile mesenteritis
  - Interloop abscess
- Cecal-appendiceal process involving terminal ileum
  - Cecal lymphoma or carcinoma
  - Appendicitis
  - Crohn's disease
  - Appendiceal tumors

The clinical history, location of the bowel involvement, and whether a single or multiple loops are involved are clues to the diagnosis. Intraperitoneal metastases cause multiple round or flat broad-based extrinsic masses on the mesenteric border of the small bowel, associated with tethered folds. The intraperitoneal implants usually involve right lower quadrant loops, the site where ascitic fluid pools in the small bowel mesentery. Ascites is usually demonstrated on cross-sectional imaging. Implants are demonstrated on CT in about 50% of cases. The site of primary tumor is usually known. The most common sites of tumors that spread to the peritoneal space are the ovary, colon, pancreas, stomach, liver, and breast.

Mid-size carcinoid tumors (1 to 2 cm) appear as a smooth-surfaced hemispheric mass with tethered plicae circulates radiating toward the tumor. When carcinoid tumors spread to the small bowel mesentery there is a desmoplastic effect on adjacent small bowel loops, resulting in numerous angulated loops with folds radiating toward the center of the small bowel mesentery. The mesenteric metastasis is demonstrated on CT as a central, spiculated mass, calcified in 60%. Thick strands radiate from the mass toward the small bowel. If smooth, thick valvulae conniventes are also seen, a diagnosis of ischemia complicating carcinoid tumor may be made. Other conditions that cause desmoplasia in the small bowel mesentery, such as retractile mesenteritis, may have a similar appearance to advanced-stage carcinoid tumor.

Pancreatitis may cause desmoplastic changes in left upper quadrant jejunal loops or the splenic flexure of the colon. An interloop abscess may splay small bowel. Smooth folds radiate toward the interloop abscess.

Separation of Bowel Loops without Tethering

Causes of separation of bowel loops (without tethering) include the following:

- Normal small bowel mesenteric fat
- Ascites
- Related to primary thickening of small bowel wall
  - Crohn's disease
  - Primary lymphoma
  - Other tumors
- Mesenteric or retroperitoneal lymphadenopathy
  - Lymphoma
  - Whipple's disease
  - AIDS-related
- Primary mesenteric tumors
- Fibrofatty proliferation in Crohn's disease

The most common cause of separated small bowel loops is a prominent amount of fat within the small bowel mesentery. During fluoroscopy, the bowel loops retain their normal pliability and mobility. The spaces between the

loops change with palpation. In patients with uncomplicated ascites, the small bowel loops also change in position with palpation. In patients with moderate to marked ascites, the small bowel loops are centrally located and move with a fluid-wave created during palpation. Masses within the small bowel mesentery may cause focal displacement of one or several small intestinal loops without tethering. The loops are relatively fixed and draped around a mesenteric mass. In some patients with mesenteric nodal lymphoma, obstruction only results when there is extensive infiltration of the intestinal wall, with narrowing and angulation of the lumen and smooth thick submucosal folds. Mesenteric desmoid tumors, most frequently seen in patients with familial adenomatous polyposis syndrome, may or may not tether the adjacent small intestine. When there is separation of small intestinal loops related to fibrofatty proliferation in Crohn's disease, other radiographic findings of Crohn's disease are present.

Dilated Lumen, Normal Folds

Small bowel dilatation is an important sign of small bowel abnormality but it does not always imply obstruction.

Normal Number of Folds (per inch)

Mechanical obstruction

- Common
  - Adhesions
  - Hernia
  - Metastases
  - Radiation
  - Colonic obstruction
- Uncommon
  - Diverticulitis
  - Crohn's disease
  - Gallstone "ileus"
  - Meckel's with volvulus or intussusception
  - Primary adenocarcinoma
  - Tumor with intussusception

Adynamic ileus

- Common
  - Postoperative
  - Prior vagotomy
  - Drug-induced atony (e.g., opiates, anticholinergics)
  - Diabetes
  - Low blood flow states (congestive heart failure, myocardial infarction, sepsis)
- Uncommon
  - Peritonitis
  - Electrolyte imbalance (uremia, hypokalemia)
  - Blunt trauma
  - Tumor in mesentery
  - Radiation
  - Hypothyroidism
  - Amyloidosis

- Scleroderma
- Congenital myopathy or neuropathy

Decreased Number of Folds in Duodenum or Jejunum

- Celiac disease

Increased Number of Folds per inch Duodenum or Jejunum

- Scleroderma
- Dermatomyositis

Diffuse small bowel dilatation may be present with a variety of causes of mechanical obstruction or adynamic (paralytic) ileus. Demonstration of a transition zone between dilated and collapsed small bowel on CT, barium study, or MR imaging is required for the diagnosis of presence, location, and etiology of an obstructing lesion. Analysis of the morphology of the focal obstructing lesion enables a more specific etiologic diagnosis of one of the more common causes of obstruction: adhesions, hernia, metastases, or radiation enteropathy.

The most common causes of adynamic ileus are the postoperative state, various medications, ischemia, and prior vagotomy. Diffusely dilated small bowel in a patient who is less than 7 days postoperative is assumed to be postoperative adynamic ileus, unless there are thick folds or other signs of ischemia or focal dilatation related to internal herniation. Hypokalemia, blunt abdominal trauma, diabetes, and hypothyroidism also cause small intestinal hypomotility. The small bowel is dilated in systemic sclerosis, amyloidosis, and peritonitis, but there are other radiographic findings on CT or barium studies.

Focal dilatation of small bowel may enable a radiologist to suggest a more specific diagnosis or a smaller differential diagnosis. If only a few loops of proximal small intestine are dilated on plain film, the radiologist should consider obtaining a CT or barium study to look for a pancreatic disease obstructing small intestine or a primary jejunal adenocarcinoma. A focal region of dilated small intestinal loops with air-fluid levels suggests diagnosis of an internal hernia or volvulus of bowel around a band. A CT should be performed to look for signs of strangulation: thick folds, target sign in wall, lack of bowel wall contrast enhancement, pneumatosis, and fluid and vascular changes in the small bowel mesentery.

When proximal small intestine is dilated and there are clearly a diminished number of folds per inch, the radiologist should consider a diagnosis of celiac disease (gluten-sensitive enteropathy). The diminished number of folds reflects the loss of mucosal surface area caused by villous atrophy. The small bowel may adapt to this loss of surface area by increasing the height and number of folds in the ileum, the so-called *jejunization of the ileum*. Celiac disease may be diagnosed in an adult for the first time, in a patient with now obvious malabsorption, or one of the sequelae of malabsorption of minerals or vitamins. If the duodenum and jejunum is diffusely dilated, yet the folds are crowded together despite luminal dilatation, a diagnosis of scleroderma should be considered. Many of these patients already carry a diagnosis of scleroderma; however, some patients carry a diagnosis of another connective tissue disorder or nothing, and the radiologist is the first physician to suggest a diagnosis of mixed connective tissue disease or scleroderma, respectively. The diagnosis of scleroderma is aided by broad-based sacculations opposite folds that are crowded together.

Abnormalities in Fold Size

Small bowel folds are composed of mucosa and submucosa. An abnormality in fold size means there is an abnormality in the mucosa, submucosa, or both. The radiologist analyzes the amount of small intestine involved and the location and morphology of the abnormal folds. Consideration of the clinical history and other radiographic findings enables a specific diagnosis or short differential diagnosis in most cases.

Thick, Smooth, and Straight Folds

Folds that have a smooth surface, are uniformly thickened, and lie perpendicular to the longitudinal axis of the small intestine suggest a diagnosis of submucosal edema or hemorrhage. Thick (>3 mm), smooth, straight folds can include the following:

Diffuse

- *Edema*
  - Hypoproteinemia (serum albumin <2 g/dL)
    - Cirrhosis
    - Nephrotic syndrome
    - Protein-losing enteropathy
  - Congestive heart failure
  - Portal hypertension

Long segment

- *Intramural hemorrhage*
  - Anticoagulant therapy
  - Ischemia
  - Coagulopathies
  - Hemophilia
  - Idiopathic thrombocytopenic purpura
- *Vasculitis*
- *Connective tissue diseases*
  - Henoch-Schönlein purpura systemic lupus (SLE)
- *Radiation enteropathy*
- *Eosinophilic enteritis (multifocal)*

Focal

- *Mesenteric venous or lymphatic obstruction*
  - Metastasis
  - Surgery
- *Early Crohn's disease*

Pseudothickening of folds

- Celiac disease
- Giardiasis
- Other inflammatory states
- Abetalipoproteinemia
- Protein-losing enteropathy.

Diffuse small bowel edema occurs in patients with elevated portal venous pressure related to cirrhosis or congestive heart failure. Patients with severe hypoproteinemia (serum albumin less than 2 g/dL) may also have diffuse small bowel edema.

Most diseases that cause submucosal edema or hemorrhage involve several contiguous loops of small intestine, resulting in a focal, but long segment of abnormality. The folds are smooth, thick, and perpendicularly aligned to the longitudinal axis of the small bowel. When folds are markedly thickened, they approach each other and have been said to resemble a "stack of coins". The most common causes of long segment smooth thick folds include

ischemia from a variety of causes, anticoagulant therapy, various vasculitides, coagulopathies, and radiation enteropathy. Radiation enteropathy is confined to the radiation portal and usually associated with radiation serositis that results in angulated loops. The clinical history aids in a more specific diagnosis. The small intestine in many forms of intramural hemorrhage (low-grade ischemia, anticoagulant related bleeding, and so forth) usually returns to normal on a small bowel study repeated within 2 to 3 weeks.

Mucosal Nodularity and Irregular Fold Thickening of Ulceration

Diseases with thick folds that favor a distal location are as follows:

- Associated with minimal, if any, luminal narrowing, and no evidence of obstruction
  - Yersinia enterocolitis
  - Salmonella and other infections
  - Crohn's disease
  - Lymphoma
  - Cecal cancer or lymphoma
- Associated with moderate to marked luminal narrowing
  - Crohn's disease
  - Tuberculosis
  - Behçet's disease

Diseases with thick folds that favor a proximal location are as follows:

- Giardiasis
- Whipple's disease
- Abetalipoproteinemia
- Lymphoma arising in celiac disease
- Ulcerative jejunoileitis
- Tropical sprue
- Gastrojejunostomy

An immunocompromised patient with thick, nodular small bowel folds suggests that an infection has supervened, such as:

- Cryptosporidiosis
- Toxoplasmosis
- Isosporiasis
- Giardiasis
- Candidiasis
- Cytomegalovirus
- *Mycobacterium avium-intracellulare*
- Actinomycosis
- *Mycobacterium tuberculosis*

Diseases with thick nodular folds can involve long segments of both jejunum and ileum:

- Primary lymphangiectasia
- Secondary lymphangiectasia
- Amyloidosis
- Eosinophilic enteritis

- Histoplasmosis
- Mastocytosis
- Graft-versus-host disease
- Lymphoma
- Waldenström's macroglobulinemia

Tubular Bowel

The small intestine may appear tubular when the valvulae conniventes have been destroyed by an acute or chronic inflammatory or ischemic process as follows:

- Jejunum
  - Celiac disease
  - Strongyloidiasis
- Ileum
  - Chronic ischemia from radiation
  - Burnt-out Crohn's disease
- Short segment
  - Lymphoma
- Diffuse
  - Graft-versus-host disease
  - Cytomegalovirus

Sacculations

Sacculations may form in bowel either opposite acute inflammation and scarring or in areas of bowel wall weakness as follows:

- Scleroderma
- Crohn's disease
- Ischemia

Gastrointestinal-Stromal Tumors (GISTs)

Introduction

Gastrointestinal-stromal tumors (GISTs), leiomyosarcomas (LMSs), and leiomyomas are nonepithelial mesenchymal tumors that occur predominantly in the gastrointestinal (GI) tract. They are most often located in the stomach and proximal small intestine, but can occur in any portion of the alimentary tract that contains smooth muscle within its wall, and occasionally in the omentum. Most are histologically high grade, and by IHC, they express smooth muscle actin, desmin, or both.

Characteristics on CT Scan

CT characteristics may predict the likelihood of malignancy. Tumors that are larger than 5 cm, lobulated, have heterogeneous enhancement, mesenteric fat infiltration, ulceration, regional lymphadenopathy, or an exophytic growth pattern on CT scan are more likely to be malignant.

Clinical Manifestations

Smooth muscle tumors of the GI tract are often asymptomatic and discovered incidentally during endoscopic or barium studies. In contrast, others are associated with nonspecific symptoms unless they ulcerate, bleed, or grow

large enough to cause pain or obstruction. In one series that included patients with leiomyomas and LMS (without separation of the GISTs within these subtypes at that time), for example, there were three major presentations:

- Gastrointestinal bleeding — 40 percent
- Abdominal mass — 40 percent
- Abdominal pain — 20 percent

In other series, approximately 25 to 40 percent of patients presented with intestinal obstruction, which may be due to the tumor serving as a lead point for intussusception. In addition, up to two-thirds of patients had overt or occult GI bleeding. Intestinal perforation, although rare, can also occur.

Diagnosis

GI mesenchymal tumors appear as a submucosal mass, which has smooth margins, may bulge into the lumen, and has normal overlying mucosa. A central ulceration is occasionally seen. On CT, the mass may appear as a hypodense lesion immediately adjacent to the lumen.

Endoscopic biopsies, using standard techniques, usually do not obtain sufficient tissue for a definite diagnosis. Newer techniques using EUS-guided fine needle biopsy forceps also may not yield enough tissue, but may be useful for excluding other submucosal lesions. The combined use of cytologic analysis, IHC, and reverse transcriptase polymerase chain reaction for c-kit mutations may permit the diagnosis of some of these lesions by EUS-guided fine needle aspiration. Snare biopsies (in which a polypectomy snare is used to remove a large piece of tissue) can lead to perforation; however, this technique has been safely performed in carefully selected cases (see below).

Esophagus: Mesenchymal tumors are commonly found in the mid to distal third of the esophagus, and are usually small and asymptomatic, but occasionally grow to enormous size and produce dysphagia. The vast majority are leiomyomas. They are more common in men and often detected incidentally on a barium swallow or endoscopy performed for other.

Lesions that are larger than 2 cm or produce dysphagia should be treated with appropriate surgical resection. Five-year survival rates of approximately 30 to 40 percent has been reported in patients with surgically resected LMS; individual survival is strongly influenced by tumor differentiation and size.

Stomach: The stomach is the most frequent site for smooth muscle tumors of the GI tract; GISTs account for 1 to 3 percent of all stomach neoplasms.

They may occur anywhere in the stomach, but are most common in the fundus. These neoplasms usually occur after the age of 50, but they can affect a broad age range, and are disproportionately common in men. The majority of GISTs and gastric leiomyomas are less than 0.5 cm, but tumors as large as 20 cm may be encountered, which grow both inwardly and outwardly forming a dumb-bell shape. Multiple small leiomyomas (microleiomyomas) have also been reported in as many as 16 to 38 percent of resected stomachs. In contrast, multiple LMSs are rare.

Most small GISTs remain asymptomatic. Large lesions may ulcerate and present with bleeding in upto 60 percent of cases. Other symptoms that may occur include anorexia, weight loss, nausea, vomiting, and pain; gastric perforation is uncommon. "Carney's triad" is a rare syndrome that has been reported in young women that includes GISTs (originally referred to as "leiomyosarcoma" of the stomach), paraganglioma, and pulmonary chondroma. This syndrome can exhibit a very different natural history from other GISTs in that the tumors can be relatively indolent even if metastatic, especially in children and young adults aged 12 to 18.

Small intestine: The small intestine is the second most frequent site for smooth muscle tumors. Tumors are most commonly found in the jejunum followed by the ileum and the duodenum.

Colon and rectum: Smooth muscle tumors are uncommon in the colon and rectum. In the rectum, they usually present as small, hard nodules less than 1 cm in diameter found incidentally during a clinical examination. Large

tumors can ulcerate and may mimic a rectal adenocarcinoma. In the colon, GISTs are more common than LMSs, and they are typically transmural, with frequent intramural and outward bulging components.

CT SCAN FEATURES OF COLONIC DISEASES

A unique imaging feature of CT is its ability to accurately demonstrate the bowel wall as well as adjacent structures. CT provides a highly sensitive method for the detection of intramural pathology as well as extraluminal extension of colonic diseases. Its used not only for detection of neoplastic disease but also for characterization of various inflammatory conditions of the colon including appendicitis, typhlitis, infectious colitis, pseudomembranous colitis, diverticulitis and inflammatory bowel disease. Colonic intussusception and volvulus.

Technique

Routine abdominal CT is usually performed after the administration of intravenous and oral contrast. Approximately 1200-1250 ml of a 2-3% oral Gastrografin solution 60-90 minutes prior to the scan. If specific colonic pathology is suspected, it is important to adequately opacify the entire colon. Therefore, oral contrast can be administered the night before the study as well as just prior to the scan. This insures that the contrast has reached the colon and is essential for optimal visualization. Alternatively in urgent cases, or in patients in whom limited rectosigmoid disease is suspected, about 350-500 ml of contrast can be gently administered as an enema.

Administration of intravenous contrast is essential for characterization of colonic pathology, it is often helpful, especially if extracolonic extension of disease is also suspected. We use 80-100 ml of watersoluble contrast at a rate of 2-3 ml/sec.

Using a single or multidetector CT scanner, the abdomen should be routinely imaged from the level of the diaphragm through the symphysis pubis. We routinely obtain delayed images at the site of pathology and for evaluating the urinary bladder (especially in cases of pelvic pathology).

Normal Colon

The colon can usually be distinguished from small bowel by its location, size and the presence of haustra. The colon normally frames the abdomen. The cecum and ascending colon lies in the right abdomen and is mostly in the retroperitoneum. The transverse colon is in the peritoneal cavity and crosses the abdomen anteriorly. The descending colon lies in the left abdomen, in the retroperitoneum, while the sigmoid is intraperitoneal and in the pelvis**.** The colon is surrounded by homogeneous fat.

Pathologic Conditions

Inflammatory Conditions

Appendicitis: The normal appendix is a finger-shaped structure that is closely related to the base of the cecum and is variable in its location. The appendix appears as tubular or ring-like structure in CT depending on the axis of the imaging plane. It may be collapsed, air filled or fluid filled. In fact, the presence of air within the appendix is considered a strong sign for excluding an inflammatory process. The wall is normally very thin and the diameter of the appendix measures less than 6 mm. The surrounding fat is clear without suggestive stranding or linear opacifications. It is important for correct localization of the appendix to trace it to its blind-ending tip, for which the cine mode of overlapping thin slices (3 mm) is most helpful.

The abnormal appendix is characterized by wall thickening (2-6 mm), distention (> 6 mm, mostly 1-1.5 cm, rarely up to 4 cm) and wall enhancement after application of intravenous contrast media. Already on an unenhanced scan the appendix wall may be denser than the intraluminal fluid; the strong enhancement of the wall after contrast application is described as target sign or ring sign. A double ring sign (in 7%) is suggestive for a necrotizing appendicitis. Other findings in necrotizing appendicitis include focal wall thinning, focal loss of wall continuity and focal loss of wall enhancement.

In appendicitis, the periappendiceal fat is typically clouded with linear streaking. Focal fluid collections in the right lower quadrant, a perityphlitic abscess or a phlegmon (ill defined soft tissue density with focal central hypodensity) are more frequent in pediatric patients than in adults. A small bowel obstruction is a complication more typical for the pediatric patient. Small extraluminal air bubbles (intraperitoneal or retroperitoneal) are suggestive for a perforation. Due to adjacent inflammation, the cecum, terminal ileum and sigmoid colon also show wall thickening. The regularly seen focal thickening of the cecal apex at the origin of the appendix is described as arrow head sign (if the imaging plane shows the funnel-shaped edema of the cecal wall en face). In upto 60% of patients there are enlarged inflammatory pericecal lymph nodes. An appendolith may be an incidental finding, not meaning in itself an inflammatory process.

Intraperitoneal appendicitis leads to circumscribed adhesion of the peritoneal leaves with associated peritoneal thickening and enhancement. With retroperitoneal appendicitis, the inflammatory process can spread along the psoas muscle.

Diverticulitis: Diverticulosis is a common condition in the western world. Diverticula can occur anywhere throughout the colon but are most common in the sigmoid. They represent small outpouchings of the colonic mucosa and submucosa through the muscular layers of the wall. Diverticula usually range in size from 2-3 mm upto 2 cm.

The most common complications of diverticular disease include bleeding, due to erosion of a feeding nutrient artery, and infection. Acute diverticulitis occurs when the neck of a diverticulum is occluded by stool, inflammation or food particles resulting in a microperforation of the diverticula and surrounding pericolonic inflammation. Left sided diverticula more commonly lead to infection, while right sided diverticula more frequently bleed.

On CT, diverticulosis appears as small air filled outpouchings of the wall of the colon, most abundant in the sigmoid colon. The wall of the colon may appear thickened due to muscular hypertrophy. Diverticulitis appears as segmental wall thickening, hyperemia and inflammatory changes in the pericolonic fat. A frank abscess can be seen in upto 30% of cases. A diverticular abscess appears as a soft tissue mass with surrounding inflammatory changes. The center of the collection may contain air or air fluid levels or have low attenuation representing necrotic debris.

CT also allows detection of other complications of diverticulitis such as colovesical fistula or perforation. Colovesical fistula is suspected when air is seen in the bladder and there is thickening of the bladder wall adjacent to a diseased segment of bowel (usually sigmoid.) Focal contained perforations appear as small extraluminal pockets of air or extravasation oral contrast material.

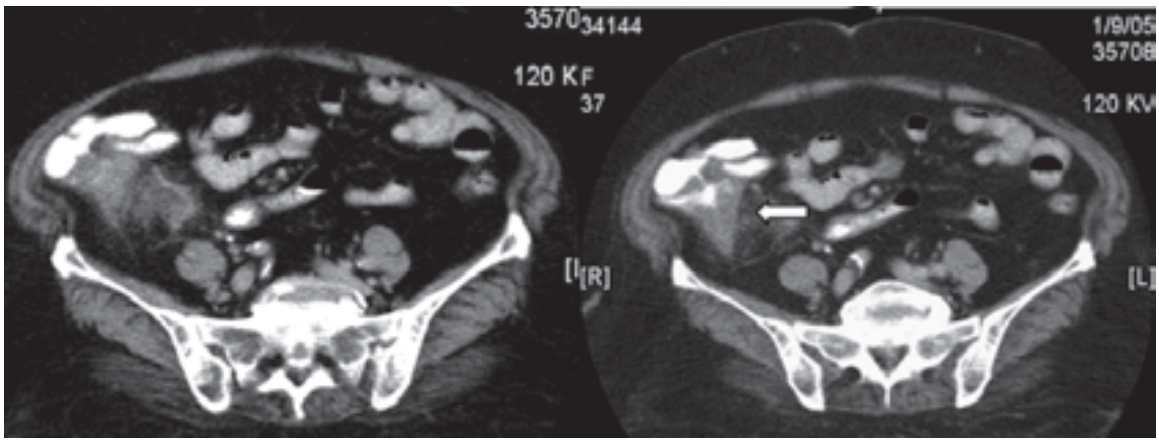

FIGURES 8.80A and B: Axial CECT in a patient with right iliac fossa pain reveals the arrowhead sign of appendicitis (arrow), note the pericecal inflammatory changes.

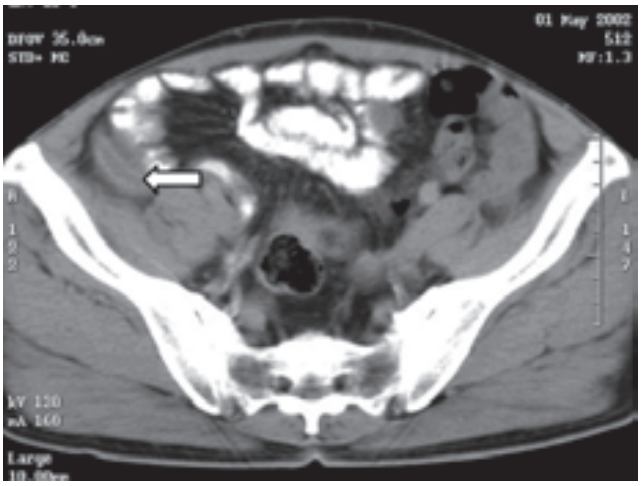

FIGURE 8.81: Axial CECT in a patient with right iliac fossa pain shows dilated fluid filled appendix with thickened enhancing wall (arrow).

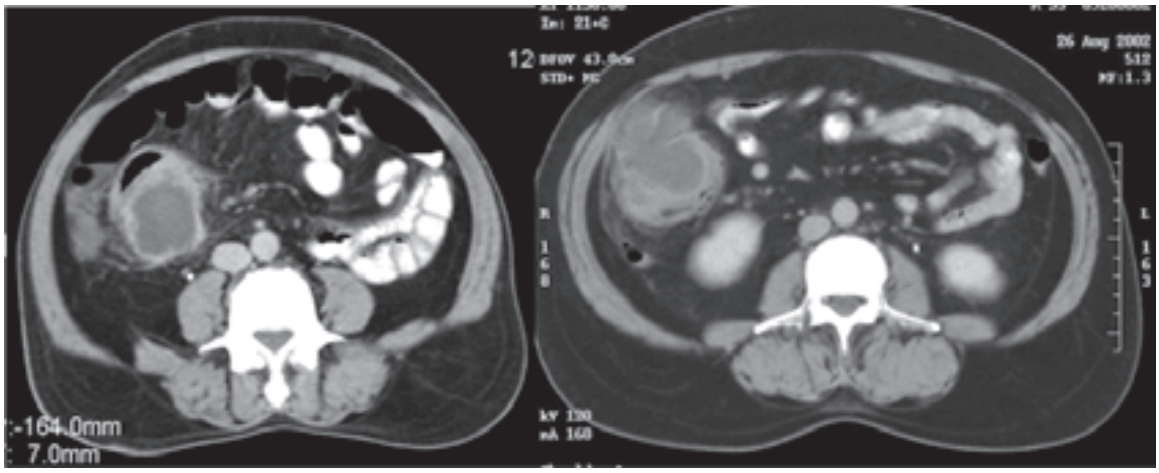

FIGURES 8.82A and B: Axial CECT showing pericecal abscess with pericolic fat stranding.

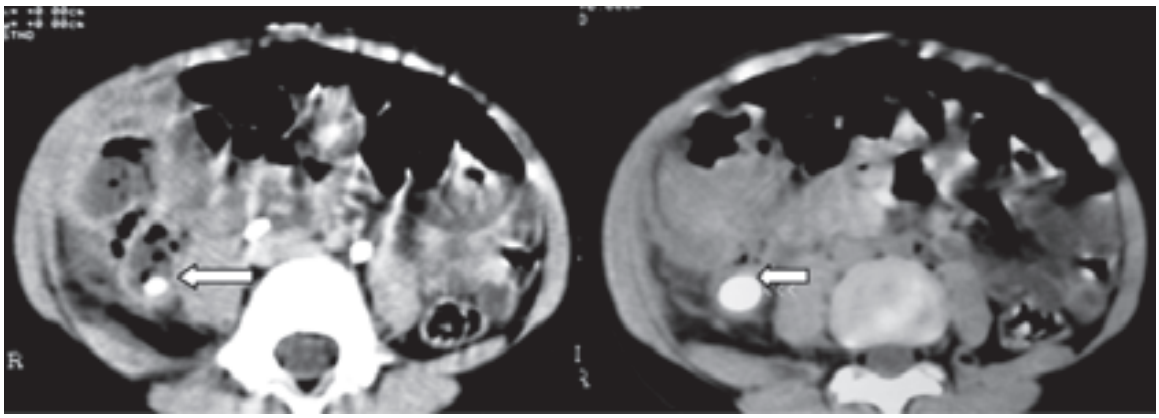

FIGURES 8.83A and B: Axial CECT showing appendicolith seen a hyperdense focus (arrow in B) with periappendiceal and pericolic abscess (arrow).

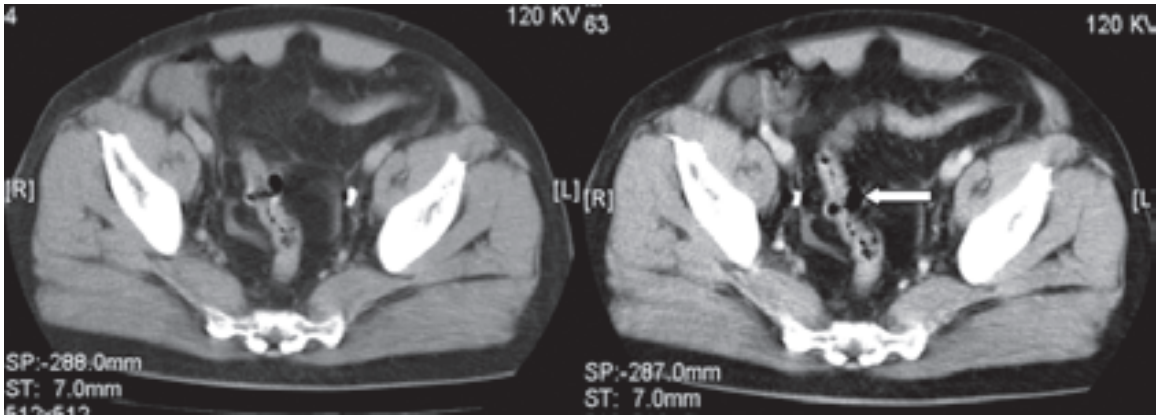

FIGURES 8.84A and B: Axial CECT showing a uninflamed sigmoid diverticulum seen as a airfilled out pouching (arrow).

Typhlitis: Typhlitis, also known as neutropenic enterocolitis, is a condition which occurs in neutropenic patients undergoing treatment for a malignancy, most frequently in patients with acute leukemia on chemotherapy. Typhlitis is characterized by edema and inflammation of the cecum, ascending colon and sometimes terminal ileum. CT is the study of choice for the diagnosis of typhlitis, due to the risk of perforation with colonoscopy or contrast enema. CT demonstrates cecal distention and circumferential thickening of the wall, which may have low attenuation secondary to the edema. Inflammatory stranding of the adjacent mesenteric fat is a common finding.

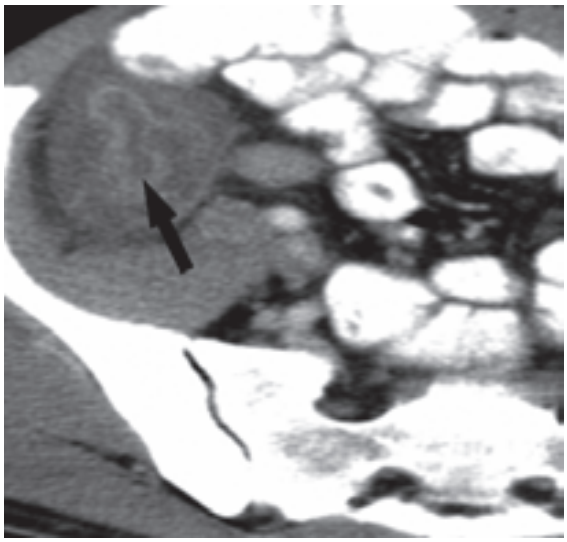

FIGURE 8.85: Axial CECT in a chemotherapy patient showing hypodense mural thickening of cecum (arrow).

Radiation colitis: Radiation therapy can result in injury to colon. More than half of patients undergoing radiation therapy to the pelvis will experience a self-limited acute proctitis. Radiation colitis tends to be left sided, as radiation therapy is often given for pelvic pathology. CT findings include nonspecific wall thickening, typically in the rectum, increased pelvic fat accumulation and thickening of the perirectal fibrous tissue are also seen. Stricturing and fistulae are possible complications.

Inflammatory bowel disease: Although contrast studies and colonoscopy remain the principal tools for the diagnosis and evaluation of suspected inflammatory bowel disease. CT plays an important role in detection of complications of inflammatory bowel disease.

There may be considerable overlap of the CT findings in Crohn's disease and ulcerative colitis. Extensive involvement of right colon and small bowel more common in Crohn's, although involvement of the left colon and rectosigmoid does occur. In contrast, ulcerative colitis is typically left sided or diffuse, and only rarely involves the right colon exclusively. On CT scan, the most frequent finding in both Crohn's disease and ulcerative colitis is wall thickening. The mean wall thickness in Crohn's colitis (11-13 mm) is usually greater than in ulcerative colitis 7-8 mm. Wall thickening in UC may be diffuse and symmetric, while wall thickening in Crohn's may be eccentric and segmental with skip regions.

The halo sign, a low attenuation ring in the bowel wall due to deposition of submucosal fat, seen more commonly in ulcerative colitis than Crohn's colitis. In Crohn's disease, the bowel wall tends to enhance homogeneously, although edema within the wall may result in low attenuation.

Proliferation of mesenteric fat is seen almost exclusively in Crohn's, while the proliferation of perirectal fat is nonspecific and can be present in Crohn's, UC, pseudomembranous colitis, or radiation colitis. The presence of mesenteric lymphadenopathy suggests Crohn's rather than UC.

Abscess formation is detected almost exclusively in Crohn's, not UC. Abscesses can be confined to the bowel wall and pericolonic fat, or can involve adjacent structures such as the bladder, psoas muscle, or pelvic sidewall. Fistulae can also be reliably detected. Enterovesical, enterocutaneous, perianal, rectovaginal fistulae have all been detected with CT.

Toxic megacolon is a severe, life-threatening fulminant transmural colitis most commonly associated with UC. Toxic megacolon, however, has also been reported to occur infrequently with Crohn's, amebiasis, salmonella, pseudomembranous colitis and ischemic colitis. The patient typically presents with profuse bloody diarrhea, abdominal pain, fever and leukocytosis. On CT, there is distention of the colon, most commonly involving the transverse colon, containing large amounts of fluid and air. The haustra appear edematous and distorted, or may be absent. The presence of pneumatosis signifies ischemia and necrosis.

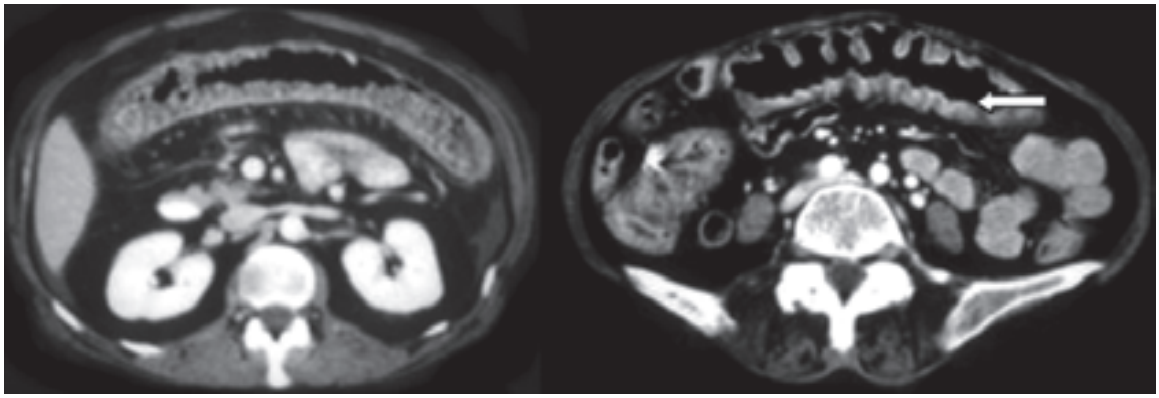

FIGURES 8.86A and B: Axial CECT without oral contrast reveals diffuse mucosal irregularity with enhancement (arrow) in a case of ulcerative colitis.

In cases with high clinical suspicion we prefer scheduling the CT scan after colonoscopy for two reasons: (1) the insufflated air provides good contrast, (2) better study planning can be done to answer specific questions if any are raised after scopy.

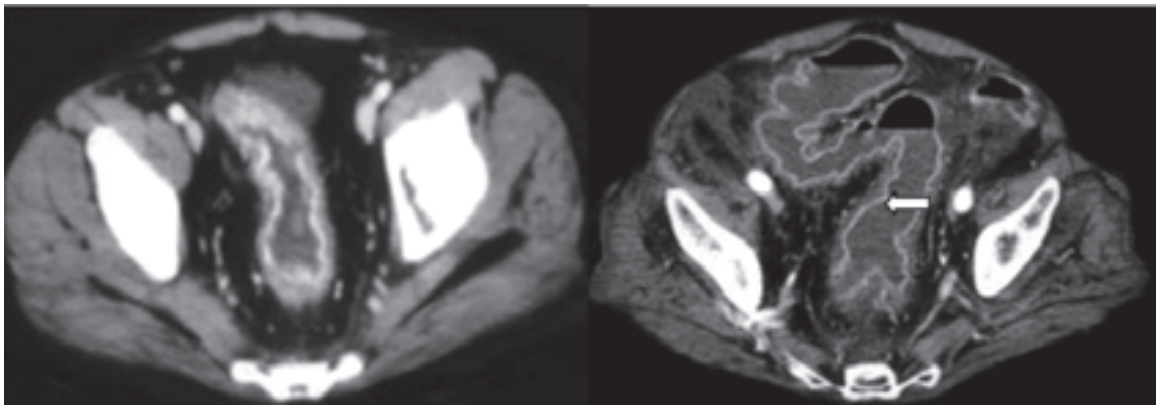

FIGURES 8.87A and B: Axial CECT in a patient with nonspecific inflammatory colitis reveals diffuse mucosal enhancement (arrow), note the fluid filled lumen.

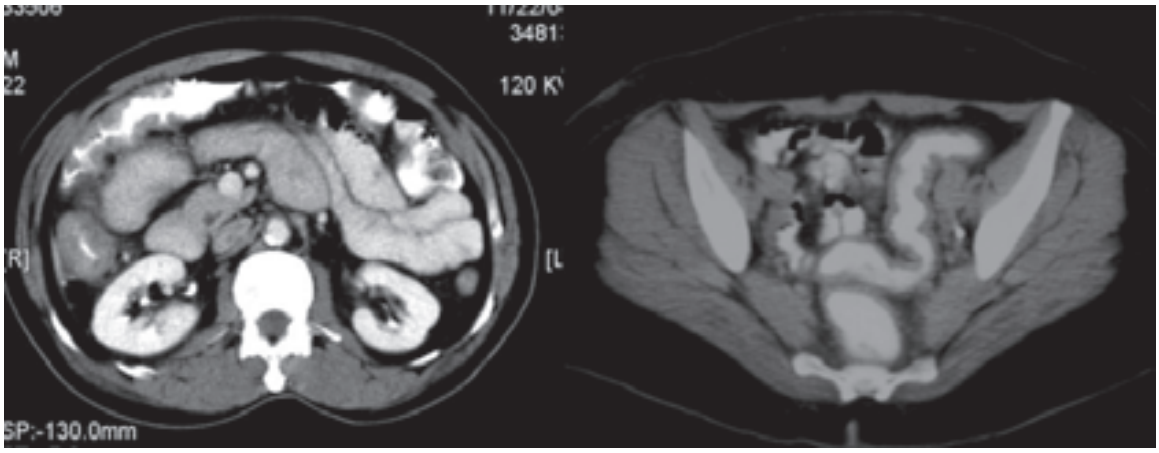

FIGURES 8.88A and B: Axial CECT in a patient with documented Crohn's disease shows mucosal thickening of ascending and proximal transverse colon.

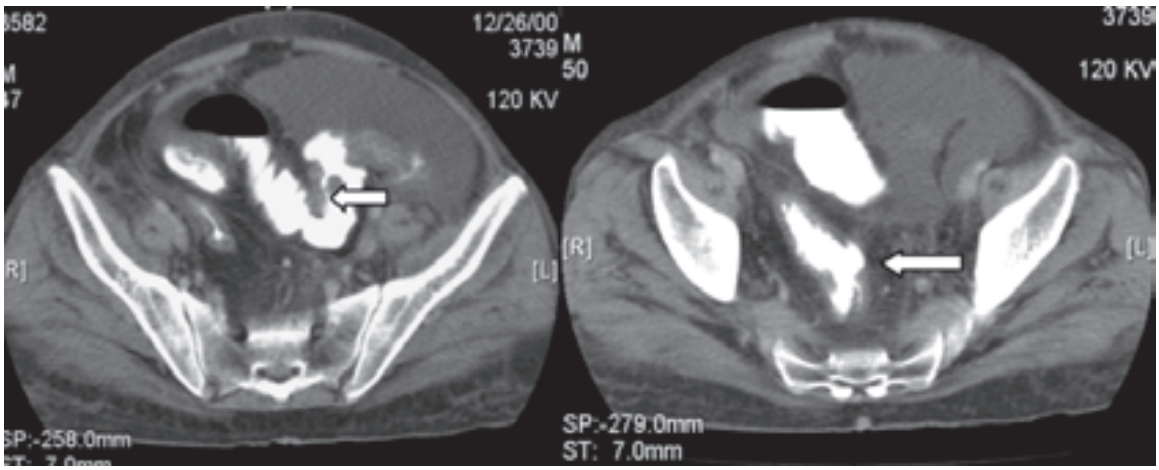

FIGURES 8.89A and B: Axial CECT with luminal contrast in a patient with chronic abdominal pain reveals mucosal polyps (Fig. A), mucosal ulcerations seen in the rectum (arrow in B) case of ulcerative colitis.

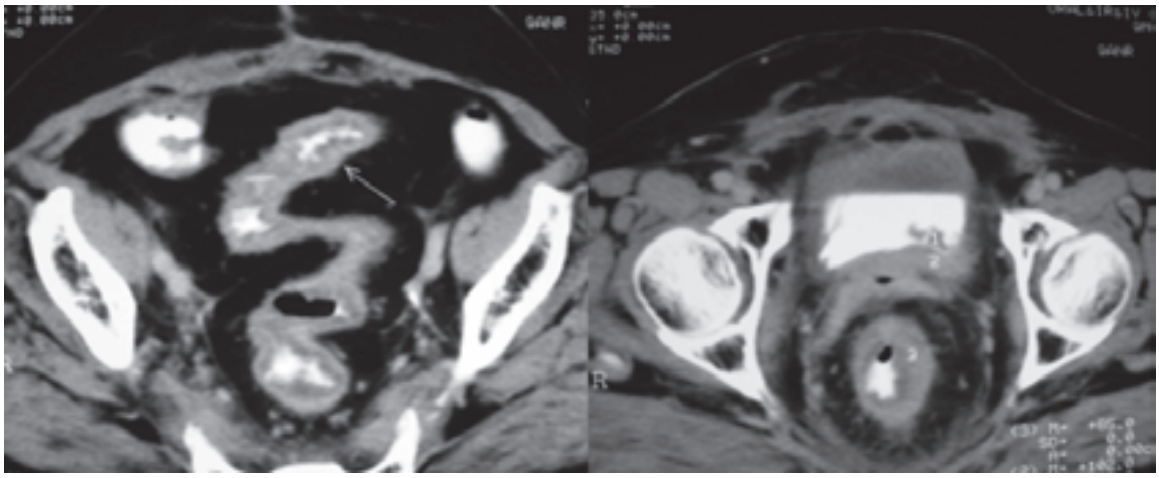

FIGURES 8.90A and B: Nonspecific colitis axial CECT showing long segment mural thickening with mucosal irregularity involving the rectum and sigmoid colon.

Ischemic Colitis

Colonic ischemia: Ischemia of the colon is considered to be the most common vascular disorder of the intestines in elderly patients. In contrast to patients with mesenteric ischemia, patients with colonic ischemia are usually not critically ill at the time of presentation. Patients usually complain of mild abdominal pain, followed by bloody diarrhea. In the majority of cases, the exact etiology cannot be established, and no evidence of vascular occlusion can be demonstrated. Since most patients are over the age of 70 and have evidence of widespread atherosclerosis, it is believed that the ischemia results from decreased blood flow to the colon. This may occur when there is an increased demand for blood by the colonic tissue in patients with only marginal blood flow or as a result of an acute decrease in blood flow to the colon.

Non-occlusive colonic ischemia usually involves the watershed areas of the colon, i.e. splenic flexure or rectosigmoid junction, but any part of the colon can be involved. The length of involved colon depends on the cause. For instance, non-occlusive ischemia usually will affect a larger segment of colon than ischemia resulting from atheromatous emboli. Most patients with non-occlusive colonic ischemia are treated conservatively with bowel rest, IV fluids and occasionally antibiotics. The injury resolves spontaneously in over 50% of cases in 1-2 weeks. Strictures are common complications of more serous episodes. If severe, ischemic bowel may become gangrenous and infarcted, which is a life-threatening condition requiring immediate surgical resection.

CT of Colonic Ischemia

Any segment of the colon can be involved, depending on the etiology. As most cases are a result non-occlusive ischemia, the watershed regions are most commonly affected, usually at the splenic flexure, left colon or rectosigmoid junction. Right sided colonic ischemia and necrosis has been reported as a complication of hemorrhagic shock after blunt or penetrating trauma. In addition, ischemic colitis has been described proximal to an obstructing colon cancer, which can be misinterpreted as tumor extension if it is adjacent to the primary tumor. However, the ischemia can occur at site remote from the obstructing tumor.

The colonic thickening is usually circumferential but may appear homogeneous or heterogeneous depending on the extent of submucosal edema, inflammation of hemorrhage. A halo may also be present. As with mesenteric ischemia, if transmural ischemia or infarction has occurred, pneumatosis may be present. Pneumatosis with or without air in the mesenteric vessels or portal vein is an ominous finding in patients with colonic ischemia and suggesting necrosis.

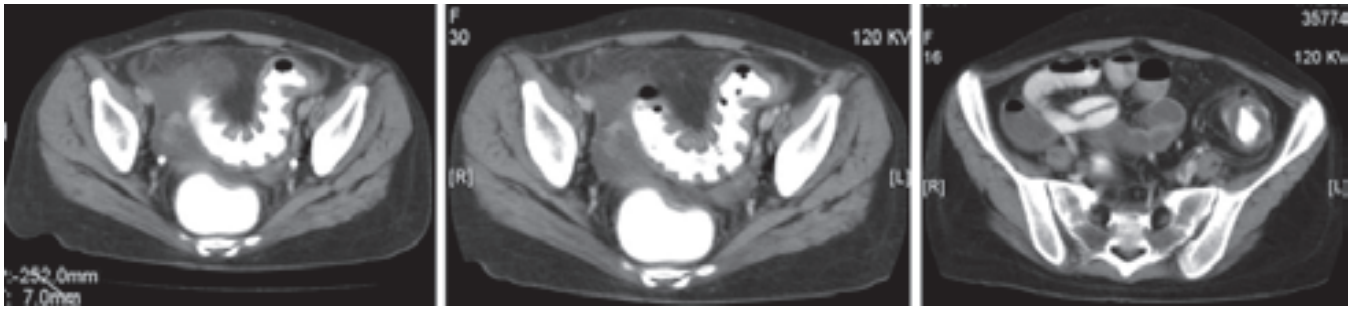

FIGURES 8.91A to C: Axial CECT in a patient with SLE presenting with acute abdominal pain and distention showing thickening of transverse colon and descending colon with enhancement of the serosa (arrow in C) typical features of nonocclusive ischemia.

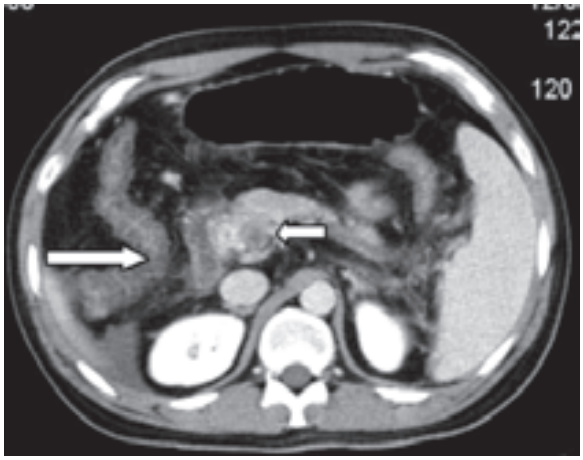

FIGURE 8.92: Axial CECT shows superior mesenteric vein thrombus (arrow), ascending colon appears thickened with mucosal edema (arrow).

Inflammation of Appendage Epiploicae

Appendices epiploicae are fat containing peritoneal outpouchings which are attached to the serosal surface of the colon.

These structures can undergo torsion resulting in ischemia and infarction. On CT, the diagnosis of inflammation of the appendices epiploicae should be suspected when there is focal localized inflammatory changes in the pericolonic fat.

Tuberculosis

Intestinal TB occurs at any age and is equally prevalent in both male and females. CXR may be positive in about 20% of patients. Intestinal TB may occur by several mechanisms including:

1. Swallowing of infected sputum in active pulmonary TB
2. Ingestion of contagious milk
3. Hematogenous spread
4. Direct extension from adjacent organs.

Once bacilli enters the GI tract, it traverses the mucosa to lodge in the submucosa. lymphangitis, endarteritis, and fibrosis ensues leading to mucosal ulceration, caseating necrosis, and narrowing of the intestinal tract.

Intestinal TB manifests as ulcerative, hypertrophic, ulcerohypertrophic forms. Pattern of involvement include bowel, peritoneum and mesenteric lymph node.

CT findings include bowel wall thickening, varying from 1-2 cm in thickness, bowel walls may show homogenous attenuation, multiple sites of involvement with skip lesions may be seen. Bowel loop separation may be seen caused by lymphadenopathy, bowel thickening, interloop fluid collection, and rarely fibrous fat proliferation.

Enlarged nodes are larger than 1cm and have low attenuation centers, caused by caseating necrosis, commonly involve the peripancreatic nodal chains. CT findings of TB peritonitis may mimic those of peritoneal carcinomatosis including diffuse omental thickening, mesenteric nodules, ascites and peritoneal thickening.

Complications include intestinal obstruction, bowel perforation, fistula, and venous thrombosis.

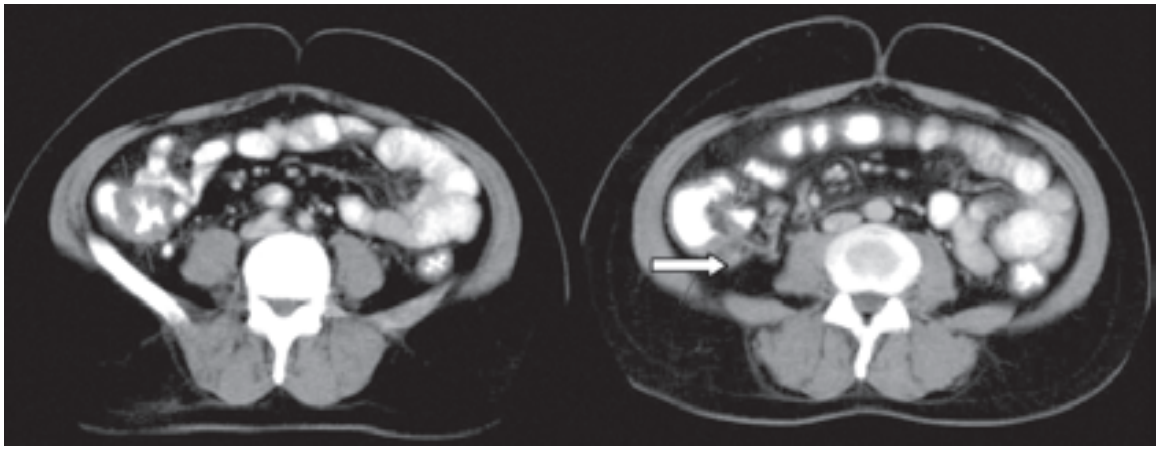

FIGURES 8.93A and B: Axial CECT showing thickening in the ileocecal region with pericecal fat stranding.

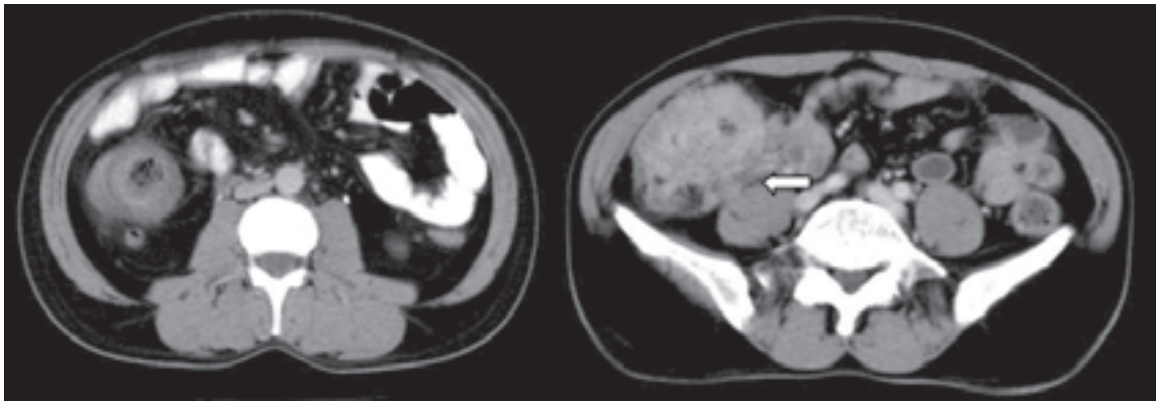

FIGURES 8.94A and B: Axial CECT reveals circumferential cecal thickening with a ileocecal enhancing phlegmonous soft tissue (arrow).

Pseudomembranous Colitis

Pseudomembranous colitis results from an overgrowth of the organism *Clostridium difficile*. Although first described as a complication of antibiotic therapy, pseudomembranous colitis has also been described with hypotensive episodes, chemotherapeutic agents, following abdominal surgery, and proximal to a large bowel obstruction.

CT findings include marked low attenuation wall thickening, which can be circumferential or eccentric. Haustral folds are thickened and can appear as broad transverse bands, referred to as "accordion pattern". The colon wall may enhance secondary to the hyperemia. Classically PMC is a pancolitis.

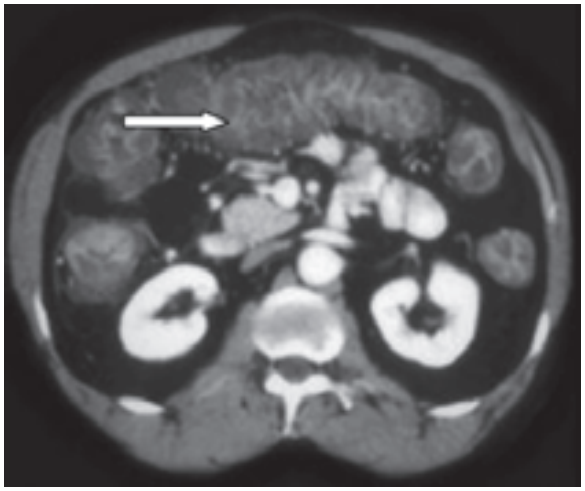

FIGURE 8.95: Axial CECT showing diffuse mural thickening of large bowel with mucosal enhancement (arrow).

Obstruction/Ileus

Mechanical obstruction of the colon can be caused by a variety of pathologic processes including malignancies, inflammatory structures, volvulus, intussusception, hernias, and fecal impaction.

The key to detection of a colonic obstruction on CT is the presence of dilated colon proximal to a transition to normal caliber or collapsed bowel distally. This distinguishes obstruction from nonobstructive ileus.

Colonic ileus occurs when there is selective distention of the colon without a mechanical obstruction. The etiology of colonic ileus is not known but is thought to relate to a problem with sympathetic and parasympathetic innervation of the colon. Colonic ileus usually occurs in hospitalized patients.

On CT, colonic ileus appears as dramatic dilation of all or part of the colon. The walls of the colon are smooth and not usually thickened or edematous, which may help distinguish ileus from obstruction. However, it may be difficult to distinguish colonic ileus from obstruction on CT and a contrast enema may be necessary to definitely exclude obstruction. Impending perforation has been reported with cecal diameters of 9-12 cm.

Specific Causes of Colonic Obstruction

Intussusception: An intussusception occurs when a segment of bowel prolapses into the lumen of an adjacent segment. Intussusception is more common in children and is usually idiopathic. In adults, however, an anatomic lead point can often be identified. Certain conditions such as celiac disease, scleroderma, Whipple's disease predispose to intussusception. Recently AIDS associated intussusception in adults has been described.

The CT appearance of intussusception is very distinctive. Intussusceptions can appear as a target mass with alternating rings of soft tissue and fat, representing the wall of the intussusceptum, mesenteric fat, and the wall of the intussuscipiens. As edema of the bowel wall increases, these distinct layers may be obscured. The presence of pneumatosis indicates significant ischemia. Dilatation and/or air fluid level in proximal loops suggests obstruction.

Volvulus: Colonic volvulus is a well recognized cause of intestinal obstruction. Approximately 3 to 5% of all cases of intestinal obstruction are caused by colonic volvulus. Of all areas of colonic volvulus, only 4% involve the transverse colon. Volvulus of the transverse colon most often occurs in the second and third decades of life with an additional peak in the seventh decade and women outnumber men 2:1. The mortality rate of transverse colon volvulus is 33%, whereas sigmoid volvulus carries a mortality rate of 21% and cecal volvulus rate of 10%.

Volvulus of the transverse colon is a closed loop obstruction. The normal anatomy of the transverse colon typically prohibits volvulus in this area. The short transverse mesocolon and the hepatic and splenic flexures act to

fix the transverse colon in position. The etiologies of transverse colon volvulus may be grouped as mechanical, physiological, and congenital. Mechanical causes include: previous volvulus of the transverse or sigmoid colons, distal colonic obstruction, adhesions, malposition of the colon following previous surgery, mobility of the right colon, inflammatory strictures, and carcinoma. The most common physiological condition which predisposes to volvulus is chronic constipation. Chronic constipation tends to elongation and redundancy of the colon, permitting volvulus even in the presence of a normal mesentery.

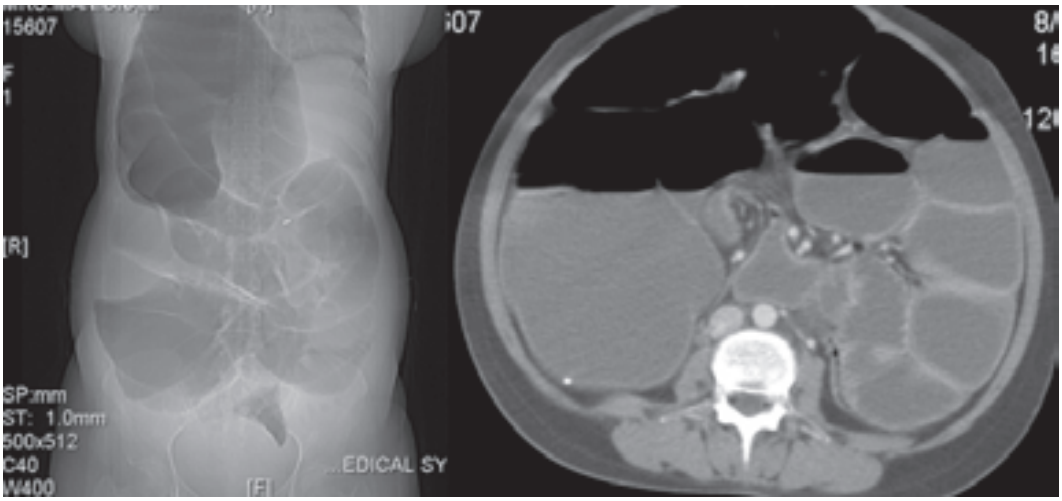

FIGURES 8.96A and B: Scanogram shows dilated large bowel with an inverted U-shaped dilatation of transverse colon. Axial CECT shows grossly dilated large bowels (postoperative finding was that of a transverse colon volvulus).

Cecal volvulus occurs in patients with an unusually long mesentery to the right colon. This results in a mobile cecum which can twist upon its luminal axis and cause obstruction. The twisted distended cecum flips superiorly and to the left so that it is now located in the left upper quadrant. This has a distinctive appearance on plain film and contrast enema. The key to the CT diagnosis is distention of the cecum which is displaced into the left upper quadrant. A "whirl" pattern of dilated bowel around twisted mesenteric vessels was first described in midgut volvulus, but has also described in volvulus of the colon.

Sigmoid volvulus occurs when a long mobile segment of sigmoid twists upon itself. This results in a closed loop obstruction which tends to fill the lower abdomen. On plain film this appears as a bean shaped collection of air representing the displaced and distended closed loop of sigmoid. CT diagnosis of volvulus is suggested when the sigmoid appears distended and displaced superiorly. A whirl sign as well as pericolonic inflammation may also be present.

Hernia: An external hernia results when a peritoneal sac herniates through a weakness in the muscular layers of the abdominal wall. Common external hernias that may contain colon include inguinal, femoral, spigelian, and incisional hernias. Obturator, sciatic notch, and umbilical hernia are much less common.

Inguinal hernias can be direct or indirect depending on their position relative to the inferior epigastric artery and vein. Indirect inguinal hernias are most common. Right sided inguinal hernias often contain small bowel while left sided inguinal hernias often contain sigmoid colon.

In a patient with an indirect inguinal hernia, bowel is identified within the inguinal ring and may extend inferiorly into the scrotum or labia.

Direct inguinal hernias are within the aponeurosis of the external oblique muscle and rarely involve the scrotum. Femoral hernias are less common than inguinal hernias and represent herniations through the femoral ring. Femoral hernia sacs lies below and lateral to the pubic tubercle (inguinal hernias are above and medial). Femoral hernias have higher incidence of incarceration. Spigelian hernias, herniation of bowel at the lateral border of the rectus sheath, along the linea semilunaris, can also contain colon.

The key to the diagnosis of an external hernia on CT is the identification of bowel in an abnormal location. The bowel loops contained within the hernia must be examined carefully. Dilation of the herniated loops or proximal bowel loops indicates obstruction. Inflammatory changes, wall thickening or pneumatosis signify incarceration and ischemia, which is a surgical emergency.

Diaphragmatic hernias can be congenital or acquired. A foramen of Morgagni hernia typically present in adults, and are located on the right side through the anteromedial foramen of Morgagni. The hernia may be comprised totally of omental fat and vessels, or may contain bowel, especially transverse colon.

Foramen of Bochdalek hernia are typically on the left and are located posterolaterally. These hernias may contain small or large bowel, stomach, omentum, liver or spleen. Most congenital hernias occur through the foramen of Bochdalek.

Miscellaneous

Pneumatosis: Pneumatosis coli is an uncommon but important condition characterized by air within the wall of the colon. Classically the condition is separated into cystic (pneumatosis cystoides intestinalis) vs. linear depending on the morphology of the thin walled noncommunicating air collections. Traditionally, cystic air collections were thought to be due to "benign" conditions such as chronic obstructive pulmonary disease or high dose corticosteroids, while linear collections were thought to be more indicative of serious conditions such as bowel ischemia or necrosis. However, it is not always possible to classify the condition based on the morphology of the air collections, as there is considerable overlap in appearance. The condition can be indolent or fatal depending on the severity and etiology which can be difficult to predict from imaging. Therefore, correlation with the patients clinical condition, possible predisposing factors, and extent of bowel involvement is necessary.

CT is more sensitive than plain film for the detection of pneumatosis and can sometimes identify the etiology. The small air collections can readily be detected within the wall of the colon, especially when lung windows are obtained. Intramural air should be demonstrated in a dependent wall, as confusion with intraluminal air can thus be avoided. Additional CT findings such as distention, wall edema, pericolonic inflammation, or portal venous air suggest bowel ischemia/infarction.

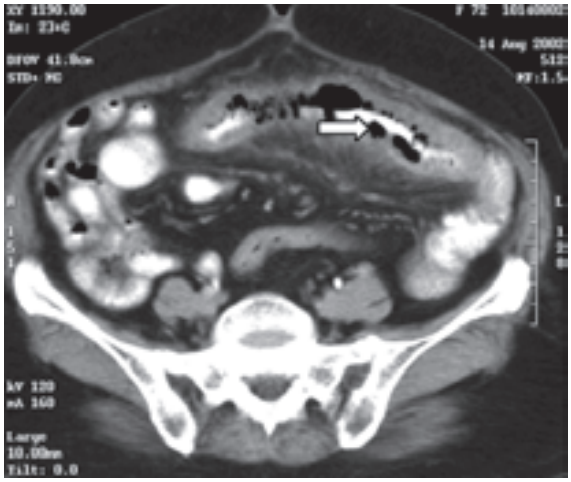

Although pneumoperitoneum can occur in benign, incidental cases or in life-threatening conditions, the clinical status of the patients will usually aid in the differential diagnosis. Portal venous air, however, is almost always a sign of serious bowel necrosis and carries a grave prognosis.

Pneumatosis coli is has recently been described as a late manifestation in patients with AIDS, typically involves the right colon, and is thought to be innocuous, not requiring emergent surgery.

FIGURE 8.97: Axial CECT showing mural air pockets in the transverse colon (arrow).

Traumatic perforation: The value of CT in the diagnosis of injury to solid abdominal organs after trauma has been well established. However, the role of CT for the diagnosis of bowel rupture after blunt abdominal trauma continues to be debated. With improvements in CT imaging techniques, more recent studies have been encouraging.

CT findings thought to be diagnostic of bowel rupture include pneumoperitoneum, pneumoretroperitoneum, or free air within the mesentery. Demonstration of oral contrast extravasation or of discontinuity in the bowel wall is also diagnostic. CT findings suspicious, but not diagnostic for colon perforation include segmental wall thickening, pericolonic fluid or blood.

The findings are often subtle.

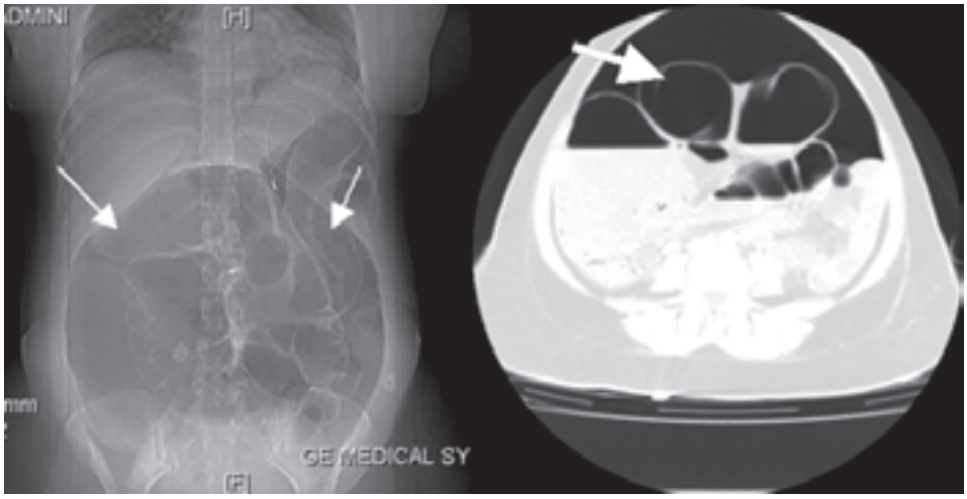

FIGURES 8.98A and B: (A) Digital scanogram showing the classical football sign of massive pneumoperitoneum (arrows). (B) Axial CT showing large amount of free air (arrow).

Colonic Malignancies

Colorectal cancer: Initial diagnoses of colorectal cancer is usually made with endoscopy or barium enema. Computed tomography continues to play a significant role in staging adenocarcinoma of the colon and rectum and in detecting recurrence.

On CT, adenocarcinoma of the colon usually appears as a soft tissue density mass. Larger masses may have a low density necrotic center or occasionally may contain gas, resembling an abscess. Rectal cancers may appear as asymmetric wall thickening which narrows the lumen. CT is able to detect extension of tumor into the pericolonic fat, invasion of adjacent organs, such as bladder or pelvic muscles, and adenopathy. CT is the study of choice for the detection of liver metastasis, which will appear as multiple hypodense lesions within the liver after injection of intravenous contrast.

Recurrent tumor after surgery usually appears as a soft tissue density mass with irregular borders. This can often be distinguished from postoperative fibrosis which usually appears more linear without a discrete mass.

Lymphoma: Primary lymphoma of the colon is rare and comprises less than 1% of all colonic neoplasms. These lesions are predominantly non-Hodgkin lymphomas and most often involve the cecum (52%) or rectum (21%).

Three distinct appearances of primary colonic lymphoma have been described on CT: a focally infiltrative lesion, a diffuse mural infiltration or a discrete mass. Classically, the appearance which should prompt consideration of lymphoma is the presence of a focal or diffuse infiltrative colonic process with abdominal or pelvic adenopathy, however, it is often difficult to distinguish primary colonic lymphoma from adenocarcinoma on CT, especially if a solitary mass is present.

CT Staging of Primary and Recurrent Colonic Tumors

Stage 1: Intraluminal polypoidal mass without thickening of clonic wall.

Stage 2: Thickened colonic wall (>6 mm) or pelvic mass without invasion of the adjacent organs or extension to the pelvic sidewalls.

Stage 3a: Thickened colonic wall or pelvic mass with invasion of adjacent muscles and/or organs.

Stage 3b: Thickened colonic wall or pelvic mass extending to pelvic sidewalls and/or abdominal wall.

Stage 4: Metastatic disease with/or without local abnormality.

Benign Neoplasms

The most common benign tumor of the colon is an adenoma. Adenomas are typically solitary, and can have significant malignant potential depending on size and histology. Certain syndromes such as familial polyposis, Gardner's, and Turcot's, are characterized by multiple colonic polyps.

The double contrast barium enema and colonoscopy are the primary imaging tools for the diagnosis of colonic polyps. Lipoma is the most common benign submucosal tumor in the colon. A colonic lipoma more commonly occurs in the cecum and ascending colon and is usually an incidental finding in asymptomatic patient. On CT, a colonic lipoma is identified as a solitary submucosal mass of uniform fat density. There is no risk of malignant degeneration. Rare complications include intussusception. Lipomatous infiltration of the ileocecal valve can also occur but is not thought to be neoplastic in nature.

Leiomyomas can occur in the colon, although they are more common in the small bowel and esophagus. On CT, the appearance of leiomyomas is nonspecific. A leiomyoma appears as a submucosal soft tissue density mass.

The most common appendiceal tumor is carcinoid. The vast majority of appendiceal carcinoid tumors are benign. They rarely metastasize or result in carcinoid syndrome. The lumen of the appendix may be obstructed and result in periappendiceal inflammation, indistinguishable for typically appendicitis. A stellate radiating pattern may be seen in the mesentery secondary to desmoplastic reaction.

Non-appendiceal large bowel carcinoids, usually involve the rectum. They are usually discovered incidentally on endoscopy or barium enema. Rectal carcinoids are low grade malignancies with metastases occurring in only 10% of cases (Figures 8.111A and B).

PATTERNS OF BOWEL MALIGNANCY

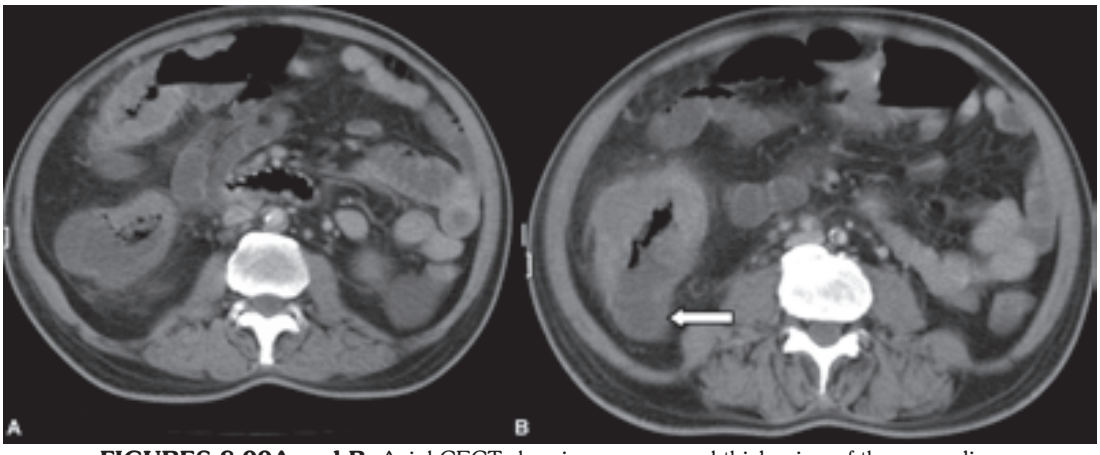

FIGURES 8.99A and B: Axial CECT showing gross mural thickening of the ascending colon with pericolic fat stranding, note focal areas of necrosis (arrow).

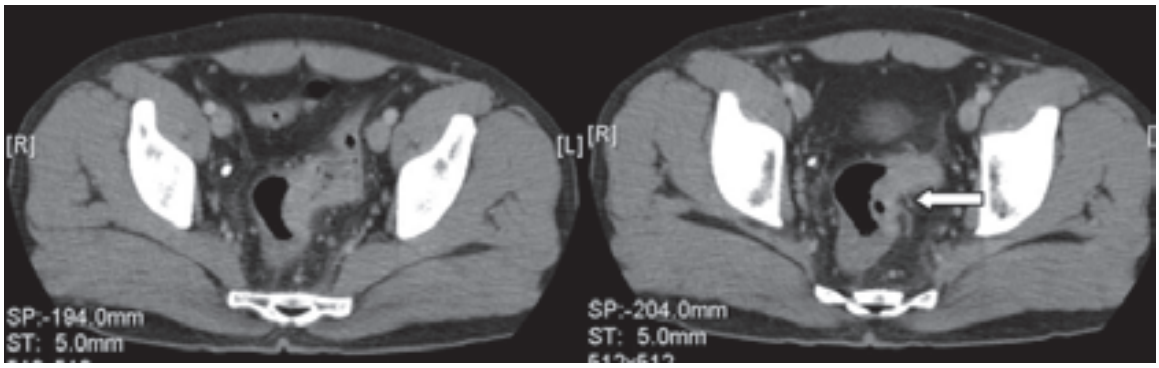

FIGURES 8.100A and B: Axial CECT showing a short segment rectal growth with shouldering (arrow).

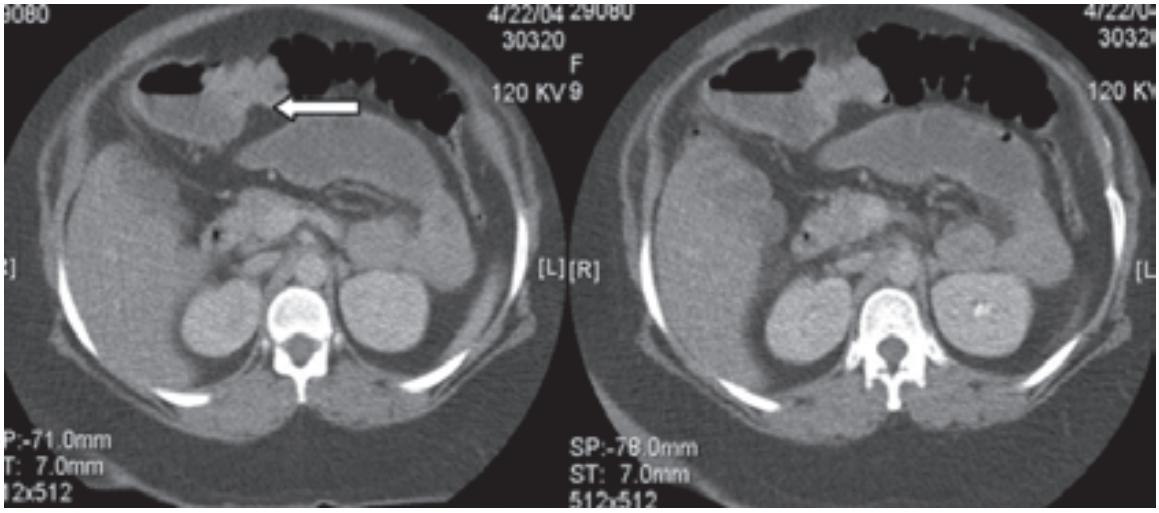

FIGURES 8.101A and B: Axial CECT reveals a short segment polypodal mass in the mid transverse colon (arrow).

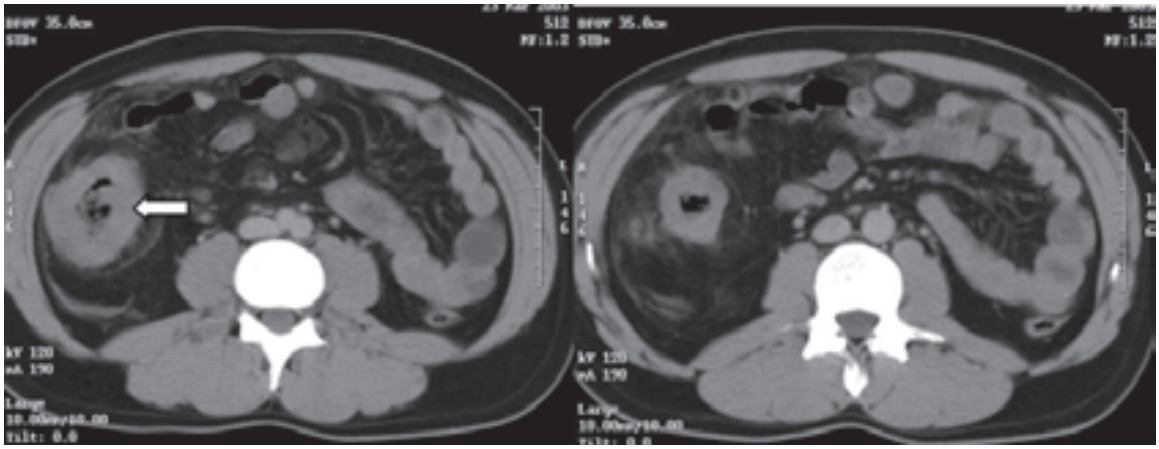

FIGURES 8.102A and B: Axial CECT showing circumferential mural thickening of ascending colon with luminal narrowing (arrow).

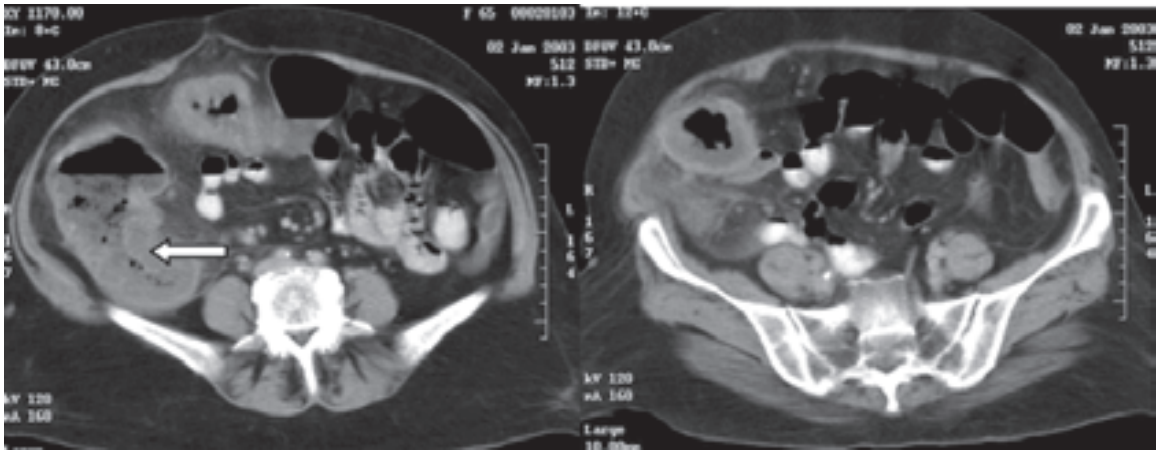

FIGURES 8.103A and B: Axial CECT showing long segment mural thickening of ascending and proximal transverse colon, note the hypodense mural thickening.

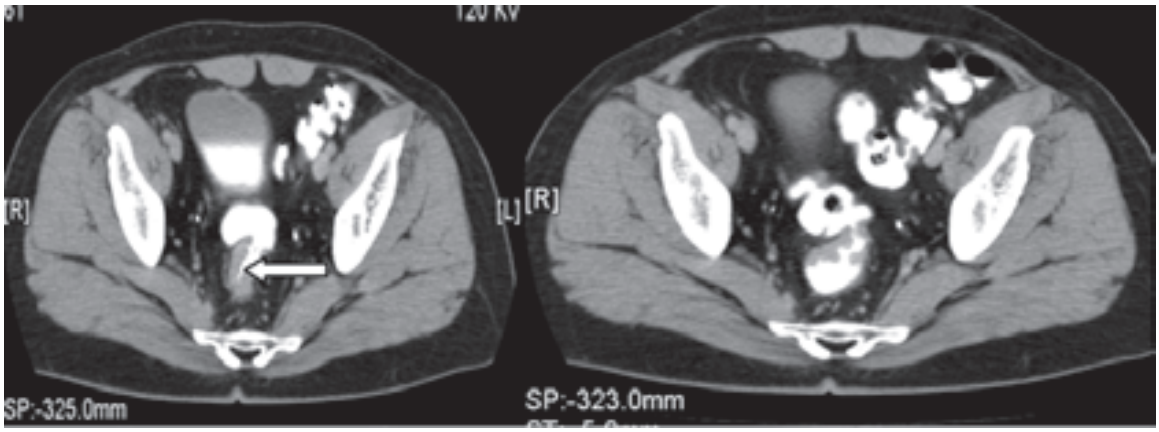

FIGURES 8.104A and B: Axial CECT with luminal contrast shows a short segment ulcerative lesion in the rectosigmoid junction.

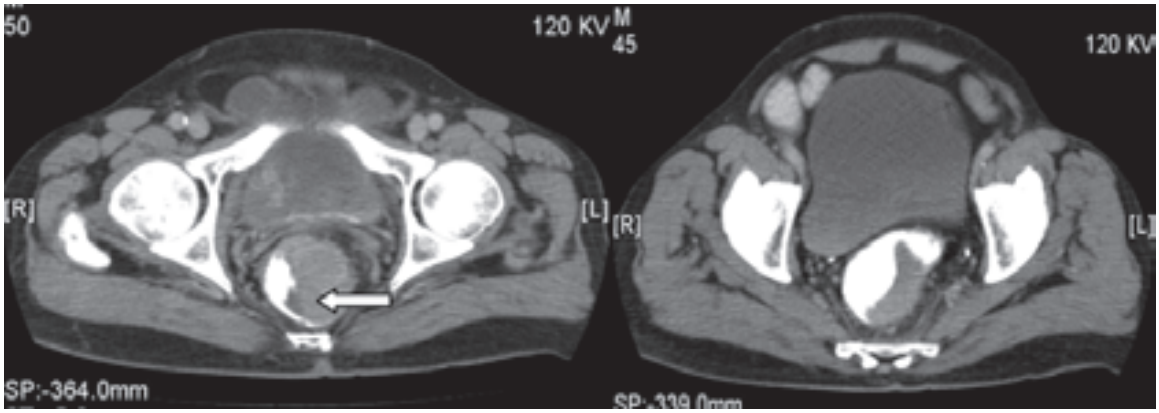

FIGURES 8.105A and B: Axial CECT with rectal contrast shows an eccentric polypoidal mass arising from the left rectal wall (arrow).

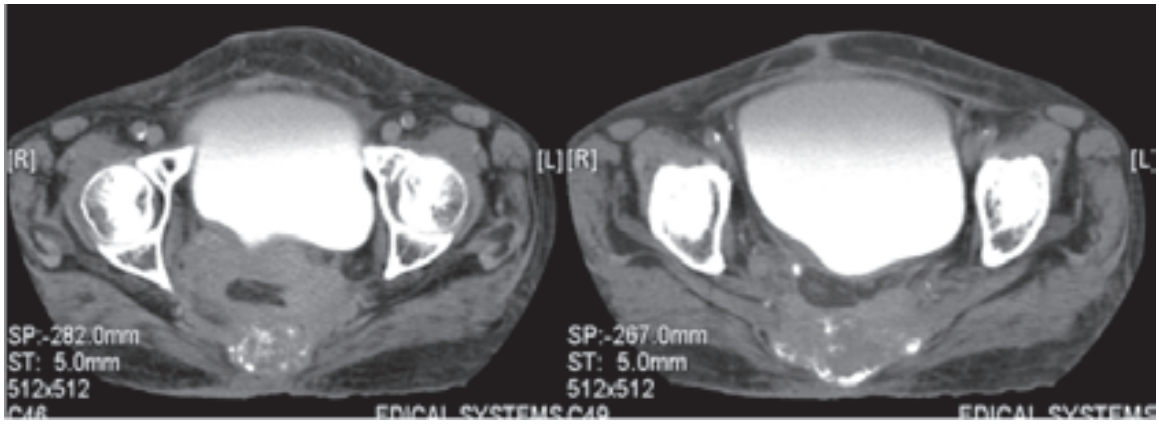

FIGURES 8.106A and B: Axial CECT (case of postoperative Ca rectum) showing destruction of sacrum with a presacral soft tissue mass–very typical pattern of local tumoral recurrence.

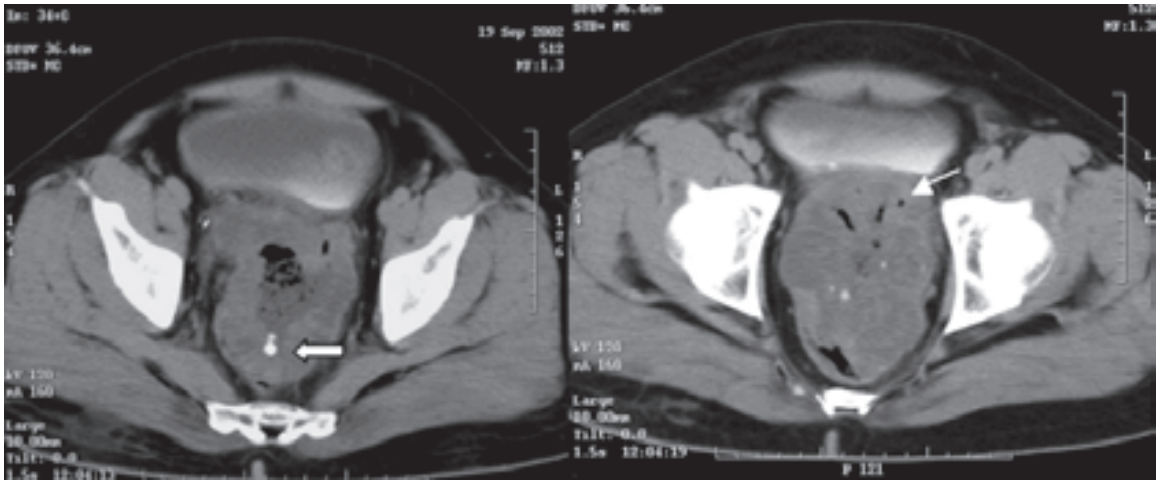

FIGURES 8.107A and B: Axial CECT showing a large circumferential thickening of rectum with luminal compromise, note the speck of calcification seen in B (suggestive of a mucinous tumor). Note the elevated bladder base with loss of fat planes suggestive of vesicle infiltration (thin arrow).

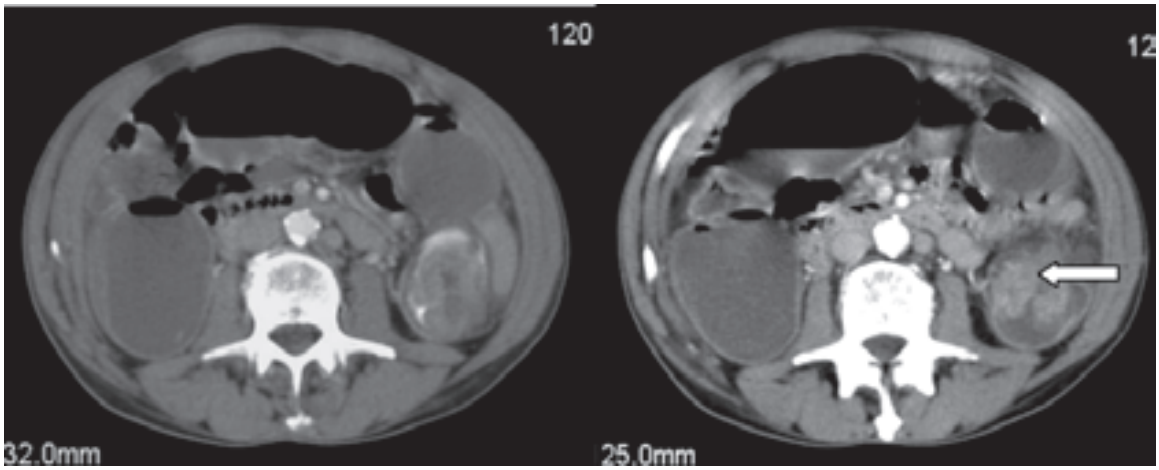

FIGURES 8.108A and B: Axial CECT showing a polypoidal mass within the descending colon causing luminal compromise (arrow).

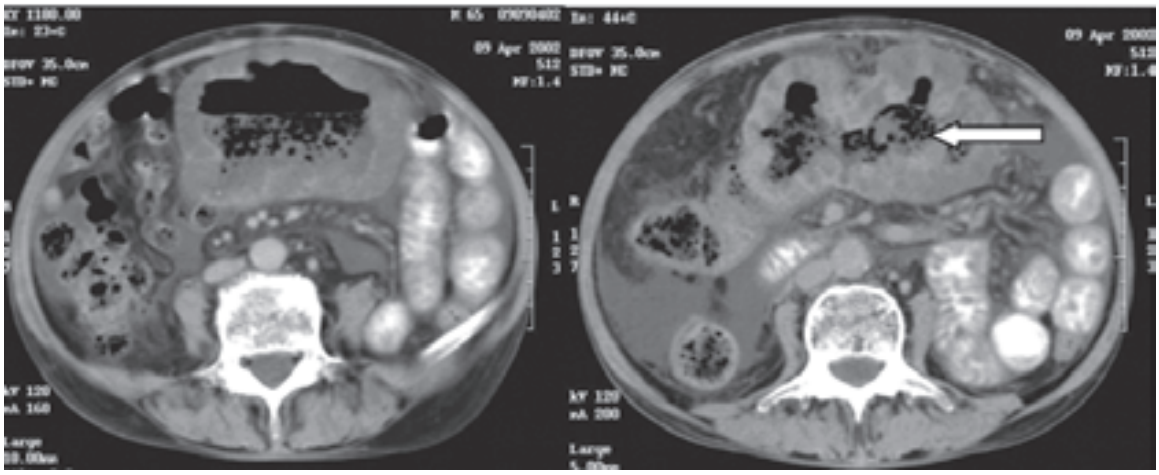

FIGURES 8.109A and B: Axial CECT showing a mid transverse colon mass with significant pericolic stranding (arrow).

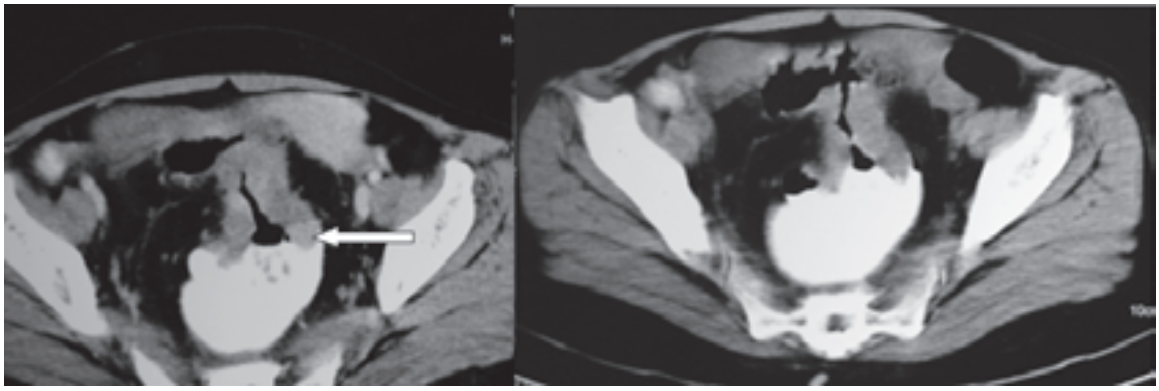

FIGURES 8.110A and B: Axial CECT showing a circumferential luminal narrowing with wall thickening in the rectosigmoid junction (arrow).

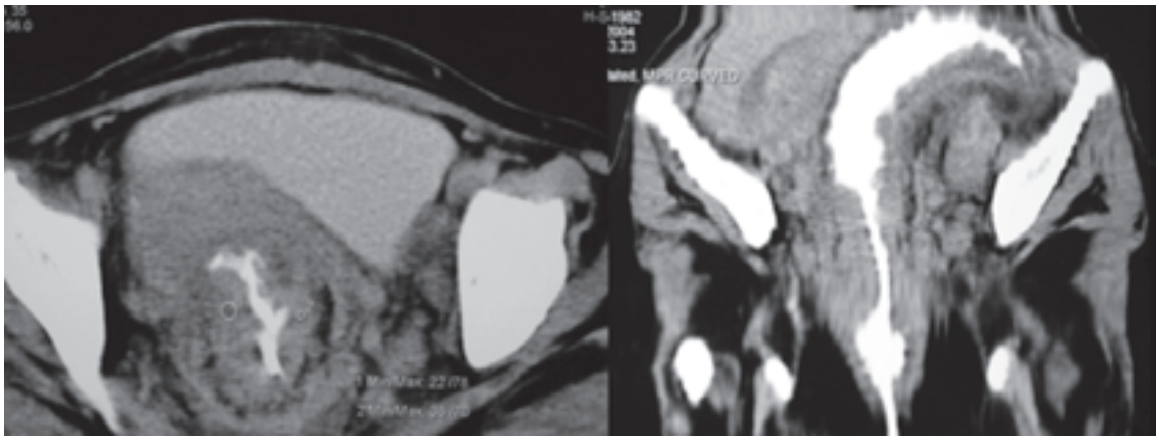

FIGURES 8.111A and B: Axial CECT in a postpartum patient with bleeding perrectum showing a long segment rectosigmoid thickening with perirectal nodular soft tissue infiltration (histopathology showed features of rectal carcinoid).

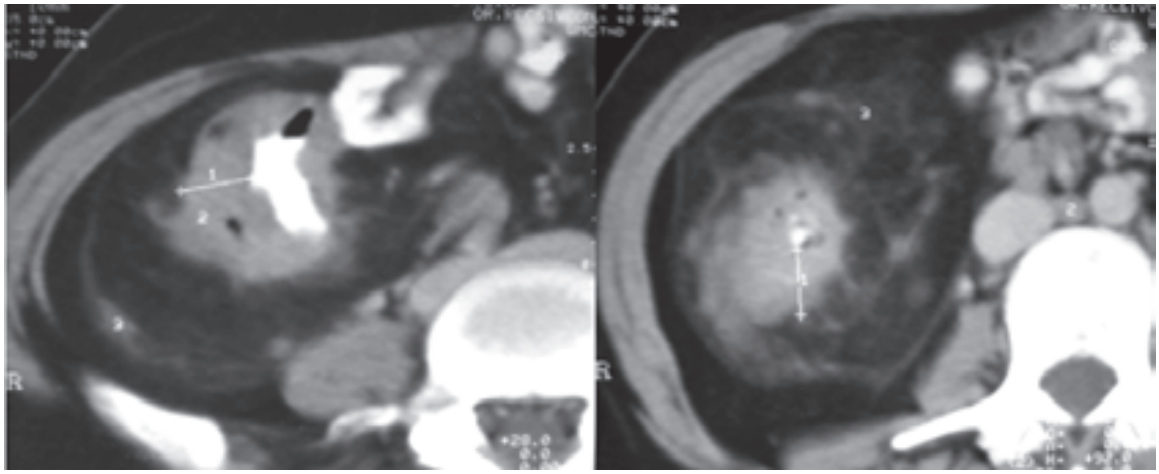

FIGURES 8.112A and B: Axial CECT with luminal contrast showing eccentric thickening of the cecum with significant pericolic fat stranding (arrow). It is unusual to see extensive pericolic stranding like this in mitotic lesions.

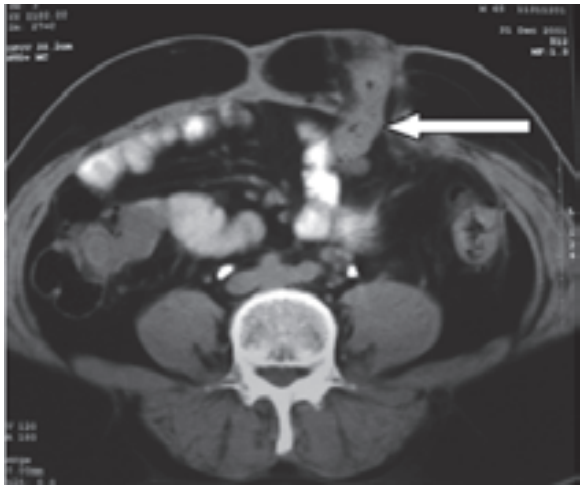

FIGURE 8.113: Axial CECT in a postoperative patient of Ca rectum showing the colostomy site (arrow).

Colovesicle Fistula

Gastrointestinal (GI) **fistulas** represent abnormal duct-like communications between the gut and another epithelial-lined surface, such as another organ system, the skin surface, or elsewhere along the GI tract itself. A GI sinus tract, in comparison, is a similar duct like passage that communicates with the gut at one end but ends blindly at the other. The development of a GI fistula can markedly increase patient morbidity and mortality, rendering detection of the fistula critical. Imaging often plays a pivotal role in the diagnosis and management of GI fistula, with fluoroscopic contrast agent–enhanced studies serving as the traditional standard bearer. The emergence of cross-sectional imaging techniques, however, has modified the radiologic approach to GI **fistulas**.

Classification of GI Fistulas

- Congenital
- Acquired
  - Internal
    - * Intestinal (gut-to-gut)
    - * Extraintestinal

    * Genitourinary
    * Biliary
    * Vascular
    * Respiratory
    * Other
  - External (cutaneous)
    * High-output
    * Low-output
  - Complex (internal and external)

Causes of GI fistulas

- Inflammation
  - Crohn disease
  - Diverticulitis
  - Infection (atypical)
  - Cholecystitis
  - Appendicitis
  - Pancreatitis
- Surgery/Iatrogenic
- Malignancy
- Radiation
- Aortic aneurysm/graft
- Peptic ulcer disease
- Trauma
- Ischemic
- Foreign body
- Idiopathic.

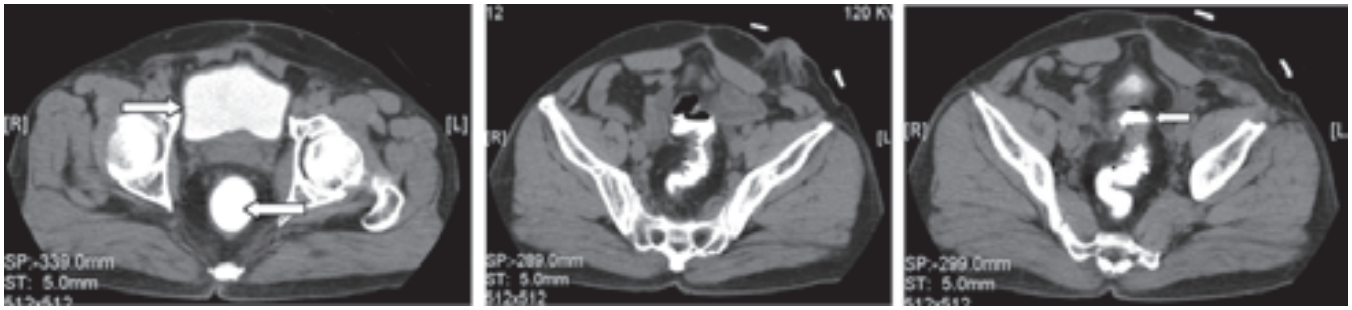

FIGURES 8.114A to C: Axial NECT with rectal contrast shows opacification of urinary bladder (arrows A), arrow in Fig. C shows the fistula. Patient had past history of AP resection for Ca rectum. In case of suspected colonic fistulas it is advisable to perform a contrast enema first without IV contrast, based on the initial findings subsequent IV contrast can be scheduled.

Extraintestinal Fistulas

The extraintestinal **fistulas** constitute a diverse and intriguing collection of acquired GI **fistulas** since they can connect the gut with virtually any other organ system. Extraintestinal **fistulas** involving the genitourinary, biliary, vascular, and respiratory systems are considered below.

Genitourinary tract—Communication between the GI and genitourinary tracts represents a major subset of extraintestinal internal **fistulas**. The bladder and vagina are most often affected, but involvement of the upper collecting system, urethra, or uterus is occasionally seen.

The term *enterovesical fistula* is often generally applied for bladder communication with the colon, small bowel, rectum, or appendix. Sigmoid diverticulitis is the single most common cause of enterovesical (specifically, colovesical) fistula. Furthermore, **fistulas** to the urinary bladder account for over half of all internal **fistulas** encountered in diverticular disease. Crohn disease accounts for most small-bowel–to-bladder **fistulas** and may be present in upto 3–4% of patients with this disease. Pelvic malignancy, especially colorectal adenocarcinoma, is the other major cause of a GI fistula to the bladder, followed by radiation- and surgically induced **fistulas**. Approximately 20% of all enterovesical **fistulas** are rectovesical, and fewer than 5% are appendicovesical.

Intestinal Fistulas

Intestinal (gut-to-gut) **fistulas** may involve any or all combinations of the small bowel, colon, and stomach. The clinical manifestation of this subset may be subtle, since only the alimentary tract is involved. Diarrhea, with or without abdominal pain, is the most common symptom overall. There are several factors that influence which segments of bowel are involved in the fistulous communication. In cases where a primary bowel abnormality is the underlying cause, the segment of diseased bowel will obviously be at highest risk. Proximity to the pathologic process, be it intestinal or extraintestinal, is also important. Finally, a preexisting or preferred pathway between certain portions of the gut, as with a connecting ligament or mesentery, explains the predisposition for some intestinal **fistulas** to form.

Enteroenteric and enterocolic **fistulas** are common complications of Crohn disease, where **fistulas** are often multiple and favor the ileocecal region. Enterocolic **fistulas** in Crohn disease are usually due to primary small-bowel disease, whereas the opposite is true for **colonic** diverticulitis. Overall, coloenteric **fistulas** constitute fewer than 10% of **fistulas** complicating diverticulitis. A more common form of intestinal fistula from diverticulitis is the so-called double-tracking colocolic fistula. This intraloop form of intestinal fistula results from localized perforation and paracolic extension that parallels the bowel lumen. A similar appearance can be seen with Crohn disease and perforated adenocarcinoma of the colon. Intestinal **fistulas** can also be seen in cases of other abdominal malignancies, radiation therapy, surgery, and foreign bodies.

Patterns of Attenuation in Bowel Wall Thickening

I. Homogeneous
- A. Common
  1. Submucosal hemorrhage
  2. Lymphoma
  3. Small adenocarcinoma
- B. Uncommon
  1. Infarcted bowel
  2. Pitfalls related to residual fluid
  3. Chronic Crohn's disease
  4. Chronic radiation injury

II. Heterogeneous
- A. Stratified attenuation
  1. Common

a. Ischemia
b. Infectious enterocolitis
c. Crohn's disease, ulcerative colitis
d. Vasculitis, lupus, Henoch-Schönlein purpura
e. Radiation
f. Bowel edema related to cirrhosis or low-protein state

2. Uncommon
a. Infiltrating scirrhous carcinoma (usually stomach or rectum)
b. Residual fluid and contrast material
c. Submucosal fat deposition
d. Pneumatosis

B. Mixed attenuation, common
1. Large adenocarcinoma
2. Gastrointestinal stromal tumor
3. Mucinous adenocarcinoma.

Degree of Bowel Wall Thickening

I. Mild Thickening (<2 cm)
A. Common
1. Infectious enterocolitis
2. Ulcerative colitis
3. Crohn's disease
4. Radiation injury
5. Ischemia
6. Bowel edema in cirrhosis
7. Submucosal hemorrhage

B. Uncommon
1. Adenocarcinoma
2. Lymphoma

II. Marked Thickening (>2 cm)
A. Common
1. Adenocarcinoma, gastrointestinal stromal tumor, metastases, lymphoma
2. Severe colitis
3. Systemic lupus erythematosus

B. Uncommon
1. Crohn's disease, tuberculosis, histoplasmosis, cytomegalovirus
2. Submucosal hemorrhage.

Symmetry of Bowel Wall Thickening

I. Symmetric
A. Infections of the small and large bowel
B. Ulcerative colitis
C. Crohn's disease
D. Radiation injury
E. Ischemia

F. Bowel edema in cirrhosis
G. Lymphoma
H. Submucosal hemorrhage

II. Asymmetric

A. Adenocarcinoma
B. Gastrointestinal stromal tumor

Length of Bowel Wall Thickening

I. Focal (<10 cm)

A. Common
   1. Diverticulitis, appendicitis
   2. Adenocarcinoma
B. Uncommon
   1. Lymphoma
   2. Tuberculosis
   3. Crohn's disease

II. Segmental (10-30 cm)

A. Common
   1. Lymphoma
   2. Crohn's disease
   3. Infectious ileitis
   4. Radiation
   5. Submucosal hemorrhage
   6. Ischemia
B. Uncommon: systemic lupus erythematosus

II. Diffuse

A. Common
   1. Ulcerative colitis
   2. Infectious enterocolitis
   3. Edema from low protein and cirrhosis
   4. Systemic lupus erythematosus
B. Uncommon: ischemia.

CT TECHNIQUE FOR RETROPERITONEUM AND PERITONEUM

Adequate bowel and vascular opacification is important so as to delineate normal bowels from pathology.
Oral contrast – 800 ml in 40 min, followed by 400 ml in 20 min
100-150 ml just before the scan
For pelvis – 300-400 ml 1% diatrizoate can be used as enema.

Patterns of Fluid Collection in Abdominal Diseases

Right Subhepatic and Subphrenic Fluid Collections

Isolated right subphrenic and subhepatic fluid collections are very common. Since the major flow of peritoneal fluid proceeds up the right pericolic gutter into the posterior subhepatic space (Morrison's pouch). An isolated abscess in these regions without fluid in any other peritoneal space is often due to a perforated peptic ulcer.

Left Subphrenic fluid

In generalized ascites, fluid does not enter the left subphrenic space unless the volume is quite large. Therefore when the spleen is present, an isolated fluid collection in the left subphrenic space is almost always due to a perforated duodenal or gastric ulcer.

Lesser Sac Fluid

Fluid in the lesser sac generally occurs only when there are large amounts of intraperitoneal fluid or when there is carcinomatosis. However, isolated lesser sac fluid is almost always due to a focal inflammatory process adjacent to the lesser sac; posterior perforating gastric ulcer or pancreatitis.

Interloop Fluid

Fluid insinuating itself between the leaves of the mesentery is quite common with generalized, massive ascites. However, isolated focal interloop fluid occurs after generalized, peritoneal sepsis either caused by bowel perforation and/or surgery. Therefore, it is very common to see multiple isolated fluid collections scattered in the interloop regions in a patient who has had partially treated peritonitis or in a postoperative patient.

Free vs Loculated Peritoneal Fluid

In the supine abdomen, free flowing peritoneal fluid should first collect in the retrovesical space. As the volume of fluid increases, the fluid spills out of the pelvis and up both pericolic gutters. The fluid then collects in the right posterior subhepatic space and then spills anteriorly, laterally, and superiorly in the subphrenic space.

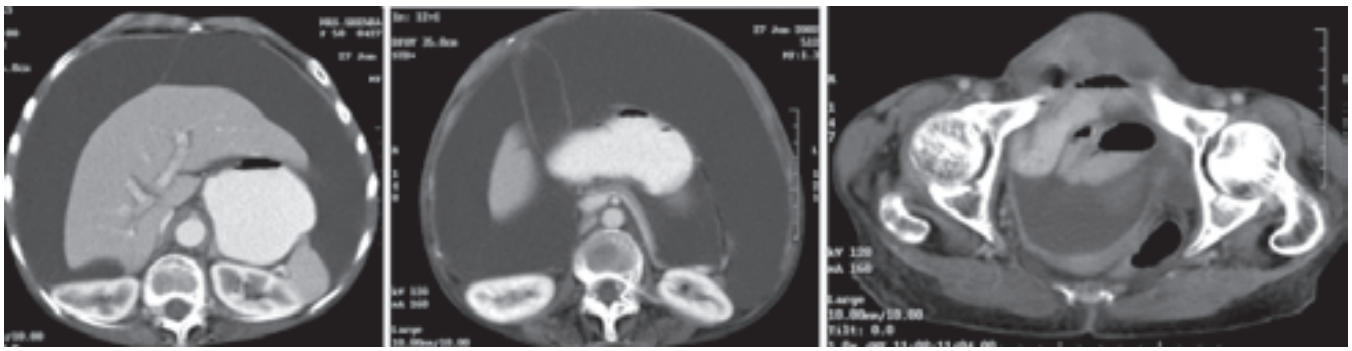

FIGURES 8.115A to C: Axial CECT in a patient with gross ascites showing the typical distribution of free fluid.

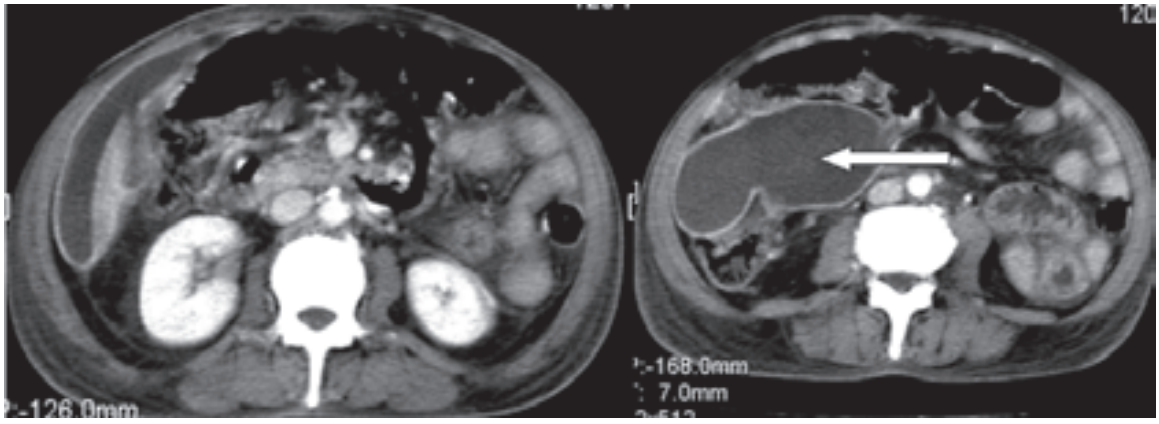

FIGURES 8.116A and B: Axial CECT showing loculated fuid in the right paracolic region (arrow).

Disparity in the volume of fluid in the abdomen by location should alert the radiologist that the fluid is loculated. This is important as infected fluid is almost always loculated but may not appear as a classic round to oval abscess. This is especially true in interloop infected collections and right subphrenic fluid from perforated ulcer disease.

Peritoneal Fluid Density

The density of the peritoneal fluid is non-specific for diagnosis unless it is above fluid attenuation. Increased attenuation to peritoneal fluid is due to the following: hemoperitoneum, extravasated contrast media form the bowel, TB peritonitis as well as delayed enhancement after intravenous contrast injection.

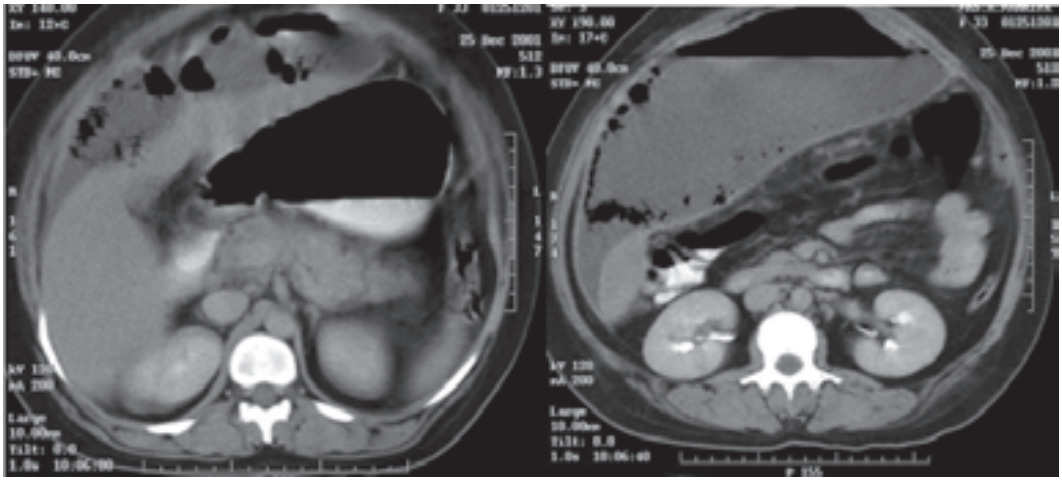

FIGURES 8.117A and B: Axial CECT showing right perihepatic and sub diaphragmatic collection with multiple air pockets and air fluid level suggestive of abscess.

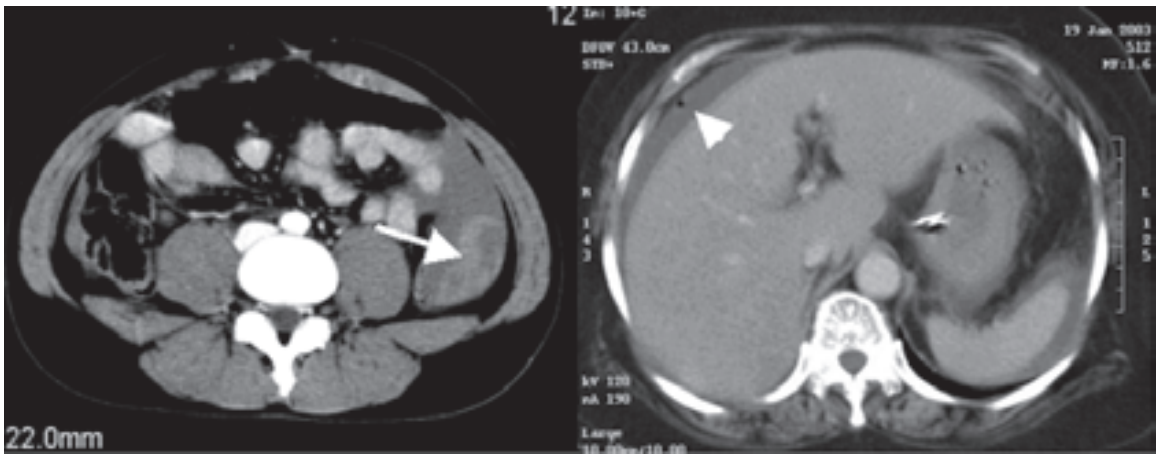

FIGURES 8.118A and B: (A) Axial CECT shows left paracolic high attenuation collection suggestive of hemoperitoneum in a patient with blunt injury. (B) perihepatic fluid with a small air pocket in a patient with duodenal perforation (arrow).

Peritoneal Pathology

Normally the peritoneum is not visualized on CT. When the peritoneal lining is visualized, it is thickened. Even when thickened, it will not be visible without accompanying fluid. Thickening of the peritoneum can occur because of inflammation or tumor.

Inflammatory Process of the Peritoneum

Generalized peritonitis is caused by bowel perforation and in patients with cirrhosis (so-called spontaneous bacterial peritonitis). The most common finding is ascites with enhancing, thickened peritoneal lining. Another cause of generalized peritonitis is from tuberculosis. The findings in this disease process are similar to those of generalized peritonitis: ascites with smoothly thickened, enhancing peritoneum.

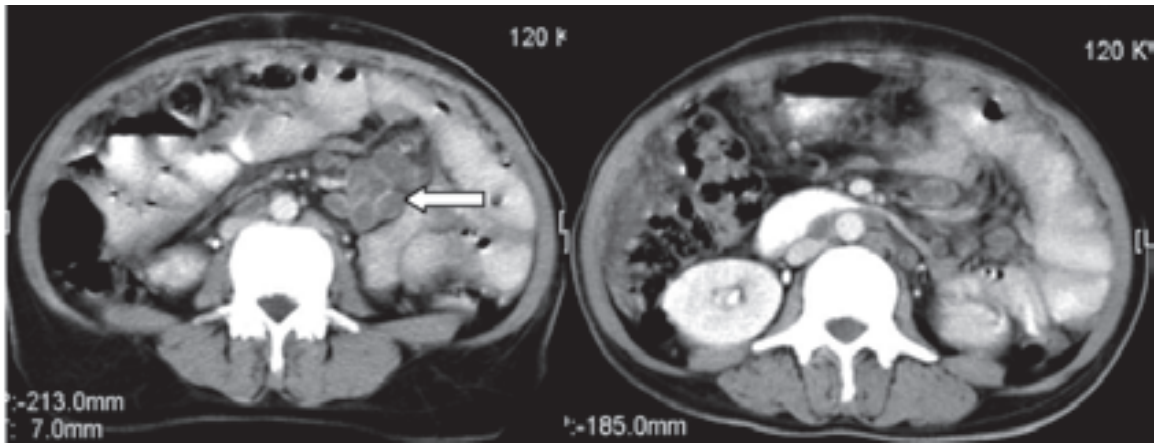

FIGURES 8.119A and B: Axial CECT in a patient with chronic abdominal distention shows multiple hypodense mesenteric lymph nodes with diffuse peritoneal enhancement and thickening. Typical finding of abdominal kochs.

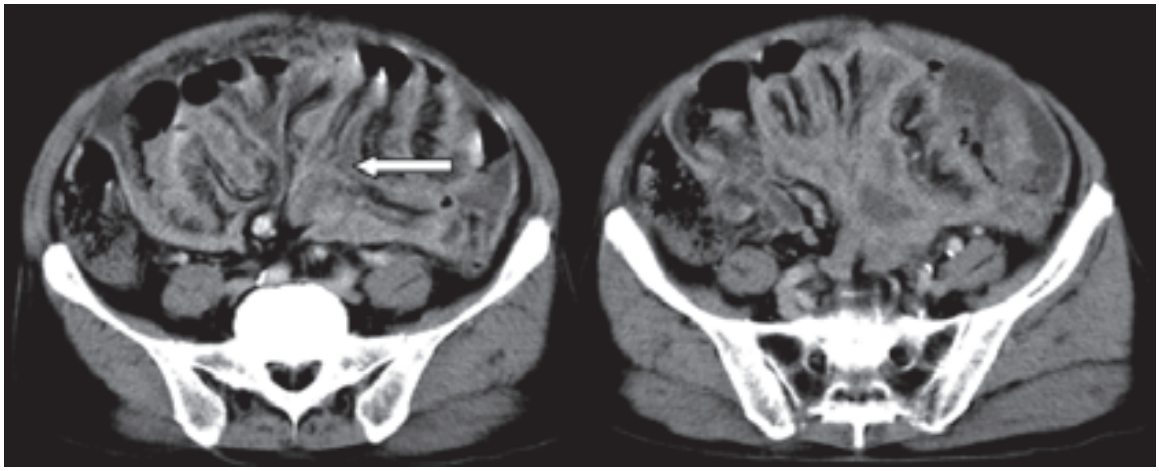

FIGURES 8.120A and B: Axial CECT showing diffuse mesenteric thickening with properitoneal fat enhancement, note typical sliced loaf appearance of peritoneal TB.

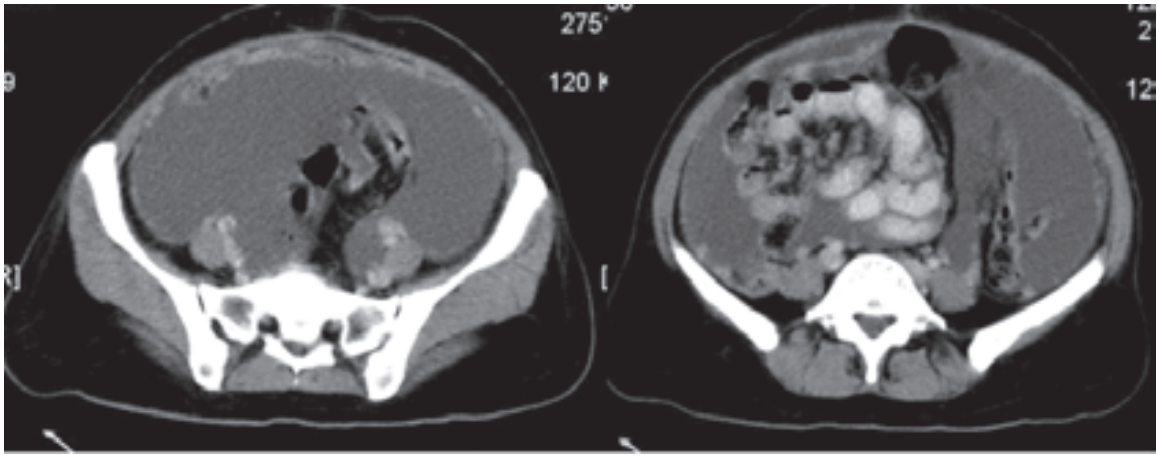

FIGURES 8.121A and B: Axial CECT shows gross peritoneal free fluid with thickening of peritoneum. Case of exudative abdominal kochs.

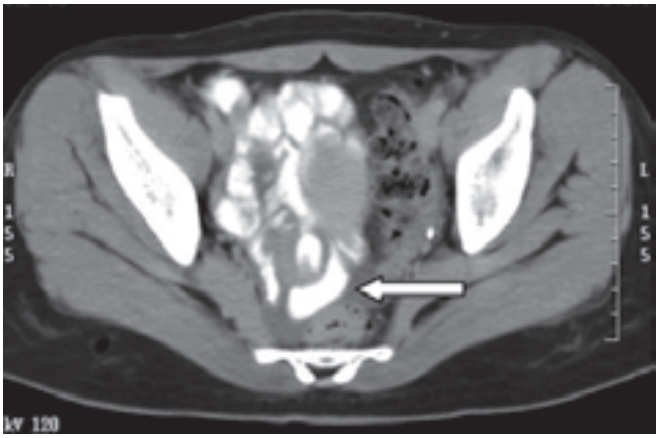

FIGURE 8.122: Axial CECT shows pelvic free fluid (arrow) in a young lady with features of pelvic inflammatory disease.

Neoplastic Peritoneal Diseases

Neoplastic processes of the peritoneum are by far the most common recognizable pathology on CT. Metastatic disease, or peritoneal carcinomatosis is much more common than primary disease. The most frequent primary tumors to involve the peritoneum are from the ovary, colon and stomach.

The most common findings in peritoneal carcinomatosis are:

1. ascites,
2. thickening of the peritoneal lining (often irregular and nodular), and
3. presence of mesenteric pathology.

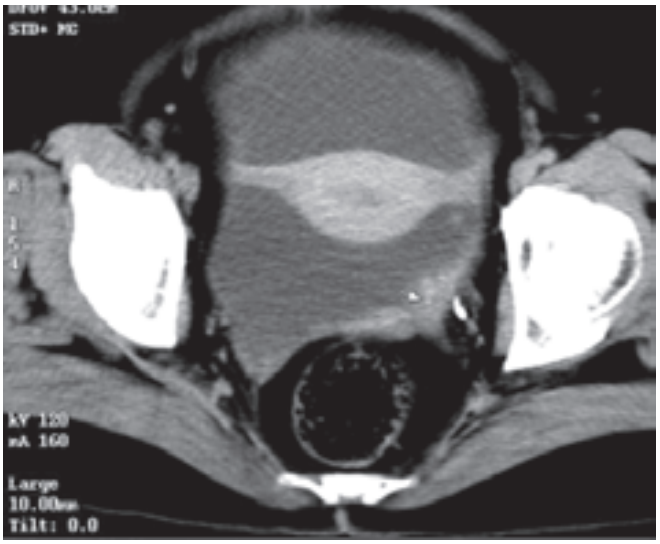

FIGURE 8.123: Axial CECT showing pelvic free fluid with nodular pelvic deposits (arrow) nodular peritoneal thickening is a strong sign of malignancy.

There is considerable overlap in findings between TB and malignancy (TB peritonitis had enhancing, smoothly-thickened parietal peritoneum. In carcinomatosis, more often tumor presents as nodular or irregular thickening of the peritoneum).

Pseudomyxoma peritonei is a specific subtype of carcinomatosis which can be seen most commonly with a mucinous adenocarcinoma of the ovary or colon. The findings are that of multiloculated, multiseptated water attenuation masses scattered throughout the entire abdomen creating localized mass effect especially on the liver and spleen. This produces a scalloping affect on the hepatic and splenic margin. It may also give the appearance of a sub-capsular fluid collection in these organs. These septae may calcify.

Primary tumors of the peritoneum are unusual. Most common tumor is peritoneal mesothelioma, which may be primary or be involved secondarily from a pleural mesothelioma. Virtually all of these patients have had asbestos exposure.

Other primary neoplasms include a cystic mesothelioma which is a rare, benign neoplasm found almost exclusively in females. On CT, these tumors have the appearance of a multi-septated, multi-loculated fluid collections with individual cysts varying in size from a few millimeters to several centimeters. These tumors tend to occupy a large space with little to no mass effect or with less mass effect than one would expect for their size. They are indistinguishable from cystic lymphangiomas.

Mesenteric Disease

Both small and large bowels have mesentery. Within the mesentery there are vessels, lymphatics, nodes, nerves, as well as variable amounts of fat and connective tissue. The predominant tissue is fat and therefore, with the exception of the vessels, the density of the normal mesentery should be that of fat. Any variation in the density of the fat indicates disease.

A misty mesentery is defined by increased density of the mesentery fat, generally between –40 and –60 H.U. This finding can occur in edema, lymphedema, inflammation, hemorrhage/trauma, neoplasms (specifically lymphoma) and mesenteric panniculitis.

Neoplasia can either be localized or generalized and mesenteric panniculitis can be both as well.

The vessels within the mesenteric fat are generally well-defined, linear, to tubular shaped structures with a sharp interface between the vessel and the adjacent fat.

Any variation in the appearance of these vessels should indicate disease. Any irregular thickening in these structures should indicate tumor although at times, it can be difficult to distinguish edema from tumor infiltration.

Inflammatory Disease of the Mesentery

Mesenteric panniculitis: This is an uncommon disease occurring in the 6th and 7th decade of life. The presentation is non-specific and includes abdominal pain, fever, nausea and vomiting and weight loss. A palpable, poorly defined abdominal mass can be detected. The cause is not known. On CT, the mesentery is involved by a well-defined, heterogeneous area of increased density. The appearance is one of soft tissue infiltrate creating some mass effect. Pathologically, these are firm or hard masses which contain normal fat as well as areas of necrosis. The differential diagnosis includes a carcinoid tumor, metastatic disease, lymphoma, liposarcoma, teratoma as well as fat necrosis.

Neoplastic Diseases of the Mesentery

The most common tumors to involve the mesentery are secondary. These include metastatic carcinoid tumors, as well as lymphoma.

Primary neoplasms of the mesentery are uncommon. These include leiomyomas, lipomas, neurofibromas and their malignant counterparts as well as lymphangiomas and teratomas. In addition, mesotheliomas can involve the

mesentery as it does the peritoneum. Solid tumors are less common than cystic ones and in general the CT findings are non-specific.

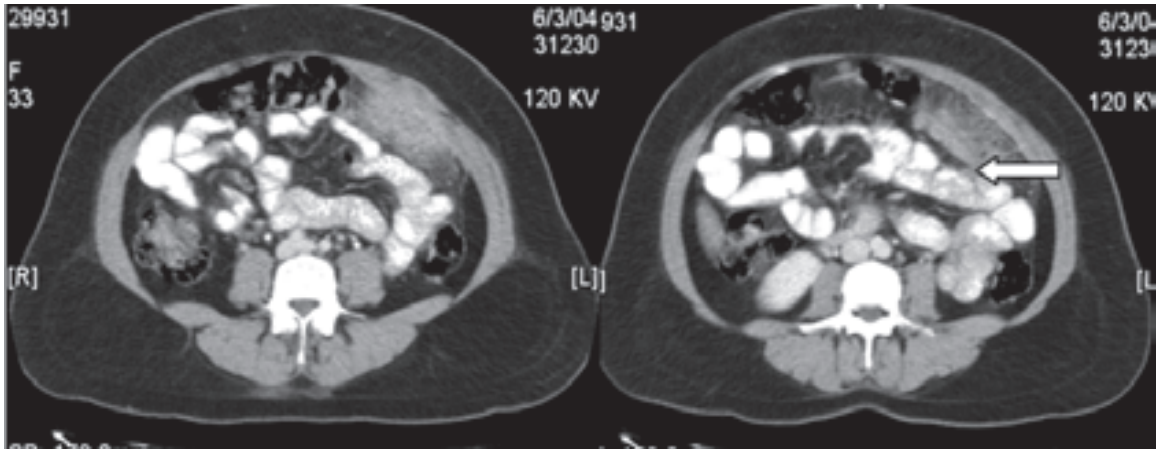

FIGURES 8.124A and B: Axial CECT in a patient with persisten pain abdomen showing infiltration with enhancement of the left paracolic and properitoneal fat planes (arrow).

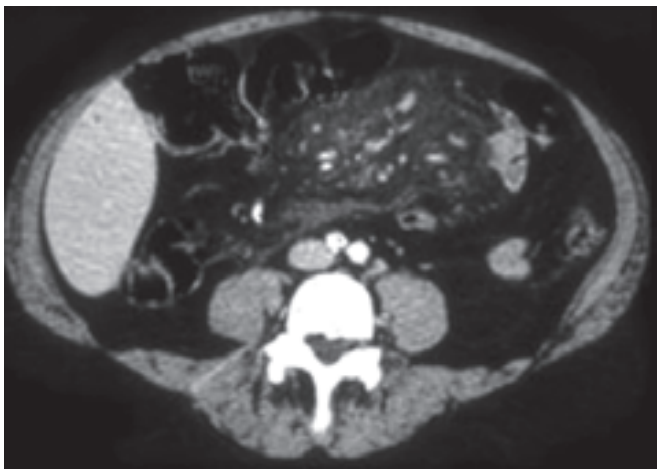

FIGURE 8.125: Axial CECT showing nodular soft tissue stranding of the mesentery – typical feature of panniculitis.

Metastatic disease involving the mesentery has distinct patterns. When omentum is involved, there is a cake-like thickening of the omentum by a linear to plaque-like soft tissue mass. Within the mesentery itself, the vessels become irregularly thickened. Small nodules or irregularly infiltrated fat may be present. Mesenteric lymphadenopathy or multiple discrete nodules may also be present.

Peritoneal Metastases

Metastases spread to the peritoneum in four ways:

- Direct spread along peritoneal ligaments, mesenteries and omenta to non-contiguous organs.
- Intraperitoneal seeding via ascitic fluid.
- Lymphatic extension.
- Embolic hematogenous spread.

Spectrum of Peritoneal Carcinomatosis

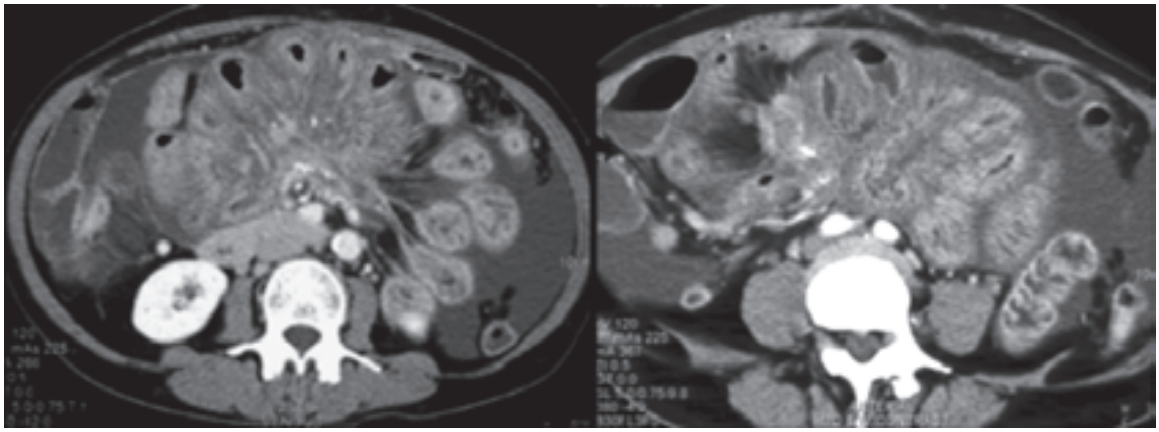

FIGURES 8.126A and B: Axial CECT reveals diffuse peritoneal stranding in a patient with carcinoma stomach with enhancement causing thickening of small bowel mesentery with thickened bowel loops – carcinomatous peritonitis.

Direct spread

Primary tumors may invade non-contiguous organs by direct invasion and spread along the peritoneal reflections.

These include:

Eight ligaments: The right and left coronary, falciform, hepatoduodenal, duodenocolic, gastrosplenic, splenorenal and phrenicocolic ligaments.

Four mesenteries: The small bowel mesentery, transverse mesocolon, sigmoid mesocolon and mesoappendix.

Two omenta: The lesser and greater omentum.

Intraperitoneal seeding

Intraperitoneal fluid is in constant circulation throughout the abdomen under the influence of gravity and negative intra-abdominal pressure. This flow allows transcoelomic dissemination of malignant cells. Their deposition, fixation and growth are favored in particular sites of relative stasis of ascitic fluid. These include:

- The pelvis, especially within the pouch of Douglas.
- The right iliac fossa at the inferior extent of the small bowel mesentery.
- The superior aspect of the sigmoid mesocolon.
- The right paracolic gutter.
- The right subhepatic and subphrenic spaces.

Non-Hodgkin's, mesenteric lymphomas have several manifestations. Mesenteric adenopathy, an isolated mesenteric mass, mass-like increased mesenteric root density (misty mesentery) with or without adenopathy (similarly to mesenteric panniculitis, confluent mesenteric retroperitoneal mass.

Carcinoids are endocrine tumors arising from the gastrointestinal tract which often secondarily involve the mesentery especially where they are malignant. These tumors incite an intense desmoplastic or fibrotic reaction.

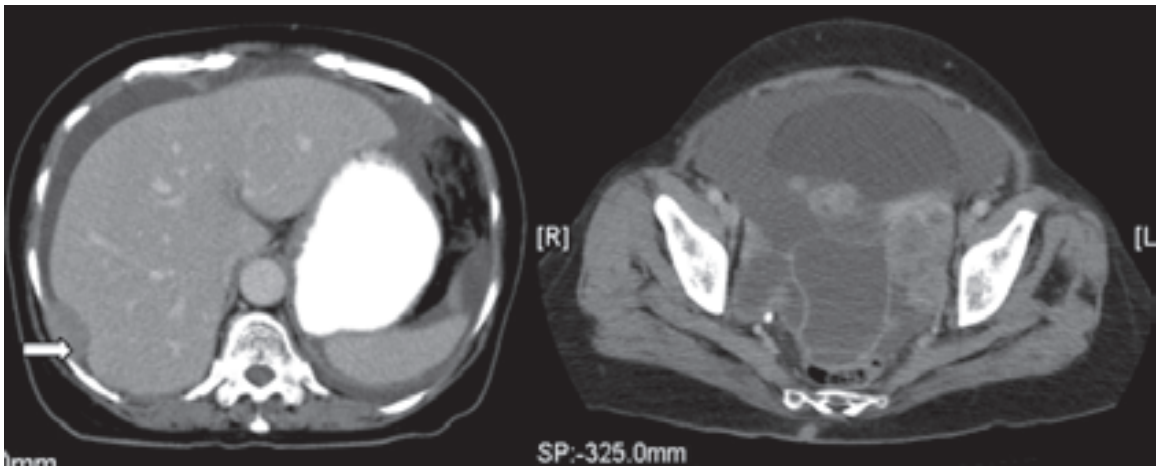

FIGURES 8.127A and B: Axial CECT in a patient with ovarian malignancy shows nodular pelvic deposits (arrow in B), peritoneal implants seen indenting the liver (arrow in A).

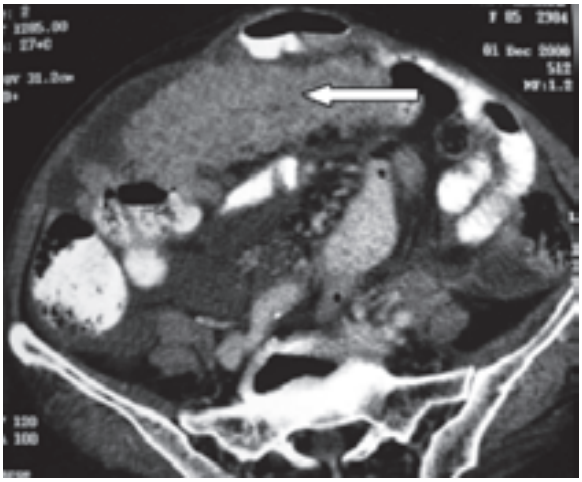

FIGURE 8.128: Axial CECT shows nodular peritoneal deposits in a patient with Ca cervix.

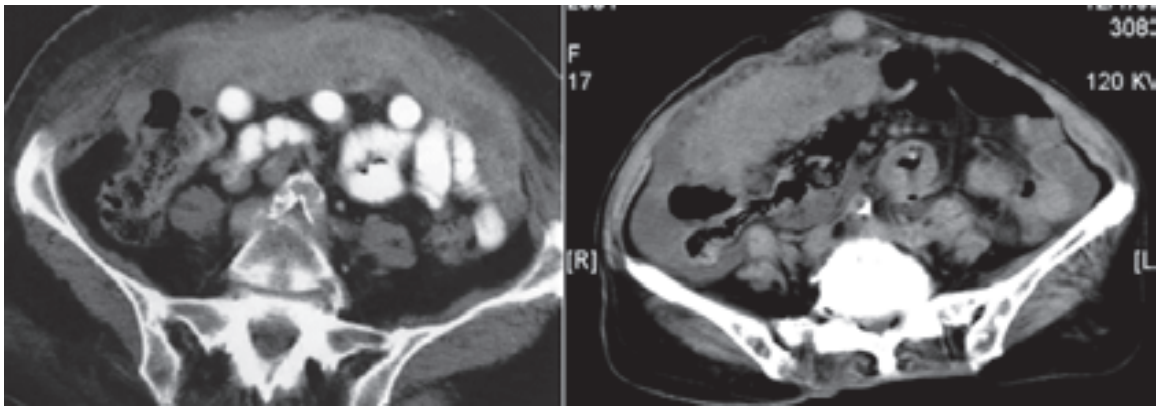

FIGURES 8.129A and B: Axial CECT showing diffuse enhancing peritoneal thickening with nodularity.

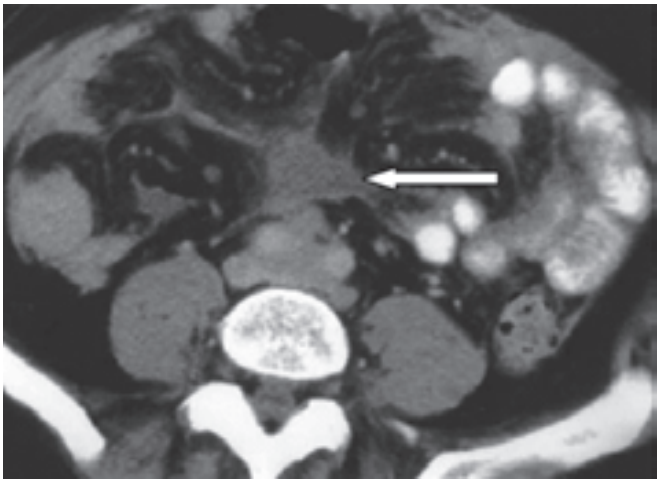

FIGURE 8.130: Axial CECT showing a stellate hypodense lesion in the mesentery with surrounding stranding.

Mesenteric cysts—Mesenteric and omental cysts are benign lesions that appear most commonly as asymptomatic abdominal masses; infrequently, however, they may present secondary to torsion, rupture, infection, or bleeding. Mesenteric and omental cysts are not a specific entity: rather, they are a group of different pathologic processes that share a similar location and radiographic and gross appearance. This category includes lymphangiomas, nonpancreatic pseudocysts, enteric duplication cysts, enteric cysts, and mesothelial cysts. Mesenteric and omental cysts are composed of chylous or serous elements, possibly complicated by hemorrhage. They arise most frequently from the small bowel mesentery but also may be located in the mesocolon and omentum. On CT scans, mesenteric and omental cysts appear as well-demarcated, fluid-attenuation masses that may have thin internal septations. Depending on their location and size, mesenteric cysts may be difficult to distinguish from cystic ovarian lesions. Similarly, large mesenteric cysts may be confused with ascites, although mesenteric cysts usually displace bowel loops posteriorly rather than centrally.

Mesothelioma—Peritoneal mesothelioma arises from the serosal lining of the peritoneum. Mesothelioma may involve the pleura, pericardium, or peritoneum, and 30 to 40% have peritoneal manifestations. Malignant peritoneal—mesothelioma is associated with asbestos exposure and is most common in middle-aged men. Radiographic findings include thickening and nodularity of the peritoneum, mesentery, and omentum, as well as ascites. This progresses to nodular masses, which eventually become confluent. The tumor spreads across serosal surfaces throughout the intra-abdominal cavity, and direct organ invasion may occur. Peritoneal mesothelioma rarely calcifies, and the omental "cake-like" masses may mimic peritoneal carcinomatosis.

Cystic mesothelioma is a rare, benign neoplasm that is a related entity; however, it is separate from the more common malignant peritoneal mesothelioma. Cystic mesothelioma also arises from the mesothelial cells lining the peritoneal cavity; although it does not metastasize, local recurrence may occur after resection. Unlike malignant peritoneal mesothelioma, cystic mesothelioma is not related to asbestos exposure and occurs most frequently in women. CT evaluation shows a multiloculated cystic mass without calcification that often arises from the pelvis.

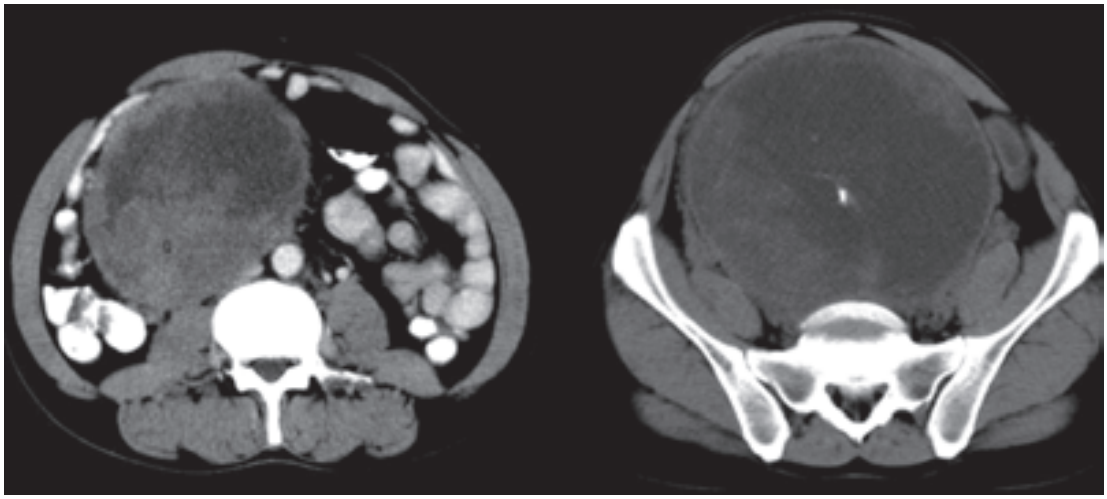

FIGURES 8.131A and B: Axial CECT shows a well marginated mesenteric cyst with internal nodularity and a central calcific speck.

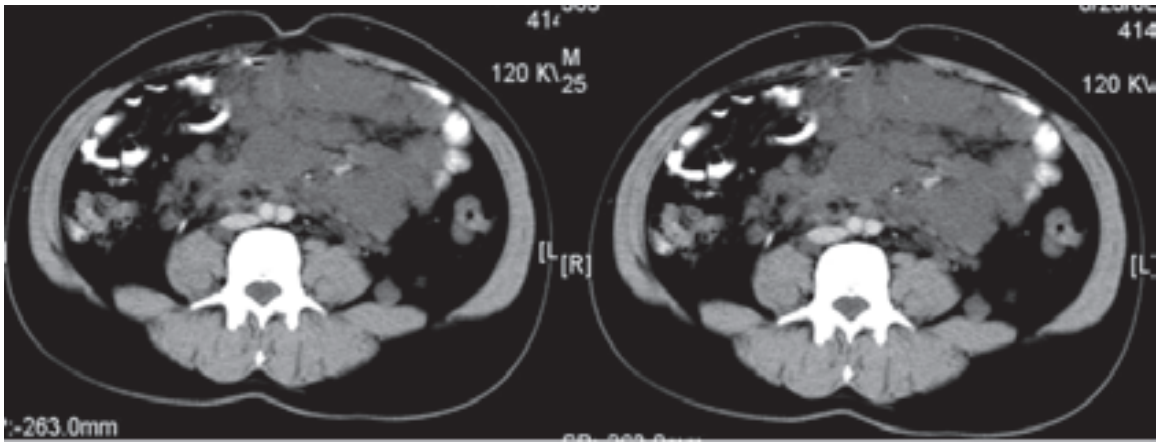

FIGURES 8.132A and B: Axial CECT showing nodular confluent peritoneal thickening displacing the bowels, differential diagnosis for this pattern of involvement would include peritoneal mesotheliomas.

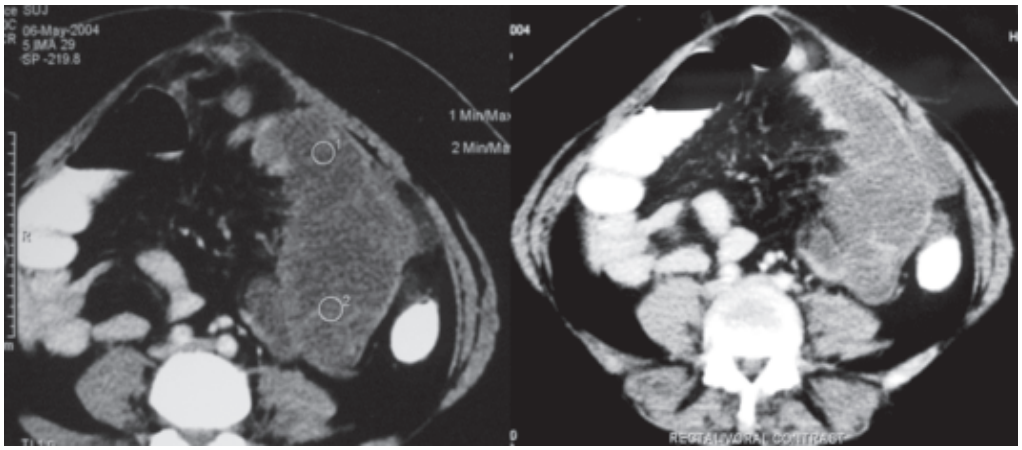

FIGURES 8.133A and B: Axial CECT shows a hypodense septated peritoneal lesion displacing the bowels – case of lymphangioma.

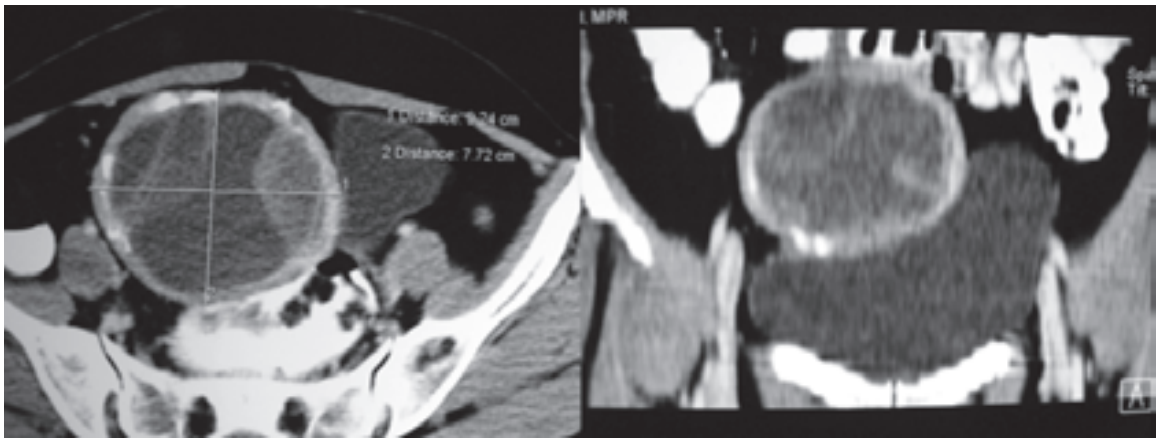

FIGURES 8.134A and B: Axial CECT shows a well marginated lesion showing a layered appearance in the pelvis indenting the bladder dome (HPE - gossibyoma) patient had previous history of surgery for hysterectomy.

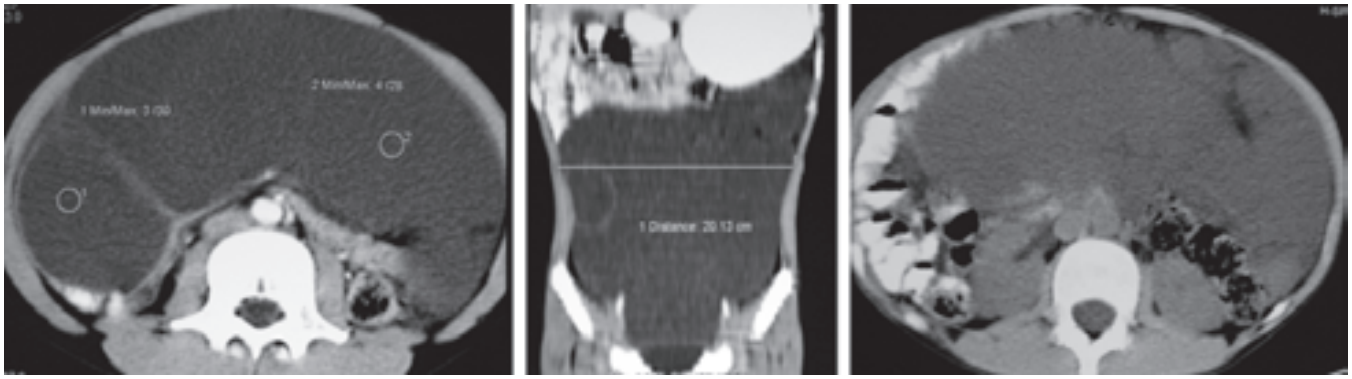

FIGURES 8.135A to C: Axial CECT in a 7-year-old boy with progressive abdominal distention reveals hypodense septated peritoneal mass involving the entire abdomen, displacing the bowel loops (HPE - lymphangioma).

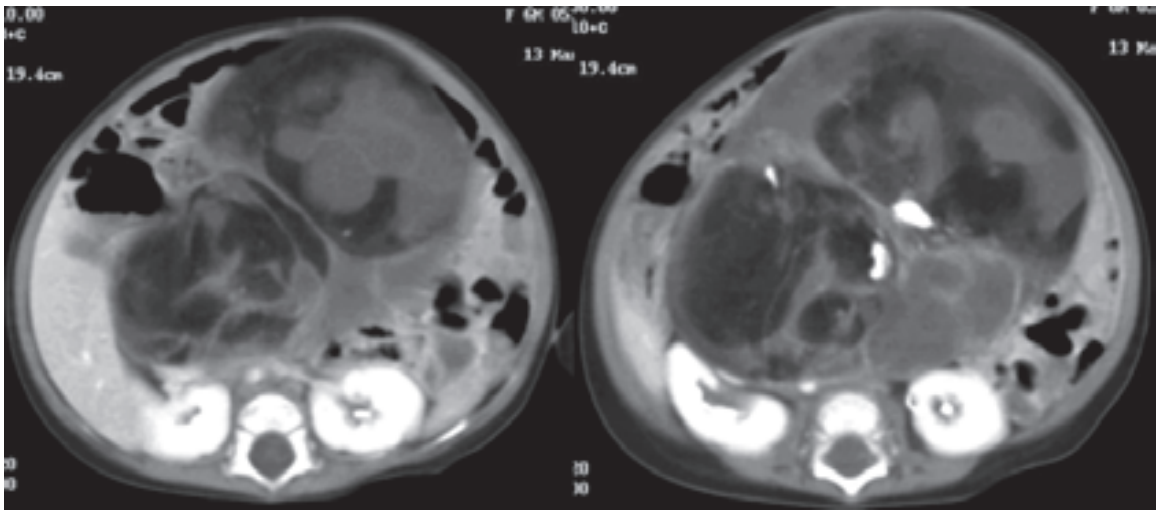

FIGURES 8.136A and B: Axial CECT showing a large mesenteric mass with areas of fat and calcific attenuation (HPE – teratoma).

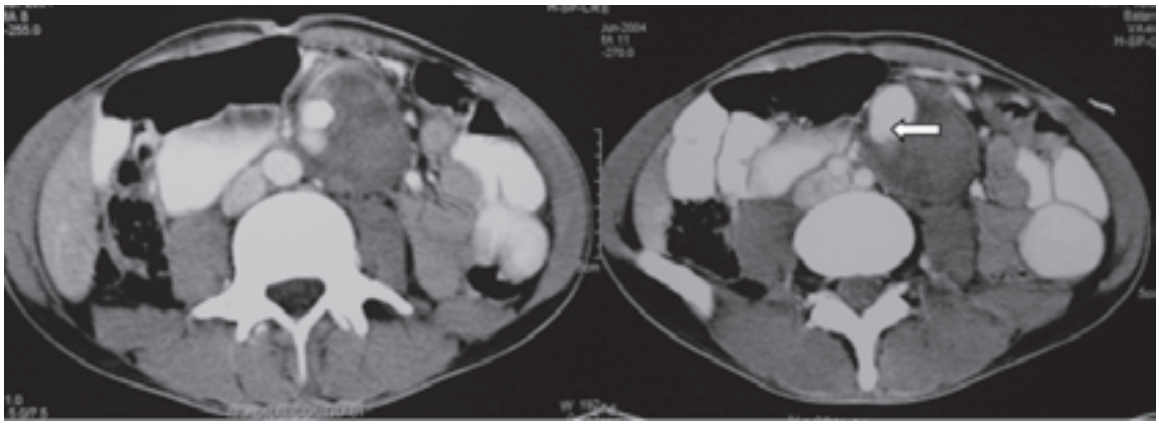

FIGURES 8.137A and B: Axial CECT in a 46-year-old male with acute lower abdominal pain reveals a well marginated lesion showing a eccentric area of intense arterial enhancement – suggestive of pseudoaneurysm arising from the branch of SMA.

Sclerosing Peritonitis

Sclerosing peritonitis (SP) is an uncommon but important complication of ambulatory peritoneal dialysis. Histologically, the small bowel is encased in a sheet of fibrous tissue comprised of fibroblastic spindle cells, at times accompanied by chronic inflammatory cells. SP was first described in 1980 in patients who received CAPD for a period of 3 months to 4 years. The prevalence increases with the duration of CAPD.

The exact etiology of SP is unknown. Antiseptics (chlorhexidene in alcohol), dextrose degradation products from heat sterilization, particulate matter in the dialysate, beta-blockers (especially practolol), bacterial peritonitis, plasticizers, and acetate-buffered dialysates have all been implicated as etiological agents. It is likely that the etiology is multifactorial.

Clinically, the onset of SP is often heralded by nonspecific symptoms such as abdominal pain, anorexia, weight loss, and, eventually, partial or complete small-bowel obstruction. Loss of ultrafiltration is common, as is bloody dialysis effluent. Mortality rates are high (50 to 80%) and are usually related to bowel obstruction and complications from surgery.

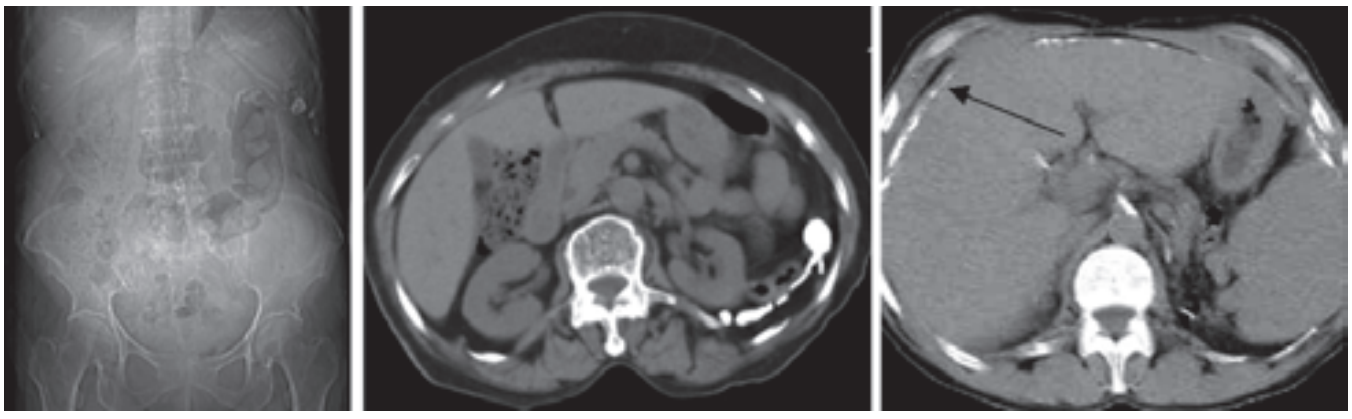

FIGURES 8.138A to C: (A and B) Digital scanogram and axial plane CT shows dense calcification of the left lateroconal facial plane in a patient with healed tuberculous peritonitis, (C) Axial plain CT in a patient who was on long-term CAPD shows uniform ring of calcification of peritoneum (arrow).

Abdominal radiographs are frequently unremarkable until late in the disease process, when curvilinear peritoneal calcification can be detected. Conventional radiographs of the abdomen may reveal centrally located, dilated loops of bowel with wall thickening or edema and "thumb printing."

Computed tomography of the abdomen in patients with SP has shown peritoneal enhancement, thickening, and calcification as well as loculated intraperitoneal fluid collections. Also seen are adherent bowel loops and dilated bowel containing air-fluid levels, both of which suggest disordered motility. In a review of the CT findings in 10 patients with SP, Stafford-Johnson et al found peritoneal thickening in all patients (100%), as well as loculated fluid collections (90%), calcification (70%), small-bowel tethering (60%), and peritoneal enhancement (50%).

Pneumoperitoneum

Background

The term pneumoperitoneum refers to air within the peritoneal cavity. The most common cause is a perforated abdominal viscus, generally a perforated ulcer, although any part of the bowel may perforate from a benign ulcer, tumor, or trauma. The exception is a perforated appendix, which seldom causes a pneumoperitoneum.

The presence of a pneumoperitoneum does not, however, always imply a perforation because a number of other (mostly nonsurgical) conditions are associated with pneumoperitoneum. A pneumoperitoneum is common after abdominal surgery and usually resolves 3-6 days after surgery, although it may persist for as long as 24 days after surgery.

The most common cause of a spontaneous pneumoperitoneum is the introduction of air through the female genital tract.

Pathophysiology

Causes of pneumoperitoneum

Air within the peritoneal cavity has several causes. Some are associated with peritonitis that needs urgent abdominal surgery, while others may be incidental findings for which only observation is required.

The causes of a pneumoperitoneum are as follows:

- Ruptured hollow viscus—Perforated peptic ulcer, ruptured or perforated Meckel sigmoid and jejunal diverticula, necrotizing enterocolitis, toxic megacolon, inflammatory bowel disease, and idiopathic gastric perforation in premature infants.
- Infection of the peritoneal cavity with gas-forming organisms and/or rupture of an adjacent abscess.
- Iatrogenic factors—Recent abdominal surgery, abdominal trauma, leaking surgical anastomosis, misplaced thoracentesis or pleural drainage tube, endoscopic perforation, injury due to the tip of an enema catheter, percutaneous needle biopsy, peritoneal catheter placement, peritoneal dialysis, paracentesis, diagnostic or therapeutic pneumoperitoneum, instrumental perforation of uterus or vagina, culdocentesis, ruptured urinary bladder, Rubin test for tubal patency, pelvic examination, intercourse, orogenital insufflation, douching, knee-to-chest movements in females (as during water skiing, horseback riding, and squatting), perforating foreign body, and application of compressed air directed towards the anus and overdistention of the stomach with gas during gastroscopy.
- Bowel obstruction due to a neoplasm, imperforate anus, Hirschsprung disease, or meconium ileus (when gas may permeate through the bowel wall).
- Pneumatosis intestinalis
- Chemoembolization of liver tumors.
- Extension from the chest: pneumomediastinum and bronchopleural fistula.

- Perforated peptic ulcer and Meckel diverticulum - Most common causes in older children.
- Necrotizing enterocolitis and spontaneous perforation of the stomach - First and second most common causes of organ perforation in the newborn and infants, respectively.

Anatomic Locations of Abdominal Gas Collections

Abnormal abdominal gas collections are subdivided by the anatomic location, which is often the key to the differential diagnosis.

Extraluminal gas: Extraluminal gas may be involved in pneumoperitoneum or gas within an abscess or fistulous tract. Gas within a pelvic abscess usually indicates that the abscess is of GI origin. Gas within an abscess of pelvic inflammatory disease (PID) is unusual. Gas within the paracolic gutter is usually associated with GI perforation. Diverticulitis may be produce extraluminal gas trapped within the adjacent mesentery.

Intraluminal gas: Intraluminal gas may be normal or abnormal. The gas may be intratumoral (within a neoplasm with infection or with bowel communication), intramural, within a paralyzed loop of bowel, within an obstructed Meckel diverticulum (secondary infection), or within the biliary tree.

Intraparenchymal gas: Within the portal vein, intraparenchymal gas may sometimes be seen as gas microbubbles moving through the liver as linear collections of hyperlucent branching gas at the periphery of the liver. Gas may be seen in a liver abscess. In most other organs, intraparenchymal gas usually indicates an abscess.

Intratumoral gas: Intratumoral gas typically occurs in a gastric leiomyoma or leiomyosarcoma, in which the gas may be seen extending from the lumen of the stomach into the tumor. Intratumoral gas may also be seen in hepatic tumors after chemoembolization, after which differentiation of the gas from an abscess may be difficult on images alone.

Intramural gas: Intramural gas may be related to ischemia. Adjacent bowel wall thickening is often present. Crohn disease and cytomegaloviral (CMV) infection are less common causes of intramural bowel gas.

Pneumatosis coli is often better shown with CT. Acute emphysematous cholecystitis, which often occurs in the diabetics and the elderly shows evidence of intramural gas.

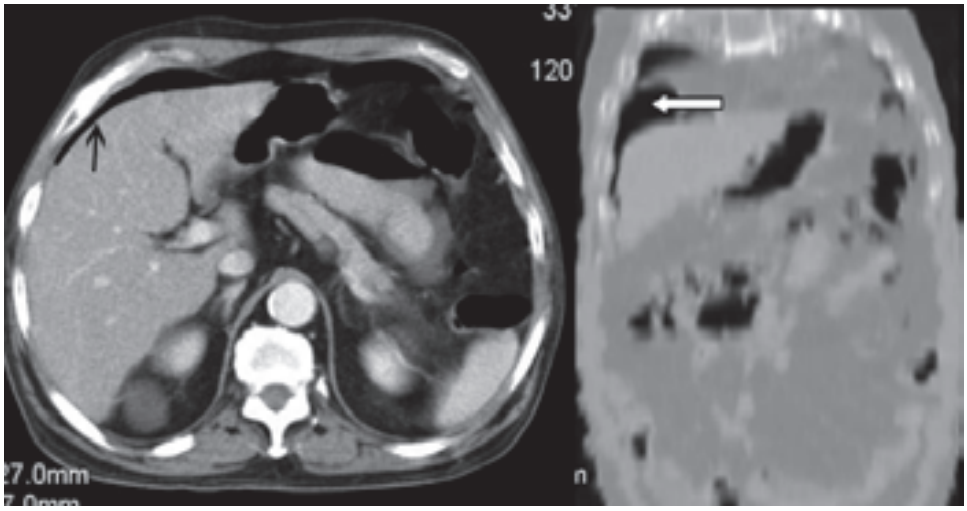

FIGURES 8.139A and B: Axial CECT showing peritoneal free air in the right subdiaphragmatic region. Figure B is coronal reformation of the same.

Perforation: CT is by far more sensitive than plain film radiography for the detection of a small pneumoperitoneum and unsuspected gastroduodenal perforation. Perforations are usually the result of an injury (seat belt, steering wheel injury or iatrogenic) rather than an intrinsic lesion (postbulbar ulcer, Crohn's disease, diverticulitis).

Scans in ***gastroduodenal ulcer disease*** may reveal local wall thickening that enhances with intravenous contrast. Perforation of the stomach or duodenal bulb cause extraluminal gas in the peritoneal cavity while perforation of the duodenal loop may lead to air bubbles in the retroperitoneum, e.g. anterior pararenal space. Small pockets of extraluminal air may be trapped beneath the mesenteric leaves or the greater omentum (lung window settings). Larger collections of air are usually localized anterior to the liver in the upper abdomen if the patient is examined in supine position.

Perforations may incite inflammatory reactions in adjacent organs (pancreas, colon, liver). Fluid extravasation (containing hydrochloric acid and digestive enzymes) from gastroduodenal perforations into the peritoneal cavity gives rise to peritonitis and abscess formation. Postinflammatory strictures may be responsible for stenotic narrowing.

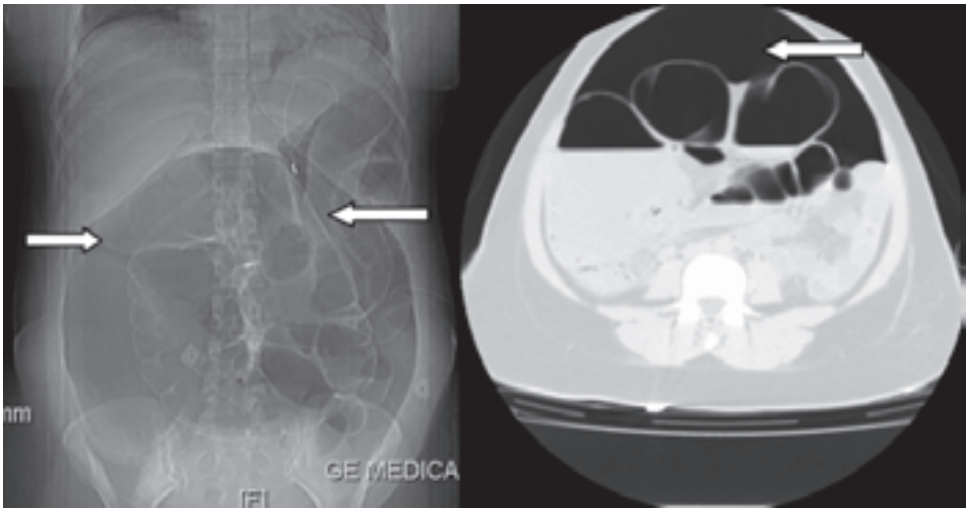

FIGURES 8.140A and B: Scanogram showing the classical football sign of pneumoperitoneum (arrows) axial CECT showing gross peritoneal free air (arrow in B). Linear sigmoid colon rent was found at surgery.

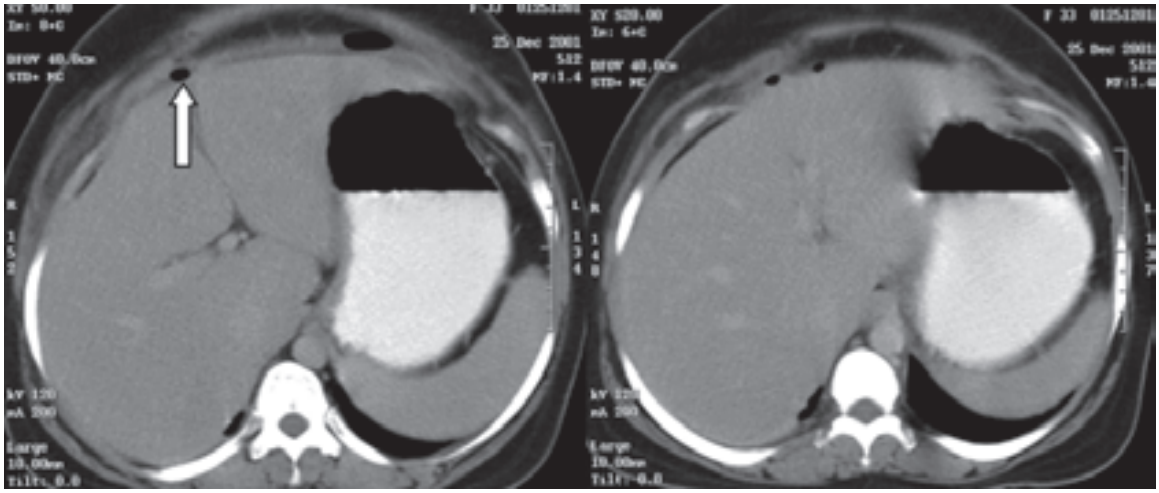

FIGURES 8.141A and B: Axial CECT in a patient with features of bowel perforation shows a small speck of air in the perihepatic and right subdiaphragmatic space (arrow).

Root of the Small-Bowel Mesentery

The root of the small-bowel mesentery (SBM) is located in the central portion of the abdomen, connecting intraperitoneal structures, and is contiguous to other peritoneal ligaments and mesocolons. It is important to know the anatomic relationships in this area as they are seen to be involved in several pathologic conditions occurring in the SBM itself, and diseases from other organs that spread via connections to the mesenteric root.

The SBM is a fat-laden peritoneal reflection that fixes the jejunum and ileum to the posterior abdominal wall. The attached parietal border, which is approximately 15 cm long, runs obliquely down from the duodenojejunal flexure to the ileocecal region. Its root is a bare area continuous with the anterior pararenal space of the retroperitoneum. The root of the SBM contains two major vessels, the superior mesenteric artery (SMA) and superior mesenteric vein (SMV).

There are many important structures and organs in the vicinity of the root of the SBM. The root of the SBM is contiguous superiorly to the hepatoduodenal ligament around the SMV and portal vein, contiguous anteriorly to the transverse mesocolon, and contiguous posterolaterally to the ascending and descending mesocolons (anterior pararenal space). The gastrocolic trunk is a landmark of the junction between the transverse mesocolon and the root of the SBM. The inferior mesenteric vein, which is a landmark of the descending mesocolon, joins the SMV or splenic vein on the left side of the root of the SBM.

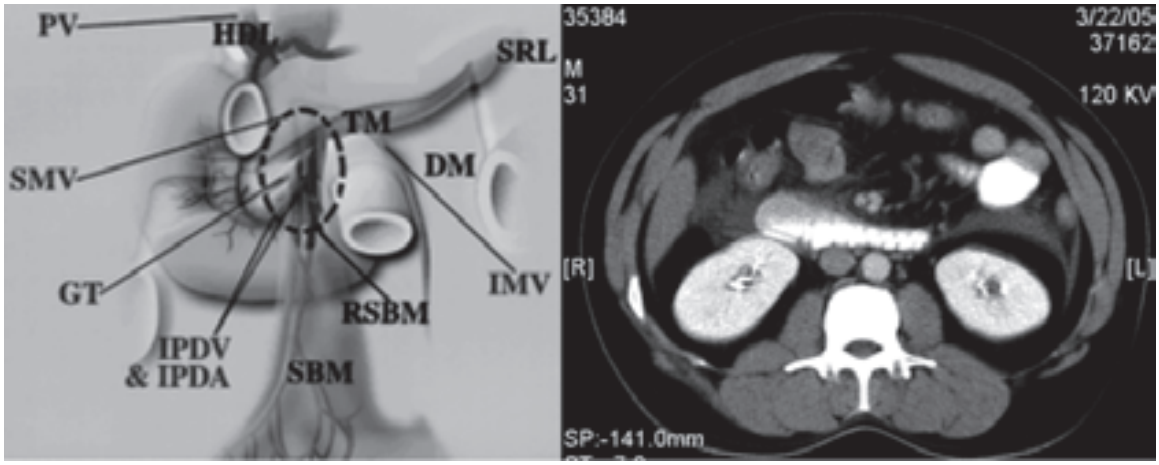

FIGURES 8.142A and B: The root of the SBM (area within dashed circle), hepatoduodenal ligament (HDL) along the SMV, anteriorly to the transverse mesocolon (TM), and posterolaterally to the ascending mesocolon and descending mesocolon (DM). The gastrocolic trunk (GT) is a landmark of the junction between the transverse mesocolon and the root of the SBM. The inferior mesenteric vein (IMV) is a landmark of the descending mesocolon and joins the SMV or splenic vein on the left side of the root of the SBM. IPDA = inferior pancreaticoduodenal artery, IPDV = inferior pancreaticoduodenal vein, PV = portal vein, SRL = splenorenal ligament.

Characterization of the Retroperitoneal Space

The first step is to decide whether the tumor is located within the retroperitoneal space. It is useful to observe the displacement of normal anatomic structures. Anterior displacement of retroperitoneal organs (e.g., kidneys, adrenal glands, ureters, ascending and descending colon, pancreas, portions of the duodenum) strongly suggests that the tumor arises in the retroperitoneum.

1. **Psoas muscle space**—Most pathologies in this space come from the neighboring structures. Pott's spine due mycobacterial TB is a common pathology to involve this space to cause abscess. Pathologies from kidneys, ureter, aortic aneurysm and trauma can involve this compartment.

   Intrinsic disease of psoas space include tumors of neural origin such as neurofibroma, and tumors of the lymphatic system such as lymphoma.

2. **Posterior pararenal space**—It has a long cephalocaudal dimension, contains no organs, has few intercoastal and lumbar nerves and fat. This space is rarely involved in pathologies from sigmoid colon and pancreas.
3. **Perirenal space**—bound by anterior and posterior renal fascia, this space contains kidney and adrenal. It is pierced medially by renal arteries and veins and ureter exits inferiorly. Pathologies are usually of renal origin contain blood, pus and urine.
4. **Anterior pararenal space**—It is a complex space made of two major components, the pancreaticoduodenal and the pericolonic space. These two compartments communicate at the root of the transverse mesentery and aggressive process in either can transgress compartmental lines.

   Pathologies in PD space include pancreatitis, penetrating duodenal ulcer, pericolonic space pathologies usually caused due colonic disease.
5. **Great vessel space**—Fat containing area surrounding the aorta and IVC usually behaves as a separate space, continues with posterior mediastinum other contents of this space include abdominal portion of ureters, paraaortic and paracaval nodes.

Identification of the Organ of Origin

Beak sign—When a mass deforms the edge of an adjacent organ into a "beak" shape, it is likely that the mass arises from that organ (beak sign).

FIGURES 8.143A and B: Positive beak sign in which *Tumor A* arises from *Organ B*, the negative beak sign in which *Tumor A* does not arise from *Organ B*.

Phantom (Invisible) organ sign— When a large mass arises from a small organ, the organ sometimes becomes undetectable. This is known as the phantom organ sign. However, false-positive findings do exist, as in cases of huge retroperitoneal sarcomas that involve other small organs such as the adrenal gland.

Embedded organ sign—When a tumor compresses an adjacent organ (e.g. gastrointestinal tract, inferior vena cava) that is not the organ of origin, the organ is deformed into a crescent shape. In contrast, when part of an organ appears to be embedded in the tumor, the tumor is in close contact with the organ and the contact surface is typically sclerotic with desmoplastic reaction. When the embedded organ sign is present, it is likely that the tumor originates from the involved organ.

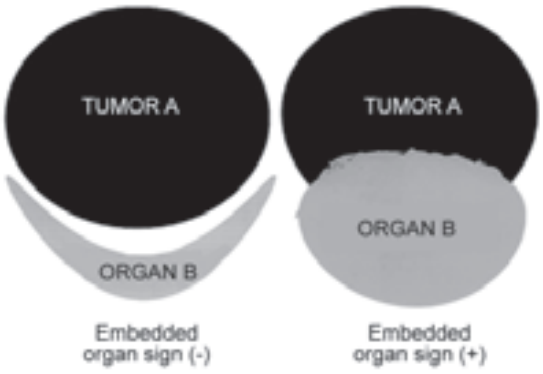

FIGURES 8.144A and B: Schematic describing the embedded organ sign.

Primary retroperitoneal neoplasms are a diverse group of benign and malignant tumors that arise within the retroperitoneum but outside the major organs. Diagnosis of these tumors is often challenging for radiologists and consists of several steps, including determining tumor location (characterizing the retroperitoneal space and identifying the organ of origin) and recognizing specific features of various retroperitoneal tumors (evaluating patterns of spread, tumor components, and vascularity.

Lesions that Extend between Normal Structures

Some tumors grow and extend into spaces between preexisting structures and surround vessels without compressing their lumina. Lymphangiomas and ganglioneuromas are examples of such tumors.

Lymphangiomas represent about 1% of all retroperitoneal neoplasms. Most cases are detected in the first 2 years of life on the basis of symptoms like abdominal distention or pain; however, they can manifest in older patients as a huge, asymptomatic mass. At imaging, they appear as fluid-filled, unilocular or multilocular cystic masses with minimal contrast enhancement.

Another entity with this growth pattern is lymphoma. This neoplasm tends to surround adjacent vessels, manifesting with the "CT angiogram sign" or "floating aorta sign".

Lesions that extend along Normal Structures

Tumors of the sympathetic ganglia (i.e. paragangliomas, ganglioneuromas) tend to extend along the sympathetic chain and have an elongated shape.

Characteristic Tumor Components

Some tumor contents can be clearly demonstrated at CT and MR imaging and provide strong clues that help narrow the differential diagnosis.

Fat

The presence of fat is easily recognized owing to its low attenuation at CT or its high signal intensity at T1-weighted MR imaging with loss of signal intensity on fat-suppressed images. The presence (or absence) of fat limits the differential diagnosis.

A mass that is homogeneous and well defined and consists almost entirely of fat represents lipoma teratomas are also characterized by the presence of fat and mature teratomas can be characterized by the presence of fluid attenuation or signal intensity, fat-fluid levels, and calcifications.

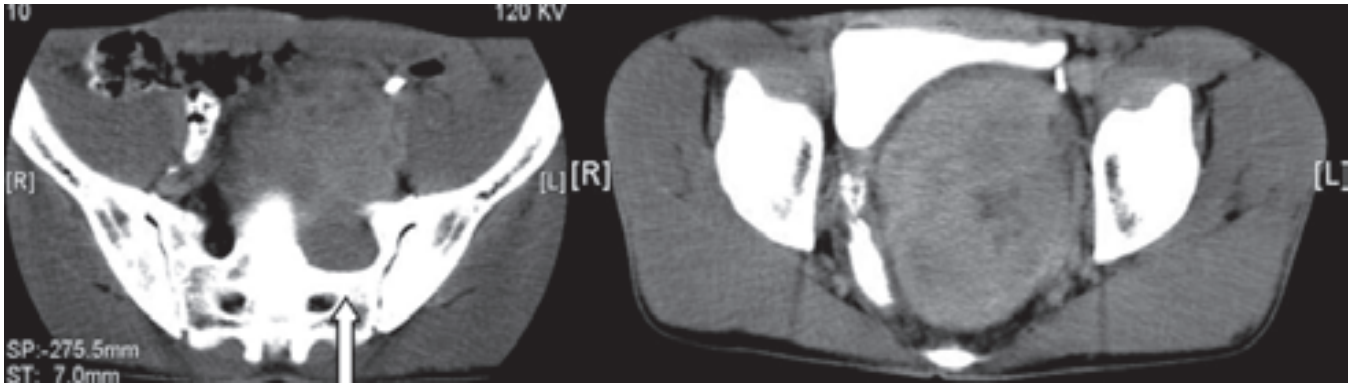

FIGURES 8.145A and B: Axial CECT showing a presacral mass displacing the rectum and bladder base, note the widened left sacral foramina (arrow). Imaging features of suggestive of a neural tumor.

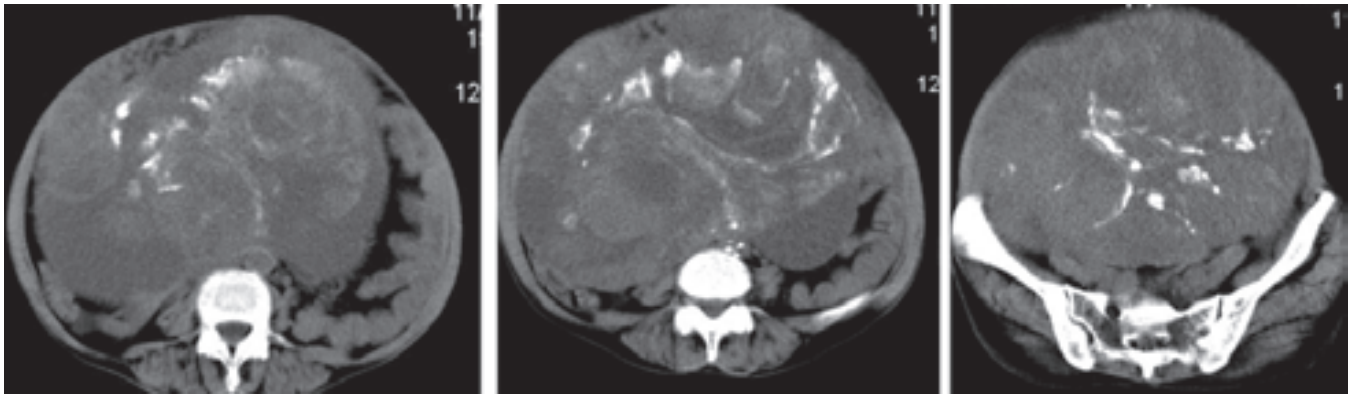

FIGURES 8.146A to C: Axial CT shows a large mixed dense mass with areas of confluent calcification in a case of teratoma.

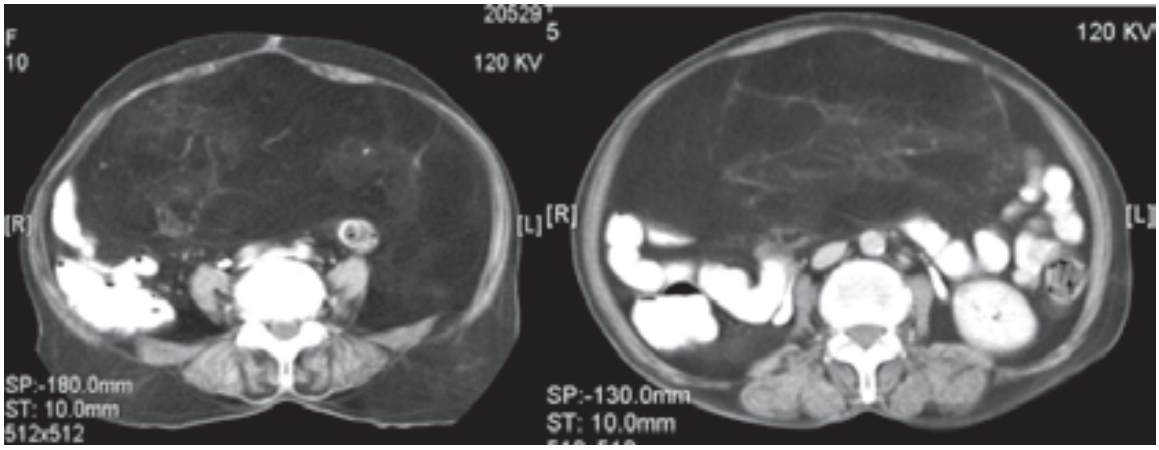

FIGURES 8.147A and B: Axial CECT showing a fat density mass displacing the bowel loops (arrow) suggestive of liposarcoma.

Myxoid Stroma

A limited number of tumors commonly contain myxoid stroma; consequently, the presence of myxoid stroma helps narrow the differential diagnosis. Myxoid stroma is characterized pathologically by a mucoid matrix that is rich in acid mucopolysaccharides.

Tumors that commonly contain myxoid stroma include neurogenic tumors (schwannomas, neurofibromas, ganglioneuromas, ganglioneuroblastomas, malignant peripheral nerve sheath tumors), myxoid liposarcomas, and myxoid malignant fibrous histiocytoma.

Myxoid liposarcomas are of intermediate-grade malignancy and have a CT attenuation lower than that of muscle.

Necrosis

Necrotic portions within tumors have low attenuation without contrast enhancement at CT. Necrosis is usually seen in tumors of high-grade malignancy such as leiomyosarcomas.

Cystic Portion

Some tumors are completely cystic in appearance. These include lymphangiomas and mucinous cystic tumors. Solid tumors with a partially cystic portion include neurogenic tumor.

Small Round Cells

Lymphomas are the most commonly encountered tumors composed of small round cells. They are homogeneous, with minimal contrast enhancement at CT.

Vascularity

Vascularity is another important feature of retroperitoneal tumors. Extremely hypervascular tumors include paragangliomas and hemangiopericytomas Moderately hypervascular tumors include myxoid malignant fibrous histiocytomas, leiomyosarcomas, and many other sarcomas. Hypovascular tumors include low-grade liposarcomas, lymphomas, and many other benign tumors.

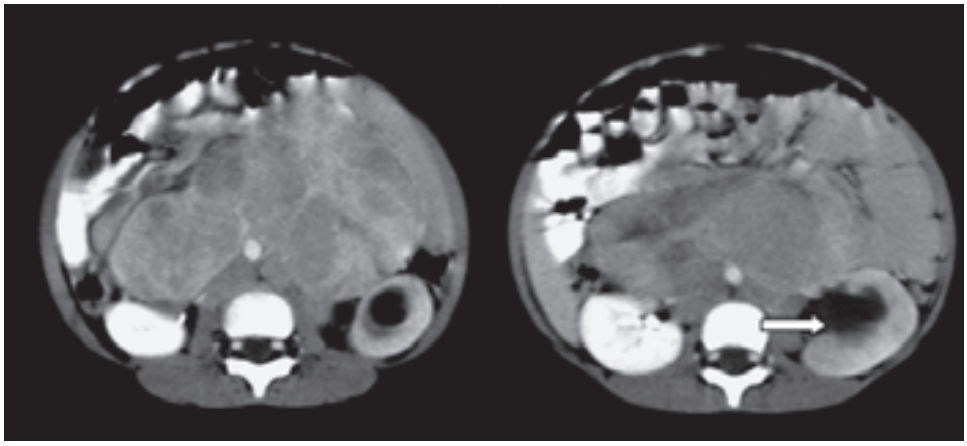

FIGURES 8.148A and B: Axial CECT showing confluent retroperitoneal nodal mass engulfing the aorta causing left ureteric obstruction (arrow) patient was 14-year-old boy with left testicular malignancy.

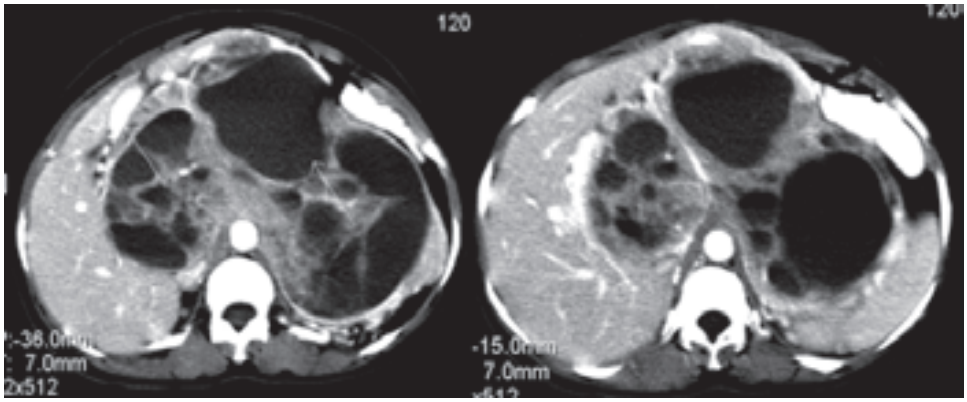

FIGURES 8.149A and B: Axial CECT shows a large retroperitoneal mass with cystic components showing fluid-fluid level encasing the mesenteric vessels. Note the displacement of the splenoportal axis superiorly (arrow) this is a useful finding which helps to localize large lesions in this area as retroperitoneal lesions displace the splenic vein anteriorly or superiorly—case of atypical carcinoid lesion.

Retroperitoneal Fibrosis

An uncommon fibrotic process involving the caudal portion of the retroperitoneum. In upto 70% of patients there is no causative factor which is found. Of late it has been postulated to occur secondary to a immune response to material leaked into the retroperitoneum from the plaques in the abdominal aorta called as ceroid which is seen in the aortic adventitia and the periaortic nodes.

Other known benign causes include drugs like methisurgide, β-blockers, methyldopa. Infections like tuberculosis, fungal like histoplasmosis, hemorrhage in upto 10% of cases, malignant processes can provoke an extensive desmoplastic reaction that cannot be distinguished from benign processes.

Usually imaging is done secondary to pain or urinary tract problems where it shows classical periaortic soft tissue with medial deviation of ureters. Usually seen at the L 4 level it generally surrounds the anterior and lateral aspect of great vessels rather than displace it.

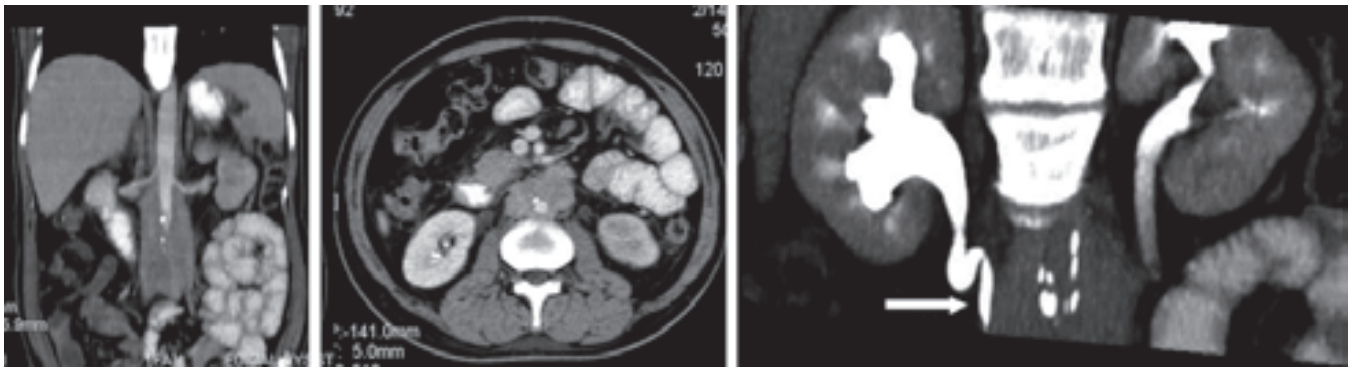

FIGURES 8.150A to C: Axial CECT showing retroperitoneal fibrosis. Note the typical periaortic soft tissue encasing the aorta from the level of renal artery to the level of iliac bifurcation. Figure C shows a coronal MPR of the kidneys with dilated medially deviated ureter encased by the periaortic soft tissue (arrow).

Aortic Aneurysms

Atherosclerotic disease is the predominant cause of abdominal aortic aneurysm. The most common atherosclerotic aneurysm is a fusiform aneurysm that begins 2 to 3 cm inferior to the renal arteries, but sometimes a juxtarenal aneurysm is observed that extends to the origin of the renal arteries, which creates problems for surgery. Abdominal aortic aneurysms often extend to the common iliac artery and may involve the internal iliac artery, causing dilatation, but aneurysm of the external iliac artery is rare.

Inflammatory Abdominal Aortic Aneurysm

Inflammatory abdominal aortic aneurysm is characterized by significant thickening of the aortic wall and adhesion to the adjacent tissues. Compared with atherosclerotic abdominal aortic aneurysm, a markedly thickened wall is observed with fibrosis extending to the retroperitoneal space, and sometimes with strong adhesions to the duodenum and mesentery, kidneys, urinary tract, and inferior vena cava. The patient has back pain and abdominal pain, and there is elevation of the erythrocyte sedimentation rate and weight loss. As with atherosclerotic aortic aneurysm, surgical intervention is the main treatment, but steroids are sometimes administered to control inflammatory process.

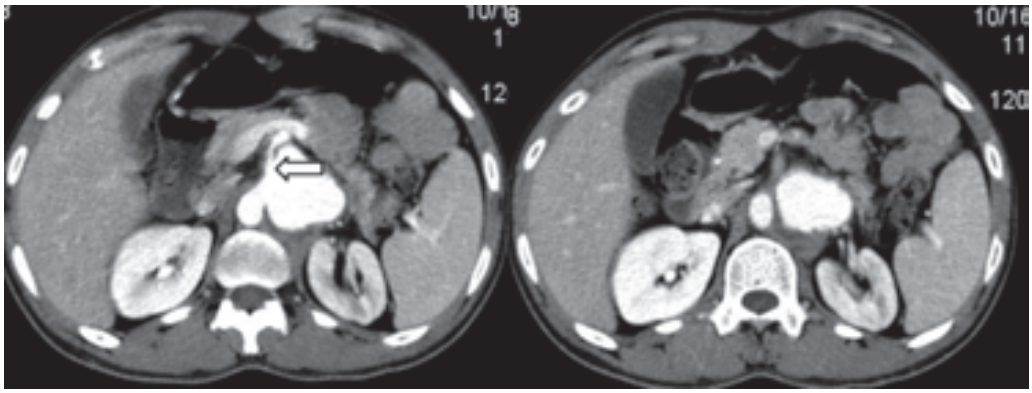

FIGURES 8.151A and B: Axial CECT shows a saccular aortic aneurysm in a 35-year-old male with complaints of persistent back pain increasing in severity on bending forward. Note the origin of SMA is from the aneurysm (arrow).

Impending Rupture

Rupture of abdominal aortic aneurysm (AAA) is a life-threatening complication. The overall mortality rate of AAA ruptures ranges from 70 to 94%. More than half of the patients die before they reach the hospital. Even among patients who reach the hospital and undergo operative repair, the average mortality rate is approximately 50%. The classic symptoms of ruptured AAA are hypotension, abdominal pain or flank pain, and pulsatile abdominal mass.

CT is usually requested in hemodynamically stable patients to confirm the diagnosis and to exclude other causes of abdominal pain, such as intra-abdominal abscess, mass, renal colic, or enlarged lymph nodes.

A high-attenuation crescent sign was first described in 1988 by Pillari et al. This was the crescentic hyperattenuation area within the aortic wall or mural thrombus of AAA, which suggested penetration of blood into the mural thrombus. As the rupture progressed, the hemorrhage extended to the outer margin of the thrombus and was limited by the aortic wall.

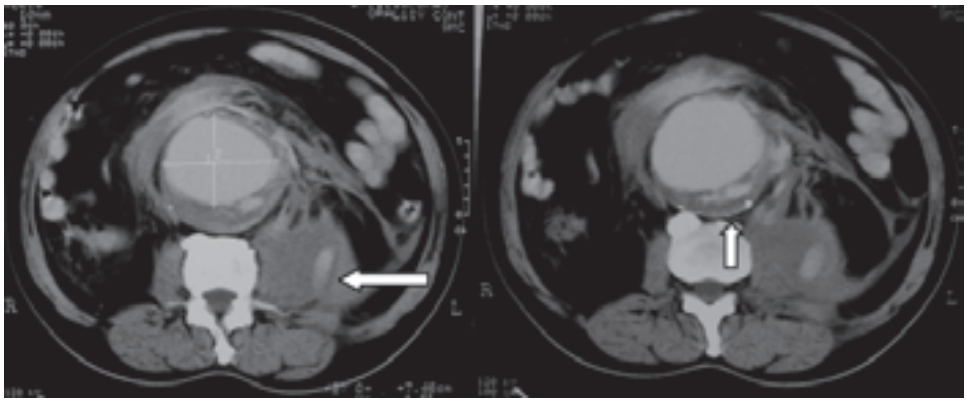

FIGURES 8.152A and B: Axial CECT showing a fusiform aortic aneurysm with a mural crescent sign (arrow in B) seen in patients with impending rupture. Left psoas bulky with areas of hemorrhage suggestive of a leaking aortic aneurysm (arrow in A).

Depending only on the size of AAA, the risk of rupture varies. For a 4 cm aneurysm, the risk was approximately 2%; but for aneurysms larger than 5 cm, the risk increased to 25-41% over 5 years. Because the risk of rupture increased substantially with larger aneurysms, most vascular surgeons would electively repair AAA larger than 5 cm in diameter unless there was a strong contraindication for surgery.

Aortic Dissection

Aortic dissection occurs in 5 to 10 cases per million population per year or 1 per 10,000 hospital admissions, and has a high rate of rupture, estimated as high as 77%, many of which occur within days of diagnosis. Complications include rupture which can lead to death in approximately 90% of untreated patients with aortic dissection, dissection into branch vessels, vascular occlusion, organ infarction, fistula formation and aortic insufficiency. Symptoms include sudden thoracic or abdominal pain which may radiate to head, back, pelvic region, lower extremities, and rarely arms.

Causes of dissection include hypertension, Marfan's syndrome, trauma, Ehlers-Danlos, coarctation, bicuspid aortic valve and relapsing polychondritis.

Etiology/Pathophysiology

Dissection refers to a tear or defect in the intima of the aorta which allows blood to enter the media, separating it into two layers. The tear occurs most frequently 1-2 cm above the aortic valve and at the isthmus near the attachment of the ligamentum arteriosum. Dissection begins as an intramural hematoma arising from ruptured vasa vasorum. Ischemia of the aortic media is the primary factor in medionecrosis.

Dissection can be described by either the De Bakey or Stanford classifications. De Bakey separates aortic dissections into three subtypes. Type1 dissections involve the entire thoracic aorta: ascending, transverse and descending. Type1 are surgical emergencies and account for 30% of dissections. Type 2 involve only the ascending and account for 12-21% (i.e. Marfan's syndrome). Type 3 are limited to the descending aorta, originating distal to the left subclavian artery and account for 50% of the cases. Stanford A involves the ascending and B involves the descending aorta.

Radiographic signs of dissection include: (1) inward displacement of the intimal calcifications, (2) intimal flap separating the true and false lumens, (3) differential contrast opacification between the true and false lumens, (4) presence of lower density material within the false lumen indicating the presence of a thrombus. The intimal tear signifying the entry or exit site are usually not seen by CT. Paraaortic hematoma or fluid may signify aortic rupture or leak.

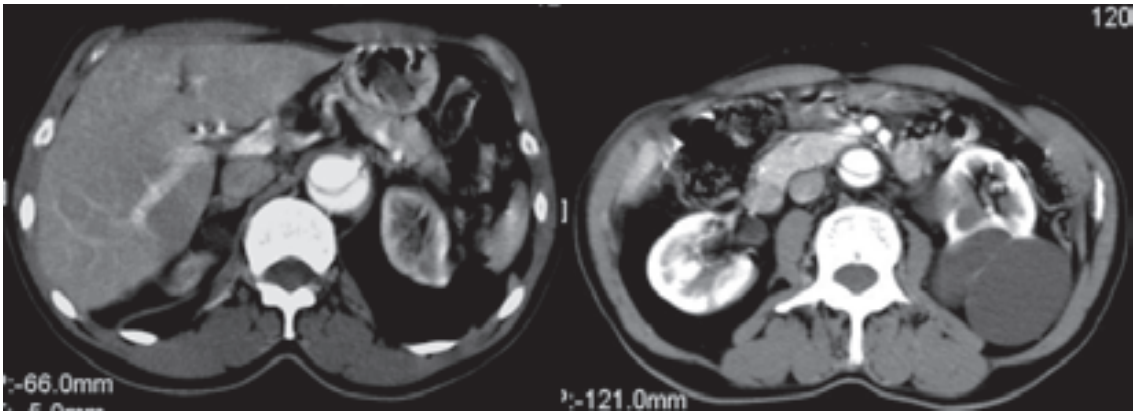

FIGURES 8.153A and B: Axial CECT showing the spiral intimal flap (arrow) in a patient with severe chest pain. Patient had a dissecting flap extending from the level of ascending aorta to the infrarenal level.

Iliopsoas Hemorrhage

Usually seen in patients with predisposing conditions, it is seen in hemophilia, von Willebrand's disease, thrombocytopenia and leaking aortic aneurysm. Acute bleeding is seen as high attenuation enlarged muscles. Fluid-fluid levels may be seen due to clot retraction.

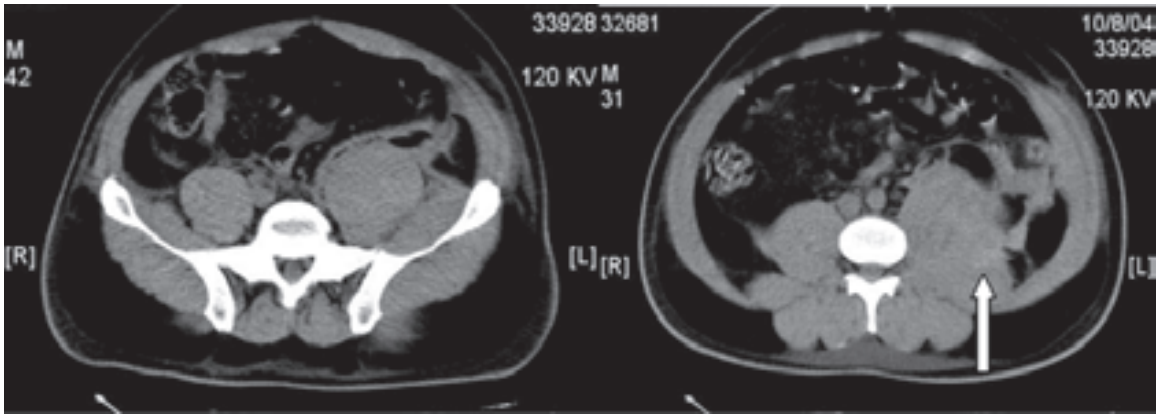

FIGURES 8.154A and B: Axial CECT showing bulky left psoas with areas of high attenuation (arrow in B) in a patient who had undergone thrombolysis for acute MI. Imaging features are suggestive of spontaneous psoas hematoma.

Inflammatory Lesions

About 50% of psoas and pararenal and colic phlegmonous lesions are due to infections, in majority of cases infection spreads from adjacent infection of kidneys, spine, pancreas, or bowel. CT shows varying findings from enlargement of the muscle mass to walled of low attenuation areas. Acute infections may show air-fluid levels. Adjacent destruction of lumbar spine can be seen.

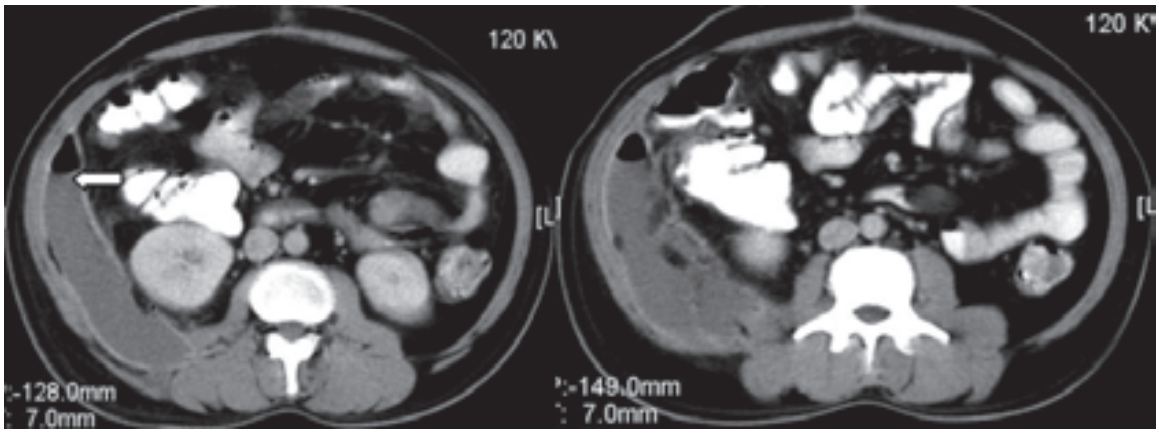

FIGURES 8.155: Axial CECT shows a left posterior pararenal, paracolic walled of abscess showing an air-fluid level (arrow).

AN APPROACH TO ABDOMINAL PAIN

Acute abdominal pain is abdominal pain that persists for more than a few hours characterized by abdominal tenderness and evidence of inflammatory reaction or visceral dysfunction.

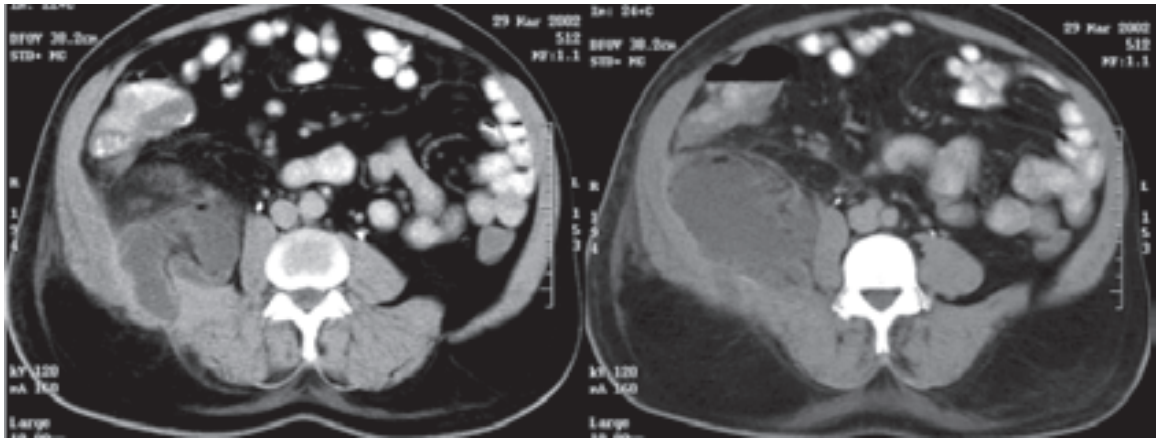

FIGURES 8.156A and B: Axial CECT showing right quadratus lumborum abscess pointing out posteriorly adjacent to the erector spine muscle.

Patient evaluation includes evaluation of the following parameters.

- History
  - past medical history
  - history of the present illness

- Physical examination
  – pelvic examination in females
- Laboratory examination
- Radiologic evaluation.

Five Principles of clinical symptoms:
- Pain
- Collapse
- Vomiting
- Muscular rigidity
- Abdominal distention.

Radiologic evaluation
- Abdominal radiographs
  – Supine (KUB) and upright abdominal films
- Ultrasound
- Computed tomography.

Non-traumatic Abdominal Emergencies

a. The peritoneal cavity
   – Ascities
   – Peritonitis
   – Abdominal abscess.
b. Liver and biliary tract
   – Jaundice: obstructive and non-obstructive
   – Cholecystitis
c. Pancreatitis
d. Urinary tract.
   – Urinary stones
   – Infection
   – Pyelonephritis
   – Renal abscess
e. Adrenal hemorrhage.
f. Gastrointestinal tract
   – Gastrointestinal hemorrhage
   – Bowel obstruction
   – Bowel infarction
   – Bowel infection
   – Appendicitis
   – Diverticulitis
   – Infectious enteritis and colitis
g. Epiploic appendagitis.
h. Inflammatory bowel disease
   – Crohn disease
   – Ulcerative colitis

The acute abdomen is a clinical diagnosis. CT has gained a prominent role in the diagnostic work-up of such patients. It is now the first-line technique for patient with acute flank pain (low-dose non-contrast CT) and vascular emergencies.

It is a second-line technique in cases in which ultrasound fails to clarify the diagnosis, such as in acute appendicitis, diverticulitis, complicated cholecystitis, pancreatitis, or abdominal abscess or hemorrhage.

Examination Technique

The required technique for imaging of abdominal emergencies varies. For CT angiography it is highest (3-5 mm collimation with helical CT) for renal stones, the collimation should also not exceed 5 mm, while for most other indications 5-7 mm collimation will be needed. For evaluation of small bowel loops, 3 mm increment may be essential.

Oral contrast may help in patients with suspected appendicitis, diverticulitis, intra-abdominal abscess, or tumor. Use of oral contrast is contraindicated in patients with suspected high-grade small bowel obstruction or ureteral colic; negative oral contrast can be used for cases with suspected gastrointestinal bleeding.

If a perforation is suspected or intraperitoneal free air is to be excluded, the images must also be evaluated in a lung window setting (level –650, width 1500 HU).

In our institution, we initially perform a noncontrast scan in patients with urolithiasis and hemorrhage, and later decide for a contrast-enhanced examination.

CT protocols in patients with acute abdomen tailored to the clinical working diagnosis

No intravenous contrast	Ureteral stone, intra-abdominal bleeding, hematoma
No oral contrast	Ureteral stone, vascular disease, small bowel obstruction, pancreatitis
Negative oral contrast (water)	Gastroduodenal ulcer, intraductal gallstone
Rectal contrast (optional.	Appendicitis, diverticulitis
Increased flow rate of IV contrast	Vascular disease, hemorrhage, bowel ischemia, renal infarct
Delayed acquisition (> 3 min)	Pyelonephritis
Narrow collimation	Ureteral stone, intraductal gallstone, vascular disease
Small recon. interval (≤ 3 mm)	As with narrow collimation, + small bowel disease

Most of the patients with acute abdominal condition present with pain, based on the nature and temporal profile of the pain, it is possible to form reasonable conclusion as to the source of the pathology.

Patients with central abdominal pain are difficult to diagnose, consider these possibilities

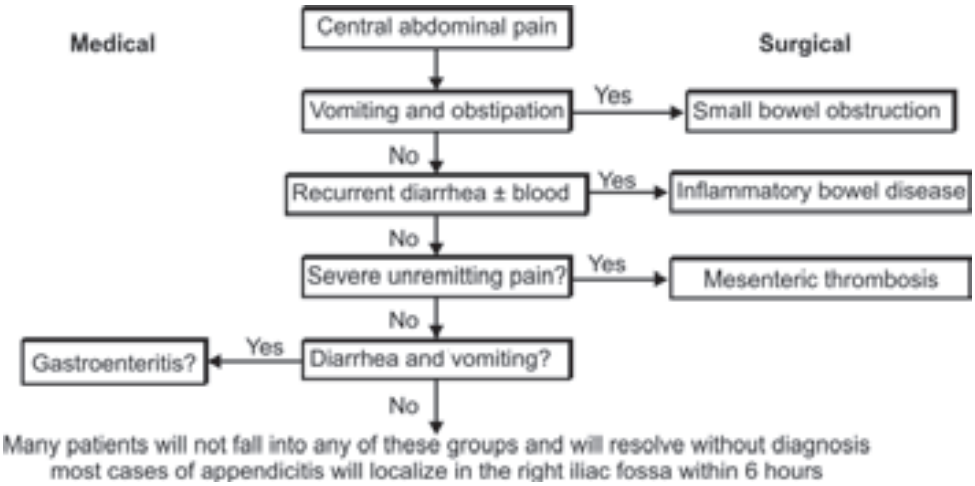

Table 8.3: Possible causes of pain by location

Location of pain	*Associated diseases*
Right upper quadrant *(liver, kidney, gallbladder)*	Acute cholecystitis, biliary colic, acute hepatitis, duodenal ulcer, right lower lobe pneumonia
Right lower quadrant *(ascending colon, appendix, ovary, fallopian tube)*	Appendicitis, cecal diverticulitis, ectopic pregnancy, tubo-ovarian abscess, ruptured ovarian cyst, ovarian torsion
Left upper quadrant *(pancreas, spleen, kidney)*	Gastritis, acute pancreatitis, splenic pathology, left lower lobe pneumonia
Left lower quadrant *(sigmoid and descending colon, ovary, fallopian tube)*	Diverticulitis, ectopic pregnancy, tubo-ovarian abscess, ruptured ovarian cyst, ovarian torsion
Midline or periumbilical	Appendicitis (early), gastroenteritis, mesenteric lymphadenitis, myocardial ischemia or infarction, pacreatitis
Flank	Abdominal aortic aneurysm, renal colic, pyelonephritis
Front to back	Acute pancreatitis, ruptured abdominal aortic aneurysm, retrocecal appendicitis, posterior duodenal ulcer
Suprapubic or lower abdominal	Ectopic pregnancy, mittelschmerz, ruptured ovarian cyst, pelvic inflammatory disease, endometriosis, urinary tract infection

Table 8.4: Referred pain

Structure irritated	*Location of referred pain*
Diaphragmatic	Supraclavicular area (Kehr's sign)
Ureteral	Hypogastrium, groin, inner thigh
Cardiac pain	Epigastrium, jaw, shoulder
Appendix	Periumbilical via T10 nerve
Duodenum	Umbilical region via greater thoracic splanchnic nerve
Hiatal hernia	Epigastrium via T7 and T8 nerves
Pancreas or gallbladder	Epigastrium
Gallbladder and bile duct	Epigastric pain that wraps around to the scapula

Table 8.5: Stereotypical localization of abdominal pain

Localization of pain	*Organs*	*Embryonic derivative*	*Nerves*
Epigastrium	• Stomach • First two parts of the duodenum • Liver • Gallbladder • Pancreas	Foregut	• Vagus nerve (parasympathetic) • Greater thoracic splanchnic nerves (sympathetic)
Periumbilical	• Third and fourth parts of duodenum • Jejunum	Midgut	• Vagus nerve (parasympathetic) • Greater thoracic splanchnic nerves (sympathetic)

Contd...

Contd...

Localization of pain	*Organs*	*Embryonic derivative*	*Nerves*
	• Ileum • Cecum • Appendix • Ascending colon • First two-thirds of transverse colon		
Hypogastrium	• Distal one-third of transverse colon • Descending and sigmoid colon • Rectum and upper portion of anal canal • Reproductive organs (ovaries, fallopian tubes, uterus, seminal vesicles, prostate) • Bladder	Hindgut, genitourinary	• Pelvic splanchnic nerves (parasympathetic) • Lesser thoracic splanchnic nerves (sympathetic)

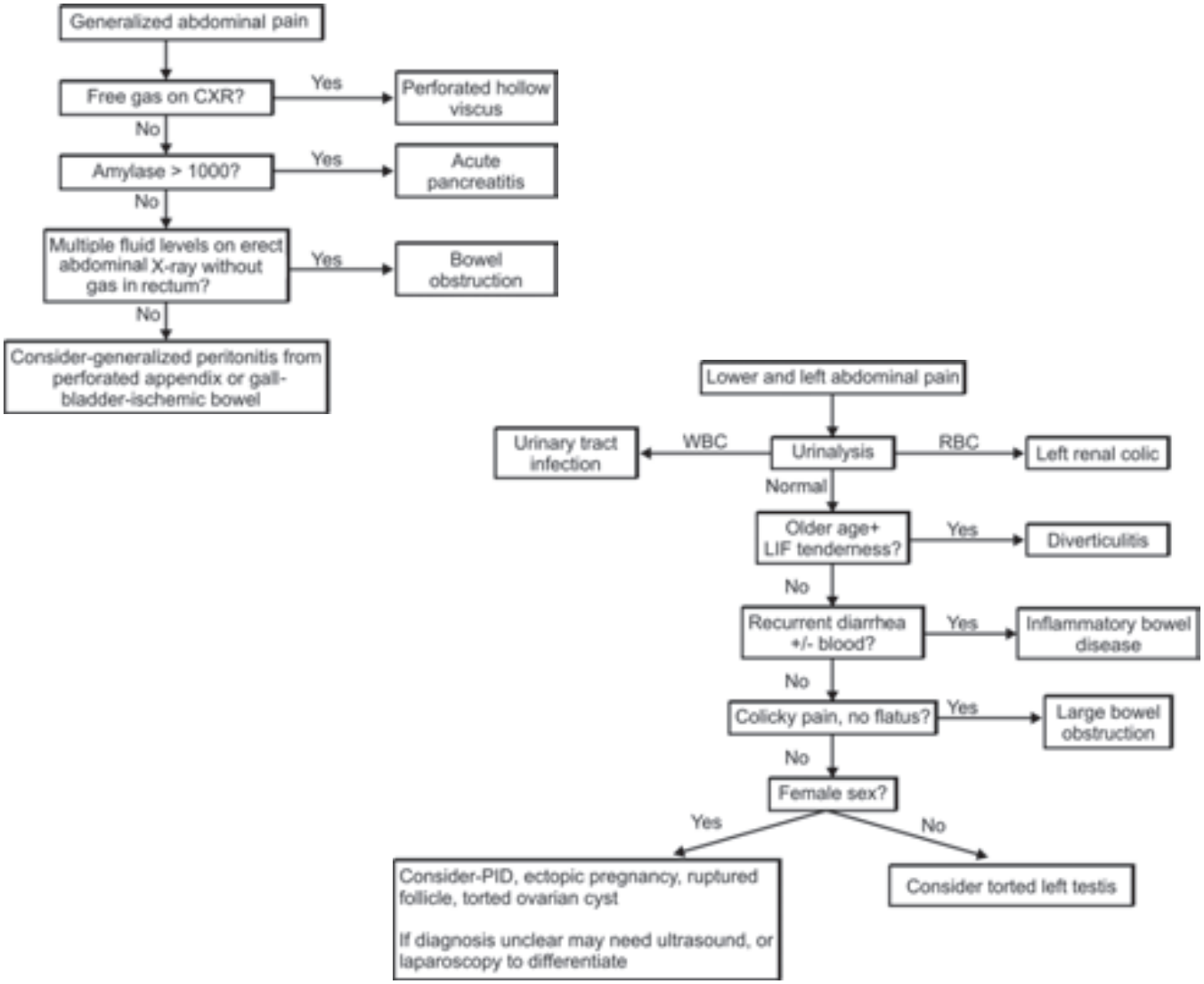

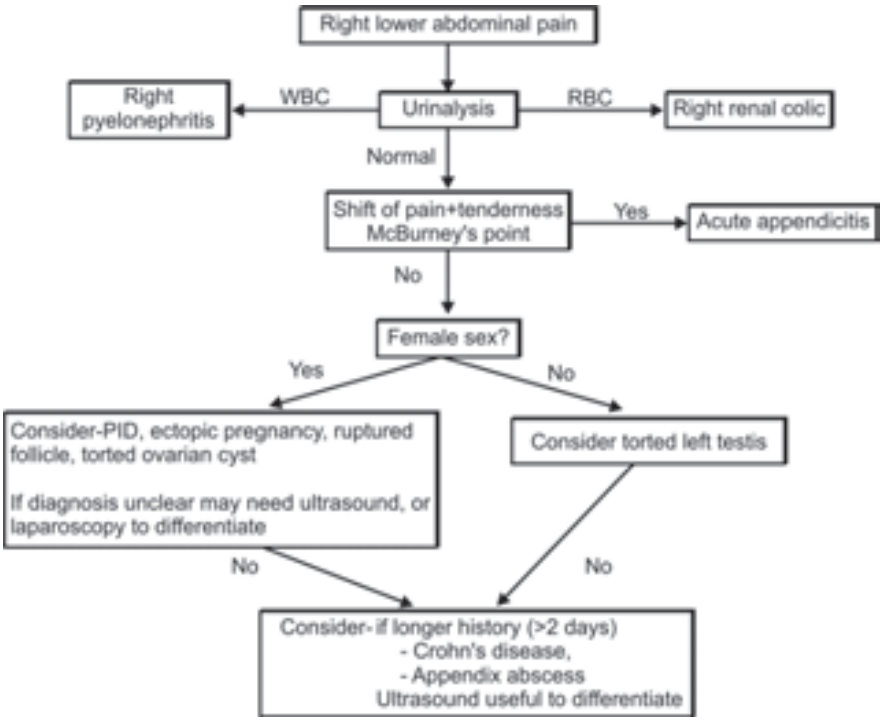

ABDOMINAL WALL

INTRODUCTION

Abdominal wall is often an overlooked source of pain. The pathologies which involve the abdominal wall are diverse and vary from the common to very rare pathologies. In this chapter we present a pictorial representation of some diverse pathological conditions.

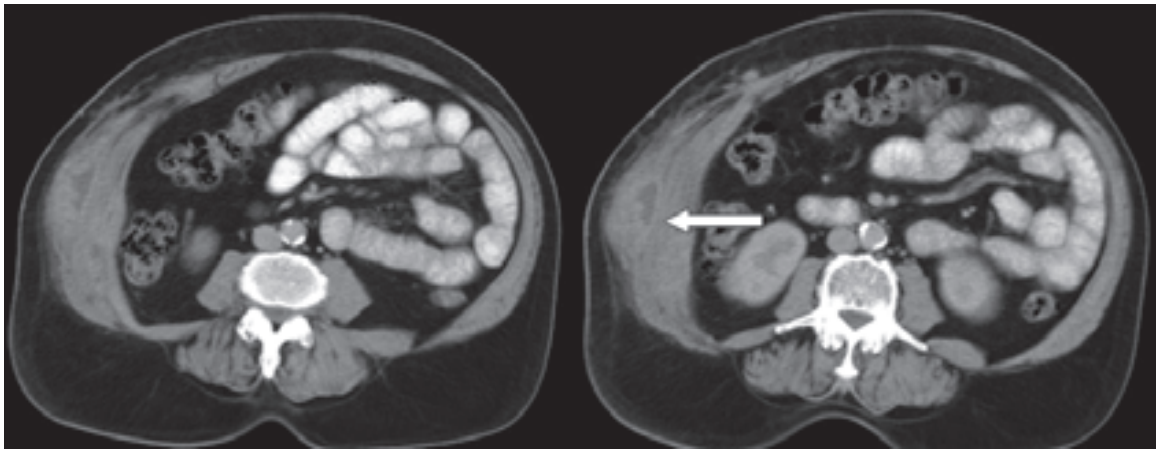

FIGURES 8.157A and B: Axial CECT in a diabetic patient presenting with fever and pain in the right flank region with skin discoloration (arrow) shows right parietal wall phlegmonous changes with abscess formation.

Table 8.6: Etiology of abdominal wall pain

Etiology	*Comments*	*Diagnosis*
Hernia	Protuberance in abdominal wall that usually decreases in size when patient is supine	Abdominal CT scanning, abdominal ultrasonography, herniography
Rectus nerve entrapment	Occurs along lateral edge of rectus sheath; worsening of pain with tensing of muscles	Injection of local anesthetic
Thoracic lateral cutaneous nerve entrapment	Occurs spontaneously, after surgery or during pregnancy	History and physical examination
Ilioinguinal and iliohypogastric nerve entrapment	Lower abdominal pain that occurs after inguinal hernia repair	History and physical examination
Endometriosis	Cyclic abdominal pain	Laparoscopy
Diabetic radiculopathy	Acute, severe truncal pain involving T6-T12 nerve roots	Paraspinal EMG
Abdominal wall tear	Occurs mainly in athletes	History and physical examination
Abdominal wall hematoma	Complication of abdominal laparoscopic procedures	Abdominal CT scanning, abdominal ultrasonography
Spontaneous rectus sheath hematoma	Presents as tender, usually unilateral mass that does not extend beyond midline	Abdominal CT scanning, abdominal ultrasonography
Desmoid tumor	Dysplastic tumor of connective tissue; occurs in young patients (females more often than males)	Surgical excision
Herpes zoster	Pain and hyperesthesia followed by vesicles along a dermatome	History and physical examination
Spinal nerve irritation	Caused by disorders of thoracic spine	CT scanning or MRI studies of thoracic spine
Slipping rib syndrome	Sharp, stabbing pain in upper abdomen caused by luxation of eighth to 10th ribs	Hooking maneuver to pull lower ribs anteriorly, which reproduces the pain and sometimes a click.
Idiopathic	Myofascial pain	History and physical examination

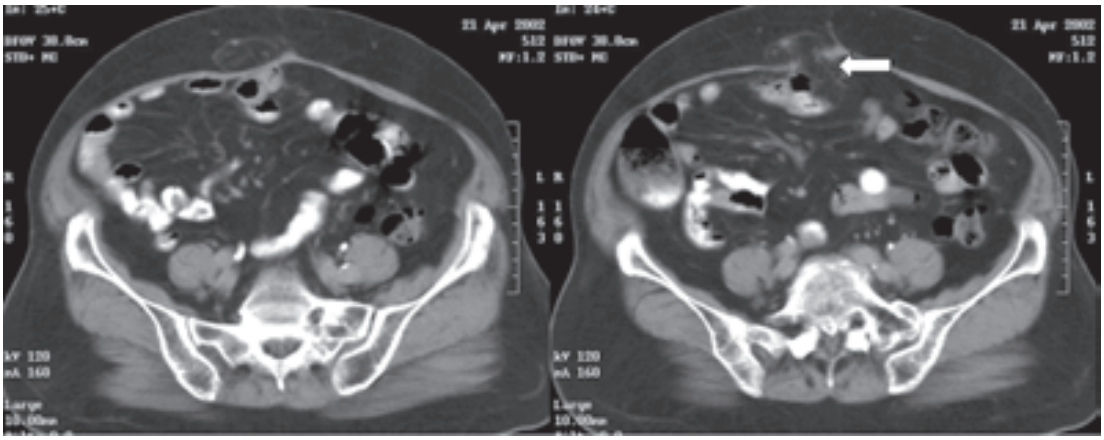

FIGURES 8.158A and B: Axial CECT in a patient with persistent periumbilical pain reveals a small paraumbilical hernia with herniation of fat (arrow).

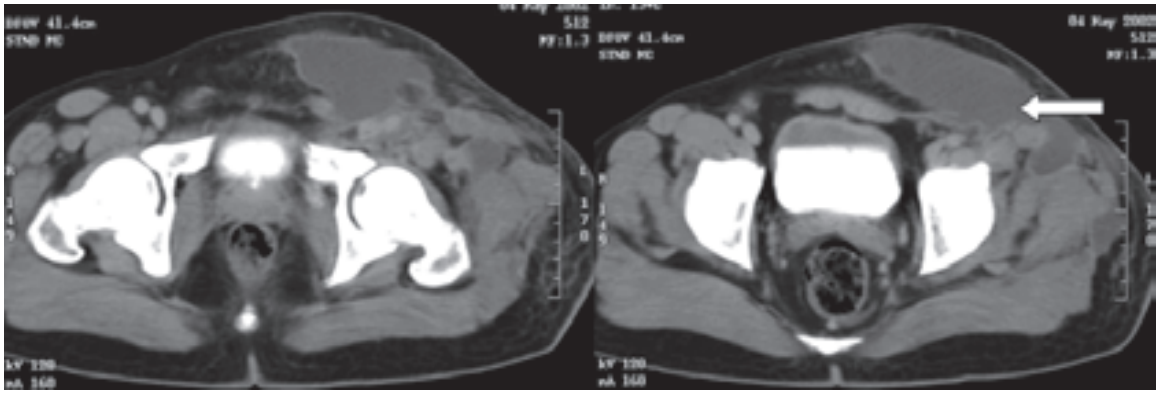

FIGURES 8.159A and B: Axial CECT in a patient with left inguinal region pain reveals a well marginated hypodense abscess collection (arrow).

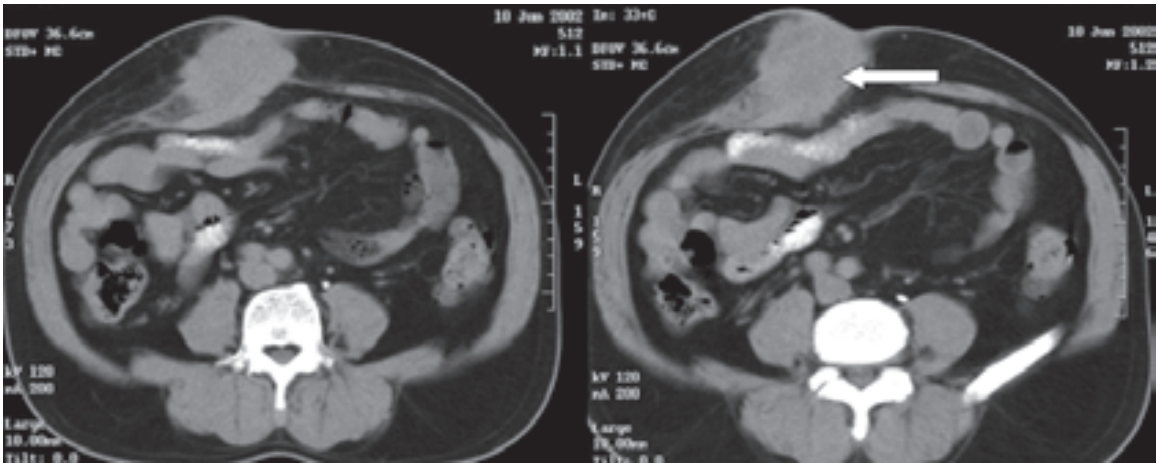

FIGURES 8.160A and B: Axial CECT in a patient with swelling in the right paraumbilical region (arrow) with dull aching pain (HPE- Desmoid tumor).

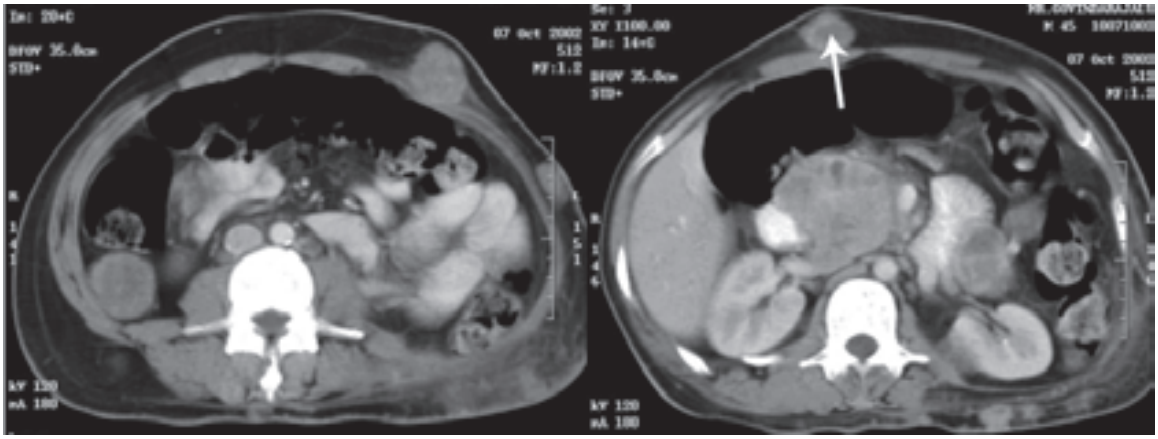

FIGURES 8.161A and B: Axial CECT in a patient with disseminated melanoma reveals multiple subcutaneous nodules (case of metastatic melanoma).

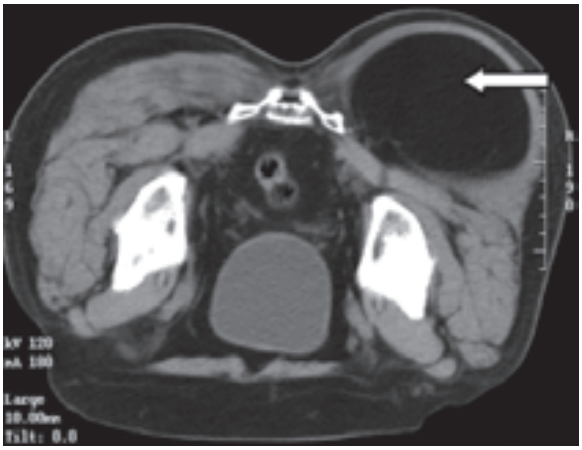

FIGURE 8.162: Axial prone CT in a patient with gluteal mass of 12 years duration reveals a large lipoma (arrow).

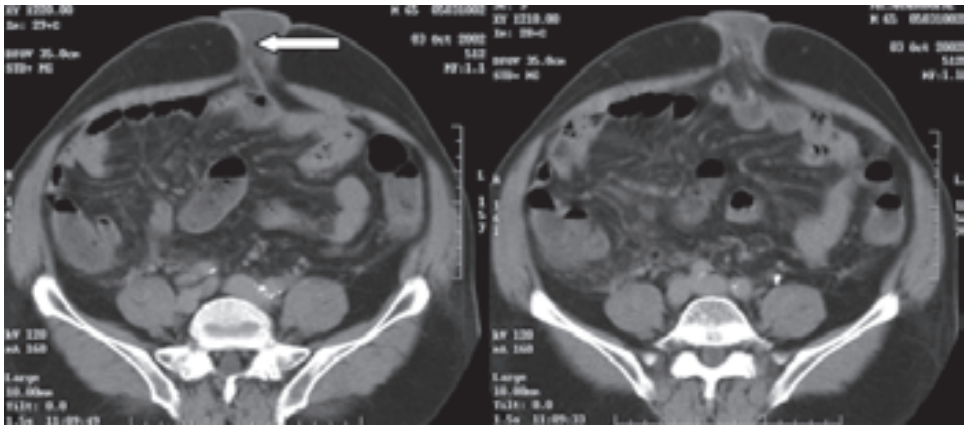

FIGURES 8.163A to C: Axial CECT reveals an umbilical hernia (arrow).

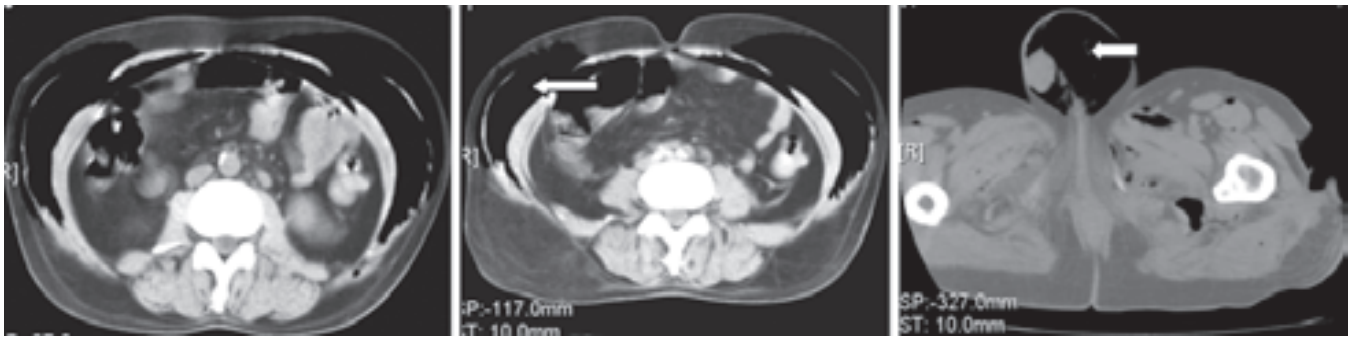

FIGURES 8.164A to C: Axial CECT in a patient with polytrauma reveals extensive subcutaneous emphysema (arrow in B). Note the pneumoscrotum (arrow in C).

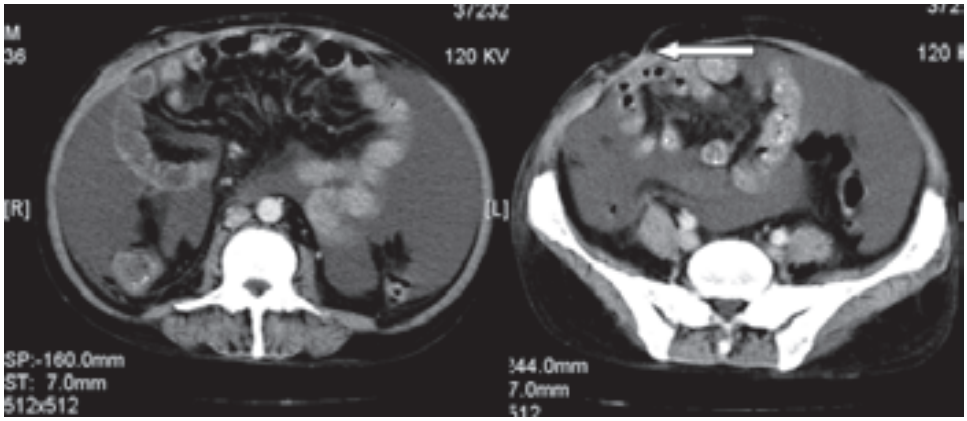

FIGURES 8.165A and B: Axial CECT in a diabetic patient with subcutaneous ulceration in the right inguinal region (arrow) with inflammatory changes in the adjacent properitoneal plane.

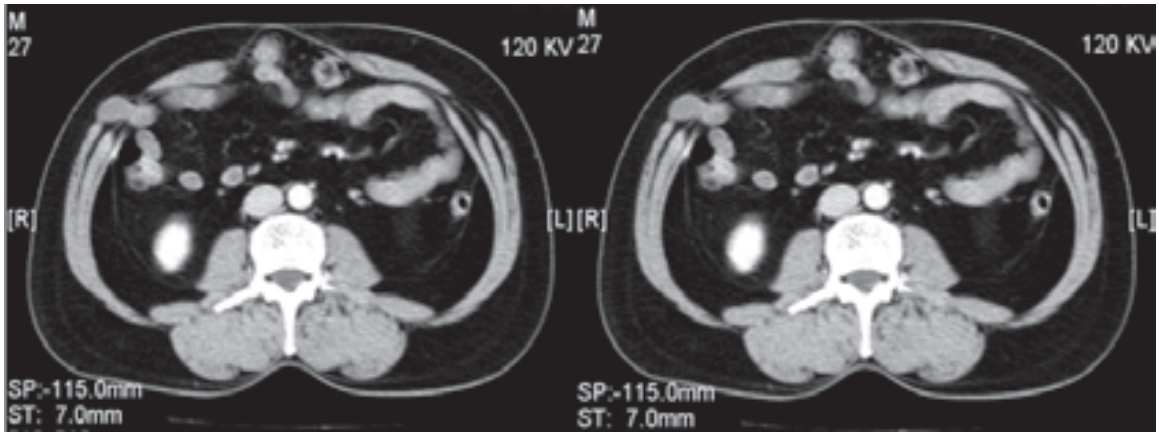

FIGURES 8.166A and B: Axial CECT in a patient with a fluctuating swelling in the right lumbar region reveals herniation of the small bowels through a defect in the muscle plane – suggestive of parietal hernia.

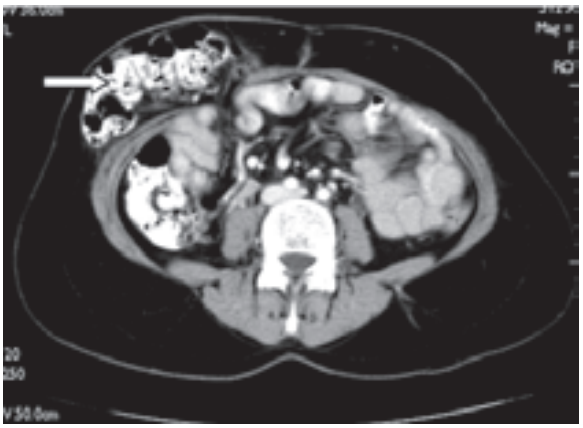

FIGURE 8.167: Axial CECT in a patient with history of laparotomy for hysterectomy 4 years ago presenting with large parietal hernia (arrow).

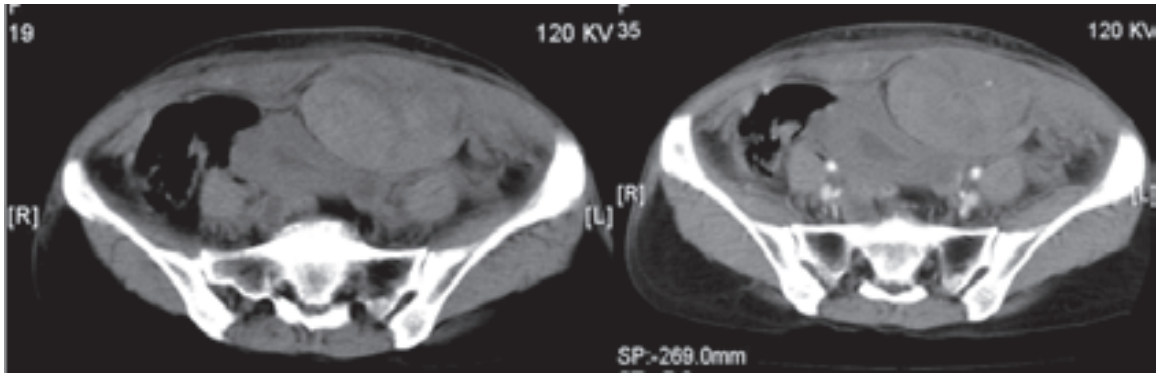

FIGURES 8.168A and B: Axial plain and CECT reveals enlargement of the left rectus muscle having hyperdense variegated appearance – case of spontaneous left rectus sheath hematoma.

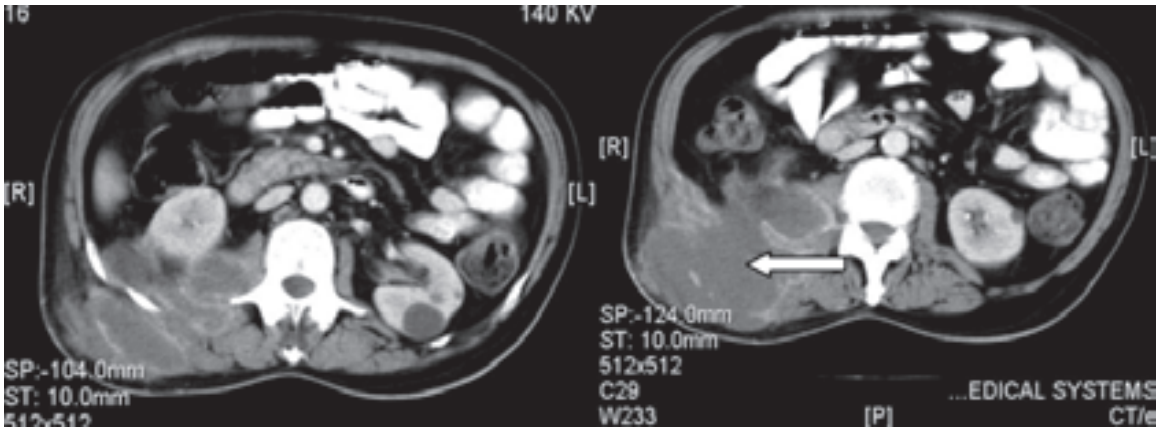

FIGURES 8.169A and B: Axial CECT in a patient with fever and right loin pain reveals a parietal wall and right psoas abscess involving the posterior pararenal facial planes (arrow).

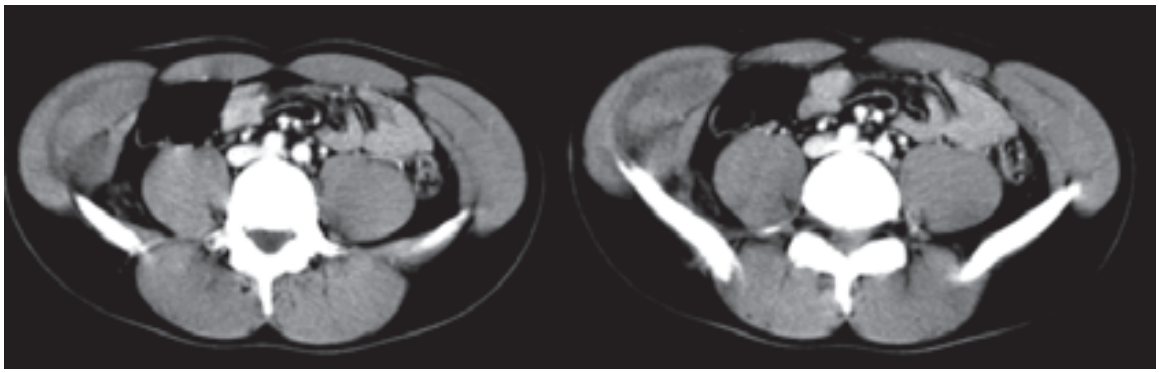

FIGURES 8.170A and B: Axial CECT in a patient with history of blunt abdominal trauma reveals a right iliac properitoneal and deep muscular hematoma.

CT ANGIOGRAM

The development of the multidetector computed tomography (MDCT) scanner, combined with state-of-the-art three-dimensional (3D) reconstruction software, has optimized the resolution of today's computed tomographic angiography (CTA) to the extent that clinicians are increasingly relying on this noninvasive means of evaluating vascular disease rather than conventional arterial angiography.

3D Rendering Techniques

The three principle techniques for 3D processing of CT datasets include surface rendering, maximum intensity projection (MIP), and volume rendering. Surface rendering was one of the first methods developed, and it relies on the comparison of a voxel intensity to some defined threshold value, which the computer uses to define an edge contour.

The MIP algorithm selects out the maximum value in a voxel along a line from the viewer's eye through the image and displays only that value in the corresponding pixel. The limitations of both MIP and surface rendering lie in the forfeiting of most of the available data in order to increase image-processing speed.

Volume rendering, on the other hand, sums the contributions of each voxel along a line from the viewer's eye through the dataset, such that all of the information is included in the final image. Therefore, volume rendering is more accurate and allows the visualization of multiple tissue types simultaneously. For these reasons, volume rendering has become the preferred method for 3D postprocessing. MIP plays a complementary role and is used in conjunction with volume rendering.

CTA of the Kidney

CT angiography has come to the forefront in the preoperative evaluation of candidates for renal transplants and partial nephrectomies. It is also a reliable noninvasive exam for the detection of renal artery stenosis. A triphasic CT vascular map is now indicated for noninvasive evaluation of both the donor organ and selection of the organ to be transplanted, identifying any aberrant vessels or anatomic variations. In addition to evaluating the vasculature, CTA has the advantage of simultaneously excluding the presence of renal cell carcinoma or renal artery stenosis in renal donors, both of which may render the patient inoperable. CT angiography has also played a key role in the presurgical evaluation of patients for laparoscopic partial nephrectomies and in the postoperative evaluation of complications including urinoma, pseudoaneurysm, and perinephric hemorrhage.

Renal Transplant Donor Evaluation

- Number and location of all renal arteries (including perihilar branching and arteries arising from the iliac vessels)
- Number and location of all renal veins (including circumaortic and retroaortic renal veins)
- Since the left kidney is usually chosen for transplant (unless complex vascular anatomy is present) definition of the left adrenal vein and gonadal vein is needed
- The presence of prominent lumbar veins or variant vascular anatomy is critical.

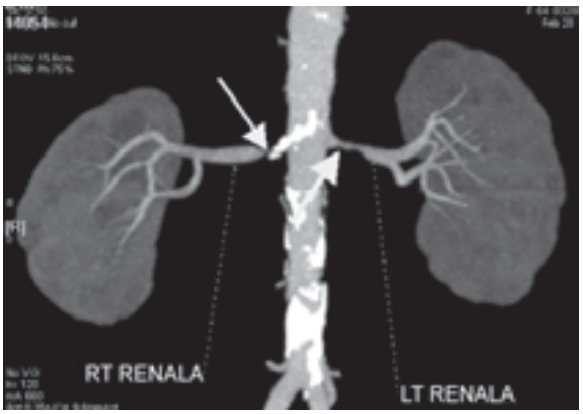

FIGURE 8.171: Coronal 3D MIP projection showing bilater osteoproximal renal artery stenosis (arrow).

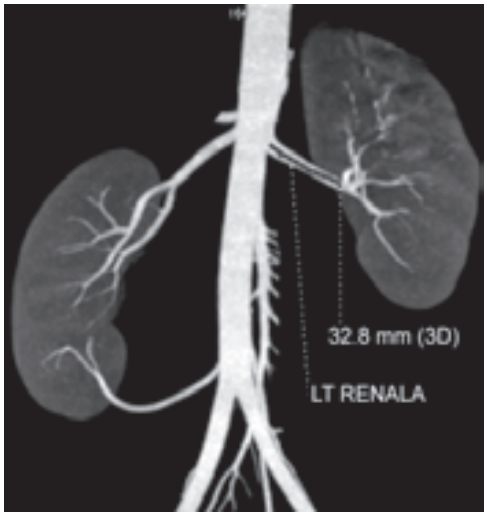

FIGURE 8.172: Coronal MIP showing accessory right renal artery to the lower pole in a renal donor.

CTA of the Pancreas

The accurate identification of vascular invasion is crucial in the staging and evaluation for resectability in patients with pancreatic cancer. In evaluating patients who are potential candidates for a Whipple procedure, the superior mesenteric artery (SMA) and the superior mesenteric vein (SMV) must be clearly defined in relation to the pancreatic mass, and a decision must be made as to whether the mass invades or just abuts the vasculature. It has been shown in the literature that while evaluation of vascular invasion with axial images alone has a poor correlation with surgical findings, 3D CTA detection has a very high accuracy. This is in part due to the multiplanar capabilities of MDCT scanning, but is also a result of enhanced resolution provided by thinner slices.

Pancreatic Tumor Evaluation

- Extent of tumor
- Encasement of the arterial supply including the SMA and the celiac artery (including the gastroduodenal artery and hepatic artery)
- Encasement of the venous system including the portal vein and SMV
- Relationship of the mass and duodenum.

CTA of the Mesentery

Timed administration of the intravenous contrast bolus for both arterial and venous phases provides a dynamic evaluation of the mesenteric vasculature that may aid in the diagnosis of bowel ischemia and inflammatory bowel disease. The CT evaluation of patients with suspected bowel ischemia has previously relied on the detection of pneumatosis, pneumoperitoneum, and bowel wall thickening. However, bowel wall edema is a relatively nonspecific inflammatory finding and benign causes of pneumatosis have been reported due to steroid use, pulmonary disease, and collagen vascular disease. Therefore, a more specific dynamic evaluation of the mesenteric vasculature is desired for the detection of low-flow states or embolic vessel occlusion, which may precipitate ischemia to the bowel.

CT angiography of affected bowel loops may demonstrate absence of enhancement, delay in enhancement, or persistent enhancement when compared with unaffected loops. Visualization of the entire data set in one image improves the detection of collateral vessels between the celiac, SMA, and inferior mesenteric artery (IMA), which may suggest chronic ischemia in selected segments of bowel. Improved resolution with MDCT allows the detailed visualization of small branching vessels that may contain tiny emboli.

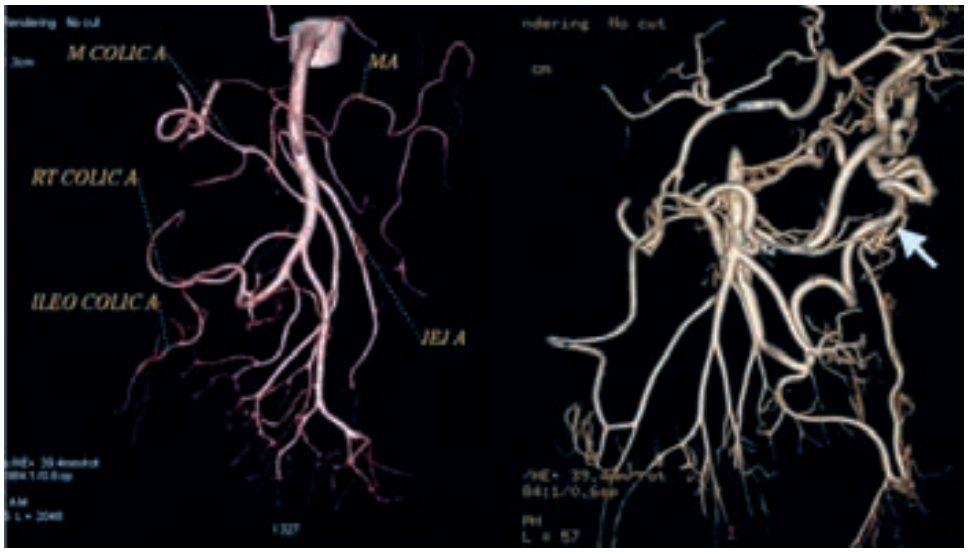

FIGURES 8.173A and B: Showing 3D volume rendering of the superior mesenteric arcade. (B) 3D VR in case of aortoarteritis showing the well formed arc of Rolon and marginal artery of Drummond (arrow).

CTA of the Abdominal Aorta

CT angiography plays an important role in the preoperative and postoperative evaluation of abdominal aortic graft placement, aneurysms, and dissections. The multiplanar capabilities of 3D CTA are extremely useful in obtaining accurate measurements of the extent and maximum diameter of tortuous aortic aneurysms. Postoperatively, CTA is a low-cost and noninvasive means of surveillance of aortic stents.

Complications after graft placement including supragraft aneurysms, distal anastomotic aneurysms, graft infections, perigraft fluid collections, and graft thrombus are also optimally detected. Imaging the entire aorta in one plane is ideal for the evaluation of aortic dissections. CT angiography is used to depict the relative patency of the true and false lumen and the origin of the renal arteries can be clearly defined.

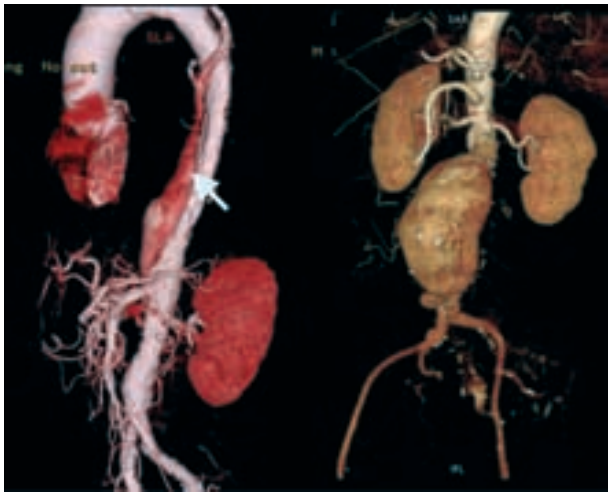

FIGURE 8.174: 3D VR image showing type 3 aortic dissection arrow shows the false lumen. Figure B shows a large fusiform infra-renal aortic aneurysm.

CTA of the Liver

CT angiography evaluation of the liver is very useful for preoperative vascular mapping in the evaluation of candidates for liver transplant as well as detecting vascular complications of cirrhosis and early identification of hepatocellular carcinoma. The "typical" hepatic arterial anatomy occurs in only 55% of the population, and at least 10 variations exist. In liver transplant patients, CTA identifies aberrant anatomy pre-operatively, and simultaneously evaluates liver volume. Another benefit of CTA is the full visualization of the extent of varices and collateral vascularization in cirrhotic patients on a single image. CT angiography is also particularly useful for the detection of small hepatomas in patients with hepatitis or cirrhosis.

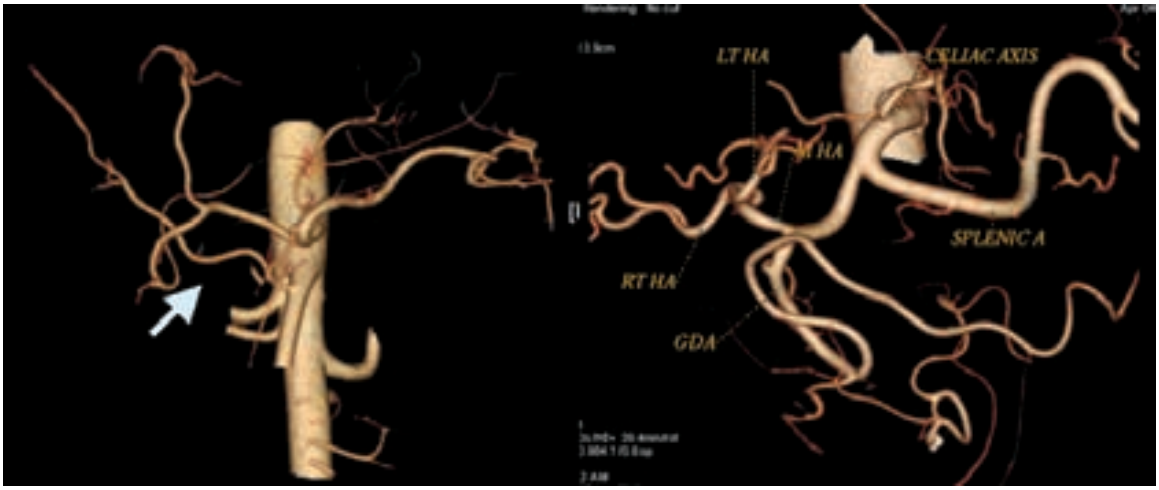

FIGURES 8.175A and B: 3D VR image of the hepatic arteries showing the right hepatic artery arising from the SMA (arrow) Figure B shows the normal branching pattern of the hepatic arteries.

Oncologic Imaging

MDCT is ideal for tumor detection and staging. The ability to acquire true volume datasets with optimized data acquisition and contrast delivery timing is a key advantage of MDCT. In oncologic imaging this means better detection of lung and liver metastases as well as more accurate staging of a wide range of neoplasms including renal, adrenal and pancreatic carcinoma lymphoma, hepatic tumors and colon cancer.

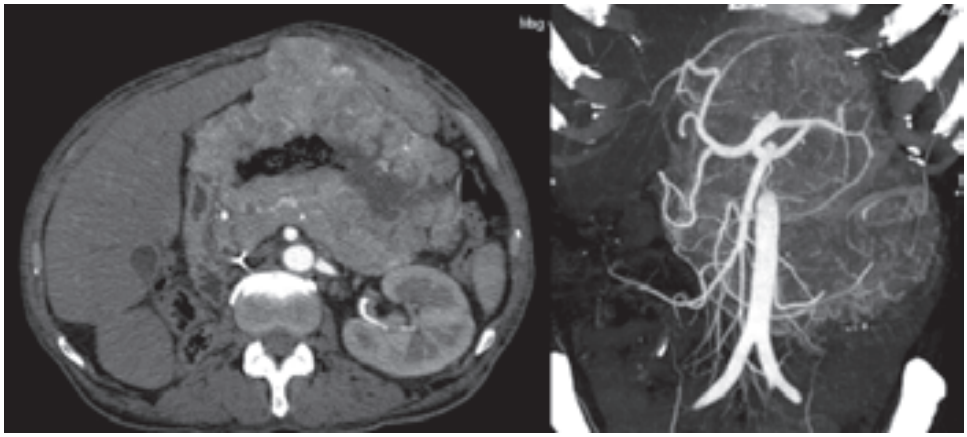

FIGURES 8.176A and B: Axial CECT showing a large mass arising from the duodenum and DJ flexure. 3D MIP showing vascular supply to the mass from the branches of both celiac and SMA branches.

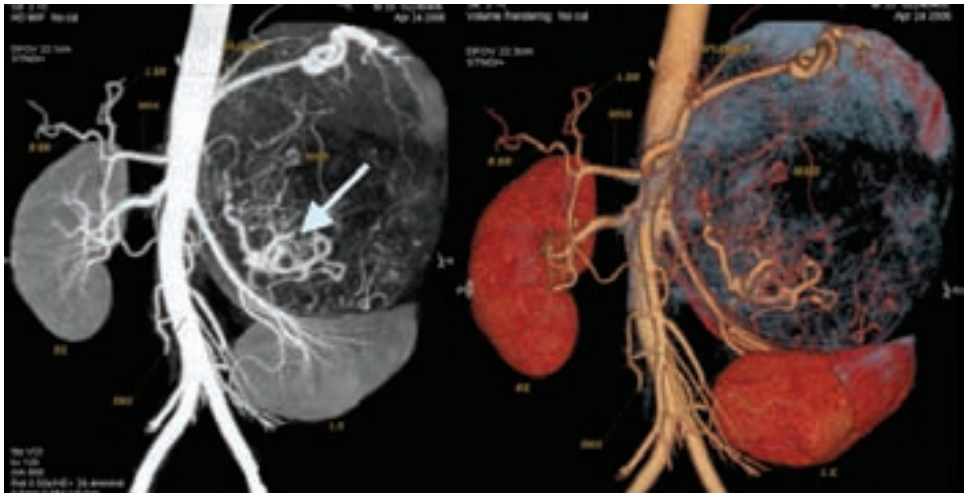

FIGURES 8.177A and B: Axial 3D MIP and VR images showing a large left suprarenal mass displacing the kidney with serpiginous neovascular vessels in the base (arrow).

CHAPTER

9 Abdominal Trauma

The diagnosis of abdominal injuries due to blunt trauma is challenging because the injuries may not manifest clinically during initial assessment. A major advance in the management of patients with abdominal trauma has been the rapid and accurate diagnosis now provided by CT. The rapid diagnostic capabilities of CT has not only contributed towards decrease in morbidity and mortality from abdominal injuries but also a decrease in non-therapeutic laparotomies in patients who can be managed conservatively.

Hemoperitoneum is easily diagnosed as are injuries of solid organs, mesentery, bowel and diaphragm. CT is also very sensitive in identifying active arterial bleeding as sites of contrast extravacation. The accuracy of CT in diagnosis of blunt abdominal trauma has been reported as high as 97%. Major advantage of helical and multislice CTs in abdominal trauma imaging has been the increased speed of examination, decreasing the scanning time for injured patients.

CT TECHNIQUE FOR BLUNT ABDOMINAL TRAUMA

Polytrauma patients who require CT imaging of head should have their head CT performed prior to abdominal CT as IV contrast required for abdominal CT could interfere with the interpretation of head CT.

The performance of high quality abdominal CT with oral and IV contrast ensures the best accuracy in the identification of abdominal injuries. In suspected cases of bowel injuries water soluble contrast agents are preferred rather than dilute barium sulfate agents which are less tolerated by the peritoneum. 400-600 ml of gastrograffin is given via a nasogastric tube (less severely injured patients can take the contrast orally). Prior to scanning the nasogastric tube is pulled back to mid esophagus so as to avoid artifacts. For IV contrast 100 ml of nonionic contrast (300 mg/I) is given at the rate of 3 ml /second scanning is started at a 30 second delay after initiation of IV contrast, using a collimation of 7 mm with a pitch of one. Additional delayed images are obtained at 3 minute intervals for opacification of the urinary tract.

Lung window images of the abdomen may be helpful in showing small amounts of extraluminal air in the peritoneal cavity or retroperitoneum. Bone window images provide identification of suspected and unsuspected spine and pelvic injuries.

HEMOPERITONEUM

Hemoperitoneum is the most frequent sign of injury and it may be the only and most obvious sign, detection of fluid in the paracolic gutter indicates at least 200 ml of blood, visualization of blood in abdomen and pelvis corresponds to more than 500 ml of blood.

CT is useful in characterization of intraperitoneal fluid collections in trauma patients, hemoperitoneum usually measure greater than 30 HU. Water dense fluids in trauma patients such as ascites, urine, bile measure 0-5 HU.

Hemoperitoneum may display a variety of densities at CT. Unclotted blood usually measures 30-45 HU, clotted blood measures about 40-60 HU. One can use a thumbrule that the densest blood is usually closest to the site of injury.

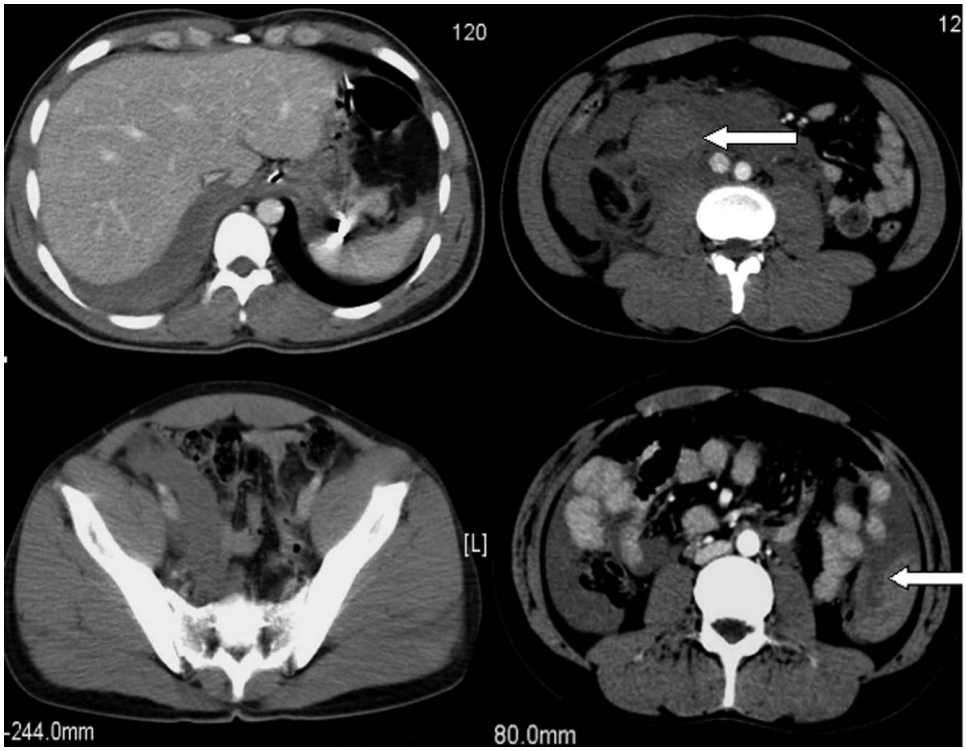

FIGURES 9.1A to D: Axial CECT in a patient with blunt trauma reveals gross hemoperitoneum in the perihepatic, perisplenic and both paracolic gutter region. Note the high attenuation clot (arrow in Fig. B and D).

HEPATIC INJURY

Liver is second only to spleen as the most frequently injured organs. Nearly 20% of organ injuries in blunt trauma involve the liver. The spectrum of hepatic injuries include laceration, subcapsular hematoma, contusion, hepatic venous and arterial injury and disruption of hepatic biliary system. Right lobe of liver is stastically found to be more frequently injured than the left. Lacerations are frequently seen to involve the posterior segment of right lobe because of its proximity to the rib cage. Zones of low attenuation paralleling the portal vein called as periportal tracking if seen in trauma patients generally denote dissection of blood along the course of portal veins.

Table 9.1: CT-based injury severity of blunt hepatic trauma

CT-based Grade	*Criteria*
1	Capsular avulsion, superficial laceration(s) less than 1 cm deep, subcapsular hematoma less than 1 cm in maximum thickness, periportal blood tracking only
2	Laceration(s) 1-3 cm deep, central-subcapsular hematoma(s) 1-3 cm in diameter
3	Laceration greater than 3 cm deep, central-subcapsular hematoma(s) greater than 3 cm in diameter
4	Massive central-subcapsular hematoma greater than 10 cm, lobar tissue destruction (maceration) or devascularization
5	Bilobar tissue destruction (maceration) or devascularization

Subcapsular hematomas have a lenticular shapes and compress the liver parenchyma, often associated with rib fractures. Contusion and hematomas may have smooth or irregular borders, laceration and fractures come in various shapes and may exhibit branching patterns.

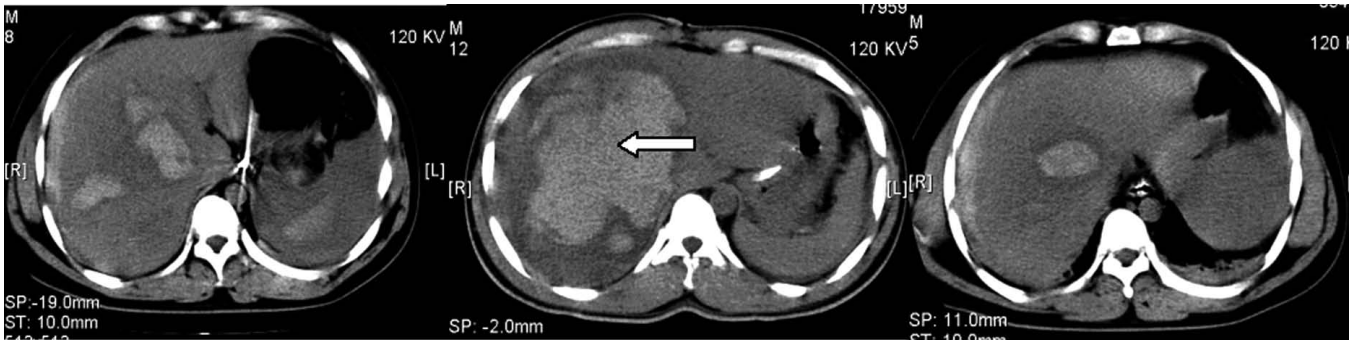

FIGURES 9.2A to C: Axial CECT reveals acute parenchymal hematoma in the right lobe of liver (arrow in B) due to laceration with suspected arterial injury.

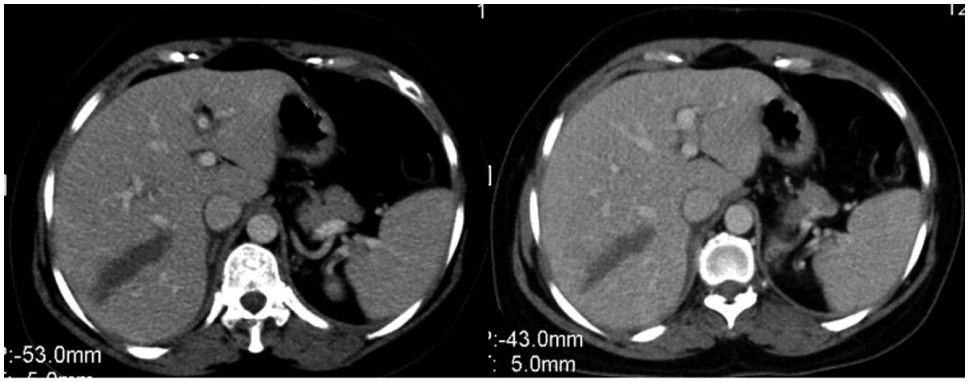

FIGURES 9.3A and B: Axial CECT reveals a linear nonenhancing lesion in the right lobe segment 6 region suggestive of laceration.

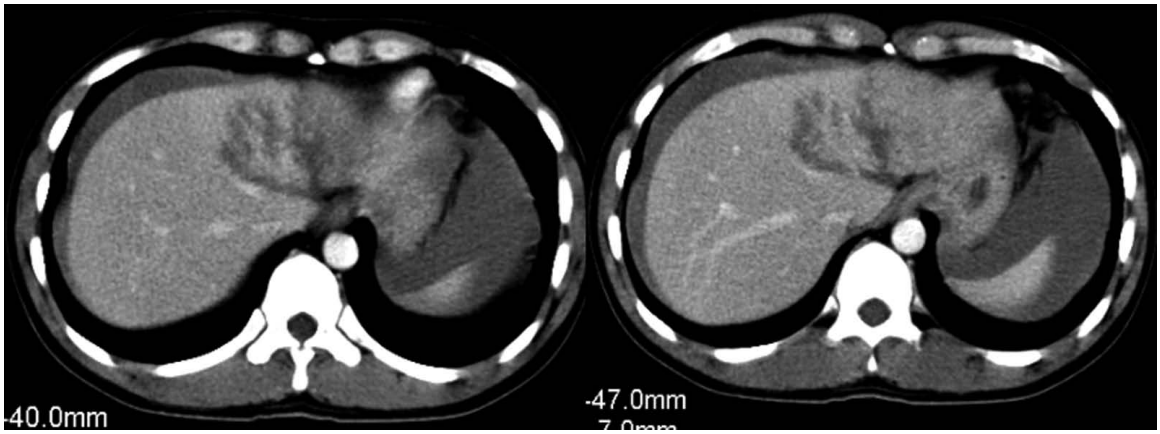

FIGURES 9.4A and B: Axial CECT reveals a stellate laceration involving segment 2 region.

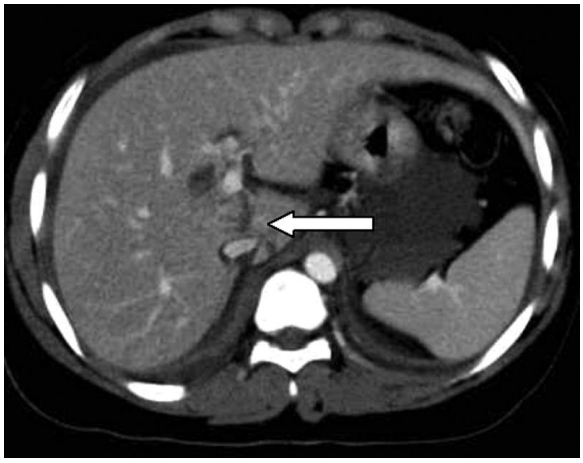

FIGURE 9.5: Axial CECT reveals laceration involving the caudate lobe (arrow) note the close relationship of IVC to the margin of laceration.

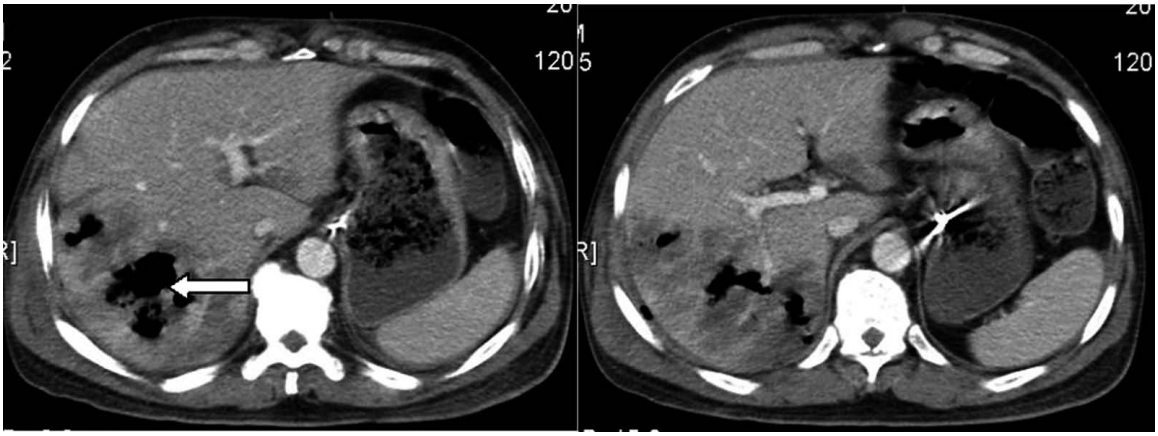

FIGURES 9.6A and B: Axial CECT postoperative follow-up study (case of blunt injury with laceration) reveals right lobe liver segment 6 air pockets (arrow) with hypodense nonenhancing areas. Air may be seen in postoperative scans.

GALLBLADDER INJURY

Trauma to the gallbladder is rare. Occurs secondary to trauma to distended gallbladder, spectrum of injuries include contusion of gallbladder wall, rupture, gallbladder avulsion, traumatic perforation may produce collections of a water density within the peritoneal cavity. CT findings of trauma include pericholecystic fluid, blurring of gallbladder contour, focal thickening or discontinuity of wall or a mucosal flap within the lumen. Hemorrhage may be seen within the gallbladder lumen. Ruptured gallbladder may be collapsed in CT.

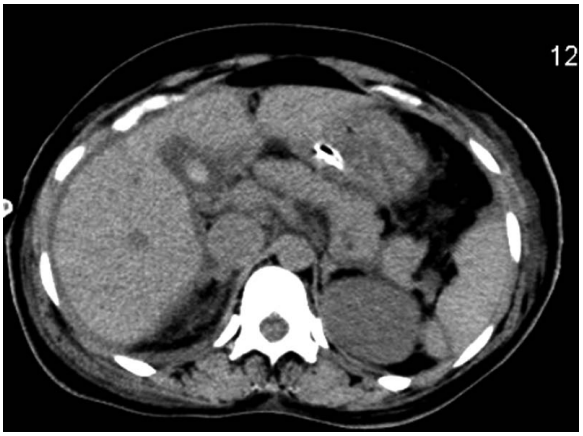

FIGURE 9.7: Axial plain CT in a patient with blunt injury shows a partially distended gallbladder with luminal high attenuation suggestive of acute hemorrhage.

SPLENIC TRAUMA

The spleen is one of the most frequently injured intraperitoneal organs in both children and adults. Upto 20% of patients with left lower rib fractures have splenic injuries. In recent years, the majority of splenic injuries have been managed nonsurgically owing to the risk of sepsis in the postsplenectomy patient.

There are varying degrees of splenic injury, which includes lacerations, fractures, rupture, intrasplenic and subcapsular hematomas. Contrast-enhanced CT is extremely sensitive in the evaluation of splenic injury. However, the grade of splenic injury at CT does not directly influence clinical management. The finding at contrast-enhanced CT that is most often considered to require surgical intervention is active extravasation of intravenously administered contrast material from the region of splenic injury.

A splenic laceration is seen at CT as an irregular, low-attenuation defect traversing the splenic parenchyma and capsule. If the cleft extends through two capsular surfaces, it is called a fracture. Lacerations are associated with free intraperitoneal fluid. If there is active arterial bleeding from the injury at the time of scanning, a focus of high attenuation that is iso- or hyperintense relative to the major arteries will be identified. At contrast-enhanced CT, an intrasplenic hematoma manifests as a well-defined lesion with decreased attenuation relative to normal splenic tissue. A subcapsular hematoma also has low attenuation but is lentiform and flattens the spleen subjacent to the capsule.

Pitfalls include splenic lobulation, cleft, Moiré spleen seen in spiral CT acquisitions, beam hardening from ribs.

Table 9.2: AAST splenic injury scale

Grade	Type	Description of injury
I	Hematoma	Subcapsular, <10% surface area
	Laceration	Capsular tear, <1 cm parenchymal depth
II	Hematoma	Subcapsular, 10–50% surface area; intraparenchymal, <5 cm in diameter
	Laceration	1–3 cm parenchymal depth; does not involve a trabecular vessel
III	Hematoma	Subcapsular, >50% surface area or expanding; ruptured subcapsular or parenchymal hematoma
	Laceration	>3 cm parenchymal depth or involved trabecular vessels
IV	Laceration	Laceration involving segmental or hilar vessels and producing major devascularization (>25% of spleen)
V	Laceration	Completely shattered spleen
	Vascular	Hilar vascular injury that devascularizes spleen

Active extravasation of contrast indicating ongoing bleed is seen as an irregular or linear high attenuation area of extravasated contrast. On excretory phase images the site of active extravasation remains high in attenuation and increases in size as contrast-enhanced blood continues to extravasate from the injured vessel.

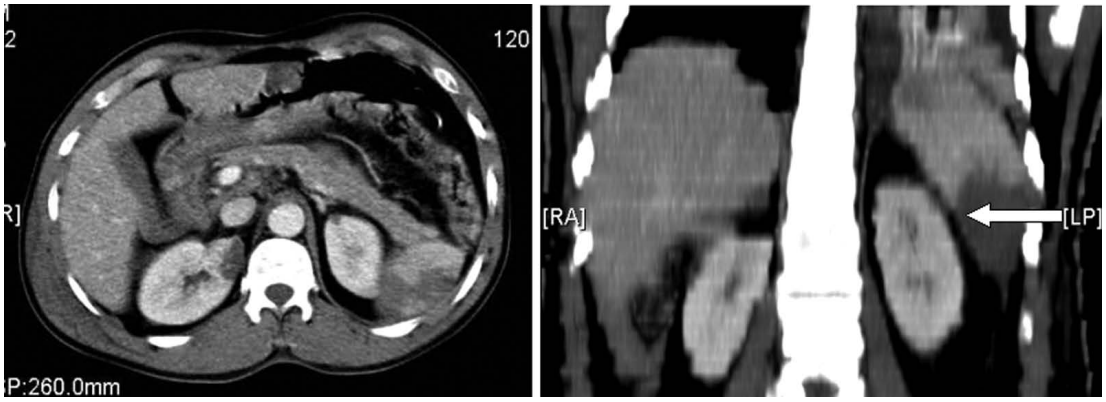

FIGURES 9.8A and B: Axial CECT reveals hypodense nonenhancing region in the lower pole of spleen suggestive of contusion (arrow).

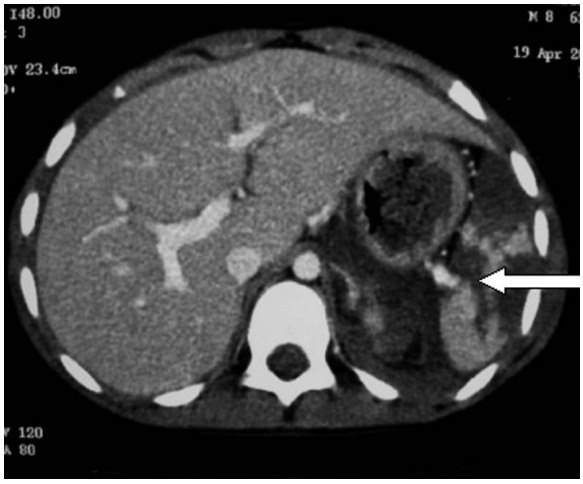

FIGURE 9.9: Axial CECT reveals a linear defect suggestive of laceration (arrow) with peripheral areas of hypodensity suggestive of contusion.

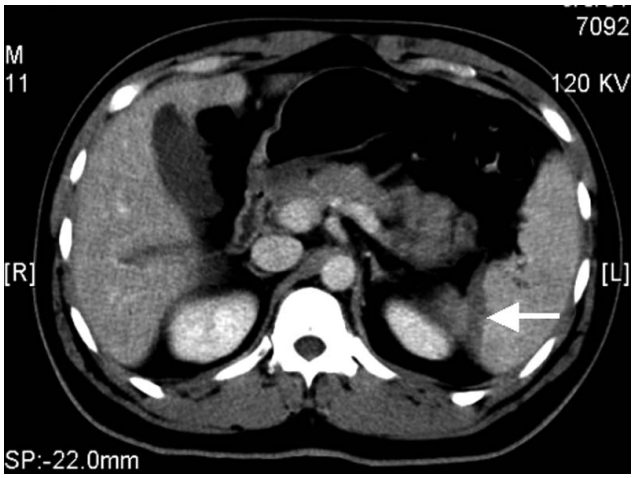

FIGURE 9.10: Axial CECT reveals a rim of perisplenic fluid around the posteromedial splenic margin (arrow).

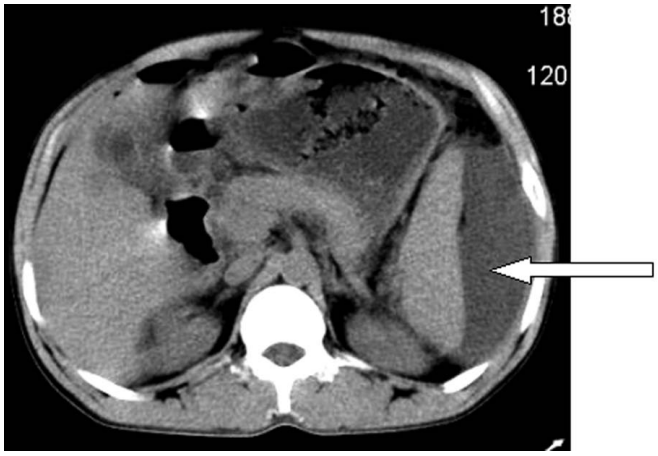

FIGURE 9.11: Axial CECT reveals a large subcapsular fluid collection indenting the spleen (arrow).

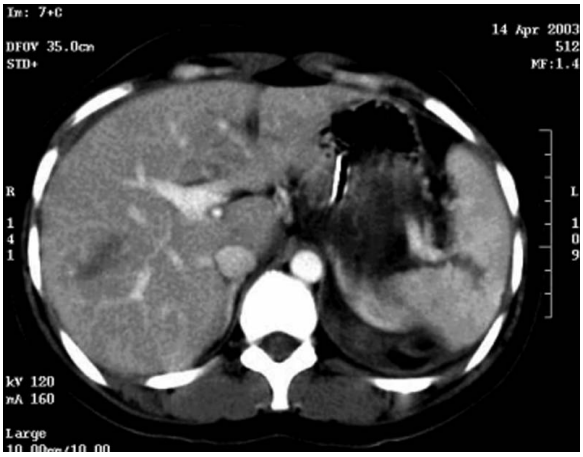

FIGURE 9.12: Axial CECT reveals a linear lucency seen in the hilum of spleen suggestive of laceration.

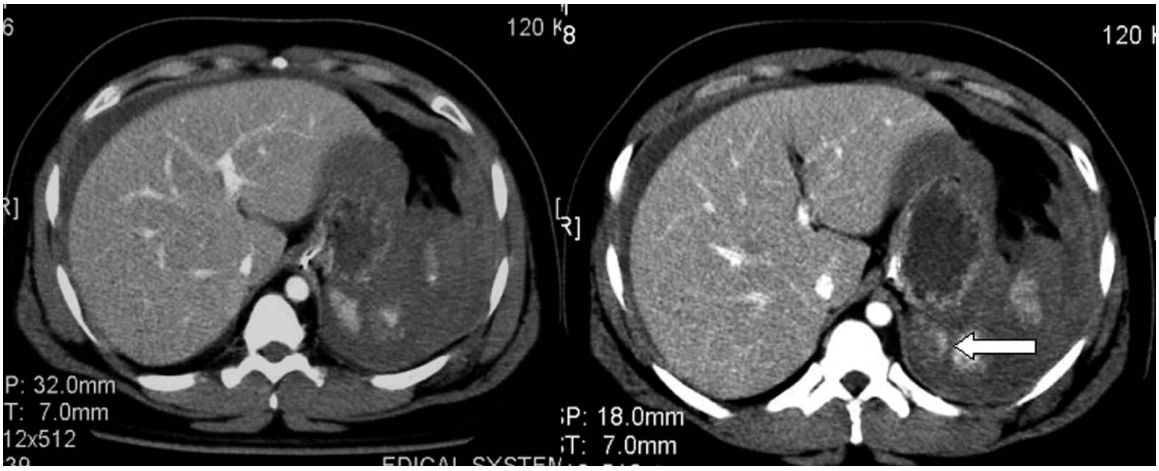

FIGURES 9.13A and B: Axial CECT reveals hypodense fragmented spleen hyperdense focus (arrow) was found to be a actively bleeding vessel at surgery.

RENAL TRAUMA

Renal injury is caused by blunt or penetrating trauma and are often associated with injuries of other organs. Major blunt trauma accounts for 80% of all urinary tract injuries. Eighty-five percent of renal injuries are minor. Five percent are shattered kidneys or have vascular pedicle injuries. Spectrum of injuries include renal contusions, cortical lacerations and fracture kidneys, shattered kidney, subcapsular hematoma, renal artery occlusion and renal vein thrombosis.

Contusions on CT are seen as focal patchy parenchymal zone of decreased IV contrast enhancement, or may appear as striated nephrogram. Lacerations appear as irregular, linear low attenuation zones extending from the periphery of the parenchyma to the intrarenal collecting system. Delayed CT images at 5-10 minutes may be needed to demonstrate extravasation of contrast material when lacerations are associated with urine leak.

Table 9.3: Renal trauma classification

Category	*Description*
I	Minor injury (renal contusion, intrarenal and subcapsular hematoma, minor laceration with limited perinephric hematoma without extension to the collecting system or medulla, small subsegmental cortical infarct)
II	Major injury (major renal laceration through the cortex extending to the medulla or collecting system with or without urine extravasation, segmental renal infarct)
III	Catastrophic injury (multiple renal lacerations, vascular injury involving the renal pedicle)
IV	Ureteropelvic junction injury [avulsion (complete transsection), laceration (incomplete tear)].

Subcapsular hematomas appear as crescent-shaped zones of low attenuation that extends along the surface of the kidney beneath the capsule, they compress and distort the normal contour of the kidney.

Traumatic renal artery injuries result from decelaration injuries that stretch the renal arteries producing intimal tears that produce thrombosis. Findings in CT include absence of nephrogram on the affected side on CECT. The cortical rim sign of peripheral renal enhancement may be seen which is due to the perfusion from the capsular arteries.

Segmental infarction may occur as a result of traumatic occlusion of one or several segmental arteries. Traumatic renal vein thrombosis may appear as persistent nephrogram on delayed scans, and the thrombus may be seen within the vein.

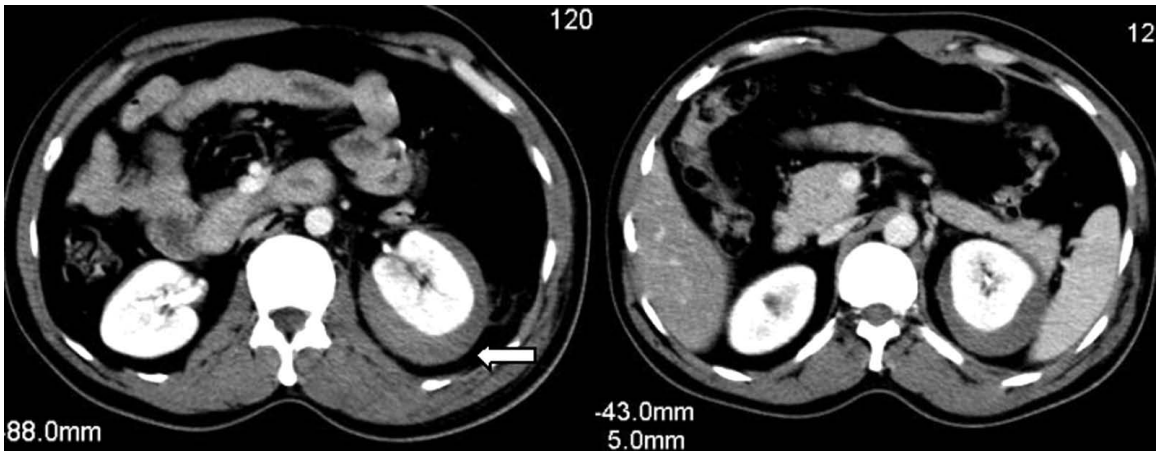

FIGURES 9.14A and B: Axial CECT reveals rim of subcapsular hemorrhage following blunt injury (arrow).

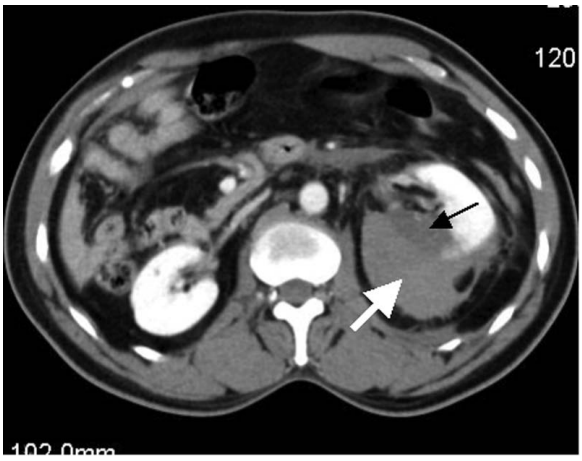

FIGURE 9.15: Axial CECT showing left perinephric hematoma medially in the left renal interpolar area displacing the kidney anteriorly (arrow). Note the nonenhancing contused medial renal cortex (thin arrow).

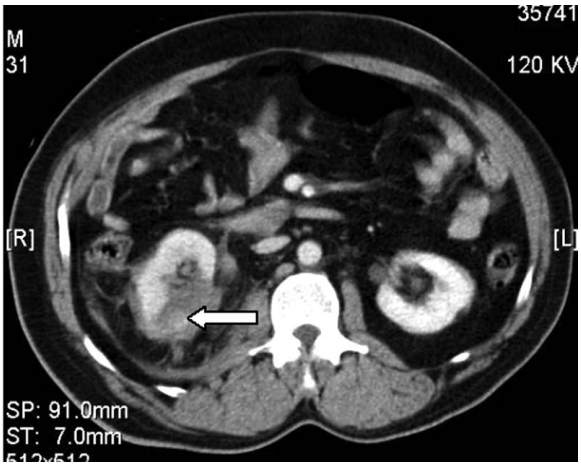

FIGURE 9.16: Axial CECT shows hypodense nonenhancing contused areas in the right renal interpolar posteromedial cortex with perinephric stranding (arrow).

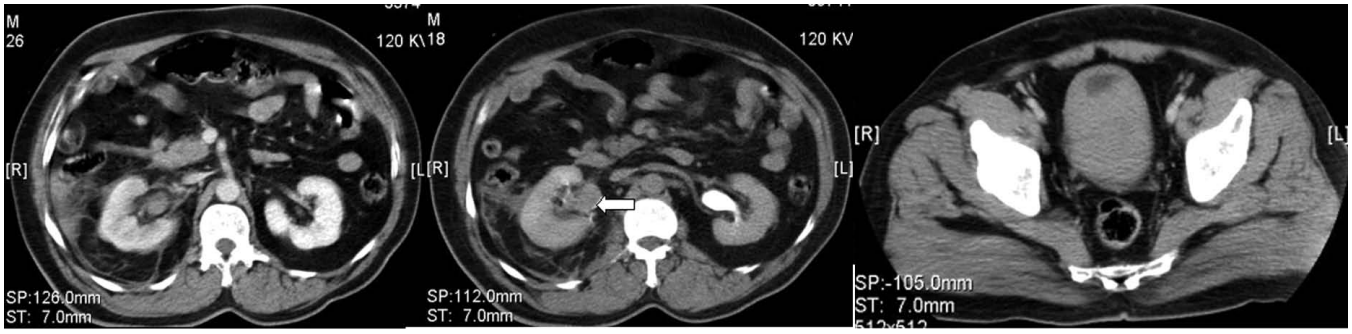

FIGURES 9.17A to C: Axial CECT reveals right renal perinephric stranding, right renal pelvis shows luminal hemorrhage (arrow). Urinary bladder shows hematoma.

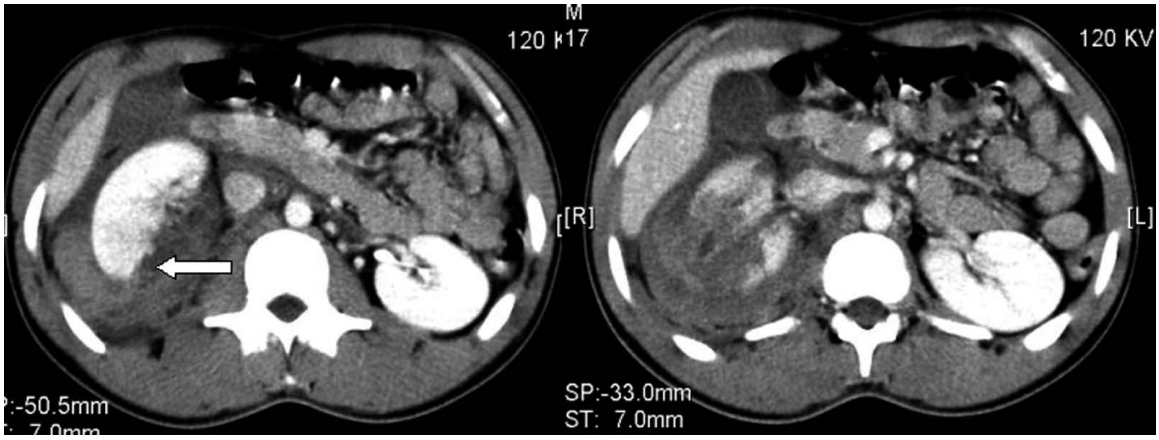

FIGURES 9.18A and B: Axial CECT shows loss of parenchyma involving the medial interpolar and postero-lateral cortex of the right kidney suggestive of contusion with laceration (arrow).

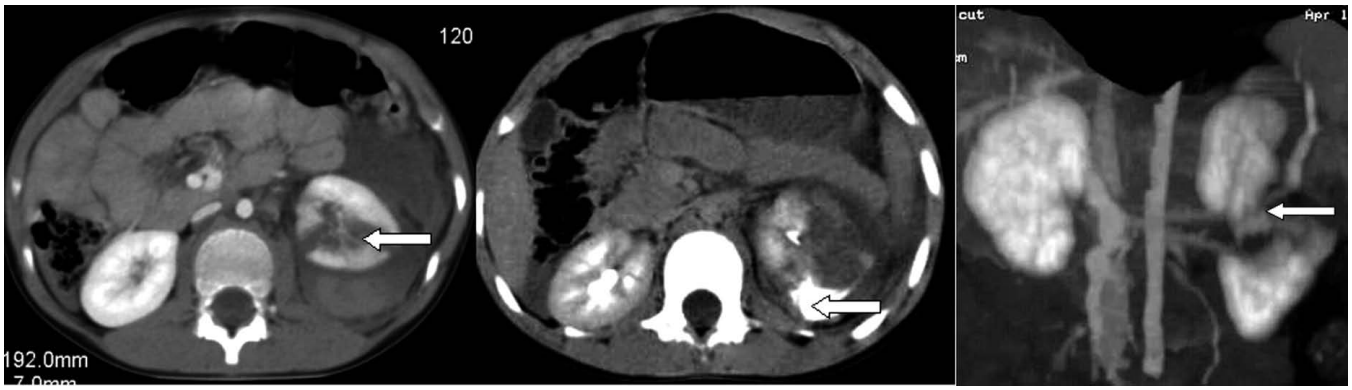

FIGURES 9.19A to C: Axial CECT showing complete laceration of the left renal interpole (Fig. A arrow) with posterior perirenal hematoma. Delayed images (arrow in Fig. B) showing contrast extravasation due to collecting system injury. Fig. C is a coronal MIP reformation showing the separated segments retaining vascularity (arrow).

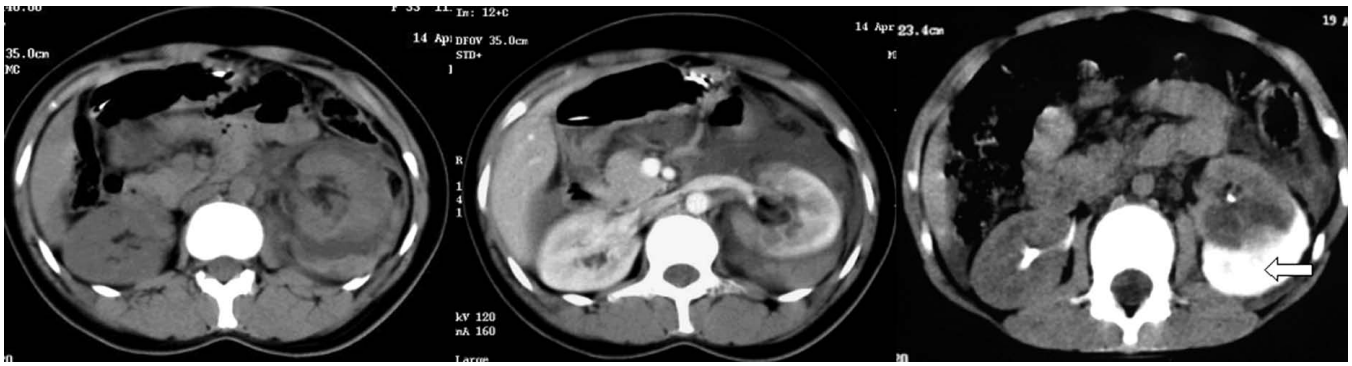

FIGURES 9.20A to C: Axial plain CT (Fig. A) showing perinephric hematoma, focal hypodense nonenhancing region seen in the posterior cortex (arrow in Fig. B) during the corticomedullary phase is suggestive of contusion. Delayed images (arrow in Fig. C) show posterior perinephric contrast extravasation. This case illustrates the need for delayed imaging so as to rule out collecting system injury as subtle injuries would be missed otherwise.

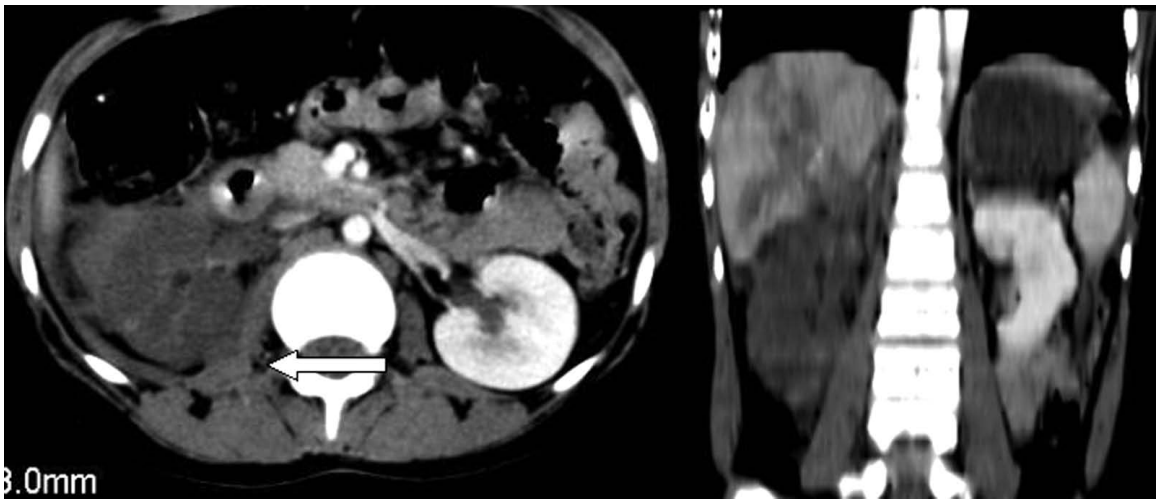

FIGURES 9.21A and B: Axial CECT with coronal reformation in a patient who sustained blunt injury to abdomen 9 hours prior to the CT scan showing nonenhancing right kidney with no enhancement or the renal vessels suggesting a dissection or thrombus of the main renal artery (arrow).

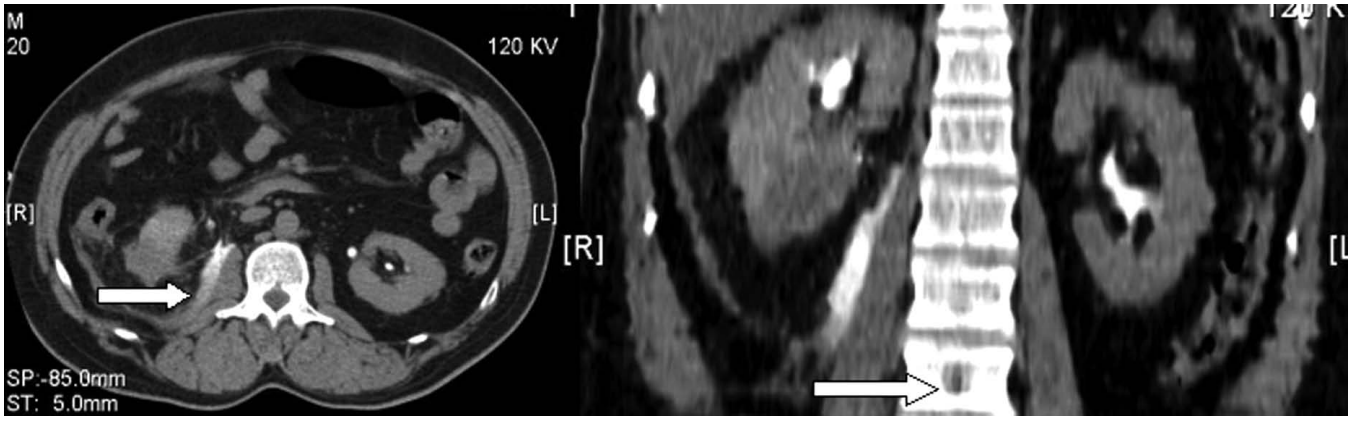

FIGURES 9.22A and B: Axial delayed phase CT with coronal reformation showing hypodense lower pole suggestive of contusion (arrow). Note the linear area of contrast extravasation (black arrow in B) due to injury to the proximal ureter just distal to PUJ.

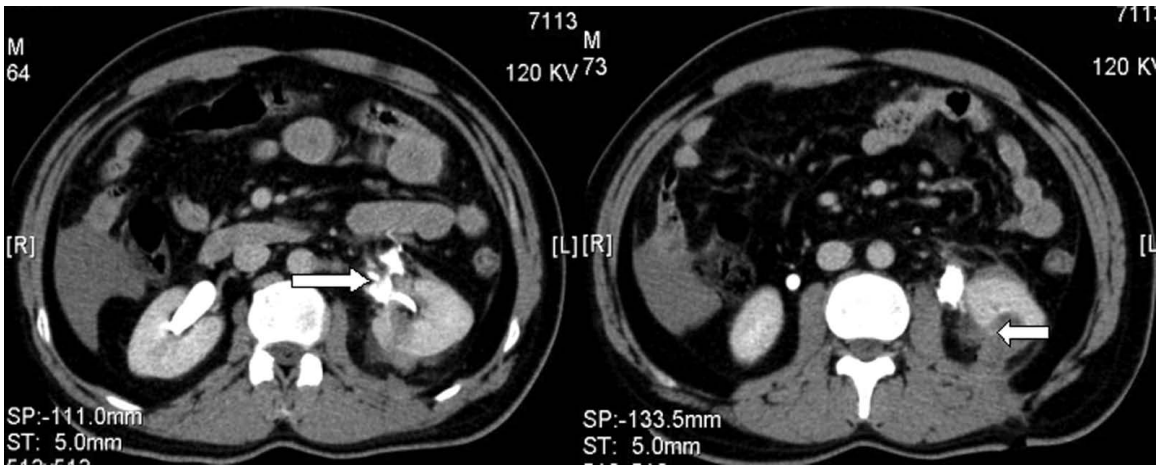

FIGURES 9.23A and B: Axial CECT reveals left renal lower pole contusion (arrow in B), renal pelvic injury with contrast extravasation (arrow in A). This emphasises the importance of delayed imaging in delineating collecting system injuries.

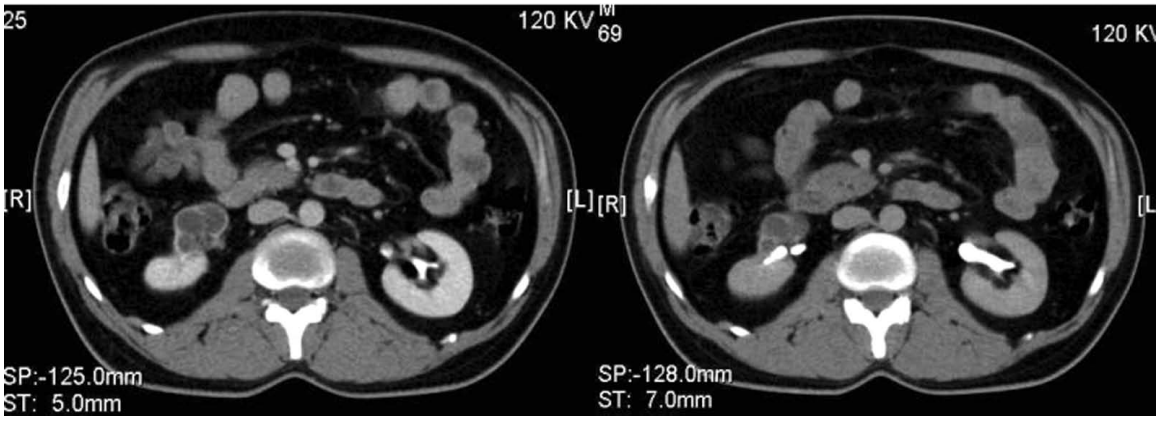

FIGURES 9.24A and B: Axial CECT follow-up study (case of renal contusion) reveals shrunken kidney with cystic changes.

BLADDER INJURY

Urinary bladder injuries occur in 10-15% of major pelvic fractures.

Mechanism of Injury

Blunt trauma is responsible for a rather large number of severe associated injuries, such as pelvic, splenic, renal, aortic, bowel, and hepatic insults. Injury is not necessarily localized to areas obviously traumatized.

Penetrating injury is often secondary to missiles, impaling objects, and knives. These injuries are of varying severity and often, but not always, result in damage to more focal areas. Some missile injuries have a vaguely estimable trajectory when one considers the entrance and exit wound, and many knife wounds still have the impaling blade in place at the time of presentation.

CT Cystographic Technique

In stable patients with suspicion of bladder injury delayed imaging of bladder following an IV contrast administration is sufficient.

In patients who are not hemodynamically stable retrograde bladder distention is required prior to CT cystography through the Foley's.

After Foley's catheter insertion, adequate bladder distention is achieved by instilling at least 350 mL of a diluted mixture of contrast material (50 mL of ioxehol and 450 mL of normal saline solution) into the bladder under gravity control). Contiguous 10 mm axial images are then obtained from the dome of the diaphragm to the perineum, thus including the upper thighs.

In our experience, postdrainage images through the decompressed bladder are not required. Removal of the Foley's catheter to identify bladder base lacerations has also proved unnecessary. Even simple deflation of the balloon with possible inadvertent removal of the catheter would be detrimental in the patient with associated urethral injury.

The normal CT cystogram will demonstrate a uniformly hyperattenuating, well-distended urinary bladder with thin walls. The adjacent fat planes will be distinct, with no evidence of extravasated contrast material.

CT Cystographic Findings in Bladder Injury

Type 1: Contusion

Bladder contusion is defined as an incomplete or partial tear of the bladder mucosa. Although patients present with hematuria, findings at conventional and CT cystography are normal. Bladder contusion is believed to be the most common bladder injury in multitrauma patients but is not in itself considered to be a major bladder injury.

Type 2: Intraperitoneal Rupture

Intraperitoneal bladder rupture occurs in approximately 10-20% of major bladder injuries. This injury is typically the result of a direct blow to the already distended bladder. The sudden increase in intravesicular pressure causes intraperitoneal rupture of the bladder dome. CT cystography demonstrates intraperitoneal contrast material around bowel loops, between mesenteric folds, and in the paracolic gutters.

Type 3: Interstitial Injury

Interstitial bladder injury is rare and is defined as an intramural or partial-thickness laceration with intact serosa.

Type 4: Extraperitoneal Rupture

Extraperitoneal rupture is the most common type of bladder injury (80–90% of cases). It is usually caused by penetrating trauma; in blunt trauma, the presumed mechanism is direct laceration of the bladder by bone fragments from a pelvic fracture. The path of extravasated contrast material is variable. Extravasation is confined to the perivesical space in simple extraperitoneal ruptures (Type 4a), whereas in complex extraperitoneal ruptures, contrast material extends beyond the perivesical space (Type 4b) and may dissect into a variety of fascial planes and spaces.

Type 5: Combined Rupture

Combined bladder rupture consists of simultaneous intraperitoneal and extraperitoneal injury. The prevalence of combined bladder rupture is 5–12% in published series that include both penetrating and blunt trauma.

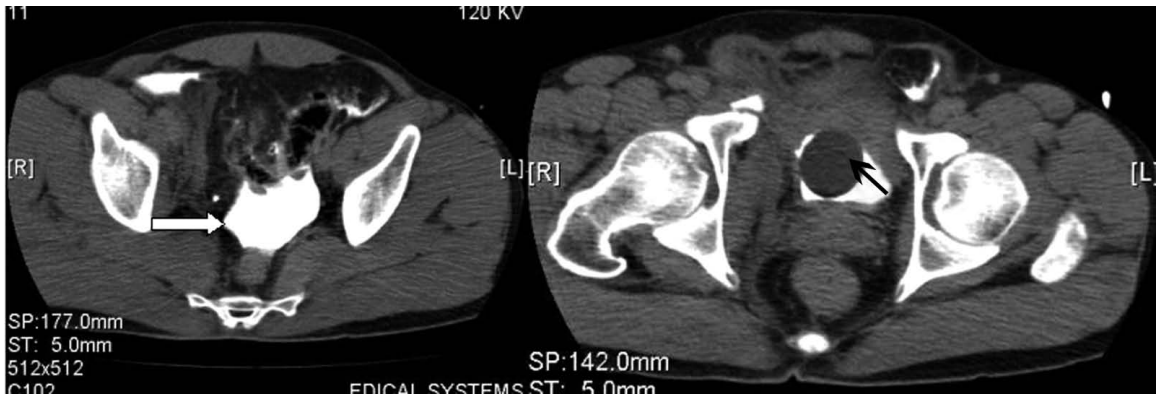

FIGURES 9.25A and B: Axial CECT showing the extravasated contrast in the pelvis (arrow in A), sections at the level of urinary bladder shows the thickened anteroinferior wall (arrow in B)—Intraperitoneal rupture.

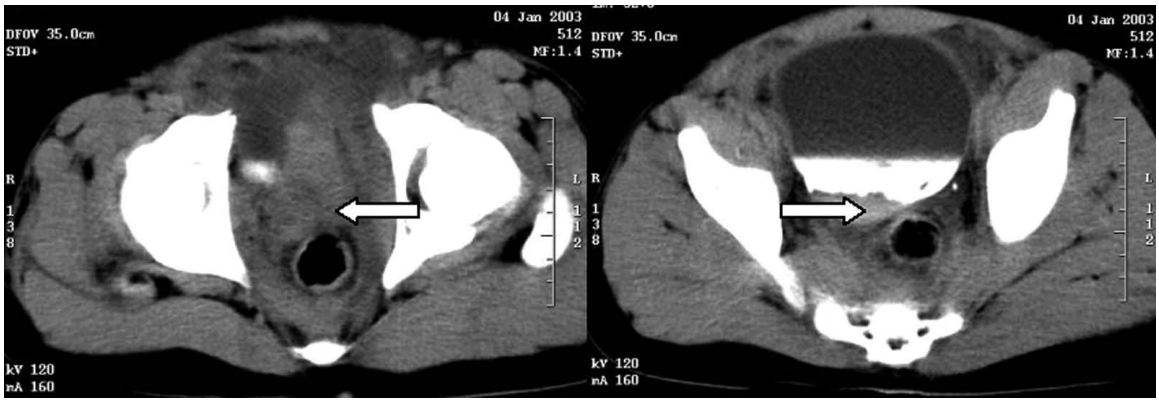

FIGURES 9.26A and B: Axial CECT showing hematoma of the bladder base indenting the left lateral wall (arrow in Fig. A), Fig. B shows a layered hematoma (arrow in B).

BOWEL AND MESENTERIC INJURIES

Hemoperitoneum is no longer an unequivocal indication for exploratory laparotomy in a stable patient. More emphasis is now placed on nonsurgical management of liver and spleen injuries. The concurrent presence of significant bowel or mesenteric injury, however, would make conservative treatment inappropriate and necessitate exploratory laparotomy.

The current surgery literature even suggests that a negative CT scan can be used as a screening tool to help identify patients who may be discharged without further evaluation. Because so much emphasis is now placed on CT its important to have a fixed protocol for evaluation of mesenteric and bowel injuries.

Bowel Discontinuity

Discontinuity of bowel is the primary finding of bowel injury. Because direct visualization is unusual, we must rely on secondary findings.

Extraluminal Oral Contrast Material

Free intraperitoneal oral contrast material is 100% specific for bowel perforation.

Extraluminal Air

The finding of pneumoperitoneum has a sensitivity of 44–55%. Pneumoretroperitoneum in the setting of duodenal injury seems to be a more sensitive finding.

Intramural Air

Major bowel injuries and minor bowel injuries have findings of bowel-wall thickening and free fluid in common. Along with extraluminal air, the presence of intramural air will highlight a probable full-thickness rather than partial-thickness injury.

Bowel-wall Thickening

Bowel-wall thickening, seen in 75% of transmural injuries, is sensitive for bowel-wall injury. Isolated mesenteric lacerations may also demonstrate this sign, probably as a result of interruption of the arterial supply or venous drainage. Disproportionate thickening compared with normal segments or bowel-wall thickness greater than 3 mm with adequate bowel distention is abnormal.

Bowel-wall Enhancement

Bowel-wall enhancement without perforation as part of the hypoperfusion complex (shock bowel) in children has been described in litreature. The proposed cause of enhancement of reduced perfusion and interstitial leak of contrast material fits into the categories of either local vascular damage related to bowel or mesenteric injury or the more systemic hypoperfusion complex.

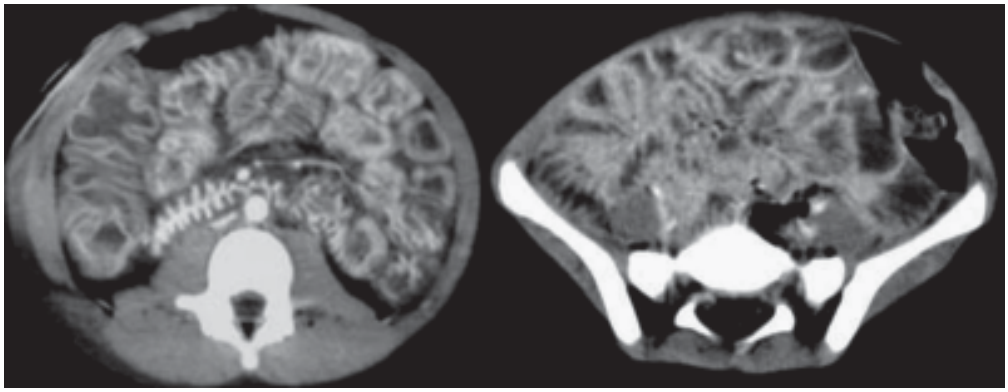

FIGURES 9.27A and B: Axial CECT showing diffusely enhancing bowels in a patient who has sustained blunt injury.

Mesenteric Infiltration

Mesenteric infiltration or "stranding" can be associated with mesenteric injury with or without bowel perforation but bowel-wall thickening associated with stranding is highly suggestive of significant bowel injury. Mesenteric findings are more common when bowel injury is along the mesenteric border. A localized hematoma within the mesentery in the absence of a bowel abnormality points to an isolated laceration of a mesenteric vessel.

Intraperitoneal and Retroperitoneal Fluids

Hematomas can occur in the peritoneal cavity, retroperitoneum, or both. Retroperitoneal hematoma along with wall thickening helps identification of duodenal trauma and is frequently present with this type of injury. Hemoperitoneum is a common finding in patients with intraperitoneal bowel or mesenteric laceration (88–100% of patients). Periduodenal hematoma is a fairly specific sign of duodenal injury because retroperitoneal blood tends to localize at the site of injury. This is in contrast with intraperitoneal blood for which the absence of restriction allows blood from solid organ injury to flow freely where it may be associated with normal bowel loops. It follows that hemoperitoneum in the absence of solid organ injury would imply bowel or mesenteric laceration as the source of bleeding.

PANCREATIC INJURY

Pancreatic injuries are uncommon with blunt abdominal trauma and when it occurs it is associated with injuries of other organs like duodenum and liver, the usual mechanism of injury is a anterior midline blow causing compression of pancreas against the vertebral column. Spectrum of injuries include contusion, hematoma, pancreatitis, laceration or fracture.

Pancreatic injuries are more common in children and young adults, complications of missed or delayed diagnosis includes recurrent pancreatitis, pseudocyst formation or pancreatic abscess.

Pancreatic lacerations and fracture appear as interruptions in the parenchyma, with associated fluid in the anterior pararenal space, subtle injuries may appear as pancreatic enlargement, masses or irregularity in contour which may be associated with peripancreatic fluid collection. Fluid around the SMA, fluid in the transverse mesocolon or lesser sac, thickening of pararenal fascial planes may also be seen in otherwise occult injury.

CLASSIFICATION

Type 1—Minor contusion or hematoma, capsule and duct intact.
Type 2—Parenchymal injury without major ductal injury.
Type 3—Major ductal injury.
Type 4—Severe crush injury.

CT FINDINGS

- Edema/fluid in peripancreatic fat.
- Focal/diffuse pancreatic enlargement.
- Irregularity of pancreatic contour.
- Areas of low attenuation, fluid around SMA.
- Fluid in transverse mesocolon/lesser sac.
- Fluid between pancreas and splenic vein.
- Thickening of anterior pararenal fascia.

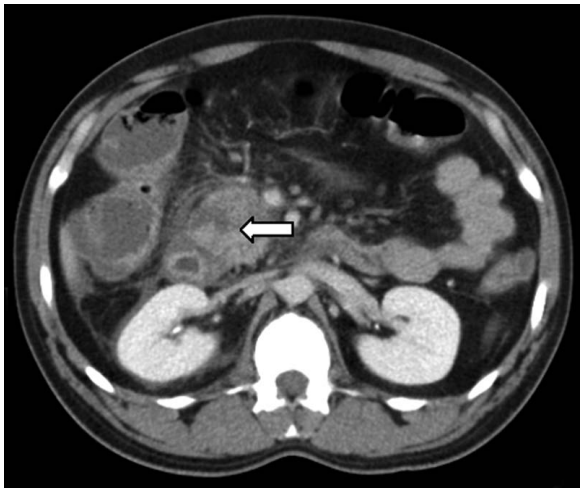

FIGURE 9.28: Axial CECT in patient with blunt abdominal trauma showing focal enlargement with hypodensity in the pancreatic head (arrow) suggestive of traumatic pancreatitis.

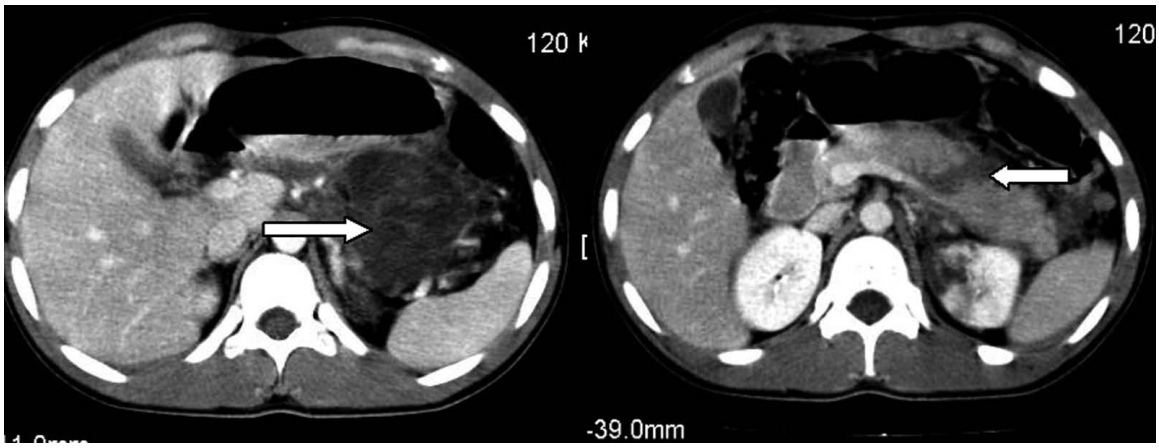

FIGURES 9.29A and B: Axial CECT showing organized collection in the lesser sac region (arrow in A) secondary to laceration of the pancreatic body seen as a hypodense longitudinal nonenhancing area (arrow in B).

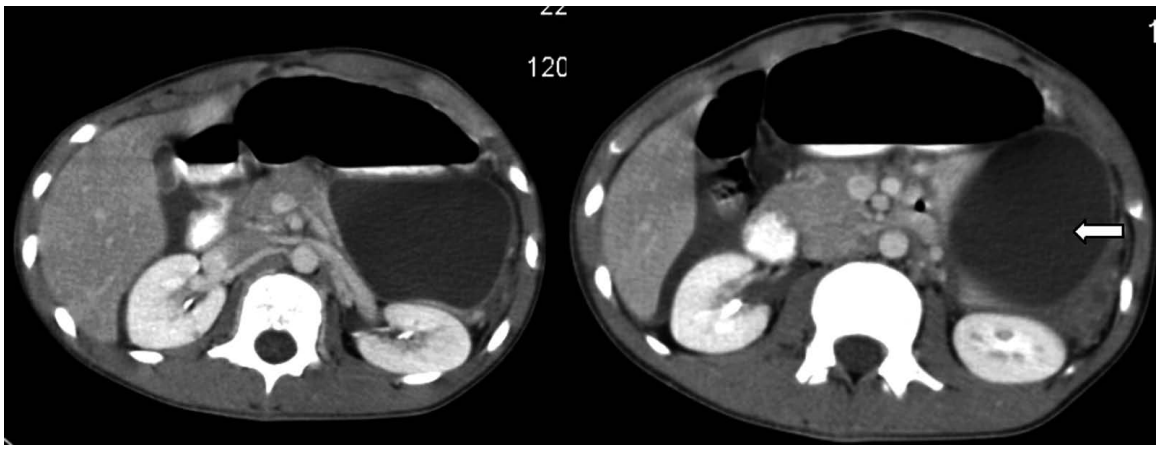

FIGURES 9.30A and B: Axial CECT showing post-traumatic pseudocyst arising from the pancreatic tail in the lesser sac region (arrow).

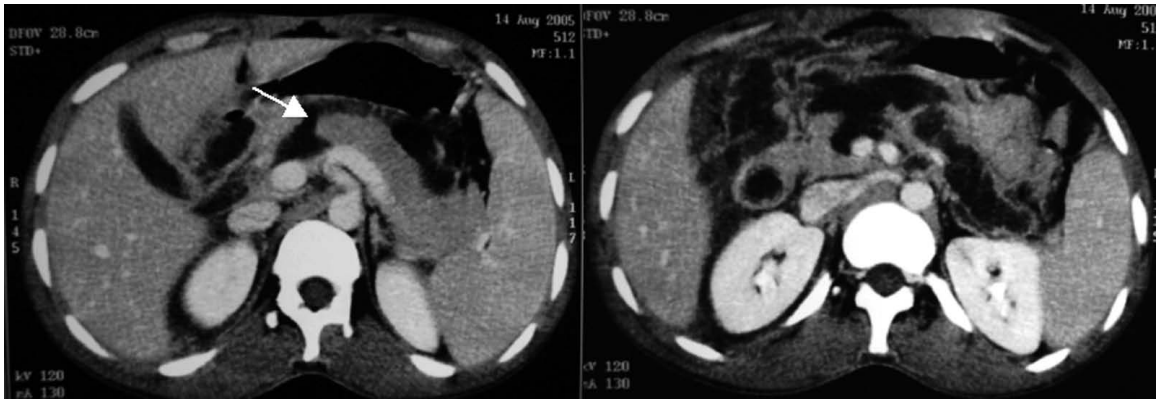

FIGURES 9.31A and B: Axial CECT in a patient with a 1-month-old blunt injury history shows a linear laceration of the pancreatic neck with peripancreatic collection (arrow).

IVC IN ABDOMINAL TRAUMA

In cases with blunt trauma its very useful to note the shape and caliber of IVC, as a useful indicator of the patients intravascular fluid volume. When IVC is oval and plump, it usual implies that fluid replacement therapy has been sufficient for the patients needs. When IVC is thin and flat on multiple CT slices it indicates insufficient fluid replacement. CT demonstration of a flat IVC is a early sign of hypovolemia.

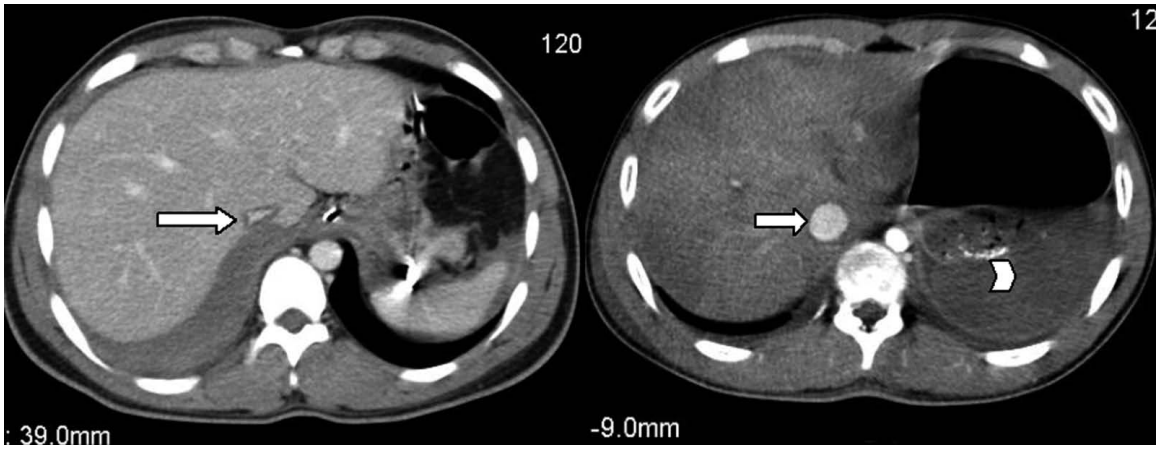

FIGURES 9.32A and B: Axial CECT in two different patients with trauma—Fig. A shows the flat IVC (arrow) due to massive hemoperitoneum. Fig. B shows a plump IVC after emergency reperfusion of fluids, note the hypodense liver and spleen reflecting a sequelae to very severe hypovolemia (arrowhead).

ADRENAL INJURY

Adrenal injuries occur secondary due to severe **trauma**, because the adrenal glands are small, relatively well-protected structures in the retroperitoneum. In 25% of cases incidental adrenal hematoma can be seen in major abdominal injuries. Two proposed mechanisms of injury include-severe hyperextension and lateral compressive force—either of which can result in direct injury that is probably due to compression against the spine. These direct injuries are often associated with other ipsilateral injuries: Left adrenal hematomas were more associated with left rib fracture and with **splenic** and left renal injuries. Right adrenal hematomas were more common and were more highly associated with right rib fracture and with hepatic and right renal injuries. The greater propensity for right

adrenal hematomas may be explained by the more confined space of the right adrenal gland between the liver and the spine and the greater mass of the liver.

The right adrenal gland, along with a very short direct adrenal vein, lies directly posterior to the inferior vena cava. With rapid deceleration injury and blunt **trauma** to the abdomen, very high abdominal pressure is probably transmitted through the vena cava, and thus through the adrenal vein, for a short duration. On the left, this pressure would dissipate through the left renal venous system, but on the right, it would be transmitted directly to the adrenal gland through the short right adrenal vein.

One potential difficulty in diagnosing **trauma**-induced adrenal hematoma is due to the common occurrence of incidental adrenal masses, particularly nonhyperfunctioning adenomas. The presence of a mass in the adrenal gland of a **trauma** patient should not be considered evidence of injury because it may be a preexisting incidental lesion. Adrenal hematomas have the typical appearance: They have a mean maximum diameter of 2.8 cm, most are ovoid, and are associated with periadrenal stranding. Most of the adrenal hematomas are slightly hyperattenuating, and they had a mean attenuation of 52 HU.

Determining the attenuation of lesions may be useful in distinguishing adrenal hematoma from incidental adenoma. Most acute adrenal hematomas are relatively hyperattenuating, while most adenomas are relatively hypoattenuating.

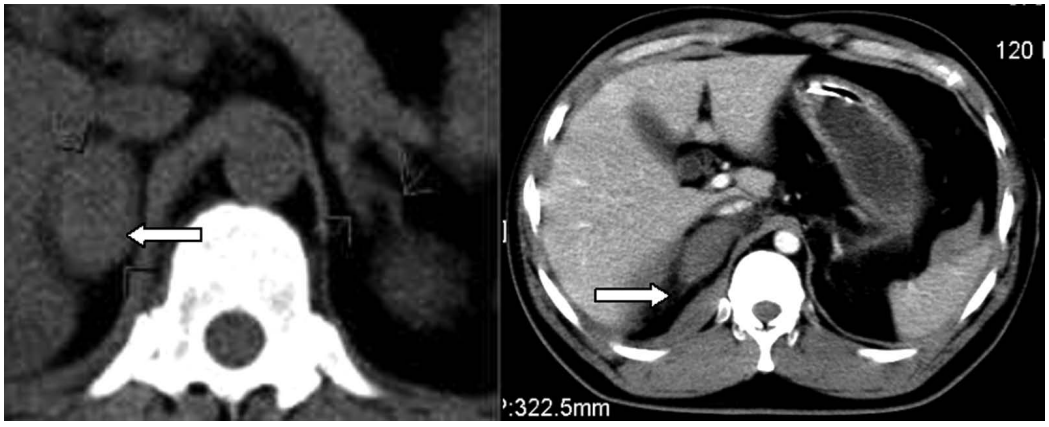

FIGURES 9.33A and B: Axial plain study in a blunt abdominal trauma reveals a ovoid high attenuation right adrenal lesion (arrows in A). Axial CECT in a patient with chest and abdominal trauma reveals right adrenal lesion with adjacent thickening of the diaphragmatic crus (arrow in B).

DIAPHRAGMATIC INJURY

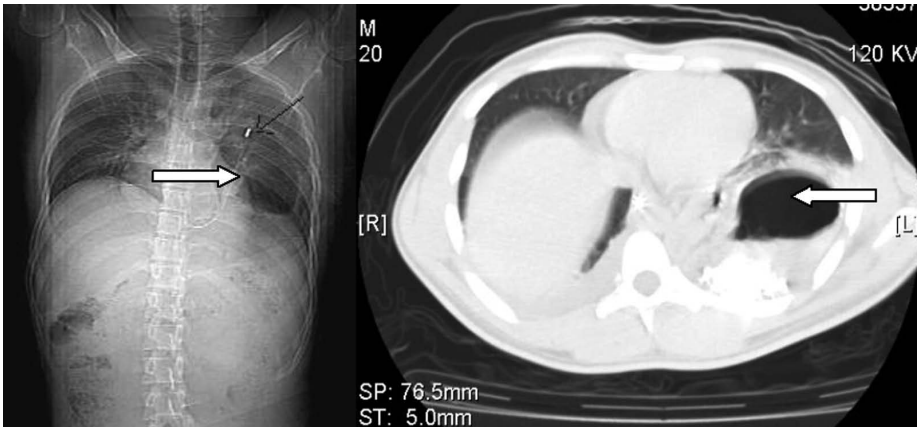

FIGURES 9.34A and B: Digital scanogram showing the presence of gastric air bubble in the left hemithorax (arrow in A). Note the tip of Ryle's tube within it. Axial images after administration of oral contrast showing the fundus of stomach within the left hemithorax.

Findings suggestive of hemidiaphragmatic tears:

1. Direct discontinuity of the hemidiaphragm was seen in 71–73% of cases. A diaphragmatic defect appears to be the most sensitive sign of rupture seen at conventional CT with a sensitivity of 73% and a specificity of 90%.
2. Intrathoracic herniation of abdominal contents has a sensitivity of 55% and a specificity of 100%. The stomach and colon are the most common viscera to herniate on the left side, and the liver is the most common viscus to herniate on the right side.
3. The collar sign, a waist-like constriction of the herniating hollow viscus at the site of the diaphragmatic tear, has a sensitivity of 63% with helical CT and is most frequently diagnosed. On the right side, the collar sign can appear as a focal indentation of the liver, a subtle sign easily overlooked on axial images.
4. The dependent viscera sign is an additional sign that is observed in 90% of cases. When a patient with a ruptured diaphragm lies supine at CT examination, the herniated viscera (bowel or solid organs) are no longer supported posteriorly by the injured diaphragm and fall to a dependent position against the posterior ribs. Consequently, the dependent viscera sign is present if the upper one-third of the liver abuts the posterior ribs on the right side or if the stomach, spleen, or bowel abuts the posterior ribs on the left side. However, this sign is rarely isolated but represents an early indication of diaphragmatic tear on axial images before visceral herniation can be confidently diagnosed by using sagittal and coronal multiplanar reformation.

Index

A

Abdominal trauma 358
Abdominal wall 347
Acute acalculous cholecystitis 77
Addison's disease 230
Adenomyomatosis 76
Adrenal cyst 230
Adrenal gland 222
Adrenal hyperplasia 229
Adrenal injury 373
Adrenal mass 225
  adrenocortical carcinoma 227
  miscellaneous 226
  myelolipomas 225
  pheochromocytoma 227
Adrenal pseudomasses 222
  hyperfunctioning adrenal cortical neoplasms 223
  hyperfunctioning adrenal medullary neoplasms 223
Alcoholic chronic pancreatitis 107
Angiomyolipoma 161
Anomalies and anatomical variants 103
  annular pancreas 104
  ectopic pancreatic tissue 104
  pancreatic divisum 103
Approach to abdominal pain 342
Approach to liver masses 34
Approach to renal cyst evaluation 170
  cystic renal disease—classification 170
    nongenetic disease 170
Autoimmune pancreatitis 107
Axial anatomy 1

B

Biliary obstruction 82
  cause of obstruction 82
  level and extent of obstruction 82
Biliary tract diseases 83
  choledocholithiasis 83
Bladder injury 368
  CT cystographic findings in bladder injury 368
    combined rupture 369
    contusion 368
    extraperitoneal rupture 369
    interstitial injury 368
    intraperitoneal rupture 368
  CT cystographic technique 368
  mechanism of injury 368
Bowel and mesenteric injuries 369
  bowel discontinuity 370
  bowel-wall enhancement 370
  bowel-wall thickening 370
  extraluminal air 370
  extraluminal oral contrast material 370
  intramural air 370
  intraperitoneal and retroperitoneal fluids 371
  mesenteric infiltration 371

C

Causes for pancreatic calcification 116
  chronic pancreatitis 116
  cystic fibrosis 116
  hyperparathyroidism 116
  tumor 116
Causes of GI fistulas 315
Characteristic tumor component 336
  aortic aneurysms 339
    inflammatory abdominal aortic aneurysm 339
  aortic dissection 340
    etiology/pathophysiology 340
    lliopsoas hemorrhage 341
  impending rupture 340
  inflammatory lesions 342
  retroperitoneal fibrosis 338
  vascularity 338
Characterization of the retroperitoneal space 334
  anterior pararenal space 335
  great vessel space 335
  perirenal space 335
  posterior pararenal space 335
  psoas muscle space 334
Cholangiocarcinoma (CCA) 83
  extrahepatic cholangiocarcinoma 86
    infiltrating extrahepatic cholangiocarcinoma 86
    polypoid extrahepatic cholangiocarcinoma 86
  intrahepatic cholangiocarcinoma 84
    exophytic hilar cholangiocarcinoma 85
    hilar cholangiocarcinoma 85
    infiltrating hilar cholangiocarcinoma 85
    intraductal intrahepatic cholangiocarcinoma 84
    mass-forming intrahepatic cholangiocarcinoma 84
    periductal infiltrating intrahepatic cholangiocarcinoma 85
    polypoid hilar cholangiocarcinoma 85
Cholecystitis 71
  acute cholecystitis 71
    complications 72
  emphysematous cholecystitis 72
  empyema 72
  gangrenous cholecystitis 72
  xanthogranulomatous cholecystitis 75
Choledochal cyst 86
  classification 87
    pyogenic cholangitis (oriental cholangitis) 87
    sclerosing cholangitis 88
Chronic calculus cholecystitis 78
Chronic myeloid leukemia 96
Chronic obstructive pancreatitis 107
Chronic pancreatitis 113
  radiographic diagnosis 113
  role of imaging in chronic pancreatitis 114
Classification of congenital renal abnormalities 139
  anomalies of rotation 142
  ask upmark kidney 141
  bilateral renal agenesis 140
  crossed renal ectopia 143
  cystic disease 145
  horseshoe kidney 144
  renal agenesis 140
  renal aplasia 141
  renal ectopia 142
  simple renal hypoplasia 141
  solitary kidney 140
Congenital adrenal cortical hyperplasia 230

Congenital lesions 69
gallbladder number 69
gallbladder position 69
gallbladder shape 69
Contour distortions of extrinsic origin 288
abnormalities in fold size 291
dilated lumen, normal folds 290
extrinsic mass effect and tethering 288
separation of bowel loops without tethering 289
CT angiogram 353
3D rendering techniques 353
CTA of the abdominal aorta 355
CTA of the kidney 353
renal transplant donor evaluation 353
CTA of the liver 356
CTA of the mesentery 354
CTA of the pancreas 354
pancreatic tumor evaluation 354
oncologic imaging 356
CT arterial portography 16
CT arteriography 17
CT protocols 17
CT arteriography 17
CT evaluation of pancreatic cancer 120
differential diagnosis of cystic lesions of the pancreas 124
abscess 124
cystadenocarcinoma 124
cystic fibrosis 124
dysontogenic cyst 124
IPMT 124
lymphangioma 124
macrocystic adenoma 124
microcystic adenoma 124
pancreatic pseudocyst 124
issues in pancreatic tumor imaging 121
adenopathy 122
CT morphology 124
intraductal papillary mucinous tumor 123
islet cell tumors 123
macrocystic cystadenoma or cystadenocarcinoma 123
metastases 122
microcystic cystadenoma 123
pancreatic adenocarcinomas 123
pancreatic mass vs inflammatory mass 121
solid papillary epithelial tumor 123
vascular encasement 121
tumor detection 120
CT indication for evaluating the GUT 232
consideration for specific areas 233
colon 234
duodenum 233
esophagus 233
stomach 233
pitfalls 232
points to be evaluated 232
regimens for abdominal survey 233
technical considerations 232
CT of duodenum 250
annular pancreas 251
CT technique 250
duodenal trauma 251
duplications and diverticula 250
hematologic abnormalities 252
infectious processes 252
inflammatory process 252
malrotation 251
neoplastic processes 252
CT pertoneogram—showing peritoneal spaces 7
inframesocolic compartment 9
left inframesocolic space 9
left supramesocolic space 8
paracolic gutters 10
pelvic peritoneal spaces 10
peritoneal spaces 7
right inframesocolic space 9
right supramesocolic space 7
supramesocolic compartment 7
CT scan features of colonic diseases 296
normal colon 296
pathologic conditions 296
CT of colonic ischemia 302
inflammation of appendage epiploicae 303
inflammatory conditions 296
ischemic colitis 302
obstruction/lleus 305
pseudomembranous colitis 304
specific causes of colonic obstruction 305
tuberculosis 303
technique 296
CT technique for blunt abdominal trauma 358
CT technique for pelvis and urinary bladder 179
bladder herniation 182
bladder stones 183
cystitis 180
extrinsic bladder compression 183
pelvic hematoma or urinoma 183
neoplasms of bladder 184
benign 184
malignant 184
urachal disease 188
outpouching from bladder 181
trabeculation 180
CT technique for retroperitoneum and peritoneum 318
patters of fluid collection in abdominal diseases 318
free vs loculated peritoneal fluid 319
interloop fluid 319
left subphrenic fluid 319
lesser sac fluid 319
peritoneal fluid density 320
right subhepatic and subphrenic fluid collections 318
peritoneal pathology 321
inflammatory disease of the mesentery 323
inflammatory process of the peritoneum 321
mesenteric disease 323
neoplastic diseases of the mesentery 323
neoplastic peritoneal diseases 322
CT techniques 68

D

Deviations of ureter 191
Differential diagnosis for adrenal lesion 231
adrenal malignancies 231
calcific adrenal lesions 231
nonmalignant adrenal disease 231
unilateral adrenal lesions 231
Differential diagnosis in pancreatic disease 135
developmental 135
focal pancreatic mass 136
inflammatory 136
miscellaneous 136
neoplastic 136
inflammatory causes 135
neoplasms 135
pancreatic and peripancreatic cystic lesions 136
pancreatic calcifications 135
pancreatic duct dilatation 136

Differential diagnosis in splenic pathology 100
patterns of involvement in splenic parenchymal disease 101
diffuse disease without focal lesion 101
multiple focal abnormalities 101
solitary lesions 101
primary causes of anomalies of splenic size 100
small spleen 101
splenomegaly 100
Differentiation inflammatory mass from carcinoma 114
Diffuse disease 98
infarction 98
primary splenic artery aneurysm 100
pseudoaneurysm 99
Diffuse liver disease 47
cirrhosis in metabolic disorders 49
hemochromatosis 49
Wilson's disease 49
CT technique 47
diffuse changes 47
cirrhosis 49
high attenuation 48
infiltrative process 48
low attenuation 47
primary biliary cirrhosis 49
primary sclerosing cholangitis 49
discussion on specific pathological processes 53
classification 53
CT findings 53
etiology 53
hepatic cirrhosis 53
geographic changes 51
focal fatty metamorphosis 51
hepatic infarction 52
lymphoma 53
metastatic disease and pseudo-cirrhosis 52
post sinusoidal hepatic disease 50
Budd-Chiari syndrome 50

G

Gallbladder and biliary tract 68
Gallbladder injury 361
Gallbladder neoplasms 78
approach to thick walled gallbladder on CT 80
carcinoma of the gallbladder 78
carcinoma as a gallbladder fossa mass 80
carcinoma as a polypoid mass 79
carcinoma with mural thickening 79
clinical features 78
imaging findings 79
vicarious contrast excretion 80
Gallstones 69
milk of calcium bile 71
Gastrointestinal-stromal tumors 294
characteristics on CT scan 294
clinical manifestations 294
diagnosis 295
Genitourinary system 137
Glossary of terms in cystic kidney 171
Graft renal artery thrombus 220
post-transplant lymphocele 221
post-transplant renal artery stenosis 221
Granulomatous lesion 94
Groove pancreatitis 106

H

Helical CT 89
Hemobilia 77
Hemoperitoneum 358
Hepatic infections 17
amebic abscess 21
hepatic granuloma 22
hydatid disease 21
tuberculous 22
benign liver tumors 24
biliary origin 24
hepatocyte origin 24
mesenchymal origin 25
diffuse inflammation 23
focal nodular hyperplasia 26
complications 27
pathology 26
fungal abscess 22
candidiasis 22
mucormycosis 23
hemangioma 25]
complications of hemangioma 25
diagnostic triad of hemangioma: peripheral filling, delayed filling, and persistence of enhancement 25
incidence 25
pathology 25
nodular regenerative hyperplasia 27
complication 28
hepatic cysts 27
incidence 28
peliosis hepatis 24
pyogenic hepatic abscess 17
Hepatic injury 359
Hernia 278
extrinsic causes 278
internal hernias 282
paraduodenal hernia 282
transmesenteric hernias 283
strangulation 279
volvulus 279
age and sex distribution 281
clinical features 281
epidemiology 280
etiology and pathogenesis 280
primary small bowel volvulus 280
secondary small bowel volvulus 281
Hodgkin's lymphoma 96

I

Identification of the organ of origin 335
Imaging of small bowel 256
benign lesions 261
adenomas 261
leiomyomas 261
normal findings and interpretation of small bowel CT 257
polyposis syndromes 262
cronkhite canada syndrome 262
Peutz-Jeghers syndrome 262
solitary polyp 262
small bowel malignancies 257
predisposing conditions 257
types of tumors in small bowel 257
adenocarcinomas 257
carcinoid tumors 259
metastatic lesions 261
neuroendocrine tumors 260
primary GI tract lymphoma 259
sarcomas 260
Individual bowel patterns 6
Inflammatory changes of the pancreas 104
acute pancreatitis 104
IVC in abdominal trauma 373

K

Kidney 137
bladder abnormalities 139
calculi 139
hematuria 139

noncontrast CT 137
corticomedullary phase 137
excretory phase 138
parenchymal phase 138
papillary necrosis 139
renal masses 139
renal pelvic and ureteral disease 139

L

Liver 14
Liver segments 1
Lymphoma 162

M

Malignant hepatic tumors 28
angiosarcoma 31
biliary cystadenocarcinoma 32
cholangiocarcinoma 30
classification of malignant tumors 28
epithelial tumors 28
mesenchymal tumors 28
epithelioid hemangioendothelioma 31
hepatic lymphoma 32
hepatocellular carcinoma 28
CT pitfalls in the diagnosis of HCC 30
risk factors for hepatoma 28
vascular effects of HCC 29
Metastasis 225
Muscles and pelvic structures 5

N

Neoplasms of the pancreas 119
rarer presentations of pancreatic carcinoma 120
types of pancreatic neoplasms 119
clinical presentation 119
incidence and prognosis 119
Neuroblastoma 229
Nonenhanced CT 15
hepatic arterial phase [HAP] 15
portal venous phase (PVP) 16
Non-Hodgkin's lymphoma 97
Non-neoplastic small bowel diseases 262
adult intussusception 274
causes of small bowel obstruction in adults 276
CT manifestations of bowel ischemia 265
GI vasculitis 270
vasculitis 270
impaired venous drainage 268
ischemia due to closed-loop small-bowel obstruction 268
ischemic bowel disorders 263
causes of acute bowel ischemia and/or ischemic colitis 263
mesenteric ischemia and infarction 263
major categories of noninfectious vasculitis 270
systemic lupus erythematosus 271
peritoneal carcinomatosis 276
persistent arterial insufficiency without reperfusion 266
portomesenteric vein gas 269
mesenteric vein gas 269
small bowel obstruction 275
specific disorders 271
antiphospholipid antibody syndrome 272
Churg-Strauss syndrome 271
Henoch-Schönlein purpura 272
Henoch-Schönlein syndrome 273
inflammatory bowel disease associated vasculitis 272
polyarteritis nodosa 271
systemic lupus erythematosus 272
transient arterial insufficiency with subsequent reperfusion 267
Normal axial CT anatomy 1

O

Omentum 10
greater omentum 10
gastrocolic ligament 11
gastrophrenic ligament 11
gastrosplenic ligament 11
lesser omentum 10
Oncocytoma 160
CT findings 160

P

Pancreas 102
examination techniques 102
technique for angiography 103
Pancreatic injury 371
classification 371
CT findings 371
Pancreatic lipomatosis 118
Pattern of inflammatory changes in acute pancreatitis 110
Patterns of bowel malignancy 309
Patterns of renal cell carcinoma 164
bosniack classification of renal cyst 170
cystic renal masses 170
renal pelvic tumors 169
Pediatric liver masses 33
classification 33
benign epithelial tumors 33
benign mesenchymal tumors 33
malignant epithelial tumors 34
malignant mesenchymal tumors 34
metastases 34
Pediatric liver tumor 35
angiosarcoma 39
atypical delayed filling is seen in hemangioma 41
diffuse liver disease 46
focal nodular hyperplasia 42
hemangioma 40
hepatic metastasic diseases 43
blood supply 43
detection by imaging 43
imaging appearances 44
hepatoblastoma 35
non-Hodgkin's lymphoma 40
patterns of hepatocellular carcinoma 36
pseudo mass 42
simple cysts 42
Pediatric renal tumor 178
abnormalities of ureteric caliber 192
approach to suspected ureteric obstruction 193
congenital anomalies 190
dilatation in the absence of intrinsic obstruction 192
entire ureter 192
lower ureter 192
upper ureter 192
lateral deviation of the ureter 192
lower ureter 192
upper ureter 192
medial deviation of the ureter 191
lower ureter 192
upper ureter 191
nonobstructive ureteral dilatation 193
Pelvicalyceal system and ureter 189
primary renal tumors in older children 179
primary renal tumors of infancy 178
secondary signs of urinary tract obstruction 193
Peritoneal folds 11

Peritoneal ligaments 10
Peritoneal pouches 12
Pneumobilia 88
anatomic locations of abdominal gas collections 332
extraluminal gas 332
intraluminal gas 332
intramural gas 332
intraparenchymal gas 332
intratumoral gas 332
causes 88
causes of pneumoperitoneum 331
pathophysiology 331
perforation 333
Pneumoperitoneum 331
Porcelain gallbladder 76
Pseudotumors 160
dromedary hump 161

R

Renal hemorrhage 216
causes of subcapsular renal or perinephric hemorrhage 217
Renal infarction 212
causes 214
Renal masses 155
approach to renal masses 156
classification 155
neoplastic 155
non-neoplastic 155
pattern of growth 156
renal cell carcinoma 158
advantages 158
corticomedullary phase 158
CT findings 159
delayed de-enhancement 159
unenhanced CT 158
Renal transplant 217
intrarenal arteriovenous fistula and pseudoaneurysm 219
parenchyma 218
parenchymal abscess 219
perirenal abscess 219
perirenal hematoma 219
perirenal lymphocele 219
pyeloureter 218
renal artery stenosis 219
renal artery thrombosis 219
renal graft torsion 220
renal vein thrombosis 220
urinoma 220
vasculature 218
Renal trauma 364
Renal vascular disorders 208
aneurysms of the renal artery 210
CT findings 210
arteriovenous communications 209
CT findings 209
polyarteritis nodosa 210
CT findings 210
renal artery stenosis 211
CT findings 212
renal neoplasms that cause renal hemorrhage 211
CT findings 211
systemic lupus erythematosus 211
CT findings 211
vasculitis 210
Renal vein thrombosis 215
causes 215
Retroperitoneum 12
anterior pararenal compartment 12
perinephric compartment 12
posterior pararenal compartment 13
Root of the small-bowel mesentery 334

S

Solid and papillary epithelial neoplasm 129
adrenal masses 134
mesenteric masses 135
pitfalls in diagnosis of pancrearic masses 129
adenopathy 133
nodes in the root of the mesentery 134
peripancreatic nodes 134
portocaval nodes 134
stomach, duodenum, and proximal jejunum 129
renal masses 134
Solitary lesions 92
cysts 92
hemangiomas 93
infection and inflammation 94
lymphangiomas 93
Spectrum of chronic pancreatitis 115
Spleen 89
Splenic calcifications 96
Splenic trauma 362
Stages of cirrhosis 54
developmental lesion 63
bile duct hamartoma 64
caroli disease 64
hepatic (bile duct) cyst 63
polycystic liver disease 64
macronodular cirrhosis 56
expanded GB fossae 56
portosystemic collaterals 57
micronodular cirrhosis 54
redistributed lobar volumes 55
neoplastic lesions 64
abscess 65
biliary cystadenoma and cystadenocarcinoma 65
cystic metastases 65
cystic subtypes of primary liver neoplasms 65
hematoma 66
hepatic extrapancreatic pseudocyst 66
intrahepatic hydatid cyst 66
undifferentiated embryonal sarcoma 64
nodular lesions in cirrhosis 57
cirrhotic nodule 57
dysplastic nodule 57
HCC 57
regenerative nodule 57
portal hypertension 58
collateral pathways in portal hypertension 59
portal venous occlusion 60
CT appearances of thrombosed veins 60
CT diagnosis of malignant thrombosis of the portal vein 61
diseases causing segmental occlusion of the portal vein 61
miscellaneous condtions 63
signs of malignant thrombi 61
Surface reformation 2

T

Technical principles of contrast enhanced CT 15
Technique for gastric CT 236
oral contrast agent 236
inflammatory conditions 237
emphysematous gastritis 237
gastritis 237
clinical features and diagnosis 238
gastric carcinoid 239
gastric lymphomas 239
miscellaneous cause of gastric wall thickening 240
post gastrojejunostomy CT 239
stromal tumors 239
CT of malignant gastric masses 240
CT of staging of gastric adeno-carcinoma 240

gastric neoplasms 238
gastric adenocarcinoma 238
gastritis 240
pathogenesis 238
Terminologies of pancreas 105
acute fluid collection 105
hemorrhage and pseudoaneurysm 106
pancreatic abscess 105
pancreatic necrosis 105
pseudocyst 105

U

Ureteral narrowing 198
neo bladder 207
continent urinary diversion 207
noncontinent urinary diversion 207
peviureteric junction obstruction 205
primary mega ureter 204
ureteral urine leaks 202
causes 202
diagnosis and imaging features 202
ureteric tumors 199
ureteroceles 203
urine leaks 201
causes 201
diagnosis and imaging features 201
Urinary infections 147
emphysematous pyelonephritis 150
renal and perirenal gas 150
etiology and pathogenesis 147
acute pyelonephritis 148
chronic pyelonephritis 148
cystitis 147
prostatitis 147
urethritis 147
xanthogranulomatous pyelonephritis 148
pyonephrosis 152
renal and perirenal abscesses 152
tuberculosis 155
Uterus and ovaries 5

W

Wandering spleen 90
atrophy 92
autosplenectomy 92
number (polysplenia, asplenia) 91
size (splenomegaly, splenic atrophy) 91